Dissertation zur Erlangung des Doktorgrades der Fakultät für Chemie und Pharmazie der Ludwig-Maximilians-Universität München

Hydrophobically Modified Polymers as a Potential siRNA Delivery System for Brain Diseases

Natascha Verena Hartl

aus Fürstenfeldbruck, Deutschland

2023

Erklärung

Diese Dissertation wurde im Sinne von § 7 der Promotionsordnung vom 28. November 2011 von Frau Prof. Dr. Olivia M. Merkel betreut.

Eidesstattliche Versicherung

Diese Dissertation wurde eigenständig und ohne unerlaubte Hilfe erarbeitet.

München, den 19.06.2023

(Natascha Verena Hartl)

Dissertation eingereicht am:	04.05.2023
1. Gutachterin:	Prof. Dr. Olivia M. Merkel
2. Gutachter:	Prof. Dr. Ernst Wagner
Mündliche Prüfung am:	06.06.2023

To my family (of choice).

Acknowledgements

The present thesis was prepared under the supervision of Prof. Dr. Olivia Monika Merkel at the Department of Pharmacy, Pharmaceutical Technology and Biopharmaceutics at the Ludwig-Maximilians-Universität München (LMU) in Munich, Germany.

First and foremost, I would like to express my deepest gratitude to Prof. Dr. Olivia Merkel for providing me the opportunity to work on such an interesting and innovative topic. I am very thankful for her excellent supervision and guidance throughout my work and her valuable advice as well as her help in preparing publications what contributed beyond measure to my scientific development over the last years. I would like to mention that she provided all this while becoming a mother for what she deserves my greatest respect as I can imagine how demanding it is to combine career and family. Furthermore, I want to thank her for all possibilities she offered me, including collaborations, additional workshops and certificates and the opportunity to present my work on several conferences.

This work was in parts further supervised by Dr. Gabriella Costabile, Dr. Aditi Mehta and Dr. Friederike Adams. Gabriella, I would like to thank you for your guidance throughout the whole research process of my first publication what includes planning, executing, documenting and interpreting of scientific experiments and the proper writing of scientific research articles. You taught me many important lessons that were of great value for my further work. Aditi I would like to thank you for your constant advice during a great period of my PhD time, for providing me guidance and expertise in especially biological issues based on your endless knowledge and additionally for the time you led and hold together our group as an excellent group leader. Rike, thank you for your excellent guidance und supervision throughout my last period of my PhD time. You not just provided me with synthesized polymers as I needed them most, you also brought new inspiring ideas into my research topic. I always enjoyed the lively discussions and meetings we had and I learned a lot during the corporate writing of our progress report.

My deepest gratitude is expressed to all other members of the Merkel as well as the Winter and Frieß group. I highly appreciate the opportunity to absolve my PhD in a team where support and cohesion are always a priority. Special thanks go to Rima, Bettina, Christoph, Domizia, Dennis, Lolo, Ute, Theresa and Fabian for a lot of fun in and outside the lab, but also deep talks and discussions and for the teamwork in so many ways. I want to put a special emphasis on Lolo and Ute: thank you for your friendship, for your support and for always being there with

an open ear no matter if work or life related. Thank you for all the conversations and special memories we made throughout this time. That would not have been the same without you!

Furthermore, I would like to thank Prof. Dr. Gerhard Winter and Prof. Dr. Wolfgang Frieß for providing such a great and welcoming working atmosphere, for fruitful discussions and valuable inputs especially within the thursday seminars, but also for numerous fun activities outside of work.

Moreover I would like to thank several colleagues and collaboration partners such as Prof. Runhui Liu from East China University of Science and Technology for providing the Nylon-3 polymers and the input for preparing the associated manuscript, Prof. Fricker and Prof. Müller for their scientific input especially regarding blood-brain barrier topics, Tobias Köthe and Viktor Balzer for the inter-laboratory exchanges and their offer for cells, Prof. Walter Mier, Dr. Philipp Uhl, Christian Kleist and Karin Leotta for their expertise and help with the *in vivo* work of this thesis that was performed with radioactive markers in the laboratories of the university of Heidelberg, Dr. Antje Appelt-Menzel and Dr. Sabrina Oerter for the joint preparation and the performance of the blood-brain barrier model experiments in the laboratories of the university of Würzburg and Dr. Stefanie Hauck and Dr. Ann-Christine König from Helmholtz Center Munich for the MS measurements within the protein corona part of this thesis.

I would moreover like to thank all students who gave me the chance to guide and teach them, Nurunnisa Özyürek, Rimsha Ahmad, Seynur Sunar, Sanja Tosheska, Nina Huber, Mara-Noel Weis and especially my bachelor student Adrian Kromer, you did great work and I wish you all the best for your future careers!

My deepest gratitude goes to my family and my friends, who supported me in any imaginable way throughout all the years. Special thanks to my mom, my little sister and my “favorite uncle” for being a family even in hard times. Eli, you always believed in me, you always offered an open ear to me, you supported me in everyday things, but also in the most challenging situations. For this I want to express my deepest gratitude to you and I want to thank you from the bottom of my heart for 15 years of friendship, for being my safe place and my partner in crime. Thank you, Tien, for more than 20 years of friendship even over long distances, then and now spending uncountable hours on the phone. Thank you, Jule, for becoming not only my roommate but also a very good friend, thank you for our balcony conversations at any time of the day or night. Thank you Nadja, for countless unforgettable moments, for always being there and all the joy you brought with you. And last but not least, a more than special thanks to Paulina for coming into my life and not leaving my side during the last phase of my PhD.

Funding Acknowledgements

This work was funded by the Else Kröner-Fresenius-Stiftung.

Table of Content

Chapter I

General Introduction

1. RNA Interference (RNAi)

RNA interference (RNAi) is a natural biologic process enabling cell defense against viruses and other foreign nucleic acids and was first discovered in 1998 by Andrew Fire and Craig Mello, for which they were awarded the Nobel Prize in Medicine or Physiology in 2006. The discovery of RNAi was the result of a study of gene expression in *Caenorhabditis elegans*, in which post – translational gene silencing of sequence specific genes occurred in response to the introduction of long double-stranded RNA (dsRNA) [1]. Based on these findings, it was further elucidated that the mediators of sequence-specific degradation of messenger RNA are 21- to 23- nucleotide small interfering RNAs (siRNAs) generated by cleavage of long dsRNAs [2], which enabled the use of RNAi to silence genes even in mammalian cells [3]. Offering the potential to theoretically silence any chosen gene with a known sequence [4], RNAi has subsequently been studied extensively as a method for therapeutic downregulation of the expression of disease-related genes. The discovery of RNAi therefore opened new avenues for the development of therapeutic options for incurable diseases.

Specifically, the first step in the process of RNAi is the production of small RNA molecules generated from long dsRNAs precursors by an RNAse III-like enzyme called "Dicer". Subsequently, the double stranded siRNA molecules consisting of a guide and a passenger strand are loaded onto a multi-protein complex called RNA-induced silencing complex (RISC), as depicted in Figure 1.

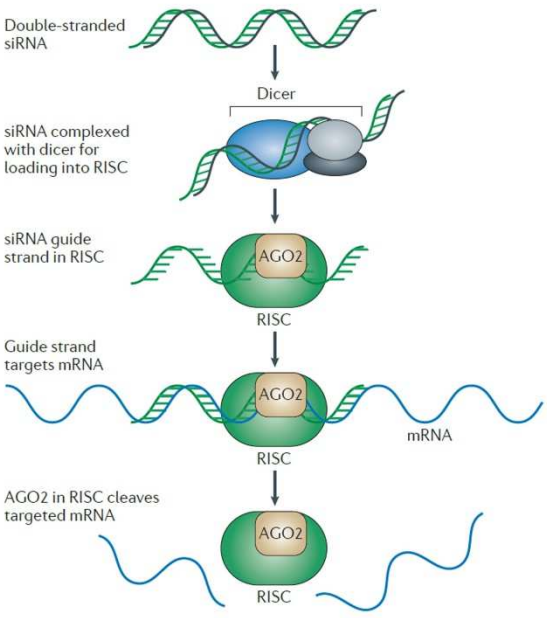

Figure 1. Mechanism of RNA interference (RNAi) induced by small interfering RNA (siRNA). Double-stranded siRNA is incorporated into RNA-induced silencing complex (RISC), which binds to targeted messenger RNA (mRNA) via the guide strand of siRNA and initiates the degradation of mRNA by Argonaute 2 (Ago2) proteins. Adopted with permission from Kole et al. [5].

One component of the RISC complex is a slicing protein called Argonaute 2 (Ago2), which cleaves and releases the passenger RNA strand [5]. The guide strand directs the RISC towards complementary sequences in the respective target messenger RNA (mRNA), and binding via intermolecular base pairing [6] initiates cleavage of the mRNA by Ago2 proteins, ultimately preventing translation of the mRNA into the respective protein [5]. Endogenous RISC is located in the cytosol of cells. Therefore, to achieve therapeutic effects, siRNA needs to be delivered into the cytosol of potential target cells.

Thus, the technique of RNAi represents a highly potential and selective tool to control disease-associated gene expression in virtually every human disease caused by pathologic gene activity, even if the disease-related genes differ solely in one or few nucleotides compared to the original gene. Taken together with much higher efficacy in comparison to other antisense strategies such as DNA oligonucleotides and ribozymes [7], RNAi holds great potential as a therapeutic strategy to tackle diseases such as autoimmune diseases, cancer, dominant genetic disorders and viral infections [8]. A variety of RNAi-based therapeutics has been developed in the laboratory; however, it remains a major challenge to translate the potential of RNAi into safe and effective drugs.

2. Delivery of siRNA

One of the major bottlenecks in developing RNAi-based therapies is the successful delivery of siRNA to the target cells since the molecule is not only featured with several unfavorable physicochemical properties but also faces many additional physiological barriers on its way to reach the site of action after systemic administration, as illustrated in Figure 2 [9]. Naked siRNA is rapidly degraded by ubiquitously present serum nucleases [10] and efficiently cleared via the kidney/urine, resulting in short plasma half-lives [11]. Furthermore, RNA molecules possess negative charges provided by the phosphate backbone, which hampers interaction with cell membranes and internalization into target cells [12]. In addition, aspects of i) immune response activation, ii) interaction with plasma proteins, iii) extravasation from blood vessels, iv) reaching target tissues, v) cell entry, vi) endosomal escape, vii) payload release, and viii)

incorporation of siRNA into the RNAi machinery needs to be addressed to achieve safe and efficient therapeutic siRNA delivery [13].

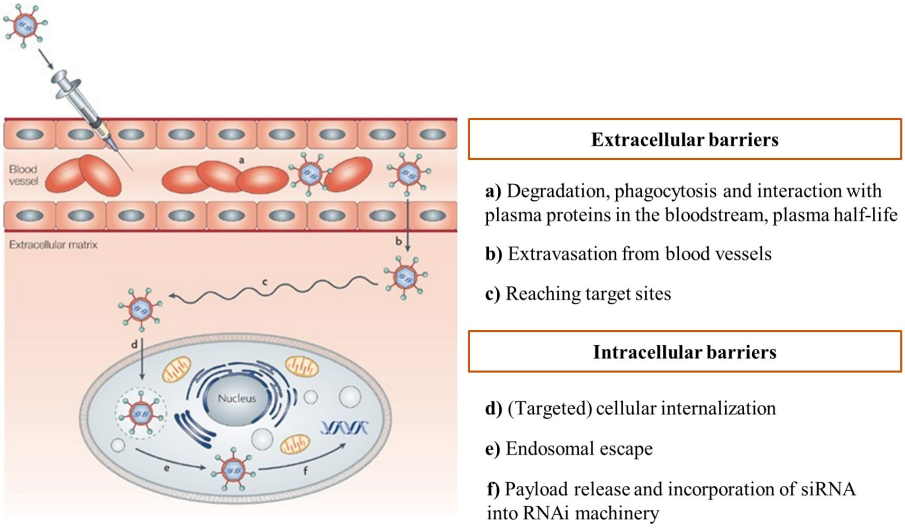

Figure 2. Physiological barriers to siRNA delivery after systemic administration exemplarily shown for a nanoparticulate formulation. Extracellular barriers comprise a) degradation by serum nucleases, immune activation, adsorption of plasma proteins and routes of elimination, b) extravasation from the blood vessels, and c) reaching the target tissues. Intracellular barriers include d) cellular internalization e) endosomal escape, f) payload release, and d) incorporation of siRNA to the RNAi machinery in the cytoplasm of the cell. Adopted with permission from Whitehead et al. [9].

Several strategies to tackle these hurdles have been developed in order to achieve improved stability, prolonged plasma half-lives and selective cell entry, including chemical modification of siRNA, forming siRNA conjugates with small molecules, aptamers, functional proteins, lipophilic molecules or polyethylene glycol (PEG), and encapsulation of siRNA into nanoparticles of various materials [14].

Carefully applied chemical alterations of siRNA bear the potential not only to improve stability against nucleases but also to reduce immune responses and off-target effects without loss of efficacy [15]. Most utilized are 2'-deoxy-2'-fluoro and 2'-O-methyl modification of ribose moieties and phosphorothioate linkages at the 5'-end of guide and passenger siRNA strands as they confer siRNAs with considerably enhanced stability against degradation by serum nucleases [16-19]. In addition, 2'-O-methyl modifications have been shown to reduce nonspecific activation of the immune system [20, 21].

Besides several conjugation approaches that improve siRNA stability, prolong circulation times and improve cellular internalization, tremendous success for targeted siRNA delivery was achieved by covalent linkage of ligands typically performed on the 3´- and 5´-terminus of the passenger strand and the 3´-terminus of the guide strand [22]. The most prominent example is the modification of siRNA with N-Acetyl-D-galactosamine (GalNac), which is a ligand for the hepatic asialoglycoprotein receptor, enabling effective hepatocyte-targeted delivery [23].

In addition, considerable research efforts have been invested in the development of nanoparticulate systems containing unmodified or less heavily modified siRNA, with a focus on lipid- and polymer- based formulations as most attractive non-viral delivery systems. Upon mixing siRNA with cationic lipids/polymers, so-called lipoplexes/polyplexes emerge due to electrostatic interactions between negative charges present in siRNA and positive charges of the nanocarriers [24].

Resulting nanoparticles can be further modified with specific ligands to achieve precise internalization into target cells via receptor-meditated endocytosis (RMT) [25]. Moreover, smart nanocarriers with unique physical and chemical properties have been developed to further improve delivery efficiency, targeting and gene silencing through the ability to respond to a complex biological environment. Stimuli-responsive moieties translate chemical or physical signals, such as acidic pH, redox gradient or even light into remarkable behavior changes [26]. Overall, numerous parameters and effective features have emerged as particularly effective for siRNA delivery, which gives prospect for successful application of RNAi in the clinic.

Even though lipid carriers require extensive formulation work to optimize the ideal composition of components and mostly possess poor drug loading [27], they are also featured with favorable pharmacokinetic and safety profiles, which allows excellent clinical translation [28]. In contrast, polymer-based vectors offer several advantages, such as a wide range of easily modifiable systems, but are characterized by a suboptimal balance between efficacy and toxicity, which has so far hampered successful translation into the clinic [27].

To date, only five RNAi-based drugs, formulated either with cationic lipids (Onpattro™) or as siRNA conjugates (Givlaari™, Oxlumo™, Leqvio™, Amvuttra™), have been approved for clinical use by regulatory authorities in various countries. Only in 2018 the very first RNAi therapeutic (Patisiran, Onpattro™) was approved by the U.S Food and Drug Administration

(FDA) and the European Medicines Agency (EMA) for the treatment of hereditary amyloid transthyretin-mediated (hATTR) amyloidosis. Patisiran contains a double-stranded siRNA encapsulated by a lipid carrier that is administered via intravenous infusion and targets the production of the abnormal form of the transthyretin protein in the liver, which is responsible for the build-up of amyloid deposits in tissues and organs [29]. The cationic lipid DLin-MC3-DMA is responsible for the formulation of siRNA, such as siRNA encapsulation, and regulates the siRNA delivery into hepatocytes, including cellular uptake and release of the payload from the endosome. The targeting ligand Apolipoprotein E (ApoE) adsorbs to the nanoparticles upon administering the formulation into the circulatory system and induces active cell uptake by RMT into hepatocytes. In addition, further components of the lipid carrier, namely 1,2-distearoyl-sn-glycero-3-phosphocholine (DSPC) and cholesterol possess structural functions, whereas PEG2000-C-DMG components confer the particles with higher hydrophilicity and thus higher circulation times for further uptake into hepatocytes [30]. Meanwhile, four further RNAi-based drugs are approved for the treatment of acute hepatic poryphyria (AHP) (Givosiran, Givlaari™, 2019), hyperoxaluria type 1 (PH1) (Lumasiran, Oxlumo™, 2020), heterozygous familial hypercholesteremia (Inclisiran, Leqvio™, 2021) and amyloid transthyretin-mediated (ATTR) amyloidosis with polyneuropathy (Vutrisiran, Amvuttra™, 2022). In all cases, a potent delivery approach based on conjugation of GalNAc molecules to the siRNA passenger strand for active targeting of hepatocytes via asialoglycoprotein receptor 1 and enhanced stabilization chemistry of the siRNA obviated the need for a nanoparticulated formulation [31-34].

3. Polymer-based gene delivery

Polymers that are used for nucleic acid delivery are chemically and structurally diverse and can derive either from one monomer (homopolymers) or from two or more subunits arranged randomly or in blocks (copolymers). Various chemical synthesis tools enable the design of macromolecules with linear, branched, dendrimer, star or graft architectures [35]. Some systems were initially investigated for DNA delivery and later additionally applied for other nucleic acids such as siRNA.

Among the earliest investigated materials are linear polycations such as poly-L-lysine (PLL) and polyethylenimine (PEI), that contain cationic charged amine groups, enabling efficient nucleic acid packaging [36, 37]. Further linear polycations such as poly (amidoamines) (PAAS)

or poly(β-amino esters) (PBAEs) were additionally studied. However, besides efficient payload protection and uptake abilities, these materials also possess unfavorable toxicity profiles and low endosomal escape abilities.

Other highly investigated classes of polymers are branched (co)polymers, e.g., PEI or PBAEs and dendrimers consisting of poly (amidoamine) PAMAM or polypropylene imine (PPI) [38-40].

Branched PEI with a high molecular weight (25kDa) is an especially high performing nanocarrier with great transfection efficacy caused by high charge density and evolved to the "golden standard" of gene carriers. PAMAM dendrimers contain hydrogen-bonding amide and tertiary amine groups in their cores and display primary amine end groups as their corona, conferring them with high cellular internalization abilities. Advantageously, due to present amine groups with different pKa values, both systems are featured with excellent endosomal escape abilities. After internalization into endosomes, the shift to lower pH values induces the protonation of further amine groups, which is hypothesized to cause an influx of chloride ions and water into the endosome and thus osmotic swelling and endosomal membrane disruption with subsequent payload release into the cytosol [41].

However, the balance between efficacy and toxicity of these systems is not ideal since high cationic charges are a prerequisite for successful cell uptake and endosomal release but also induce severe cytotoxic effects. In an effort to enable the successful implementation of polymer-based delivery into the clinic, the development of various approaches to overcome these hurdles has been explored.

One of them is the modification of polymers with hydrophobic moieties resulting in cationic amphiphiles that can self-assemble in aqueous solution to micelles and form micelle-like particles upon mixing with nucleic acids. These unique systems potentially possess advantageous features such as improved cellular internalization abilities due to additional hydrophobic interactions with cell membranes and enhanced toxicity profiles achieved by reduced charge density. Amphiphilic polymers can be obtained by modification of cationic polymers with hydrophobic subunits, such as alkanes [42, 43], fatty acids [44] or phospholipids [45, 46]. In terms of PEI, the group of Aliabadi et al., for instance, demonstrated increased uptake ability and gene silencing efficacy taken together with tolerable cytotoxicity of fatty acid

modified PEI polyplexes compared to unmodified PEI [44]. In addition, various chemical synthesis methods provide the possibility to obtain versatile amphiphilic polymer compositions by incorporation of cationic and hydrophobic subunits [35].

Another key factor that needs to be considered for successful development of safe polymer-based RNAi therapeutics is the biodegradability and biocompatibility of materials. Most of the commonly used cationic polymeric vectors, such as PLL and PEI, consist of non-degradable vinyl and amide bonds, leading to significant accumulation in the body, which may cause high cytotoxic effects [47, 48], especially after repeated administration [49]. As already described in literature, there are some suitable natural polymers for gene delivery exhibiting great biocompatibility, such as chitosan, dextran or β-cyclodextrin [50]. Spermines, as naturally occurring small, linear tetraamines represent a further potential siRNA delivery agent with high biodegradability [51-53]. However, the synthesis of higher molecular weight spermine-containing substances is necessary to achieve efficient siRNA encapsulation and cellular internalization. Synthetic biodegradable polymers possess labile chemical bonds such as esters, anhydrides, carbonates, amides and urethans that can be degraded into metabolites which can be easily excreted [54]. Several polymerization methods, mainly step polymerization and ring-opening polymerization (ROP), are utilized to synthesize a myriad of biodegradable polymers such as poly (4-hydroxy-L-proline ester) (PHP), PBAEs, poly(δ-valerolactone) (PVL), aminated poly(α-hydroxy acids) (PAHA), polyphosphoester (PPE), polylactide (PLA), and polycarbonate (PC). A particular class of biodegradable polyamides (nylon-3 polymers) that can be synthesized via ROP with tailored amounts of hydrophobic subunits has recently been shown to hold great potential for siRNA delivery [55].

4. Drug delivery to the brain

With regard to tremendous population growth and increased life expectations, the number of people suffering from CNS diseases will significantly increase in the next decades. Therefore, there is an urgent demand for effective therapeutic systems delivering potent CNS drugs to their target sites in the brain.

The use of RNAi-based therapeutics holds great potential for treatment of CNS diseases derived from improper functioning mutated genes such as Parkinson's disease (PD), Alzheimer's disease (AD) or brain cancers. In terms of PD, it was recently shown that translation of mutated

genes into misfunctioning proteins, in particular α-synuclein, was reduced after administration of a multifunctional superparamagnetic nanoparticle containing a small hairpin RNA against α-synuclein [56]. Moreover, BACE1 protein represents a therapeutic target in AD that has been successfully addressed applying an siRNA/chitosan approach [57].
In the case of brain cancers, such as glioblastoma multiforme, it was previously demonstrated that siRNA can successfully induce glioma-related gene knockdown using dendrimer or PEI entrapped gold nanoparticles [58, 59].

However, drug development for CNS diseases is a challenging task since the brain is separated from the circulating blood by an especially tight blood-brain barrier (BBB), which considerably limits the entry of small molecules and in particular macromolecular drugs. In addition, several other concerns, such as the lack of predictive *in vitro* and *in vivo* models, impede successful clinical translation of CNS drugs.

As illustrated in Figure 3, the BBB is composed of brain endothelial cells, pericytes and astrocytes and is further characterized by the presence of extremely tight junction complexes in the interendothelial spaces, formed by claudin and occludin and the expression of export proteins such as p-glycoprotein. It controls the brain homeostasis as well as ion and molecule movement and protects the brain against metabolites, xenobiotics and pathogens [60].

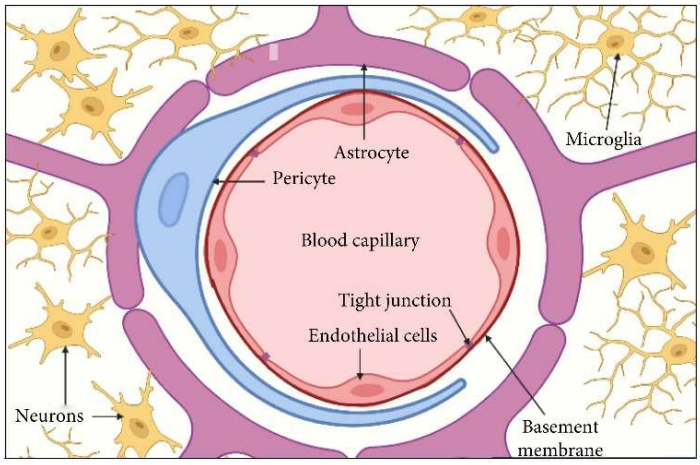

Figure 3. Structure of the Blood – Brain Barrier (BBB). A physical barrier is formed by the brain endothelial cells connected by tight junctions as well as by the surrounding vascular basement membrane, pericytes and end feet of astrocytes. Adopted from Alahmari et al. [61].

The high compactness of the BBB layer precludes the paracellular diffusion by anionic, hydrophilic and high molecular weight substances [62, 63]. Passive transcellular transport occurs solely for lipid-soluble compounds, whereas larger and more hydrophilic substances need to be taken up in an active way [64]. Active transport pathways include carrier-, receptor-, and adsorptive transcytosis through the endothelial cells into the brain stroma [65].

Various strategies for direct and local drug administration in the brain have been employed, such as intrathecal and intraventricular injection [66] or osmotic [67] and focused ultrasound induced opening of the BBB [68]. Also, alternative routes to bypass the BBB, e.g., intranasal drug administration, have been investigated [69].

One of the most intensively applied strategies to deliver nanoparticles into the brain represents their functionalization with specific targeting ligands to make use of the receptor-mediated transcytosis (RMT) pathway to cross the BBB, as depicted in Figure 4. The process of transcytosis describes the internalization of the cargo after binding to respective receptors expressed at the apical side of the endothelial cell membrane into vesicles, which consequently moves through the cytoplasm to the basolateral side of the endothelial cell where they are exocytosed. Endothelial brain cells possess several receptors that can initiate RMT, e.g., insulin, lactoferrin, Transferrin, leptin, mannose-6-phosphate, low-density lipoprotein (LDL) and lipoprotein receptor-related protein (LRP) receptors [70, 71]. This pathway exhibits an excellent possibility for the transport of large molecules such as nanoparticles into the brain.

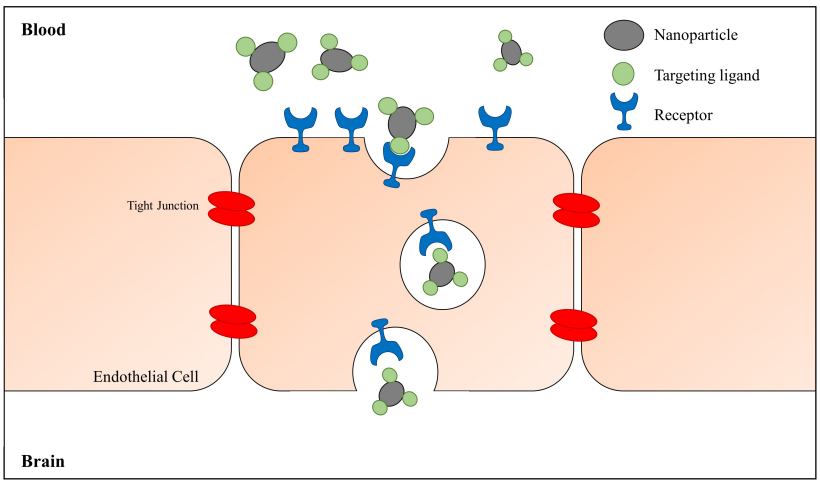

Figure 4. Receptor-mediated transcytosis (RMT) of nanoparticles functionalized with a targeting ligand at the blood-brain barrier (BBB). The interaction of the targeting ligand with the respective receptor triggers endocytosis of the complex. The vesicles transport their cargo through the brain endothelial cells and finally release it into the brain stroma.

Numerous brain targeted delivery systems have been designed by several functionalization strategies of carriers with specific targeting ligands. The most intensively investigated systems were decorated with, for instance, Transferrin or ApoE. Transferrin is a native plasma glycoprotein responsible for iron transport in biological fluids, and respective Transferrin receptors were found to be highly expressed on brain endothelial cells to meet the iron requirement of the brain [72, 73]. By functionalization of nanoparticles with the endogenous Transferrin ligand, or antibodies and peptides binding to different epitopes of the receptor, delivery of nanoparticles into the brain has been successfully achieved as measured either by quantification of the nanoparticles in the brain or with therapeutic outcomes of the delivered drugs [73-75]. In a study by Huang et al., a brain-targeting non-viral vector based on PAMAM dendrimer conjugated to Transferrin via a bifunctional PEG linker for successful delivery of a nucleic acid payload into the brain was reported [76]. ApoE is a component of the lipoprotein classes of very low-density lipoproteins (VLDL) and chylomicrons that regulate the transport of triglycerides and cholesterol from sites of synthesis to sites of utilization. Interactions of ApoE with LDL or LRP receptors expressed by target cells initiate the endocytic uptake of the complex [77]. Both receptors are expressed on brain endothelial cells to ensure the supply of the brain with essential lipids. Several ApoE functionalization strategies for polymeric nanoparticles containing small molecules or peptide/protein drugs such as i) direct coating ii) surfactant induced binding iii) PEG induced binding or iv) covalent linkage for brain delivery have been successfully applied in *in vitro* and *in vivo* experiments. Consequently, the ApoE approach holds great potential to implement precise brain targeting also for polymeric RNAi-based drugs. In this context, it is worth mentioning that it is also possible that plasma ApoE is adsorbed onto specifically tailored nanoparticles upon administering them into the blood stream. It has been reported that precoating of nanoparticles, in particular with the surfactant polysorbate 80 as a hydrophobic anchor, induces the adsorption of plasma ApoE, finally leading to active targeting effects in the body [78].

The surface of nanoparticles interacts with many classes of blood proteins resulting in formation of the so-called protein corona, which remarkably influences the fate of the nanoparticle in the body. The non-specific interaction with proteins is highly influenced by the nanoparticle's material and should be considered by designing delivery systems for systemic application [79]. Depending on the composition of the protein corona, not only active targeting effects can be initiated, but also remarkable changes in interactions with RES and thus biodistribution and even loss of efficacy of beforehand attached targeting ligands have been reported [80].

Furthermore, the success of bench-to-bedside translation of brain-targeted systems highly depends on available BBB models. In order to study the drug transmigration across the BBB, simplified *in vitro* models have been developed, such as monolayer models, co-culture models, dynamic models, stem cell-based models and microfluidic models [81]. Primary cells, which are accompanied with time and cost-intensive isolation processes have been replaced by immortalized endothelial cell lines of different species [82-84]. However, discrepancies of transendothelial electrical resistance (TEER) values, that characterizes the tightness of the barrier, are still significant. Immortalized cell lines forms barriers with TEER values below 150 $\Omega \cdot cm^2$, whereas physiological TEER values can reach up to 1500 $\Omega \cdot cm^2$ [85]. Even the use of *in vivo* models (besides general ethical and scientific concerns [86-89]) is characterized by some considerable drawbacks, such as remarkable species differences concerning the biodistribution or the expression and functionality of important transporters at the BBB [72]. With regard to barrier tightness, remarkable advancements have been achieved by the use of stem cell-derived endothelial-like cells reaching TEER values up to 5000 $\Omega \cdot cm^2$, that can be further enhanced by co-culturing with other cell types such as neural cells, astrocytes and pericytes [90].

5. Aim of the thesis

The overall aim of this thesis was to extend the knowledge in the field of polymeric nanoparticle mediated drug delivery to achieve transfer of siRNA across the blood-brain barrier (BBB) for the potential treatment of glioblastoma multiforme or other CNS disorders. A special emphasis is laid on the question, whether hydrophobic modification of nanoparticles mediates a beneficial effect on cellular internalization for overcoming the BBB to reach target sites in the brain. Furthermore, it was aimed to generate a greater understanding on the role of proteins as functional components of the protein corona of polymer-siRNA complexes to achieve active brain targeting.

Part I of the thesis (**Chapter II**) therefore focuses on the investigation of highly promising amphiphilic polymers regarding their potential of siRNA delivery into glioblastoma cells. Part II of the thesis (**Chapter III**) concentrates on proteins as functional components of the protein corona of nanoparticles for active brain targeting, whereas Part III of the thesis (**Chapter IV**) describes the evaluation of the blood-brain permeability of nanoparticles in *in vitro* and *in vivo* models.

Amphiphilic polymers are hypothesized to exhibit fusogenic properties due to additional hydrophobic interactions with cell membranes. Improved particle – cell interactions in comparison to cationic polymers would be of great advantage in terms of overcoming the extremely tight BBB. Hence, **Chapter II** reports on the evaluation of new classes of siRNA nanocarriers depending on their structural parameters. *Subchapter II.1* describes the synthesis of a set of poly-β-peptides (nylon-3 polymers) with varying hydrophobic content and compares the physicochemical properties, cellular uptake and gene silencing efficiency as well as the tolerability of the polymer-siRNA complexes (polyplexes) concluding in the superior suitability of the polymer with the highest hydrophobic content. *Subchapter II.2* investigates the performance of a series of poly(spermine acrylamides) homo- and copolymers with varying amounts of hydrophobic decylacrylamide subunits as an siRNA delivery agent for glioblastoma cells with special emphasis on the cell tolerability of polyplexes.

In the context of targeted brain delivery, **Chapter III** illuminates the role of proteins as functional components of nanoparticles. *Subchapter III.1* reviews the topic of active brain targeting with a particular focus on the composition of the blood-brain barrier (BBB) and summarizes approaches for Apolipoprotein E (ApoE) functionalization of polymeric nanoparticles as a successful strategy to overcome the BBB via low density lipoprotein receptor-mediated transcytosis by brain endothelial cells, rounded off with information on relevant *in vitro* BBB-models and *in vivo* studies. *Subchapter III.2* deals with evaluating an appropriate method for protein corona investigations on polyplexes to gain insight into this important aspect of drug delivery. Proteins that bind to nanoparticles after intravenous injection not only considerably affect their fate *in vivo* but might also be involved in receptor-mediated active targeting processes. This study describes the successful optimization of a purification method for polyplexes incubated in serum by centrifugation, which subsequently allowed the identification of bound proteins on nylon-3 and PEI polyplexes by a mass spectrometric method and a comparison of their protein corona profiles. *Subchapter III.3* attempts to answer the question whether the successful surfactant-based approach of direct coating of nanoparticles with ApoE for active brain targeting is transferable from solid nanoparticles to polyplexes depending on their structural parameters. In this study, polyplexes obtained with a highly hydrophobically modified nylon-3 polymer selected in *Subchapter II.1* and PEI are coated with ApoE with and without polysorbate 80 precoating and examined regarding cellular uptake and gene knockdown efficacy *in vitro* using an LDL and LRP1 receptor expressing model cell line.

In addition, biodistribution and brain targeting ability of formulations are investigated *in vivo* utilizing a radiolabeling approach of siRNA.

Chapter IV emerged out of the findings of the former chapters and describes the evaluation of the blood-brain barrier permeability of hydrophobically modified PEI polyplexes in a serum dependent manner with BBB models *in vitro* and *in vivo.* For this purpose, polyplexes properties, stability and cell tolerability are investigated in detail, and protein corona composition is examined depending on polyplex composition by applying the methods developed in *Subchapter III.2*. A sophisticated cell-based *in vitro* BBB model derived from human pluripotent stem cells is established for the prediction of the BBB permeability of polyplexes. Moreover, results are compared to *in vivo* data generated with a siRNA-radiolabeling and gamma-counting approach.

Chapter V provides a concluding summary of all results and gives indications of further possible parameters and developments that still need to be addressed in future investigations.

References

[1] A. Fire, S. Xu, M.K. Montgomery, S.A. Kostas, S.E. Driver, C.C. Mello, Potent and specific genetic interference by double-stranded RNA in Caenorhabditis elegans, nature, 391 (1998) 806-811.
[2] P.D. Zamore, T. Tuschl, P.A. Sharp, D.P. Bartel, RNAi: Double-Stranded RNA Directs the ATP-Dependent Cleavage of mRNA at 21 to 23 Nucleotide Intervals, Cell, 101 (2000) 25-33.
[3] S.M. Elbashir, J. Harborth, W. Lendeckel, A. Yalcin, K. Weber, T. Tuschl, Duplexes of 21-nucleotide RNAs mediate RNA interference in cultured mammalian cells, nature, 411 (2001) 494-498.
[4] S. Mocellin, M. Provenzano, RNA interference: learning gene knock-down from cell physiology, Journal of translational medicine, 2 (2004) 1-6.
[5] R. Kole, A.R. Krainer, S. Altman, RNA therapeutics: beyond RNA interference and antisense oligonucleotides, Nature reviews Drug discovery, 11 (2012) 125-140.
[6] G. Tang, siRNA and miRNA: an insight into RISCs, Trends in biochemical sciences, 30 (2005) 106-114.
[7] J. Martinez, A. Patkaniowska, H. Urlaub, R. Lührmann, T. Tuschl, Single-stranded antisense siRNAs guide target RNA cleavage in RNAi, Cell, 110 (2002) 563-574.
[8] L. Aagaard, J.J. Rossi, RNAi therapeutics: principles, prospects and challenges, Advanced drug delivery reviews, 59 (2007) 75-86.
[9] K.A. Whitehead, R. Langer, D.G. Anderson, Knocking down barriers: advances in siRNA delivery, Nature Reviews Drug Discovery, 8 (2009) 129-138.
[10] D. Guo, B. Wang, F. Han, T. Lei, RNA interference therapy for glioblastoma, Expert opinion on biological therapy, 10 (2010) 927-936.
[11] F.M. van de Water, O.C. Boerman, A.C. Wouterse, J.G.P. Peters, F.G.M. Russel, R. Masereeuw, Intravenously administered short interfering RNA accumulates in the kidney and selectively suppresses gene function in renal proximal tubules, Drug Metabolism and Disposition, 34 (2006) 1393.
[12] Y. Wan, P.M. Moyle, M.P. Christie, I. Toth, Nanosized, peptide-based multicomponent DNA delivery systems: optimization of endosome escape activity, Nanomedicine, 11 (2016) 907-919.
[13] R. Kanasty, J.R. Dorkin, A. Vegas, D. Anderson, Delivery materials for siRNA therapeutics, Nature materials, 12 (2013) 967-977.
[14] K. Nishina, T. Unno, Y. Uno, T. Kubodera, T. Kanouchi, H. Mizusawa, T. Yokota, Efficient in vivo delivery of siRNA to the liver by conjugation of α-tocopherol, Molecular therapy, 16 (2008) 734-740.
[15] J.K. Watts, G.F. Deleavey, M.J. Damha, Chemically modified siRNA: tools and applications, Drug discovery today, 13 (2008) 842-855.
[16] F. Czauderna, M. Fechtner, S. Dames, H. AyguÈn, A. Klippel, G.J. Pronk, K. Giese, J. Kaufmann, Structural variations and stabilising modifications of synthetic siRNAs in mammalian cells, Nucleic Acids Res, 31 (2003) 2705-2716.
[17] M. Takahashi, N. Minakawa, A. Matsuda, Synthesis and characterization of 2′-modified-4′-thioRNA: a comprehensive comparison of nuclease stability, Nucleic Acids Res, 37 (2009) 1353-1362.
[18] C.R. Allerson, N. Sioufi, R. Jarres, T.P. Prakash, N. Naik, A. Berdeja, L. Wanders, R.H. Griffey, E.E. Swayze, B. Bhat, Fully 2 ‘-modified oligonucleotide duplexes with improved in vitro potency and stability compared to unmodified small interfering RNA, Journal of medicinal chemistry, 48 (2005) 901-904.
[19] J.M. Layzer, A.P. McCaffrey, A.K. Tanner, Z. Huang, M.A. Kay, B.A. Sullenger, In vivo activity of nuclease-resistant siRNAs, Rna, 10 (2004) 766-771.
[20] V. Hornung, M. Guenthner-Biller, C. Bourquin, A. Ablasser, M. Schlee, S. Uematsu, A. Noronha, M. Manoharan, S. Akira, A. de Fougerolles, Sequence-specific potent induction of

IFN-α by short interfering RNA in plasmacytoid dendritic cells through TLR7, Nature medicine, 11 (2005) 263-270.
[21] A.D. Judge, V. Sood, J.R. Shaw, D. Fang, K. McClintock, I. MacLachlan, Sequence-dependent stimulation of the mammalian innate immune response by synthetic siRNA, Nature biotechnology, 23 (2005) 457-462.
[22] J.H. Jeong, H. Mok, Y.-K. Oh, T.G. Park, siRNA conjugate delivery systems, Bioconjugate chemistry, 20 (2009) 5-14.
[23] Y. Dong, D.J. Siegwart, D.G. Anderson, Strategies, design, and chemistry in siRNA delivery systems, Advanced drug delivery reviews, 144 (2019) 133-147.
[24] C. Tros de Ilarduya, Y. Sun, N. Düzgüneş, Gene delivery by lipoplexes and polyplexes, European Journal of Pharmaceutical Sciences, 40 (2010) 159-170.
[25] L. Nobs, F. Buchegger, R. Gurny, E. Allémann, Current methods for attaching targeting ligands to liposomes and nanoparticles, Journal of Pharmaceutical Sciences, 93 (2004) 1980-1992.
[26] Y. Lu, A.A. Aimetti, R. Langer, Z. Gu, Bioresponsive materials, Nature Reviews Materials, 2 (2016) 1-17.
[27] A. Wahane, A. Waghmode, A. Kapphahn, K. Dhuri, A. Gupta, R. Bahal, Role of Lipid-Based and Polymer-Based Non-Viral Vectors in Nucleic Acid Delivery for Next-Generation Gene Therapy, Molecules, 25 (2020) 2866.
[28] S. Doktorovova, A.B. Kovačević, M.L. Garcia, E.B. Souto, Preclinical safety of solid lipid nanoparticles and nanostructured lipid carriers: Current evidence from in vitro and in vivo evaluation, European Journal of Pharmaceutics and Biopharmaceutics, 108 (2016) 235-252.
[29] S.M. Hoy, Patisiran: first global approval, Drugs, 78 (2018) 1625-1631.
[30] S.S. Titze-de-Almeida, P.R.d.P. Brandão, I. Faber, R. Titze-de-Almeida, Leading RNA interference therapeutics part 1: silencing hereditary transthyretin amyloidosis, with a focus on patisiran, Molecular diagnosis & therapy, 24 (2020) 49-59.
[31] P.R. de Paula Brandão, S.S. Titze-de-Almeida, R. Titze-de-Almeida, Leading RNA interference therapeutics part 2: silencing delta-aminolevulinic acid synthase 1, with a focus on givosiran, Molecular diagnosis & therapy, 24 (2020) 61-68.
[32] L.J. Scott, S.J. Keam, Lumasiran: First Approval, Drugs, 81 (2021) 277-282.
[33] J.M. Migliorati, J. Jin, X.-b. Zhong, siRNA drug Leqvio (inclisiran) to lower cholesterol, Trends in pharmacological sciences, 43 (2022) 455.
[34] S.J. Keam, Vutrisiran: First Approval, Drugs, 82 (2022) 1419-1425.
[35] L.Y. Qiu, Y.H. Bae, Polymer Architecture and Drug Delivery, Pharmaceutical Research, 23 (2006) 1-30.
[36] W. Zauner, M. Ogris, E. Wagner, Polylysine-based transfection systems utilizing receptor-mediated delivery, Advanced drug delivery reviews, 30 (1998) 97-113.
[37] O. Boussif, F. Lezoualc'h, M.A. Zanta, M.D. Mergny, D. Scherman, B. Demeneix, J.-P. Behr, A versatile vector for gene and oligonucleotide transfer into cells in culture and in vivo: polyethylenimine, Proceedings of the National Academy of Sciences, 92 (1995) 7297-7301.
[38] D.A. Tomalia, A.M. Naylor, W.A. Goddard III, Starburst dendrimers: molecular-level control of size, shape, surface chemistry, topology, and flexibility from atoms to macroscopic matter, Angewandte Chemie International Edition in English, 29 (1990) 138-175.
[39] D.M. Lynn, R. Langer, Degradable poly (β-amino esters): synthesis, characterization, and self-assembly with plasmid DNA, Journal of the American Chemical Society, 122 (2000) 10761-10768.
[40] B.H. Zinselmeyer, S.P. Mackay, A.G. Schatzlein, I.F. Uchegbu, The lower-generation polypropylenimine dendrimers are effective gene-transfer agents, Pharmaceutical research, 19 (2002) 960-967.
[41] G. Sahay, D.Y. Alakhova, A.V. Kabanov, Endocytosis of nanomedicines, Journal of Controlled Release, 145 (2010) 182-195.

[42] P.Y. Teo, C. Yang, J.L. Hedrick, A.C. Engler, D.J. Coady, S. Ghaem-Maghami, A.J. George, Y.Y. Yang, Hydrophobic modification of low molecular weight polyethylenimine for improved gene transfection, Biomaterials, 34 (2013) 7971-7979.
[43] A. Schroeder, J.E. Dahlman, G. Sahay, K.T. Love, S. Jiang, A.A. Eltoukhy, C.G. Levins, Y. Wang, D.G. Anderson, Alkane-modified short polyethyleneimine for siRNA delivery, Journal of controlled release, 160 (2012) 172-176.
[44] H.M. Aliabadi, B. Landry, R.K. Bahadur, A. Neamnark, O. Suwantong, H. Uludağ, Impact of Lipid Substitution on Assembly and Delivery of siRNA by Cationic Polymers, Macromolecular Bioscience, 11 (2011) 662-672.
[45] G. Navarro, S. Essex, R.R. Sawant, S. Biswas, D. Nagesha, S. Sridhar, C.T. de Ilarduya, V.P. Torchilin, Phospholipid-modified polyethylenimine-based nanopreparations for siRNA–mediated gene silencing: Implications for transfection and the role of lipid components, Nanomedicine: Nanotechnology, Biology and Medicine, 10 (2014) 411-419.
[46] R.R. Sawant, S.K. Sriraman, G. Navarro, S. Biswas, R.A. Dalvi, V.P. Torchilin, Polyethyleneimine-lipid conjugate-based pH-sensitive micellar carrier for gene delivery, Biomaterials, 33 (2012) 3942-3951.
[47] T.G. Park, J.H. Jeong, S.W. Kim, Current status of polymeric gene delivery systems, Advanced drug delivery reviews, 58 (2006) 467-486.
[48] D. Fischer, Y. Li, B. Ahlemeyer, J. Krieglstein, T. Kissel, In vitro cytotoxicity testing of polycations: influence of polymer structure on cell viability and hemolysis, Biomaterials, 24 (2003) 1121-1131.
[49] J. Luten, C.F. van Nostrum, S.C. De Smedt, W.E. Hennink, Biodegradable polymers as non-viral carriers for plasmid DNA delivery, Journal of Controlled Release, 126 (2008) 97-110.
[50] T.G. Barclay, C.M. Day, N. Petrovsky, S. Garg, Review of polysaccharide particle-based functional drug delivery, Carbohydrate polymers, 221 (2019) 94-112.
[51] H. Eliyahu, A. Makovitzki, T. Azzam, A. Zlotkin, A. Joseph, D. Gazit, Y. Barenholz, A. Domb, Novel dextran–spermine conjugates as transfecting agents: comparing water-soluble and micellar polymers, Gene therapy, 12 (2005) 494-503.
[52] H.-L. Jiang, H.-T. Lim, Y.-K. Kim, R. Arote, J.-Y. Shin, J.-T. Kwon, J.-E. Kim, J.-H. Kim, D. Kim, C. Chae, J.-W. Nah, Y.-J. Choi, C.-S. Cho, M.-H. Cho, Chitosan-graft-spermine as a gene carrier in vitro and in vivo, European Journal of Pharmaceutics and Biopharmaceutics, 77 (2011) 36-42.
[53] M. Elsayed, V. Corrand, V. Kolhatkar, Y. Xie, N.H. Kim, R. Kolhatkar, O.M. Merkel, Influence of oligospermines architecture on their suitability for siRNA delivery, Biomacromolecules, 15 (2014) 1299-1310.
[54] Q. Liu, L. Jiang, R. Shi, L. Zhang, Synthesis, preparation, in vitro degradation, and application of novel degradable bioelastomers—A review, Progress in polymer science, 37 (2012) 715-765.
[55] V. Nadithe, R. Liu, B.A. Killinger, S. Movassaghian, N.H. Kim, A.B. Moszczynska, K.S. Masters, S.H. Gellman, O.M. Merkel, Screening Nylon-3 Polymers, a New Class of Cationic Amphiphiles, for siRNA Delivery, Molecular Pharmaceutics, 12 (2015) 362-374.
[56] S. Niu, L.-K. Zhang, L. Zhang, S. Zhuang, X. Zhan, W.-Y. Chen, S. Du, L. Yin, R. You, C.-H. Li, Inhibition by multifunctional magnetic nanoparticles loaded with alpha-synuclein RNAi plasmid in a Parkinson's disease model, Theranostics, 7 (2017) 344.
[57] Y. Gao, Z.-Y. Wang, J. Zhang, Y. Zhang, H. Huo, T. Wang, T. Jiang, S. Wang, RVG-Peptide-Linked Trimethylated Chitosan for Delivery of siRNA to the Brain, Biomacromolecules, 15 (2014) 1010-1018.
[58] L. Kong, J. Qiu, W. Sun, J. Yang, M. Shen, L. Wang, X. Shi, Multifunctional PEI-entrapped gold nanoparticles enable efficient delivery of therapeutic siRNA into glioblastoma cells, Biomaterials Science, 5 (2017) 258-266.

[59] J. Qiu, L. Kong, X. Cao, A. Li, P. Wei, L. Wang, S. Mignani, A.-M. Caminade, J.-P. Majoral, X. Shi, Enhanced Delivery of Therapeutic siRNA into Glioblastoma Cells Using Dendrimer-Entrapped Gold Nanoparticles Conjugated with β-Cyclodextrin, Nanomaterials, 8 (2018) 131.
[60] P. Ballabh, A. Braun, M. Nedergaard, The blood–brain barrier: an overview: structure, regulation, and clinical implications, Neurobiology of disease, 16 (2004) 1-13.
[61] A. Alahmari, Blood-Brain Barrier Overview: Structural and Functional Correlation, Neural Plasticity, 2021 (2021) 6564585.
[62] L. Crawford, J. Rosch, D. Putnam, Concepts, technologies, and practices for drug delivery past the blood–brain barrier to the central nervous system, Journal of Controlled Release, 240 (2016) 251-266.
[63] S. Fumoto, T. Yamamoto, K. Okami, Y. Maemura, C. Terada, A. Yamayoshi, K. Nishida, Understanding in vivo fate of nucleic acid and gene medicines for the rational design of drugs, Pharmaceutics, 13 (2021) 159.
[64] W.M. Pardridge, Drug transport across the blood–brain barrier, Journal of cerebral blood flow & metabolism, 32 (2012) 1959-1972.
[65] N.J. Abbott, A.A. Patabendige, D.E. Dolman, S.R. Yusof, D.J. Begley, Structure and function of the blood–brain barrier, Neurobiology of disease, 37 (2010) 13-25.
[66] Y.-L. Kwong, D.Y. Yeung, J.C. Chan, Intrathecal chemotherapy for hematologic malignancies: drugs and toxicities, Annals of hematology, 88 (2009) 193-201.
[67] K. Jahnke, D.F. Kraemer, K.R. Knight, D. Fortin, S. Bell, N.D. Doolittle, L.L. Muldoon, E.A. Neuwelt, Intraarterial chemotherapy and osmotic blood-brain barrier disruption for patients with embryonal and germ cell tumors of the central nervous system, Cancer: Interdisciplinary International Journal of the American Cancer Society, 112 (2008) 581-588.
[68] L.H. Treat, N. McDannold, N. Vykhodtseva, Y. Zhang, K. Tam, K. Hynynen, Targeted delivery of doxorubicin to the rat brain at therapeutic levels using MRI-guided focused ultrasound, International journal of cancer, 121 (2007) 901-907.
[69] B. Gabold, F. Adams, S. Brameyer, K. Jung, C.L. Ried, T. Merdan, O.M. Merkel, Transferrin-modified chitosan nanoparticles for targeted nose-to-brain delivery of proteins, Drug Delivery and Translational Research, 13 (2023) 822-838.
[70] J.E. Preston, N.J. Abbott, D.J. Begley, Transcytosis of macromolecules at the blood–brain barrier, Advances in pharmacology, 71 (2014) 147-163.
[71] K.B. Johnsen, A. Burkhart, L.B. Thomsen, T.L. Andresen, T. Moos, Targeting the transferrin receptor for brain drug delivery, Progress in Neurobiology, 181 (2019) 101665.
[72] I. van Rooy, S. Cakir-Tascioglu, W.E. Hennink, G. Storm, R.M. Schiffelers, E. Mastrobattista, In Vivo Methods to Study Uptake of Nanoparticles into the Brain, Pharmaceutical Research, 28 (2011) 456-471.
[73] I. van Rooy, E. Mastrobattista, G. Storm, W.E. Hennink, R.M. Schiffelers, Comparison of five different targeting ligands to enhance accumulation of liposomes into the brain, Journal of controlled release, 150 (2011) 30-36.
[74] Y. Zhang, F. Calon, C. Zhu, R.J. Boado, W.M. Pardridge, Intravenous nonviral gene therapy causes normalization of striatal tyrosine hydroxylase and reversal of motor impairment in experimental parkinsonism, Human gene therapy, 14 (2003) 1-12.
[75] Y. Zhang, W.M. Pardridge, Neuroprotection in transient focal brain ischemia after delayed intravenous administration of brain-derived neurotrophic factor conjugated to a blood-brain barrier drug targeting system, Stroke, 32 (2001) 1378-1384.
[76] R.-Q. Huang, Y.-H. Qu, W.-L. Ke, J.-H. Zhu, Y.-Y. Pei, C. Jiang, Efficient gene delivery targeted to the brain using a transferrin-conjugated polyethyleneglycol-modified polyamidoamine dendrimer, The FASEB journal, 21 (2007) 1117-1125.
[77] R.W. Mahley, Apolipoprotein E: cholesterol transport protein with expanding role in cell biology, Science, 240 (1988) 622-630.

[78] J. Kreuter, D. Shamenkov, V. Petrov, P. Ramge, K. Cychutek, C. Koch-Brandt, R. Alyautdin, Apolipoprotein-mediated transport of nanoparticle-bound drugs across the blood-brain barrier, J Drug Target, 10 (2002) 317-325.
[79] K.E. Wheeler, A.J. Chetwynd, K.M. Fahy, B.S. Hong, J.A. Tochihuitl, L.A. Foster, I. Lynch, Environmental dimensions of the protein corona, Nature Nanotechnology, 16 (2021) 617-629.
[80] M. Mahmoudi, I. Lynch, M.R. Ejtehadi, M.P. Monopoli, F.B. Bombelli, S. Laurent, Protein–Nanoparticle Interactions: Opportunities and Challenges, Chemical Reviews, 111 (2011) 5610-5637.
[81] A. Wolff, M. Antfolk, B. Brodin, M. Tenje, In Vitro Blood–Brain Barrier Models—An Overview of Established Models and New Microfluidic Approaches, Journal of Pharmaceutical Sciences, 104 (2015) 2727-2746.
[82] K. Vu, B. Weksler, I. Romero, P.-O. Couraud, A. Gelli, Immortalized human brain endothelial cell line HCMEC/D3 as a model of the blood-brain barrier facilitates in vitro studies of central nervous system infection by Cryptococcus neoformans, Eukaryotic cell, 8 (2009) 1803-1807.
[83] O. Steiner, C. Coisne, B. Engelhardt, R. Lyck, Comparison of Immortalized bEnd5 and Primary Mouse Brain Microvascular Endothelial Cells as in vitro Blood–Brain Barrier Models for the Study of T Cell Extravasation, Journal of Cerebral Blood Flow & Metabolism, 31 (2011) 315-327.
[84] D.E. Eigenmann, G. Xue, K.S. Kim, A.V. Moses, M. Hamburger, M. Oufir, Comparative study of four immortalized human brain capillary endothelial cell lines, hCMEC/D3, hBMEC, TY10, and BB19, and optimization of culture conditions, for an in vitro blood–brain barrier model for drug permeability studies, Fluids and Barriers of the CNS, 10 (2013) 1-17.
[85] C. Crone, S.P. Olesen, Electrical resistance of brain microvascular endothelium, Brain Research, 241 (1982) 49-55.
[86] H.R. Ferdowsian, N. Beck, Ethical and Scientific Considerations Regarding Animal Testing and Research, PLOS ONE, 6 (2011) e24059.
[87] P. Perel, I. Roberts, E. Sena, P. Wheble, C. Briscoe, P. Sandercock, M. Macleod, L.E. Mignini, P. Jayaram, K.S. Khan, Comparison of treatment effects between animal experiments and clinical trials: systematic review, BMJ, 334 (2007) 197.
[88] S.K. Doke, S.C. Dhawale, Alternatives to animal testing: A review, Saudi Pharmaceutical Journal, 23 (2015) 223-229.
[89] P. Croce, Vivisection or science? An investigation into testing drugs and safeguarding health, (1999).
[90] A. Appelt-Menzel, A. Cubukova, K. Günther, F. Edenhofer, J. Piontek, G. Krause, T. Stüber, H. Walles, W. Neuhaus, M. Metzger, Establishment of a Human Blood-Brain Barrier Co-culture Model Mimicking the Neurovascular Unit Using Induced Pluri- and Multipotent Stem Cells, Stem Cell Reports, 8 (2017) 894-906.

Chapter II

Hydrophobically Modified Polymers for siRNA Delivery to Glioblastoma Cells

II.1 The Impact of Nylon-3 Copolymer Composition on the Efficiency of siRNA Delivery to Glioblastoma Cells

This chapter was published as research article in the Journal Nanomaterials:

Natascha Hartl, Friederike Adams, Gabriella Costabile, Lorenz Isert, Markus Döblinger, Ximian Xiao, Runhui Liu and Olivia M. Merkel

"The Impact of Nylon-3 Copolymer Composition on the Efficiency of siRNA Delivery to Glioblastoma Cells"

Nanomaterials 2019, 9(7), 986; https://doi.org/10.3390/nano9070986

Graphical Abstract

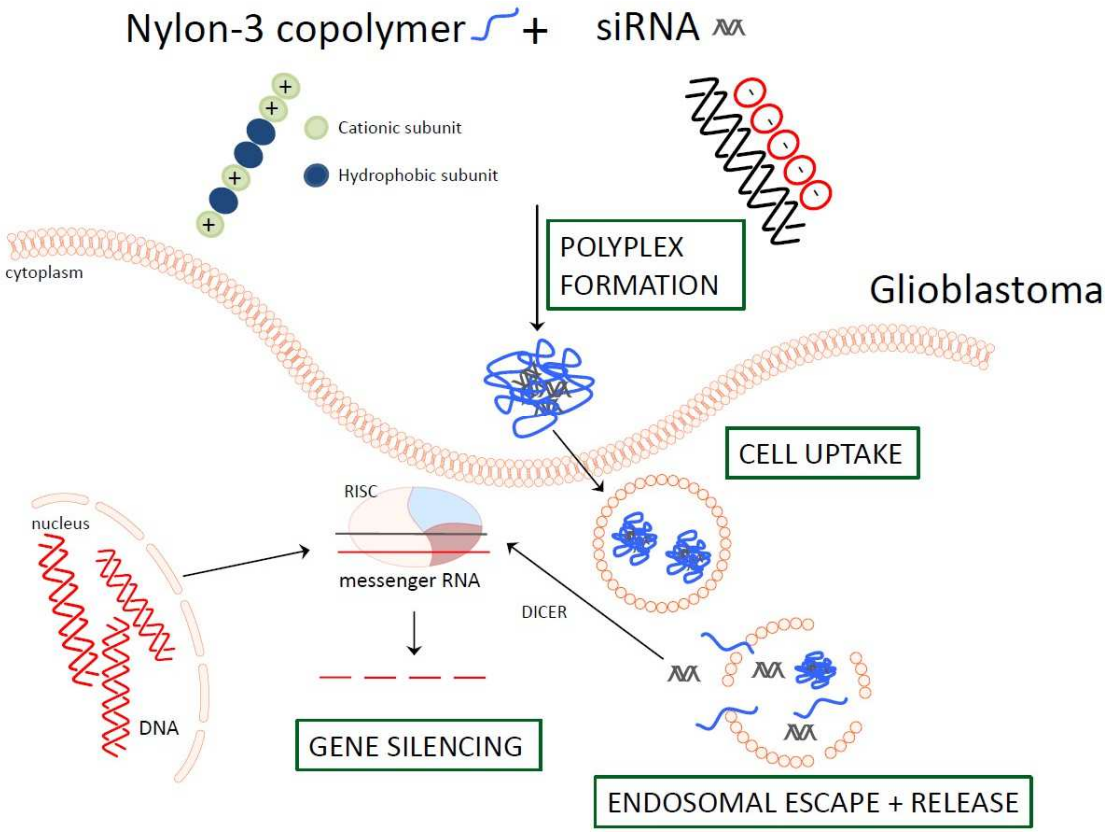

Abstract

Glioblastoma multiforme is a devastating disease which attracts enormous attention due to poor prognosis and high recurrence. Small interfering RNA (siRNA) in principle offers a promising therapeutic approach by downregulation of disease-related genes via RNA interference. For efficient siRNA delivery to target sites cationic polymers are often used in preclinical studies for protection of siRNA and complex formation based on electrostatic interactions. In an effort to develop biocompatible and efficient nanocarriers with translational outlook for optimal gene silencing at reduced toxicity, we synthesized two sets of Nylon-3 copolymers with variable content of cationic (DM or NM monomer) and hydrophobic subunits (CP monomer) and evaluated their suitability for in vitro siRNA delivery into glioblastoma cells. $DM_{0.4}/CP_{0.6}$ and $NM_{0.4}/CP_{0.6}$ polymers with similar subunit ratios were synthesized to compare the effect of different cationic subunits. Additionally, we utilized $NM_{0.2}/CP_{0.8}$ polymers to evaluate the impact of the different hydrophobic content in the polymer chain. The siRNA condensation ability and polymer-siRNA complex stability was evaluated by unmodified and modified SYBR Gold assays, respectively. Further physicochemical characteristics, e.g., particle size and

surface charge, were evaluated by dynamic light scattering and laser Doppler anemometry, whereas a relatively new method for polyplex size distribution analysis – tunable resistive pulse sensing – was additionally developed and compared to DLS measurements. Transfection efficiencies, the route of cell internalization and protein knockdown abilities in glioblastoma cells were investigated by flow cytometry. Furthermore, cellular tolerability was evaluated by MTT and LDH assays. All polymers efficiently condensed siRNA at N/P ratios of 3, whereas polymers with NM cationic subunits demonstrated smaller particle size and lower polyplex stability. Furthermore, $NM_{0.2}/CP_{0.8}$ polyplexes with the highest hydrophobic content displayed significantly higher cellular internalization in comparison to more cationic formulations and successful knockdown capabilities. Detailed investigations of the cellular uptake route demonstrated that these polyplexes mainly follow clathrin-mediated endocytotic uptake mechanisms implying high interaction capacity with cellular membranes. Taken together with conducive toxicity profiles; highly hydrophobic Nylon-3 polymers provide an appropriate siRNA delivery agent for potential treatment of glioblastoma.

1. Introduction

Glioblastoma multiforme (GBM) is the most common devastating type of primary malignant tumor of the central nervous system. The current standard treatment includes surgical resection followed by radiation and chemotherapy with temozolomide and the use of the monoclonal antibody bevacizumab that inhibits vascular endothelial growth factors [1]. However, even with aggressive treatment, patient outcomes remain poor with median survival times of only 12 to 15 months [2]. Thus, any new therapeutic strategy to target this disease is of significant benefit. Small interference RNA (siRNA) is a promising therapeutic approach due to its ability to potentially knock down disease-related genes and is intensively investigated for the treatment of a broad range of disorders [3–7]. In case of glioblastoma treatment, it was recently shown by various groups that siRNA can successfully induce glioma-related gene knockdown and tumor growth inhibition in *in vitro* as well as *in vivo* experiments [8–10]. Successful siRNA delivery and silencing of glioma-related genes, e.g. B-cell lymphoma/leukemia-2 (Bcl-2), was enabled by dendrimer - or polyethylenimine (PEI) - entrapped gold nanoparticles by the groups of Qiu et al. and Khong et al., respectively [11,12]. In these treatments and also in most other cases of siRNA delivery, limitations in application of naked siRNA caused by rapid degradation, immune response and low passive cell uptake [13] are bypassed by using suitable delivery systems to encapsulate the nucleic acids by electrostatic interactions in order to shield them

from the environment and to assist cellular internalization. Several non-viral siRNA formulation approaches such as liposomes and especially cationic polymeric delivery systems have been extensively investigated [14]. However, the main hurdle of high cellular toxicity due to high positive charge density and poor transfection efficiencies of cationic nucleic acid carriers still remains [15]. As an advancement, hydrophobically modified cationic polymers, e.g. phospholipid-modified PEI [16], poly(amidoamine) dendrimers (PAMAM) [17] and PEI-poly(caprolactone)-poly(ethylene glycol) (PEI-PCL-PEG) polymers [18] were investigated by various groups due to improved performance as siRNA carriers coupled with considerably decreased cytotoxicity [19]. In addition, Nylon-3 polymers, which have a similar backbone to biocompatible and biodegradable peptides, were tested for various medical/biological applications by the groups of Gellman and Liu. Due to their high altering amenability, they were successfully used for mimicking antimicrobial host-defense peptides [20], lung surfactant [21], natural polysaccharides [22] and as cell adhesion promoters [23], which also laid promising foundations for application as a potential gene delivery agent. The first siRNA delivery performance study on these polymers was investigated in non-small cell lung cancer cells (H1299) indicating hydrophobic structures made from a considerable amount of hydrophobic subunits might be superior siRNA delivery agents [24]. Nylon-3 polymers can be synthesized via anionic ring-opening polymerization (ROP) via statistical copolymerization of various β-lactams using lithium bis(trimethylsilylamide) (LiHMDS) as initiator to incorporate both cationic and lipophilic/hydrophobic subunits, providing the opportunity to obtain versatile and tailor-made polymer compositions by regulation of the monomer feed [25]. Herein, we synthesized a tailored set of random Nylon-3 copolymers via ROP with increased amount of hydrophobic subunits derived from β-lactam cyclopentyl (CP) and cationic subunits either from β-lactam dimethyl (DM) or nomethyl (NM). Differently designed Nylon-3 polymers concerning the ratio between the hydrophobic and cationic subunit as well as the use of different cationic monomers were used to investigate the suitability for siRNA delivery into glioblastoma cells depending on the polymer's microstructure. Optimized NM monomer was used to decrease sterically demand and hydrophobicity of cationic subunits in order to enable more compact siRNA complexation potentially leading to more favorable particle sizes. The obtained siRNA-polymer complexes (polyplexes) were characterized in detail regarding physicochemical characteristics such as siRNA encapsulation ability, polyplex stability, particle size and surface charge. Tunable resistive pulse sensing (TRPS) was established as a suitable method for polyplex size distribution analysis by comparison to dynamic light scattering (DLS) data. Furthermore, cellular internalization, route of uptake and gene

knockdown efficiency was assessed by flow cytometry and cell tolerability was examined by MTT and LDH assays. Based on these findings, the most hydrophobic Nylon-3 polymers provide optimal properties regarding particle characteristics and ability to fuse with cell membranes leading to excellent transfection efficiencies and successful gene knockdown in glioblastoma cells at minimal cytotoxic effects.

2. Materials and Methods

2.1 Materials

HEPES (4-(2-hydroxyethyl)–1-piperazineethanesulfonic acid), sodium acetate, potassium chloride, Tween® 20, heparin sodium salt, thiazolyl blue tetrazolium bromide (MTT), Nystatin, Wortmannin, chlorpromazine hydrochloride, methyl–ß-cyclodextrin, chloroquine diphosphate, paraformaldehyde solution, 4′,6–diamidino–2-phenylindole dihydrochloride (DAPI), FluorSave Reagent and for cell culture U87 cells (human glioblastoma astrocytoma), Eagle's Minimum Essential Medium (EMEM), RPMI-1640 Medium, Fetal Bovine Serum (FBS), Penicillin-Streptomycin solution, Dulbecco's Phosphate Buffered Saline (PBS), trypsin-EDTA solution 0.25%, L-glutamine solution 200 mM, dimethyl sulfoxide (DMSO) and Geniticin (G418) disulfate solution were purchased from Sigma-Aldrich (Taufkirchen, Germany). Green fluorescent protein (eGFP) reporter cell line–NCI-H1299 (human non-small cell lung carcinoma) was purchased from ATCC (Manassas, VA, USA). SYBR Gold Dye, Lipofectamin 2000 transfection reagent, AlexaFluor 488 (AF488) and 647 (AF647) dyes were purchased from Life Technologies (Carlsbad, California, USA). HyClone trypan blue solution 0.4% in phosphate buffered saline was obtained from FisherScientific (Hampton, New Hampshire, USA) and CytoTox 96® Non-Radioactive Cytotoxicity Assay was purchased from Promega (Madison, Wisconsin, USA). Amine-modified eGFP siRNA (5′-pACCCUGAAGUUCAUCUGCACCACcg, 3′- ACUGGGACUUCAAGUAGACGGGUGG C), human glyceraldehyde 3–phosphate dehydrogenase (GAPDH) siRNA (5′-pGGUCGGAGUCAACGGAUUUGGUCgt, 3′- UUCCAGCCUCAGUUGCCUAAACCAGC A), and scrambled siRNA (5′-pCGUUAAUCGCGUAUAAUACGCGUat, 3′-CAGCAAUUAGCGCAUAUUAUGCGCAUAp) were purchased from Integrated DNA Technologies (Leuven, Belgium). Indication of modified nucleotides: "p" denotes a phosphate residue, lower case letters are 2′-deoxyribonucleotides, capital letters are ribonucleotides, and underlined capital letters are 2′-O-methylribonucleotides.

2.2 Synthesis and characterization of Nylon-3 random copolymers

Nylon-3 random copolymers were synthesized via anionic ring-opening polymerization (ROP) of racemic β-lactams. Polymer $DM_{0.4}/CP_{0.6}$ (DM as cationic monomer and CP as hydrophobic monomer) was synthesized as described previously [24, 25]. The polymerization was conducted in the presence of (±)-7-(2-tritylthioacetyl)-7-azabicyclo[4,2,0]octan-8-one (I) as the co-initiator and lithium bis(trimethylsilylamide) (LiHMDS) as the base to afford the desired polymer with one N-terminal thiol-end group per polymer chain (Figure S1, Supplementary Material) [23]. Monomers β-NM (cationic monomer) and CP (hydrophobic monomer) for NM/CP copolymers were prepared according to literature procedures [26]. Random copolymers from β-NM and CP were synthesized by following previously reported procedures [20]. The polymerization was conducted in the presence of 4-tert-butyl-benzoyl chloride (II) as the co-initiator and LiHMDS as the base to afford the desired polymers with an N-terminal tert-butyl-benzoyl group (Figure S2, Supplementary Material) [27]. Deprotection of all Boc-protected polymers was performed in trifluoroacetic acid (TFA) to obtain the TFA-salts of the desired polymers [28]. To determine the average molecular weight and polydispersity of DM/CP polymers, characterization was conducted with Boc-protected side chains via gel permeation chromatography (GPC) using a Shimadzu GPC instrument equipped with two Waters columns (Styragel HR 4E, particle size 5 µm) linked in series, equipped with a multiangle light scattering detector (Wyatt miniDAWN, 690 nm, 30 mW), and a refractive index detector (Wyatt Optilab-rEX, 690 nm). THF was used as the mobile phase at a flow rate of 1 mL/min. ^{1}H - NMR spectra of DM/CP polymer were measured on a Varian Mercury Nuclear Magnetic Resonance (NMR) Spectrometer at 300 MHz in deuterium oxide with 512 scans. ^{1}H - NMR spectra of NM/CP polymers were measured on a Bruker AV500 in deuterium oxide with 128 scans. Molar masses of NM/CP polymers were directly calculated via ^{1}H-NMR in D_2O performed with unprotected TFA salts by comparing the signal between 4.0 and 4.5 ppm (one proton per repeating unit p (p = n + m)), and the tert-butyl group of the end-group (1.33 ppm) or the aromatic benzylic protons (7.5 – 8.0 ppm).

2.3 Preparation of polyplexes

To prepare polymer-siRNA complexes (polyplexes), aqueous polymer stock solutions were diluted with freshly filtered 10 mM HEPES buffer (pH 7.2) to predetermined concentrations, added to a defined amount of siRNA in a microcentrifuge tube to obtain polyplexes at various N/P ratios and incubated for 30 min to permit stable polyplex formation. The N/P ratio is defined as the molar ratio between the polymer amine groups (N) and the siRNA phosphate

groups (P). The amount of polymer needed to obtain different N/P ratios was calculated according to following equation:

m (polymer in pg) = n siRNA (pmol) x M protonable unit (g/mol) x N/P x number of nucleotides siRNA

The protonable unit of each polymer was calculated by dividing its molar mass by number of protonable primary amines present in each polymer and illustrated in Scheme 1. (Number of nucleotides of 25/27mer siRNA = 52)

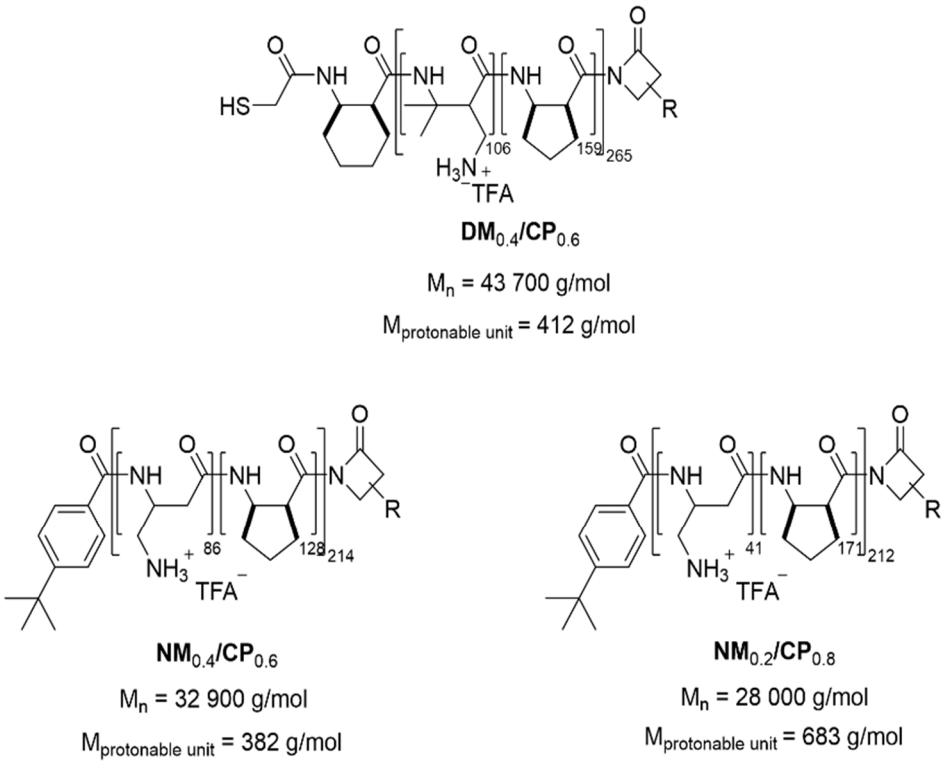

Scheme 1. Nylon-3 polymers used in this study.

2.4 siRNA encapsulation Assay by SYBR Gold Assay

SYBR Gold assay was used to evaluate the capacity of the polymers to condense siRNA at various N/P ratios analogous to procedures previously described [29]. Polyplexes with 50 pmol siRNA were prepared in HEPES buffer and 100 µl of each polyplex solution was distributed in a white FluoroNunc 96 well plate (FisherScientific, Hampton, New Hampshire, USA). A 4X SYBR Gold solution (30 µl) was added to each well and the plate was incubated for 10 min in the dark. Fluorescence signal was determined by using a fluorescence plate reader (FLUOstar

Omega, BMG Labtech, Ortenberg, Germany) at 492 and 555 nm excitation and emission wavelengths, respectively. An analogous procedure with free siRNA was used as 100% value. Measurements were performed in triplicates and results are shown as mean values (n = 3).

2.5 Size and (ζ)-Potential Analysis by Dynamic Light Scattering and Laser Doppler Anemometry

Particle size, polydispersity index (PDI) and zeta potential of polyplexes were measured using a Zetasizer Nano ZS (Malvern Instruments, Malvern, UK). Polyplexes were formed at various N/P ratios in HEPES buffer. A total volume of 100 µl of each sample was added to a disposal cuvette (Malvern Instruments, Malvern; UK) and used for particle size and PDI measurements by dynamic light scattering at 173° backscatter angle running 15 scans three times per sample. Zeta potentials were measured using a Zeta Cell (Zetasizer Nano series, Malvern, UK) containing a 7X dilution of another 100 µl sample aliquot by laser Doppler anemometry (LDA) with each run consisting of 30 scans. Results are expressed as mean ± standard deviation (n = 3).

2.6 Size Measurements by Tunable Resistive Pulse Sensing

Measurements were conducted using a qNano Gold system (Izon Science, Oxford, UK) equipped with an upper and a lower fluid cell and a separating polyurethane membrane between the cells possessing a single nanopore at its center. All measurements were performed with a NP 200 Nanopore (size range 85 – 500 nm) (Izon Science, Oxford, UK) with a minimum particle count of 500. The lower and upper fluid cells were filled with 75 µl and 40 µl of electrolyte (30 mM HEPES, 100 mM potassium chloride, 2 mM EDTA and 0.03% Tween®20), respectively. The instrument was calibrated according to the manufacturer´s protocol with defined 200 nm polystyrene calibration particles. Subsequently, the calibration particle suspension in the upper fluid cell was replaced by 40 µl polyplexes dilution. As 10 mM HEPES buffer was not suitable for polyplex preparation to achieve a stable signal and baseline during the measurements due to insufficient electrical conductivity (σ = 44 µS/cm), samples were prepared as usual, incubated for 30 mins and 1X diluted with a freshly filtered electrolyte solution containing 30 mM HEPES, 100 mM potassium chloride, 2 mM EDTA and 0.03% Tween®20 (σ = 8.5 mS/cm). All samples were used within 30 min after dilution. Membrane stretching was maintained between 44 and 48 mm, voltage was adjusted to achieve an appropriate baseline current for each sample and additional pressures ranging from 6 to 18 mbar

were applied to the system. The current pulse signals were collected and exported for analysis using Izon Control Suite software 3.3 (Izon Science, Oxford, UK).

2.7 Polyplex morphology by scanning transmission electron microscopy coupled with energy-dispersive X-ray spectroscopy

The morphology and the composition of the polyplexes were analyzed with a Titan Themis transmission electron microscope (TEM) equipped with a Super-X energy dispersive X-ray (EDX) spectrometer. The measurements were performed in scanning transmission electron microscopy (STEM) annular dark field (ADF) mode at an acceleration voltage of 300 kV. STEM-ADF delivers atomic number sensitive contrast, thereby areas of different composition may be distinguished from their surroundings. $NM_{0.2}/CP_{0.8}$ polyplexes were prepared in water to avoid buffer crystallization at N/P 4 and diluted 1:5 with water. A drop of particle suspension was dispensed on a plasma activated carbon-coated copper grid and left to dry for 60 s before blotting.

2.8 Cells and Cell culture

U87 cells (human glioblastoma cell line) were cultured in EMEM media supplemented with heat inactivated FBS (10%) and Penicillin-Streptomycin (1%). eGFP reporter cell line-NCI-H1299 was cultivated in RPMI-1640 media supplemented with heat inactivated FBS (10%), Penicillin-Streptomycin (1%) and 0.4% (v/v) Geneticin (G418). The plasmid for eGFP expression also contains an antibiotic resistance for Geniticin to enable the selection of only stably eGFP expressing cells. All cells were subcultured, maintained and grown in an incubator in humidified air with 5% CO_2 at 37 °C.

2.9 Quantification of cellular Uptake by Flow Cytometry

Flow cytometry was used to quantify the *in vitro* cellular uptake of polyplexes. Amine modified siRNA was labeled with the fluorescence dye Alexa Fluor 488 (AF488) following the manufacturer´s protocol and purified by ethanol precipitation and spin column binding as described previously [30]. U87 cells were seeded in 24 well plates at a density of 100.000 cells per well and incubated for 24 h at 37 °C and 5% CO_2. For all uptake experiments, polyplexes were prepared with 50 pmol siRNA-AF488 at different N/P ratios, negative controls consisted of untreated and free siRNA treated cells, while positive control cells were transfected with Lipofectamine 2000 lipoplexes, which were prepared with 50 pmol siRNA-AF488 according to the manufacturer's protocol. After transfection of cells for 24 h, incubation medium was

removed, cells were washed with PBS and detached using 0.25% trypsin-EDTA. Samples were washed two times with PBS and resuspended in 500 µl PBS/2 mM EDTA. Additionally, trypan blue quenching was used to exclude surface fluorescence signals of not completely internalized siRNA-complexes. Results were compared to those obtained with cells that did not undergo trypan blue quenching. Median fluorescence intensities (MFI) were analyzed using an Attune NxT Acoustic Focusing Cytometer (Thermo Fisher Scientific, Waltham, Massachusetts, USA) by exciting the siRNA-AF488 at 488 nm and measuring the fluorescence signal with a 530/30 nm emission filter. Samples were run in triplicates, each sample consisting of a minimum of 10000 viable cells. Results are given as mean ± standard deviation (n = 3).

2.10 Route of cellular Uptake

To investigate the route of polyplexes uptake, experiments with different types of specific uptake inhibitors were performed [31]. U87 cells (100000 per well) seeded 24 h prior to experiment were incubated with nystatin (10 µg/ml), wortmannin (12 ng/ml), chlorpromazine (10 µg/ml) and methyl-beta-cyclodextrin (3 mg/ml) for 1 h followed by incubation with polyplexes containing AF488 labelled siRNA for 24 h. Positive control cells without inhibitor treatment were transfected with polyplexes and untreated cells served as a blank control. After trypsinizing, 20 µl of cell suspension was stained with 0.4% trypan blue solution to investigate the cytotoxicity of used inhibitors. Number of living and dead cells was counted in a Neubauer chamber using an Axio Vert.A1 microscope (Zeiss, Oberkochen, Germany). The percentage of viable cells was calculated. Remaining samples were washed, one half mixed with 0.4% trypan solution to quench surface fluorescence and all samples were subjected to flow cytometric detection of siRNA uptake as described above. The experiments were performed in triplicates. Results are shown as percentage of median fluorescence intensity related to not inhibited positive control samples (100%).

2.11 siRNA Release by Heparin Competition Assay

To evaluate the polyplex stability in the presence of competing polyanions under neutral and acidic conditions a heparin competition assay was performed. Polyplexes were prepared in the presence of two different buffers, a 10 mM HEPES buffer (pH 7.4) and a 10 mM sodium acetate buffer (pH 4.5) to enable comparison of polyplexes stability at different pH as well as at various ionic strengths. Polyplexes sample aliquots of 60 µl were dispersed into a white FluoroNunc 96 well plate and 10 µl of beforehand prepared heparin concentrations (0.12, 0.16, 0.21, 0.27, 0.35, 0.46, 0.59, 0.77, 1 USP units/well) were added to the wells each. After incubation for 30 min

at room temperature, 30 µl of a 4X SYBR Gold solution was added to each well and the plate was incubated for 10 min under light exclusion. Fluorescence measurement and calculation of percentage of free siRNA was performed as described under section 2.4. To obtain more precise results each heparin concentration was added to the respective buffer and used as blank for related samples. Measurements were performed in triplicates and results are shown as mean values (n = 3).

2.12 In vitro eGFP Knockdown by Flow Cytometry

To determine if polyplexes can efficiently knock down protein levels in cells, silencing of enhanced green fluorescent protein reporter gene eGFP was quantified by flow cytometry. H1299/eGFP cells (25000 per well) were seeded in 24 well plates in 500 µl medium and grown for 24 h at 37 °C in humidified atmosphere with 5% CO_2. As positive control Lipofectamin 2000 lipoplexes formulated with 50 pmol of siRNA against eGFP (siGFP) and as negative control poly - and lipoplexes containing scrambled siRNA were included. Cells were transfected with siGFP-polyplexes and controls for 48 h with or without chloroquine treatment. Subsequently, cells were trypsinized and prepared for flow cytometry measurements as described for cellular uptake experiments. MFIs of samples were quantified using an Attune Cytometer (Thermo Fisher Scientific, Waltham, Massachusetts, USA) with a 488 nm excitation laser and a 530/30 nm emission filter. Experiments were conducted in triplicates, each sample consisting of a minimum of 10000 cells. Results are shown as percentage of knockdown compared with the expression level in non-transfected cells.

2.13 Cytotoxicity

2.13.1 MTT Assay

Cytotoxicity of free polymers and polyplexes was tested via MTT assay. Therefore 8000 U87 cells per well were plated 24 h prior in a transparent 96 well plate (FisherScientific, Hampton, New Hampshire, USA). Free polymers were diluted in pre-warmed EMEM medium to a final concentration of 5 µg/ml and 20 µg/ml. Polyplexes were freshly prepared and 10X diluted with medium as well. After consumed medium was completely removed, 100 µl of polymer or polyplex containing medium was added to each well and incubated for 24, 48, 72 h at 37°C and 5% CO_2. As a positive control, DMSO 25% in medium was used. After the respective incubation times, medium was aspirated and 100 µl of MTT containing medium (0.5 mg/ml in EMEM media) was added to each well. Cells were incubated for another 3 h in the incubator. Subsequently, the cell culture medium was completely removed and insoluble purple formazan

crystals, converted from water soluble MTT by metabolically active mitochondria [32] was dissolved in 200 µl iso-propanol. The absorption was quantified at 570 nm and corrected with background values measured at 680 nm using a microplate reader (FLUOstar Omega, BMG Labtech, Ortenberg, Germany). The experiment was performed in triplicate and results are shown as mean ± standard deviation normalized to percentage of viable cells in comparison to untreated cells representing 100% viability.

2.13.2 LDH Assay

Cytotoxicity, caused by membrane damage after polymer/polyplex treatment, was evaluated using a CytoTox 96® Non-Radioactive Cytotoxicity Assay Kit (containing lysis buffer, Cytotox 96 reagent and stop solution) according to the manufacturer´s protocol. Briefly, U87 cells were plated 24 h prior in a 96 well plate at a density of 8000 cells per well and were treated with polymer or polyplex solutions similar as described for the MTT assay. Samples treated with lysis buffer were used as positive control and represent 100% LDH release; untreated cells were cultivated as blank controls. In another 96 well plate, 50 µl media aliquots were mixed with 50 µl Cytotox 96 reagent. Plates were incubated under light protection for 30 min to allow the conversion of tetrazolium salt into a red formazan product mediated via lactate dehydrogenase (LDH) enzyme [33]. Subsequently, 50 µl stop solution was added and absorbance was measured at 490 nm by using a microplate reader (FLUOstar Omega, BMG Labtech, Ortenberg, Germany). The percentage of cytotoxicity was calculated by the ratio of experimental LDH release and maximum LDH release. Results are graphed as mean ± standard deviation (n = 3).

2.14 Confocal Laser Scanning Microscopy

2.14.1 Endosomal entrapment

To visualize the cellular distribution of polyplexes, 50000 eGFP H1299 cells were seeded on 13 mm microscope cover glasses (VWR, Pennsylvania, USA) which were placed in each well of a 24 well plate. Cells were transfected with or without chloroquine treatment for 24 h with poly- and lipoplexes formulated with 50 pmol AlexaFluor 647-labeled siRNA. Subsequently, cells were washed with PBS twice, incubated with a 75 nM Lysotracker red™ dnd 99 solution for 1 h at 37°C and 5% CO_2, washed again with PBS and fixed using freshly prepared 4% paraformaldehyde in PBS. After washing cells with PBS twice, their nucleus was stained with DAPI at a final concentration of 1 µg/ml. The cells were finally washed with PBS twice and mounted utilizing FluorSave reagent. Fluorescence images were acquired using a laser scanning

microscope (Leica SP8 inverted, Software: LAS X, Leica microsystems GmbH, Wetzlar, Germany). Diode lasers (405 and 638 nm) and an argon laser (552 nm) were chosen for excitation, emission was detected in blue (410 – 480 nm, DAPI), red (660 – 785 nm, AF647) and yellow (600 – 700 nm, Lysotracker red) channels, respectively.

2.14.2 In vitro eGFP Knockdown

For eGFP knockdown experiments, 50000 eGFP H1299 cells were seeded on coverslips placed in a 24 well plate and treated as described for eGFP knockdown experiments. Subsequently, cells were washed with PBS twice and fixed using 4% paraformaldehyde in PBS. After washing cells with PBS twice, their nucleus was stained with DAPI at a final concentration of 1 µg/ml. The cells were finally washed with PBS twice and mounted utilizing FluorSave reagent. Slides were imaged as described above; for excitation a diode laser (405 nm) and an argon laser (488 nm) were used, emission was detected in blue (410 - 483 nm, DAPI) and green (493 - 778 nm, eGFP) channels, respectively.

2.15 Statistics

Unless otherwise stated, results are given as mean value ± standard deviation. One-way ANOVA with Bonferroni multiple comparison test and two-way ANOVA were performed in GraphPad Prism software (Graph Pad Software, La Jolla, CA) to calculate p-values at 95% confidence.

3. Results and Discussion

3.1 Polymers synthesis and characterization

Polymers were prepared with varying ratios of hydrophobic and hydrophilic ß-lactams via anionic ring-opening polymerization (ROP) as described above, by simple modulation of the monomer feed. The synthesis led to two sets of random Nylon-3 copolymers that contain both, a hydrophobic and a cationic, subunit. The hydrophobic monomer was in every case cyclopentadienyl ß-lactam (CP). The cationic monomer was either a dimethyl ß-lactam (DM) or a ß-lactam without methyl group (NM). $DM_{0.4}/CP_{0.6}$ and $NM_{0.4}/CP_{0.6}$ polymers with similar subunit ratios were synthesized to compare the effect of different cationic subunits. Additionally, we altered the proportion of hydrophobic subunit in the NM/CP set ($NM_{0.4}/CP_{0.6}$ and $NM_{0.2}/CP_{0.8}$) to be able to evaluate the impact of different hydrophobic fractions of the polymer chains regarding particle formation, cellular internalization and endosomal escape

ability. To determine molecular weights of the NM/CP polymers and to confirm subunit ratios, polymers were characterized by ^{1}H-NMR spectroscopy as described above. Molar masses and degree of polymerization obtained for $NM_{0.4}/CP_{0.6}$ and $NM_{0.2}/CP_{0.8}$ polymers were 32900 g/mol and 214 and 28000 g/mol and 212, respectively (Figure S5 and S6, Supplementary Material). Due to the lack of visible end-groups in the ^{1}H-NMR spectra (Figure S4, Supplementary Material), to determine the polydispersity and to confirm monomodal distribution of Nylon-3 polymers, $DM_{0.4}/CP_{0.6}$ was characterized by gel permeation chromatography (GPC) in THF using the boc-protected polymer. Values derived from GPC analysis of $DM_{0.4}/CP_{0.6}$ are shown in Figure S3 (Supplementary Material). Based on the GPC results, a degree of polymerization of 265 and a molar mass of 43700 g/mol for unprotected $DM_{0.4}/CP_{0.6}$ was calculated.

3.2 siRNA encapsulation Assay

In order to enable delivery of siRNA molecule to target sites and especially to protect the sensitive backbone from various sources of degradation after application such as nucleases [34], an effective method of protection is encapsulation by charge complexation. Positively charged polymers electrostatically interact with negative charges provided by phosphate groups present in the siRNA molecule [35]. Consequently, siRNA encapsulation ability of polymers represents an important property in evaluating their suitability as siRNA carrier. Although, exact mechanism for complex formation between Nylon-3 polymers and siRNA are still unknown, a combination of electrostatic and hydrophobic interactions due to polymers structural properties is implicated [24]. As previously described, polycationic structures cause dose-dependent toxicity, therefore optimal polymer concentrations for efficient siRNA condensation and protection needs to be evaluated [15]. In order to determine optimal amounts of polymer, we performed siRNA encapsulation assays at various N/P ratios (Figure 1) by using the fluorescent dye SYBR Gold.

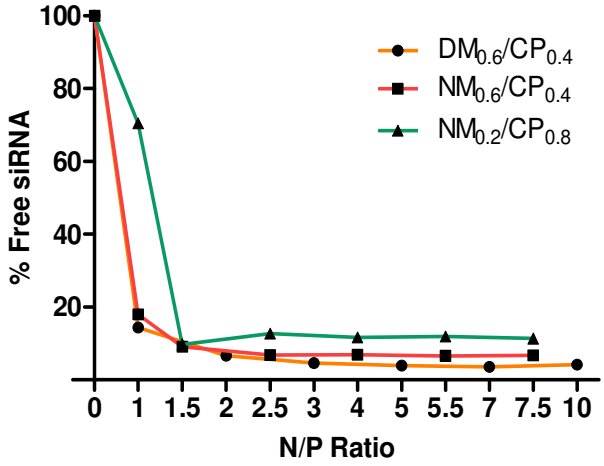

Figure 1. siRNA encapsulation profiles of polyplexes as measured by SYBR Gold assay at various N/P ratios. 100% values (N/P = 0) are represented by determined fluorescence of uncondensed siRNA. (Data points indicate mean, n = 3).

In this assay, free and unbound siRNA is completely accessible to the intercalating nucleic acid dye SYBR Gold causing a fluorescence signal enhancement, measured fluorescence signal decreases as soon as siRNA is protected in a polyplex. $DM_{0.4}/CP_{0.6}$ and $NM_{0.4}/CP_{0.6}$ polymers showed comparable siRNA encapsulation profiles with approximately 15% free siRNA at N/P 1 and maximum condensation at N/P 3 with 4.63% and 6.8% of non-encapsulated siRNA, respectively. $NM_{0.2}/CP_{0.8}$ polymer left 70.45% of siRNA uncondensed at N/P 1 and showed maximum protection of siRNA payload at N/P 2.5 with 12.68% free siRNA. As the $NM_{0.2}/CP_{0.8}$ polymer has the lowest charge density, it can be concluded that a certain amount of electrostatic interaction is needed to encapsulate siRNA efficiently. Furthermore, $NM_{0.2}/CP_{0.8}$ polymer was not able to condense siRNA as efficiently as $DM_{0.4}/CP_{0.6}$ and $NM_{0.4}/CP_{0.6}$ polymers. However, all polymers showed highly efficient siRNA encapsulation at rather low N/P ratios in comparison to low molecular weight polyethylenimine based polymers for example [36]. Using the latter, complete condensation of siRNA was achieved only at N/P ratio of 5 and higher. In contrast, as described elsewhere, amphiphilic PEI-PCL-PEG polymers achieved full siRNA condensation comparable to Nylon-3 polymers at N/P ratio 2 indicating a high nucleic acid-binding affinity of amphiphilic materials that condense with siRNA electrostatically and due to hydrophobic interactions [18]. Advantageously, the use of low polymer concentrations helps avoid unwanted side or toxic effects and reduces costs caused of the polymer excipient.

3.3 Particle characterization

3.3.1 Size and Zeta (ζ)-Potential Analysis by Dynamic Light Scattering and Laser Doppler Anemometry

In order to investigate whether Nylon-3 polymer–siRNA polyplexes fulfill general requirements for efficient nanoparticle drug delivery in glioblastoma cells [37], the first step of our study was the characterization of nanoparticles physicochemical characteristics, as these are two major determinants for intracellular uptake and transfection abilities. To determine optimal N/P ratios for further experiments, hydrodynamic diameter, PDIs and zeta potentials were measured at N/P ratios from 1 to 15 using protocols described above and are exemplarily shown for $NM_{0.2}/CP_{0.8}$ polymer (Figure S7, Supplementary Material). At N/P ratio 4 $NM_{0.2}/CP_{0.8}$ polyplexes demonstrated smallest particle sizes in combination with slightly positive zeta potentials indicating optimal encapsulation efficiency at this N/P ratio. In an analogous procedure and in combination with uptake experiments (vide infra) N/P ratios for $NM_{0.4}/CP_{0.6}$ and $DM_{0.4}/CP_{0.6}$ polymers were selected. In detail, and as shown in Figure 2A, $DM_{0.4}/CP_{0.6}$ polyplex sizes increased with increasing N/P ratios from 128.2 nm at N/P 1 to 253.0 nm at N/P 5, whereas $NM_{0.4}/CP_{0.6}$ and $NM_{0.2}/CP_{0.8}$ polyplexes showed smallest sizes at N/P 4 with 107.1 nm and 101.1 nm and PDIs of 0.298 and 0.193, respectively. This finding is in line with previously published data for the $DM_{0.4}/CP_{0.6}$ polymer [24]. NM/CP polymers both displayed a similar trend as reported for high molecular weight PEI and for PEI-PCL-PEG polymers that show a minimum in hydrodynamic diameter at N/P ratio of 2 (133 nm) and 10 (128 nm), respectively. Increasing the N/P ratio beyond this optimal value was shown to cause larger hydrodynamic diameters and PDIs [38]. Zeta potentials of polyplexes increased with rising N/P ratios (Figure 2B), showing negative values at lower N/P ratios, while at N/P 4 or 5 all polyplexes revealed positive values ranging from 2.24 mV for $DM_{0.4}/CP_{0.6}$ polyplexes to 17.03 mV for $NM_{0.2}/CP_{0.8}$ polyplexes. $NM_{0.4}/CP_{0.6}$ polyplexes showed a slightly higher positive charge at N/P ratio 2.5 compared to that at N/P 5, which is comparable with findings for PEI/siRNA complexes [38].

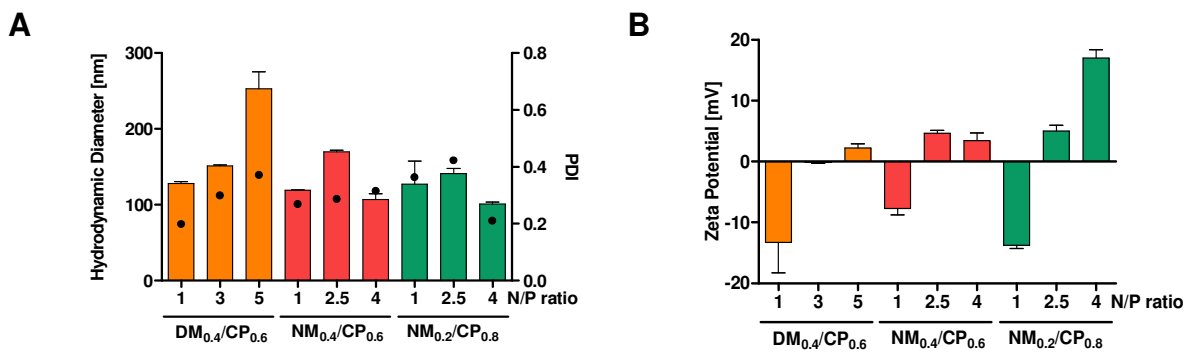

Figure 2. Dynamic light scattering and laser Doppler anemometry measurements of polyplexes formed with $DM_{0.4}/CP_{0.6}$, $NM_{0.4}/CP_{0.6}$ and $NM_{0.2}/CP_{0.8}$ (**A**) Hydrodynamic diameters (left y-axis), polydispersity indices (PDI, right y-axis) and (**B**) zeta potentials of $DM_{0.4}/CP_{0.6}$ polyplexes at N/P ratio 1, 3 and 5 and of NM/CP polyplexes at N/P ratio 1, 2.5 and 4. (Data points indicate mean ± SD, n = 3).

On the basis of this data, we suggest that at N/P 1 siRNA is incompletely and loosely attached to the polymer leading to a negative zeta potential. By increasing N/P ratios, siRNA is more efficiently embedded in the polymers. N/P 5 for $DM_{0.4}/CP_{0.6}$ and 2.5 for both NM/CP polymers offer sufficient polymer excess for positive surface charges. Upon addition of further polymer, it is possible that either further polymer layers form on the surface of the polyplex or a redistribution of siRNA and polymer may occur [38]. Interestingly, NM/CP polymers demonstrated smallest particle sizes with narrow size distributions at N/P ratio 4 indicating higher packing efficiencies probably due to missing methyl groups, and therefore less steric hinderance in the cationic subunits. The NM subunit is in addition more hydrophilic, which supports interactions with siRNA molecules. These results confirmed our assumption that NM monomer makes polymer highly capable to form compact particles with siRNA at favorable sizes. Increasing the N/P ratio beyond this optimal value was shown to cause larger hydrodynamic diameters and PDIs [38]. In conclusion all polymers at optimal N/P ratios were able to form particles with siRNA at appropriate size and surface charges.

3.3.2 Size measurements by Tunable Resistive Pulse Sensing

Particle diameter measurements were also performed by tunable resistive pulse sensing (TRPS). This technique has already been used in the field of drug delivery as it provides accurate characterization possibilities of drug delivery systems to ensure effectivity and quality control [39]. The system is equipped with an upper and a lower fluid cell filled with electrolyte and separated by a polyurethane membrane containing a centered single nanopore. When a voltage is applied ions move through the nanopore and generate a baseline current. As soon as a particle traverses the pore a reduction in the ionic current occurs and the magnitude of the measured blockade signal is directly proportional to the particle volume, allowing determination of particle size. Consequently, and in contrast to DLS measurements, TRPS performs particle-by particle-measurements and provides statistical number-weighted distributions rather than average results. To allow a consistent comparison between DLS and TRPS technique, DLS data were also expressed as number-weighted distributions calculated from scattered light intensity values and various other parameters [37]. To optimize a protocol for the measurement of polyplexes as dynamic charged systems with TRPS, different aspects had to be taken into account. As complex formation between siRNA and polymer is mainly

caused by electrostatic interactions, an increase in the salt concentration, as present in measurement electrolyte, leads to a decreased binding affinity between siRNA and polymer due to charge shielding effects [40]. Furthermore, as the TRPS technique was initially optimized to measure particles with negative surface charges, we expected interactions of positively charged polyplexes with the polyurethane membrane. Modifications optimized for negatively charged particles might lead to nanopore blockades by measuring polyplexes with positive loads. In order to circumvent these limitations, we used $NM_{0.2}/CP_{0.8}$ with the lowest cationic amount for TRPS protocol optimization. By using SYBR Gold assays, performed in HEPES buffer and in TRPS-electrolyte solutions, we confirmed no significant difference in encapsulation efficiencies (Figure S8 A, Supplementary Material). To determine influence on polyplex size, we performed DLS measurements in HEPES buffer and electrolyte solution over time at various N/P ratios. In line with our expectations, hydrodynamic diameters of polyplexes increased after diluting polyplexes with electrolyte solution after 10 min incubation due to decreased binding affinities, whereas the most distinct effect of size increase was displayed at N/P 4 (Figure S8, B, Supplementary Material). However, after 1 h incubation time, diameters remained quite stable. TRPS and DLS measurements were conducted within 30 mins after sample dilution to avoid destabilizing effects of electrolytes. In Table 1, DLS and TRPS diameters are listed for $NM_{0.2}/CP_{0.8}$ polyplexes at N/P ratios 4, 5.5, 7.5 and 11.5.

Table 1. Particle diameters of $NM_{0.2}/CP_{0.8}$ polyplexes at N/P ratios 4, 5.5, 7.5 and 11.5 diluted 1X with electrolyte solution (30 mM HEPES, 100 mM potassium chloride, 2 mM EDTA and 0.03% Tween®20) obtained by DLS and TRPS measurements. (Data shown as mean ± standard deviation, n=3).

N/P ratio	DLS (mean size ± SD) [nm]	TRPS (mean size ± SD) [nm]
4	158.00 ± 5.18	177.00 ±15.56
5.5	133.37 ± 1.79	100.50 ± 0.71
7.5	144.30 ± 1.76	164.00 ± 22.63
11.5	164.00 ± 3.8	193.00 ± 5.66

With both techniques, the smallest particles were measured at N/P 5.5 with 133.37 nm (DLS) and 100.5 nm (TRPS). At N/P ratio 7.5 and 11.5 diameters increased further to 144.3 nm and 164.0 nm (DLS) and to 164.00 nm and 193.00 nm (TRPS). Particle sizes depending on used N/P ratios followed the same trend as already described above, however, due to higher ionic concentrations in the TRPS electrolyte solution, smallest particles and consequently most efficient siRNA packing occurred at N/P 5.5 instead of N/P 4 as determined under standard conditions in HEPES buffer. TRPS data displayed slightly higher mean diameters, but average sizes as well as number-weighted distribution profiles are in acceptable agreement with DLS data (Figure S9, Supplementary Material) as estimated for monodisperse size distributions, proving successful protocol optimization. TRPS provides a promising technique for further applications in the field of polymeric drug delivery, e.g., polyplex concentration analysis and, is especially suitable for multiple population analysis, for protein corona experiments as well as for payload release studies.

3.3.3 Polyplex morphology

STEM imaging revealed non-spherical structures, as known for dynamic systems such as polyplexes [38]. The bright areas in the STEM images correspond to areas of larger electron density which can be a matter of higher atomic number (Figure 3, area 1 (bright) and 2 (darker) in red boxes). The analysis of the compositions of brighter and darker areas by EDX elemental analysis revealed the presence of significant amounts of phosphorous and considerably lower relative nitrogen content in area 1. The area-integrated EDX spectra indicate that bright signals are enriched in phosphorous-containing siRNA and contain less polymer which is characterized by a large number of amines and amides less prominent in the bright areas.

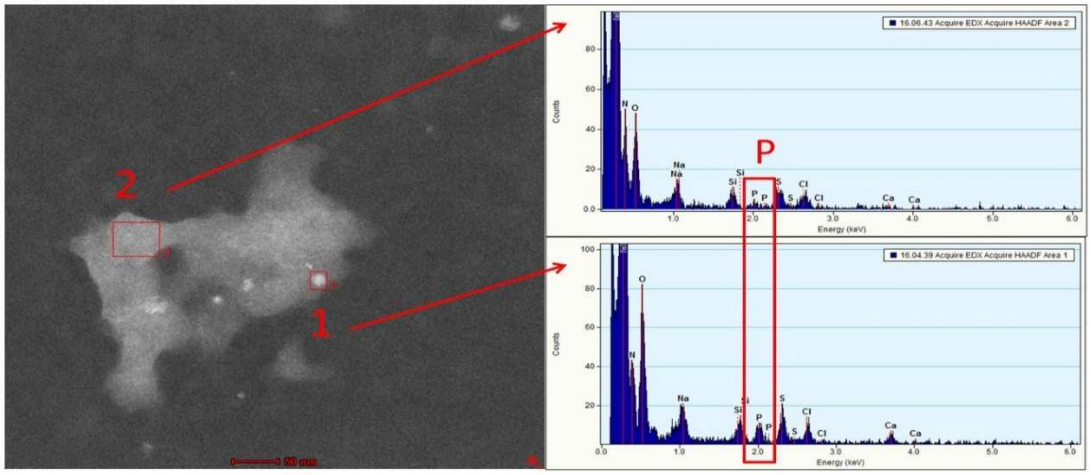

Figure 3. STEM-ADF image of a typical polyplex and EDX spectra obtained from the red boxes (1) and (2). Both spectra show carbon, nitrogen and oxygen as main constituents. Smaller amounts of sodium, chlorine, sulfur and calcium can be detected due to residuals of the buffer solution. Importantly, a significant amount of phosphorous can only be detected for area 1. In addition, the relative nitrogen content is considerably lower for area 1.

3.4 Quantification of Cellular Uptake by Flow Cytometry

As initial experiments indicated that Nylon-3 polymers are suitable for siRNA delivery regarding siRNA encapsulation efficiency and physicochemical characteristics, the next step was to investigate their ability to mediate internalization into glioblastoma cells depending on structural characteristics. In this regard, cellular uptake of Alexa Fluor 488-labeled siRNA was quantified by flow cytometry. As cellular internalization ability can be different depending on utilized cell lines [41] a preliminary uptake experiment was conducted in H1299, in which successful transfection has been previously shown [24] and in U87 cells in order to confirm transfection abilities also in glioblastoma cells. As illustrated in Figure S10 (Supplementary Material), median fluorescence intensity (MFI) measured in U87 cells eventuated in overall lower MFI values, nonetheless showing the same trends regarding tested polymers and N/P ratios. This result confirmed comparable cell entry mechanism of polyplexes in H1299 and U87 cells, however, indicated that U87 cells are generally harder to transfect. Based on these data, incubation times of 24 h were chosen for further experiments in U87 cells. In addition, uptake measurements at N/P ratios from 1 to 15 were conducted using protocols described above and are exemplarily shown for $NM_{0.2}/CP_{0.8}$ polymer (Figure S7, Supplementary Material) to verify N/P 4 as the most suitable N/P ratio for $NM_{0.2}/CP_{0.8}$. Fluorescence signals of cellular internalized siRNA-AF488 increased for N/P ratios from 4 to 7.5 and decreased for N/P ratios from 11.5 to 15. However, as significant uptake was already reached at N/P ratio 4, this N/P ratio was identified as optimal and used for further experiments. In an analogous procedure N/P ratio 4 and 5 for $NM_{0.4}/CP_{0.6}$ and $DM_{0.4}/CP_{0.6}$ polymers were determined. Figure 4 shows the

MFI of U87 cells transfected with polyplexes formulated with different polymers at the preassigned N/P ratios for 24 h, in comparison to untreated cells and free siRNA treated cells as negative controls and Lipofectamin 2000 (LF) lipoplexes treated cells as positive control.

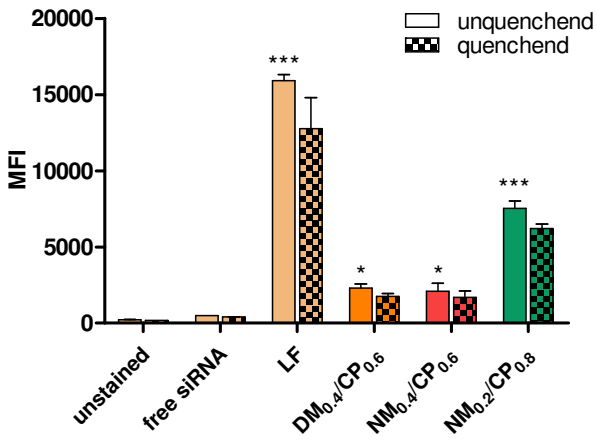

Figure 4. Cellular uptake of polyplexes ($DM_{0.4}/CP_{0.6}$ polyplexes: N/P 5, $NM_{0.4}/CP_{0.6}$ and $NM_{0.2}/CP_{0.8}$ polyplexes: N/P 4) after 24 h incubation as quantified by flow cytometry performed with and without trypan quenching and presented as median fluorescence intensity. Negative control: untreated cells and with free siRNA treated cells, positive control: with Lipofectamin (LF) lipoplexes transfected cells. (Data points indicate mean ± SD, n = 3, two-way ANOVA with Bonferroni post-hoc test, *$p < 0.05$, **$p < 0.01$, ***$p < 0.005$).

All polyplexes displayed significantly higher uptake compared to negative control as indicated by the statistics in Figure 4, whereby signals of cells treated with $NM_{0.2}/CP_{0.8}$ polyplexes (MFI = 7536) were approximately four times higher than those of cells treated with formulations containing higher amounts of cationic monomers ($DM_{0.4}/CP_{0.6}$ polyplexes: MFI = 2303, $NM_{0.4}/CP_{0.6}$ polyplexes: MFI = 2098). Trypan blue quenching, that was additionally performed in order to exclude extracellular fluorescent signals caused by cell surface-bound siRNA, resulted in insignificantly lower MFI values for all tested polyplexes indicating that inconsiderable amounts of polyplexes stuck to the outer cell membranes. Most efficient siRNA delivery in glioblastoma cells was observed by the most hydrophobic $NM_{0.2}/CP_{0.8}$ polyplexes. Besides already described interactions of cationic polyplex structures with anionic cell surface proteoglycans [42], we therefore suggest that also hydrophobic interactions with lipid bilayers might play an important role in polyplex uptake procedure. As recently described various hydrophobically modified polymers were used to enhance transfection efficiencies at low cytotoxicity. For example oleic and stearic acid modified PEI 2kDa resulted in 3-fold increased siRNA delivery to B16 melanoma cells in comparison to unmodified PEI [43] and triblock copolymeric systems of poly(amidoamine) (PAMAM) dendrimers modified with PEG and dioleoylphosphatidyl ethanolamine (DOPE) displayed

significantly higher uptake of siRNA in A549 cells [44]. These results strongly support our findings where hydrophobization of polymers enhanced siRNA delivery to target cells even at low N/P ratios. In general nanoparticles with a size range of 100-200 nm and slight positive surface charges have been shown to achieve the best cellular uptake [45]. Altogether these results indicate that due to accumulation of favorable properties especially $NM_{0.2}/CP_{0.8}$ polyplexes exhibit great potential as siRNA delivery agent.

3.5 Route of cellular uptake

As the route of cellular uptake determines intracellular processing and subsequent transfection efficiencies of delivery systems it is important to profile their cellular endocytotic pathways. It was recently shown that lipoplexes are internalized solely by clathrin-mediated endocytosis, whereas polyplexes are taken up both by clathrin-mediated and caveolae-mediated endocytosis. However, it was also stated that only the caveolae-dependent route leads to successful transfection due to lysosomal degradation of polyplexes and their payload after clathrin-mediated cell entry [41]. To investigate the route of uptake of Nylon-3 polyplexes, we performed a modified cellular uptake experiment with $DM_{0.4}/CP_{0.6}$ and $NM_{0.2}/CP_{0.8}$ polyplexes. In this regard, we incubated cells with different chemical uptake inhibitors (nystatin, wortmannin, chlorpromazine and methyl-β-cyclodextrin) prior to transfection. Subsequently, samples were treated as described above and subjected to flow cytometric measurements. Nystatin is known to inhibit the internalization of caveolae and lipid rafts through depletion of cholesterol in the cell membrane [46], wortmannin has been shown to block micropinocytosis, which is discussed as an alternative endocytic pathway for polyplexes, chlorpromazine suppresses clathrin-coated pit formation by reversible translocation of clathrin from the plasma membrane to intracellular vesicles [47], and methyl-β- cyclodextrin inhibits cholesterol-dependent clathrin-mediated glycolipids and is involved in lipid raft depletion [48]. Several chemical inhibitors are described in the literature as substances with cell line dependent toxic effects, leading to inaccurate experimental results. Therefore, applied concentrations needed to be optimized. Herein cell viabilities of U87 cells at chosen inhibitor concentrations were confirmed by trypan blue staining of dead cells after inhibitor incubation (Figure S11, Supplementary Material). As shown in Figure 5 cellular uptake after inhibitor treatment is given as a percentage of MFI related to uninhibited samples.

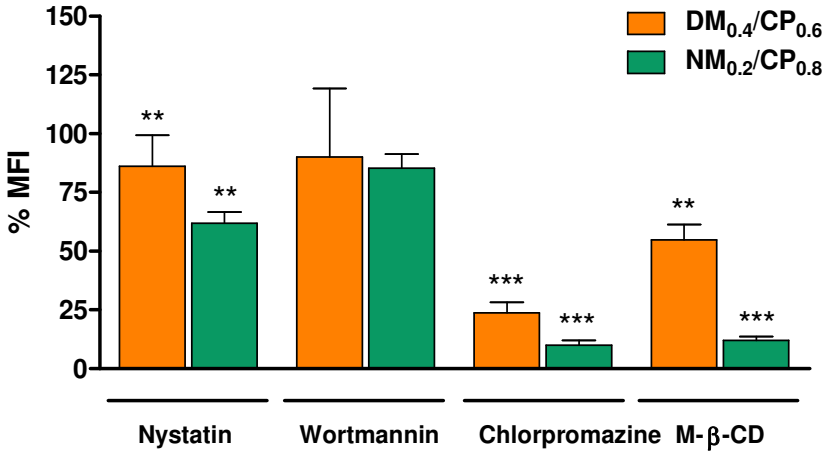

Figure 5. Cellular uptake of polyplexes ($DM_{0.4}/CP_{0.6}$ polyplexes: N/P ratio = 5 and $NM_{0.2}/CP_{0.8}$ polyplexes: N/P ratio = 4) after treatment with nystatin (10 µg/ml), wortmannin (12 ng/ml), chlorpromazine (10 µg/ml) and methyl-β-cyclodextrin (M-β-CD) (3 mg/ml) as evaluated by flow cytometry and presented as MFI. (Results are shown as mean ± SD as percentage of median fluorescence intensity related to not inhibited samples, n = 3, two-way ANOVA with Bonferroni post-hoc test, **p < 0.01, ***p < 0.005).

Wortmannin led to insignificant signal reduction, implying that micropinocytosis did not play a considerable role in polyplex internalization. Using nystatin, chlorpromazine and methyl-ß-cyclodextrin, the observed remaining signals in comparison to uninhibited polyplex uptake for $DM_{0.4}/CP_{0.6}$ were 86.17%, 23.77% and 54.80% and for $NM_{0.2}/CP_{0.8}$ polyplexes 61.9%, 9.95% and 12.03%, respectively. In summary, chlorpromazine and methyl-β-cyclodextrin most strongly inhibited polyplex cellular uptake for both formulations, indicating both polyplexes were predominantly internalized via cholesterol-dependent clathrin-mediated endocytosis and only partially by caveolae-mediated endocytosis. However, due to stronger inhibitory effects on $NM_{0.2}/CP_{0.8}$ polyplexes, we suggest that polyplexes with higher hydrophobic content share more similarity with lipoplexes regarding their uptake route. As illustrated in Figure S11 (Supplementary Material), the inhibition treatment was well tolerated by the treated glioblastoma cells. Taken together with the fact that MFI values insignificantly decreased after performed trypan blue quenching as shown in Figure S12 (Supplementary Material), it was concluded that the fluorescence decrease shown in Figure 5 was not a result from cellular toxicity of the inhibitors but that it also represented mainly internalized siRNA rather than polyplexes considerably accumulated on the cell surface. In line with our assumptions are recently reported data which show that DOTAP lipoplexes are mainly taken up by clathrin-mediated endocytosis, whereas PEI polyplexes no longer show transfection efficiency if caveolae-mediated endocytosis is blocked [41]. Furthermore, Lu et al. recently suggested a fusogenic mechanism between lipoplexes and cell membranes as depletion of cholesterol from

the cell membrane prevented successful siRNA delivery[49]. In conclusion, clathrin-mediated endocytosis and fusogenic uptake mechanisms as described for lipoplexes seems to play an important role for amphiphilic polyplexes as well.

3.6 siRNA Release Assay

The stability of polyplexes, which is influenced by the presence of competing anions after addition to serum containing cell culture medium or administration *in vivo*, is also an important parameter to screen the potential efficiency of polymers as siRNA vectors [50]. Therefore, release assays were performed to confirm the protection ability of Nylon-3 polymers for siRNA in the presence of polyanions under physiologically relevant conditions (pH 7.4). Moreover, as free siRNA present in the cytoplasm is a prerequisite to induce the RNAi machinery, siRNA release ability under acidic conditions (pH 4.5), mimicking the endosomal compartment, was determined also. As illustrated in Figure 6A siRNA displacement at pH 7.4 from $DM_{0.4}/CP_{0.6}$ polyplexes was observed at low heparin concentrations and reached maximum release of approximately 60% as of 0.455 USP units heparin per well. $NM_{0.2}/CP_{0.8}$ polyplexes displayed a comparable release profile upon addition of 0.455 USP units per well and more. $NM_{0.4}/CP_{0.6}$ polyplexes demonstrated to be the most stable complexes, as only up to 30.5% nucleic acid was displaced when the maximum amount of heparin was added. This observation goes in line with our suggestion that missing methyl groups in NM subunits lead to both, more hydrophilic character and lack of steric hindrance, and finally to stronger interactions with siRNA molecules. $NM_{0.4}/CP_{0.6}$ polymer contains highest amount of NM subunits and most strongly condenses siRNA at pH 7.4. Consequently, just a small amount of siRNA molecules could be replaced by competing heparin anions. From $NM_{0.2}/CP_{0.8}$ polyplexes siRNA was more easily replaced mostly due to lower charge density within the polymer. Methyl groups present in $DM_{0.4}/CP_{0.6}$ polymers sterically hinders complex formation with siRNA leading to more loosely assembled polyplexes and consequently to highest siRNA release after heparin addition. Furthermore, we assume that the effect of the dimethyl group in DM subunit on the pKa value for primary amines present in NM and DM subunit is negligible. We expect that same amount of primary amines is protonated in DM as well as in NM subunit at pH 7.4 and therefore that obtained differences in siRNA release profiles are not influenced by grade of protonation but can be mainly explained by sterically hindrance mechanisms during polyplex formation.

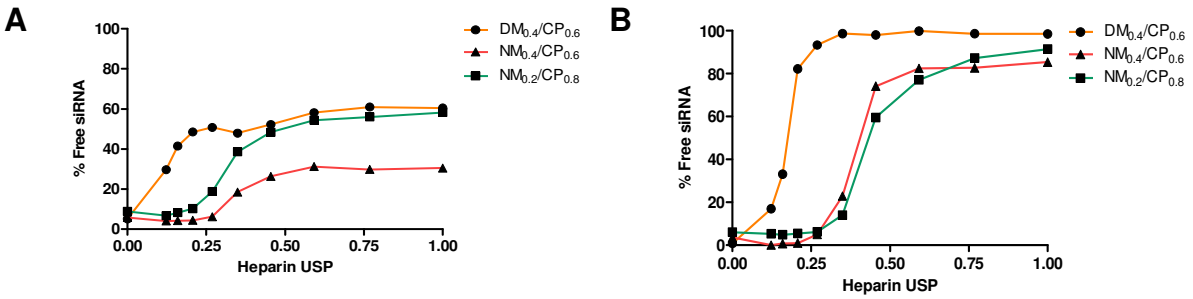

Figure 6. Release profiles of siRNA from $DM_{0.4}/CP_{0.6}$ polyplexes at N/P 5 and $NM_{0.4}/CP_{0.6}$ and $NM_{0.2}/CP_{0.8}$ polyplexes at N/P 4 as a function of heparin concentration (0.0 - 1.0 USP heparin per well) at pH (**A**) 7.4 and (**B**) 4.5. (Data points indicate mean normalized fluorescence, n = 3).

Under acidic conditions, as illustrated in Figure 6B and in accordance with our former observations, siRNA was very easily released from $DM_{0.4}/CP_{0.6}$ polyplexes reaching almost 100% release already at low heparin concentrations of 0.269 USP units heparin per well. $NM_{0.4}/CP_{0.6}$ and $NM_{0.2}/CP_{0.8}$ showed similar release profiles by reaching siRNA displacement of approximately 87% when using the highest heparin concentration of 1.000 USP units per well indicating appropriate payload release abilities. SiRNA release at lower pH values might occur through charge repulsion after amine protonation leading to complex destabilization [51]. These data indicate that especially $NM_{0.4}/CP_{0.6}$ polyplexes provide a stable system in circulation and that all polyplexes are able to efficiently release their payload in presence of competing anions at low pH upon being endocytosed. As described in literature PEI25kDa polyplexes release about 20% of siRNA at N/P 5 under physiological conditions when treated with heparin concentrations as low as 0.1 international units [36]. In comparison to Nylon-3 polyplexes they represent a system that only relies on the presence of high charge density. Under acidic conditions PEI25kDa polyplexes were described to release up to 50% of siRNA. Due to protonation of amines in the endosomal compartment it was hypothesized that the high amount of positive charges within the polymer may on the one hand lead to electrostatic repulsion, complex destabilization and endosomal escape [52]. One the other hand it is possible that said electrostatic repulsion causes sponge-like loose complex association but strong charge-charge interaction in specific complex areas which may be too strong for payload release. However, release of siRNA is a prerequisite for incorporation into the RNAi machinery and consequently therapeutic effects. In contrast, it was furthermore described that polymers containing hydrophobic functionalities, e.g., triazine dendrimers modified with alkyl chains, showed increased stability against heparin displacement under physiological conditions in comparison to PEI25kDa [53]. This shows very well that amphiphilic polymers interact with siRNA also based on hydrophobic interactions which are not affected by competing anions such as heparin.

This is especially true for $NM_{0.2}/CP_{0.8}$ polyplexes which show comparably high stability in particular in an acidic environment despite rather low cationic content.

3.7 In vitro eGFP Knockdown

To further evaluate gene silencing efficiency of $NM_{0.2}/CP_{0.8}$ polyplexes on the protein level, we utilized H1299/eGFP cells that stably express the 'enhanced green fluorescent protein' reporter gene (eGFP). H1299/eGFP cells were transfected with $NM_{0.2}/CP_{0.8}$ polyplexes formulated with siRNA against eGFP (siGFP) or with scrambled siRNA (siNC) as negative control. As positive control Lipofectamin (LF) 2000 lipoplexes were used. Additionally, cells were treated with the endosomolytic drug chloroquine that is able to increase the endosomal release of siRNA in order to investigate whether poor knockdown efficiencies may be caused by endosomal entrapment of polyplexes [50]. After treatment, the median fluorescence intensity of eGFP in each sample was quantified via flow cytometry. As seen in Figure 7, lipoplexes and $NM_{0.2}/CP_{0.8}$ polyplexes achieved a significant silencing effect even without chloroquine treatment indicating endogenous endosomal escape capacity of at least parts of the siRNA.

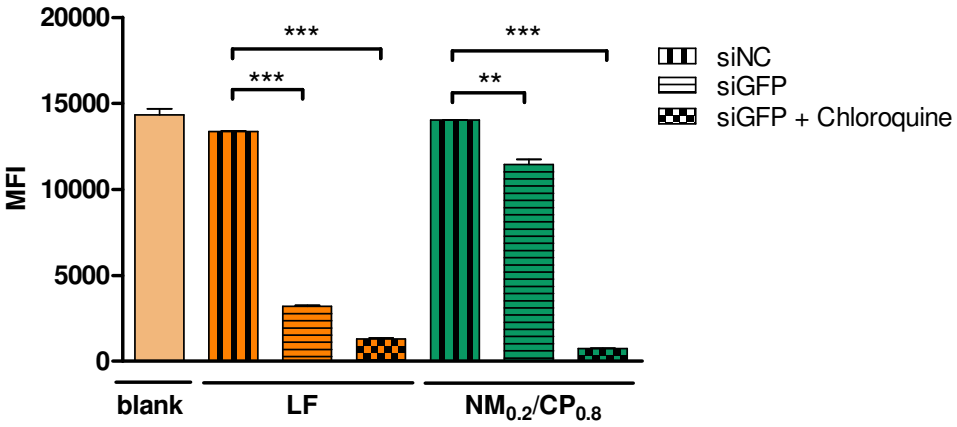

Figure 7. eGFP knockdown of $NM_{0.2}/CP_{0.8}$ polyplexes in human non-small cell lung carcinoma cells expressing eGFP (H1299/eGFP) quantified by flow cytometry as median fluorescence intensity (MFI) of eGFP after transfection with polyplexes at N/P 4 with eGFP siRNA or scrambled control siRNA (siNC) for 48 h with and without chloroquine treatment. Blank samples consisted of H1299/eGFP untreated cells. The positive control consisted of Lipofectamin (LF) 2000 lipoplexes formulated with eGFP siRNA or scrambled control siRNA with and without chloroquine treatment. (Data points indicate mean ± SD, n = 3, two-way ANOVA with Bonferroni post-hoc test, $^{**}p < 0.01$, $^{***}p < 0.005$).

However, the use of chloroquine increased the silencing effect for $NM_{0.2}/CP_{0.8}$ polyplexes tremendously, implying that endosomal entrapment of polyplexes hampers their full effect. Furthermore, $NM_{0.2}/CP_{0.8}$ polyplexes and LF lipoplexes containing scrambled control siRNA did not reduce the MFI of eGFP, indicating that the observed protein knockdown was not

mediated by the polymer system or any non-specific effects, but was RNAi mediated by eGFP siRNA delivered into the cytoplasm. It can be suggested that parts of the siRNA were able to escape the endosome and were released into the cytoplasm. A potential endosomal membrane rupture caused by Nylon-3 polyplexes might have a beneficial effect regarding endosomal escape ability. As recently described in literature, endosome disruption can be caused by cationic as well as hydrophobic moieties of polymeric nanoparticles, both present in Nylon-3 polymers [54]. Transbilayer flip-flop of negatively charged phospholipids from the cytoplasmatic leaflet to the luminal leaflet of the endosome was suggested to result in the formation of charge-neutral ion pairs for cationic-hydrophobic based delivery systems. Thereby weakening of the electrostatic interactions between siRNA and cationic charges can cause a release of the siRNA from the complexes [54]. Furthermore, destabilization of the endosomal membrane caused by direct interactions with hydrophobic domains in the polyplexes may help to release payload into the cytoplasm [55]. Altogether, the results shown here demonstrated knockdown ability of eGFP siRNA delivered by $NM_{0.2}/CP_{0.8}$ polyplexes, endosomal entrapment remains to be the major bottleneck to achieve efficient knockdown as described elsewhere [56]. Therefore, we suggest that, in comparison to PEI, buffering capacities of Nylon-3 polymers were not sufficient to enable similar escape of the endosomal compartment as known for PEI formulations. This drawback can be addressed in future approaches by precise optimization of polymer compositions. To test the nanocarriers for glioblastoma treatment in an *in vivo* setting in the future it needs also to be considered that formulations have to be able to overcome the blood brain barrier. The ability to overcome this important barrier will be currently assessed in a blood-brain barrier *in vitro* model.

3.8 Cytotoxicity

3.8.1 MTT Assay

One major drawback of cationic delivery systems is toxicity caused by high positive charge densities, which leads to cellular loss of outer membrane integrity and pore formation [15]. To test cytotoxicity of free polymer and polyplexes, MTT assays were conducted with U87 cells that had been incubated for 24, 48 and 72 h with free polymers at two concentrations (5 and 20 µg/ml per well) and polyplex formulations at two different N/P ratios. Thereby, lower concentration and N/P ratio represented treatment relevant conditions in *in vitro* experiments. Strongest toxic effect for all polymers and polyplexes was observed after 48 h treatments, indicating that cells were able to recover after an incubation period of 72 h (Figure 8). Both concentrations tested for free polymers led to similar toxicity profiles. $DM_{0.4}/CP_{0.6}$ polymer

demonstrated the highest negative influence on cell viability with survival rates of 70%, followed by $NM_{0.2}/CP_{0.8}$ polymer with 78.8% and $NM_{0.4}/CP_{0.6}$ polymer showing 100% viability after 48 h incubation time (Figure 8 A). In comparison to free polymers, polymer-siRNA complexes were overall better tolerated due to, as suggested, a shielding effect of positive charges after complexation with siRNA molecules (Figure 8B) [57].

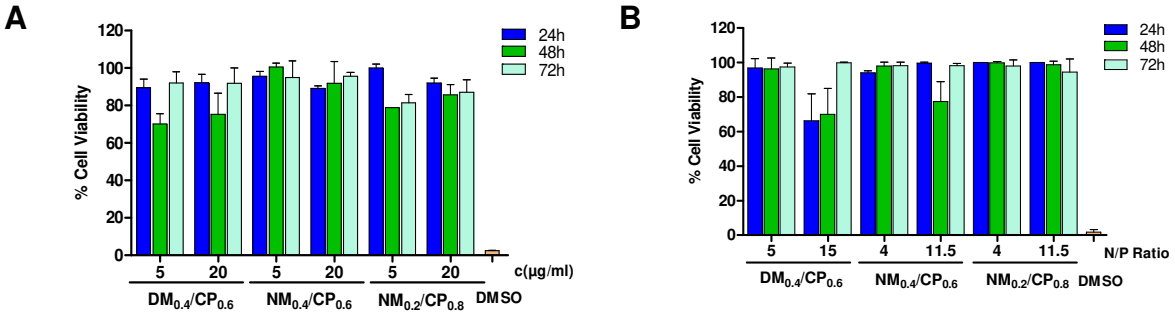

Figure 8. Cell viability as determined by MTT assay for free polymers with concentrations of 5 and 20 µg/ml per well (**A**) and formulated polyplexes at suitable N/P ratios (**B**) after incubation periods of 24, 48 and 72 h. (Results are shown as mean ± SD as percentage of viable cells in comparison to untreated cells representing 100% viability, n = 3).

At lower N/P ratios polyplexes demonstrated no significant toxic effects. In line with results for free polymers, $DM_{0.4}/CP_{0.6}$ polyplexes at N/P 15 caused the strongest toxic effect with approximately 70% survival rates after incubation periods of 24 and 48 h. $NM_{0.4}/CP_{0.6}$ and $NM_{0.2}/CP_{0.8}$ polyplexes displayed survival rates of 77.4% and 98.8% after 48 h incubation, respectively. In conclusion, acceptable cell compatibility for U87 cells could be confirmed for all free polymers as well as for all polyplexes. Free polymers with a maximum cationic content of 40% and polyplexes formulated from them demonstrated suitable toxicity profiles in U87 cells. An already published set of Nylon-3 polymers [24] showed cell viabilities ranging from 60 to 95% after 24 h incubation at concentrations of 20 µg/ml. PEI25kDa showed significant cellular toxicity (less than 50% cell viability) even at low concentrations of 5 µg/ml of the polymer [24]. Importantly, all Nylon-3 polymers were less toxic than broadly used high molecular weight PEI. Furthermore, this observation is especially important for future *in vivo* experiments as it demonstrates that our delivery systems are well tolerated even after potential internalization into healthy cells of the brain tissue. Moreover, to avoid side effects in healthy cells, a promising strategy is the use of therapeutic siRNA that target genes only present in tumor cells, e.g mutated growth factor receptor genes. In line with our assumptions toxicity of Nylon-3 polymers could be further reduced by optimizing the content of cationic subunits within the polymer chains, however, in future designs a critical balance should be considered

between cationic charge density for siRNA complexation and adjustments that decrease polymer toxicity.

3.8.2 LDH Assay

We utilized lactate dehydrogenase (LDH) assays to focus additionally on cytotoxicity caused by loss of membrane integrity. Measurements were performed with free polymers and polyplexes in U87 cells after 24, 48 and 72 h of incubation times. Percentage of LDH release for each sample was calculated in comparison to the signal of positive control cells treated with lysis buffer (100% LDH release). No considerable influence on LDH release could be found after free polymer or polyplex treatment (Figure 9).

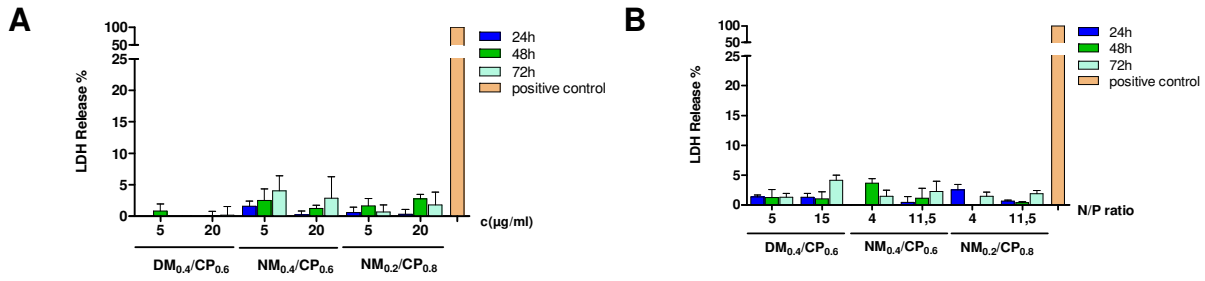

Figure 9. Cell membrane integrity determined by LDH assay for free polymers with concentrations of 5 and 20 µg/ml per well (**A**) and formulated polyplexes at suitable N/P ratios (**B**) with incubation periods of 24, 48 and 72 h. (Results are shown as mean ± SD as percentage of LDH release in comparison to blank cells treated with lysis buffer representing 100% LDH release, n = 3).

The strongest effect on membrane integrity was demonstrated after treatment with $NM_{0.4}/CP_{0.6}$ polymers (c = 5 µg/ml, t = 72h) and $DM_{0.4}/CP_{0.6}$ polyplexes (N/P ratio 15, t = 72h) with 4% LDH release. Summing up, these data show that neither free polymers nor polyplexes formulated with siRNA are expected to have a noticeable effect on membrane stability. Altogether these results demonstrated that all formulations are well tolerated by the cellular membranes.

3.9 Confocal Laser Scanning Microscopy

3.9.1 In vitro eGFP Knockdown

In order to visualize eGFP knockdown ability of $NM_{0.2}/CP_{0.8}$ polyplexes we performed confocal microscopy experiments. H1299/eGFP cells were transfected with polyplexes formulated with siRNA against eGFP (siGFP) or with scrambled siRNA (siNC) as negative control. As positive control Lipofectamin (LF) 2000 lipoplexes were used. As illustrated in Figure 10 lipoplexes as well as polyplexes achieved a decrease in eGFP fluorescence in comparison to negative control

samples. In line with the observations from *in vitro* eGFP knockdown experiments, confocal images verified partly endogenous endosomal escape capacity even without using chloroquine as cell organelle disruption agent.

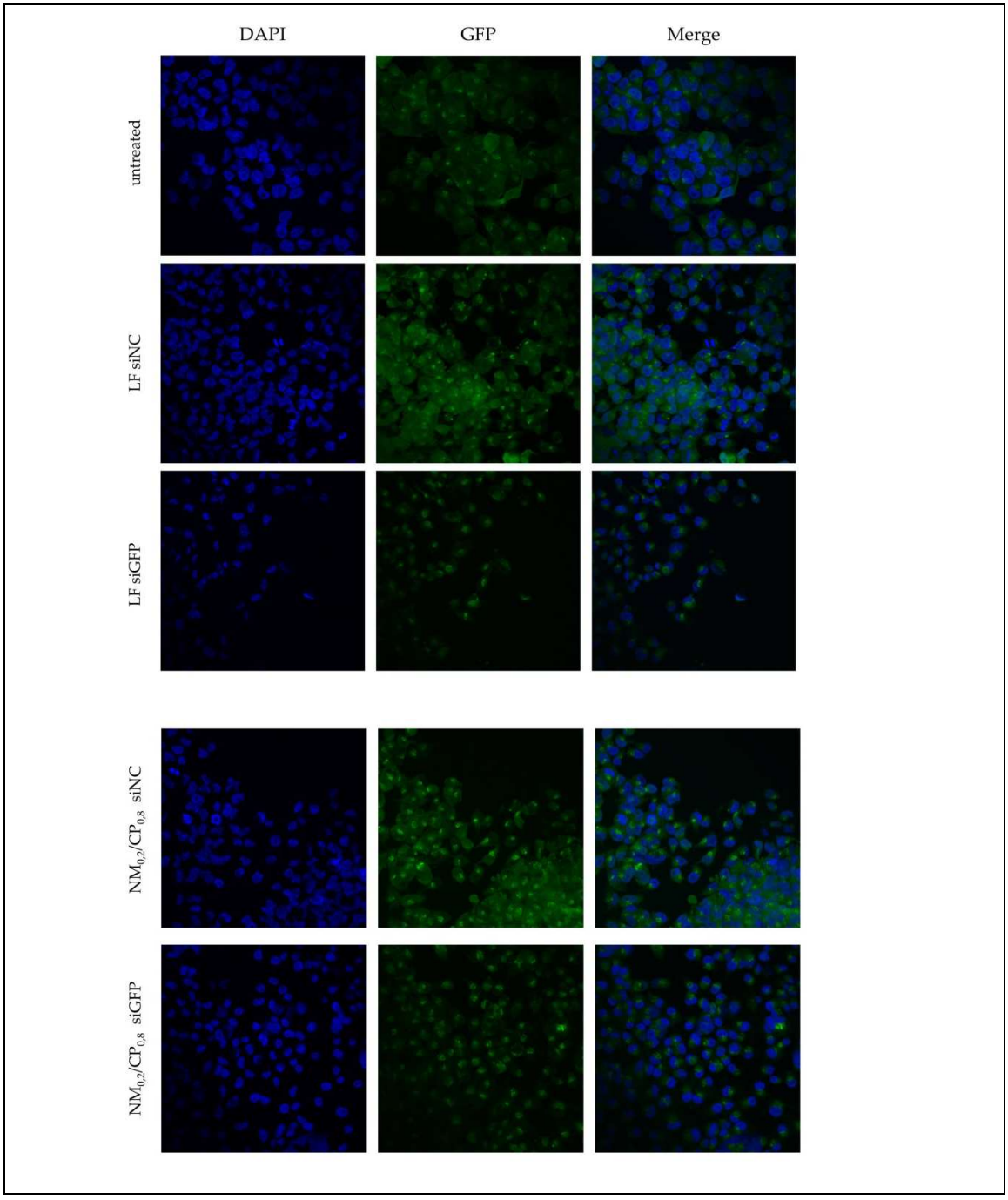

Figure 10. Confocal images after treatment of H1299/eGFP cells with NM0.2/CP0.8 polyplexes and Lipofectamin 2000 (LF) lipoplexes formulated with siGFP or siNC as negative control and staining with DAPI. eGFP fluorescence is shown in green, DAPI signal is shown in blue and depicts cell nuclei.

3.9.2 Endosomal entrapment

The endosomal compartment represents a substantial barrier to successful cytosolic siRNA delivery and plays a significant role for most polyplex-based siRNA delivery systems [58]. Once polyplexes are internalized into cells via endocytotic pathways, the release of the siRNA from the endosomal compartment is a crucial prerequisite for undergoing the RNAi machinery taking place in the cytoplasm. In order to further investigate cellular distribution of polyplexes, $NM_{0.2}/CP_{0.8}$ polyplexes were formulated with Alexa Fluor 647 labeled siRNA (shown in red). We performed a series of confocal microscopy experiments after transfection with $NM_{0.2}/CP_{0.8}$ polyplexes at N/P 4 for 24 h and staining of acidic cell organelles such as endosomes and lysosomes with Lysotracker red™ dnd 99 (shown in yellow) and of cell nuclei with DAPI (shown in blue) utilizing Alexa Fluor 647 labelled siRNA for transfection with $NM_{0.2}/CP_{0.8}$ polyplexes at N/P 4 for 24 h (shown in red). Samples treated with endosomolytic drug chloroquine were included as positive controls. Figure 11 illustrates resulting subcellular distribution profiles for $NM_{0.2}/CP_{0.8}$ polyplexes and Lipofectamin (LF) 2000 lipoplexes as positive control with and without chloroquine treatment. Both formulations exhibited cell internalization with rather punctuated distribution and showed colocalization with lysotracker signal indicating localization in endo- and lysosomes. Chloroquine treatment and thus disruption of endosomal membranes in positive control cells resulted in a more even distribution of AF647 labeled siRNA in the cytoplasm due to facilitated endosomal escape of siRNA. These observations were consistent with our previous experiments in which $NM_{0.2}/CP_{0.8}$ polyplexes demonstrated significant cellular uptake, successful knockdown ability but also entrapment in endosomal compartments. Future approaches may focus on polymer modification to address the bottleneck of endosomal entrapment.

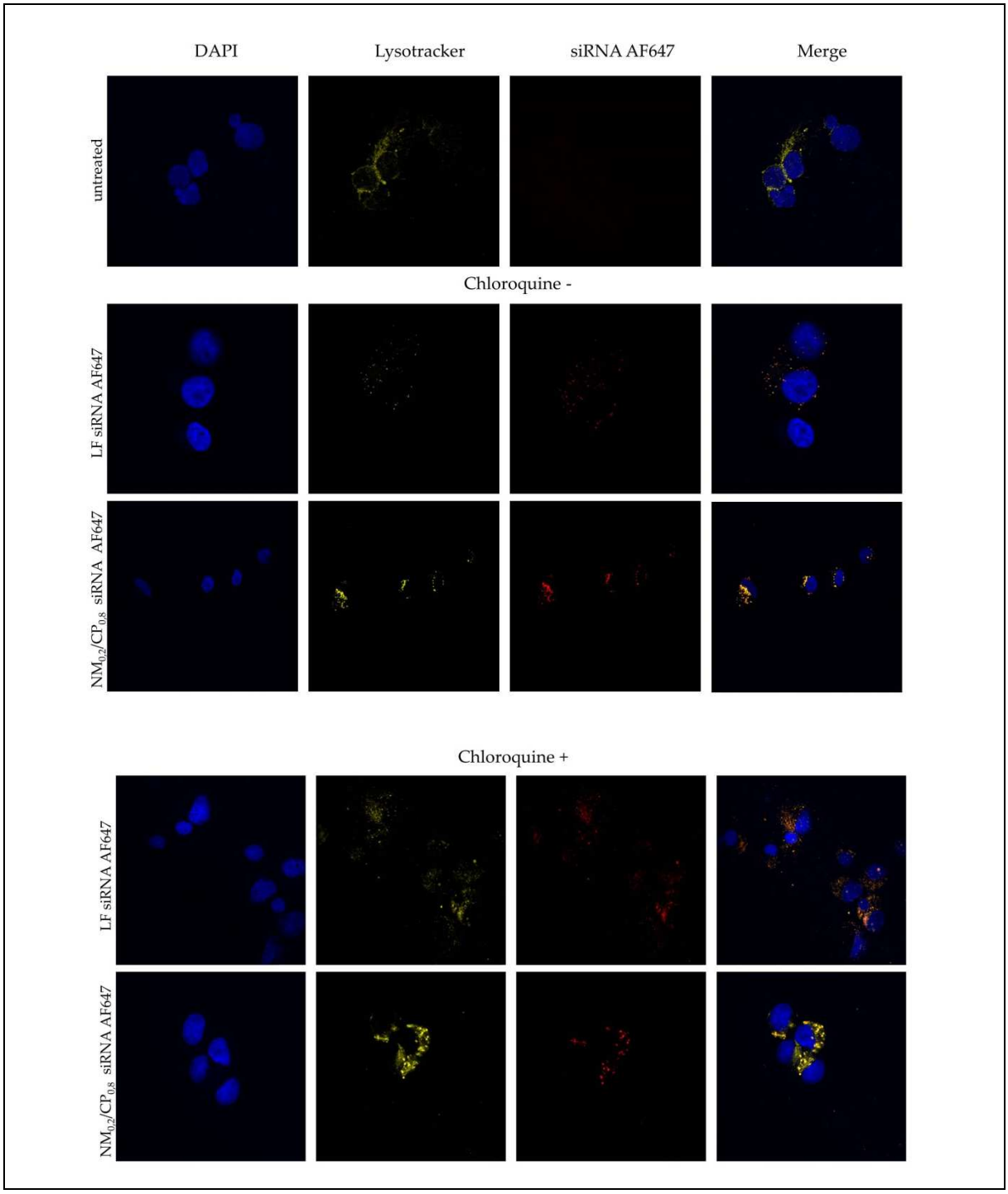

Figure 11. Confocal images after treatment of H1299 cells with Lipofectamin (LF) 2000 lipoplexes and $NM_{0.2}/CP_{0.8}$ polyplexes formulated with AF647 labeled siRNA (shown in red) and staining with Lysotracker red™ dnd 99 (representing lysosomes, shown in yellow) and DAPI (staining cell nuclei, shown in blue). Experiment was performed without (chloroquine -) and with chloroquine (chloroquine +) treatment.

4. Conclusion

Many cationic polymers exhibit great potential for siRNA delivery though demonstrating high cytotoxicity, relatively low transfection efficiencies and poor biocompatibility profiles. Herein, we presented the synthesis and application of Nylon-3 copolymers, consisting of hydrophobic and cationic moieties, for the encapsulation and *in vitro* delivery of siRNA to glioblastoma cells. Hydrophobic subunits within the polymer are derived from β - lactam monomer CP and cationic subunits either from β-lactam monomer DM or NM. $DM_{0.4}/CP_{0.6}$, $NM_{0.4}/CP_{0.6}$ and $NM_{0.2}/CP_{0.8}$ polymers were designed to study the impact of the ratio between the hydrophobic and cationic subunit as well as of the use of different cationic monomers. Efficient siRNA condensation was demonstrated for all tested polymers even at comparably low polymer concentrations. Regarding zeta potentials and uptake ability of polyplexes, optimal N/P ratios of 5 for $DM_{0.4}/CP_{0.6}$ and 4 for NM/CP were investigated. Assembly of polyplexes with optimal polymer amount led to particles with hydrodynamic diameters of < 250 nm and slightly positive surface charges, whereby $NM_{0.2}/CP_{0.8}$ polymer formed the smallest particles at approximately 100 nm with narrow size distributions (PDI < 0.2). TRPS was established as a suitable method for polyplex size distribution analysis and provided results which were in acceptable agreement with DLS data. The method can be further investigated to enable polyplex concentration measurements in the future. In a modified SYBR Gold assay, $NM_{0.4}/CP_{0.6}$ displayed most stable complexes under physiological conditions leading to the assumption that NM subunits interact more strongly with siRNA molecules than DM subunits. Nevertheless, all polyplexes were able to release acceptable amounts of siRNA under acidic conditions, mimicking endosomal compartment conditions. Cellular uptake experiments, conducted by flow cytometry, exhibited higher internalization abilities of $NM_{0.2}/CP_{0.8}$ polyplexes in comparison to $DM_{0.4}/CP_{0.6}$ and $NM_{0.4}/CP_{0.6}$ polyplexes. By using specific uptake inhibitors, it was confirmed that $NM_{0.2}/CP_{0.8}$ polyplexes follow endocytic uptake pathways similar to lipid nanocarriers, more precisely clathrin- and lipid-raft-mediated endocytosis. Therefore, it appears that higher hydrophobic content has a beneficial effect on the internalization ability. Knockdown experiments showed that $NM_{0.2}/CP_{0.8}$ polyplexes were able to slightly reduce protein expression in the cytoplasm, but also that siRNA stayed predominantly entrapped in the endosome. In conclusion, the polymer composition indeed had an effect on various crucial properties of the polyplexes, whereas $NM_{0.2}/CP_{0.8}$ with highest hydrophobic content exhibited most favorable characteristics. This led to excellent transfection efficiencies and successful gene knockdown in glioblastoma cells. Taken together with minimal cytotoxic effects, Nylon-3 polymers were demonstrated to

be a promising type of siRNA delivery agents for future approaches. Due to the simple synthesis and structure versatility of Nylon-3 polymers, which have a similar backbone to biocompatible and biodegradable peptides, adjustments regarding chemical and physical properties are easily available to enhance characteristics for further improvements as siRNA delivery agents. It was proved that hydrophobically modification of cationic polymers in general is a suitable tool to design drug delivery systems with enhanced cellular internalization abilities at low toxicity; however, buffering capacities of our set of polymers were not sufficient to enable escape of the endosomal compartment. This critical point can be addressed in future approaches by precise adjustment of polymer compositions. Ongoing work currently also focuses on including, e.g., stimulus-responsive monomers in the optimized polymer to overcome the major hurdle of endosomal release.

References

[1] A.F. Hottinger, R. Stupp, K. Homicsko, Standards of care and novel approaches in the management of glioblastoma multiforme, Chinese journal of cancer, 33 (2014) 32-39.
[2] J.P. Thakkar, T.A. Dolecek, C. Horbinski, Q.T. Ostrom, D.D. Lightner, J.S. Barnholtz-Sloan, J.L. Villano, Epidemiologic and Molecular Prognostic Review of Glioblastoma, Cancer Epidemiology, Biomarkers & Prevention, 23 (2014) 1985-1996.
[3] M. Jinek, J.A. Doudna, A three-dimensional view of the molecular machinery of RNA interference, Nature, 457 (2009) 405-412.
[4] M.E. Davis, J.E. Zuckerman, C.H.J. Choi, D. Seligson, A. Tolcher, C.A. Alabi, Y. Yen, J.D. Heidel, A. Ribas, Evidence of RNAi in humans from systemically administered siRNA via targeted nanoparticles, Nature, 464 (2010) 1067-1070.
[5] T. Coelho, D. Adams, A. Silva, P. Lozeron, P.N. Hawkins, T. Mant, J. Perez, J. Chiesa, S. Warrington, E. Tranter, Safety and efficacy of RNAi therapy for transthyretin amyloidosis, New England Journal of Medicine, 369 (2013) 819-829.
[6] T. Zimmermann, V. Karsten, J. Harrop, A. Chan, J. Chiesa, G. Peters, R. Falzone, J. Cehelsky, S. Nochur, A. Vaishnaw, J. Gollob, Phase I First-in-Humans Trial of ALN-TTRsc, a Novel RNA Interference Therapeutic for the Treatment of Familial Amyloidotic Cardiomyopathy (FAC), Journal of Cardiac Failure, 19 (2013) S66.
[7] M.G. Kim, S.D. Jo, J.Y. Yhee, B.S. Lee, S.J. Lee, S.G. Park, S.-W. Kang, S.H. Kim, J.H. Jeong, Synergistic anti-tumor effects of bevacizumab and tumor targeted polymerized VEGF siRNA nanoparticles, Biochemical and Biophysical Research Communications, 489 (2017) 35-41.
[8] M. Grzelinski, B. Urban-Klein, T. Martens, K. Lamszus, U. Bakowsky, S. Höbel, F. Czubayko, A. Aigner, RNA Interference-Mediated Gene Silencing of Pleiotrophin Through Polyethylenimine-Complexed Small Interfering RNAs In Vivo Exerts Antitumoral Effects in Glioblastoma Xenografts, Human Gene Therapy, 17 (2006) 751-766.
[9] R. Zukiel, S. Nowak, E. Wyszko, K. Rolle, I. Gawronska, M.Z. Barciszewska, J. Barciszewski, Suppression of human brain tumor with interference RNA specific for tenascin-C, Cancer biology & therapy, 5 (2006) 1002-1007.
[10] J. Bruun, T.B. Larsen, R.I. Jølck, R. Eliasen, R. Holm, T. Gjetting, T.L. Andresen, Investigation of enzyme-sensitive lipid nanoparticles for delivery of siRNA to blood–brain barrier and glioma cells, Int J Nanomedicine, 10 (2015) 5995.
[11] J. Qiu, L. Kong, X. Cao, A. Li, P. Wei, L. Wang, S. Mignani, A.-M. Caminade, J.-P. Majoral, X. Shi, Enhanced Delivery of Therapeutic siRNA into Glioblastoma Cells Using Dendrimer-Entrapped Gold Nanoparticles Conjugated with β-Cyclodextrin, Nanomaterials, 8 (2018) 131.
[12] L. Kong, J. Qiu, W. Sun, J. Yang, M. Shen, L. Wang, X. Shi, Multifunctional PEI-entrapped gold nanoparticles enable efficient delivery of therapeutic siRNA into glioblastoma cells, Biomaterials Science, 5 (2017) 258-266.
[13] Y. Wan, P.M. Moyle, M.P. Christie, I. Toth, Nanosized, peptide-based multicomponent DNA delivery systems: optimization of endosome escape activity, Nanomedicine, 11 (2016) 907-919.
[14] G.R. Rettig, M.A. Behlke, Progress Toward In Vivo Use of siRNAs-II, Molecular Therapy, 20 (2012) 483-512.
[15] S.M. Moghimi, P. Symonds, J.C. Murray, A.C. Hunter, G. Debska, A. Szewczyk, A two-stage poly(ethylenimine)-mediated cytotoxicity: implications for gene transfer/therapy, Molecular Therapy, 11 (2005) 990-995.
[16] G. Navarro, S. Essex, R.R. Sawant, S. Biswas, D. Nagesha, S. Sridhar, C.T. de Ilarduya, V.P. Torchilin, Phospholipid-modified polyethylenimine-based nanopreparations for siRNA–mediated gene silencing: Implications for transfection and the role of lipid components, Nanomedicine: Nanotechnology, Biology and Medicine, 10 (2014) 411-419.

[17] A. Bielinska, J.F. Kukowska-Latallo, J. Johnson, D.A. Tomalia, J.R. Baker, Jr, Regulation of in vitro Gene Expression Using Antisense Oligonucleotides or Antisense Expression Plasmids Transfected Using Starburst PAMAM Dendrimers, Nucleic Acids Res, 24 (1996) 2176-2182.
[18] L. Liu, M. Zheng, D. Librizzi, T. Renette, O.M. Merkel, T. Kissel, Efficient and Tumor Targeted siRNA Delivery by Polyethylenimine-graft-polycaprolactone-block-poly(ethylene glycol)-folate (PEI–PCL–PEG–Fol), Molecular Pharmaceutics, 13 (2016) 134-143.
[19] G. Navarro, J. Pan, V.P. Torchilin, Micelle-like Nanoparticles as Carriers for DNA and siRNA, Molecular Pharmaceutics, 12 (2015) 301-313.
[20] B.P. Mowery, S.E. Lee, D.A. Kissounko, R.F. Epand, R.M. Epand, B. Weisblum, S.S. Stahl, S.H. Gellman, Mimicry of Antimicrobial Host-Defense Peptides by Random Copolymers, Journal of the American Chemical Society, 129 (2007) 15474-15476.
[21] M.T. Dohm, B.P. Mowery, A.M. Czyzewski, S.S. Stahl, S.H. Gellman, A.E. Barron, Biophysical Mimicry of Lung Surfactant Protein B by Random Nylon-3 Copolymers, Journal of the American Chemical Society, 132 (2010) 7957-7967.
[22] E.L. Dane, M.W. Grinstaff, Poly-amido-saccharides: Synthesis via Anionic Polymerization of a β-Lactam Sugar Monomer, Journal of the American Chemical Society, 134 (2012) 16255-16264.
[23] M.-R. Lee, S.S. Stahl, S.H. Gellman, K.S. Masters, Nylon-3 Copolymers that Generate Cell-Adhesive Surfaces Identified by Library Screening, Journal of the American Chemical Society, 131 (2009) 16779-16789.
[24] V. Nadithe, R. Liu, B.A. Killinger, S. Movassaghian, N.H. Kim, A.B. Moszczynska, K.S. Masters, S.H. Gellman, O.M. Merkel, Screening Nylon-3 Polymers, a New Class of Cationic Amphiphiles, for siRNA Delivery, Molecular Pharmaceutics, 12 (2015) 362-374.
[25] R. Liu, K.S. Masters, S.H. Gellman, Polymer Chain Length Effects on Fibroblast Attachment on Nylon-3-Modified Surfaces, Biomacromolecules, 13 (2012) 1100-1105.
[26] R. Liu, X. Chen, Z. Hayouka, S. Chakraborty, S.P. Falk, B. Weisblum, K.S. Masters, S.H. Gellman, Nylon-3 Polymers with Selective Antifungal Activity, Journal of the American Chemical Society, 135 (2013) 5270-5273.
[27] R. Liu, X. Chen, S.P. Falk, B.P. Mowery, A.J. Karlsson, B. Weisblum, S.P. Palecek, K.S. Masters, S.H. Gellman, Structure–Activity Relationships among Antifungal Nylon-3 Polymers: Identification of Materials Active against Drug-Resistant Strains of Candida albicans, Journal of the American Chemical Society, 136 (2014) 4333-4342.
[28] J. Zhang, D.A. Kissounko, S.E. Lee, S.H. Gellman, S.S. Stahl, Access to Poly-β-Peptides with Functionalized Side Chains and End Groups via Controlled Ring-Opening Polymerization of β-Lactams, Journal of the American Chemical Society, 131 (2009) 1589-1597.
[29] M. Elsayed, V. Corrand, V. Kolhatkar, Y. Xie, N.H. Kim, R. Kolhatkar, O.M. Merkel, Influence of oligospermines architecture on their suitability for siRNA delivery, Biomacromolecules, 15 (2014) 1299-1310.
[30] O.M. Merkel, D. Librizzi, A. Pfestroff, T. Schurrat, M. Béhé, T. Kissel, In Vivo SPECT and Real-Time Gamma Camera Imaging of Biodistribution and Pharmacokinetics of siRNA Delivery Using an Optimized Radiolabeling and Purification Procedure, Bioconjugate Chemistry, 20 (2009) 174-182.
[31] M. Benfer, T. Kissel, Cellular uptake mechanism and knockdown activity of siRNA-loaded biodegradable DEAPA-PVA-g-PLGA nanoparticles, European Journal of Pharmaceutics and Biopharmaceutics, 80 (2012) 247-256.
[32] Y. Liu, D.A. Peterson, H. Kimura, D. Schubert, Mechanism of Cellular 3-(4,5-Dimethylthiazol-2-yl)-2,5-Diphenyltetrazolium Bromide (MTT) Reduction, Journal of Neurochemistry, 69 (1997) 581-593.

[33] X. Han, R. Gelein, N. Corson, P. Wade-Mercer, J. Jiang, P. Biswas, J.N. Finkelstein, A. Elder, G. Oberdörster, Validation of an LDH assay for assessing nanoparticle toxicity, Toxicology, 287 (2011) 99-104.
[34] D. Guo, B. Wang, F. Han, T. Lei, RNA interference therapy for glioblastoma, Expert opinion on biological therapy, 10 (2010) 927-936.
[35] H. de Martimprey, C. Vauthier, C. Malvy, P. Couvreur, Polymer nanocarriers for the delivery of small fragments of nucleic acids: Oligonucleotides and siRNA, European Journal of Pharmaceutics and Biopharmaceutics, 71 (2009) 490-504.
[36] S.K. Jones, V. Lizzio, O.M. Merkel, Folate receptor targeted delivery of siRNA and paclitaxel to ovarian cancer cells via folate conjugated triblock copolymer to overcome TLR4 driven chemotherapy resistance, Biomacromolecules, 17 (2016) 76-87.
[37] A. Aigner, D. Kögel, Nanoparticle/siRNA-based therapy strategies in glioma: which nanoparticles, which siRNAs?, Nanomedicine, 13 (2018) 89-103.
[38] M. Zheng, G.M. Pavan, M. Neeb, A.K. Schaper, A. Danani, G. Klebe, O.M. Merkel, T. Kissel, Targeting the blind spot of polycationic nanocarrier-based siRNA delivery, ACS nano, 6 (2012) 9447-9454.
[39] E. Weatherall, G.R. Willmott, Applications of tunable resistive pulse sensing, Analyst, 140 (2015) 3318-3334.
[40] A.V. Kabanov, V.A. Kabanov, Interpolyelectrolyte and block ionomer complexes for gene delivery: physico-chemical aspects, Advanced Drug Delivery Reviews, 30 (1998) 49-60.
[41] J. Rejman, A. Bragonzi, M. Conese, Role of clathrin-and caveolae-mediated endocytosis in gene transfer mediated by lipo-and polyplexes, Molecular therapy, 12 (2005) 468-474.
[42] M. Ruponen, S. Ylä-Herttuala, A. Urtti, Interactions of polymeric and liposomal gene delivery systems with extracellular glycosaminoglycans: physicochemical and transfection studies, Biochimica et Biophysica Acta (BBA) - Biomembranes, 1415 (1999) 331-341.
[43] A. Alshamsan, A. Haddadi, V. Incani, J. Samuel, A. Lavasanifar, H. Uludag, Formulation and delivery of siRNA by oleic acid and stearic acid modified polyethylenimine, Molecular pharmaceutics, 6 (2009) 121-133.
[44] S. Biswas, P.P. Deshpande, G. Navarro, N.S. Dodwadkar, V.P. Torchilin, Lipid modified triblock PAMAM-based nanocarriers for siRNA drug co-delivery, Biomaterials, 34 (2013) 1289-1301.
[45] K.Y. Win, S.-S. Feng, Effects of particle size and surface coating on cellular uptake of polymeric nanoparticles for oral delivery of anticancer drugs, Biomaterials, 26 (2005) 2713-2722.
[46] A.I. Ivanov, Pharmacological inhibition of endocytic pathways: is it specific enough to be useful?, Exocytosis and endocytosis, (2008) 15-33.
[47] L.-H. Wang, K.G. Rothberg, R. Anderson, Mis-assembly of clathrin lattices on endosomes reveals a regulatory switch for coated pit formation, The Journal of cell biology, 123 (1993) 1107-1117.
[48] S.K. Rodal, G. Skretting, Ø. Garred, F. Vilhardt, B. Van Deurs, K. Sandvig, Extraction of cholesterol with methyl-β-cyclodextrin perturbs formation of clathrin-coated endocytic vesicles, Molecular biology of the cell, 10 (1999) 961-974.
[49] J.J. Lu, R. Langer, J. Chen, A novel mechanism is involved in cationic lipid-mediated functional siRNA delivery, Molecular pharmaceutics, 6 (2009) 763-771.
[50] O.M. Merkel, D. Librizzi, A. Pfestroff, T. Schurrat, K. Buyens, N.N. Sanders, S.C. De Smedt, M. Béhé, T. Kissel, Stability of siRNA polyplexes from poly(ethylenimine) and poly(ethylenimine)-g-poly(ethylene glycol) under in vivo conditions: Effects on pharmacokinetics and biodistribution measured by Fluorescence Fluctuation Spectroscopy and Single Photon Emission Computed Tomography (SPECT) imaging, Journal of Controlled Release, 138 (2009) 148-159.

[51] T.F. Martens, K. Remaut, J. Demeester, S.C. De Smedt, K. Braeckmans, Intracellular delivery of nanomaterials: how to catch endosomal escape in the act, Nano Today, 9 (2014) 344-364.
[52] J. Nguyen, F.C. Szoka, Nucleic acid delivery: the missing pieces of the puzzle?, Accounts of chemical research, 45 (2012) 1153-1162.
[53] O.M. Merkel, M.A. Mintzer, D. Librizzi, O. Samsonova, T. Dicke, B. Sproat, H. Garn, P.J. Barth, E.E. Simanek, T. Kissel, Triazine Dendrimers as Nonviral Vectors for in Vitro and in Vivo RNAi: The Effects of Peripheral Groups and Core Structure on Biological Activity, Molecular Pharmaceutics, 7 (2010) 969-983.
[54] Y. Xu, F.C. Szoka, Mechanism of DNA release from cationic liposome/DNA complexes used in cell transfection, Biochemistry, 35 (1996) 5616-5623.
[55] A. Elouahabi, J.-M. Ruysschaert, Formation and intracellular trafficking of lipoplexes and polyplexes, Molecular therapy, 11 (2005) 336-347.
[56] H.K. Shete, R.H. Prabhu, V.B. Patravale, Endosomal escape: a bottleneck in intracellular delivery, Journal of nanoscience and nanotechnology, 14 (2014) 460-474.
[57] B. Urban-Klein, S. Werth, S. Abuharbeid, F. Czubayko, A. Aigner, RNAi-mediated gene-targeting through systemic application of polyethylenimine (PEI)-complexed siRNA in vivo, Gene therapy, 12 (2005) 461-466.
[58] O.M. Merkel, T. Kissel, Quo vadis polyplex?, Journal of Controlled Release, 190 (2014) 415-423.

Supplementary Material

1. Polymer synthesis and characterization

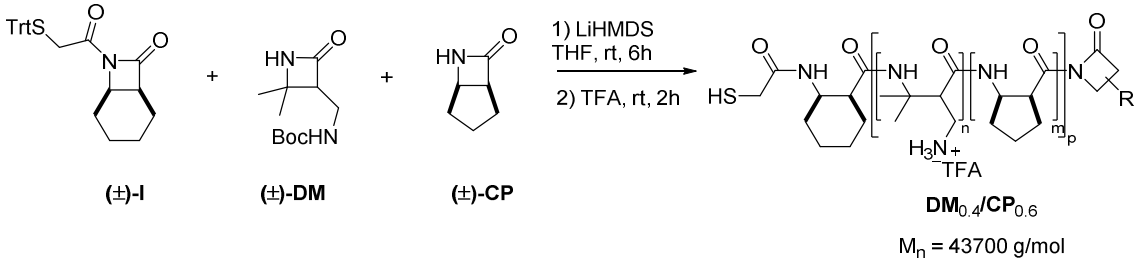

Figure S1. Synthesis of TFA-salt of Nylon-3 polymer $DM_{0.4}/CP_{0.6}$ in presence of a co-initiator **I** and a base LiHMDS. DM = dimethyl, CP = cyclopentyl, R = side chain groups of DM or CP. Adapted from [1].

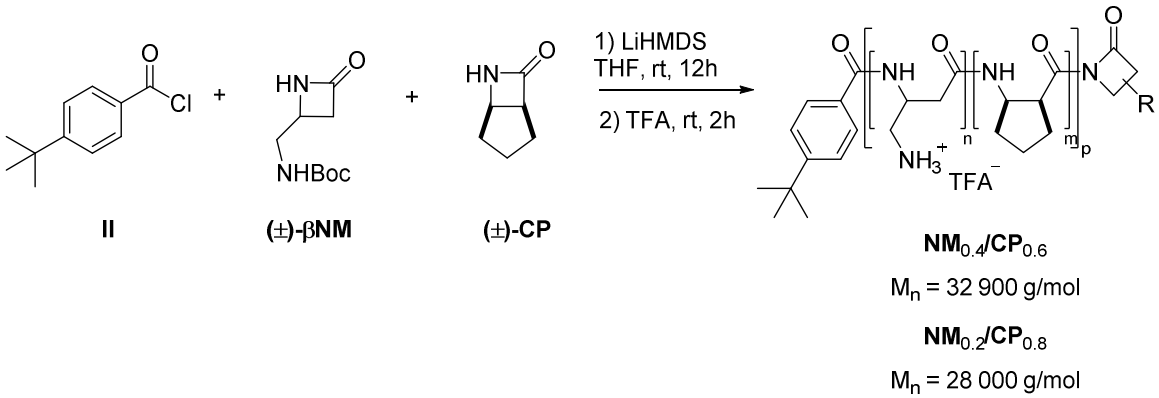

Figure S2. Synthesis of TFA-salts of gene delivery Nylon-3 polymers (NM/CP) in presence of a co-initiator **II** and a base LiHMDS. R = side chain groups of NM or CP. Adapted from [2].

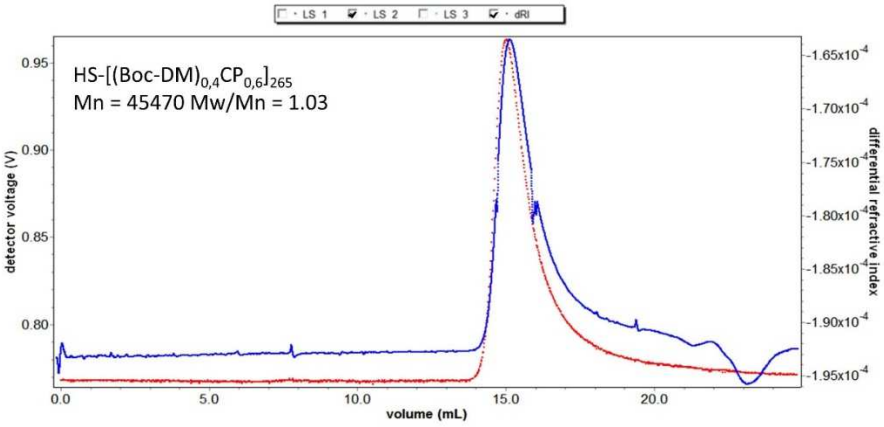

Figure S3. GPC chromatograph of Boc-protected HS-$[(Boc\text{-}DM)_{0.4}CP_{0.6}]_{265}$ copolymer measured with light-scattering (red) and refractive index (blue) detectors, mobile phase: THF.

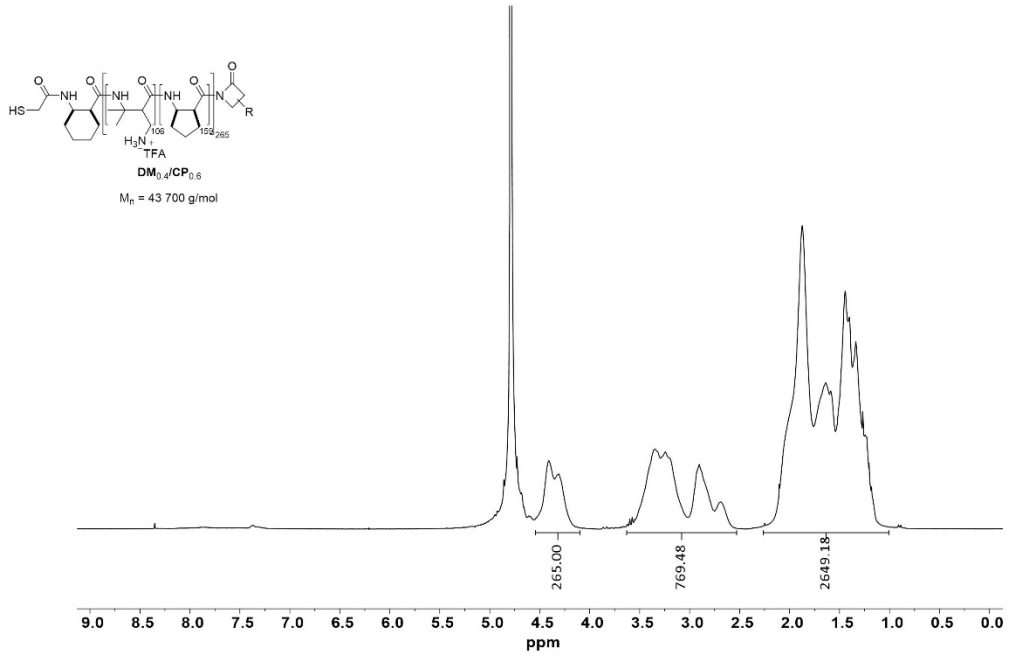

Figure S4. ^{1}H-NMR spectrum of unprotected $DM_{0.4}/CP_{0.6}$ polymer measured in D_2O (300 MHz, 512 scans).

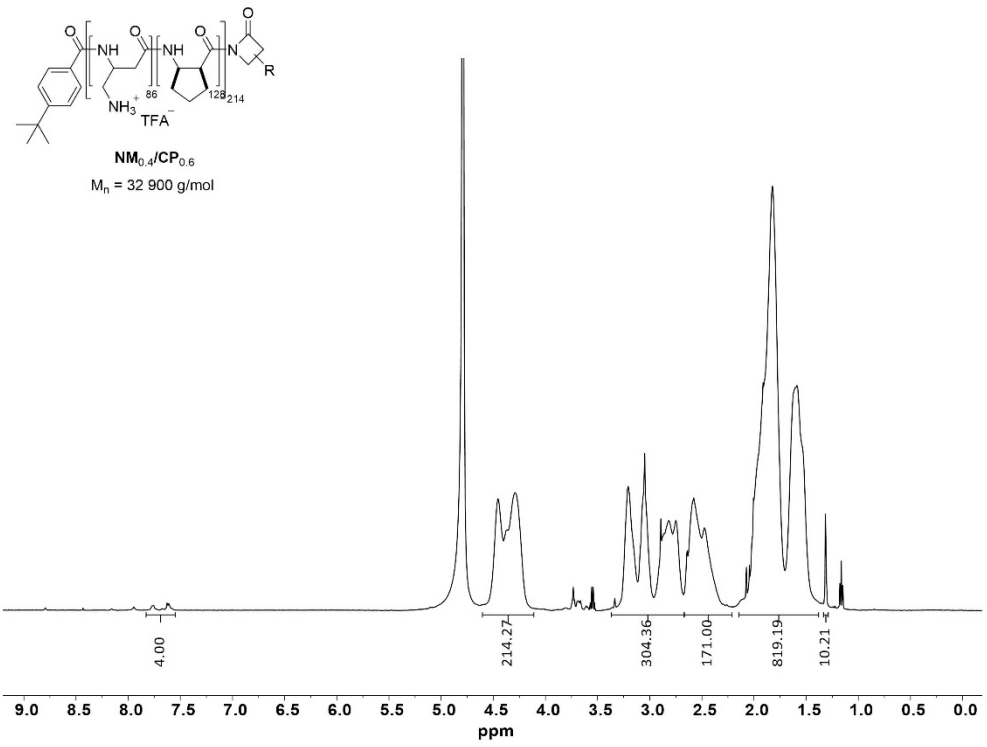

Figure S5.^{1}H-NMR spectrum in D_2O of unprotected $NM_{0.4}/CP_{0.6}$ polymer measured in D_2O (500 MHz, 126 scans).

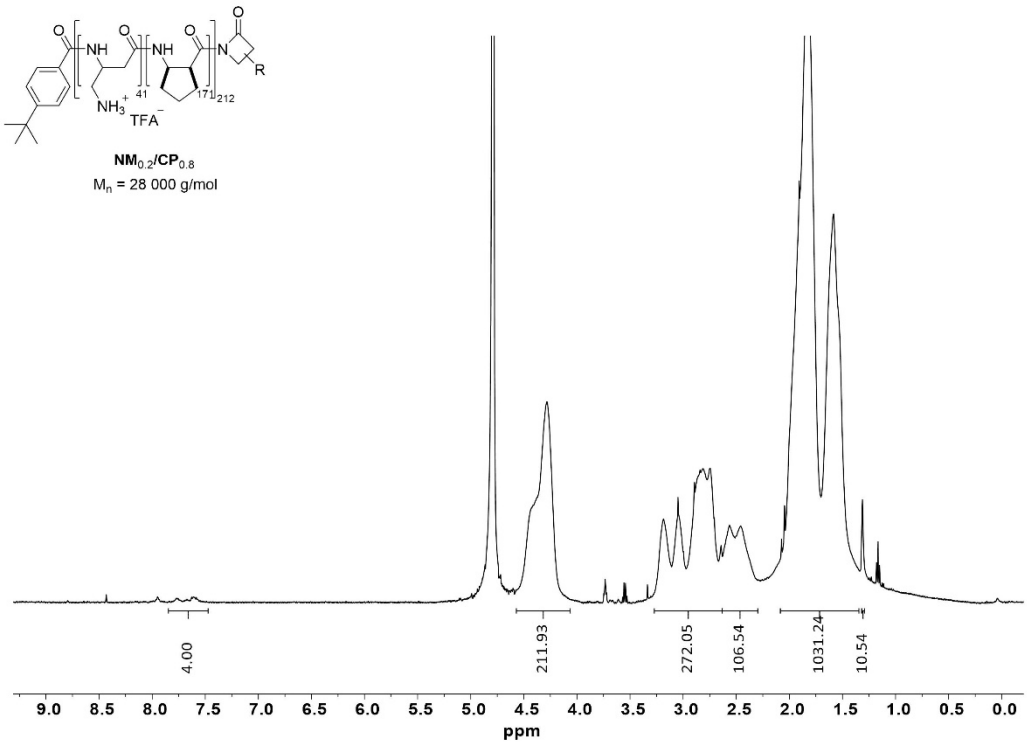

Figure S6. ^{1}H-NMR spectrum of unprotected $NM_{0.2}/CP_{0.8}$ polymer measured in D_2O (500 MHz, 126 scans).

2. Polyplex characterization

2.1 N/P ratio optimization

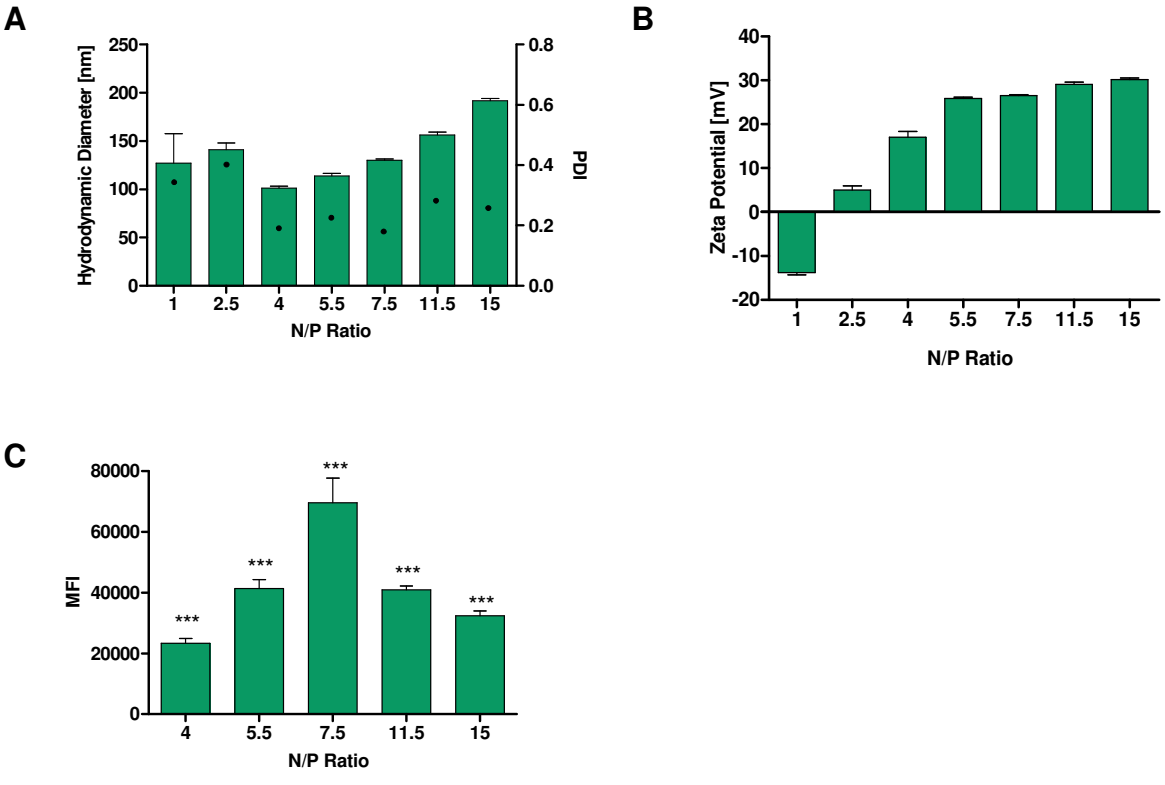

Figure S7. (**A**) Hydrodynamic diameters investigated by DLS (left y-axis) and polydispersity indices (PDI, right y-axis), (**B**) zeta potentials measured by LDA and (**C**) MFIs of $NM_{0.2}/CP_{0.8}$ cells treated with respective polyplexes determined by flow cytometry. (Data points indicate mean ± SD, n = 3).

2.2 Size measurements by TRPS

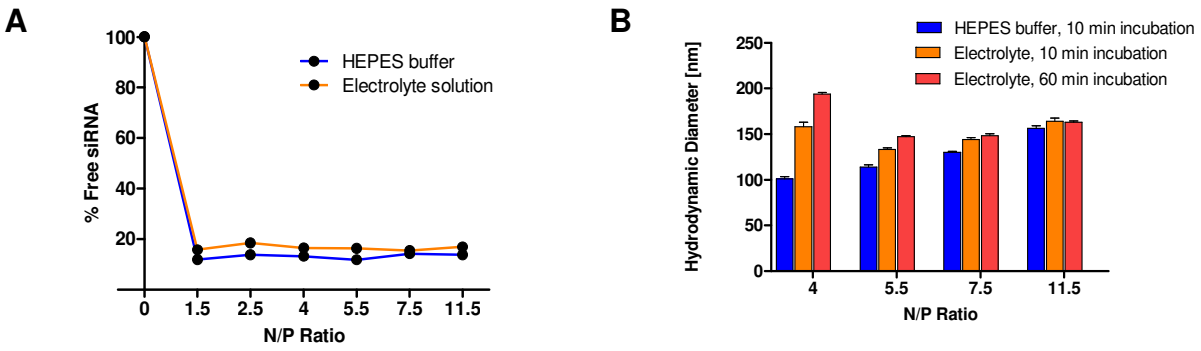

Figure S8. (**A**) siRNA encapsulation profiles of $NM_{0.2}/CP_{0.8}$ polyplexes prepared in 10 mM HEPES buffer at N/P 4 and 1X diluted with either 10 mM HEPES buffer or TRPS electrolyte solution (30 mM HEPES, 100 mM potassium chloride, 2 mM EDTA and 0.03% Tween®20). 100% values (N/P = 0) are determined by fluorescence of uncondensed siRNA. (Data points indicate mean, n = 3). (**B**) DLS measurements of $NM_{0.2}/CP_{0.8}$ polyplexes prepared in 10 mM HEPES buffer at N/P 4 and 1X diluted with either 10 mM HEPES buffer or TRPS electrolyte solution, measured after 10 and 60 min incubation period (Data points indicate mean ± SD, n = 3).

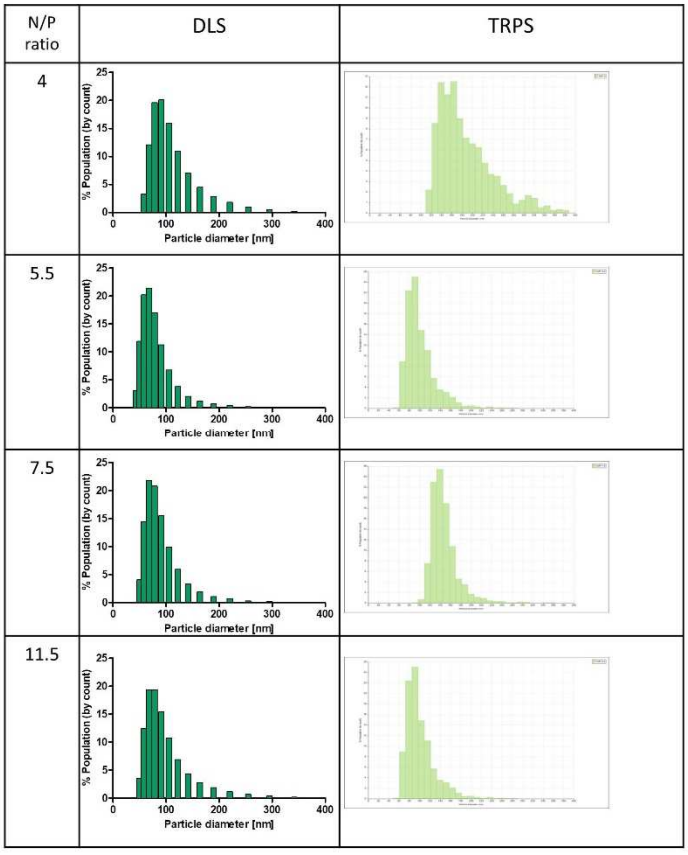

Figure S9. Number-weighted size distributions of $NM_{0.2}/CP_{0.8}$ polyplexes at N/P ratios 5, 5.5, 7.5 and 11.5. 1:1 diluted with electrolyte solution and measured by DLS and TRPS, respectively.

3. Quantification of cellular Uptake

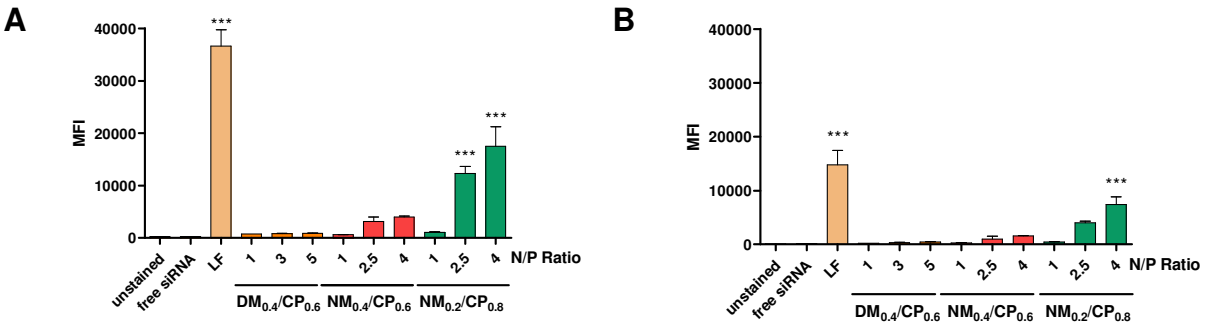

Figure S10. Cellular uptake of polyplexes performed at various N/P ratios in (**A**) H1299 cells and (**B**) U87 cells after 5 h incubation as determined by flow cytometry presented as median fluorescence intensity. Negative control: untreated cells and cells treated with free siRNA, positive control: cells transfected with Lipofectamin (LF) lipoplexes. (Data points indicate mean ± SD, n = 3, two-way ANOVA with Bonferroni post-hoc test, ***p < 0.005).

4. Route of cellular Uptake

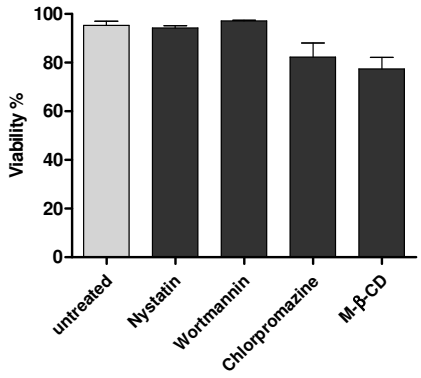

Figure S11. U87 cell viabilities after treatment with nystatin (10 µg/ml), wortmannin (12ng/ml), chlorpromazine (10 µg/ml) and methyl-beta-cyclodextrin (3 mg/ml); determined by trypan blue staining. Number of living and dead cells was counted in a Neubauer chamber using an Axio Vert.A1 microscope. The percentage of viable cells was calculated. (Results are given as mean ± SD, n = 3).

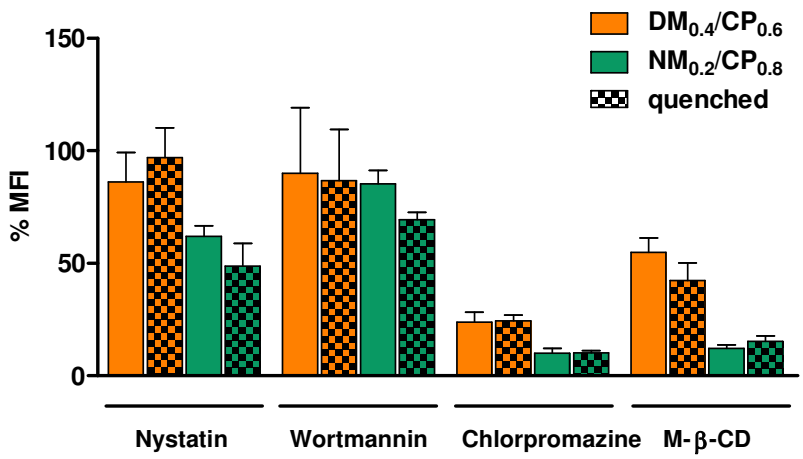

Figure S12. Cellular uptake of polyplexes ($DM_{0.4}/CP_{0.6}$ polyplexes: N/P ratio= 5 and $NM_{0.2}/CP_{0.8}$ polyplexes: N/P ratio = 4) after treatment with nystatin (10 µg/ml), wortmannin (12 ng/ml), chlorpromazine (10 µg/ml) and methyl-β-cyclodextrin (M-ß-CD) (3 mg/ml) conducted with and without trypan quenching as evaluated by flow cytometry and presented as MFI. (Results are shown as mean ± SD as percentage of median fluorescence intensity related to not inhibited samples, n = 3).

References

[1] R. Liu, K.S. Masters, S.H. Gellman, Polymer Chain Length Effects on Fibroblast Attachment on Nylon-3-Modified Surfaces, Biomacromolecules, 13 (2012) 1100-1105.
[2] R. Liu, X. Chen, S.P. Falk, B.P. Mowery, A.J. Karlsson, B. Weisblum, S.P. Palecek, K.S. Masters, S.H. Gellman, Structure–Activity Relationships among Antifungal Nylon-3 Polymers: Identification of Materials Active against Drug-Resistant Strains of Candida albicans, Journal of the American Chemical Society, 136 (2014) 4333-4342.

Chapter II

Hydrophobically Modified Polymers for siRNA Delivery to Glioblastoma Cells

II.2 Evaluation of Spermine-based Poly(acrylamides) with Varying Hydrophobicity as siRNA Delivery System for Glioblastoma Cells Transfection

Abstract

To this day Glioblastoma multiforme is one of the deadliest cancer types known due to poor prognosis and the lack of therapies. Small interfering RNA (siRNA) has shown high potential in offering a new therapeutic approach in cancer treatment by the downregulation of disease-related genes via RNA interference (RNAi). However, in the human body siRNA is quickly degraded, and passive uptake in target cells is limited. For this reason, research in carrier systems for siRNA has caught a lot of attention. Especially cationic polymers provide suitable characteristics for siRNA delivery and have been used often in preclinical studies. They can protect siRNA from any degrading influences by forming polyplexes due to the electrostatic interactions between negative and positive charges of siRNA and polymer, respectively. A disadvantage of this approach is that the high cationic charge densities which are needed for successful cell transfection are known to induce cytotoxicity. To address this problem, endogenous cationic molecules, such as spermine, were investigated as promising biocompatible cationic siRNA carrier systems. To overcome the hurdle of limited cell transfection success by low molecular weight molecules we synthesized various spermine-based poly(acrylamides) with different molecular weights and varying hydrophobicity to evaluate their physicochemical characteristics, cell tolerability and their cellular internalization and gene knockdown ability in glioblastoma cells depending on their microstructures. Poly(spermine acrylamides) displayed minimal cytotoxic effects in comparison to transfection standards such as polyethylenimine and Lipofectamine 2000, as well as appropriate particle sizes and efficient siRNA encapsulation and release abilities. Polyplexes prepared with hydrophobic modified polymers showed enhanced uptake and gene-silencing efficiency among the poly(spermine acrylamides) tested and therefore especially provide a promising group of delivery agents for highly efficient intracellular siRNA delivery for the potential treatment of glioblastoma.

1. Introduction

Glioblastoma multiforme (GBM) is the most common devastating type of primary malignant tumor of the central nervous system. [1]. Current standard treatment includes surgical resection and radiation combined with temozolomide chemotherapy as aftercare. As additional approach the monoclonal antibody bevacizumab was approved by the FDA and Swissmedic, which inhibits the vascular endothelial growth factor (VEGF), an important factor for tumor growth and supply [2]. Approved therapies show only limited efficiency so that the average survival rate is only 15 months [3]. The development of gene therapy approaches for treatment of glioma related genes might therefore be of great potential. RNA interference (RNAi), a post-transcriptional gene-silencing mechanism, for example, has been rapidly progressed from basic research to clinical trials. Small interfering RNA (siRNA) is an intermediate in the RNAi process and comprises double stranded RNA of 21 – 25 nucleotides in length. siRNA can be used to achieve RNAi and to downregulate overexpressed genes [4, 5]. The primary challenge of siRNA therapeutics, however, is the hurdle of intracellular delivery. In most cases of siRNA delivery, limitations in the application of naked siRNA caused by rapid degradation, immune response, and low passive cell uptake [6] are bypassed by using suitable delivery systems to encapsulate the nucleic acids by electrostatic interactions in order to shield them from the environment and to assist cellular internalization. Several non-viral delivery strategies for siRNA molecules such as liposomes and especially cationic polymeric systems have been extensively investigated [7]. However, the main hurdle of high cellular toxicity due to high positive charge density and the poor transfection efficiencies of cationic nucleic acid carriers, as especially investigated for polyethylenimine (PEI) based materials, still remains [8]. Therefore, intensive research is being carried out to find suitable cationic polymeric materials for nucleic acid transport with appropriate transfection efficiencies on the one hand but also biodegradability and thus fewer toxic effects on the other. As endogenous spermines are safe, naturally occurring, small, linear tetraamines with two primary and two secondary amines, they are promising candidates for nucleic acid carrier agents. In the body, spermine aids in packaging cellular DNA into compact state, which is essential in cell growth processes in eukaryotic cells [9, 10]. Due to its low molecular weight, naturally occurring spermine is not able to encapsulate siRNA and to transfect cells efficiently. Therefore, it is necessary to modify the spermine units to increase their molecular weight. One way of creating higher molecular weight spermine-containing substances is conjugation of monoprotected bis-boc spermine with various reactive linkers to obtain respective oligospermines as already described in literature [11]. As it was

shown for phospholipid-modified PEI [12] that hydrophobic modifications of cationic polymers can lead to improved performances as siRNA carrier coupled with considerably decreased cytotoxicity [13], we manufactured a set of poly(spermine acrylamides) (P(SpAA)) of homopolymers with different molecular weights and copolymers with varying amounts of hydrophobic modifications of decylacrylamide subunits to examine the influence on the performance as an siRNA delivery agent for glioblastoma cells depending on the polymer´s microstructure. Herein, we synthesized poly(spermine acrylamide) homo- and copolymers via free-radical polymerization (FRP) using azobisisobutyronitrile (AIBN) as a radical starter. These cationic polymers were used to condense siRNA molecules and resulting siRNA-polymer complexes (polyplexes) were characterized regarding their physicochemical characteristics such as siRNA encapsulation and release ability, particle size and surface charge. Furthermore, cell tolerability was examined by MTT assays, cellular internalization ability by flow cytometry and gene knockdown efficiency was assessed by qRT-PCR. Based on these findings, especially poly(spermine acrylamides) with hydrophobic moieties provides optimal properties regarding particle characteristics, excellent transfection efficiencies and successful gene knockdown in glioblastoma cells with minimal toxic effects.

2. Materials and Methods

2.1 Materials

HEPES (4-(2-hydroxyethyl)-1-piperazineethansulfonic acid), sodium acetate, sodium hydrogen carbonate, thiazolyl blue tetrazolium bromide (MTT), Ethylenediaminetetraacetic acid (EDTA), heparin sodium salt, for cell culture U87 cells (human glioblastoma astrocytoma), Eagle´s Minimum Essential Medium (EMEM), Dulbecco´s Phosphate Buffered Saline (PBS), trypsin-EDTA solution 0.25%, fetal bovine serum (FBS), dimethyl sulfoxide (DMSO), dried DMSO, branched polyethyleneimine (PEI) 10 kDa, and Penicillin-Streptomycin solution were purchased from Sigma-Aldrich (Taufkirchen, Germany). SYBR Gold dye, Lipofectamine 2000 transfection reagent, AlexaFluor488 (AF488) were purchased from Life Technologies (Carlsbad, Ca, USA). HyClone trypan blue solution 0.4% in phosphate-buffered saline was purchased from FisherScientific (Hampton, NH, USA). PureLink™ RNA Mini Kit, high capacity cDNA synthesis kit and powerSYBR green PCR master mix were purchased from Thermofisher Scientific (Waltham, MA, USA), QuantiTect® primer assays Hs_GAPDH_1_SG and Hs_ACTB_2_SG were purchased from Qiagen (Venlo, Netherlands). Amine-modified eGFP siRNA (5´-pACCCUGAAGUUCAUCUGCACCACcg, 3´-

ACUGGGACUUCAAGUAGACGGGUGGC), human glyceraldehyde-3-phosphate-dehydrogenase (GAPDH) siRNA (5´-pGGUCGGAGUCAACGGAUUUGGUCgt, 3´-UUCCAGCCUCAGUUGCCUAAA-CCAGCA) and scrambled siRNA (5´-pCGUUAAUCGCGUAUAAUACGCGUat, 3´-CAGCAAUUAGCGCAUAUUAUGCGCAUAp) were purchased from Integrated DNA Technologies (Leuven, Belgium). Modified nucleotides are indicated as follows: ''p'' denotes a phosphate residue, lower case letters are 2´-deoxyribonucleotides, capital letters are ribonucleotides, and underlined capital letters are 2´-O-methyribonucleotides.

2.2 Synthesis and characterization of Homo- and Copolymers

The synthesis of poly(spermine acrylamide) homo- and copolymers was performed as illustrated in Scheme 1 according to procedures previously described in literature [14]. In brief, the monomers N-acryloxysuccinimide (NAS) and N-decylacrylamide (DAA) were synthesized starting from acryloyl chloride, triethylamine and N-hydroxysuccinimide or N-decylamine, respectively, using modified literature procedures [15, 16]. To use spermine as a functional molecule, tri-boc spermine (TBSp), protected with three boc-protection groups and with only one reactive primary amine was synthesized using orthogonal protection group chemistry in an adapted literature procedure [17]. FRP was performed with AIBN and N-acryloxysuccinimide (NAS) in toluene with varying ratios of AIBN to obtain different poly(N-acryloxysuccinimide) (P(NAS)) homopolymers. Structure and purity of the (P(NAS) 1 – 3) polymers were analyzed via NMR spectroscopy in DMSO according to protocols described elsewhere [14] (Figure S1, Supplementary Material). The number-averaged molecular weight (Mn) and polydispersity (Đ) of the (P(NAS) 1 – 3) polymers were determined via size-exclusion chromatography (SEC) in dimethylformamide (DMF) (Figure S12-S13, Supplementary Material) relative to polystyrene standards as depicted in Table S1. Additionally, copolymers (P(NAS-co-DAA)1-2) with varying ratios of NAS and DAA were synthesized via FRP by simply modulating the monomer feed and subsequently analyzed by SEC (Figure S14-S15, Table S1, Supplementary Material) and NMR (Figure S2-S3, Supplementary Material). Post-polymerization functionalization of P(NAS) and P(NAS-co-DAA) polymers was performed by reacting TBSp with the respective polymer at 40°C in DMF. Reaction products poly(tri-boc spermine acrylamide) (P(TBSpAA) 1-3) and poly(tri-boc spermine acrylamide-co-N-decylacrylamide) (P(TBSpAA-co-DAA) 1-2) were again evaluated using SEC (Figure S16-S19, Table S1, Supplementary Material) and NMR analysis methods (Figure S4-S6, Supplementary Material). To remove Boc-protection groups, tri-fluoroacetic acid (TFA) was added generating poly(spermine acrylamide) (P(SpAA)

1-3) and poly(spermine acrylamide-co-N-decylacrylamide) (P(SpAA-co-DAA) 1-2) TFA salts. Deprotected polymers were analyzed by ^{1}H-NMR in D_2O as shown in Figure S7-S11 (Supplementary Material). A final cationic to hydrophobic ratio (SpAA:DAA) of 90:10 and 75:25 was obtained as determined via ^{1}H-NMR spectra for P(SpAA-co-DAA) 1 and 2, respectively.

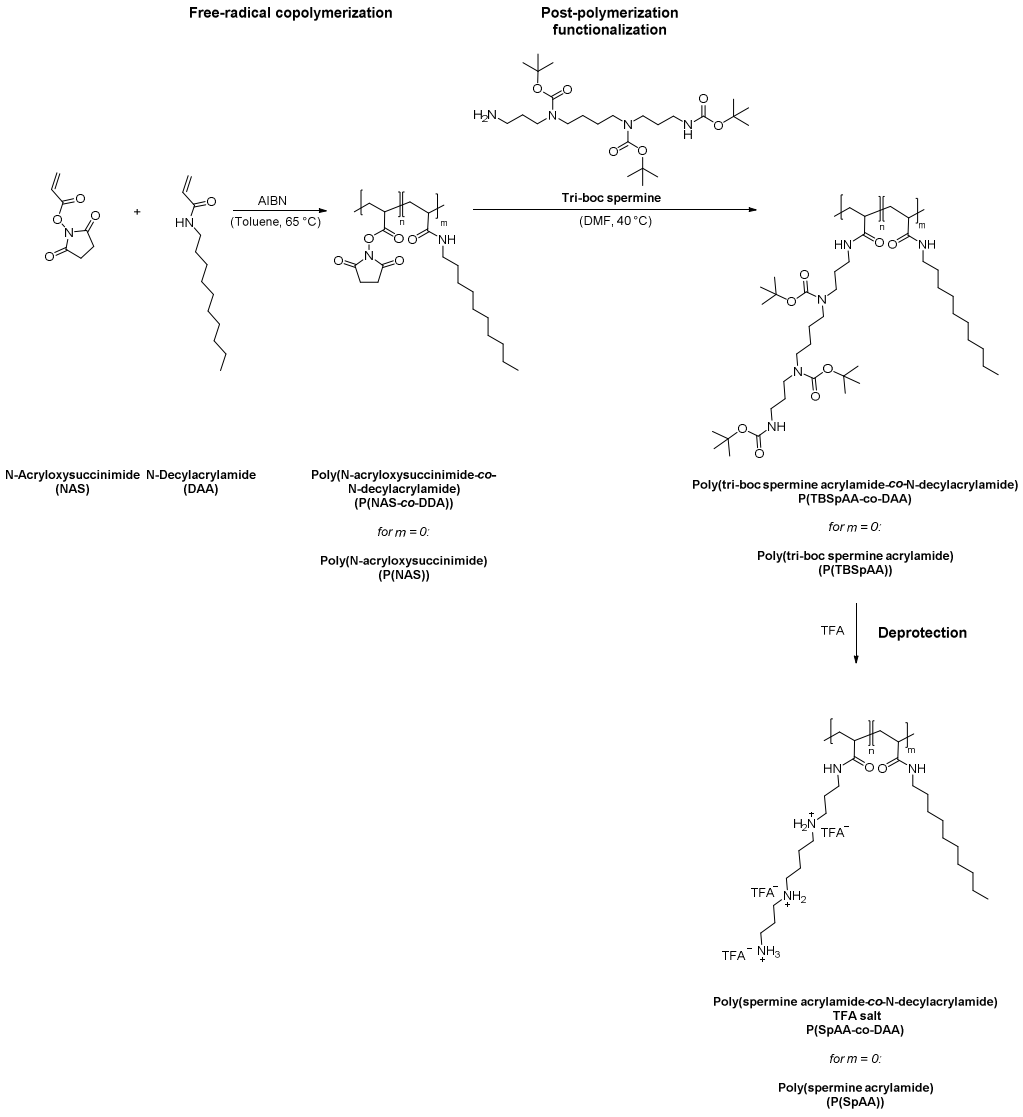

Scheme 1. Synthesis of poly(spermine acrylamide) (P(SpAA)) and poly(spermine acrylamide-co-N-decylacrylamide) (P(SpAA-co-DAA) via radical (co)polymerization of N-Acryloxysuccinimide (NAS) and N-Decylacrylamide (DAA), followed by post-polymerization with tri-boc spermine and deprotection using trifluoroacetic acid (TFA).

An overview of the P(SpAA) (1a-c) and P(SpAA-co-DAA) (2a, 2b) polymers finally utilized in this study is depicted in Table 1.

Table 1. Overview of P(SpAA) and P(SpAA-co-DAA) polymers used in this study.

		Number of repeating units			SpAA/DAA [mol%][a]
		n	m	i = n+m	
Homopolymers P(SpAA)					
1a	$P(SpAA)_{268}$	268	0		100/0
1b	$P(SpAA)_{327}$	327	0		100/0
1c	$P(SpAA)_{485}$	485	0		100/0
Copolymers P(SpAA-co-DAA)					
2a	$P(SpAA_{0.9}/DAA_{0.1})_{461}$	415	46	461	90/10
2b	$P(SpAA_{0.75}/DAA_{0.25})_{526}$	395	131	526	75/25

n = number of cationic subunits SpAA, m = number of hydrophobic subunits DAA, i = (n + m) number of total repeating units, [a]Ratio between SpAA/DAA calculated via ^{1}H-NMR spectroscopy (see supporting material).

2.3 Preparation of polyplexes

Aqueous polymer stock solutions were prepared by diluting predetermined amounts of lyophilized polymer in deionized water. The polymer stock solutions were then diluted with freshly filtered 10 mM HEPES buffer (pH 7.2) to precalculated concentrations and combined with defined amounts of siRNA in a microcentrifuge tube to obtain polyplexes at various N/P ratios and incubated for 30 min to enable stable polyplex formation. The N/P ratio is defined as the molar ratio between the polymer amine groups (N) and the siRNA phosphate groups (P). The amount of polymer needed to obtain different N/P ratios was calculated according to the following equation:

$$\text{m (polymer in pg)} = \text{n siRNA (pmol)} \times \text{M protonable unit (g/mol)} \times \text{N/P} \times \text{number of nucleotides siRNA}$$

The protonable unit of the homopolymers was calculated by dividing the mass of the repeating unit by the number of protonable primary and secondary amines present in the polymer (Scheme 2, A). The protonable unit of the different copolymers was calculated by using the ratio of the two repeating units and the number of protonable primary and secondary amines present in the polymer (Scheme 2, B). Branched PEI (10kDa) has a protonable unit of 43.1 g/mol. The number of nucleotides of 25/27mer siRNA is set to 52.

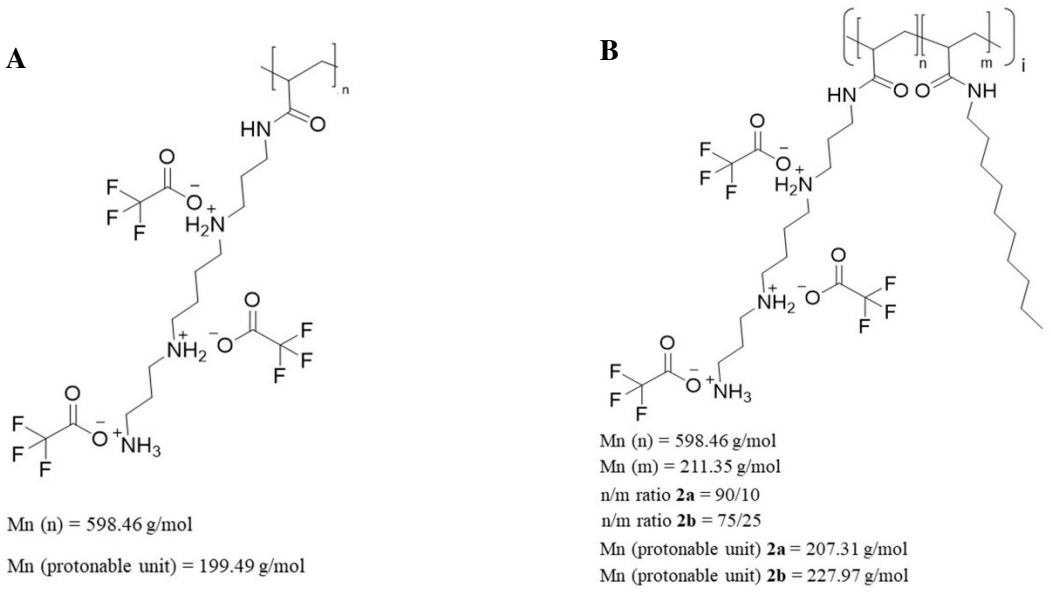

Scheme 2. TFA salts of poly(spermine acrylamide) (P(SpAA)) homo- (**A**) and poly(spermine acrylamide-co-decylacrylamide) (P(SpAA-co-DAA)) copolymers (**B**), M_n: number-averaged molecular weight of polymer subunits n or m, M_n (protonable unit): molecular weight of protonable units.

2.4 siRNA encapsulation by SYBR Gold Assay

The SYBR Gold assay is a commonly used method to detect free nucleic acids. In our experiments it was used to determine the amount of free siRNA after the encapsulation via polyplex formation at various N/P ratios. Therefore, different N/P ratio polyplexes were prepared following the formula from above. Polyplexes were formed in HEPES buffer with 50 pmol of scrambled siRNA, and 100 µL of each polyplex solution was distributed in a white FluoroNunc 96-well plate (FisherScientific, Hampton, NH, USA). A 4X SYBR Gold solution (30 µL) was added to each well, and the plate was incubated for 10 min in the dark before measuring the fluorescence signal by using a fluorescence plate reader (FLUOstar Omega, BMG Labtech, Ortenberg, Germany) at 492 and 555 nm excitation and emission wavelengths, respectively. An analogous procedure with free siRNA was used as 100 % value. Measurements were performed in triplicates, and results are shown as mean values (n = 3).

2.5 siRNA Release by Heparin Competition Assay

To evaluate the polyplex stability in the presence of competing polyanions under neutral and acidic conditions, a heparin competition assay was performed. Polyplexes were prepared in the presence of two different buffers, a 10 mM HEPES buffer (pH 7.4) and a 10 mM sodium acetate buffer (pH 4.5) to enable comparison of polyplexes stability at different pH as well as at various

ionic strengths. Polyplex sample aliquots of 60 µl (N/P 3) were dispersed into a white FluoroNunc 96 well plate and 10 µl of beforehand prepared heparin concentrations (0.12, 0.16, 0.21, 0.27, 0.35, 0.46, 0.59, 0.77, 1 USP units/well) were added to the wells. After incubation for 30 min at room temperature, 30 µl of a 4X SYBR Gold solution was added to each well and the plate was incubated for 10 min under light exclusion. Fluorescence measurements and calculation of percentage of free siRNA were performed as described under 2.4. To obtain more precise results, each heparin concentration was added to the respective buffer and used as blank for related samples. Measurements were performed in triplicates and results are shown as mean values (n = 3).

2.6 Size and (ζ)-Potential Analysis by Dynamic Light Scattering and Laser Doppler Anemometry

To investigate the particle size and the polydispersity index (PDI) as well as the zeta potential of the different polyplexes a Zetasizer Nano ZS (Malvern Instruments, Malvern, UK) was used. Polyplexes were formed in HEPES buffer at various N/P ratios. To determine the average particle size and PDI, 100 µL polyplex solution was pipetted into disposable cuvettes (Malvern Instruments, Malvern, UK) and used for measurements by dynamic light scattering at 173° backscatter angle running 10 scans three times per sample. Zeta potentials were measured using a Zeta Cell (Zetasizer Nano series, Malvern, UK) containing a 7X dilution of another 100 µL sample aliquot by laser Doppler anemometry (LDA) with each run consisting of 30 scans. Results are expressed as mean ± standard deviation (n = 3).

2.7 Cells and Cell culture

U87 cells (human glioblastoma cell line) were cultured in EMEM media supplemented with heat inactivated FBS (10%) and Penicillin-Streptomycin (1%). The cells were subcultured, maintained and grown in an incubator in humidified air with 5% CO_2 at 37 °C.

2.8 Evaluation of cytotoxicity via MTT Assay

Cytotoxicity of free polymers and polyplexes was tested via MTT assay on U87 glioblastoma cells. Therefore, the cells were seeded in a 96 well plate at a density of 8.000 cells per well and grown for 24 h. Free polymer (in concentrations that correspond to concentrations used for polyplex preparation for N/P ratios of 3, 5 and 10) and polyplex suspensions (N/P ratios 3, 5 and 10) were added to the wells and incubated for 24 h. After removing the medium, 0.5 mg/mL MTT containing fresh medium was added and incubated for 3 h at 37 °C and 5 % CO_2. Finally,

insoluble purple formazan crystals were dissolved in 200 µL isopropanol, and the absorption was quantified at 570 nm wavelength and corrected with background values measured at 680 nm using a microplate reader (FLUOstar Omega, BMG Labtech, Ortenberg, Germany). The experiment was performed in triplicate and results are shown as mean ± standard deviation normalized to percentage of viable cells in comparison to untreated cells representing 100% viability. In our context we further wanted to investigate the polymer concentrations (IC_{50} values) that reduce mitochondrial activity of the treated cells by 50% after a specific incubation period in comparison to well-known transfection agents. Therefore, U87 cells were seeded in a 96-well plate at a density of 8000 cells per well and incubated for 24 h. $P(SPAA)_{327}$ (**1b**), PEI and Lipofectamine with varying concentrations (0.01 mg/mL to 1 mg/mL for PEI and 0.01 mg/mL to 0.1 mg/mL for LF) were added and incubated for 24 h. An MTT Assay was performed as described above. Cell viability profiles were constituted as a function of log concentration values and IC_{50} values were calculated using the GraphPad Prism 5 Software by using a nonlinear fit.

2.9 Quantification of Cellular Uptake by Flow Cytometry

The *in vitro* cellular uptake of polyplexes was quantified by flow cytometry. Amine modified siRNA was labeled with the fluorescent dye Alexa Fluor 488 (AF488) following the manufacturer´s protocol and purified by ethanol precipitation and spin column binding as described previously [18]. U87 cells were seeded 24 h prior to the experiment in 24-well plates at a density of 50.000 cells per well and incubated at 37 °C and 5 % CO_2 atmosphere. All uptake experiments were performed using 50 pmol of siRNA-AF488 at N/P ratio of 3, negative controls consisted of untreated and free siRNA-AF488 treated cells. Positive controls consisted of Lipofectamine 2000 lipoplexes which were prepared with 50 pmol of siRNA-AF488 according to the manufacturer´s protocol. After the transfection of cells for 24 h, the incubation medium was removed, and cells were washed with PBS and detached using 0.25 % trypsin-EDTA. Samples were washed twice with 500 µL PBS and resuspended in 500 µL PBS/2 mM EDTA. Additionally, trypan blue quenching was used to exclude the surface fluorescence signals of not completely internalized siRNA complexes. Median fluorescence intensities (MFI) were analyzed using an Attune NxT Acoustic Focusing Cytometer (Thermo Fisher Scientific, Waltham, MA, USA) by exciting the siRNA-AF488 at 488 nm and measuring the fluorescence signal with a 530/30 nm emission filter. Samples were run in triplicates, each sample consisting of a minimum of 10000 viable cells. Results are given as mean ± standard deviation (n = 3).

2.10 In vitro GAPDH gene Knockdown by PCR measurements

To test gene silencing abilities of the polyplexes, 120.000 glioblastoma cells per sample were seeded in a 6-well plate and grown for 24 h. Cells were transfected with polyplexes containing 50 pmol siRNA at N/P 3 either directed against GAPDH (siGAPDH) or scrambled negative control siRNA (siNC), respectively. After a 24-hour incubation period, cells were harvested and total RNA was isolated with the PureLink^{TM} RNA mini kit (ThermoFisher Scientific, Waltham, MA, USA) according to the manufacturer´s protocol with additional DNase digestion. cDNA was synthesized from RNA with a high-capacity cDNA synthesis kit (ThermoFisher Scientific, Waltham, MA, USA) using a qTOWER real-time PCR thermal cycler (Analytik Jena, Jena, Germany). cDNA was amplified with powerSYBR green PCR master mix (ThermoFisher Scientific, Waltham, MA, USA) and Quantitect® primer assays Hs_GAPDH_1_SG and Hs_ACTV_2_SG (Qiagen, Venlo, Netherlands) using the thermal cycler mentioned above. Cycle threshold (Ct) values were obtained with the qPCRsoft software (Analytik Jena). The experiment was performed in triplicates for each sample with additional water samples as negative controls. GAPDH gene expression was calculated according to the delta - delta Ct method and normalized by corresponding β-actin expression for each sample related to siNC negative control values. Results are given as mean ± standard deviation (n = 3).

2.11 Statistics

Unless otherwise stated, results are given as mean value ± standard deviation. One-way ANOVA with Bonferroni multiple comparison test was performed in GraphPad Prism software (Graph Pad Software, La Jolla, CA) to calculate p-values at 95% confidence.

3. Results and Discussion

3.1 siRNA encapsulation Assay

Negatively charged phosphate groups present in the siRNA molecule and positively charged polymers can form polyplexes. This is due to electrostatic attraction inducing charge complexation when they are combined in solutions [19]. Within this complex the siRNA molecule and especially its sensitive phosphate backbone is protected against various sources of degradation after *in vitro* or *in vivo* application such as nucleases [20] and therefore is enabled to reach its target side in an intact manner. Consequently, the siRNA encapsulation ability of polymers represents an important property in evaluating their suitability as siRNA carriers. Due to induced cytotoxicity by high cationic charge densities, full encapsulation of siRNA at low

N/P ratios and therefore low amounts of polymer is desirable. To determine the optimal polymer amounts for condensation of a specific siRNA amount, siRNA encapsulation assays were performed at various N/P ratios by using the fluorescent dye SYBR Gold.

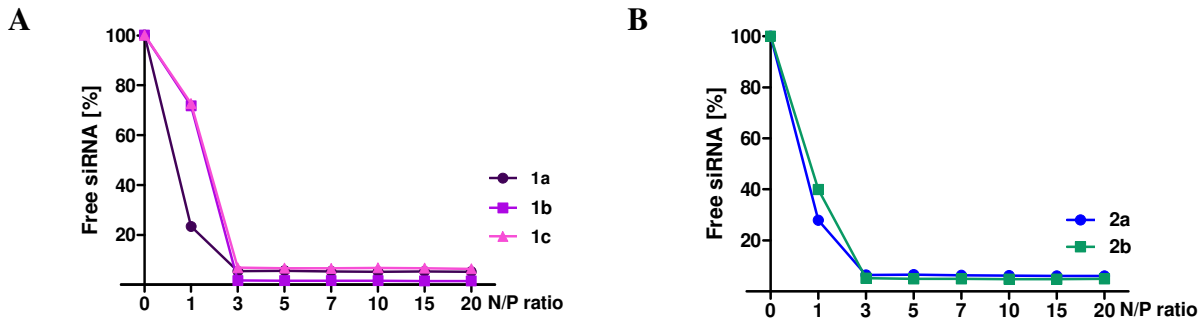

Figure 2. Small Interfering RNA (siRNA) encapsulation profiles of polyplexes formed with homopolymers (**A**) and copolymers (**B**) as measured by SYBR Gold assay at various N/P ratios. 100 % values (N/P = 0) are represented by the determined fluorescence of uncondensed siRNA. (Data points indicate mean, n = 3).

As displayed in Figure 2 all polymers showed comparably efficient siRNA condensation abilities with maximum protection of the payload at N/P ratio 3 with 5.4%, 1.7% and 6.8% non-encapsulated siRNA for polymers **1a** – **c** and 6.6% and 5.2% for polymers **2a** and **2b**, respectively. An increase in the concentration of the polymers did not further lead to a more efficient siRNA encapsulation. At lower N/P ratios, the smallest polymer (**1a**) showed most efficient condensation of the nucleic acids. At N/P ratio 1 already 77% siRNA were encapsulated, whereas polymers **1b** and **1c** had only encapsulated 28% of available siRNA molecules. This suggests that steric hindrance of larger polymer molecules may make encapsulation less efficient while using low polymer concentrations. The hydrophobically modified polymers exhibited a comparable condensation ability as polymer **1a** with 77% and 60% of free siRNA, respectively at N/P 1. One could conclude from these results that hydrophobic interactions of the additional subunits may contribute to the formation of polyplexes [21]. In summary, all the polymers showed highly efficient siRNA condensation abilities at rather low N/P ratios in comparison to low molecular weight polyethylenimine-based polymers, for example [22]. Advantageously, the use of low polymer concentrations helps avoid unwanted side or toxic effects and reduces the incurred costs of the polymer excipient.

3.2 siRNA Release by Heparin Competition Assay

The stability of polyplexes, which is influenced by the presence of competing anions after addition to serum containing cell culture medium or administration *in vivo*, is also an important parameter to screen the potential efficiency of polymers as siRNA vectors [23]. After *in vivo*

administration polyplexes need to remain stable for successful delivery of their payload to their specific target sites. Therefore, release assays were performed to confirm the protection ability of P(SPAA) and P(SPAA-co-DAA) polymers for siRNA in the presence of polyanions under physiologically relevant conditions (pH 7.4) as present in the blood stream. On the other hand, as free siRNA present in the cytoplasm is a prerequisite to induce the RNAi machinery, siRNA release ability under acidic conditions (pH 4.5), mimicking the endosomal compartment, was determined also. As illustrated in Figure 3A solely slight siRNA displacement at pH 7.4 from P(SPAA) polyplexes occurred for all heparin concentrations and reached siRNA release of approximately 12% for **1a** and **1b** polyplexes and 7% for **1c** polyplexes for the highest used heparin concentration of 1 USP units per well. **1a** polyplexes showed one additional peak with maximal free siRNA concentrations of 24% at 0.12 USP units heparin per well. **2a** and **2b** polyplexes displayed a comparable release profile to **1b** and **1c** polyplexes with a maximum of free siRNA amount (7.3% for **2a** polyplexes and 8.9% for **2b** polyplexes) at 1 USP units per well (Figure 3B). Consequently, just a small amount of siRNA molecules could be replaced by competing heparin anions what leads to the conclusion that all used polymers are able to form polyplexes which are stable under physiologic conditions. Under these conditions hydrophobic modifications commonly exhibit enhanced siRNA retention by additional hydrophobically reflected here by small differences between the homo- and copolymers.

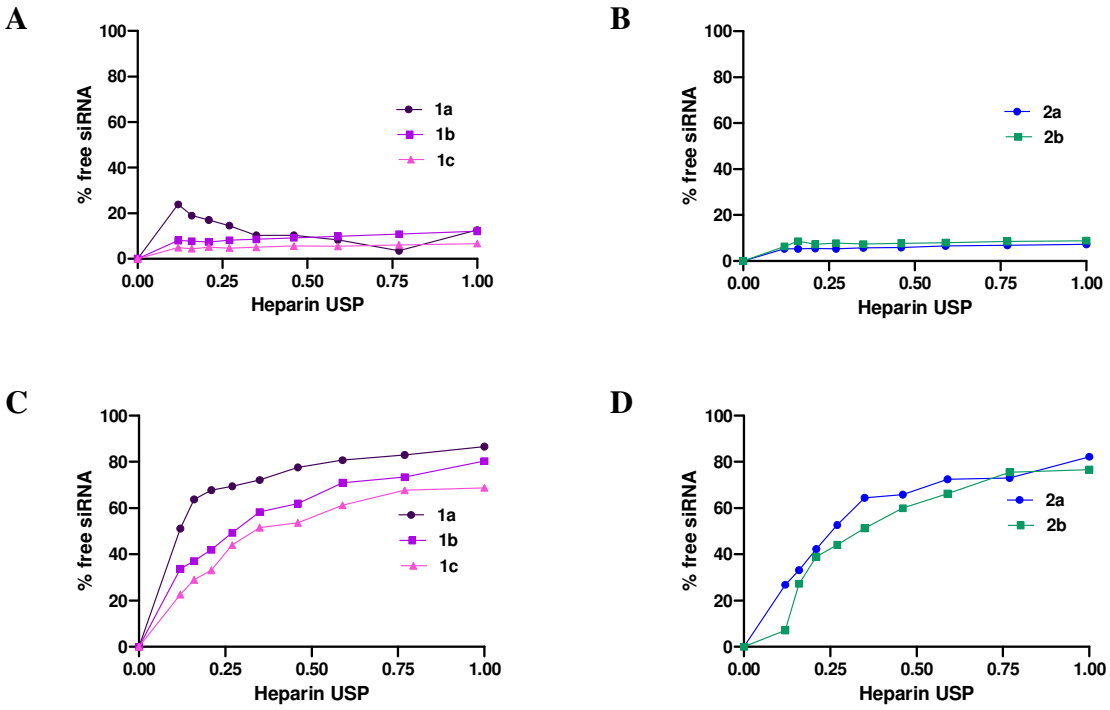

Figure 3. Release profiles of siRNA from polyplexes formed at N/P 3 with homopolymers **1a** – **c** (**A** and **C**) and copolymers **2a** and **2b** (**B** and **D**) as a function of heparin concentration (0.0 - 1.0 USP heparin per well) at pH 7.4 (**A** and **B**) and 4.5 (**C** and **D**). (Data points indicate mean normalized fluorescence, n = 3).

As illustrated in Figure 3C and 3D and in accordance with our former observations, siRNA was very easily released from all kinds of used polyplexes indicating appropriate payload release abilities under mimicked endosomal conditions. siRNA release at lower pH values might occur through charge repulsion after amine protonation leading to complex destabilization and payload release [24]. Release of siRNA is a prerequisite for incorporation into the RNAi machinery and consequent therapeutic effects. At highest used heparin concentration, 87%, 80% and 69% for **1a** – **c** polyplexes and 82% and 77% for **2a** and **2b** polyplexes of free siRNA were found, respectively. Payload release abilities shown by homopolymers indicate in accordance with data for encapsulation ability, that variations in polymer sizes lead to differences in the stability of the formed complexes. It seems that replacement of siRNA from complexes formed with the low molecular weight polymer **1a** (87%) is easier that from complexes built with higher molecular weight polymer **1c** (69%). Therefore, we suggest that lower molecular weight can impair the stable complex formation ability. This finding is in line with already described observations for PEI polyplexes [25]. Hydrophobically modified copolymer **2b** showed slightly lower siRNA release for analogous heparin concentrations than copolymer **2a** indicating that higher number of hydrophobic interactions within this polymer-siRNA complexes may protect RNA better against competing anions such as heparin. It was already described in literature that polymers containing hydrophobic functionalities, e.g., triazine dendrimers modified with alkyl chains, showed increased stability against heparin displacement under physiological conditions [26].

3.3 Particle characterization

3.3.1 Size and Zeta (ζ)-Potential Analysis by Dynamic Light Scattering and Laser Doppler Anemometry

As the nanoparticles' physicochemical characteristics are major determinants for intracellular uptake and transfection abilities, one aim of the study was to investigate whether P(SpAA) and P(SpAA-co-DAA) complexes fulfill the general requirements regarding polyplex properties for successful RNA delivery. It is known that there is a limit in size by which particles get internalized into cells [27] but also that very small particles are quickly excreted by the kidneys [28]. Another important factor is the surface charge of the nanoparticles, as slight positive charges can help to enter cells via interaction with negatively charged proteoglycans present in the cell membrane. However, high charge densities can also induce cytotoxicity [29]. Size, PDI

and zeta potentials measurements were performed at N/P ratios of 3, 5 and 10 as the increasing polymer concentration might also have an effect on the polyplex properties.

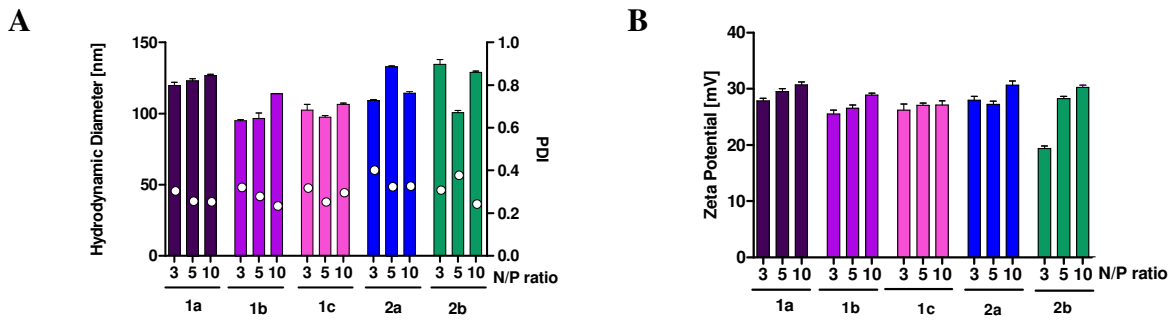

Figure 4. Dynamic light scattering measurements of polyplexes formed with homo- and copolymers (**A**) Hydrodynamic diameters (left y-axis) and polydispersity indices (PDI, right y-axes) for N/P ratios of 3; 5 and 10 and (**B**) zeta potentials of polyplexes formed with homo- and copolymers at N/P ratios of 3; 5 and 10. (Data points indicate mean ± SD, n = 3).

Our data revealed, as illustrated in Figure 4A, that all polymers encapsulated the siRNA firmly and formed polyplexes at very favorable size ranges between 95 and 135 nm. If considered at which N/P ratios these sizes were reached, our spermine-based polyacrylamides showed advantages against many other hydrophobically modified polymers or PEI. Most other polymers require much higher N/P ratios to achieve encapsulated particles within comparable size ranges [30]. Low molecular weight polymer **1c** formed largest particles (**1a**: 126 nm, **1b**: 114nm and **1c**: 106 nm for N/P 10) what supports our thesis that these kinds of polymers form more loosely bound complexes with siRNA molecules. To generate reproduceable data in further experiments the polyplexes investigated should be as uniform as possible. In our study we found a PDI range from 0.23 to 0.4 indicating appropriate size distribution profiles. For subsequent experiments the PDIs could be further improved by optimizing synthesis and purification of the polymer or controlled assembly of the polyplexes for example with a microfluidic polyplex preparation approach as already described in literature [31]. As expected, zeta potential values as shown in Figure 4B were correlating with the N/P ratio. The zeta potentials were in a desirable range from 19.3 to 30.8 mV. This seems understandable because the increasing amount of positively charged polymer added to the polyplexes impacts the particle charge. Interestingly the polyplexes formed with the most hydrophobic polymer **2a** showed a decrease in surface charge. This indicates that the hydrophobic modifications are capable to shield the cationic charge to a certain degree. These results hint to promising uptake capabilities since all physicochemical characteristics lay inside the narrow requirement ranges explained in the beginning.

3.4 Evaluation of cytotoxicity via MTT Assay

As previously described, structures with high cationic charge density induce severe cytotoxicity. On the other hand, they can strengthen the polyplexes against destabilizing polyanionic structures which are abundant in the blood and extracellular fluids [32]. Furthermore, they support cell internalization of the particles and endosomal escape of siRNA molecules, and consequently they are a mandatory requirement for successful siRNA delivery leading to therapeutic effects. This is one of the biggest challenges to overcome in developing siRNA carrier systems since cytotoxicity on the one hand and polyplex stability, transfection efficiency, gene knockdown ability and biocompatibility on the other need to be balanced against each other. This is one of the reasons poly(spermine acrylamides) were investigated by our group. One aspect was to introduce endogenous cationic structures to reduce cytotoxicity. Additionally, the hypothesis was developed, that the hydrophobic subunits might be able to shield the cationic charge and thereby can reduce cytotoxicity. To check this hypothesis, a thiazolyl blue tetrazolium bromide (MTT) assay was performed in U87 glioblastoma cells after 24 h exposure with free polymers at various concentrations (same concentrations of free polymers were used as needed for corresponding polyplex preparation for N/P 3 and 10) as well as formed polyplexes at N/P ratio 3 and 10. N/P 3 represents the working N/P ratio for further experiments in this study, whereas N/P 10 was chosen to generate data also for higher polymer amounts to get more insight of the toxicity profiles of the used materials. To be able to compare cell tolerability of poly(spermine acrylamides) and currently used transfection standards the IC_{50} values of $P(SPAA)_{327}$ (**1b**), branched PEI (10 kDa) as well as Lipofectamine 2000 (LF) were determined. Therefore, an MTT assay in U87 glioblastoma cells after 24 h of exposure was performed. Absorbance signal of untreated cells was set to 100 %. With the GraphPad Prism 5 Software the IC_{50} values for our tested dilution series were calculated. Therefore, the logarithmic concentrations were plotted against the percentage of cell viability. The software then calculated the inflexion point which resembles the IC_{50} value. This value is not only substance specific but also cell line specific. The calculated concentrations indicated circumstances under which only half of all cells of a certain type showed full mitochondrial activity.

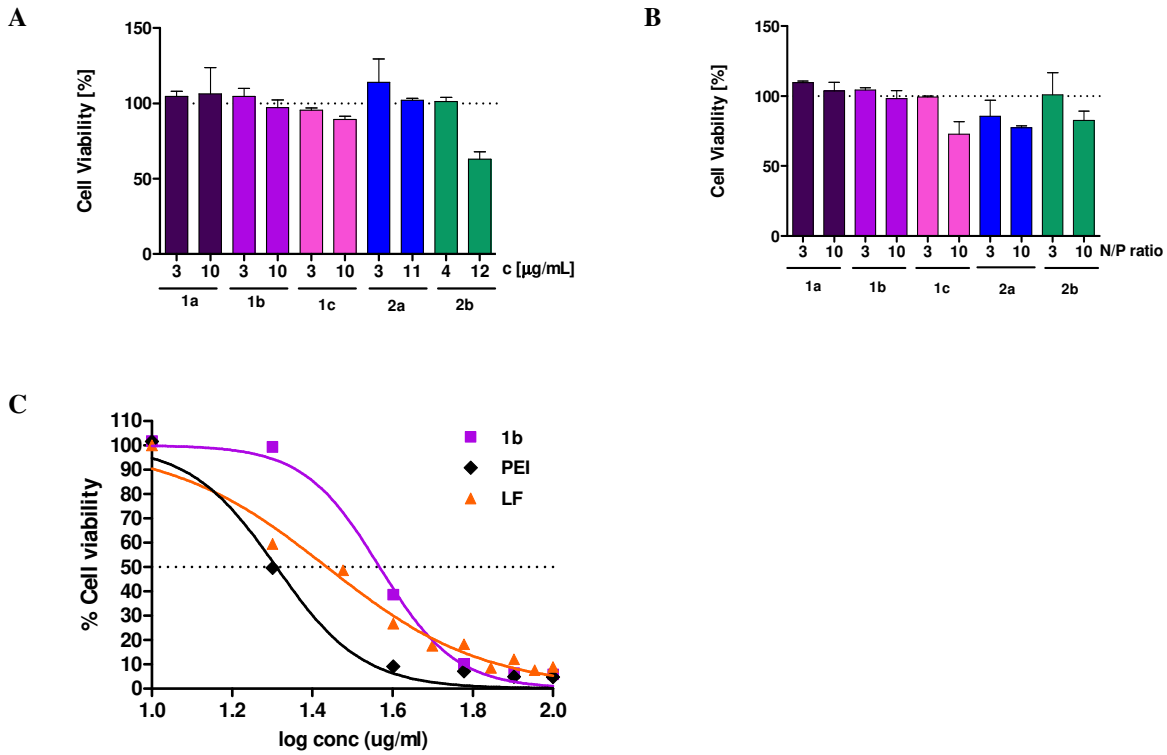

Figure 5. Cell viability of U87 glioblastoma cells as determined by thiazolyl blue tetrazolium bromide (MTT) assay after 24 h of polymer/polyplexes incubation time. Cell viability for various concentrations of homo- and copolymers (**A**). Cell viability for polyplexes with N/P ratios of 3 and 10 (**B**). Cell viability profiles and IC50 value determination for 1b polymer, poly(ethylenimine) (PEI) as well as Lipofectamine 2000 (LF) as a function of log concentration values (**C**).

The obtained results (Figure 5A and 5B) indicated that free polymers and polyplexes at low concentrations and N/P ratios showed no toxic effects. Only at higher concentrations and N/P ratios cytotoxicity became a minor factor for some formulations. Thus, free polymer **1c** and **2b** displayed survival rates of 89 % at 10 µg/mL and 63 % at 12 µg/mL, respectively. Decreased cell viabilities could displayed for polyplexes prepared with **1c** (73 % for N/P 10), **2a** (86% for N/P 3 and 77% for N/P 10) and **2b** (83% for N/P 10) and therefore hydrophobically modified copolymers appeared to be slightly more toxic than homopolymers what may be caused by their surface activity or the synthesis process. However, acceptable cell compatibility for U87 cells could be confirmed for all free polymers as well as for all polyplexes. This promises high potential for the use of our polymers as carrier systems especially regarding *in vivo* experiments in the future. As displayed in Figure 5C IC_{50} values for $P(SPAA)_{327}$, branched PEI and LF were determined as a function of log values of used concentration and were for PEI and LF 20.43 µg/mL and 27.28 µg/mL, respectively. With an IC_{50} concentration of 36.93 µg/mL $P(SPAA)_{327}$ demonstrated increased cell tolerability. This data highlights that $P(SPAA)_{327}$ was indeed superior regarding cytotoxicity in comparison to LF and PEI. We could thereby confirm our

hypothesis that spermines as endogenous structures are promising source materials for cationic polymer delivery systems with low cytotoxic effects. This suggests high potential for therapeutic approaches.

3.5 Quantification of Cellular Uptake by Flow Cytometry

With the promising data regarding physicochemical characteristics and siRNA encapsulation ability the next step in our research was to determine the capability of our polyplexes to enter cells. Therefore, polyplexes were prepared with a previously labelled AF488-siRNA. The cellular internalization in glioblastoma cells was measured by flow cytometry after polyplex incubation of 24 h. Preliminary experiments with varying N/P ratios were performed to identify the N/P ratio with the best uptake capabilities. The most efficient N/P was 3 for all tested polyplexes and then chosen as working N/P ratio for following experiments. Labelled siRNA or formed polyplexes which are adherently bound to the cell surface but not internalized can cause wrong fluorescence signals and therefore falsify the generated data. To evaluate the influence of this phenomenon, samples were measured with and without trypan quenching. Trypan blue does not diffuse across cell membranes [33] and therefore erases all fluorescence signals from the surface of cells. Obtained data displayed no statistical difference from the quenched data (data not shown). This confirmed that cellular internalization was measured without additional signals generated by adherently bound fluorophores. Interestingly, with further rising polymer concentration, uptake capabilities constantly decreased. The cytotoxicity on the other hand rose with the N/P ratio and thereby might be the cause for decreased uptake. Figure 6 shows the median fluorescent intensity (MFI) of U87 glioblastoma cells transfected with preformed polyplexes, compared to free siRNA and untreated cells as negative control as well as Lipofectamine 2000 (LF) lipoplexes as positive control after trypan blue quenching.

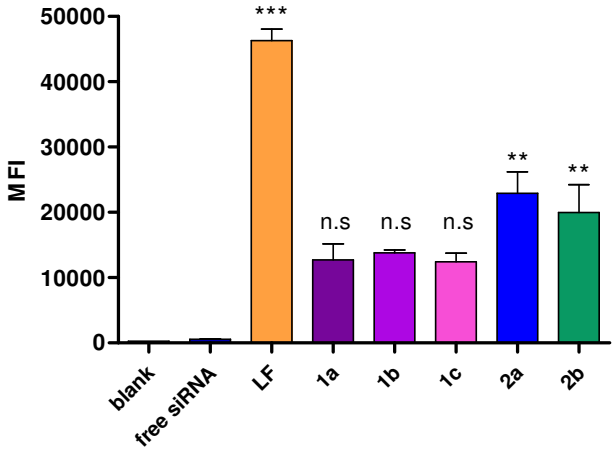

Figure 6. Cellular uptake of polyplexes after 24 h incubation time, as quantified by flow cytometry performed with trypan quenching and presented as median fluorescent intensity (MFI, y-axis) compared to free siRNA and untreated cells as negative controls as well as Lipofectamine 2000 (LF) lipoplexes as positive control. (Statistical evaluation was performed by one-way ANOVA, ** $p < 0,01$, *** $p < 0,001$).

The cells transfected with P(SPAA)-polyplexes showed no significant increase in cellular uptake in comparison to free siRNA, and MFIs were in a range from 12409 (**1c**) to 13771 (**1a**). The P(SpAA-co-DAA) polyplexes displayed significantly higher uptake with MFI values of 22907 for $P(SpAA_{0.9}/DAA_{0.1})_{461}$ and 19999 for $P(SpAA_{0.75}/DAA_{0.25})_{526}$. Therefore, suitable cell internalization capabilities were confirmed especially for hydrophobically modified ones. This data implied that the hydrophobic subunits support cell internalization as previously shown for many other hydrophobically modified polymers [34]. We suggest that hydrophobic interactions of the aliphatic side chains within the polymer with lipid bilayers of the cells might play an important role in the polyplex uptake procedure [35]. Enhanced cellular internalization abilities of hydrophobically polymers were already described for palmitic acid modified chitosan [36] and poly-L-lysine polymers (PLL) [37], for amino acid modified poly(amidoamines) (PAA) [38], for oleic and stearic acid-modified PEI 2kDa [39], for triblock copolymeric systems of poly(amidoamine) (PAMAM) dendrimers modified with PEG and dioleoylphosphatidyl ethanolamine (DOPE) [40] and Nylon-3 polymers modified with hydrophobic subunits [41]. A next step might be to investigate the route of cellular uptake to evaluate potential differences between homo- and copolymers. Nonetheless, we achieved considerable uptake levels for both types of polymers highlighting the potential of poly(spermine acrylamides) for siRNA delivery in general, whereas hydrophobic modified ones are especially promising.

3.6 GAPDH Knockdown measured by RT-PCR

To investigate whether cellular uptake also correlates with corresponding gene silencing we performed a GAPDH Knockdown experiment. Gene downregulation on the mRNA level was examined using siRNA specifically targeting the house-keeping gene GAPDH (GAPDH-siRNA) followed by isolation of the RNA, reverse transcription in cDNA and quantification of respective cDNA templates via real time PCR (RT-PCR). All tested formulations were also applied containing scrambled non-targeting siRNA (NC-siRNA) as a negative control. Figure 7 shows GAPDH expression normalized to beta-actin gene expression related to negative control values for each sample calculated by the delta-delta Ct method.

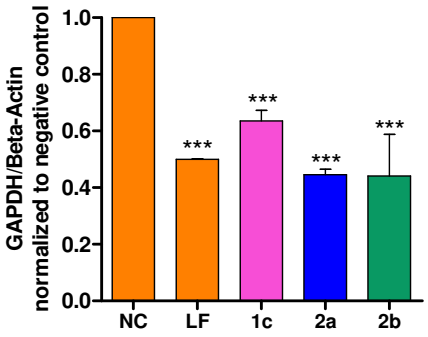

Figure 7. GAPDH knockdown of **1c**, **2a** and **2b** polyplexes at N/P 3 in U87 glioblastoma cells quantified by polymerase chain reaction (PCR) and calculated by the delta-delta Ct method normalized to beta-actin gene expression and scrambled siRNA values used as negative control for each polymer. (Data points indicate mean ± SD, n = 3. Statistical evaluation was performed by one-way ANOVA, *** $p < 0{,}001$).

All tested formulations displayed a significant silencing effect of GAPDH gene expression compared to their respective NC-siRNA controls. Most efficient knockdown ability of hydrophobically modified copolymers **2a** and **2b** (66 %) was observed, followed by LF positive control (50%) and homopolymer **1c** (36%). More efficient gene silencing effect of hydrophobically modified polymers might be attributed on the one hand to enhanced cellular internalization ability that led to higher amounts of siRNA molecules within the cells. On the other hand, after endocytosis, free siRNA molecules need to be released from the polymer-siRNA complex and be able to escape the endosomal compartment to undergo the RNAi machinery. All formulations exhibited also appropriate siRNA release abilities at conditions present in the endosomolytical compartment (pH = 4.5). Furthermore, as hydrophobic moieties facilitate internalization into cells via hydrophobic interactions with the cellular lipid bilayer, we hypothesize, that these interactions may also be helpful to escape the endosomal compartment besides the buffering capacity of primary and secondary amines (proton sponge effect) [9]. Consequently, free siRNA molecules are present in the cytoplasm and available for knocking down their specific gene expression on the mRNA level. The higher extent of DAA subunits within the **2b** polymer, however, could not further improve the knockdown ability. Taken together modified poly(spermine acrylamides) exhibited more efficient GAPDH knockdown than unmodified ones, what leads to the assumption, that additional hydrophobic interactions with the membrane of the endosome might cause an improved siRNA release into the cytoplasm and, taken together with appropriate siRNA release and cellular internalization abilities, this leads to a highly efficient gene silencing effect. P(SpAA-co-DAA) polyplexes therefore provide a highly promising system for siRNA delivery into glioblastoma cells.

4. Conclusion

Many carrier systems for siRNA delivery exhibit great potential. However, low cytotoxicity as well as appropriate transfection efficiencies and endosomal escape capabilities remain big challenges for successful gene knockdown and therapeutic effects. Herein, we presented a way to synthesize a new type of polymer following the approach of using NAS as monomers for FRP reactions leading to poly(tri-boc spermine acrylamides) after post-polymerization functionalization with tri-boc spermine molecules. Additionally, we described a way to synthesize hydrophobically modified copolymers with hydrophobic decylacrylamide subunits to gain insight into the effect of the modifications. . All polymers were able to form polyplexes with high maximum encapsulation values of 94-95%. They uniformly reached maximum siRNA encapsulation from N/P 3 which was determined by SYBR Gold assay. DLS measurements showed that all polyplexes were in favourable size ranges of 95-140 nm and that the size distribution was in an acceptable range from 0.23 to 0.4. Zeta potentials determined with LDA were between 19.3 mV and 30.8 mV. Therefore, our polymers formed polyplexes with very favorable physicochemical characteristics. Using MTT assays to determine cell viability via metabolic activity we found that at working N/P ratios, none of our polymers showed any sign of cytotoxicity. To gain more insights regarding cytotoxic effects of the materials IC_{50} concentrations of $P(SpAA)_{327}$, branched PEI and the cationic lipid LF 2000 were additionally determined. Herein, we confirmed, in line with our assumption a superior cell tolerability for $P(SpAA)_{327}$ polymer in comparison to currently used standards LF 2000 and branched PEI. Tested on U87 glioblastoma cells, all polyplexes showed favourable cell internalization capabilities whereas hydrophobically modified polymers performed best. GAPDH gene silencing experiments were used to evaluate the knockdown ability of the polyplexes on RNA level. Copolymers were able to induce the strongest GAPDH gene knockdown effect of 66% compared to negative control, whereas higher hydrophobic extent does not lead to a more efficient gene-silencing effect. Consequently, siRNA molecules seem to be released from polyplexes in an appropriate manner and moreover, hydrophobic moieties even might facilitate the escape from the endosome. The mechanism for this postulation is still not investigated and needs to be addressed in future projects. The comparison between oligospermines and P(SpAA) homo- and copolymers in which the molecular masses were further increased underlined that higher molecular masses of spermine-containing substances did not result in improved uptake and knockdown abilities, whereas hydrophobic modifications were shown to be able to achieve such an effect. Controversially, there is also evidence in the

literature of hydrophobically modified formulations that have promoted cell entry but not endosomal escape what suggest, that it is not possible to make a general statement about the behavior *in vitro* [9]. The success of the material might considerably depend on type and extent of the hydrophobic modifications as well as the cell membrane composition of utilized cell lines and needs to be investigated in every single case. Furthermore, as the composition of the outer cell membrane differs to the one of the endosomes, enhanced cellular internalization does not necessarily mean that endosomal escape is also improved. In conclusion, synthesized spermine-based poly(acrylamides) provide a suitable group of materials for siRNA delivery into glioblastoma cells with minimal toxic effects. Especially hydrophobic modification of polymers is a suitable tool to design drug delivery systems with enhanced cellular internalization and gene-silencing abilities via additional hydrophobic interactions with cell membranes. To further enhance their intracellular uptake abilities, synthesis methods, that enable higher number of hydrophobic subunits within the polymers are under investigation. Ongoing work currently also focuses on improvement of endosomal escape with the use of e.g., trans-activator of transcription (TAT) peptides from HIV or similar cell penetrating peptides combined with histidine residues or covalently bound melittin to osmotically disrupt the endosomes. To enable selective targeting a Transferrin-based delivery directly towards tumor cells might be possible. Finally, to reach glioblastoma cells after intravenous injection, a mechanism to overcome the blood-brain barrier is necessary as well. The final objective is the delivery of therapeutic siRNAs for glioma-related genes to decrease tumor proliferation. This might be a promising therapy advancement for glioblastoma multiforme patients all over the world.

References

[1] E.A. Maher, R.M. Bachoo, Glioblastoma, Rosenberg's Molecular and Genetic Basis of Neurological and Psychiatric Disease, Elsevier2020, pp. 173-182.
[2] A.F. Hottinger, R. Stupp, K. Homicsko, Standards of care and novel approaches in the management of glioblastoma multiforme, Chinese journal of cancer, 33 (2014) 32-39.
[3] J.P. Thakkar, T.A. Dolecek, C. Horbinski, Q.T. Ostrom, D.D. Lightner, J.S. Barnholtz-Sloan, J.L. Villano, Epidemiologic and Molecular Prognostic Review of Glioblastoma, Cancer Epidemiology, Biomarkers & Prevention, 23 (2014) 1985-1996.
[4] M.T. McManus, P.A. Sharp, Gene silencing in mammals by small interfering RNAs, Nature reviews genetics, 3 (2002) 737-747.
[5] J.K.-W. Lam, W. Liang, H.-K. Chan, Pulmonary delivery of therapeutic siRNA, Advanced drug delivery reviews, 64 (2012) 1-15.
[6] Y. Wan, P.M. Moyle, M.P. Christie, I. Toth, Nanosized, peptide-based multicomponent DNA delivery systems: optimization of endosome escape activity, Nanomedicine, 11 (2016) 907-919.
[7] G.R. Rettig, M.A. Behlke, Progress Toward In Vivo Use of siRNAs-II, Molecular Therapy, 20 (2012) 483-512.
[8] S.M. Moghimi, P. Symonds, J.C. Murray, A.C. Hunter, G. Debska, A. Szewczyk, A two-stage poly(ethylenimine)-mediated cytotoxicity: implications for gene transfer/therapy, Molecular Therapy, 11 (2005) 990-995.
[9] H. Eliyahu, S. Siani, T. Azzam, A.J. Domb, Y. Barenholz, Relationships between chemical composition, physical properties and transfection efficiency of polysaccharide–spermine conjugates, Biomaterials, 27 (2006) 1646-1655.
[10] H.-L. Jiang, H.-T. Lim, Y.-K. Kim, R. Arote, J.-Y. Shin, J.-T. Kwon, J.-E. Kim, J.-H. Kim, D. Kim, C. Chae, J.-W. Nah, Y.-J. Choi, C.-S. Cho, M.-H. Cho, Chitosan-graft-spermine as a gene carrier in vitro and in vivo, European Journal of Pharmaceutics and Biopharmaceutics, 77 (2011) 36-42.
[11] M. Elsayed, V. Corrand, V. Kolhatkar, Y. Xie, N.H. Kim, R. Kolhatkar, O.M. Merkel, Influence of oligospermines architecture on their suitability for siRNA delivery, Biomacromolecules, 15 (2014) 1299-1310.
[12] G. Navarro, S. Essex, R.R. Sawant, S. Biswas, D. Nagesha, S. Sridhar, C.T. de Ilarduya, V.P. Torchilin, Phospholipid-modified polyethylenimine-based nanopreparations for siRNA–mediated gene silencing: Implications for transfection and the role of lipid components, Nanomedicine: Nanotechnology, Biology and Medicine, 10 (2014) 411-419.
[13] G. Navarro, J. Pan, V.P. Torchilin, Micelle-like Nanoparticles as Carriers for DNA and siRNA, Molecular Pharmaceutics, 12 (2015) 301-313.
[14] F. Adams, C.M. Zimmermann, D. Baldassi, Amphiphilic poly(spermine acrylamides): A new class of sophisticated non-viral vectors for pulmonary siRNA delivery, Advanced Healthcare Materials, (to be submitted for publication).
[15] T.J. Prazeres, M. Beija, M.-T. Charreyre, J.P.S. Farinha, J.M. Martinho, RAFT polymerization and self-assembly of thermoresponsive poly (N-decylacrylamide-bN, N-diethylacrylamide) block copolymers bearing a phenanthrene fluorescent α-end group, Polymer, 51 (2010) 355-367.
[16] S. Sharma, K.C. Basavaraju, A.K. Singh, D.-P. Kim, Continuous Recycling of Homogeneous Pd/Cu Catalysts for Cross-Coupling Reactions, Organic Letters, 16 (2014) 3974-3977.
[17] A.J. Geall, I.S. Blagbrough, Homologation of polyamines in the rapid synthesis of lipospermine conjugates and related lipoplexes, Tetrahedron, 56 (2000) 2449-2460.
[18] O.M. Merkel, D. Librizzi, A. Pfestroff, T. Schurrat, M. Béhé, T. Kissel, In Vivo SPECT and Real-Time Gamma Camera Imaging of Biodistribution and Pharmacokinetics of siRNA

Delivery Using an Optimized Radiolabeling and Purification Procedure, Bioconjugate Chemistry, 20 (2009) 174-182.
[19] H. de Martimprey, C. Vauthier, C. Malvy, P. Couvreur, Polymer nanocarriers for the delivery of small fragments of nucleic acids: Oligonucleotides and siRNA, European Journal of Pharmaceutics and Biopharmaceutics, 71 (2009) 490-504.
[20] A. Aied, U. Greiser, A. Pandit, W. Wang, Polymer gene delivery: overcoming the obstacles, Drug Discovery Today, 18 (2013) 1090-1098.
[21] L. Liu, M. Zheng, D. Librizzi, T. Renette, O.M. Merkel, T. Kissel, Efficient and Tumor Targeted siRNA Delivery by Polyethylenimine-graft-polycaprolactone-block-poly(ethylene glycol)-folate (PEI–PCL–PEG–Fol), Molecular Pharmaceutics, 13 (2016) 134-143.
[22] S. Jones, O. Merkel, Indium-labeling of siRNA for small animal SPECT imaging, RNA Imaging, Springer2016, pp. 79-88.
[23] O.M. Merkel, D. Librizzi, A. Pfestroff, T. Schurrat, K. Buyens, N.N. Sanders, S.C. De Smedt, M. Béhé, T. Kissel, Stability of siRNA polyplexes from poly(ethylenimine) and poly(ethylenimine)-g-poly(ethylene glycol) under in vivo conditions: Effects on pharmacokinetics and biodistribution measured by Fluorescence Fluctuation Spectroscopy and Single Photon Emission Computed Tomography (SPECT) imaging, Journal of Controlled Release, 138 (2009) 148-159.
[24] T.F. Martens, K. Remaut, J. Demeester, S.C. De Smedt, K. Braeckmans, Intracellular delivery of nanomaterials: how to catch endosomal escape in the act, Nano Today, 9 (2014) 344-364.
[25] M. Neu, D. Fischer, T. Kissel, Recent advances in rational gene transfer vector design based on poly(ethylene imine) and its derivatives, The Journal of Gene Medicine, 7 (2005) 992-1009.
[26] O.M. Merkel, M.A. Mintzer, D. Librizzi, O. Samsonova, T. Dicke, B. Sproat, H. Garn, P.J. Barth, E.E. Simanek, T. Kissel, Triazine Dendrimers as Nonviral Vectors for in Vitro and in Vivo RNAi: The Effects of Peripheral Groups and Core Structure on Biological Activity, Molecular Pharmaceutics, 7 (2010) 969-983.
[27] S.E.A. Gratton, P.A. Ropp, P.D. Pohlhaus, J.C. Luft, V.J. Madden, M.E. Napier, J.M. DeSimone, The effect of particle design on cellular internalization pathways, Proceedings of the National Academy of Sciences, 105 (2008) 11613.
[28] M. Longmire, P.L. Choyke, H. Kobayashi, Clearance properties of nano-sized particles and molecules as imaging agents: considerations and caveats, Nanomedicine, 3 (2008) 703-717.
[29] E. Fröhlich, The role of surface charge in cellular uptake and cytotoxicity of medical nanoparticles, Int J Nanomedicine, 7 (2012) 5577-5591.
[30] A. Dinari, T.T. Moghadam, M. Abdollahi, M. Sadeghizadeh, Synthesis and Characterization of a Nano-Polyplex system of GNRs-PDMAEA-pDNA: An Inert Self-Catalyzed Degradable Carrier for Facile Gene Delivery, Scientific Reports, 8 (2018) 8112.
[31] D.P. Feldmann, Y. Xie, S.K. Jones, D. Yu, A. Moszczynska, O.M. Merkel, The impact of microfluidic mixing of triblock micelleplexes on in vitroin vivo gene silencing and intracellular trafficking, Nanotechnology, 28 (2017) 224001.
[32] A. Hall, U. Lächelt, J. Bartek, E. Wagner, S.M. Moghimi, Polyplex evolution: understanding biology, optimizing performance, Molecular Therapy, 25 (2017) 1476-1490.
[33] E.S. Van Amersfoort, J.A. Van Strijp, Evaluation of a flow cytometric fluorescence quenching assay of phagocytosis of sensitized sheep erythrocytes by polymorphonuclear leukocytes, Cytometry: The Journal of the International Society for Analytical Cytology, 17 (1994) 294-301.
[34] Z. Liu, Z. Zhang, C. Zhou, Y. Jiao, Hydrophobic modifications of cationic polymers for gene delivery, Progress in Polymer Science, 35 (2010) 1144-1162.

[35] C.E. Nelson, J.R. Kintzing, A. Hanna, J.M. Shannon, M.K. Gupta, C.L. Duvall, Balancing Cationic and Hydrophobic Content of PEGylated siRNA Polyplexes Enhances Endosome Escape, Stability, Blood Circulation Time, and Bioactivity in Vivo, ACS Nano, 7 (2013) 8870-8880.
[36] I.F. Uchegbu, L. Sadiq, A. Pardakhty, M. El-Hammadi, A.I. Gray, L. Tetley, W. Wang, B.H. Zinselmeyer, A.G. Schätzlein, Gene Transfer with Three Amphiphilic Glycol Chitosans—the Degree of Polymerisation is the Main Controller of Transfection Efficiency, J Drug Target, 12 (2004) 527-539.
[37] B.A. Clements, V. Incani, C. Kucharski, A. Lavasanifar, B. Ritchie, H. Uludağ, A comparative evaluation of poly-l-lysine-palmitic acid and Lipofectamine ™ 2000 for plasmid delivery to bone marrow stromal cells, Biomaterials, 28 (2007) 4693-4704.
[38] K. Kono, H. Akiyama, T. Takahashi, T. Takagishi, A. Harada, Transfection Activity of Polyamidoamine Dendrimers Having Hydrophobic Amino Acid Residues in the Periphery, Bioconjugate Chemistry, 16 (2005) 208-214.
[39] A. Alshamsan, A. Haddadi, V. Incani, J. Samuel, A. Lavasanifar, H. Uludağ, Formulation and Delivery of siRNA by Oleic Acid and Stearic Acid Modified Polyethylenimine, Molecular Pharmaceutics, 6 (2009) 121-133.
[40] S. Biswas, P.P. Deshpande, G. Navarro, N.S. Dodwadkar, V.P. Torchilin, Lipid modified triblock PAMAM-based nanocarriers for siRNA drug co-delivery, Biomaterials, 34 (2013) 1289-1301.
[41] N. Hartl, F. Adams, G. Costabile, L. Isert, M. Döblinger, X. Xiao, R. Liu, O.M. Merkel, The Impact of Nylon-3 Copolymer Composition on the Efficiency of siRNA Delivery to Glioblastoma Cells, Nanomaterials, 9 (2019) 986.

Supplementary Material

1. NMR spectra of polymers

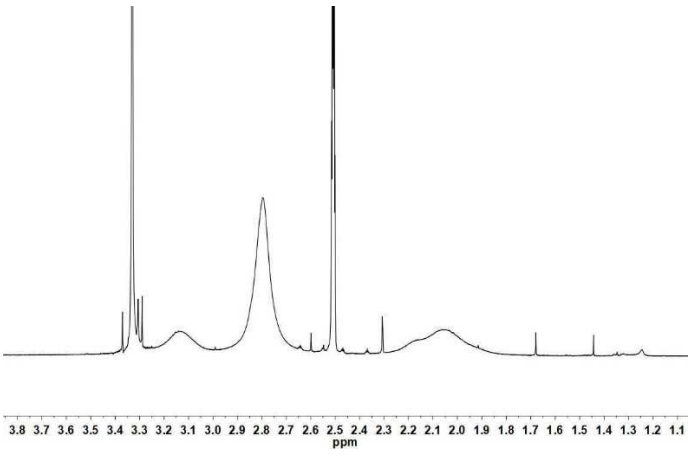

Figure S1. ^{1}H-NMR spectrum of P(NAS) homopolymer (exemplarily) in DMSO.

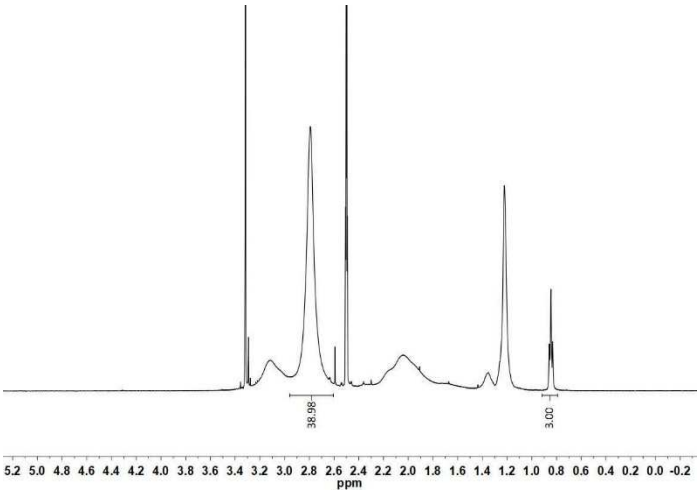

Figure S2. ^{1}H-NMR spectrum of P(NAS-co-DAA) 1 in DMSO.

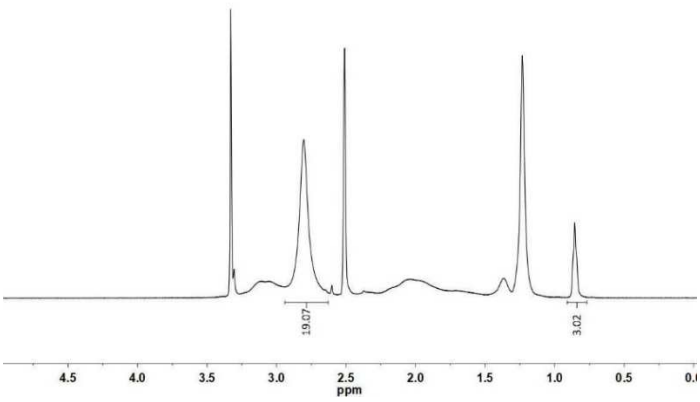

Figure S3. [1]H-NMR spectrum of P(NAS-co-DAA) 2 in DMSO.

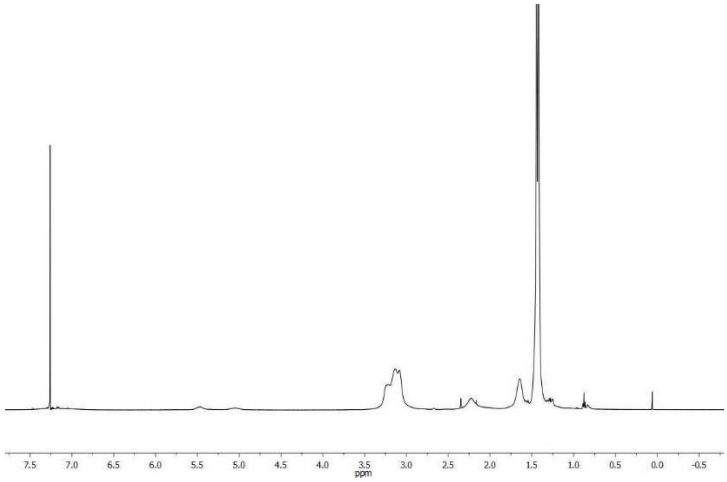

Figure S4. [1]H-NMR spectrum of P(TBSpAA) homopolymer (exemplarily).

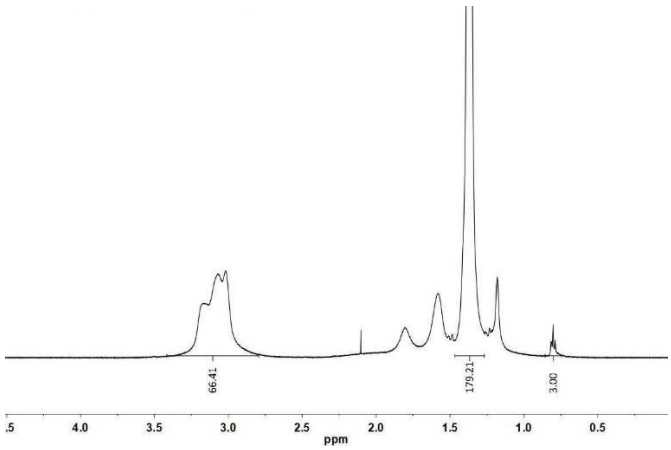

Figure S5. [1]H-NMR spectrum of P(TBSpAA-co-DAA) 1 in CDCl3.

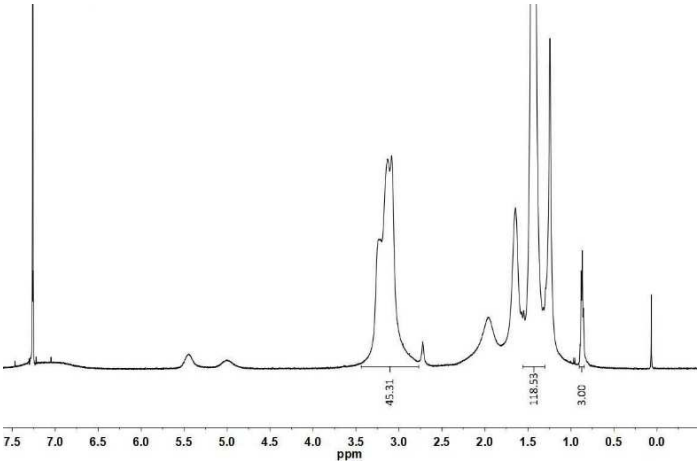

Figure S6. [1]H-NMR spectrum of P(TBSpAA-co-DAA) 2 in CDCl3.

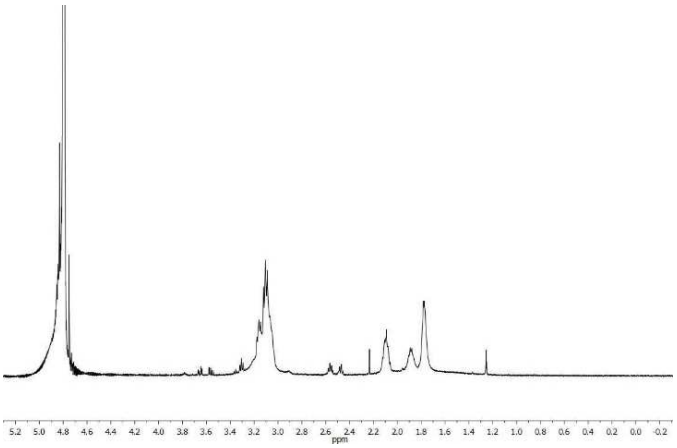

Figure S7. ^{1}H-NMR spectrum of P(SpAA) 1 (**1a**) TFA salt in D_2O.

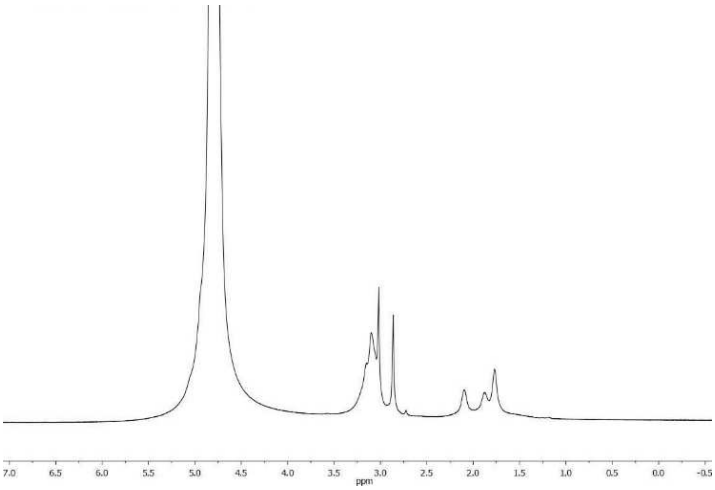

Figure S8. ^{1}H-NMR spectrum of P(SpAA) 2 (**1b**) TFA salt in D_20.

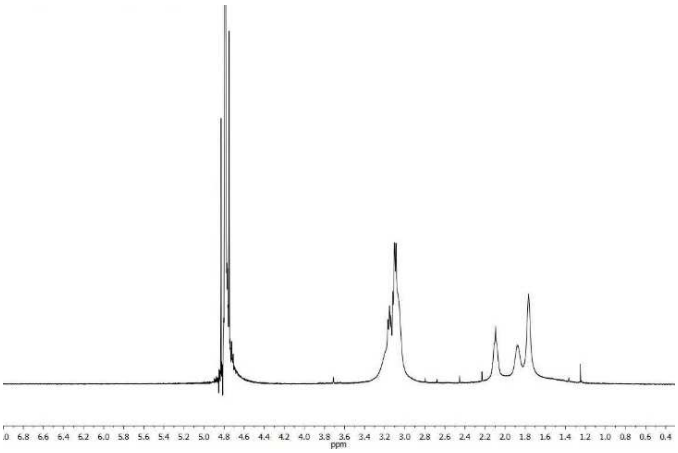

Figure S9. ^{1}H-NMR spectrum of P(SpAA) 3 (**1c**) TFA salt in D_2O.

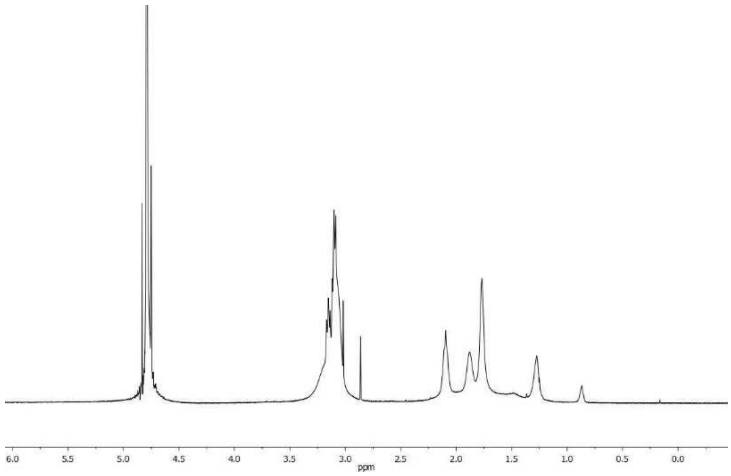

Figure S10. ^{1}H-NMR spectrum of P(SpAA-co-DAA) 1 (**2a**) TFA salt in D_2O.

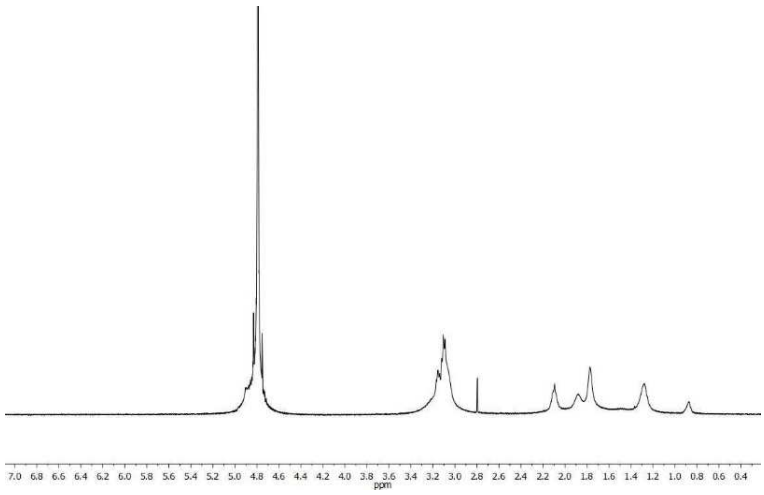

Figure S11. ^{1}H-NMR spectrum of P(SpAA-co-DAA) 2 (**2b**) TFA salt in D_2O.

2. GPC traces

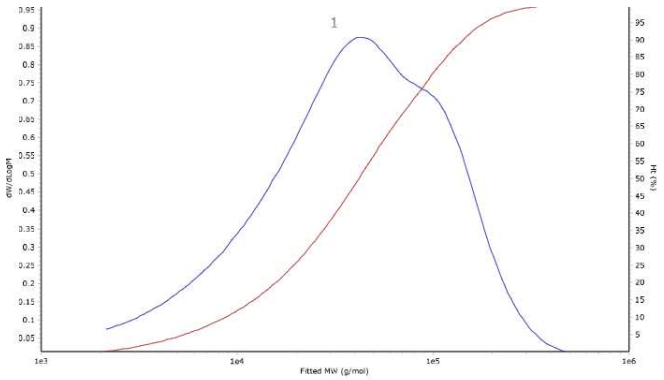

Figure S12. GPC trace of P(NAS) 2 measured via SEC in DMF.

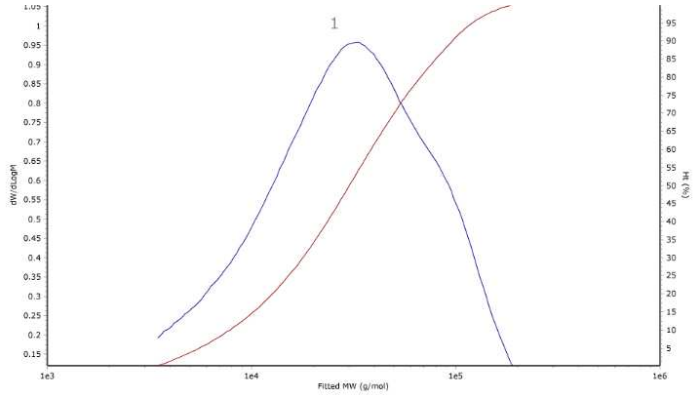

Figure S13. GPC trace of P(NAS) 3 measured via SEC in DMF.

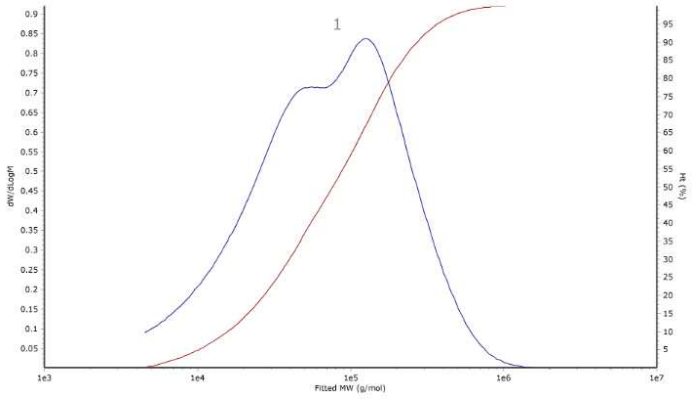

Figure S14. GPC trace of P(NAS-co-DAA) 1 measured via SEC in DMF.

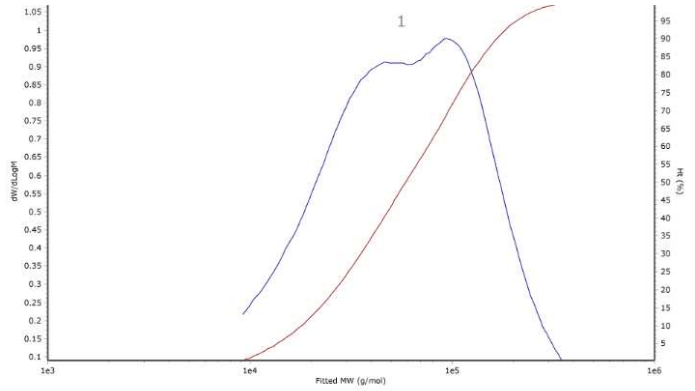

Figure S15. GPC trace of P(NAS-co-DAA) 2 measured via SEC in DMF.

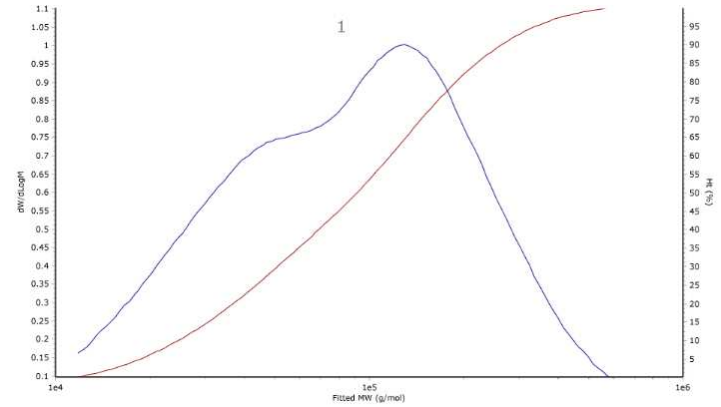

Figure S16. GPC trace of P(TBSpAA) 1 measured via SEC in DMF.

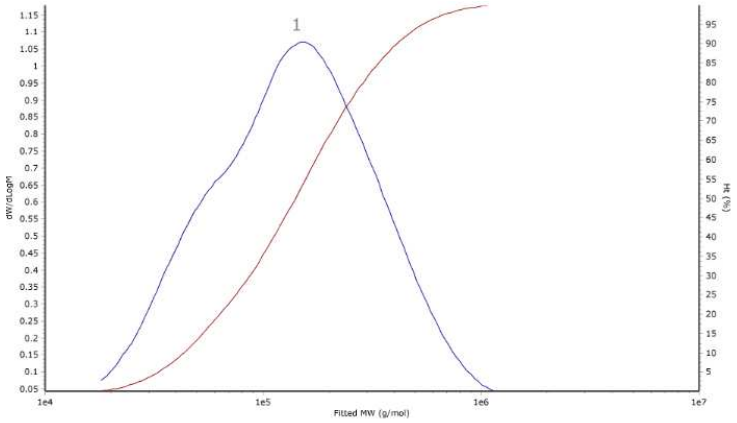

Figure S17. GPC trace of P(TBSpAA) 3 measured via SEC in DMF.

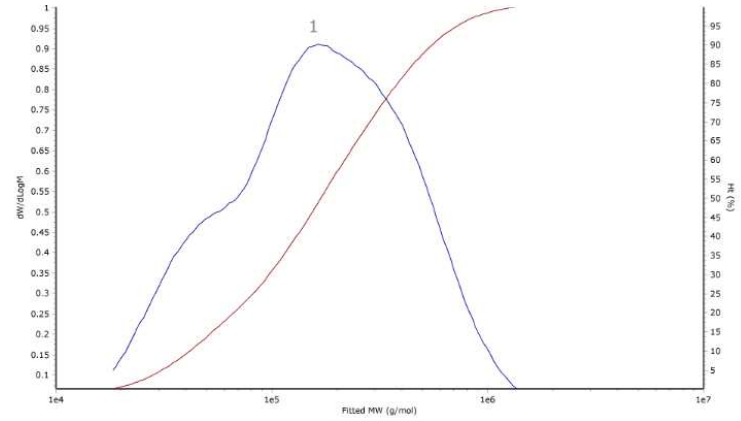

Figure S18. GPC trace of P(TBSpAA-co-DAA) 1 measured via SEC in DMF.

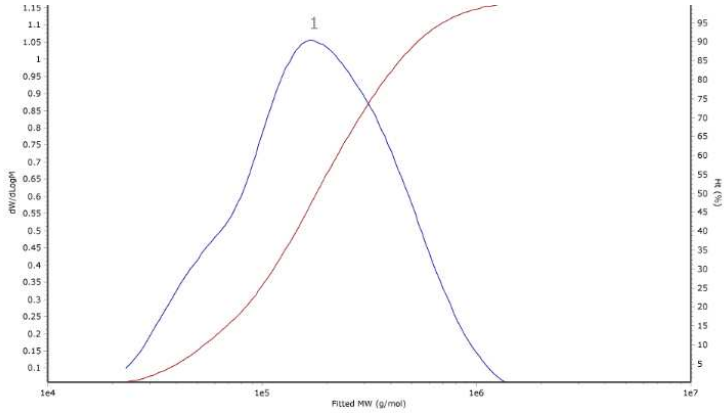

Figure S19. GPC trace of P(TBSpAA-co-DAA) 2 measured via SEC in DMF.

3. Molar masses and polydispersities

Table S1. Molar masses and polydispersities of polymers calculated via SEC.

Name	M_n [x10^3 g mol^{-1}][a]	Đ[a]	Name Postpoly.	M_n [x10^3 g mol^{-1}][a]	Đ[a]
P(NAS)1	24.0	2.46	P(TBSpAA)1	57.7	2.11
P(NAS)2	20.9	2.96	P(TBSpAA)2	39.3	2.08
P(NAS)3	18.8	2.24	P(TBSpAA)3	95.8	2.02
P(NAS-co-DAA)1	38.5	3.08	P(TBSpAA-co-DAA)1	10.3	2.37
P(NAS-co-DAA)2	40.5	1.93	P(TBSpAA-co-DAA)2	12.3	2.01

[a] M_n as obtained via SEC in DMF relative to polystyrene standards, Đ = M_w/M_n calculated via SEC in DMF or chloroform

Chapter III

Proteins as Functional Components of Nanoparticles for Brain Targeting

III.1 From Adsorption to Covalent Bonding: Apolipoprotein E Functionalization of Polymeric Nanoparticles for Drug Delivery Across the Blood-Brain Barrier

This chapter was published as progress report in the Journal Advanced Therapeutics:

Natascha Hartl, Friederike Adams and Olivia M. Merkel

"From Adsorption to Covalent Bonding: Apolipoprotein E Functionalization of Polymeric Nanoparticles for Drug Delivery across the Blood-Brain Barrier"

Advanced Therapeutics 2021,4: 2000092, https://doi.org/10.1002/adtp.202000092

Top Cited Article 2021/2022

Abstract

The blood-brain barrier (BBB) is composed of brain endothelial cells, pericytes, and astrocytes, which build a tight cellular barrier. Therapeutic (macro)molecules are not able to transit through the BBB in their free form. This limitation is bypassed by Apolipoprotein E (ApoE)-functionalized polymeric nanoparticles (NPs) that are able to transport drugs (e.g. dalargin, loperamide, doxorubicin, nerve growth factor) across the BBB via low density lipoprotein (LDL) receptor mediated transcytosis. Coating with polysorbate 80 or poloxamer 188 facilitates ApoE adsorption onto polymeric NPs enabling recognition by LDL receptors of brain endothelial cells. This effect is even enhanced when NPs are directly coated with ApoE without surfactant anchor. Similarly, covalent coupling of ApoE to NPs that bear reactive groups on their surface leads to significantly improved brain uptake while avoiding the use of surfactants. Several *in vitro* BBB models using brain endothelial cells or co-cultures with astrocytes/pericytes/glioma cells are described which provide first insights regarding the ability of a drug delivery system to cross this barrier. *In vivo* models are employed to simulate central nervous system-relevant diseases such as Alzheimer's or Parkinson's disease and cerebral cancer.

1. Introduction

According to the World Health Organization (WHO), approximately 20% of all humans suffer from damages of the central nervous system (CNS), such as depression, epilepsy, Parkinson´s disease, dementia/Alzheimer's disease, stroke, cerebral cancer or CNS-relevant metabolic diseases. Due to the strong protective function of the blood-brain barrier (BBB), the ability of therapeutic agents to reach their targets in the CNS is extremely limited. Less than 2% of small molecule drugs are able to cross this barrier with even lower numbers for macromolecules due to their high molecular weight [1]. Furthermore, those few drugs that are capable of crossing the BBB can be actively transported back into the vasculature by efflux transporters [2]. Consequently, the delivery and release of drugs into the brain is a challenging topic that requires specific systems for drugs to transit the BBB. In the past, several approaches have been tested to transiently open or to passage this barrier. Intrathecal or intraventricular injection of drugs represents an invasive method which has been used for chemotherapy with methotrexate or cytarabine/cortisol in patients with aggressive lymphoma or acute lymphatic leukemia [3]. With infusion of hyperosmotic solutions via the arteria carotis interna, a shrinkage of endothelial cells and opening of tight junctions is achieved [4]. This approach has clinically been used, but the unselective opening of the BBB was accompanied by the risk of edema formation [5]. Moreover, shear forces of microcurrents induced by applied focused ultrasound in the area of treatment cause a local disruption of the BBB, which was shown by the group of Treat in animal trials [6]. Schinkel et al. showed that the CNS concentration of various drugs is significantly increased by blockage or knock-out of efflux transporters in the BBB [7]. However, these transporters are also blocked in other barriers of the body leading to altered pharmacokinetics of many endogenous and exogenous compounds. Due to unspecific side effects of the above described disrupting methods, the design of efficient non-invasive nanocarrier systems that can facilitate controlled and targeted drug delivery to the specific regions of the brain is the goal of many current research efforts, but is also a major challenge [8]. As a promising nanocarrier system, liposomes have been investigated initially for small molecule drug encapsulation and delivery. To achieve specific targeting of the brain endothelium the transport pathway of receptor-mediated transcytosis (RMT) was utilized with these systems after surface modification with target seeking ligands [9]. Ligand-decorated liposomes bind to specific receptors, are endocytosed and the liposomal content is transported across the BBB [10]. As ligands directed against Transferrin receptors overexpressed on the BBB, i.e Transferrin receptor antibodies were coupled to liposomes [9].

Also the low density lipoprotein-(LDL) receptor family, a group of cell surface receptors that transport several macromolecules into cells, is expressed in several different tissues and can also be found in the brain [11]. These receptors play a crucial role in the homeostasis of triglycerides and cholesterol by mediating cellular uptake of apolipoprotein-containing lipoprotein particles [12]. An alternative to liposomes are polymeric nanoparticles (NPs), consisting of low-cost, stable, tailored and biodegradable materials, e.g poly(lactic-co-glycolic acid) (PLGA) or poly(n-butylcyanoacrylate) (PBCA), making them advantageous over liposomes [13]. Up to date, there is a very urgent need to also use macromolecules as therapeutics for CNS diseases. Promising compounds are high molecular weight biologicals, e.g antibodies for Alzheimer's disease and multiple sclerosis, enzymes for lysosomal storage diseases or peptides for ischemic brain diseases [14]. Especially polymeric NPs systems provide a promising delivery tool for embedding these macromolecules as well as small molecule drugs. The following progress report will focus on the latest developments in LDL receptor mediated brain targeting with ApoE-functionalized polymeric NPs. Special emphasis is given on the different polymeric materials, encapsulated drugs, *in vitro* BBB models and *in vivo* setups simulating different CNS-relevant diseases.

2. Blood-brain barrier

2.1 Structure and physiological function of the blood-brain barrier

The CNS is the most critical and sensitive organ in the human body and needs a regulated extracellular environment. Neurons, astrocytes, endothelial cells of the BBB, myocytes, pericytes and extracellular matrix components form the neurovascular unit (NVU) that serves to maintain CNS homeostasis. The capillaries of the CNS have evolved to restrain the movement of molecules and cells between blood and the brain. The BBB is a highly regulated and efficient biological barrier between the peripheral circulation and the CNS. The BBB controls brain homeostasis as well as ion and molecule movement and protects the brain against metabolites, xenobiotics, pathogens and a multitude of drugs. The cellular barrier of the BBB is composed of brain microvessel endothelial cells, pericytes, as a second line of defense, and astrocyte end feet, which tightly ensheath the vessel wall (Figure 1). Pericytes are known to have various functions in the CNS such as modulation of endothelial permeability, stabilization of microvessel walls by intimate contact to endothelial cells, supply of BBB-specific enzymes and phagocytotic activity. Astrocytes, solely or in combination with neurons, act as mediators in regulation of CNS microvascular permeability. Their end feet cover pericytes and endothelial

cell walls, release trophic factors that are essential for the induction and maintenance of the BBB and are involved in water and ion balance regulation [15]. BBB endothelial cells differ from endothelial cells in the rest of the body by the absence of fenestration and presence of extremely tight junction complexes in the inter-endothelial space that includes tight junction proteins, adhesion junctions, junctional adhesion molecules and accessory proteins. The presence of junction complexes and the lack of aqueous pathways between cells greatly restricts permeation of polar solutes through paracellular diffusional pathways from the blood plasma to the brain extracellular fluid [16]. The tight junctions consist of three integral membrane proteins, namely, claudin, occludin and junction adhesion molecules (JAM) and a number of cytoplasmatic accessory proteins including zonula occludens proteins and cingulin [15]. Occludin appears to be a regulatory protein that can alter the paracellular permeability. JAM is involved in cell-to-cell adhesion and monocyte transmigration through BBB [17]. All described components are essential for the normal function and stability of the BBB.

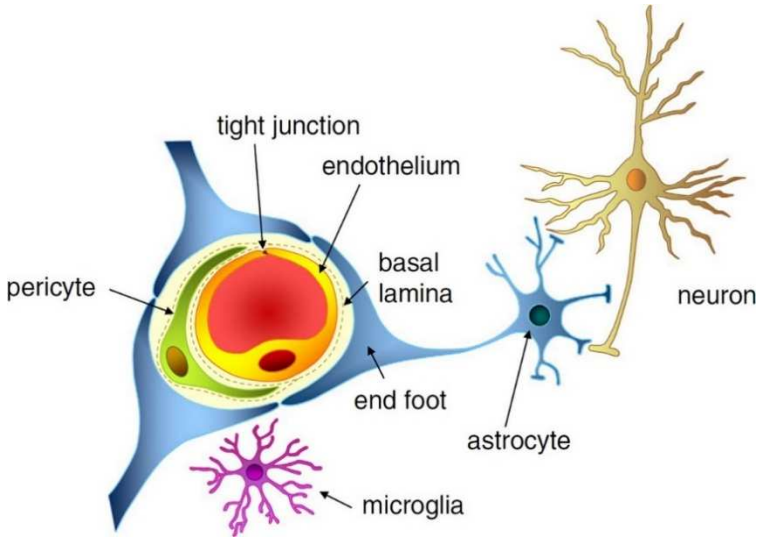

Figure 1. The neurovascular unit and structures that contribute to the BBB i.e., endothelial cells, tight junctions, pericytes, and astrocytic end feet. With permission from Ref. 117. Copyright 2013, John Wiley and Sons.

2.2 Transport routes across the BBB

Substances can cross the BBB via different pathways (Figure 2). The first route is paracellular transport, which involves passing in between the endothelial cells across the tight junctions. Through simple passive diffusion water and small water-soluble substances are capable of passing the BBB (Figure 2, A). The second pathway is transcellular transport and occurs via diffusion of small lipophilic gases and some lipid-soluble compounds, such as alcohol and steroid hormones, from the endothelial cells into the brain stroma in a passive way (Figure 2, B) [8]. Larger and more hydrophilic nutrients and metabolites, that are essentially required by

the nervous tissue, need to be taken up in an active way [18]. Therefore, specific transport mechanisms for these active pathways, i.e., carrier-, receptor-, and adsorptive-mediated transcytosis or efflux transporters, are embedded in the BBB to guarantee an adequate supply and export of these substances [19]. In case of carrier-mediated transcytosis (CMT), solutes such as glucose, amino acids or essential fatty acids bind to a transport protein which is embedded in the membrane of the endothelium (Figure 2, C). This interaction leads to a change in the carrier protein conformation, resulting in transport through the endothelial cell along or against a concentration gradient [8]. Specific efflux transporters, inserted predominantly in the apical membrane, act as extremely efficient efflux pumps and are capable of rapidly pumping back potentially toxic components into the blood stream (Figure 2, D). These efflux transporters include members of the ATP-binding casette (ABC) gene family, e.g., P-glycoprotein, multidrug resistance proteins (MRPs) and breast cancer resistance proteins (BCRP) that are highly overexpressed by endothelial cells of the BBB [20]. The vesicular mechanism that provides the main route for the entry of macromolecules, such as proteins, into the brain involve either receptor-mediated transcytosis (RMT) or adsorptive-mediated transcytosis (AMT). In RMT, binding of macromolecular ligands to specific receptors on the cell surface triggers endocytosis (Figure 2, E). Receptors and their bound ligands form complexes that are internalized into the endothelial cells as pinocytotic vesicles. These vesicles move through the cytoplasm to the basolateral sides of the endothelial cells where they are exocytosed. Dissociation of the ligand-receptor complex presumably occurs during cellular transit or exocytosis [21]. So far, several receptors have been identified that can initiate RMT, e.g., insulin, epidermal growth factor, Transferrin and LDL-related protein receptors [22]. AMT is induced by ligands bearing a positive charge, so that they can interact electrostatically with negatively charged cell surface binding sites and subsequently are absorbed and transcytosed (Figure 2, F) [23]. In both pathways, the degradative lysosomal compartment within the cell needs to be avoided to ensure entry of intact compounds to the brain [24].

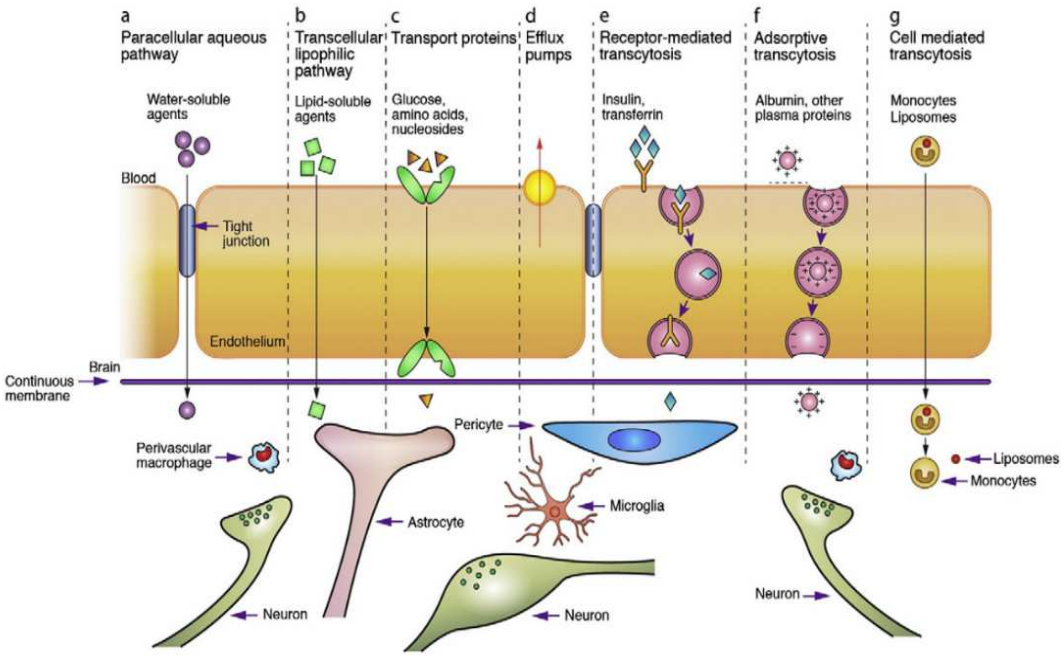

Figure 2. Different transport pathways to passage the BBB. With permission from Ref. 8. Copyright 2012, Elsevier.

3. Apolipoprotein E and its associated receptors

3.1 Apolipoprotein E

Lipoproteins are biological carriers transporting both lipids and proteins systemically through the body. Lipoproteins, which consist of lipids and proteins, are classified based on the proportions of these two substances and their density into five main categories, namely chylomicrons, very low-density lipoproteins (VLDL), intermediate-density lipoproteins (IDL), LDL and high-density lipoproteins (HDL) [11a]. Lipoproteins are composed of an insoluble core of cholesteryl ester and triglycerides surrounded by a shell of amphiphilic phospholipids and specialized proteins called apolipoproteins (Apo) [25]. Plasma lipoprotein metabolism is regulated and controlled by these specific apolipoprotein parts, as they are involved in the redistribution of lipids among cells and tissues, in the maintenance of the lipoprotein structures as well as in enzyme activation levels. The most common apolipoproteins are ApoE, ApoB, ApoA-I, ApoA-IV, ApoC-I, ApoC-II and ApoC-III [26]. Apolipoprotein E (ApoE) is a component found in lipoprotein classes VLDL and chylomicrons. Therefore, the major function of ApoE is the transport of triglycerides and cholesterol from sites of synthesis or adsorption to sites of utilization (peripheral tissues) or excretion (liver) [27]. ApoE-mediated lipid transport and delivery into cells operates mainly via two receptor-mediated pathways: on the one hand via the LDL receptor and on the other hand via the LDL receptor-related protein (LRP) receptor,

which was recently discovered [22]. Lipoprotein-binding to the receptors induced by interactions with ApoE initiates an endocytotic cellular uptake of the ligand – receptor complex and degradation of the lipoproteins within the cells [28]. Lipoprotein metabolism is influenced by the primary, secondary and supramolecular apolipoprotein conformation in solution [29]. ApoE is composed of 299 amino acids possessing a molecular mass of approximately 34 kDa [30]. The secondary structure of ApoE possesses two separate structural domains: the amino terminal two-thirds of the molecule and the carboxy-terminal one-third of the molecule, connected by a hinge region (Figure 3). The amino-terminal domain, composed of a four-helix bundle, contains lysine and arginine rich receptor-binding sites, whereas the carboxyl-terminal domain includes the major lipid-binding site located in amphipathic alpha-helices. The three major isoforms (ApoE2, -E3 and -E4) differ only in single amino acid substitutions at two positions, which profoundly affect their structures and explain their different ability to bind lipids and receptors [31].

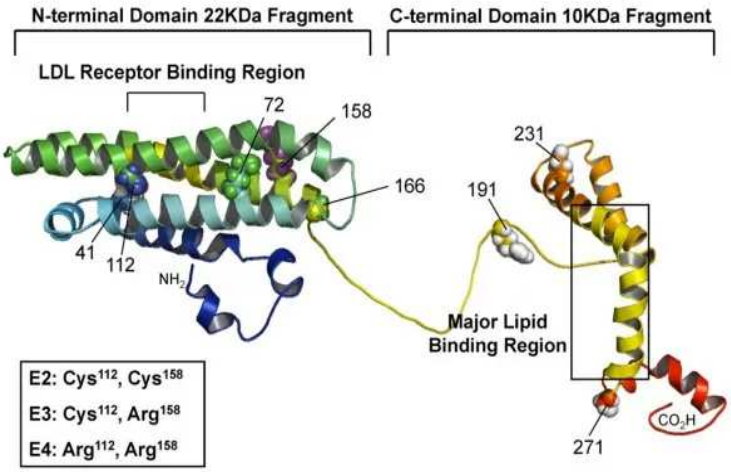

Figure 3. Structure of ApoE. Reprinted with permission from Ref. 118.

3.2 LDL and LRP receptors

The groups of LDL and LRP receptors belong both to the LDL receptor family, a group of cell surface receptors that transport several macromolecules into cells. In humans, the LDL receptor family includes in addition the very low-density lipoprotein (VLDL), the ApoER2 and the sorLA/LRP11 receptors. Each member is expressed in several different tissues, has a wide range of suitable ligands and is involved in various physiological functions [11]. LDL receptors are mainly expressed by liver and adrenal tissues, but can, amongst others, also be found in the brain, lung, heart and kidney. LRP receptors are highly expressed in liver, brain and lung tissues [11a]. The LDL and LRP receptors play a crucial role in the homeostasis of triglycerides and

cholesterol by mediating cellular uptake of ApoE (and also ApoB in case of LDL receptor)-containing lipoprotein particles. The receptors consist of several distinct domains with individual function. The LDL receptor ligand binding domain, a cluster of seven complement-like cysteine-rich repeating units can be found on the extracellular side. This domain is followed by a sequence with similarities to the membrane-bound precursor of the epidermal growth factor (EGF) which is important for ligand uncoupling in acidified endosomes [12]. The receptor is anchored in the plasma membrane by a third important functional region, followed by several cytoplasmatic domains for endocytosis and interaction motifs for a variety of cytoplasmatic adaptor and scaffolding proteins. The LRP receptor is more complex and larger than the LDL receptor [32]. In contrast to the LDL receptor, which specifically interacts with ApoE and ApoB ligands, the LRP receptor is a multifunctional multi-ligand receptor and is therefore able to bind several ligands, such as ApoE, plasminogen activators and protease/inhibitor complexes [11a]. So far, controversial information has been reported regarding the function of the LRP receptor in literature. In several studies LRP1 is described as the main brain clearance receptor, especially in the case of amyloid β (Aβ) peptides [11b,c]. However, other studies indicate that LRP1 is more likely expressed in pericytes than in endothelial cells and may not be involved in the efflux of Aβ peptides on the endothelial level [11d]. This discrepancy could be related to the different cell models used and points out that the function of the receptor is not yet fully clarified. As lipoprotein transport across the BBB is of crucial importance for the delivery of essential lipids to the brain, endothelial cells of the BBB are equipped with LDL and LRP receptors [33]. An ApoE-based transport system which is recognized by LDL receptors offers the possibility to traffic substances across the BBB and therefore provides a highly promising pathway for drug delivery into the brain.

4. Approaches for ApoE-functionalization of polymeric nanoparticles

Organ distribution of drug-loaded NPs, in this regard also for reaching the brain, is regulated by the immediate adsorption of plasma proteins onto these particles after intravenous injection [34]. These protein adsorption patterns on the surface can depend on the physicochemical characteristics of the particles [35]. Thereafter, amount of proteins as well as adsorption of specific proteins influence macrophage uptake and in turn the organ distribution [34]. In addition, uptake into different organs can be shifted by attachment of receptor-specific ligands to the particles.

4.1 Surfactant-based approach

4.1.1 Initial protein adsorption experiments using model carrier

First attempts on organ biodistributions with surfactant-coated polymers were performed by Illum and Davis using poly(styrene) (PS) as a model carrier (Figure 4). PS is a hydrophobic, but not biodegradable polymer, which was coated with poloxamer or poloxamine followed by intravenous injection. As a consequence of coating, nanoparticle uptake was shifted from reticuloendothelial system (RES)-organs (liver and spleen) to other tissues [36].

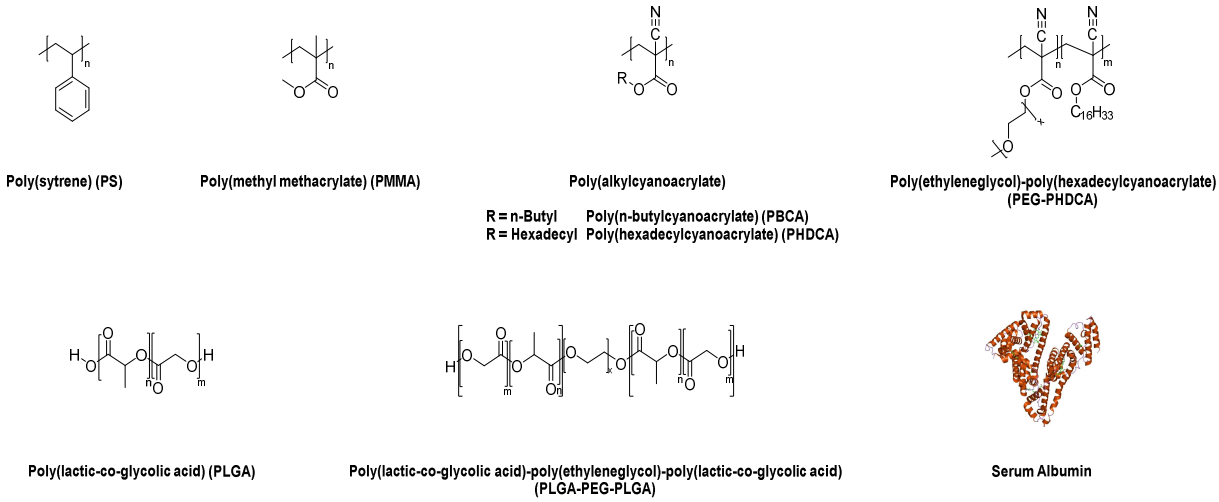

Figure 4. Commonly used (bio)polymers for investigation on ApoE-mediated brain targeting.

The specific adsorption pattern of proteins was tested in 1993 by Müller et al. with well-defined hydrophobic polystyrene beads using poloxamers [34]. Poloxamers adsorb with their hydrophobic part (poly(propylene oxide) (PPO)) at the nanoparticle, whereas the hydrophilic part (poly(ethylene oxide) (PEO or PEG) protrudes into the dispersion medium, exposing a hydrophilic surface, which can be modified when using poloxamers with different polarity by varying hydrophobic/hydrophilic ratio (Figure 5).

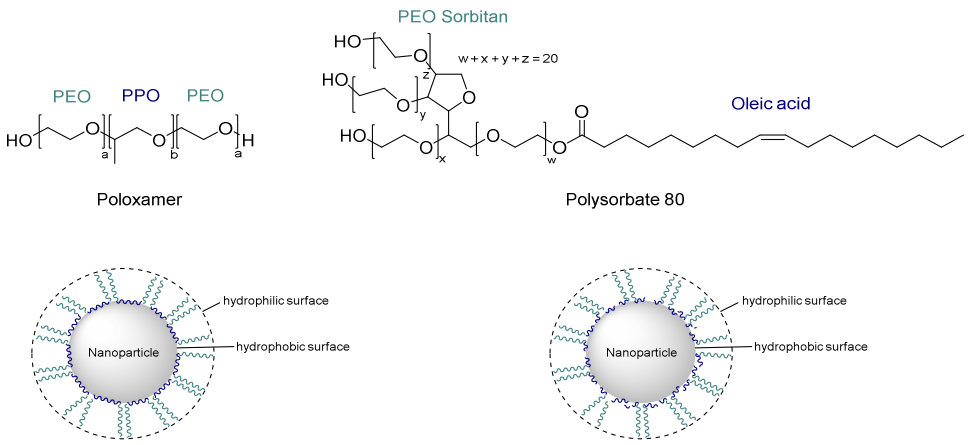

Figure 5. Poloxamer- and polysorbate-coating of hydrophobic nanoparticles [34].

These differently constituted poloxamers facilitate the adsorption of specific proteins. To determine amounts of adsorbed proteins (e.g., albumin, fibrinogen, apolipoproteins), the patterns of protein adsorption onto coated beads were analyzed after incubation with plasma by high-resolution two-dimensional polyacrylamide gel electrophoresis (2-D PAGE). Increased amounts of proteins on the surface in comparison to the amount of these proteins in the plasma were found for e.g., Transferrin or ApoC-III, which are proteins facilitating receptor-mediated uptake of nanoparticles. In general, the amount of an adsorbed protein is related to surface hydrophobicity. Over-proportional fractions were found for ApoE on particles with the lowest hydrophilicity (Figure 6, A). In contrary, quantitative differences for single proteins could not solely be correlated to the differences in surface hydrophobicity. Therefore, only measuring surface hydrophobicity is not sufficient for statements about protein adsorption patterns [34]. The same group further intensified their studies on adsorption of plasma proteins on various surfaces by synthesizing polymers in a very complex and multifaceted approach. Five different latex type particles using styrene and different functionalized (meth)acrylates with different hydrophobicities, surface properties and surface charges were obtained. Protein adsorption onto these colloidal surfaces depended on surface properties such as hydrophobicity, charge density, and accessibility due to sterical hinderance of the surface groups. Apolipoproteins were adsorbed in slightly higher amounts on type 4 latex particles which bear different functional groups (OH, NR3) located at the end of flexible polyethylene glycol (PEG) chains. The PEG chains seem to protect the surface of the particles against adsorption of larger proteins. Hence, small proteins, such as apolipoproteins, despite having a lower affinity to the surface, probably could adsorb to binding sites of particle type 4, when they are not occupied by larger proteins. Nevertheless, the impact of apolipoproteins on the total adsorbed protein amount was very low compared to that of the larger proteins [35].

First attempts in determining *in vivo* organ distribution were realized with coated and uncoated radiolabeled poly(methyl methacrylate) (PMMA) particles (Figure 4). 14C-labeled nanoparticles were prepared by radiation-induced polymerization of methyl[2-14C]methacrylate [38]. Coating was performed with non-ionic surfactants such as poloxamers/poloxamines, polysorbates or polyoxyethylene lauryl ether [37]. A prolonged circulation time in the blood stream was induced by steric repulsion of these surfactant-coated PMMA NPs and led to reduction of adsorption onto surfaces of macrophages. Thus, a lower particle concentration in RES organs and tissues such as liver, spleen, bone marrow and lymph nodes was observed. Significantly higher levels in the blood and non-RES organs (heart, gastrointestinal tract, ovary, kidneys, muscles and brain) were obtained after coating with either

surfactant. Poloxamer and poloxamine (i.e. poloxamer 338 and poloxamine 908) were the most efficient ones in decreasing liver uptake, while increasing the blood levels of NPs by a factor of 100 or higher. In the brain, the uptake of nanoparticles was increased for all surfactants up to 13-fold, especially nanoparticle coatings with polysorbate 80 and 60 and different poloxamers, except poloxamer 188, were the most efficient [37].

These surfactant-coated radiolabeled PMMA NPs were also tested in an uptake study using bovine microvessel endothelial cell (BMEC) monocultures. Coating with polysorbate 80, the most efficient surfactant for *in vivo* brain targeting, showed also a promising performance in *in vitro* nanoparticle uptake, which was enhanced by a factor of 5 compared to the control group (uncoated PMMA NPs). However, distinction between uptake and cell attachment could not be made using their experimental setup [39].

4.1.2 Poly(alkylcyanoacrylates)

Not only the surfactant, but also the type of solid particle, i.e. the hydrophilicity of the particle, has an influence on the body distribution. Because PMMA and PS are quite similar regarding their hydrophobicity, similar affinity to surfactants was expected [40]. Poly(alkylcyanoarylates), especially PBCA (Figure 4), show a much higher hydrophilicity. In addition, a very rapid degradation via ester hydrolysis was confirmed, so that drug release for these polymers occurs due to degradation [41]. In addition, *in vivo* and *in vitro* studies demonstrated that PBCA is non-toxic, but until now poly(alyklcyanoacrylates) are not approved for intravenous administration by the US Food and Drug Administration (FDA) [42].

First attempts to use PBCA NPs for transport of drugs across the BBB were performed with the hexapeptide dalargin. The analgesic effects of this drug were studied simultaneously by two independent groups using different pain assessment methods (tail flick test [43] vs. hot-plate test [44]). Both drug delivery systems consisted of PBCA, dalargin and polysorbate 80. Nanoparticles were prepared using n-butyl cyanoacrylate and dextran 70000 as stabilizer in an acidic polymerization medium. The peptide dalargin was then adsorbed onto the nanoparticle surface and afterwards polysorbate 80 was added. These studies demonstrated that binding of dalargin to the PBCA NPs as well as coating of these NPs with polysorbate 80 are mandatory to promote dalargin uptake into the brain [43-45]. In a further in-depth study, 12 different surfactants for coating onto dalargin-containing PBCA NPs were tested. Solely polysorbate coating with polysorbate 20, 40, 60 and 80 had a significant effect on the successful passage of dalargin across the BBB *in vivo*, in which polysorbate 80 was the most efficient one. In addition, NPs with polysorbate 80 coating, but without dalargin had no effect. The authors suggested a

specific alteration of the PBCA surface properties due to coating with polysorbates. In accordance with previous studies, adsorption of only specific substances from the blood which induce endocytosis from the blood by the endothelial cells of the BBB was assumed [46]. Body distribution of ^{3}H-dalargin-loaded, polysorbate 80-coated PBCA was analyzed after intravenous injection into mice. Radioactivity levels, caused by ^{3}H-dalargin, were three-times higher in the brain and reduced in the liver when the drug-loaded and polysorbate-coated PBCA NPs were used [45, 47].

The influence of polysorbate 80-coated and uncoated PBCA NPs on the BBB integrity of porcine brain capillary endothelial cells (PBCEC) cultured on microporous Transwell® filter inserts was studied via transendothelial electrical resistance (TEER) measurements. The integrity of the BBB was also analyzed by measuring the passage of ^{14}C-sucrose and FITC-BSA (fluorescein isothiocyanate labelled bovine serum albumin) as reference substances. The application of polysorbate 80-coated PBCA NP led to a reversible disruption of the barrier. After 24 h the TEER of cells treated with 13 µg/mL NP recovered to about 80% of the starting value. Further lowering the NPs concentration led to a nearly complete recovery of the barrier integrity. The obtained increased permeability of ^{14}C-sucrose and FITC-BSA about 4 h after nanoparticle application were conflicting with other measurements regarding the permeability of the BBB after treatment with polysorbate 80-coated PBCA [48]. Another criticism that brain delivery with polysorbate 80-coated PBCA NPs occurs due to toxic effects of the carrier arose after using an *in vitro* BBB model of a coculture of bovine brain capillary endothelial cells (BBCEC) and rat astrocytes. The observed toxicity led to opening of the tight junctions allowing the penetration of drugs through the BBB and thus leading to therapeutic limitations of PBCA NPs when NPs with concentrations of 10 µg/mL and above were used [49]. As a consequence of these statements, prior binding of dalargin to the nanoparticles is not mandatory and the drug can also diffuse into the brain after carrier-induced opening of the tight junctions when polymer and drug are injected shortly after each other. This assumption was rejected by Begley and coworkers in 2002 using *in vivo* and *in vitro* human, bovine, and rat models. In order to evaluate this hypothesis *in vivo*, free dalargin was injected intravenously into mice after the injection of polysorbate 80-coated, but empty NPs. Analgesic effects were only obtained when the drug was adsorbed onto the NPs and the thesis of diffusional dalargin entry was not supported. *In vitro*, the permeability of ^{14}C-sucrose and ^{3}H-inulin, as model substances, was not changed after PBCA preincubation at concentrations of 10 or 20 µg/ml. Incubation of uncoated and polysorbate-80-coated PBCA NPs showed a normal morphology of the endothelial cells, again emphasizing a lack of toxicity. The bovine endothelial cells appeared intact without any

evidence of available paracellular pathways. However, the authors observed undefined changes at the cell membranes by electron microscopy when using polysorbate-80-coated PBCA NPs [50].

Cultured microvessel brain endothelial cells of human and bovine origin were used, to gain deeper insights into the uptake mechanism of polysorbate 80-coated PBCA NPs. These cells express high levels of LDL receptor, which seems to play an important role in the uptake of polysorbate 80-coated NPs, due to adsorption of apolipoproteins onto the NPs' surface. Indeed, the uptake of polysorbate-coated PBCA NPs in these cells was 20-times higher compared to uncoated counterparts. Inhibition experiments revealed that nanoparticles were taken up via an endocytic mechanism. Phagocytosis, which is caused by apolipoprotein components, provoked uptake. This was concluded because uptake was inhibited by cytochalasin, a phagocytic uptake inhibitor. Pinocytosis was not observed, since uptake was not inhibited by colchicin, a pinocytic uptake inhibitor [13].

Besides intravenous injection, oral delivery of dalargin-loaded PBCA NPs coated with polysorbate 80 was tested as another administration route. For comparison reasons, dalargin-bound PBCA NPs were applied intravenously and orally and *in vivo* dalargin-induced analgesia was used to amount the efficiency of BBB passage by hot-plate test. PBCA NPs were prepared in acidic medium using polysorbate 85, dextran 12000 or poloxamer 188 as stabilizers. Similar to the before mentioned methods, dalargin was subsequently attached to the nanoparticles before coating with polysorbate 80 was performed. Polysorbate 85-stabilized, dalargin-loaded, but uncoated PBCA NPs were able to induce analgesic effects in mice after intravenous and oral application even when NPs were not coated. Dextran 12000 or poloxamer 188-stabilized, dalargin-loaded, uncoated NPs showed no significant effect after oral administration [51]. Oral administration was also tested with double-coated dalargin-loaded PBCA NPs. Tail-flick tests showed that dalargin-induced analgesia was higher with PBCA NPs prepared with double-coating of polysorbate and PEG compared to single-coating. As a result, surfactant-coated PBCA NPs are able to cross the gastrointestinal barrier after oral administration. Nevertheless, the exact mechanisms of nanoparticular uptake through the gastrointestinal barrier was not elucidated [52].

4.1.3 Poly(lactic-co-glycolic acid)

Poly(lactic-co-glycolic acid) (PLGA) is considered for brain targeting across the BBB due to FDA approval of other drug formulations containing PLGA for human use combined with conducive biocompatibility and biodegradability profiles (Figure 4) [53]. The first study on

surfactant-coated, drug-loaded PLGA NPs for brain delivery after intravenous injection was performed by Kreuter et al. in 2010 with poloxamer 188 and polysorbate 80 as surfactants. The PLGA NPs were prepared by a multistep emulsification–solvent evaporation technique with different modifications depending on which drug was used (i.e. doxorubicin or loperamide). For PLGA, the most efficient brain delivery was achieved by binding of these drugs to poly(vinyl alcohol) (PVA)-stabilized NPs coated with poloxamer 188. The anti-tumor effect of doxorubicin was evaluated in a rat model of glioblastoma. To compare PLGA to PBCA NPs, experiments were planned similarly to PBCA experiments regarding surfactants, drugs and animal models. For both polymers, uncoated NPs were ineffective. Coating with polysorbate 80 led to highest efficiencies for PBCA NPs, whereas poloxamer 188-coating performed best for PLGA NPs [54].

The mechanism by which doxorubicin-loaded poloxamer 188-coated PLGA NPs enter brain tumor cells was elucidated by uptake experiments in human glioblastoma cells without investigating the passage of the BBB. The main mechanism of the NP internalization was clathrin-mediated endocytosis. It was demonstrated that the main mechanism of release of the drug was due to doxorubicin diffusion from the NPs rather than by intracellular degradation of the polymer, because free doxorubicin reached the nuclei, whereas PLGA was still present in the endosomes/lysosomes [85].

A similar drug delivery system was developed by Lee et al. who used poly(lactide-co-glycolide)-poly(ethylene glycol)-poly(lactide-co-glycolide) (PLGA-PEG-PLGA) triblock copolymers (Figure 4). This polymer was synthesized by ring-opening polymerization using PEG as a macroinitiator. Loperamide-loaded PLGA-PEG-PLGA (PEP) NPs were prepared by a nanoprecipitation method and then the NPs were coated with poloxamer 188 or polysorbate 80. For an *in vitro* BBB penetration study, a co-culture of immortalized rat brain endothelial cell line and C6 glioma cells was established. It was shown that surfactant-coated PEP NPs had a better penetration than uncoated PEP NPs and poloxamer 188-coated PEP NPs showed higher cellular uptake than polysorbate 80-coated ones. However, the group did not include TEER measurements during their study to validate the intact co-culture setup [55].

4.1.4 Other Materials

In addition to the before mentioned polymers, individual investigations were also performed with other polymeric NPs (Table 1 and 2).

Polycaprolactone (PCL) NPs loaded with the small drug pentamidine were compared to liposomes regarding *in vitro* transport across the BBB with the aim of treating Human African

Trypanosomiasis. These pentamidine-loaded PCL NPs were obtained by double solvent evaporation method. Polysorbate 80 was used as a surfactant to obtain ApoE adsorption facilitating transport across the BBB. The study revealed that liposome nanocarriers were able to transport a larger dose percentage of pentamidine compared to PCL NPs and that drug loading in PCL NPs needed optimization [56]. Based on these observations, PCL NPs seem not to exhibit the desired carrier properties for drug delivery across the BBB.

Superparamagnetic iron oxide nanoparticles (SPIONs) decorated with PEG, poly(ethylenimine) and polysorbate 80 resulting in Tween-SPIONs were prepared for brain targeting. Intravenously administrated Tween-SPIONs actively crossed the BBB of rats under an external magnetic field (EMF), and a significant amount of SPIONs was found in the cortex. Both, the surfactant and the magnetic field, played a crucial role in transportation of SPIONs across the BBB. It was suggested that the positively charged Tween-SPIONs adsorb apolipoproteins in the blood. With the assistance of EMF, the contact with the endothelial cells is improved promoting receptor-mediated endocytosis [57]. A similar approach was conducted with magnetic nanoparticles (MNPs) made from PS nanospheres. These Fe_3O_4/PS nanospheres were suspended in a polysorbate aqueous solution and can cross the intact BBB after intravenous injection when subjected to an EMF. The role of the surfactant was not discussed in this manuscript. In addition, a large fraction of the magnetic NPs was cleared from the circulation by liver and spleen [58].

4.2 Direct coating with ApoE

To further investigate the involvement of apolipoproteins in the transport of drug-loaded NPs across the BBB, dalargin- and loperamide-loaded PBCA NPs were directly coated with apolipoproteins AII, B, CII, J and E with and without additional precoating with polysorbate 80 (Figure 6, B). Afterwards, these different nanoparticular formulations were intravenously injected into mice and their efficiency was calculated by tail-flick test, since both drugs induce an analgesic effect. It was shown that solely drug-bound NPs coated with polysorbate 80 and/or with ApoB or ApoE induced the desired effects [59]. In general, these effects were higher in case of ApoE-functionalization than with ApoB, making ApoE an ideal candidate for brain targeting across the BBB. The most pronounced effect was observed after precoating with polysorbate 80 and additional coating with apolipoproteins, caused by additional adsorption of apolipoproteins from blood plasma after intravenous injection [59-60]. These finding were substantiated by *in vivo* experiments with genetically modified ApoE-deficient mice in which drug-containing NPs showed lower effects compared to experiments using non-modified mice.

These experiments confirm the suggestion that apolipoproteins are involved in the uptake mechanism of polysorbate 80-coated NPs by adsorption of these proteins from the blood after intravenous injection. ApoE-functionalized NPs mimic lipoproteins that are able to enter the brain capillary endothelial cells via LDL receptor-mediated endocytosis. Drugs are then further transported by diffusion or by transcytosis. The authors also mentioned in this context that apolipoproteins only facilitate the interaction with the endothelial cells, but are not taken up together with the NPs [59].

One approach to directly coat NPs with ApoE was carried out by Kuo et al. using rosmarinic acid-loaded poly(acrylamide)-chitosan-poly(lactide-co-glycolide) (RA-PAAM-CH-PLGA) NPs anchoring two targeting biomolecules. Rosmarinic acid, an antioxidant with antiallergenic and anti-inflammatory activity was encapsulated for the potential treatment of Alzheimer's disease. Cross-reacting material 197 (CRM197), a ligand of the diphtheria toxin receptor, and ApoE, which can recognize LDL receptors, were expected to facilitate transcytosis across brain-microvascular endothelial cells. PLGA was used as the hydrophobic core and hydrophilic PAAM and chitosan entrapped the drug. The polymeric nanocarriers were prepared by a complex method consisting of microemulsion, solvent diffusion, grafting, and surface modification to obtain CRM197-ApoE-RA-PAAM-CH-PLGA NPs. For uptake experiments RAW264.7 cells and for viability and permeability measurements SK-N-MC cells and co-cultures of human BMECs (HBMECs) and astrocytes were used. The results revealed that a higher PAAM-percentage decreased the grafting efficiency of CRM197 and ApoE. Additionally, an increase in CRM197 and ApoE enhanced the ability of rosmarinic acid to cross the BBB and inhibited apoptosis of Aβ-insulted SK-N-MC cells to a larger extent [61].

4.3 PEG approach

An advanced system was developed by Couvreur et al. who incorporated PEG-chains to poly(alkylcyanoacrylates) to induce an *in vivo* long-circulating ("stealth") effect and investigated the biodistribution of such systems after intravenous administration to mice. PEG-cyanoacrylate copolymers were prepared by condensation of methoxy-poly(ethylene glycol)cyanoacrylate and [3-^{14}C]-n-hexadecyl-cyanoacrylate in different ratios (Figure 4). It was observed that these [^{14}C]-radiolabeled PEGylated poly(hexadecylcyanoacrylate) (PEG-PHDCA) NPs remained longer in the blood circulation and had a reduced cytotoxicity compared to non-PEGylated PHDCA NPs which were cleared in a few minutes [62]. Further increasing the PEG-amount in the PEG-PHDCA copolymers had no effect on *in vivo* blood circulation time in this study, but had a positive effect regarding toxicity in *in vitro* studies on

PEG-coated poly(alkylcyanoacrylates) [62-63]. Liver accumulation was drastically reduced, however an increased spleen uptake was shown [62]. Accumulation in the brain was first tested with these systems in 2001 by the same group by investigating biodistribution profiles, brain concentrations and brain distributions of radiolabeled PEG-PHDCA in comparison to polysorbate 80- or poloxamine 908-coated PHDCA NPs *in vivo* in rats and mice. Based on the before observed long-circulating characteristics of PEGylated PHDCA NPs, these NPs enter the brain to a larger extent than NPs without PEGylation or with surfactant-coated NPs. In addition, the stealth effect was more pronounced in mice than in rats. BBB permeability was not influenced after injection of PEG-PHDCA as measured *in vivo* by diffusion of ^{14}C-sucrose into the brain [64]. Detailed analytical investigation on absorbed proteins on the surface of PEG-PHDCA NPs after incubation with serum revealed that ApoE and ApoB adsorbed more onto PEGylated PHDCA than on unmodified PHDCA NPs (Figure 6, C). As a consequence, ApoE or ApoB-100 preadsorbed onto PEG-PHDCA NPs were more efficient than unmodified PEG-PHDCA in penetrating into rat brain endothelial cells, suggesting the involvement of LDL receptor-mediated endocytosis also for PEGylated PHDCA [65]. In addition, cellular uptake was also increased with increasing the concentrations of ApoE in ApoE-preincubated NPs.

Inhibition of the cellular uptake of fluorescent-labeled PEG-PHDCA NPs with chlorpromazine and sodium azide, which inhibit clathrin and energy-dependent endocytosis, respectively, caused a significant decrease in uptake. Inhibition of the caveolae-mediated pathway by preincubation with filipin and nystatin did not alter the cellular uptake. The confirmation of involvement of LDL receptor was confirmed by blocking ligand-binding LDL receptors using anti-LDLR mAb which caused a drastic decrease in uptake of ApoE-precoated PEG-PHDCA [66].

However, in preclinical tests, doxorubicin-loaded PEG-PHDCA failed to induce a therapeutic effect in 9L gliosarcoma models and accumulation was about 3 times lower in the tumor in comparison to unloaded PEG-PHDCA NPs. Aggregation with plasma proteins due to higher positive charge of the doxorubicin-loaded PEG-PHDCA NPs is suggested which might hinder efficient therapeutic effects which is not observed using surfactant-coated NPs (e.g. PBCA or PLGA) in the same gliosarcoma model. As a conclusion, stealth properties alone might not be sufficient for effective brain targeting [67].

4.4 Covalent linkage with ApoE

Taken together the findings of studies on polysorbate 80-coated PBCA NPs, adsorption of ApoE and subsequent binding of ApoE to the LDL receptor facilitate endocytosis and/or transcytosis which can be applied for drug transport to the brain [59].

Another delivery system are albumin-NPs prepared from human serum albumin (HSA), which are biodegradable, easy to prepare and bear reactive groups on their surfaces e.g., amino and carboxylic acid groups (Figure 4). These groups facilitate direct covalent ligand binding/surface modification, which can be advantageous to surfactant-coating due to concerns and contradictions regarding surfactant's toxicity [68].

In 2006, ApoE was coupled by chemical methods covalently to HSA NPs by the group of Langer to investigate the transport of loperamide to the brain. These NPs were prepared by a desolvation method and afterwards these NPs were activated using a sulfhydryl-modified PEG cross-linker (NHS-PEG-Mal). NeutrAvidin was conjugated to the activated HSA-NP by reaction of avidin with the amino group of the bifunctional spacer. ApoE was biotinylated to enable the attachment of ApoE to NeutrAvidin-modified NPs (Figure 6, D). This modification was chosen since avidin and biotin form the most stable naturally occurring complex. Investigation of these ApoE-coupled and loperamide-coated HSA NPs revealed strong antinociceptive effects, whereas non-modified HSA-NP were unable to transport the drug across the BBB. These effects were even more pronounced than with polysorbate-coated HSA-NPs [68]. When using HSA NPs, loperamide is only adsorbed to the surface of the NPs, but all experiments revealed a stable drug attachment even in the presence of various concentrations of serum or surfactants [68].

HSA NPs with covalently bound ApoE are taken up into brain endothelial cells by endocytosis after intravenous injection tested *in vivo* and *in vitro* with mouse endothelial (b.End3) cells. In addition, transcytosis took place as well because some of these particles were found in the brain parenchyma [69]. Studies on the exact uptake mechanism revealed the LRP1 as the receptor responsible for ApoE-HSA NPs uptake after performing *in vitro* experiments with b.End3 cells using specific antibodies against the LRP1, the LDL, the ApoE-receptor and Megalin and co-incubation experiments [70]. A similar method for covalent binding was used to determine if a shorter linkage is possible by using thiolated apolipoproteins (reaction with Traut's reagent) and direct reaction with the heterobifunctional NHS-PEG-Mal linker without use of avidin-biotin (Figure 6, E). Supplementary to ApoE, covalent attachment of ApoA-I (recognized by scavenger receptor class B type I) and ApoB-100 (recognized by LDL receptor), which interact with the brain endothelial cells partially by different mechanisms, was performed. Nevertheless,

NPs with ApoE3 showed the highest antinociceptive effects [71]. In conclusion, ApoE-coupled HSA NPs are a surfactant-free and well-defined system for efficient transport of loperamide across the BBB.

One of the first approaches for direct coupling of PLGA to ApoE was performed with an ApoE-modified peptide (pep-apoE) which was previously successfully evaluated with lipid NPs [72]. A single emulsion solvent evaporation method was used for preparing the PLGA NPs. PLGA NPs were conjugated with pep-apoE using an appropriate linker for the carboxylic acid groups of PLGA and thiol-groups of the peptide (Figure 6, F). After intravenous injection in mice, ApoE-functionalized, but not non-functionalized, fluorescent PLGA NPs were detected in the cerebral cortex parenchyma. However, a weak fluorescence signal was also detected after injection of ApoE-functionalized PLGA NPs in liver sections [72a].

A new preparation strategy for surface modified poly(lactic acid) (PLA) NPs was established by Langer and coworkers in 2018 to enhance uptake by endothelial cells. In order to achieve an active targeting to the brain, a covalent linkage of ligands i.e. ApoE, penetratin and ovalbumin to the nanoparticles' surface was performed by a vinyl sulfone-modified poly(vinyl alcohol)-derivative (VS-PVA), a newly developed steric stabilizer bearing reactive vinyl sulfone-groups (Figure 6, G). This modified stabilizer was introduced as a facile route for ligand coupling reactions directly to PVA-stabilized NPs. The problem of inaccessibility of the polymers' carboxylic groups hindering covalent surface modification by coating with commonly used, but unreactive PVA was overcome by this approach. NPs were prepared by an emulsification-diffusion method. For preparation of protein-modified PLA NPs, the surface of the NPs was PEGylated by reaction of the vinyl-sulfone groups of VS-PVA-PLA with the amino groups of α-amino-ω-carboxy PEG chains. Afterwards, ApoE and ovalbumin were coupled to the PEG-chains by esterification. Penetratin was coated onto the surface of the NP without using PEG-spacer. Penetratin- (a cell-penetrating peptide) and ApoE-modified VS-PVA-PLA NPs showed a significantly higher cellular uptake than ovalbumin-modified or unmodified NPs as control formulations. In conclusion, an effective approach to couple ligands to PLA surfaces was established, [73] but *in vivo* studies were not conducted.

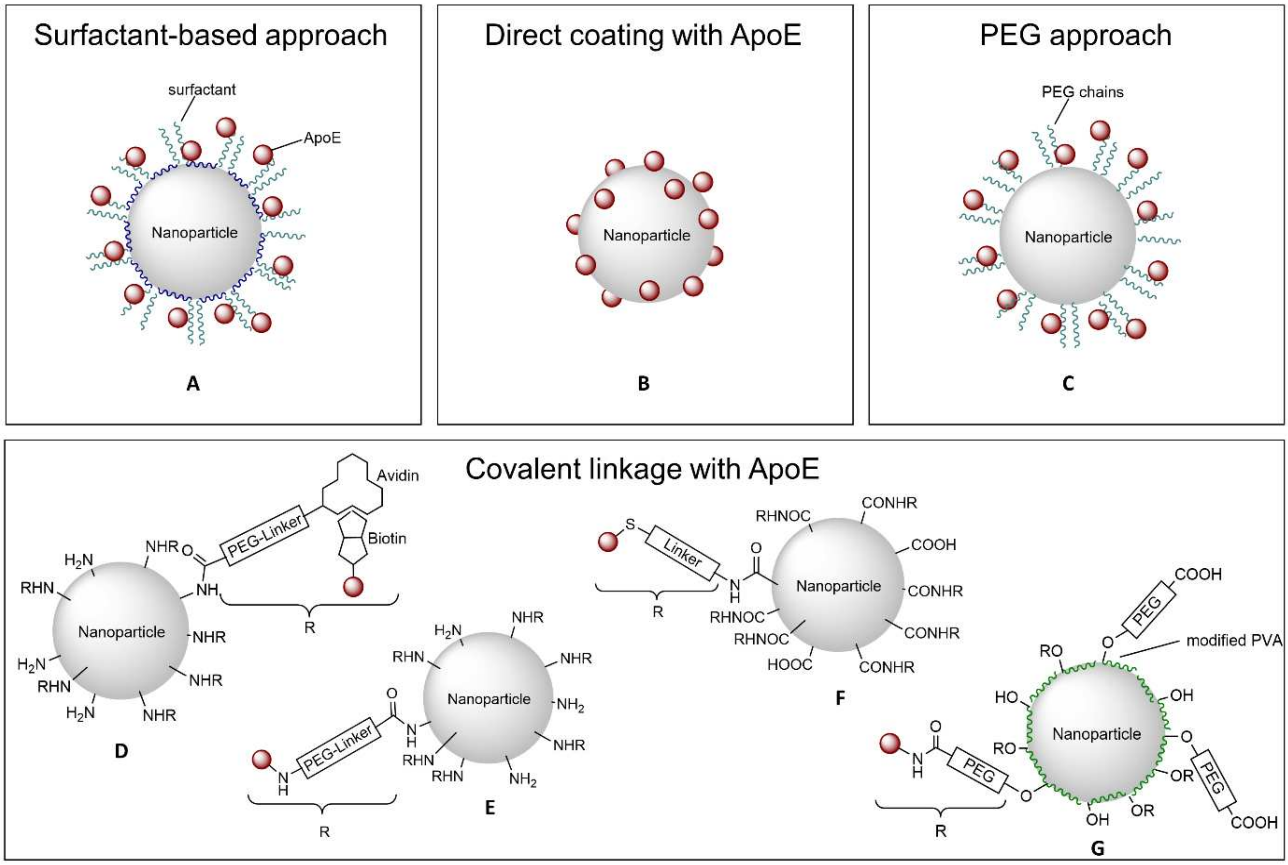

Figure 6. Approaches for ApoE-functionalization of polymeric nanoparticles.

5. Drug Formulation

5.1 Peptides and Proteins

To investigate another neuropeptide besides dalargin (vide supra) which induces analgesia, Schröder et al. used kyotorphin, a dipeptide which normally does not cross the BBB, because of its hydrophilicity (**Table 1**). NPs modified with kyotorphin, dalargin and amitriptyline, which is known to normally penetrate the BBB as a drug, were compared. After the adsorption of the peptide dalargin on polysorbate 85-stabilized PBCA NPs, analgesia was observed by hot-plate test in mice after intravenous application even when NPs were not coated with polysorbate 80. The use of Dextran 70000 as stabilizer during acidic nanoparticle preparation in parallel experiments led to the need of polysorbate coating after attachment of the drug (dalargin or kyotorphin) to be capable of inducing analgesia. In addition, even the amitriptyline level was significantly increased in the brain with amitriptyline-loaded PBCA NPs in comparison to the free drug [74].

Nerve growth factor (NGF), a neuropeptide, adsorbed on polysorbate-80 PBCA NPs was used to study the antiparkinsonian effect in the CNS. C57B1/6 mice were treated with 1-methyl-4-

phenyl-1,2,3,6-tetrahydropyridine to provoke parkinsonian syndrome. After treatment of NGF-adsorbed polysorbate 80-coated PBCA NPs, symptoms of Parkinson's disease were decreased as shown by a lower rigidity and increased locomotor activity [75]. Brain delivery of similar NPs was also evaluated in the model of acute scopolamine-induced amnesia in rats. Using the passive avoidance reflex (PAR) test, intravenous administration of NGF polysorbate 80-coated PBCA NPs successfully reversed scopolamine-induced amnesia and enhanced recognition and memory. Direct measurement of NGF concentrations in the murine brain confirmed that polysorbate 80-coated PBCA NPs enable transit across the BBB after intravenous injection [76]. For the treatment of stroke, therapeutic NGF and ultra-small iron oxide particles (USPIO), for diagnostic functionality to track the *in vivo* biodistribution, were co-encapsulated into a chemically crosslinked HSA matrix. Modification of the particle surface with ApoE was realized by reacting a maleimide group of a PEG-crosslinking agent and thiolated ApoE. *In vitro* studies with an artificial BBB confirmed that NGF remains bioactive after encapsulation and is released from the carrier which induced neurite outgrowth in PC12 cells. The transport of NGF was investigated using a Transwell® system and b.End3 cells, and ApoE-functionalized HSA NPs caused significantly higher NGF levels in the basolateral compartment [77].

In an animal model of stroke (transient middle cerebral artery occlusion model), a combination treatment using NGF-loaded theranostic nanocarriers and the small molecular MEK inhibitor U0126 was tested. A reduction of the infarct volume indicated also an effect of NGF, when using this combinatory therapy, however, no significant difference between this combinatory approach or the use of only U0126 was observed. Consequently, benefits of ApoE-mediated therapy were not clearly perceived [77].

PLGA NPs coated with poloxamer 188 were used to enable the delivery of BDNF (brain-derived neurotrophic factor) into the brain of mice with traumatic brain injury (TBI). BDNF regulates neuronal plasticity, neuronal cell growth, proliferation, cell survival and long-term memory. The closed head injury weight-drop TBI model was used to induce trauma in mice. BNDF levels were higher after intravenous injection when BNDF was embedded in poloxamer-coated PLGA NPs in comparison to injection of free BNDF and improved neurological and cognitive deficits in TBI mice [78].

For further approaches using peptide- or protein-loaded polymeric NPs for ApoE-mediated brain-targeting see Table 1.

Table 1: Peptides/proteins encapsulated in polymeric nanoparticles for ApoE-mediated brain targeting.[a]

Drug	Disease/Effect of drug	Nanoparticular formulation	Type of ApoE-functionalization	In Vivo	[Ref.]
Dalargin (Hexapeptide)	Analgesia	PBCA	Indirect by PS80 coating	yes	[43-45, 51, 74, 110, 119]
		PBCA	Indirect by different PS coatings	yes	[46, 119a]
		PBCA	Indirect by PEG 20000 and/or PS80 coating	yes	[52]
		PBCA	Coating with ApoE (and PS80)	yes	[59-60]
Kyotorphin (Dipeptide)	Analgesia	PBCA	Indirect by PS80 coating	yes	[74]
Morphiceptin (Tetrapeptide)	Analgesia	PBCA	Indirect by PS80 coating	yes	[120]
Endomorphin-1 (Tetrapeptide)	Analgesia	PBCA	Indirect by PS80 coating	yes	[121]
Nerve growth factor	Alzheimer's disease Parkinson's disease	PBCA	Indirect by PS80 coating	yes	[75-76]
	Stroke	Iron oxide and HSA	Covalent linkage of ApoE	yes	[77]
BDNF	Traumatic brain injury	PLGA	Indirect by poloxamer 188-coating	yes	[78]
Arylsulfatase A	Metachromatic leukodystrophy	PBCA	Indirect by PS80 coating	no	[122]
		PLA	Indirect by poloxamer 188-coating	no	[122]
		PLGA	Indirect by poloxamer 188-coating	no	[122]
		HSA	Indirect by PS80 coating	no	[122]

[a] **Abbreviation: PS80 = polysorbate 80.**

5.2 Small Molecules

Brain-delivery of smaller drugs, bound to PBCA NPs, was also tested to study whether transport of dalargin across the BBB with polysorbate-coated PBCA NPs is transferable in a similar way to drugs that completely differ in their chemical structure (Table 2). New drug delivery systems based on small molecules were obtained by encapsulation of e.g. loperamide, doxorubicin or tubocurarine into PBCA NPs [79]. For tubercurarine-loaded NPs, used for muscle relaxation, an in situ perfused rat brain technique was used together with simultaneous EEG recording as an experimental model. Solely when tubocurarine was embedded in PBCA NPs which were then coated with polysorbate 80, a significant increase in the transport of this drug across the BBB occurred [79a].

As lipophilic and polar drugs, respectively, it was assumed that loperamide and doxorubicin are unable to passage the BBB. Loperamide-loaded particles were obtained by embedding the drug in PBCA NPs which are then coated with polysorbate 80. Nanoparticles were prepared by emulsion polymerization in the presence of loperamide. The obtained particles were able to cross the BBB after coating with polysorbate 80 shown by induced analgesic effects [79b]. Other loperamide-delivery systems were described under section 4 and in Table 2.

Doxorubicin, as one of the most prominent antitumoral drugs, e.g. for the treatment of glioblastomas [80], is not able to cross the BBB by itself. Therefore, delivery with polysorbate 80-coated PBCA NPs across the intact BBB was studied, and maximum levels after 2 to 4 h after intravenous injection were achieved. The uptake to the brain in comparison to other tissues was a very low, but effective process, whereas administration of free doxorubicin in a polysorbate solution had no effect on brain passage. Thus, nanoparticles are required to mediate transport when they reach the endothelial cells. Doxorubicin levels in spleen, liver and lung were decreased by about 1.5 times when PBCA NPs were coated with polysorbate. In addition, opening of the tight junctions of the BBB was not detected [79c]. Drug distribution in brain tissue after crossing the intact BBB was determined in a subsequent study via a capillary depletion technique to distinguish between amounts of doxorubicin in the whole brain and in the brain parenchyma. Therefore, rats were treated with doxorubicin solutions in polysorbate 80 or doxorubicin-loaded PBCA NPs with and without polysorbate 80 coating via intravenous injection. Clinically effective doxorubicin concentrations in all brain fractions were only found when polysorbate 80-coated PBCA NPs were used indicating significant transcytosis of the drug into the post-capillary parenchymal compartment [81].

The manufacturing parameters of poly(alkylcyanoacrylate) doxorubicin-loaded NPs were optimized regarding surfactants, polymer and doxorubicin-loading using glioblastoma-bearing rats [80, 82]. Due to the BBB, glioblastomas are nearly inaccessible for commonly used chemotherapeutics. Rats treated with doxorubicin-loaded and polysorbate-coated PBCA NPs showed significantly higher survival times, lower tumor sizes and lower values for proliferation and apoptosis without showing short-term neurotoxicity [80]. The blood half-life of the particles and in turn the uptake due to the so-called enhanced permeability and retention (EPR) effect was also improved by coating with poloxamers/poloxamines instead of polysorbate 80. These surfactants increased the anti-tumor effect of doxorubicin-loaded PBCA NPs in tumorous brain, but not in healthy brain tissue and across an intact BBB since the permeability of the BBB at the tumor site is significantly increased [82-83]. Modifications of variables, such as polymer to surfactant ratio, only led to insignificant effects [82]. Poly(iso-hexylcyanoacrylate)

(PIHCA) shows a similar efficiency as PBCA for treating cancer in rats, but is better tolerated due to a slightly slower degradation rate. In addition, doxorubicin-loaded PIHCA NPs without surfactant coating are FDA approved for *hepatocellular* carcinoma (BioalliancePharma, 2009), but not for brain therapy [67b, 84].

Other polymeric NPs such as PS-, PLGA- and starch-derivatives were investigated as well with regard to transport of doxorubicin for brain targeting across the BBB *in vivo*, into brain endothelial cells and into glioblastoma cells (Table 2) [54, 85-86].

Further successfully tested antitumoral drugs used for brain targeting *in vivo* and *in vitro* with polysorbate 80-coated PBCA were methotrexate [87], temozolomide [88] and cisplatin [89].

ApoE-functionalization by coating with ApoE was utilized for curcumin transport in PBCA NPs for the potential treatment of cancer and Alzheimer's disease. Curcumin, a natural antioxidant, was hypothesized to inhibit beta amyloid and beta amyloid induced oxidative stress and shows anticancer activities. For Alzheimer's disease therapy, release of curcumin from ApoE-NPs induced reduction in reactive oxygen species and in beta amyloid caused apoptosis in SH-SY5Y neuroblastoma cells. In both disease models, curcumin transport was increased when applying the drug in ApoE-coated PBCA NPs *in vitro* [90]. However, *in vivo* studies were not performed to validate the findings.

Several other drugs were investigated for Alzheimer's treatment *in vivo*. Tacrine and rivastigmine-loaded polysorbate 80-coated PBCA NPs were applied to healthy rats, but merely increased brain concentrations were measured [91].

Advanced effects were shown for oral administration of estradiol-loaded polysorbate 80-coated PLGA NPs in an ovariectomized rat model of Alzheimer's disease that mimics the postmenopausal conditions. These NPs provoked a significant increase of estradiol in the brain in comparison to uncoated PLGA NPs. *In vitro* data in simulated fluids showed that polysorbate 80-coated PLGA NPs were conserved in the gastrointestinal tract transit without loss of coating concentration on the particle. Orally administered estradiol had the same effect as intramuscular drug injection, which simplifies drug administration for patients in post-menopausal Alzheimer's disease [92].

For further approaches using small molecule-loaded polymeric NPs for ApoE-mediated brain-targeting see Table 2.

Table 2: Small molecules encapsulated in polymeric nanoparticles for ApoE-mediated brain targeting

Drug	Disease/Effect of drug	Nanoparticular formulation	Type of ApoE-functionalization	*In vivo*	[Ref.]
Loperamide	Analgesia	PBCA	Indirect by PS80-coating	yes	[79b]
		PBCA	Coating with ApoE	yes	[59]
		HSA	Covalent linkage of ApoE	yes	[68, 71]
		PLGA	Indirect by PS80- or poloxamer 188-coating	yes	[54]
		PLGA-PEG-PLGA	Indirect by PS80- or poloxamer 188-coating	yes	[55]
Doxorubicin	Cerebral Cancer	PBCA	Indirect by PS80-coating	yes	[79c, 80, 82]
		PLGA	Indirect by PS80- or poloxamer 188-coating	yes	[54, 85]
		PDMA-PS	Coating with mApoE	no	[86a]
Doxorubicin	Brain metastases	PMA-PS80-starch	Indirect by PS80	yes	[86b]
Methotrexate	Cerebral Cancer	PBCA	Indirect by PS80-coating	yes	[87]
Temozolomide	Cerebral Cancer	PBCA	Indirect by PS80-coating	yes	[88]
Cisplatin	Cerebral Cancer	PBCA	Indirect by PS80-coating	yes	[89]
Carboplatin	Cerebral Cancer	PLGA	Indirect by PS80-coating	yes	[123]
Docetaxel	Brain metastases	PMA-PS80-maltodextrin-dodecane	Indirect by PS80	yes	[124]
Docetaxel	Cerebral Cancer	PLGA-PEG-DHA	Indirect by PEG and DHA	yes	[125]
Gemcitabine	Cerebral Cancer	PBCA	Indirect by PS80-coating	yes	[126]
Curcumin	Cerebral Cancer	PBCA	Coating with ApoE	no	[90a]
Curcumin	Alzheimer's disease	PBCA	Coating with ApoE	no	[90b]
Tacrine	Alzheimer's disease	PBCA	Indirect by PS80-coating	yes	[91a, 127]
		PBCA-PEG	Indirect by PEG	yes	[127]
Rivastigmine	Alzheimer's disease	PBCA	Indirect by PS80-coating	yes	[91b]
Estradiol	Alzheimer's disease	PLGA	Indirect by PS80-coating	yes	[92]
Rosmarinic acid	Alzheimer's disease	PAAM-CH-PLGA	Coating with ApoE	yes	[61]
Salvianolic Acid B	Neurodegenerative diseases	PECA	Indirect by PS80-coating	yes	[128]
Tubocurarine	Muscle relaxation	PBCA	Indirect by PS80-coating	yes	[79a]
Pentamidine	Human African Trypanosomiasis	PCL	Indirect by PS80-coating	no	[56]
Amitriptyline	Depression	PBCA	Indirect by PS80-coating	yes	[74]
MRZ 2/576	Epilepsy	PBCA	Indirect by PS80-coating	yes	[129]
Valproic acid	Epilepsy	PBCA	Indirect by PS80-coating	yes	[130]

Breviscapine	Cerebrovascular diseases	PLA	Indirect by poloxamer 188-coating	yes	[131]
Puerarin	Stroke	PBCA	Indirect by PS80-coating	yes	[132]
Gatifloxacin	Central nervous system tuberculosis	PLGA	Indirect by PS80-coating	yes	[133]
Amphotericin B	Cryptococcal meningitis	PBCA	Indirect by PS80-coating	yes	[134]
		PLA-PEG	Indirect by PS80-coating and PEG	yes	[135]
Quercetin	Antioxidant	PBCA	Indirect by PS80-coating	yes	[136]
Stavudine	Human immunodeficiency virus	PBCA	Indirect by PS80-coating	no	[137]
Delavirdine	Human immunodeficiency virus	PBCA	Indirect by PS80-coating	no	[137]
Saquinavir	Human immunodeficiency virus	PBCA	Indirect by PS80-coating	no	[137]
Obidoxime	Acetylcholinesterase reactivator	HSA	Covalent linkage of ApoE	no	[138]
Sumatriptan Succinate	Migraine	PBCA	Indirect by PS80-coating	yes	[139]
		BSA	Covalent linkage of ApoE	yes	[139]

[a] Abbreviations: PS80 = polysorbate 80; PDMA = poly(dimethylacrylamide); PMA = poly(methacrylic acid); PECA = poly(ethylcyanoacrylate), BSA = bovine serum albumin.

6. *In vitro* blood-brain barrier models

In the field of brain delivery several *in vitro* blood-brain barrier models have been investigated, which mimic critical functionalities of the BBB and provide first insights in the suitability of a drug delivery system to overcome this barrier. The basic models consist of one type of cells (monoculture), mainly brain endothelial cells of different origin, with which the cellular uptake mechanisms and internalization profiles of the nanocarriers as well as their cytotoxicity and permeability can be assessed. The group of Langer used human brain microvascular endothelial cells (HBMECs) to investigate the uptake of ApoE, penetratin or ovalbumin modified PLA NPs. Therefore, cells were incubated with different nanoparticle formulations that contained the fluorescent dye Lumogen® Red. Cellular uptake was investigated by two methods, first an HPLC-FLD method for quantification, and second, for visualization, a fluorescence microscopy method. In both experiments, the group was able to show increased cellular uptake for ApoE and penetratin (a cell penetrating peptide used as positive control) containing NPs in comparison to unmodified particles, thus assuming an active targeting of cells by specific interactions between the ApoE ligand and the LRP1 receptor expressed on HBMECs [73]. Primary cerebral endothelial cells (CEC) are frequently used for such *in vitro* BBB models [93]

and can be harvested from bovine [94], porcine [95], rat [96], mouse [97] or human [94] sources. The advantage of using primary cells is that a large number of cells from one single brain can be isolated and especially the mouse and human endothelial cells provide an important tool for studying the BBB at a cellular and molecular level. However, the isolation process is complex, time consuming and provides cells with high batch-to-batch variability, which leads to low reproducibility of experimental results [98]. In order to circumvent these disadvantages of primary cultures, several immortalized CEC lines were created with the potential to provide a stable source with high homogeneity throughout numerous passages [99]. These cell lines, from bovine (e.g BBECs) [100], porcine (e.g PBMECs) [101], rat (e.g RBE4s) [102], mouse (e.g b.End.3s) [103] or human (e.g hCMEC/D3s) [104] sources, preserve basic cerebral endothelium-like features, such as tight junction formation, expression of influx and efflux transporters and endothelial-specific markers. However, immortalized cell lines are generally more permeable than primary cultures [104]. One indicator for the tightness of CEC monolayers, and consequently an indirect parameter for the paracellular permeability, is their TEER value, which is evaluated with two voltage-measuring electrodes. The cell layer should display a sufficiently high TEER value to constitute an adequate model system [105]. *In vitro* BBB assays are mostly carried out in multi-well plates, in which compartments simulating the blood (apical) and brain (basolateral) sides are separated by a microporous filter on/under which the cells are seeded. Thus, the cells can develop a monolayer in contact with different culture media in each compartment. In this regard, filters usually include Transwell® polycarbonate or polyethylene terephthalate inserts [106]. To achieve a better representation of the BBB and to improve barrier functions, co-culture and triple co-culture systems have been developed (Figure 7). Through the combination of CECs with other elements of the *in vivo* BBB, i.e., astrocytes, astrocytic cell lines, C6 glioma cell lines, pericytes and/or mixed glia cells, the physiological conditions can be simulated because all compartments of the neurovascular unit strongly contribute to the development and maintenance of the BBB phenotype. In this regard, the second type of cells can either be seeded in close proximity to the endothelial cells at the opposite site of the filter membrane (contact co-culture, Figure 7, B, D), or without contact at the bottom of the wells (non-contact co-culture, Figure 7, A, C) [107]. In triple co-culture models, a third cell type of the neurovascular unit is added (triple co-culture, Figure 7, E, F), that leads, with regard to the stabilization of tight junctions, to a synergistic effect [108] and thus, to a higher correlation with *in vivo* permeability data [109]. In these models higher TEER values can be achieved, if optimal culture conditions parameters are guaranteed [73]. The group of Appelt-Menzel recently established a BBB co-culture model by using human induced

pluripotent stem cells (hiPSC) that advantageously provides a virtually unlimited independent cell source. BBB endothelial cells differentiated from hiPSCs which are cultured with hiPS-neuronal stem cells and pericytes in a triple culture as well as with astrocytes in a quadruple culture form tight cell layers with TEER values near to physiological conditions. Together with further enhancements in the development of BBB properties this model provides an advanced tool for drug delivery investigations for future approaches [140]. For BBB permeability investigations so far, for example the group of Lee used a Transwell® contact co-culture model containing a rat brain endothelial cell line (RBE4), which was seeded on the apical side of the filter, and a rat glioma cell line (C6), which was grown on the bottom of the filter. Poloxamer 188- or polysorbate 80-coated PLGA-PEG-PLGA (PEP) NP formulations, containing the centrally analgesic drug loperamide, were added to the apical side and samples from apical and basal compartments were analyzed after an incubation period to quantify the amount of loperamide via HPLC. The group confirmed that surfactant-coated PEP NPs significantly enhanced the permeation percentage compared to unmodified PEP NPs as mandatory tool for BBB penetration [55].

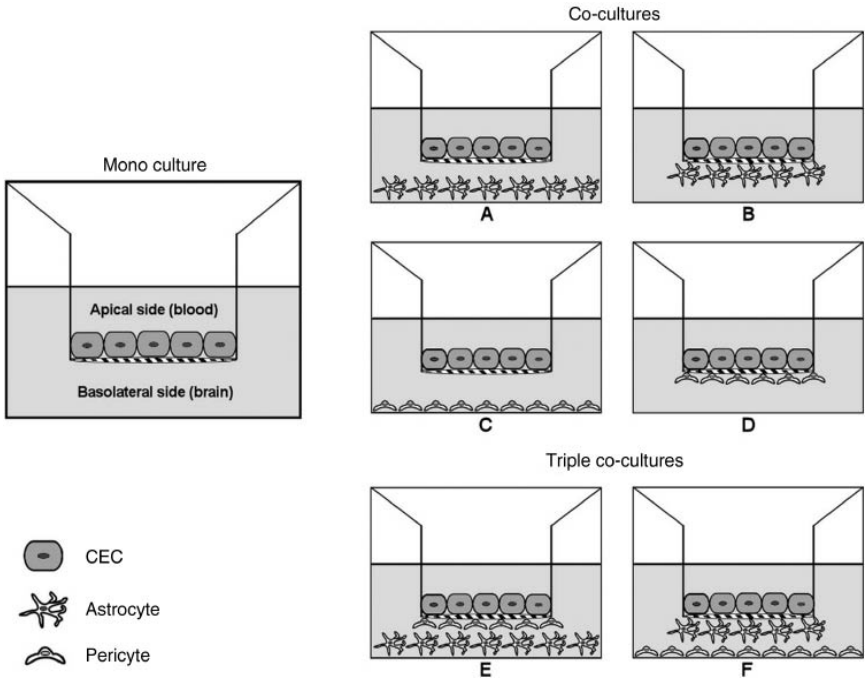

Figure 7. Transwell® systems to simulate the BBB *in vitro*. Mono-, co- (A-D), and triple co-cultures (E-F) of CECs with astrocytes and/or pericytes in contact (B, D) or non-contact (A, C) set-up. Reprinted with permission of Ref. 98. Copyright 2014, Elsevier.

7. *In vivo* studies

ApoE-mediated drug delivery across the BBB has been investigated in with regard to therapeutic effects in a variety of animal models. As depicted in examples described above, therapeutic cargoes for delivery into the brain have a wide range of effects, which explains why different *in vivo* models are necessary to assess successful delivery to their site of action within the brain. While analgesic drugs need to be studied in pain assessment tests (7.1), relevant effects of chemotherapeutics can only be determined in cancer models such as glioblastoma models (7.2) and measuring the effects of anti-AD drug delivery or NGF delivery for the treatment of Parkinson's disease require neurodegenerative animal models (7.3) in which histology and behavior as well as potential side effects due to off-target delivery can be tested. The following sub-sections summarize animal models used in the current literature within the context of either pain management (7.1), brain cancer therapy (7.2), or neurodegenerative diseases (7.3), and discuss advantages as well as disadvantages of the models.

7.1. Analgesia

First attempts in brain delivery with ApoE modified NPs were made mainly with centrally analgesic model drugs dalargin and loperamide, a P-glycoprotein substrate. These drugs cause a central analgesic effect if efficiently delivered into the brain by binding with μ-opioid receptors for pain perception and are expected to be released from drug loaded NPs once they are located in the brain. Hence, central analgesic effects would demonstrate the brain targeting of NPs after administration, since free drugs are not able to pass the BBB [52]. To confirm efficient delivery, two established pain assessment methods were utilized.

7.1.1 Hot-plate test

In general, the hot-plate test is performed by using a water-heated concealed plate that is kept at a constant temperature of approximately 55°C on which animals are placed. Immediately when they show symptoms of pain perception such as "paw-lick" reaction or jumping, they are removed from the plate. Hot-plate response latencies are measured after several defined incubation times after drug administration. To not further harm animals, a cut-off time is set. The inhibition of the paw-jumping responses due to administration of analgesic drugs is calculated in comparison to the response without treatment and is expressed as the percent of maximum possible effect (MPE) [110]. In 1998, Schröder and Sabel administered dalargin-loaded polysorbate 80-coated PBCA NPs as well as control formulations intravenously into NMRI mice. Surfactant precoated NPs showed an enhancement over 50% in hot-plate response

latency time and therefore improved brain targeting, without being able to state a mechanism at that time [44]. In a similar manner, the Lee group reported significantly improved MPE values for loperamide-loaded polysorbate 80-coated PLGA-PEG-PLGA NPs after intravenous injection in ICR mice. However, they also concluded solely that brain targeting with polysorbate 80 was improved without giving any further explanations [55]. Lemmer and coworkers reported in a similar study with dalargin-loaded polysorbate 80-coated PBCA NPs a circadian-phase dependency of NPs transport across the BBB. Therefore, treated mice were subjected to 12 h light-dark cycles and pain reactions were measured by hot-plate test performance. A significant dose-dependent antinociceptive effect was achieved with polysorbate 80-coated NPs which were shifted about 12 h compared to the normal circadian phase-dependent pain reaction of the mice. This result indicated a circadian-time dependent fluctuation in the permeability as well as in the transcytosis capacity of the small cerebral vessels [110]. This functional test, however, does not allow for quantitative measurements of bioavailability in the brain but is one of the established nociception methods available in pain research.

7.1.2 Tail-flick test

The tail-flick test is conducted with a specific device containing a slit and a quartz projection bulb. The tail of the animal is placed over the slit through which the bulb is focused and the time until the tail is withdrawn is recorded. To prevent tissue damage, the experiments are terminated after a specific time, if no response was evoked. Tail flick latency is measured after defined incubation times after drug administration and the maximum possible effect (MPE) is calculated in percent. In 2001, Kreuter et al. used the tail-flick test to investigate the brain targeting effect of dalargin-loaded PBCA NPs modified with ApoE with and without polysorbate 80 precoating. The formulations were administered intravenously into ICR mice and MPEs were calculated. It was shown that surfactant precoating additionally to ApoE overcoating achieved significantly higher MPEs in comparison to control groups. Furthermore, polysorbate 80 coating alone demonstrated improved results in comparison to ApoE coating without surfactant. Additionally, tail-flick test results obtained with ApoE-deficient (ApoEtm1Unc) mice demonstrated that ApoE has a crucial role in mediating the delivery of the NPs across the BBB [59]. These findings contributed to a better understanding of polysorbate 80 and/or ApoE modified delivery systems to the brain. As discussed above, functional assays cannot estimate bioavailability of the drug in the brain but need to be put into context of pharmacokinetic/pharmacodynamic (PK/PD) correlation.

7.2 Glioblastoma multiforme

Glioblastoma multiforme (GBM) is a devastating type of primary malignant tumor of the CNS that develops from astrocytes. Several GBM *in vivo* models have been established to investigate the brain delivery and therapeutic effects of anticancer drugs, such as doxorubicin, methotrexate, temozolamide, gemcitabine, cisplatin, carboplatin, curcumin and docetaxel (**Table 2**).

7.2.1 Capillary depletion method

Before assessing therapeutic effects in a model of disease, biodistribution assays can lay the ground for therapeutic approaches. To determine the amount of drug that is distributed within the whole brain, a sophisticated method in case of nanoparticle delivery is capillary depletion, which in contrast to models described above provides the possibility of quantifying the drug that indeed has passed the BBB and appears in the brain parenchyma. For capillary depletion, the brain of treated animals is excised and homogenized in a mortar. After centrifugation, the drug is analyzed in the supernatant which represents the brain parenchyma as well as in the pellet representing the cell debris of vascular elements [111]. In a doxorubicin-loaded and polysorbate 80-coated PBCA NP study, the group of Kreuter utilized this method to determine doxorubicin concentrations via HPLC after extraction in different healthy rat brain fractions, whereby whole homogenate, supernatant and pellet represented whole brain, brain parenchyma and brain capillaries, respectively. It was shown, that at one specific time point, the drug concentrations, only when delivered with polysorbate 80-coated NPs, were significantly higher in the supernatant in comparison to the concentrations in the pellet, which indicated a successful transport of the drug across the brain blood capillary endothelium into the brain parenchyma [81]. While this bioavailability test did not yet imply therapeutic efficacy, it helped determine optimal time points for further experiments in the disease model.

7.2.2 101/8 glioblastoma model

The 101/8 glioblastoma rat model is produced by local injection of an α-dimethylbenzanthracene (DMBA) pellet into the brain of Wistar rats. The developed tumor material is transplanted in new Witstar rat brains. As soon as these animals develop clinical signs, the tumor is removed and inoculated in the brain of further experimental animals. This model was used by Kreuter and coworkers to test the anti-tumoral effects of doxorubicin-loaded PBCA NPs precoated with different surfactants. After intravenously injection of the formulations, mean survival times of rats were determined and results were shown by Kaplan-

Meier plots. Polysorbate 80-coated NPs were shown to be the most effective formulations [82]. The same group also utilized this tumor model in another study to investigate the body distribution and BBB permeability using radiolabeled [14C]-PBCA NPs. These results showed reduced RES organ concentrations for unloaded polysorbate 80-coated NPs, whereas concentrations of drug loaded polysorbate 80-coated NPs were similar to drug loaded, but uncoated NPs. In addition, it was reported that NP concentrations in the brain of tumor bearing rats were significantly higher compared to concentrations in healthy animals. An experiment with Evans Blue, a dye commonly used to demonstrate a defective BBB, confirmed that the permeability of the BBB in tumor bearing rats is significantly increased after several days due to tumor development, which is described by the ERP effect. Therefore, the authors concluded, that besides the ability of polysorbate 80-coated NPs to cross the BBB, also the ERP effect plays an import role regarding the capability of nanocarriers to reach a tumorous brain [83]. This approach combined drug bioavilability in the brain, biodistribution to assess potential side effects and histological observations to explain the observed results. Considering the principles of the 3Rs (Replacement, Reduction and Refinement), such experiments ideally reduce the number of animals necessary in a study. However, for such refined models, often preliminary experiments are necessary to determine optimal time points, drug doses and other parameters.

7.2.3 C6 brain tumor model

The C6 brain tumor model is obtained by an intracerebral C6 murine glioma cell inoculation into the brain of rats [112]. The resulting model was utilized by the group of Akbarzadeh in a cisplatin-loaded polysorbate 80-coated PBCA NP approach. After animal treatment with different formulations, the antitumor efficacy was investigated by measuring mean survival times. None of the formulations significantly improved survival times in comparison to the control [89]. The group used merely free drug as control, which made the interpretation of the results rather difficult. However, Wang and Chen reported that rats treated with gemcitabine-loaded and polysorbate 80-coated PBCA NPs survived for a significantly longer time than those in the control group by using the same brain tumor model [113].

7.3 Neurodegenerative diseases

Alzheimer's disease is a progressive neurodegenerative disorder and is characterized by cerebral deposition of beta-amyloid peptides (Aβ) as amyloid plaques which are generated by proteolytic processing of the amyloid precursor protein (APP). The major symptoms include a variety of behavioral disturbances and neuropsychiatric symptoms, such as personality change,

intellectual debility, and dementia [91b]. So far, several anti-AD drugs have been delivered into the brain with nanoparticulate systems, such as tacrine, rivastigmine, estradiol and rosmarinic acid in preclinical studies (Table 2). Parkinson's disease is caused by a neurodegenerative process with degeneration of dopamine-containing neurons of the nigrostriatal bundle which leads to deficiencies in the motor system, such as bradykinesia, muscular rigidity, and tremor and in a later stage of the disease to behavioral problems, dementia, depression and anxiety. As therapeutic drug, NGF, which is known to prevent degeneration of dopaminergic neurons, has been delivered to the brain via NP formulations preclinically [75]. While plaque formation can be best assessed in histologic specimen, the detection of whole body biodistribution provides information about brain bioavailability and potential side effects, and numerous behavioral assays are available to determine pharmacodynamics.

7.3.1 Alzheimer's disease rat model

An AD rat model was established facilitating the analysis of the change in Aβ plaque accumulation in the brain in a physiological environment and therefore the effect of e.g rosmarinic acid which is known to reduce amyloid-β aggregation [114]. The rat model is obtained by injecting Aβ1-42 peptides in the fixed brain of Wistar rats, stitching up the cut in the scalp and observing the rat for one further week. Kuo et al. utilized such an AD model in a study with rosmarinic acid-loaded, ApoE-modified PAAM-CH-PLGA NPs. Nanoparticular formulations and control formulations were administered intravenously three times every two days, then the hippocampus of the rats was removed and sectioned using a cryostat microtome. To visualize Aβ plaques, samples were treated with an anti-Aβ monoclonal antibody and a goat anti-rabbit immunoglobulin G antibody, coupled with horseradish peroxidase (HRP) and reacted with a common substrate for HRP. Images of stained Aβ plaques within the samples were acquired with an inverted microscope and showed that the amount of Aβ plaques in samples treated with ApoE modified NPs were lower in comparison to controls [61]. The advantage of such invasive histology-based experiments clearly is the need for additional sets of animals for each time point to be determined at fixed endpoints.

7.3.2 Biodistribution analysis

Surfactant-coating of NPs and attachment of ApoE can also lead to LDL receptors-mediated uptake in other organs, such as the RES in which clearance of NPs can occur, specifically described for hepatocytes overexpressing LDL [115]. Increased delivery into other organs can hinder drugs from reaching their target sites in adequate concentrations and can be solely

evaluated in animal models. In the case of AD treatment with tacrine and rivastigmine, Wilson et al. performed biodistribution analyses of the drugs in the organs of Wistar rats (brain, liver, lungs, spleen and kidney) after intravenous injection of nanoparticulate systems and controls via HPLC methods. The results indicated significantly higher tacrine and rivastigmine concentrations in the brain with polysorbate 80-precoated PBCA NPs. However, the group of Wilson reported lower tacrine and rivastigmine accumulation in liver and spleen and higher accumulation in the kidney for polysorbate 80-coated systems, without giving any further explanations or assumptions [91]. Kumar and co-workers administered estradiol containing polysorbate 80-PLGA NPs into Sprague-Dawley rats and analyzed the drug concentration after several time points in the brain, small intestine, kidney, spleen, heart, liver and lung after homogenization with estradiol ELISA kits. The results were in line with previous reports, confirming significantly increased drug levels in the brain after treatment with surfactant-coated NPs in comparison to uncoated NPs. In case of estradiol, accumulation in liver and spleen was found to be reduced as well. The authors therefore suggested that the surfactant coating of NPs alters their surface properties and thus, leads to a lower interaction with cells of the RES and hence to a lower accumulation tendency in RES organs [92]. While the techniques used in these experiments detect the actual drug, they are very tedious and require sacrificing sets of animals for each time point. The advantage of image-based biodistribution techniques such as continuous monitoring or various time points in the same animal, however, bear the disadvantage of detecting a label rather than the drug itself.

7.3.3 Passive avoidance reflex test

In this passive avoidance reflex test in an induced amnesia mouse model, healthy mice are placed in a two-chamber cage on the side which is brightly illuminated, whereas the other side is dark. To avoid the light, mice rapidly move into the dark side, where they are exposed to an electric shock [116]. After one week of training, the latency time of the animals of remaining on the lighted side is expanded. After induced amnesia in these mice through subcutaneous injection of scopolamine, the animals forget what they have learned and return to basic latency times. Kreuter and co-workers administered NGF-loaded polysorbate 80-coated PBCA NPs into amnesia mice and reported a total reverse of the scopolamine-induced amnesia and even improved recognition and memory [76]. As in functional assays described above, this test allows for the assessment of pharmacodynamics but doesn’t allow for detection of actual drug levels in the brain.

7.3.4 Open-field test in Parkinson´s disease mice model

In the open-field test, mice are placed in the center of a locomotor activity arena and are allowed to move freely for a certain time in which activity is monitored by an automated video tracking system and behavioral parameters, such as locomotor activity, hyperactivity and exploratory pattern are observed. The group of Kreuter used mice with methylphenyltetrahydropyridine (MPTP)-induced parkinsonian symptoms for this test, characterized by reduction in the quantity and quality of spontaneous movements (oligokinesia). The degree of oligokinesia was estimated by alteration in locomotor activity of the mice tested by open-field test. Administration of NGF-loaded polysorbate 80-coated PBCA NPs yielded a significant reduction of the main extrapyramidal symptoms compared to control groups and verified therapeutic promise of designed nanocarrier system for Parkinson's disease [76]. This test can be used to complement biodistribution and pharmacokinetic assays but does not provide quantitative information about drug levels in the brain.

8. Conclusion

Because the BBB is composed of brain microvessel endothelial cells, tight junctions, pericytes, and astrocytes, which all together build a tight cellular barrier, therapeutic (macro)molecules are not able to transit through the BBB by themselves, limiting therapeutic approaches of drugs for brain diseases. CNS diseases are versatile, e.g. depression, epilepsy, Parkinson's disease, dementia/Alzheimers's disease, stroke or brain tumors, and would require efficient therapeutic agents. Polymeric NPs, consisting of low-cost, tailored and biodegradable materials have been studied for their suitability as drug delivery tools to the brain. A very efficient way to target the brain was achieved by coating these drug-loaded NPs with surfactants, leading to adsorption of specific proteins on the particle's surface from blood plasma. Thereupon, prolonged circulation time in the blood stream, induced by steric repulsion, led to inhibition/reduction of adsorption onto surfaces of macrophages and thus to a lower particle concentration in organs and tissues belonging to the RES, especially in the liver. Significantly higher levels in the blood and non-RES organs were achieved. In addition, these surfactant-decorated NPs facilitate ApoE anchoring enabling recognition by LDL receptors of brain endothelial cells and can subsequently transit the BBB via receptor-mediated transcytosis. PBCA NPs coated with polysorbate 80 facilitate the brain delivery of a number of drugs that are unable to cross the BBB in free form. Intensive studies were performed with the analgesic drugs dalargin (peptide) and loperamide (small molecule) as well as with the anticancer drug doxorubicin. Several *in*

vitro BBB models were investigated using mono and co-cultures of brain endothelial cells with astrocytes/pericytes or glioma cells, which mimic critical functionalities of the BBB and provide first insights in the suitability of a drug delivery system to passage this barrier. *In vivo* models were developed with modified rats and mice models to simulate various CNS-relevant diseases such as Alzheimer's disease, Parkinson's disease, cerebral cancer or stroke. Subsequently, polysorbate 80 was considered as the 'gold standard' for brain delivery, but also poloxamer 188 showed high potential when coated onto PLGA NPs. Direct coating of ApoE onto PLGA or PBCA NPs further enhanced the efficiency of brain targeting by RMT. Alternatively, PEG-PHDCA are able to cross the BBB due to an *in vivo* long-circulating/stealth effect and adsorption of significant amounts of ApoE on PEG-PHDCA NPs.

Covalent coupling of ApoE to nanoparticles, via avidin/biotin interaction or direct conjunction, was first enabled by the use of HSA NPs, because these specific types of NPs bear reactive groups on their surfaces. These ApoE-NP complexes led to significantly improved brain uptake without using surfactants. Over the past decades, polymeric NPs have been investigated since they deliver not only small molecule therapeutics, but also proteins and diagnostic agents. These NPs are highly promising drug delivery systems for macromolecules and small molecules in the field of CNS diseases due to their ability to protect the drug during blood circulation and guide them to an appropriate receptor without damaging the BBB. However, to the best of our knowledge, none of these described formulations using the ApoE-approach are on the market until today, partially because these investigations so far sparked only little interest in the pharmaceutical industry. It will be up to programs such as the BRAIN initiative® to translate preclinical findings into medicines.

References

[1] W.M. Pardridge, The blood-brain barrier: Bottleneck in brain drug development, NeuroRX, 2 (2005) 3-14.
[2] O. van Tellingen, B. Yetkin-Arik, M.C. de Gooijer, P. Wesseling, T. Wurdinger, H.E. de Vries, Overcoming the blood–brain tumor barrier for effective glioblastoma treatment, Drug Resistance Updates, 19 (2015) 1-12.
[3] Y.-L. Kwong, D.Y. Yeung, J.C. Chan, Intrathecal chemotherapy for hematologic malignancies: drugs and toxicities, Annals of hematology, 88 (2009) 193-201.
[4] K. Dorovini-Zis, P.D. Bowman, A. Lorris Betz, G.W. Goldstein, Hyperosmotic arabinose solutions open the tight junctions between brain capillary endothelial cells in tissue culture, Brain Research, 302 (1984) 383-386.
[5] a) K. Jahnke, D.F. Kraemer, K.R. Knight, D. Fortin, S. Bell, N.D. Doolittle, L.L. Muldoon, E.A. Neuwelt, Intraarterial chemotherapy and osmotic blood-brain barrier disruption for patients with embryonal and germ cell tumors of the central nervous system, Cancer: Interdisciplinary International Journal of the American Cancer Society, 112 (2008) 581-588.
b) P.J. Robinson, S.I. Rapoport, Model for Drug Uptake by Brain Tumors: Effects of Osmotic Treatment and of Diffusion in Brain, Journal of Cerebral Blood Flow & Metabolism, 10 (1990) 153-161.
[6] L.H. Treat, N. McDannold, N. Vykhodtseva, Y. Zhang, K. Tam, K. Hynynen, Targeted delivery of doxorubicin to the rat brain at therapeutic levels using MRI-guided focused ultrasound, International journal of cancer, 121 (2007) 901-907.
[7] A.H. Schinkel, J.J.M. Smit, O. van Tellingen, J.H. Beijnen, E. Wagenaar, L. van Deemter, C.A.A.M. Mol, M.A. van der Valk, E.C. Robanus-Maandag, H.P.J. te Riele, A.J.M. Berns, P. Borst, Disruption of the mouse mdr1a P-glycoprotein gene leads to a deficiency in the blood-brain barrier and to increased sensitivity to drugs, Cell, 77 (1994) 491-502.
[8] Y. Chen, L. Liu, Modern methods for delivery of drugs across the blood–brain barrier, Advanced Drug Delivery Reviews, 64 (2012) 640-665.
[9] J. Huwyler, W.M. Pardridge, Examination of Blood-Brain Barrier Transferrin Receptor by Confocal Fluorescent Microscopy of Unfixed Isolated Rat Brain Capillaries, Journal of Neurochemistry, 70 (1998) 883-886.
[10] A. Cerletti, J. Drewe, G. Fricker, A. Eberle, J. Huwyler, Endocytosis and Transcytosis of an Immunoliposome-Based Brain Drug Delivery System, J Drug Target, 8 (2000) 435-446.
[11] a) N.S. Chung, K.M. Wasan, Potential role of the low-density lipoprotein receptor family as mediators of cellular drug uptake, Advanced Drug Delivery Reviews, 56 (2004) 1315-1334.
b) S. Ito, S. Ohtsuki, T. Terasaki, Functional characterization of the brain-to-blood efflux clearance of human amyloid-β peptide (1–40) across the rat blood–brain barrier, Neuroscience Research, 56 (2006) 246-252.
c) M. Shibata, S. Yamada, S.R. Kumar, M. Calero, J. Bading, B. Frangione, D.M. Holtzman, C.A. Miller, D.K. Strickland, J. Ghiso, B.V. Zlokovic, Clearance of Alzheimer's amyloid-β1-40 peptide from brain by LDL receptor–related protein-1 at the blood-brain barrier, The Journal of Clinical Investigation, 106 (2000) 1489-1499.
d) P. Candela, J. Saint-Pol, M. Kuntz, M.-C. Boucau, Y. Lamartiniere, F. Gosselet, L. Fenart, In vitro discrimination of the role of LRP1 at the BBB cellular level: Focus on brain capillary endothelial cells and brain pericytes, Brain Research, 1594 (2015) 15-26.
[12] C.G. Davis, J.L. Goldstein, T.C. Südhof, R.G.W. Anderson, D.W. Russell, M.S. Brown, Acid-dependent ligand dissociation and recycling of LDL receptor mediated by growth factor homology region, Nature, 326 (1987) 760-765.
[13] P. Ramge, R.E. Unger, J.B. Oltrogge, D. Zenker, D. Begley, J. Kreuter, H. Von Briesen, Polysorbate-80 coating enhances uptake of polybutylcyanoacrylate (PBCA)-nanoparticles by

human and bovine primary brain capillary endothelial cells, European Journal of Neuroscience, 12 (2000) 1931-1940.
[14] S. Bhaskar, F. Tian, T. Stoeger, W. Kreyling, J.M. de la Fuente, V. Grazú, P. Borm, G. Estrada, V. Ntziachristos, D. Razansky, Multifunctional Nanocarriers for diagnostics, drug delivery and targeted treatment across blood-brain barrier: perspectives on tracking and neuroimaging, Particle and Fibre Toxicology, 7 (2010) 3.
[15] P. Ballabh, A. Braun, M. Nedergaard, The blood–brain barrier: an overview: structure, regulation, and clinical implications, Neurobiology of disease, 16 (2004) 1-13.
[16] D.J. Begley, The Blood-brain Barrier: Principles for Targeting Peptides and Drugs to the Central Nervous System, Journal of Pharmacy and Pharmacology, 48 (1996) 136-146.
[17] M. Aurrand-Lions, C. Johnson-Leger, C. Wong, L. Du Pasquier, B.A. Imhof, Heterogeneity of endothelial junctions is reflected by differential expression and specific subcellular localization of the three JAM family members, Blood, 98 (2001) 3699-3707.
[18] W.M. Pardridge, Drug transport across the blood–brain barrier, Journal of cerebral blood flow & metabolism, 32 (2012) 1959-1972.
[19] N.J. Abbott, A.A. Patabendige, D.E. Dolman, S.R. Yusof, D.J. Begley, Structure and function of the blood–brain barrier, Neurobiology of disease, 37 (2010) 13-25.
[20] W. Löscher, H. Potschka, Role of drug efflux transporters in the brain for drug disposition and treatment of brain diseases, Progress in Neurobiology, 76 (2005) 22-76.
[21] S. Gupta, S. Dhanda, R. Sandhir, 2 - Anatomy and physiology of blood-brain barrier, in: H. Gao, X. Gao (Eds.) Brain Targeted Drug Delivery System, Academic Press2019, pp. 7-31.
[22] J.E. Preston, N.J. Abbott, D.J. Begley, Transcytosis of macromolecules at the blood–brain barrier, Advances in pharmacology, 71 (2014) 147-163.
[23] I. Sauer, I.R. Dunay, K. Weisgraber, M. Bienert, M. Dathe, An Apolipoprotein E-Derived Peptide Mediates Uptake of Sterically Stabilized Liposomes into Brain Capillary Endothelial Cells, Biochemistry, 44 (2005) 2021-2029.
[24] R.D. Broadwell, B.J. Balin, M. Salcman, Transcytotic pathway for blood-borne protein through the blood-brain barrier, Proceedings of the National Academy of Sciences, 85 (1988) 632-636.
[25] D.W. Russell, M.S. Brown, J.L. Goldstein, Different combinations of cysteine-rich repeats mediate binding of low density lipoprotein receptor to two different proteins*, Journal of Biological Chemistry, 264 (1989) 21682-21688.
[26] R.W. Mahley, T.L. Innerarity, S.C. Rall Jr, K.H. Weisgraber, Plasma lipoproteins: apolipoprotein structure and function, Journal of lipid research, 25 (1984) 1277-1294.
[27] R.W. Mahley, J. Stanley C. Rall, Apolipoprotein E: Far More Than a Lipid Transport Protein, Annual Review of Genomics and Human Genetics, 1 (2000) 507-537.
[28] R.W. Mahley, Apolipoprotein E: Cholesterol Transport Protein with Expanding Role in Cell Biology, Science, 240 (1988) 622-630.
[29] A. Dergunov, Apolipoprotein E structure and substrate and receptor-binding activities of triglyceride-rich human plasma lipoproteins in normo-and hypertriglyceridemia, Biochemistry (Moscow), 69 (2004) 720-737.
[30] C.-C. Liu, T. Kanekiyo, H. Xu, G. Bu, Apolipoprotein E and Alzheimer disease: risk, mechanisms and therapy, Nature Reviews Neurology, 9 (2013) 106-118.
[31] J. Ribalta, J.-C. Vallvé, J. Girona, L. Masana, Apolipoprotein and apolipoprotein receptor genes, blood lipids and disease, Curr Opin Clin Nutr Metab Care, 6 (2003) 177-187.
[32] D.K. Strickland, S.L. Gonias, W.S. Argraves, Diverse roles for the LDL receptor family, Trends in Endocrinology & Metabolism, 13 (2002) 66-74.
[33] B. Dehouck, M.-P. Dehouck, J.-C. Fruchart, R. Cecchelli, A New Function for the LDL Receptor: Transcytosis of LDL Through the Blood-Brain Barrier, Vascular Endothelium: Responses to Injury, (1996) 254-254.

[34] T. Blunk, D.F. Hochstrasser, J.-C. Sanchez, B.W. Müller, R.H. Müller, Colloidal carriers for intravenous drug targeting: Plasma protein adsorption patterns on surface-modified latex particles evaluated by two-dimensional polyacrylamide gel electrophoresis, Electrophoresis, 14 (1993) 1382-1387.
[35] M. Lück, B.-R. Paulke, W. Schröder, T. Blunk, R.H. Müller, Analysis of plasma protein adsorption on polymeric nanoparticles with different surface characteristics, Journal of Biomedical Materials Research, 39 (1998) 478-485.
[36] a) L. Illum, S.S. Davis, The organ uptake of intravenously administered colloidal particles can be altered using a non-ionic surfactant (Poloxamer 338), FEBS Letters, 167 (1984) 79-82.
b) L. Illum, S.S. Davis, R.H. Müller, E. Mak, P. West, The organ distribution and circulation time of intravenously injected colloidal carriers sterically stabilized with a blockcopolymer - poloxamine 908, Life Sciences, 40 (1987) 367-374.
[37] S.D. Tröster, U. Müller, J. Kreuter, Modification of the body distribution of poly(methyl methacrylate) nanoparticles in rats by coating with surfactants, International Journal of Pharmaceutics, 61 (1990) 85-100.
[38] J. Kreuter, U. Täuber, V. Illi, Distribution and elimination of poly(methyl-2-14C-methacrylate) nanoparticle radioactivity after injection in rats and mice, Journal of Pharmaceutical Sciences, 68 (1979) 1443-1447.
[39] G. Borchard, K.L. Audus, F. Shi, J. Kreuter, Uptake of surfactant-coated poly(methyl methacrylate)-nanoparticles by bovine brain microvessel endothelial cell monolayers, International Journal of Pharmaceutics, 110 (1994) 29-35.
[40] S.D. Tröster, J. Kreuter, Contact angles of surfactants with a potential to alter the body distribution of colloidal drug carriers on poly (methyl methacrylate) surfaces, International Journal of Pharmaceutics, 45 (1988) 91-100.
[41] V. Lenaerts, P. Couvreur, D. Christiaens-Leyh, E. Joiris, M. Roland, B. Rollman, P. Speiser, Degradation of poly (isobutyl cyanoacrylate) nanoparticles, Biomaterials, 5 (1984) 65-68.
[42] a) G. Tosi, L. Costantino, B. Ruozi, F. Forni, M.A. Vandelli, Polymeric nanoparticles for the drug delivery to the central nervous system, Expert Opinion on Drug Delivery, 5 (2008) 155-174.
b) N. Voigt, P. Henrich-Noack, S. Kockentiedt, W. Hintz, J. Tomas, B.A. Sabel, Toxicity of polymeric nanoparticles in vivo and in vitro, Journal of Nanoparticle Research, 16 (2014) 2379.
c) A.M. Hall, R. Hemmer, R. Spaulding, H.N. Wetzel, J. Curcio, B.A. Sabel, P. Henrich-Noack, S. Pixley, T. Hopkins, R.L. Boyce, P.J. Schultheis, K.L. Haik, Cytotoxicity and apoptotic gene expression in an in vitro model of the blood–brain barrier following exposure to poly(butylcyanoacrylate) nanoparticles, J Drug Target, 24 (2016) 635-644.
[43] J. Kreuter, R.N. Alyautdin, D.A. Kharkevich, A.A. Ivanov, Passage of peptides through the blood-brain barrier with colloidal polymer particles (nanoparticles), Brain Research, 674 (1995) 171-174.
[44] U. Schröder, B.A. Sabel, Nanoparticles, a drug carrier system to pass the blood-brain barrier, permit central analgesic effects of i.v. dalargin injections, Brain Research, 710 (1996) 121-124.
[45] R.N. Alyaudtin, A. Reichel, R. Löbenberg, P. Ramge, J. Kreuter, D.J. Begley, Interaction of Poly(butylcyanoacrylate) Nanoparticles with the Blood-Brain Barrier in vivo and in vitro, J Drug Target, 9 (2001) 209-221.
[46] J. Kreuter, V.E. Petrov, D.A. Kharkevich, R.N. Alyautdin, Influence of the type of surfactant on the analgesic effects induced by the peptide dalargin after its delivery across the blood–brain barrier using surfactant-coated nanoparticles, Journal of Controlled Release, 49 (1997) 81-87.

[47] U. Schroeder, H. Schroeder, B.A. Sabel, Body distribution of 3HH-labelled dalargin bound to poly(butyl cyanoacrylate) nanoparticles after I.V. injections to mice, Life Sciences, 66 (2000) 495-502.
[48] R. Rempe, S. Cramer, S. Hüwel, H.-J. Galla, Transport of Poly(n-butylcyano-acrylate) nanoparticles across the blood–brain barrier in vitro and their influence on barrier integrity, Biochemical and Biophysical Research Communications, 406 (2011) 64-69.
[49] J.-C. Olivier, L. Fenart, R. Chauvet, C. Pariat, R. Cecchelli, W. Couet, Indirect Evidence that Drug Brain Targeting Using Polysorbate 80-Coated Polybutylcyanoacrylate Nanoparticles Is Related to Toxicity, Pharmaceutical Research, 16 (1999) 1836-1842.
[50] J. Kreuter, P. Ramge, V. Petrov, S. Hamm, S.E. Gelperina, B. Engelhardt, R. Alyautdin, H. von Briesen, D.J. Begley, Direct Evidence That Polysorbate-80-Coated Poly(Butylcyanoacrylate) Nanoparticles Deliver Drugs to the CNS via Specific Mechanisms Requiring Prior Binding of Drug to the Nanoparticles, Pharmaceutical Research, 20 (2003) 409-416.
[51] U. Schroeder, P. Sommerfeld, B.A. Sabel, Efficacy of Oral Dalargin-loaded Nanoparticle Delivery across the Blood–Brain Barrier, Peptides, 19 (1998) 777-780.
[52] D. Das, S. Lin, Double-coated poly (butylcynanoacrylate) nanoparticulate delivery systems for brain targeting of dalargin via oral administration, Journal of Pharmaceutical Sciences, 94 (2005) 1343-1353.
[53] a) L. Costantino, F. Gandolfi, G. Tosi, F. Rivasi, M.A. Vandelli, F. Forni, Peptide-derivatized biodegradable nanoparticles able to cross the blood–brain barrier, Journal of Controlled Release, 108 (2005) 84-96.
b) G. Tosi, L. Costantino, F. Rivasi, B. Ruozi, E. Leo, A.V. Vergoni, R. Tacchi, A. Bertolini, M.A. Vandelli, F. Forni, Targeting the central nervous system: In vivo experiments with peptide-derivatized nanoparticles loaded with Loperamide and Rhodamine-123, Journal of Controlled Release, 122 (2007) 1-9.
[54] S. Gelperina, O. Maksimenko, A. Khalansky, L. Vanchugova, E. Shipulo, K. Abbasova, R. Berdiev, S. Wohlfart, N. Chepurnova, J. Kreuter, Drug delivery to the brain using surfactant-coated poly(lactide-co-glycolide) nanoparticles: Influence of the formulation parameters, European Journal of Pharmaceutics and Biopharmaceutics, 74 (2010) 157-163.
[55] Y.-C. Chen, W.-Y. Hsieh, W.-F. Lee, D.-T. Zeng, Effects of surface modification of PLGA-PEG-PLGA nanoparticles on loperamide delivery efficiency across the blood–brain barrier, Journal of Biomaterials Applications, 27 (2013) 909-922.
[56] G. Omarch, Y. Kippie, S. Mentor, N. Ebrahim, D. Fisher, G. Murilla, H. Swai, A. Dube, Comparative in vitro transportation of pentamidine across the blood-brain barrier using polycaprolactone nanoparticles and phosphatidylcholine liposomes, Artificial cells, nanomedicine, and biotechnology, 47 (2019) 1428-1436.
[57] Y. Huang, B. Zhang, S. Xie, B. Yang, Q. Xu, J. Tan, Superparamagnetic Iron Oxide Nanoparticles Modified with Tween 80 Pass through the Intact Blood–Brain Barrier in Rats under Magnetic Field, ACS Applied Materials & Interfaces, 8 (2016) 11336-11341.
[58] S.D. Kong, J. Lee, S. Ramachandran, B.P. Eliceiri, V.I. Shubayev, R. Lal, S. Jin, Magnetic targeting of nanoparticles across the intact blood–brain barrier, Journal of Controlled Release, 164 (2012) 49-57.
[59] J. Kreuter, D. Shamenkov, V. Petrov, P. Ramge, K. Cychutek, C. Koch-Brandt, R. Alyautdin, Apolipoprotein-mediated Transport of Nanoparticle-bound Drugs Across the Blood-Brain Barrier, J Drug Target, 10 (2002) 317-325.
[60] D.A. Shamenkov, V.E. Petrov, R.N. Alyautdin, Effects of apolipoproteins on dalargin transport across the blood-brain barrier, Bulletin of Experimental Biology and Medicine, 142 (2006) 703-706.
[61] Y.-C. Kuo, R. Rajesh, Targeted delivery of rosmarinic acid across the blood–brain barrier for neuronal rescue using polyacrylamide-chitosan-poly(lactide-co-glycolide) nanoparticles

with surface cross-reacting material 197 and apolipoprotein E, International Journal of Pharmaceutics, 528 (2017) 228-241.
[62] M.T. Peracchia, E. Fattal, D. Desmaële, M. Besnard, J.P. Noël, J.M. Gomis, M. Appel, J. d'Angelo, P. Couvreur, Stealth® PEGylated polycyanoacrylate nanoparticles for intravenous administration and splenic targeting, Journal of Controlled Release, 60 (1999) 121-128.
[63] M.T. Peracchia, S. Harnisch, H. Pinto-Alphandary, A. Gulik, J.C. Dedieu, D. Desmaële, J. d'Angelo, R.H. Müller, P. Couvreur, Visualization of in vitro protein-rejecting properties of PEGylated stealth® polycyanoacrylate nanoparticles, Biomaterials, 20 (1999) 1269-1275.
[64] P. Calvo, B. Gouritin, H. Chacun, D. Desmaële, J. D'Angelo, J.-P. Noel, D. Georgin, E. Fattal, J.P. Andreux, P. Couvreur, Long-Circulating PEGylated Polycyanoacrylate Nanoparticles as New Drug Carrier for Brain Delivery, Pharmaceutical Research, 18 (2001) 1157-1166.
[65] H.R. Kim, K. Andrieux, S. Gil, M. Taverna, H. Chacun, D. Desmaële, F. Taran, D. Georgin, P. Couvreur, Translocation of Poly(ethylene glycol-co-hexadecyl)cyanoacrylate Nanoparticles into Rat Brain Endothelial Cells: Role of Apolipoproteins in Receptor-Mediated Endocytosis, Biomacromolecules, 8 (2007) 793-799.
[66] H.R. Kim, S. Gil, K. Andrieux, V. Nicolas, M. Appel, H. Chacun, D. Desmaële, F. Taran, D. Georgin, P. Couvreur, Low-density lipoprotein receptor-mediated endocytosis of PEGylated nanoparticles in rat brain endothelial cells, Cellular and Molecular Life Sciences, 64 (2007) 356-364.
[67] a) I. Brigger, J. Morizet, L. Laudani, G. Aubert, M. Appel, V. Velasco, M.-J. Terrier-Lacombe, D. Desmaële, J. d'Angelo, P. Couvreur, G. Vassal, Negative preclinical results with stealth® nanospheres-encapsulated Doxorubicin in an orthotopic murine brain tumor model, Journal of Controlled Release, 100 (2004) 29-40.
b) J. Kreuter, Drug delivery to the central nervous system by polymeric nanoparticles: What do we know?, Advanced Drug Delivery Reviews, 71 (2014) 2-14.
[68] K. Michaelis, M.M. Hoffmann, S. Dreis, E. Herbert, R.N. Alyautdin, M. Michaelis, J. Kreuter, K. Langer, Covalent Linkage of Apolipoprotein E to Albumin Nanoparticles Strongly Enhances Drug Transport into the Brain, Journal of Pharmacology and Experimental Therapeutics, 317 (2006) 1246.
[69] A. Zensi, D. Begley, C. Pontikis, C. Legros, L. Mihoreanu, S. Wagner, C. Büchel, H. von Briesen, J. Kreuter, Albumin nanoparticles targeted with Apo E enter the CNS by transcytosis and are delivered to neurones, Journal of Controlled Release, 137 (2009) 78-86.
[70] S. Wagner, A. Zensi, S.L. Wien, S.E. Tschickardt, W. Maier, T. Vogel, F. Worek, C.U. Pietrzik, J. Kreuter, H. von Briesen, Uptake mechanism of ApoE-modified nanoparticles on brain capillary endothelial cells as a blood-brain barrier model, PloS one, 7 (2012) e32568.
[71] J. Kreuter, T. Hekmatara, S. Dreis, T. Vogel, S. Gelperina, K. Langer, Covalent attachment of apolipoprotein A-I and apolipoprotein B-100 to albumin nanoparticles enables drug transport into the brain, Journal of Controlled Release, 118 (2007) 54-58.
[72] a) C. Portioli, M. Bovi, D. Benati, M. Donini, M. Perduca, A. Romeo, S. Dusi, H.L. Monaco, M. Bentivoglio, Novel functionalization strategies of polymeric nanoparticles as carriers for brain medications, Journal of Biomedical Materials Research Part A, 105 (2017) 847-858.
b) F. Re, I. Cambianica, S. Sesana, E. Salvati, A. Cagnotto, M. Salmona, P.-O. Couraud, S.M. Moghimi, M. Masserini, G. Sancini, Functionalization with ApoE-derived peptides enhances the interaction with brain capillary endothelial cells of nanoliposomes binding amyloid-beta peptide, Journal of Biotechnology, 156 (2011) 341-346.
c) F. Re, I. Cambianica, C. Zona, S. Sesana, M. Gregori, R. Rigolio, B. La Ferla, F. Nicotra, G. Forloni, A. Cagnotto, M. Salmona, M. Masserini, G. Sancini, Functionalization of liposomes with ApoE-derived peptides at different density affects cellular uptake and drug transport across

a blood-brain barrier model, Nanomedicine: Nanotechnology, Biology and Medicine, 7 (2011) 551-559.
[73] B. Raudszus, D. Mulac, K. Langer, A new preparation strategy for surface modified PLA nanoparticles to enhance uptake by endothelial cells, International Journal of Pharmaceutics, 536 (2018) 211-221.
[74] U. Schroeder, P. Sommerfeld, S. Ulrich, B.A. Sabel, Nanoparticle technology for delivery of drugs across the blood–brain barrier, Journal of Pharmaceutical Sciences, 87 (1998) 1305-1307.
[75] K.B. Kurakhmaeva, T.A. Voronina, I.G. Kapica, J. Kreuter, L.N. Nerobkova, S.B. Seredenin, V.Y. Balabanian, R.N. Alyautdin, Antiparkinsonian effect of nerve growth factor adsorbed on polybutylcyanoacrylate nanoparticles coated with polysorbate-80, Bulletin of Experimental Biology and Medicine, 145 (2008) 259-262.
[76] K.B. Kurakhmaeva, I.A. Djindjikhashvili, V.E. Petrov, V.U. Balabanyan, T.A. Voronina, S.S. Trofimov, J. Kreuter, S. Gelperina, D. Begley, R.N. Alyautdin, Brain targeting of nerve growth factor using poly(butyl cyanoacrylate) nanoparticles, J Drug Target, 17 (2009) 564-574.
[77] T. Feczkó, A. Piiper, S. Ansar, F.W. Blixt, M. Ashtikar, S. Schiffmann, T. Ulshöfer, M.J. Parnham, Y. Harel, L.L. Israel, J.-P. Lellouche, M.G. Wacker, Stimulating brain recovery after stroke using theranostic albumin nanocarriers loaded with nerve growth factor in combination therapy, Journal of Controlled Release, 293 (2019) 63-72.
[78] I. Khalin, R. Alyautdin, T.W. Wong, J. Gnanou, G. Kocherga, J. Kreuter, Brain-derived neurotrophic factor delivered to the brain using poly (lactide-co-glycolide) nanoparticles improves neurological and cognitive outcome in mice with traumatic brain injury, Drug Delivery, 23 (2016) 3520-3528.
[79] a) R.N. Alyautdin, E.B. Tezikov, P. Ramge, D.A. Kharkevich, D.J. Begley, J. Kreuter, Significant entry of tubocurarine into the brain of rats by adsorption to polysorbate 80–coated polybutylcyanoacrylate nanoparticles: An in situ brain perfusion study, Journal of Microencapsulation, 15 (1998) 67-74.
b) R.N. Alyautdin, V.E. Petrov, K. Langer, A. Berthold, D.A. Kharkevich, J. Kreuter, Delivery of loperamide across the blood-brain barrier with polysorbate 80-coated polybutylcyanoacrylate nanoparticles, Pharmaceutical research, 14 (1997) 325-328.
[80] S.C.J. Steiniger, J. Kreuter, A.S. Khalansky, I.N. Skidan, A.I. Bobruskin, Z.S. Smirnova, S.E. Severin, R. Uhl, M. Kock, K.D. Geiger, S.E. Gelperina, Chemotherapy of glioblastoma in rats using doxorubicin-loaded nanoparticles, International Journal of Cancer, 109 (2004) 759-767.
[81] S. Wohlfart, A.S. Khalansky, S. Gelperina, D. Begley, J. Kreuter, Kinetics of transport of doxorubicin bound to nanoparticles across the blood–brain barrier, Journal of Controlled Release, 154 (2011) 103-107.
[82] A. Ambruosi, S. Gelperina, A. Khalansky, S. Tanski, A. Theisen, J. Kreuter, Influence of surfactants, polymer and doxorubicin loading on the anti-tumour effect of poly(butyl cyanoacrylate) nanoparticles in a rat glioma model, Journal of Microencapsulation, 23 (2006) 582-592.
[83] A. Ambruosi, A.S. Khalansky, H. Yamamoto, S.E. Gelperina, D.J. Begley, J. Kreuter, Biodistribution of polysorbate 80-coated doxorubicin-loaded [14C]-poly(butyl cyanoacrylate) nanoparticles after intravenous administration to glioblastoma-bearing rats, J Drug Target, 14 (2006) 97-105.
[84] M. Wacker, Nanocarriers for intravenous injection—The long hard road to the market, International Journal of Pharmaceutics, 457 (2013) 50-62.
[85] Y. Malinovskaya, P. Melnikov, V. Baklaushev, A. Gabashvili, N. Osipova, S. Mantrov, Y. Ermolenko, O. Maksimenko, M. Gorshkova, V. Balabanyan, J. Kreuter, S. Gelperina, Delivery of doxorubicin-loaded PLGA nanoparticles into U87 human glioblastoma cells, International Journal of Pharmaceutics, 524 (2017) 77-90.

[86] a) M. Gregori, D. Bertani, E. Cazzaniga, A. Orlando, M. Mauri, A. Bianchi, F. Re, S. Sesana, S. Minniti, M. Francolini, A. Cagnotto, M. Salmona, L. Nardo, D. Salerno, F. Mantegazza, M. Masserini, R. Simonutti, Investigation of Functionalized Poly(N,N-dimethylacrylamide)-block-polystyrene Nanoparticles As Novel Drug Delivery System to Overcome the Blood–Brain Barrier In Vitro, Macromolecular Bioscience, 15 (2015) 1687-1697.
b) J. Li, P. Cai, A. Shalviri, J.T. Henderson, C. He, W.D. Foltz, P. Prasad, P.M. Brodersen, Y. Chen, R. DaCosta, A.M. Rauth, X.Y. Wu, A Multifunctional Polymeric Nanotheranostic System Delivers Doxorubicin and Imaging Agents across the Blood–Brain Barrier Targeting Brain Metastases of Breast Cancer, ACS Nano, 8 (2014) 9925-9940.
[87] K. Gao, X. Jiang, Influence of particle size on transport of methotrexate across blood brain barrier by polysorbate 80-coated polybutylcyanoacrylate nanoparticles, International Journal of Pharmaceutics, 310 (2006) 213-219.
[88] X.-H. Tian, X.-N. Lin, F. Wei, W. Feng, Z.-C. Huang, P. Wang, L. Ren, Y. Diao, Enhanced brain targeting of temozolomide in polysorbate-80 coated polybutylcyanoacrylate nanoparticles, Int J Nanomedicine, (2011) 445-452.
[89] H. Ebrahimi Shahmabadi, F. Movahedi, M. Koohi Moftakhari Esfahani, S.E. Alavi, A. Eslamifar, G. Mohammadi Anaraki, A. Akbarzadeh, Efficacy of Cisplatin-loaded polybutyl cyanoacrylate nanoparticles on the glioblastoma, Tumor Biology, 35 (2014) 4799-4806.
[90] a) R.S. Mulik, J. Mönkkönen, R.O. Juvonen, K.R. Mahadik, A.R. Paradkar, ApoE3 mediated polymeric nanoparticles containing curcumin: Apoptosis induced in vitro anticancer activity against neuroblastoma cells, International Journal of Pharmaceutics, 437 (2012) 29-41.
b) R.S. Mulik, J. Mönkkönen, R.O. Juvonen, K.R. Mahadik, A.R. Paradkar, ApoE3 Mediated Poly(butyl) Cyanoacrylate Nanoparticles Containing Curcumin: Study of Enhanced Activity of Curcumin against Beta Amyloid Induced Cytotoxicity Using In Vitro Cell Culture Model, Molecular Pharmaceutics, 7 (2010) 815-825.
[91] a) B. Wilson, M.K. Samanta, K. Santhi, K.P.S. Kumar, N. Paramakrishnan, B. Suresh, Targeted delivery of tacrine into the brain with polysorbate 80-coated poly(n-butylcyanoacrylate) nanoparticles, European Journal of Pharmaceutics and Biopharmaceutics, 70 (2008) 75-84.
b) B. Wilson, M.K. Samanta, K. Santhi, K.P.S. Kumar, N. Paramakrishnan, B. Suresh, Poly(n-butylcyanoacrylate) nanoparticles coated with polysorbate 80 for the targeted delivery of rivastigmine into the brain to treat Alzheimer's disease, Brain Research, 1200 (2008) 159-168.
[92] G. Mittal, H. Carswell, R. Brett, S. Currie, M.N.V.R. Kumar, Development and evaluation of polymer nanoparticles for oral delivery of estradiol to rat brain in a model of Alzheimer's pathology, Journal of Controlled Release, 150 (2011) 220-228.
[93] S. Lundquist, M. Renftel, The use of in vitro cell culture models for mechanistic studies and as permeability screens for the blood–brain barrier in the pharmaceutical industry—Background and current status in the drug discovery process, Vascular Pharmacology, 38 (2002) 355-364.
[94] D. Zenker, D. Begley, H. Bratzke, H. Rübsamen-Waigmann, H. von Briesen, Human blood-derived macrophages enhance barrier function of cultured primary bovine and human brain capillary endothelial cells, The Journal of Physiology, 551 (2003) 1023-1032.
[95] A. Patabendige, R.A. Skinner, N.J. Abbott, Establishment of a simplified in vitro porcine blood–brain barrier model with high transendothelial electrical resistance, Brain Research, 1521 (2013) 1-15.
[96] N. Perrière, P. Demeuse, E. Garcia, A. Regina, M. Debray, J.-P. Andreux, P. Couvreur, J.-M. Scherrmann, J. Temsamani, P.-O. Couraud, M.A. Deli, F. Roux, Puromycin-based purification of rat brain capillary endothelial cell cultures. Effect on the expression of blood–brain barrier-specific properties, Journal of Neurochemistry, 93 (2005) 279-289.

[97] C. Weidenfeller, S. Schrot, A. Zozulya, H.-J. Galla, Murine brain capillary endothelial cells exhibit improved barrier properties under the influence of hydrocortisone, Brain Research, 1053 (2005) 162-174.
[98] J. Bicker, G. Alves, A. Fortuna, A. Falcão, Blood–brain barrier models and their relevance for a successful development of CNS drug delivery systems: A review, European Journal of Pharmaceutics and Biopharmaceutics, 87 (2014) 409-432.
[99] T. Yang, K.E. Roder, T.J. Abbruscato, Evaluation of bEnd5 cell line as an in vitro model for the blood–brain barrier under normal and hypoxic/aglycemic conditions, Journal of Pharmaceutical Sciences, 96 (2007) 3196-3213.
[100] K. Sobue, N. Yamamoto, K. Yoneda, M.E. Hodgson, K. Yamashiro, N. Tsuruoka, T. Tsuda, H. Katsuya, Y. Miura, K. Asai, T. Kato, Induction of blood–brain barrier properties in immortalized bovine brain endothelial cells by astrocytic factors, Neuroscience Research, 35 (1999) 155-164.
[101] W. Neuhaus, R. Lauer, S. Oelzant, U.P. Fringeli, G.F. Ecker, C.R. Noe, A novel flow based hollow-fiber blood–brain barrier in vitro model with immortalised cell line PBMEC/C1–2, Journal of Biotechnology, 125 (2006) 127-141.
[102] A. Cestelli, C. Catania, S. D'Agostino, I. Di Liegro, L. Licata, G. Schiera, G.L. Pitarresi, G. Savettieri, V. De Caro, G. Giandalia, L.I. Giannola, Functional feature of a novel model of blood brain barrier: studies on permeation of test compounds, Journal of Controlled Release, 76 (2001) 139-147.
[103] T. Yang, K.E. Roder, T.J. Abbruscato, Evaluation of bEnd5 cell line as an in vitro model for the blood–brain barrier under normal and hypoxic/aglycemic conditions, Journal of Pharmaceutical Sciences, 96 (2007) 3196-3213.
[104] E. Urich, S.E. Lazic, J. Molnos, I. Wells, P.-O. Freskgård, Transcriptional profiling of human brain endothelial cells reveals key properties crucial for predictive in vitro blood-brain barrier models, PloS one, 7 (2012) e38149.
[105] S. Nakagawa, M.A. Deli, H. Kawaguchi, T. Shimizudani, T. Shimono, Á. Kittel, K. Tanaka, M. Niwa, A new blood–brain barrier model using primary rat brain endothelial cells, pericytes and astrocytes, Neurochemistry International, 54 (2009) 253-263.
[106] Y.-C. Kuo, C.-H. Lu, Effect of human astrocytes on the characteristics of human brain-microvascular endothelial cells in the blood–brain barrier, Colloids and Surfaces B: Biointerfaces, 86 (2011) 225-231.
[107] K.C.-K. Malina, I. Cooper, V.I. Teichberg, Closing the gap between the in-vivo and in-vitro blood–brain barrier tightness, Brain Research, 1284 (2009) 12-21.
[108] G. Schiera, E. Bono, M.P. Raffa, A. Gallo, G.L. Pitarresi, I. Di Liegro, G. Savettieri, Synergistic effects of neurons and astrocytes on the differentiation of brain capillary endothelial cells in culture, Journal of Cellular and Molecular Medicine, 7 (2003) 165-170.
[109] É. Hellinger, S. Veszelka, A.E. Tóth, F. Walter, Á. Kittel, M.L. Bakk, K. Tihanyi, V. Háda, S. Nakagawa, T. Dinh Ha Duy, M. Niwa, M.A. Deli, M. Vastag, Comparison of brain capillary endothelial cell-based and epithelial (MDCK-MDR1, Caco-2, and VB-Caco-2) cell-based surrogate blood–brain barrier penetration models, European Journal of Pharmaceutics and Biopharmaceutics, 82 (2012) 340-351.
[110] P. Ramge, J. Kreuter, B. Lemmer, Circadian Phase-Dependent Antinociceptive Reaction in Mice Determined by the Hot-Plate test and the Tail-Flick Test After Intravenous Injection of Dalargin-Loaded Nanoparticles, Chronobiology International, 16 (1999) 767-777.
[111] D. Triguero, J. Buciak, W.M. Pardridge, Capillary Depletion Method for Quantification of Blood–Brain Barrier Transport of Circulating Peptides and Plasma Proteins, Journal of Neurochemistry, 54 (1990) 1882-1888.
[112] F.K. Miura, M.J.F. Alves, M.C. Rocha, R.S. Silva, S.M. Oba-Shinjo, M. Uno, C. Colin, M.C. Sogayar, S.K. Marie, Experimental nodel of C6 brain tumors in athymic rats, Arquivos de neuro-psiquiatria, 66 (2008) 238-241.

[113] C.-X. Wang, L.-S. Huang, L.-B. Hou, L. Jiang, Z.-T. Yan, Y.-L. Wang, Z.-L. Chen, Antitumor effects of polysorbate-80 coated gemcitabine polybutylcyanoacrylate nanoparticles in vitro and its pharmacodynamics in vivo on C6 glioma cells of a brain tumor model, Brain Research, 1261 (2009) 91-99.
[114] T. Hase, S. Shishido, S. Yamamoto, R. Yamashita, H. Nukima, S. Taira, T. Toyoda, K. Abe, T. Hamaguchi, K. Ono, M. Noguchi-Shinohara, M. Yamada, S. Kobayashi, Rosmarinic acid suppresses Alzheimer's disease development by reducing amyloid β aggregation by increasing monoamine secretion, Scientific Reports, 9 (2019) 8711.
[115] a) D.E. Owens, N.A. Peppas, Opsonization, biodistribution, and pharmacokinetics of polymeric nanoparticles, International Journal of Pharmaceutics, 307 (2006) 93-102.
b) J.-H. Kang, R. Toita, M. Murata, Liver cell-targeted delivery of therapeutic molecules, Critical Reviews in Biotechnology, 36 (2016) 132-143.
[116] V. Petkov, A. Mosharrof, V. Petkov, Comparative studies on the effects of the nootropic drugs adafenoxate, meclofenoxate and piracetam, and of citicholine on scopolamine-impaired memory, exploratory behavior and physical capabilities (experiments on rats and mice), Acta Physiologica Et Pharmacologica Bulgarica, 14 (1988) 3-13.
[117] N.J. Abbott, Blood–brain barrier structure and function and the challenges for CNS drug delivery, Journal of Inherited Metabolic Disease, 36 (2013) 437-449.
[118] Y.-H. Hsieh, C.-Y. Chou, Structural and functional characterization of human apolipoprotein E 72-166 peptides in both aqueous and lipid environments, Journal of biomedical science, 18 (2011) 1-9.
[119] a) J. Kreuter, Influence of the surface properties on nanoparticle-mediated transport of drugs to the brain, Journal of nanoscience and nanotechnology, 4 (2004) 484-488.
b) J. Kreuter, Application of nanoparticles for the delivery of drugs to the brain, International Congress Series, 1277 (2005) 85-94.
[120] G. David, I.M. Jaba, B. Tamba, C. Bohotin, A. Neamtu, X. Patras, B.C. Simionescu, O.C. Mungiu, Antinociceptive effect of morphiceptin loaded poly (butylcyanoacrylate) nanoparticles, Rev Roum Chim, 55 (2010) 923-931.
[121] H. Liu, J. Ni, R. Wang, In vitro release performance and analgesic activity of endomorphin-1 loaded nanoparticles, Die Pharmazie-An International Journal of Pharmaceutical Sciences, 61 (2006) 450-452.
[122] T. Schuster, A. Mühlstein, C. Yaghootfam, O. Maksimenko, E. Shipulo, S. Gelperina, J. Kreuter, V. Gieselmann, U. Matzner, Potential of surfactant-coated nanoparticles to improve brain delivery of arylsulfatase A, Journal of Controlled Release, 253 (2017) 1-10.
[123] S. Jose, B.C. Juna, T.A. Cinu, H. Jyoti, N.A. Aleykutty, Carboplatin loaded Surface modified PLGA nanoparticles: Optimization, characterization, and in vivo brain targeting studies, Colloids and Surfaces B: Biointerfaces, 142 (2016) 307-314.
[124] C. He, P. Cai, J. Li, T. Zhang, L. Lin, A.Z. Abbasi, J.T. Henderson, A.M. Rauth, X.Y. Wu, Blood-brain barrier-penetrating amphiphilic polymer nanoparticles deliver docetaxel for the treatment of brain metastases of triple negative breast cancer, Journal of Controlled Release, 246 (2017) 98-109.
[125] Z. Li, J. Zhu, Y. Wang, M. Zhou, D. Li, S. Zheng, L. Yin, C. Luo, H. Zhang, L. Zhong, In situ apolipoprotein E-enriched corona guides dihydroartemisinin-decorating nanoparticles towards LDLr-mediated tumor-homing chemotherapy, Asian journal of pharmaceutical sciences, 15 (2020) 482-491.
[126] C.-X. Wang, L.-S. Huang, L.-B. Hou, L. Jiang, Z.-T. Yan, Y.-L. Wang, Z.-L. Chen, Antitumor effects of polysorbate-80 coated gemcitabine polybutylcyanoacrylate nanoparticles in vitro and its pharmacodynamics in vivo on C6 glioma cells of a brain tumor model, Brain Research, 1261 (2009) 91-99.

[127] B.A. Abdel-Wahab, M.M. Abdel-Latif, A.A. Abdel-Hafez, Comparative study for brain delivery of tacrine using polysorbate 80-coated poly(butylcyanoacrylate) and pegylated-poly(butylcyanoacrylate) nanoparticles, International Journal of Nano and Biomaterials, 2 (2009) 360-374.
[128] C. Grossi, C. Guccione, B. Isacchi, M.C. Bergonzi, I. Luccarini, F. Casamenti, A.R. Bilia, Development of blood-brain barrier permeable nanoparticles as potential carriers for salvianolic acid B to CNS, Planta Medica, 83 (2017) 382-391.
[129] A. Friese, E. Seiller, G. Quack, B. Lorenz, J. Kreuter, Increase of the duration of the anticonvulsive activity of a novel NMDA receptor antagonist using poly(butylcyanoacrylate) nanoparticles as a parenteral controlled release system, European Journal of Pharmaceutics and Biopharmaceutics, 49 (2000) 103-109.
[130] J. DARIUS, F.P. MEYER, B.A. SABEL, U. SCHROEDER, Influence of Nanoparticles on the Brain-to-serum Distribution and the Metabolism of Valproic Acid in Mice, Journal of Pharmacy and Pharmacology, 52 (2000) 1043-1047.
[131] M. Liu, H. Li, G. Luo, Q. Liu, Y. Wang, Pharmacokinetics and biodistribution of surface modification polymeric nanoparticles, Archives of Pharmacal Research, 31 (2008) 547-554.
[132] L.-x. Zhao, A.-c. Liu, S.-w. Yu, Z.-x. Wang, X.-q. Lin, G.-x. Zhai, Q.-z. Zhang, The Permeability of Puerarin Loaded Poly(butylcyanoacrylate) Nanoparticles Coated with Polysorbate 80 on the Blood–Brain Barrier and Its Protective Effect against Cerebral Ischemia/Reperfusion Injury, Biological and Pharmaceutical Bulletin, 36 (2013) 1263-1270.
[133] P. Marcianes, S. Negro, L. García-García, C. Montejo, E. Barcia, A. Fernández-Carballido, Surface-modified gatifloxacin nanoparticles with potential for treating central nervous system tuberculosis, Int J Nanomedicine, 12 (2017) 1959.
[134] N. Xu, J. Gu, Y. Zhu, H. Wen, Q. Ren, J. Chen, Efficacy of intravenous amphotericin B-polybutylcyanoacrylate nanoparticles against cryptococcal meningitis in mice, Int J Nanomedicine, (2011) 905-913.
[135] T. Ren, N. Xu, C. Cao, W. Yuan, X. Yu, J. Chen, J. Ren, Preparation and Therapeutic Efficacy of Polysorbate-80-Coated Amphotericin B/PLA-b-PEG Nanoparticles, Journal of Biomaterials Science, Polymer Edition, 20 (2009) 1369-1380.
[136] M. Bagad, Z.A. Khan, Poly (n-butylcyanoacrylate) nanoparticles for oral delivery of quercetin: preparation, characterization, and pharmacokinetics and biodistribution studies in Wistar rats, Int J Nanomedicine, 10 (2015) 3921.
[137] Y.-C. Kuo, F.-L. Su, Transport of stavudine, delavirdine, and saquinavir across the blood–brain barrier by polybutylcyanoacrylate, methylmethacrylate-sulfopropylmethacrylate, and solid lipid nanoparticles, International Journal of Pharmaceutics, 340 (2007) 143-152.
[138] S. Wagner, J. Kufleitner, A. Zensi, M. Dadparvar, S. Wien, J. Bungert, T. Vogel, F. Worek, J. Kreuter, H.v. Briesen, Nanoparticulate transport of oximes over an in vitro blood-brain barrier model, PLoS One, 5 (2010).
[139] P. Girotra, S.K. Singh, A Comparative Study of Orally Delivered PBCA and ApoE Coupled BSA Nanoparticles for Brain Targeting of Sumatriptan Succinate in Therapeutic Management of Migraine, Pharmaceutical Research, 33 (2016) 1682-1695.
[140] A. Appelt-Menzel, A. Cubukova, K. Günther, F. Edenhofer, J. Piontek, G. Krause, T. Stüber, H. Walles, W. Neuhaus, M. Metzger, Establishment of a Human Blood-Brain Barrier Co-culture Model Mimicking the Neurovascular Unit Using Induced Pluri- and Multipotent Stem Cells, Stem Cell Reports, 8 (2017) 894-906.

Chapter III

Proteins as Functional Components of Nanoparticles for Brain Targeting

III.2 Protein Corona Investigations of Polyplexes with Varying Hydrophobicity - from Method Development to *in vitro* Studies

This chapter was submitted as research article as a shortened version in the International Journal of Pharmaceutics (04/2023):

Natascha Hartl, David C. Jürgens, Simone Carneiro, Ann-Christine König, Ximian Xiao, Runhui Liu, Stefanie M. Hauck, Olivia M. Merkel

"Protein Corona Investigations of Polyplexes with Varying Hydrophobicity – from Method Development to *in vitro* Studies"

Graphical Abstract

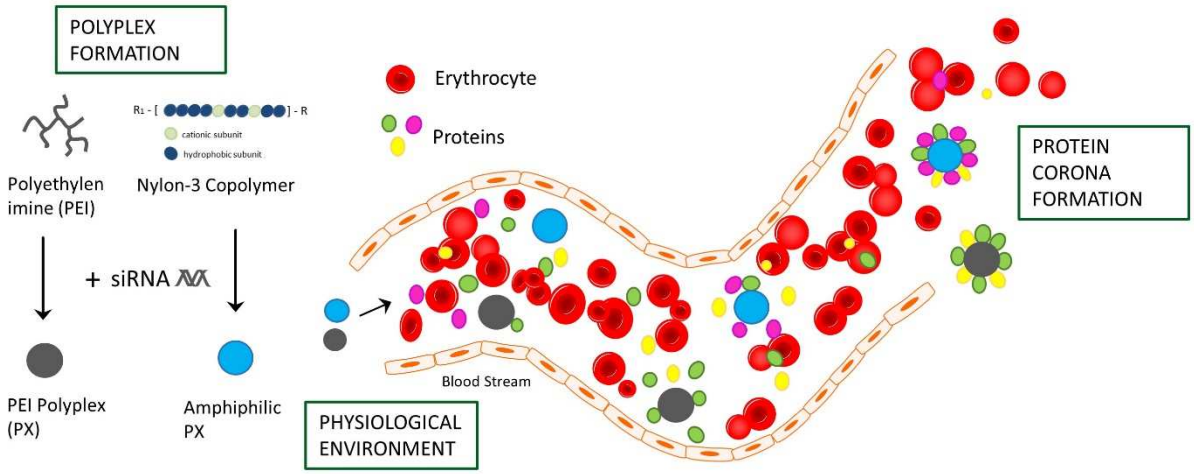

Abstract

In the field of non-viral drug delivery, polyplexes (PXs) represent an advanced investigated and highly promising tool for the delivery of nucleic acids. PXs are dynamic systems obtained via electrostatic interactions between cationic polymers and anionic nucleic acids. Upon encountering physiological fluids, they adsorb biological molecules to form a biocorona. The protein corona (PC) consists of the hard PC, which is formed by proteins strongly associated with the surface of the PX, and the soft corona, which represents the outer layer with weakly bound proteins. Once the PC is formed, solely the hard corona dictates the subsequent fate of the PX as a therapeutic agent in the body. The absorbed proteins influence PXs biodistribution, transfection efficiencies and targeting abilities. So far, PC formation is an overlooked parameter in the development process of safe and efficient nucleic acid carriers, especially due to a lack of methodologies for investigations on dynamic systems. In an effort to understand protein – PX interactions and the effect of PX material on corona composition, we utilized cationic branched 10kDa polyethyleneimine (b-PEI) and a hydrophobically modified nylon-3 polymer ($NM_{0.2}/CP_{0.8}$) within this study to develop appropriate methods for PC investigations. A centrifugation procedure for isolating hard corona – PX complexes (PCPXs) from soft corona proteins after incubating the PXs in fetal bovine serum (FBS) for PC formation was optimized by applying dynamic light scattering and SYBR Gold assay techniques. Successfully isolated PCPXs were characterized regarding their physicochemical characteristics, such as particle size and surface charge by dynamic light scattering and laser Doppler anemometry. First insight into the PC composition was provided by visualization of separated proteins via sodium dodedyclsulfate polyacrylamide gel electrophoresis (SDS-PAGE) after protein quantification with bicinchoninic assay (BCA assay). The identification of hard corona proteins for b-PEI and

$NM_{0.2}/CP_{0.8}$ PXs was enabled by a liquid chromatography-tandem mass spectrometry (LC-MS-MS) method. To determine the influence of protein adsorption on the cellular internalization abilities of PXPCs, uptake experiments were conducted by flow cytometry. The purification of PCPXs via centrifugation was successfully optimized without any significant loss of material or aggregation phenomena, leading to particles with appropriate sizes and PDI values. Negative zeta potentials measured after the purification process confirmed that hard corona proteins are still present on the surface of the PXs. LC-MS-MS results clearly demonstrated the differences in PC composition in dependency of the underlying PXs material. Particularly, transport proteins were found to reveal higher binding affinities to the hydrophobic $NM_{0.2}/CP_{0.8}$ PXs. With regard to especially interesting functional proteins, which might be able to induce active targeting effects, several well-known candidates, e.g., albumin, Transferrin or apolipoproteins could be detected to a similar extent on b-PEI and $NM_{0.2}/CP_{0.8}$ PXs. Interestingly, a specific functional protein, the hyaluronan binding protein (HAPB2), was detected with a significantly higher amount on $NM_{0.2}/CP_{0.8}$ PXs. Cellular internalization studies with a CD44 receptor-positive cell line displayed significantly higher cellular internalization of $NM_{0.2}/CP_{0.8}$ PCPXs in comparison to plain $NM_{0.2}/CP_{0.8}$ PXs. These results indicated a potential correlation between uptake capabilities and adsorbed proteins.

1. Introduction

During the past several decades, nanomedicines have gained increasing attention as they provide efficient and safe approaches for applications in the field of diagnostics, therapeutics and targeted drug delivery [1]. The increasing number of nanomedicines on the market supports their relevance as therapeutics [2]. Driven by the pandemic, the current research focus in the area of nucleic acid delivery is on non-viral delivery systems, such as liposomes, polymers or inorganic nanoparticles. These systems feature low immunogenicity, excellent biocompatibility and facile synthesis and modification possibilities [3]. As an encapsulated drug, small interfering RNA (siRNA) offers a promising therapeutic approach by downregulating disease-related genes via RNA interference [4-8]. Cationic polymers have been extensively investigated as they form complexes with the siRNA molecule via electrostatic interactions, thus enabling efficient siRNA delivery to target sites [9]. Among cationic polymers, polyethyleneimines (PEI) are the most pre-clinically evaluated ones and are considered the “gold standard” for successful delivery of nucleic acids [10]. In order to improve transfection efficiency and target specificity of delivery systems, considerable efforts have been made by modifying polymers

with targeting ligands. This strategy leads to preferential and efficient internalization of particles into target cells and thus, a tremendous decrease of side effects [11]. However, an overlooked parameter in understanding the nanoparticle's (NP) fate *in vivo* after intravenous injection is the interaction of the nanocarriers with blood components. Once NPs are administered into the body, they are immediately covered by proteins from the bloodstream, leading to the formation of the so-called protein corona (PC) [12, 13]. The corona forms due to the high surface free energy of NPs, resulting in the adsorption of various molecules, most notably proteins. The binding forces that are responsible for such interactions include van der Waals interactions, hydrogen bonds, hydrophobic interactions, electrostatic interactions and $\pi - \pi$ stacking [14]. The current hypothesis states that the corona consists of a hard and soft layer surrounding the NPs [15]. The hard layer is generally defined as the corona composed of tightly bound proteins that are slowly exchanging on the NPs' surface. Hard corona proteins ensure cell interactions, the initiation of tissue responses and many other biological processes in a biological milieu. The soft PC is referred to as a layer of weakly bound proteins that are able to rapidly exchange due to weak interactions with proteins of the hard layer. Therefore, they are irrelevant to the functional response of the nanoparticulate system *in vivo* [1]. The composition of biomolecules covering the NPs' surface depends to a large extent on the NPs' material, size, shape and surface charge. Thus, NPs with different properties acquire various new "biological identities" in a biological environment. Protein binding is established as one of the most important factors influencing biodistribution as well as the effectiveness of the delivery systems [16-19], as it affects the entire range of pharmacokinetic and -dynamic processes [20-23]. For most protein identification studies, NPs are incubated with plasma to ensure an excess of the plasma protein concentration regarding the available particle surface area. This is the most reliable method to mimic the conditions in the bloodstream. The effect of the bound proteins also implies that they can i) hamper the interaction between targeting ligands of NPs with their respective target cells [24] and ii) induce interactions through newly adsorbed targeting ligands [25]. This highlights the urgent need for appropriate methods for PC investigations in the early stage of the research to understand the identity of bound proteins and their influence on the physicochemical properties of the NPs, their biodistribution, and their ability to reach target sites. Most of the previous studies regarding protein adsorption were focused on solid NPs, whereas the investigation of dynamic systems, with some exceptions [26-30], remains a vital research question. Due to the lack of purification and characterization methods for corona proteins bound to dynamic polyplex (PX) systems, the aim of this study was to develop appropriate techniques that enable isolation, quantification and identification of

the proteins in order to gain a better understanding of protein–PX interactions. Besides a large number of inert proteins, numerous functional proteins can adsorb to a drug delivery system. Some of them are able to induce targeting effects via receptor-mediated endocytosis [25]. NPs material and physicochemical properties strongly influence the adsorbed protein profile, whereby hydrophobicity emerged as one of the most important factors [12]. Therefore, in addition to the well-known cationic branched – PEI (b-PEI) polymers, highly hydrophobic nylon-3 polymers were used in this study, enabling the examination of variations in the PC profiles depending on the NPs properties. Nylon-3 polymers can be synthesized via anionic ring-opening polymerization by the statistical copolymerization of various ß-lactams to incorporate both cationic and hydrophobic subunits. This strategy provides the opportunity to obtain tailor-made polymer compositions by regulation of the monomer feed [31]. Herein, we utilized a highly hydrophobic nylon-3 copolymer ($NM_{0.2}/CP_{0.8}$) that was previously established as a promising siRNA delivery vehicle [32]. Dynamic siRNA-polymer PXs were formed by complexing negatively charged siRNA molecules with cationic b-PEI and $NM_{0.2}/CP_{0.8}$ polymers via electrostatic interactions. Thereafter, the PC formation was simulated by incubating the particles in fetal bovine serum (FBS). In the first step, purification protocols for the separation of protein corona-polyplex complexes (PCPXs) from unbound and loosely attached proteins were successfully established. Purified PCPXs were then characterized in detail regarding physicochemical characteristics such as hydrodynamic diameters, size distributions, and surface charges. Furthermore, to answer the question of the composition of the PC and to identify functional key proteins, SDS-PAGE and LC-MS-MS techniques were applied. Based on these findings, we correlated the obtained protein binding profiles with the cellular internalization ability of PCPXs in comparison to plain PXs via flow cytometry *in vitro*.

2. Materials and Methods

2.1 Materials for analytical analysis

Branched PEI (b-PEI) 10kDa, HEPES (4-(2-hydroxyethyl)–1-piperazineethanesulfonic acid) and fetal bovine serum (FBS) were purchased from Sigma-Aldrich (Taufkirchen, Germany). Novex™ 10% tris-glycine gel, PageRuler™ Plus Prestained Protein Ladder (10 to 250 kDA), Pierce™ Lane Marker Reducing Sample Buffer, Pierce™ BCA Protein Assay Kit and HyClone trypan blue solution 0.4% in phosphate buffered saline were purchased from Thermo Fisher Scientific (Waltham, MA, USA). Rotiphorese®10x SDS-PAGE buffer was obtained from Carl Roth (Karlsruhe, Germany) and Protein Assay Dye Reagent Concentrate was purchased from

Bio-Rad (Hercules, CA, U.S.A.). Lys-C was obtained from Wako Chemicals (Neuss, Germany) and trypsin was purchased from Promega (Mannheim, Germany). Amine-modified eGFP siRNA (5′- pACCCUGAAGUUCAUCUGCACCACcg, 3′- ACUGGGACUUCAAGUAGAC GGGUGGC), and scrambled siRNA (5′-pCGUUAAUCGCGUAUAAUACGCGUat, 3′- CAGCAAUUAGCGCAUAUUAUGCGCAUAp) were purchased from Integrated DNA Technologies (Leuven, Belgium). Indication of modified nucleotides: "p" denotes a phosphate residue, lower case letters are 2′-deoxyribonucleotides, capital letters are ribonucleotides, and underlined capital letters are 2′-O-methylribonucleotides.

2.2 Materials for cell culture experiments

For cell culture experiments U87 cells (human glioblastoma astrocytoma), MCF7 cells (human breast cancer), Eagle's Minimum Essential Medium (EMEM), Dulbecco's Phosphate Buffered Saline (PBS), radioimmunoprecipitation (RIPA) lysis buffer, cOmplete™ Mini, EDTA-free Protease Inhibitor Cocktail, Phosphatase Inhibitor Cocktail 2, protein and analytical standard, bovine serum albumin (BSA), Amersham™ Protran Western blotting membranes (nitrocellulose, pore size 0.45 μm), Tris Buffered Saline with Tween®20 (TBST) and trypsin-EDTA solution 0.25% were purchased from Sigma-Aldrich (Taufkirchen, Germany). NHS-modified AlexaFluor 488 (AF488) dye was obtained from Life Technologies (Carlsbad, California, USA) and Novex™ Tris-Glycine Transfer Buffer (25X), SuperSignal™ West Pico PLUS Chemiluminescent Substrate and HyClone trypan blue solution 0.4% in phosphate buffered saline were purchased from Thermo Fisher Scientific (Waltham, MA, USA). In addition, the following antibodies were used: anti-CD44s antibody BBA10 (R&D Systems, Minneapolis, MN, U.S.A.), anti-Actin sc-1616 (Santa Cruz Biotechnology, Inc., Dallas, TX, U.S.A.), donkey anti-Mouse IgG (H+L) secondary antibody, A16011 (Invitrogen, Waltham, MA, U.S.A.) and donkey anti-goat IgG-HRP sc-2020 (Santa Cruz Biotechnology, Inc., Dallas, TX, U.S.A.).

2.3 Synthesis and Characterization of Nylon-3 random Copolymer

Nylon-3 copolymer $NM_{0.2}/CP_{0.8}$ was synthesized via anionic ring-opening polymerization (ROP) of racemic β-lactams as previously described [32]. Briefly, monomers β-NM (cationic monomer) and CP (hydrophobic monomer) were prepared according to literature procedures [33]. Random copolymers from β-NM and CP were synthesized by following previously reported procedures [34]. The polymerization was conducted in the presence of the co-initiator 4-tert-butyl-benzoyl chloride (II) and the base lithium bis(trimethylsilylamide) to afford the

desired polymers with an N-terminal tert-butyl-benzoyl group [35]. Deprotection of Boc-protected polymers was performed in trifluoroacetic acid (TFA) to obtain the TFA-salts of the desired polymers [36]. ^{1}H-NMR spectra of NM/CP polymer were measured on a Bruker AV500 in deuterium oxide with 128 scans. The molar masses of NM/CP polymers were directly calculated via ^{1}H-NMR in D_2O performed with unprotected TFA salts by comparing the signal between 4.0 and 4.5 ppm (one proton per repeating unit p (p = n + m)), and the tert-butyl group of the end-group (1.33 ppm) [32].

2.4 Preparation of Polyplexes

To prepare polymer-siRNA complexes (PXs), aqueous b-PEI as well as $NM_{0.2}/CP_{0.8}$ polymer stock solutions were diluted with freshly filtered 10 mM HEPES buffer (pH 7.2) to predetermined concentrations. A defined amount of siRNA was added to these polymer solutions in a microcentrifuge tube to obtain PXs at various N/P ratios. The mixed polymer:siRNA solutions were incubated for 30 min to permit stable PX formation. The N/P ratio is defined as the molar ratio between the polymer amine groups (N) and the siRNA phosphate groups (P). The amount of polymer needed to obtain different N/P ratios was calculated according to the following equation:

$$\text{m (polymer in pg)} = \text{n siRNA (pmol)} \times \text{M protonable unit (g/mol)} \times \text{N/P} \times \text{number of nucleotides siRNA}$$

The protonable unit of each polymer was calculated by dividing its molar mass by the number of protonable primary amines present in each polymer as illustrated in Scheme 1. The number of nucleotides of 25/27mer siRNA is set to 52.

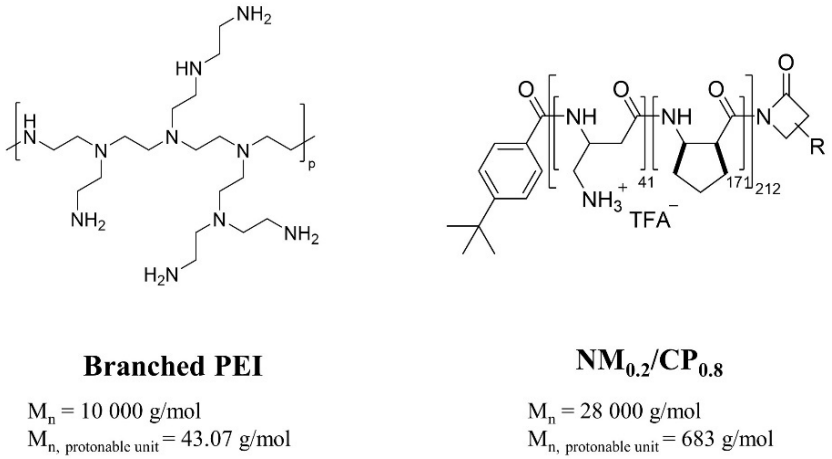

Branched PEI

M_n = 10 000 g/mol

$M_{n,\ protonable\ unit}$ = 43.07 g/mol

$NM_{0.2}/CP_{0.8}$

M_n = 28 000 g/mol

$M_{n,\ protonable\ unit}$ = 683 g/mol

Scheme 1. b-PEI and $NM_{0.2}/CP_{0.8}$ polymers used in this study.

2.5 Optimization of Protein Corona – Polyplex Complex Isolation by Centrifugation

Besides size exclusion chromatography [37-39], centrifugation is described in the literature as the most widely used method for solid NPs to remove the loosely bound soft PC [40-43]. To test the suitability of this method for b-PEI and $NM_{0.2}/CP_{0.8}$ PXs as dynamic NP systems, different centrifugation protocols were initially tested. The stability of PXs after multiple centrifugation steps and resuspension was assessed by size measurements using dynamic light scattering (DLS). Furthermore, the stability of the PXs was determined by measuring the released siRNA molecules from the siRNA-polymer complexes using SYBR Gold assay. PXs were formed with scrambled siRNA at an N/P ratio of 8 and in total volume of 500 µL. The PX suspension was centrifuged at different gravitational forces for 10 min. After centrifugation, 400 µL of the supernatant was removed, and the resulting pellet was carefully resuspended in 400 µL of fresh 10 mM HEPES buffer and incubated for 10 min to allow stable PX reassembly. Centrifugation was repeated three times at 10.000g, 12.500g and 20.000g, respectively, and particle sizes and polydispersity indices (PDIs) of redispersed PXs were subsequently measured. Since 12.500g was determined to be the optimal gravitational force, the experiment was repeated with this setting. This time, supernatants (S1 – S3) were collected after each centrifugation step and the resuspended PXs (R3) were collected after the third centrifugation step. The supernatants S1 - S3 and the resuspended PXs R3 were measured for free siRNA content by SYBR Gold assay and the PX suspension R3 was measured by DLS to obtain hydrodynamic diameters and PDI values of the formed PXs.

2.5.1 Size Measurement by Dynamic Light Scattering

Particle size and PDI were measured from resuspended PXs using a Zetasizer Nano ZS (Malvern Instruments, Malvern, UK) after 3X centrifugation with 10.000g, 12.500g and 20.000g, respectively and after every centrifugation step (1X – 3X) conducted with 12.500g. A total volume of 100 µL of each sample was added to a disposal cuvette (Malvern Instruments, Malvern; UK) and used for particle size and PDI measurements by DLS. The parameters were set as 173 ° backscatter angle and 15 scans running three times per sample. Uncentrifuged PX suspensions were used as references. Results are expressed as mean ± standard deviation (n = 3).

2.5.2 SYBR Gold Assay

Analogous to previously described procedures [44], the SYBR Gold assay was used to evaluate the amount of free siRNA molecules in the supernatants after centrifugation, and the ability of the polymers to stably condensd siRNA molecules during centrifugation and resuspension. Supernatants (S1 – S3), resuspended PXs (R3) and uncentrifuged PX solutions (N/P 8) as references were distributed in a white FluoroNunc 96 well plate (FisherScientific, Hampton, New Hampshire, USA). A 4X SYBR Gold solution (30 µL) was added to each well and the plate was incubated for 10 min in the dark. The fluorescence signal was determined with a fluorescence plate reader (FLUOstar Omega, BMG Labtech, Ortenberg, Germany) at 492 and 555nm excitation and emission wavelengths, respectively. Free siRNA, which was also subjected to the corresponding centrifugation steps, was measured analogously and used as a 100% value. Measurements were performed in triplicates and results are shown as mean ± standard deviation (n = 3).

2.6.Formation of the Protein Corona by FBS Coating

To ensure the PC formation, b-PEI and $NM_{0.2}/CP_{0.8}$ PXs were incubated with FBS at final concentrations of either 10% or 50% (v/v) FBS. Therefore, one part of the PX suspension was mixed with equal volumes of FBS to achieve a 50% FBS dilution. In addition, one part of this solution was further diluted with 10 mM HEPES buffer (pH 7.2) to achieve a final concentration of 10% FBS, which corresponds to a particle-to-serum ratio used in the *in vitro* experiments performed in this study. PX – FBS mixtures were incubated at 37°C for 30 min in a Thermomixer (Eppendorf AG, Hamburg, Germany) and used for further experiments after cooling down to room temperature (20-25 °C).

2.7 Size and Zeta Potential Analysis of PCPXs by Dynamic Light Scattering and Laser Doppler Anemometry

Particle size, PDI, and zeta potential of PCPXs were measured using a Zetasizer Nano ZS (Malvern Instruments, Malvern, UK). PXs were formed at an N/P ratio of 8 and incubated either in 10% or 50% FBS for PC formation as described above. Samples were purified by using the optimized purification procedure (12.500g, 10 min, 3X). After the last centrifugation, the pellet was resuspended in 10 mM HEPES buffer under slight vortexing and then incubated for 10 min. Particle sizes and PDI were measured as described above (see 2.4.1). Zeta potentials were measured by laser Doppler anemometry (LDA). A 100 µL sample aliquot was 7X diluted and placed in a Zeta Cell (Zetasizer Nano series, Malvern, UK). Each run consisted of 30 scans and zeta potentials were measured in triplicates. Uncoated PXs (0% FBS) were treated analogously and used as references. Results are expressed as mean ± standard deviation (n = 3).

2.8 Evaluation of Hard Protein Corona Composition

2.8.1 Protein Quantification by Bicinchoninic Acid (BCA) Assay

PXs prepared at an N/P ratio of 8 were incubated either in 10% or 50% FBS and purified by centrifugation as described above. The total protein amount of the tightly bound proteins of the hard corona was detected following the manufacturer´s protocol by bicinchoninic assay (BCA), which also allows the measurement of proteins that are covalently bound to surfaces [45]. Briefly, buffer diluted samples were added to the BCA working reagent (50 parts reagent A containing BCA detection reagent to 1 part reagent B containing copper sulfate) at a ratio of 1:10. Samples were distributed in a transparent 96-well plate (FisherScientific, Hampton, NH, USA) and incubated at 37°C for 30 min to allow the bicinchoninic acid/Cu2+ reaction with proteins. The absorbance at 562 nm was determined by using a microplate reader (FLUOstar Omega, BMG Labtech, Ortenberg, Germany). A standard curve of BSA with known protein concentrations (2 mg/mL, 1 mg/mL, 0.5 mg/mL, 0.25 mg/mL, 0.125 mg/mL, 0.065 mg/mL) was included for the protein quantification.

2.8.2 Visualization of Hard Corona Proteins by Sodium Dodecylsulfate Polyacrylamide Gel Electrophoresis (SDS-PAGE)

PXs prepared at N/P 8 were incubated in either 10% or 50% FBS and purified by centrifugation as described above. The total protein amount of the hard corona was determined by BCA assay as described above and the total protein content of each sample was adjusted to equal concentrations by diluting the samples with highly purified water. Samples were mixed with

Pierce™ Lane Marker Reducing Sample Buffer and incubated at 95°C for 5 min to denature proteins in a Thermomixer (Eppendorf AG, Hamburg, Germany). The gel electrophoresis chamber Novex® Mini-Cell was prepared with a polyacrylamide-gel 10% placed in 10-fold diluted rotiphorese® 10x SDS-PAGE buffer. The slots of the gel were loaded with 5µL of PageRuler™ Plus Prestained protein ladder (10 to 250 kDA) as a molecular marker, 25µL FBS as a control, and 25µL of b-PEI and $NM_{0.2}/CP_{0.8}$ PXs samples pre-incubated in 10% and 50% FBS, each containing 5µg total protein. The gel was run at 150 mV for 90 min, rinsed twice with deionized water, and stained overnight in Brilliant Blue G solution to visualize the proteins. Subsequently, the gel staining was removed in a mixture of 50% highly purified water for 24 h, 40% methanol, and 10% acetic acid. The gel was scanned using a Biorad Chemidoc (Bio-Rad Laboratories, Hercules, CA, USA) and data were processed using Image Lab 6.0.1 software.

2.8.3 Hard Corona Protein Identification by Mass Spectrometry (MS) measurements

2.8.3.1 Filter Aided Sample Preparation (FASP) Digest

PXs prepared with 100 pmol scrambled siRNA at N/P 8 were incubated in 10% FBS and purified by centrifugation as described above. PCPXs were reduced and alkylated using dithiothreitol (DTT) and indole-3-acetic acid (IAA), respectively, followed by a modified FASP procedure [46]. The proteins were centrifuged on a 30 kDa cutoff filter device (Sartorius), washed thrice with UA buffer (8 M urea in 0.1 M Tris/HCl pH 8.5) and twice with 50 mM ammonium bicarbonate. The proteins were digested for 2 h at room temperature using 0.5 µg Lys-C and for 16 h at 37°C using 1 µg trypsin. After centrifugation (10 min, 14.000g) the eluted peptides were acidified with 0.5% TFA and stored at -20 °C.

2.8.3.2 Mass Spectrometric (MS) Measurements

Liquid chromatography with tandem mass spectrometry (LC-MSMS) analysis was performed in data-dependent acquisition (DDA) mode. MS data were acquired on a Q-Exactive HF-X mass spectrometer (Thermo Fisher Scientific, Waltham, Massachusetts, USA) each online coupled to a nano-RSLC (Ultimate 3000 RSLC; Dionex). Tryptic peptides were automatically loaded on a C18 trap column (300 µm inner diameter (ID) × 5 mm, Acclaim PepMap100 C18, 5 µm, 100 Å, LC Packings) at 30 µL/min flow rate. For chromatography, a C18 reversed-phase analytical column (nanoEase MZ HSS T3 Column, 100Å, 1.8 µm, 75 µm x 250 mm, Waters) was used at a flow rate of 250 nL/min and following a 95-min non-linear acetonitrile gradient from 3 to 40% in 0.1% formic acid. The high-resolution (60 000 full width at half-maximum)

MS spectrum was acquired with a mass range from 300 to 1500 m/z with an automatic gain control target set to 3 x 106 and a maximum of 30 ms injection time. From the MS prescan, the 15 most abundant peptide ions were selected for fragmentation (MS-MS) if at least doubly charged, with a dynamic exclusion of 30 seconds. MS-MS spectra were recorded at 15 000 resolutions with an automatic gain control target set to 5 x 102 and a maximum of 50 ms injection time. The normalized collision energy was 28, and the spectra were recorded in profile mode.

2.8.3.3 Data Processing - Protein Identification

Proteome Discoverer 2.5 software (Thermo Fisher Scientific; Waltham, Massachusetts, USA, version 2.5.0.400) was used for peptide and protein identification via a database search (Sequest HT search engine) against Ensemble Cow data base (Release 2014_75, 22118 sequences). Search settings were 10 ppm precursor tolerance, 0.02 Da fragment tolerance, one missed cleavage allowed. Carbamidomethylation of Cys was set as a static modification. Dynamic modifications included deamidation of Asn, Gln and Arg, oxidation of Pro and Met; and a combination of Met loss with acetylation on protein N-terminus. Percolator was used for validating peptide spectrum matches and peptides, accepting only the top-scoring hit for each spectrum, and satisfying the cutoff values for false discovery rate (FDR) < 1%, and posterior error probability < 0.01.

2.8.3.4 Data Processing – Label-Free Quantification

The quantification of proteins was based on abundance values for unique peptides. Abundance values were normalized on the total peptide amount to account for sample loading errors. The protein abundances were calculated as the average of the three most abundant (Top 3N) distinct peptide groups. The final protein ratio was calculated from the grouped protein abundances and an ANOVA was used for the determination of p-values (< 0.05). To overcome the problem of missing values, match between run (MBR) was used to to transfer identified peptides in one run to another by inference based on 1ppm mass tolerance and 30sec retention time shift. Additionaly missing values were replaced by low abundant imputation from the lower five percent of detected values.

2.9 Cells and Cell Culture

U87 cells (human glioblastoma cell line) and MCF7 cells (human breast cancer cell line) were cultured in EMEM media supplemented with heat-inactivated FBS (10%) and Penicillin-

Streptomycin (1%). All cells were subcultured, maintained, and grown in an incubator in humidified air with 5% CO_2 at 37 °C.

2.10 Correlation of Protein Binding Profile with Cellular Uptake Ability in a Glioblastoma Cell Line

2.10.1 Detection of CD44 Receptor Expression of Glioblastoma Cells by Western Blot

U87 glioblastoma and MCF-7 breast cancer cells were seeded in a 6-well plate at a density of 500.000 cells per well and incubated for 24h. For harvesting, the medium was aspirated and cells were washed twice with ice-cold PBS. Cells were lysed for 30min on ice using 100 µL lysis reagent (RIPA lysis buffer, 1x protease inhibitor, 1x phosphatase inhibitor). Cell lysates were transferred to a conical tube and centrifuged (15 min, 15.000g). The supernatant was collected and total protein concentration was determined with Bradford Protein assay. Therefore, 10 µL cell lysates and BSA standards were mixed with 200 µL protein assay reagent, and absorbance (A=595nm) was measured using a Tecan Spark multi-plate reader (Tecan Group Ltd., Maennedorf, Switzerland). For protein separation, SDS-PAGE was conducted applying 120 mV for 1h. For gel loading, cell lysates containing 30 µg total protein (calculated via Bradford Protein assay data) were mixed with 5X reducing sample buffer to reach 1X final concentration and samples were further diluted with HPW to a final volume of 30 µL. Samples were boiled for 5 min at 95°C and cooled down to room temperature before transferring them to 10% Tris-Glycine Gel in Rotiphorese® 1x SDS-PAGE buffer. Western blot protein transfer was performed at 100 mV for 1h using an Amersham™ Protran Western blotting membrane. Membrane blocking was carried out with blocking buffer (5% non-fat dry milk in TBS containing 1% Tween-20) for 1 h at room temperature while shaking. The membrane was cut at 50 kDa and incubated overnight at 4°C using anti-CD44s antibody and anti-Actin primary antibodies, diluted at 1:250 and 1:1000 ratios, respectively. Membranes were washed three times for 10 min with blocking buffer and incubated for 1 h with secondary antibodies diluted 1:5000 each. For protein detection, membranes were washed three times for 10 min with TBST and incubated with SuperSignal™ West Pico PLUS chemiluminescent substrate. Subsequently, chemiluminescence was measurered using a ChemiDoc visualizer (Bio-Rad, Hercules, CA, U.S.A.). Images were acquired by using the Bio-Rad Image Lab™ software suite.

2.10.2 Quantification of Cellular Uptake into Glioblastoma Cells by Flow Cytometry

Flow cytometry was used to quantify the *in vitro* cellular uptake of b-PEI and $NM_{0.2}/CP_{0.8}$ PXs in glioblastoma cells as a functionof the present PC. Amine-modified siRNA was labeled with

the fluorescent dye Alexa Fluor 488 (AF488) according to the manufacturer´s protocol and purified by ethanol precipitation and spin column binding as described previously [47]. U87 cells were seeded in 24 well plates at a density of 50.000 cells per well and incubated for 24 h at 37 °C and 5% CO_2. Right before cell transfection, the cell culture medium was replaced with either FBS free medium or a cell culture medium containing 10% FBS. PXs were prepared with 50 pmol siRNA-AF488 at previously optimized N/P ratios for cell transfection, specifically, N/P 7 for b-PEI and N/P 9 for $NM_{0.2}/CP_{0.8}$ PXs. Negative controls consisted of untreated cells and cells treated with free siRNA. In addition, the positive control cells were transfected with Lipofectamine 2000 (LF) lipoplexes prepared with 50 pmol siRNA-AF488 according to the manufacturer's protocol. After a 24 h incubation period, the incubation medium was removed, and cells were washed with PBS and detached with 0.25% trypsin-EDTA. Samples were washed twice with PBS and resuspended in 500 µL PBS/2 mM EDTA. Additionally, trypan blue quenching was performed to exclude surface fluorescence signals of not completely internalized siRNA complexes. Median fluorescence intensities (MFI) after quenching were analyzed using an Attune NxT Acoustic Focusing Cytometer (Thermo Fisher Scientific, Waltham, Massachusetts, USA) by exciting the siRNA-AF488 at 488 nm and measuring the fluorescence signal with a 530/30 nm emission filter. Samples were run in triplicates, each sample consisting of a minimum of 10.000 viable cells. One-way ANOVA with Bonferroni multiple comparison tests were performed in GraphPad Prism software (Graph Pad Software, La Jolla, CA) to calculate p-values at 95% confidence. Results are given as mean ± standard deviation (n = 3).

3. Results and Discussion

3.1 Synthesis and Characterization of Nylon-3 Random Copolymer

$NM_{0.2}/CP_{0.8}$ polymer was prepared with hydrophobic and hydrophilic ß-lactams via anionic ring-opening polymerization (ROP) as described in section 2.3. The synthesis led to a Nylon-3 copolymer that contains randomly arranged hydrophobic and cationic subunits in a 1:4 ratio. The hydrophobic monomer was cyclopentadienyl ß-lactam (CP), and the cationic monomer was a ß-lactam without a methyl group (no methyl, NM). To determine the molecular weight of the $NM_{0.2}/CP_{0.8}$ polymer and to confirm subunit ratios, polymers were characterized by ^{1}H-NMR spectroscopy (Figure S2, Supplementary Material). Molar masses and degree of polymerization obtained for $NM_{0.2}/CP_{0.8}$ polymers were 28000 g/mol and 212 as previously indicated [32]. The suitability for siRNA delivery into glioblastoma cells in comparison to various other Nylon-3

polymers was described previously by our group and $NM_{0.2}/CP_{0.8}$ polymer revealed to hold most favorable characteristics regarding siRNA delivery into glioblastoma cells due to the high hydrophobic content [32]. Furthermore, since hydrophobic moieties of polymers have been shown to strongly influence the composition of the PC, $NM_{0.2}/CP_{0.8}$ polymer was selected in this study to investigate the PC formation in comparison to highly cationic and hydrophilic b-PEI polymers.

3.2 Optimization of Hard Protein Corona–Polyplex Complex (PCPX) Isolation by Centrifugation

Within the current understanding of the structure of the PC, it is assumed that it consists of a hard layer of proteins firmly bound to the nanoparticle (hard PC) and a soft layer of proteins (soft PC) that is solely loosely attached to the hard corona proteins (Figure 1) [15, 48].

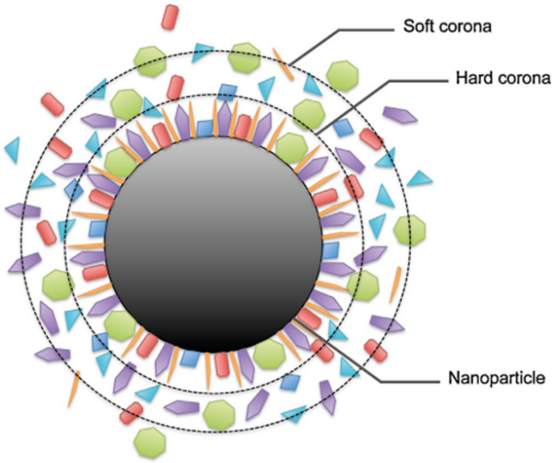

Figure 1. Schematic representation of the current understanding of the PC assembly with a hard and soft layer of proteins that cover the surface of the nanoparticle. Hard corona proteins are tightly associated with the particle surface, whereas soft corona proteins are solely loosely bound to the layer of hard corona proteins. (Adopted with permission from Ref. [14], Copyright 2014, Elsevier)

As hard corona proteins are estimated to influence the *in vivo* behavior of the nanoparticulate system within a biological environment [43], it is of great interest to analyze the composition of the absorbed PC. Therefore, there is a great need for suitable purification methods to separate soft corona proteins from the PCPXs. In this context, repeated centrifugation of formed protein–NP complexes after incubation in various types of sera, followed by resuspension of the obtained pellet is described as an appropriate and common purification method. It can be used for solid and therefore stable nanoparticulate systems; for instance, unmodified and modified polystyrene nanoparticles [41, 43, 48, 49], sulfonated polystyrene and silica nanoparticles [42]

and gold nanoparticles [40]. PC studies with soft materials are not yet addressed in the literature, with some exceptions describing washing protocols with PBS for purification of b-PEI-25k-grafted magnetic beads [26] or centrifugation of cationic gemini surfactant SS14-plasmid DNA lipoplexes [27]. The group of Zhu et al. conducted initial PC studies of PEI-DNA PXs without purification processes [28, 29], while a study by Maiolo's group demonstrated a centrifugation method for purification to be superior to a dialysis protocol [30]. As our group is working with delivery vehicles that are created by blending various polycations with siRNA molecules and therefore constitute soft and dynamic systems containing sensitive nucleic acids, the described procedures need to be tested regarding their suitability for these formulations. We investigated in preliminary experiments with bare siRNA – polymer complexes, whether the PXs remain stable during centrifugation for 10 min at 10.000g, 12.500g, and 20.000g, respectively. To ensure the removal of the unbound or weakly bound proteins of the soft corona, the purification procedure was repeated three times as suggested in the literature [28]. We made use of DLS measurements to investigate particle stability during centrifugation by determining their hydrodynamic diameters and size distributions. To underpin DLS data, we measured the free siRNA amount by SYBR Gold assay in the supernatants (S1 – S3) and resuspensions (R3) (Scheme 2) to evaluate if, when, and to which extent PXs are potentially disrupted during the centrifugation process.

3.2.1 Size Measurement by Dynamic Light Scattering

In order to investigate whether centrifugation is a suitable purification method for b-PEI and $NM_{0.2}/CP_{0.8}$ PXs, the first step of our study was the characterization of PXs after threefold centrifugation for 10 min at 10.000g, 12.500g, and 20.000g, respectively. As shown in Figure 2, for b-PEI as well as for $NM_{0.2}/CP_{0.8}$ polymers, PXs with slightly increased hydrodynamic sizes compared to the uncentrifuged control were detected. In detail, and as shown in Figure 2A, the b-PEI PX sizes increased with increasing gravitational forces from 102.3 nm for the uncentrifuged control to 109.1 nm, 205.3 nm, and 230.3 nm for 10.000g, 12.500g, and 20.000g, respectively. The $NM_{0.2}/CP_{0.8}$ PXs showed a maximum size of 287.1 nm after centrifugation at 12.500g and the smallest size of 225.9 nm at 10.000g, and 227.3 nm after centrifugation at 20.000g. The size of the uncentrifuged reference particles was 177.1 nm. The PDIs of b-PEI PXs increased with rising gravitational forces from 0.091 (control) to 0.050, 0.262, and 0.352. For $NM_{0.2}/CP_{0.8}$ PXs, PDI values increased after centrifugation in comparison to uncentrifuged control to a larger extent from 0.219 to 0.321, 0.444, and 0.476 for 10.000g, 12.500g, and 20.000g, respectively.

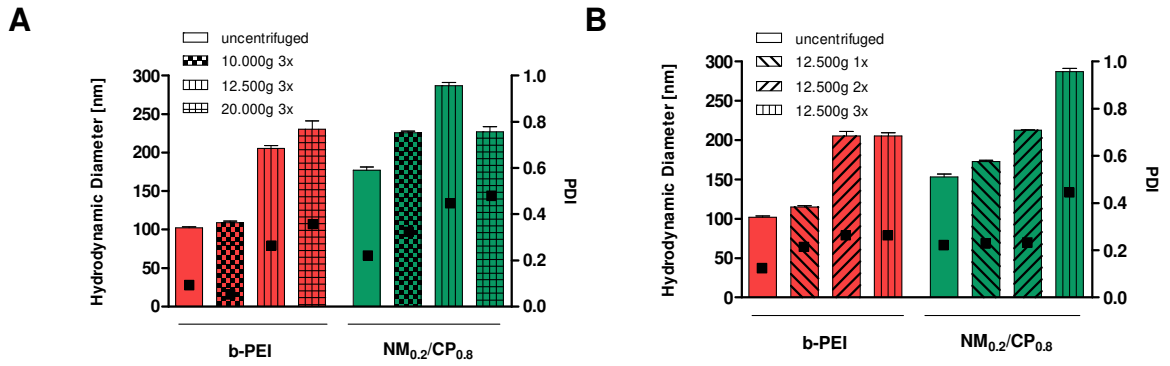

Figure 2. Hydrodynamic diameters (left y-axis) and polydispersity indices (PDI, right y-axis) of PXs composed by b-PEIor $NM_{0.2}/CP_{0.8}$ polymers at N/P ratio 8, resuspended in 10 mM HEPES buffer measured (**A**) after the third centrifugation for 10 min at 10.000g, 12.500g and 20.000g and (**B**) after the first, second and third centrifugation steps for 10 min at 12.500g. (Data points indicate mean ± SD, n = 3).

Based on the obtained data, it was concluded that stability of siRNA – polymer complexes was maintained after resuspension of the obtained pellet, although the purification procedure led to slightly bigger and more polydisperse particles. Hydrodynamic diameters and PDI values of centrifuged and washed b-PEI PXs steadily increased with rising gravitational forces, whereas $NM_{0.2}/CP_{0.8}$ PXs showed a size increase until 12.500g. After three-time centrifugation at 20.000g, particles with smaller sizes but higher polydisperse size distributions were obtained. As hydrodynamic diameters, as well as narrow size distributions, are two major determinants for intracellular uptake and transfection efficiency, and thus, notable parameters for further experiments, a gravitational force of 12.500g was chosen as the most appropriate one. The final optimized centrifugation protocol for PCPX purification is illustrated in Scheme 2. To obtain insights into the particle stability after less centrifugation steps at 12.500g, DLS measurements were additionally performed with resuspended pellets R 1 – 3 (Scheme 2). As expected, PX sizes and PDI values increased with each further centrifugation step probably due to aggregate formation or loss of material (Figure 2B). This effect was even more noticeable for $NM_{0.2}/CP_{0.8}$ PXs, therefore, it was suggested that the lower number of cationic subunits within the polymer impede the stability of PX that are based on electrostatic interactions between positive charged polymer chains and negatively charged siRNA phosphate groups. In conclusion, these results indicate that for both polymers, acceptable PX stability was maintained after three centrifugation steps with solely slight aggregation and that centrifugation is therefore an appropriate purification method for PXs.

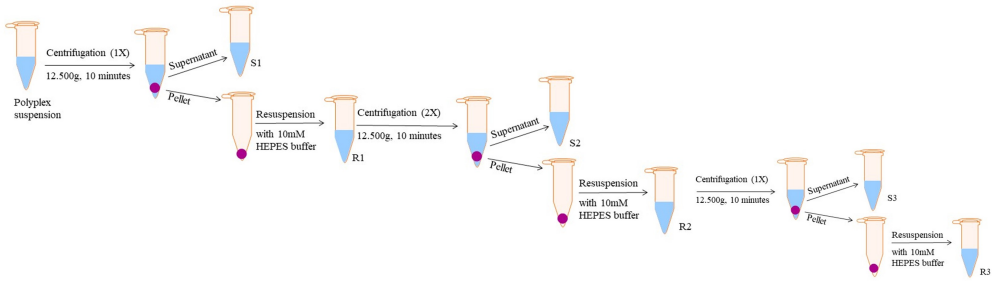

Scheme 2. Optimized centrifugation procedure for hard protein corona–polyplex complex (PCPX) purification via three centrifugation steps at 12.500g for 10 min and subsequent pellet resuspension in 10mM HEPES buffer.

3.2.2 SYBR Gold Assay

SYBR Gold assay takes advantage of the fact that free and unbound siRNA is fully accessible to the intercalating nucleic acid dye SYBR Gold, resulting in an enhancement of the fluorescent signal. The encapsulated siRNA is not available for the intercalation of dye molecules and thus, no enhancement of the fluorescence signal can be measured. Positively charged polymers electrostatically interact with negative charges provided by the phosphate groups present in the siRNA molecule [50]. Although the exact mechanism for complex formation between nylon-3 polymers and siRNA is still unknown, a combination of electrostatic and hydrophobic interactions due to polymers' structural properties is implicated [51]. In order to evaluate free siRNA amounts and the ability of siRNA re-encapsulation, SYBR Gold assay was performed with supernatants S 1 – 3 and in the final PX suspension (R3) analogously to procedures previously described [43].

Table 1. Free siRNA amounts of b-PEI and $NM_{0.2}/CP_{0.8}$ PXs at N/P ratio 8 as measured by SYBR Gold assay in uncentrifuged (0x) PX reference solutions, in supernatants after the first (1x), second (2x) and third (3x) centrifugation step and in resuspensions of PXs after the third (3x) centrifugation step (10 min, 12.500g) calculated relating to respective uncondensed siRNA amounts representing 100% values. (Results indicate mean ± SD, n = 3).

Centrifugation 12.500g, 10min	**Sample**	**Free siRNA amount [%]** (mean ± SD)	
		b – PEI	**$NM_{0.2}/CP_{0.8}$**
0x	Reference	1.15 ± 0.030	3.63 ± 0.094
1x	Supernatant S1	1.56 ± 0.017	3.20 ± 0.041
2x	Supernatant S2	1.43 ± 0.014	2.14 ± 0.004
3x	Supernatant S3	1.65 ± 0.009	1.39 ± 0.003
3x	Resuspension R3	1.72 ± 0.017	1.18 ± 0.092

Reference PX suspensions at an N/P ratio of 8 revealed free siRNA amounts of 1.15% for b – PEI and 3.63% for $NM_{0.2}/CP_{0.8}$ PXs (Table 1), which goes in line with previously reported data [32]. For b-PEI as well as for $NM_{0.2}/CP_{0.8}$ PX samples, no significant amount of free siRNA

was detected in supernatants S 1 - 3, indicating virtually no loss of siRNA molecules during the washing procedure. Furthermore, since low amounts of free siRNA were detected also in the resuspended sample R3 (1.72% free siRNA for b – PEI PXs and 1.18% for $NM_{0.2}/CP_{0.8}$ PXs), it was concluded that both types of polymers were able to stably encapsulate siRNA molecules highly efficiently even after resuspension. Taken together, these results together with the DLS data indicate that reconstitution of the siRNA-polymer complexes takes place even after the third centrifugation step, which led to PXs with suitable sizes and PDI values. In summary, these data confirmed the suitability of centrifugation under controlled conditions as a purification method for dynamic systems allowing more detailed PC investigations in this and in future studies.

3.3 Size and Zeta Potential Analysis by Dynamic Light Scattering and Laser Doppler Anemometry

After determining the optimal parameters for the purification process, the physicochemical properties of purified PCPXs after incubation in either 10% or 50% FBS were investigated in comparison to plain PXs using DLS and LDA techniques. As previously reported, DLS is a suitable method for indirect studies of the PC by measuring size changes of the underlying nanoparticles that occur due to protein adsorption [52]. In addition, LDA is used to measure the differences in the zeta potential of the particles before and after corona formation, as the absorbed proteins affect the resulting zeta potential values depending on their identity and charge [1]. Hence, b-PEI and $NM_{0.2}/CP_{0.8}$ PXs formed at an N/P ratio of 8 were incubated in either 10% or 50% FBS and purified from soft corona proteins as described above. Hydrodynamic diameters, PDIs, and zeta potentials were determined in comparison to plain PXs treated with an analogous centrifugation procedure and results are illustrated in Figure 3.

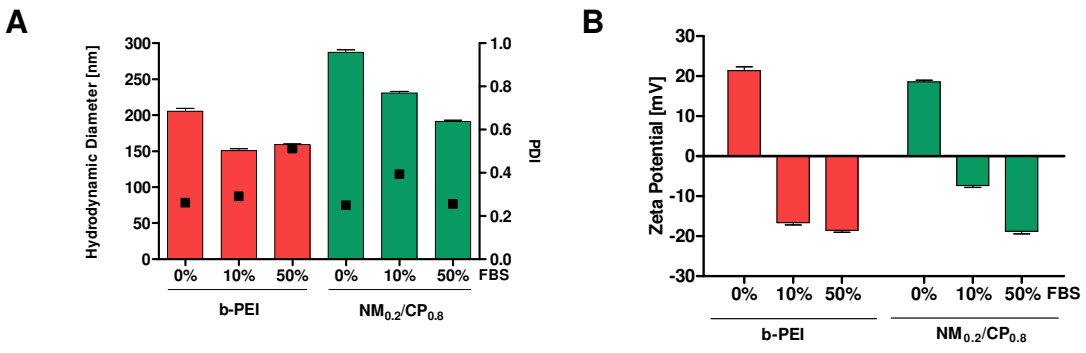

Figure 3. Dynamic light scattering (DLS) and laser Doppler anemometry (LDA) measurements of PXs formed with b-PEI and $NM_{0.2}/CP_{0.8}$ polymers at an N/P ratio 8, incubated in FBS (10% or 50%) and resuspended in 10 mM

HEPES buffer measured after the third centrifugation step (12.500g, 10min). Uncoated particles (0%) were treated analogously and used as a reference. Hydrodynamic diameters (left y-axis) and polydispersity indices (PDI, right y-axis) (**A**) and zeta potentials of particles with and without PC (**B**). (Data points indicate mean ± SD, n = 3).

Hydrodynamic diameters for b-PEI PXs were 205.3 nm, 150.8 nm, and 159.0 nm for samples incubated in 0%, 10%, and 50% FBS, respectively. PDI values increased with rising FBS concentration from 0.262 to 0.291 and 0.513, respectively. However, $NM_{0.2}/CP_{0.8}$ PXs displayed the smallest sizes of 191.0 nm after incubation in 50% FBS in comparison to reference particles (287.1 nm) and the sample incubated in 10% FBS (230.9 nm). A similar trend emerged regarding the PDI values, which yielded 0.250, 0.394, and 0.256 for 0%, 10%, and 50% FBS samples, respectively (Figure 3 A). The zeta potentials of the PXs decreased with increasing FBS concentration (Figure 3 B) for both types of polymers. In detail, both b-PEI and $NM_{0.2}/CP_{0.8}$ reference PXs displayed positive zeta potentials of +21.3 mV and +18.5 mV, respectively. The zeta potential turned into negative values for FBS-treated samples, namely -16.6 mV and -7.4 mV for 10% FBS samples and -18.6 mV and -18.8 mV for 50% FBS samples, respectively. In case of b-PEI PXs, the particles with the smallest size were obtained with the sample incubated in 10% FBS, followed by particles incubated in 50% FBS. These particles, however, exhibited the highest PDI value, indicating a less monodisperse particle composition and, probably, aggregation events during the purification process. Compared to this observation, the $NM_{0.2}/CP_{0.8}$ PXs displayed the smallest sizes and PDI values after incubation in 50% FBS. This observation may lead to the assumption that the properties of the nanoparticles, such as size, charge or material, cause different interactions with serum proteins. For both types of polymers, it was found that reference samples demonstrated the largest particle sizes. The fact that particles with adsorbed proteins displayed smaller sizes compared to reference particles was unexpected. One would assume that the adsorption of proteins would lead to larger particles, especially since this phenomenon has already been described in the literature. The groups of Nicoli et al., Zhu et al. and Maiolo et al. reported an increase in the size of b - PEI-nucleic acid complexes after decoration with various sera, such as HSA, BSA, and FBS [28, 30, 53]. In contrast and based on our data, we hypothesize that FBS proteins might stabilize our particles by reorganizing the PX into a more thermodynamically stable structure or by preventing particle/particle contacts due to serum protein adsorption on the surface. A comparable effect was already observed by our group in a project in which b - PEI/siRNA PXs modified with Transferrin illustrated smaller sizes than the unmodified ones. Here it was discussed that Transferrin, as a very soluble glycoprotein that decorates the particle surface, contributes to the smaller sizes of the particles by steric stabilization [54]. Additionally, zeta potential measurements were performed to gain further insight into the adsorption of proteins

onto our formulations, since changes in zeta potential values can be directly correlated with the number of adsorbed proteins [52]. Both b-PEI and $NM_{0.2}/CP_{0.8}$ PXs demonstrated a reduction in zeta potential values after incubation in FBS, suggesting that adsorbed proteins are present on the nanoparticles' surface even after the purification process. In summary, DLS and zeta potential measurements suggest that a protein layer forms on the particles and the interactions with the proteins of this layer might depend on the nanoparticle material. Ultimately, it was observed that both formulations interact with FBS proteins in a way that, contrary to previous observations, might stabilize PXs and consequently lead to smaller particles.

3.4 Evaluation of Hard Protein Corona Composition

3.4.1 Evaluation of Hard Protein Corona Composition by Sodium Dodecylsulfate Polyacrylamide Gel Electrophoresis (SDS-PAGE)

SDS-PAGE is a commonly used electrophoretic technique for the separation and analysis of complex protein mixtures based on their molecular weight. Protein bands within the gel can be visualized with colorimetric staining such as Comassie [55]. To get a first insight into the protein composition of the hard PC of our formulations, an SDS-PAGE was performed after b-PEI and $NM_{0.2}/CP_{0.8}$ PX preparation, FBS incubation (10% and 50%) and purification as described above. First, a BCA assay was performed to quantify the number of proteins bound to the nanoparticles for further SDS-PAGE calculations. The protein content of each sample was adjusted to equal concentrations to allow a comparison between the intensity of bands of specific proteins. For b-PEI and $NM_{0.2}/CP_{0.8}$ protein – complexes, a total protein amount of 0.246 mg/mL and 0.309 mg/mL after incubation in 10% FBS and 0.418 mg/mL and 1.540 mg/mL after incubation in 50% FBS were detected by BCA assay, respectively. These results, in agreement with the literature, indicate that hydrophobic properties of $NM_{0.2}/CP_{0.8}$ polymers have enhanced general protein adsorption capacity [39, 56].

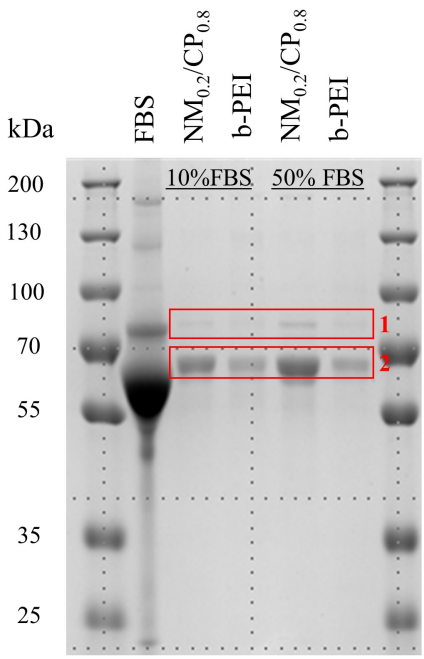

Figure 4. Protein pattern of the hard PC of purified $NM_{0.2}/CP_{0.8}$ and b-PEI PXs after incubation in either 10% or 50% FBS visualized by SDS-PAGE. The wells of the gel were loaded with a molecular marker (10 to 250kDa), FBS as a control, and $NM_{0.2}/CP_{0.8}$ and b-PEI samples (10% and 50% FBS), each one containing 5 µg total protein. Proteins were separated in a 10% polyacrylamide-gel and stained with Brilliant Blue G.

As demonstrated in Figure 4, b-PEI and $NM_{0.2}/CP_{0.8}$ formulations exhibited a different profile of bands than the FBS control, indicating, as expected, that the composition of the hard corona differs from the original FBS composition. The molecular weights of the protein bands observed for b-PEI and $NM_{0.2}/CP_{0.8}$ formulations were approximately 80 kDa (lane 1) and 65 kDa (lane 2), demonstrating that most abundant proteins within the hard PC of both types of PXs were quite similar. Since the intensity of protein bands of $NM_{0.2}/CP_{0.8}$ PXs was comparable for both 10% and 50% FBS samples, we suggest that saturation of binding of protein 1 and 2 for the $NM_{0.2}/CP_{0.8}$ PXs was already accomplished in an environment containing 10% FBS. In contrast, the protein band 2 of b-PEI PXs detected after incubation in 50% FBS was stronger than the band after incubation in 10% FBS. This leads to the assumption that b-PEI PXs have a lower binding affinity and that saturation of protein binding is probably to be reached at higher FBS concentrations than for $NM_{0.2}/CP_{0.8}$ PXs for this specific protein. It is tempting to speculate that lane 1 might depict albumin, a highly abundant protein in serum with a molecular weight of 66 kDa, as interactions between albumin and b-PEI (25 kDa) have been already described in the literature [26]. However, the SDS-PAGE results only provided the first insights into the hard PC composition, as proteins were not further identified here. For this purpose, more specific investigations regarding protein identification were conducted in additional experiments.

3.4.2 Evaluation of Hard Protein Corona Composition by Mass Spectrometry Measurements

The previously described experiments led to the assumption that the isolation of the hard corona after incubation in FBS was successful and that the composition of hard PC differs from that of FBS. Therefore, we used an LC-MS-MS method to identify the components of the PC for each type of PCPXs, as well as determine the major differences in PC composition. Both types of PXs were incubated in 10% FBS and the PCPXs were further isolated, as described above. The purified proteins were subjected to trypsin digestion. The resulting peptides were measured by an LC-MS-MS method and the identified proteins of the hard PC of b-PEI and $NM_{0.2}/CP_{0.8}$ PXs were listed and sorted by their relative abundance, excluding proteins identified by a single unit peptide. Table 2 lists the 20 most abundant proteins present in FBS as a reference according to the literature [57]. Table 3 shows the 20 most abundant proteins in the hard PC of b-PEI (Table 2, A) and $NM_{0.2}/CP_{0.8}$ PXs (Table 2, B), respectively. In addition, we classified the functions of the identified proteins (UniProtKB) into the following groups: “receptor”, “hormone”, “cell adhesion”, “coagulation”, “transport”, “immune response” and “other”.

Table 2. List of the 20 most abundant proteins in FBS [56]. Functions of proteins according to UniProtKB are also given.

Score	Gene	Protein	Function
1	ALB	Albumin	regulation of the colloidal osmotic pressure of blood, transport
2	PDE6C	cone cGMP-specific 3′,5′-cyclic phosphodiesterase R-subunit	phototransduction
3	SERPINA1	Serpin peptidase inhibitor, clade A (alpha-1 antiproteinase, antitrypsin)	blood coagulation
4	PLG	Plasminogen	blood coagulation
5	LPO	Lactoperoxidase	antimicrobial agent
6	KNG1	Kininogen 1	blood coagulation
7	NDUFS1	NADH-ubiquinone oxidoreductase 75 kDa subunit, mitochondrial	mitochondrail membrane respiratory chain
8	AHSG	Alpha-2-HS-glycoprotein	mineral balance
9	TF	Transferrin	iron binding transport protein, Transferrin receptor ligand
10	F2	Coagulation factor II Prothrombin	blood coagulation
11	APOA1	Apolipoprotein A-I	lipid metabolism and transport, major component of HDL
12	AMBP	Alpha-1-microglobulin/bikunin precursor	Host-virus interaction
13	SERPINC1	Serpin peptidase inhibitor, clade C (antithrombin), member 1	blood coagulation
14	N/A	Integrin-beta 1	cell adhesion
15	APOH	Apolipoprotein H (beta-2-glycoprotein I)	lipoprotein metabolism
16	SERPINF2	Serpin peptidase inhibitor, clade F (alpha-2 antiplasmin)	immune response
17	HBB	Hemoglobin, beta	oxygen transport
18	APOA2	Apolipoprotein A-II	lipid transport, stabilization of HDL
19	HBA2	Hemoglobin, alpha 2	oxygen transport
20	ACT	Alpha 1-antichymotrypsin	endopeptidase inhibitor activity

Table 2. List of the 20 most abundant proteins identified in the hard corona of purified (**A**) b-PEI and (**B**) $NM_{0.2}/CP_{0.8}$ PXs after exposure to 10% FBS. Functions of proteins according to UniProtKB classified in 7 groups ("receptor", "hormone", "cell adhesion", "coagulation", "transport", "immune response" and "other") are also given. Proteins were analyzed by LC-MS-MS in three independent measurements and were sorted by the average of their relative normalized abundances. Proteins identified by a single unique peptide are not considered. False discovery rates (FDR) of shown proteins are < 1% and coefficients of variation are ≤ 25%).

A

Score	Gene	Protein	Function
1	ALB	Albumin	other
2	AHSG	Alpha-2-HS-glycoprotein	other
3	SERPINA1	Serpin peptidase inhibitor, clade A (alpha-1 antiproteinase, antitrypsin)	immune response
4	GC	Group-specific component (vitamin D binding protein)	transport
5	TF	Transferrin	transport
6	FETUB	Fetuin B	other
7	APOA1	Apolipoprotein A-I	transport
8	A2M	Alpha-2-macroglobulin	other
9	AFP	Alpha-fetoprotein	other
10	SERPINA3-1	Serpin peptidase inhibitor, clade A (alpha-1 antiproteinase, antitrypsin), member 3	immune response
11	ITIH2	Inter-alpha-trypsin inhibitor, heavy chain 2	other
12	HPX	Hemopexin	transport
13	HBG2	Hemoglobin, gamma 2	transport
14	A1BG	Alpha-1-B glycoprotein	other
15	ITIH4	Inter-alpha-trypsin inhibitor heavy chain family, member 4	immune response
16	PPARD	Peroxisome proliferator-activated receptor delta	cell adhesion
17	ORM1	Orosomucoid 1	transport
18	ADIPOQ	Adiponectin	hormone
19	VTN	Vitronectin	cell adhesion
20	SERPINF2	Serpin peptidase inhibitor, clade F (alpha-2 antiplasmin)	immune response

B

Score	Gene	Protein	Function
1	ALB	Albumin	other
2	AHSG	Alpha-2-HS-glycoprotein	other
3	SERPINA1	Serpin peptidase inhibitor, clade A (alpha-1 antiproteinase, antitrypsin)	immune response
4	TF	Transferrin	transport
5	FETUB	Fetuin B	other
6	GC	Group-specific component (vitamin D binding protein)	transport
7	ITIH2	Inter-alpha-trypsin inhibitor, heavy chain 2	other
8	HBG2	Hemoglobin, gamma 2	transport
9	APOA1	Apolipoprotein A-I	transport
10	HBA2	Hemoglobin, alpha 2	transport
11	AMBP	Alpha-1-microglobulin/bikunin precursor	immune response
12	PPARD	Peroxisome proliferator-activated receptor delta	cell adhesion
13	SERPINF2	Serpin peptidase inhibitor, clade F	immune response
14	SERPINC1	Serpin peptidase inhibitor, clade C (antithrombin), member 1	blood coagulation

15	ITIH1	Inter-alpha-trypsin inhibitor heavy chain 1	other
16	CFB	Complement factor B	immune response
17	AGT	Angiotensinogen	other
18	ADIPOQ	Adiponectin	hormone
19	MAP2K5	Mitogen-activated protein kinase kinase 5	other
20	CFH	Complement factor H	immune response

The most abundant proteins present in FBS include albumin (ALB), which is responsible for regulating osmotic pressure in the blood, some proteins involved in blood coagulation processes (antitrypsin (SERPINA1), plasminogen (PLG), kininogen 2 (KNG1), coagulation factor II prothrombin (F2) and antithrombin (SERPINC1)), and some transport proteins such as Transferrin (TF), Apolipoprotein A-I, A-II and H (APOA1, APOA2, APOH) and hemoglobin alpha 2 and beta (HBA2, HBB) [57]. For b-PEI and $NM_{0.2}/CP_{0.8}$ PXs, albumin was identified as the highest scoring protein. Hard corona protein profiles for the 20 most abundant proteins showed that some proteins were identified in the profiles of the PCPXs although they are not among the most abundant components of FBS, such as fetuin B (FETUB), vitamin D binding protein (GC); inter-alpha-trypsin-inhibitor (ITIH2), hemoglobin gamma (HBG2), peroxisome proliferator-activated receptor delta (PPARD) and adiponectin (ADIPOQ). In addition, antitrypsin clade A member 3 (SERPINA3-1), inter-alpha-trypsin inhibitor (ITIH4), alpha-2-macroglobulin (A2M), alpha-fetoprotein (AFP) and alpha-1-B glycoprotein (A1BG) were solely identified for b-PEI PXs, while inter-alpha-trypsin inhibitor, heavy chain 2 (ITIH1) complement factor B and H (CFB, CFH, angiotensinogen (AGT) and mitogen-activated protein kinase kinase 5 (MAP2K5) and were solely found in the 20 most abundant proteins of the hard corona of $NM_{0.2}/CP_{0.8}$ PXs. Furthermore, when comparing the molecular weights of the proteins detected by MS with the protein bands of the SDS-PAGE (3.4.1), we conclude that albumin and Transferrin, which are confirmed by LC-MS-MS measurements to be highly abundant in the hard corona of b-PEI and $NM_{0.2}/CP_{0.8}$ PXs, were indeed visualized on the SDS-PAGE as lane 1 (Transferrin, M_w = 80 kDa) and lane 2 (albumin, M_w = 66.5 kDa).

The protein composition differs strongly in both formulations. This observation is supported by the assumption that affinities and amounts of proteins adsorbed on the surfaces of NPs depend on the nanomaterial composition and its surface chemistry. Previous studies with mainly solid NPs examined the influences of NP size, morphology, shape, and surface properties such as charge, hydrophobicity, and present functional groups [12, 58]. In summary, it was shown that the size, morphology, and shape of nanoparticles from same materials influence the amount but not the type of bound proteins [39]. The group of Cedervall et al. used model nanoparticles that

consist of essentially random, cross-linked copolymers of N-isopropylacrylamide (NIPAM) and N-tert-butylacrylamide (BAM) with controlled sizes (70-700 nm) and compositions (two comonomer ratios of 50:50 and 85:15). They reported a difference in the degree of protein surface coverage of the NPs depending on their size, with a higher degree of protein coverage of the larger particles [39]. Additionally, NP surface properties such as charge and hydrophobicity have a greater influence on protein binding. It has been observed that charged/hydrophobic particles have a higher adsorption rate than neutral/hydrophilic particles [59, 60]. The group of Gessner et al. prepared a variety of polystyrene NPs with different surface charge densities, but constant particle size and hydrophobicity. They demonstrated an increase in plasma protein adsorption with increasing surface charge density, while the profile of the detected proteins was virtually not affected [17]. Furthermore, in some studies using various particulate systems, it was found that the hydrophobicity of particles influences both the quantity and the identities of the bound proteins. In the above-mentioned study by the group of Cedervall et al., the influence of hydrophobicity on the formation of the PC was additionally demonstrated using two different compositions of NIPAM-BAM NPs, a less hydrophobic 85:15 NIPAM/BAM polymer, and its more hydrophobic 50:50 counterpart. It was shown that the protein adsorption profiles of both types of particles were different and that the more hydrophobic 50:50 NIPAM-BAM copolymer was preferentially covered by apolipoproteins as well as HAS, fibrinogen, and various other proteins [39]. Göppert et al. modified cetyl palmitate solid lipid nanoparticles with various hydrophobic poloxamers and poloxamines and reported a remarkable difference in the amount and type of proteins adsorbed onto NPs surface [37, 61]. A study of hydrophobic and hydrophilic NIPAM/BAM copolymers with a particle size of 200 nm showed that for the same protein pattern, the more hydrophobic particles bound approximately 50-fold more APOA-I than the hydrophilic copolymers. Thus, a strong correlation between the amount of adsorbed APOA-I and the hydrophobicity of the particles was indicated [37]. Taken together, the results clearly show that the physicochemical properties and the hydrophobicity of the NP strongly determine the composition of the PC. Another understanding is that the formation of the PC is a complex process that cannot be predicted by considering only a single parameter of the nanoparticulate system, especially since the change of one parameter also influences the others.

To gain a first insight into the differences in the hard PC composition of b-PEI and $NM_{0.2}/CP_{0.8}$ PXs regarding the function of proteins, we classified quantified proteins into 7 functional groups (functions of proteins according to UniProtKB). We also calculated the proportions regarding the total quantified proteins in % for the respective functional group of proteins bound

to b-PEI and $NM_{0.2}/CP_{0.8}$ PXs and presented them in Figure 5. In general, serum consists of approximately two-thirds albumin and one-third globulins, which can be further subdivided into alpha-, beta- and gamma-fraction. Albumin is a major contributor to maintaining the osmotic pressure and assists, as a carrier, the transport of lipids and steroid hormones. Each globulin fraction is a mixture of many different proteins, which fulfill a wide variety of functions such as the transport of substances, cell adhesion, or blood coagulation. The alpha-globulin fraction is a mixture of several conjugated proteins such as lipo- and mucoproteins. The beta-globulin fraction of serum contains, in addition to lipoproteins and mucoproteins, two metal-binding proteins, Transferrin and ceruloplasmin, which bind iron and copper, respectively. The gamma globulin fraction includes macroglobulins, which act in the field of immune response [62].

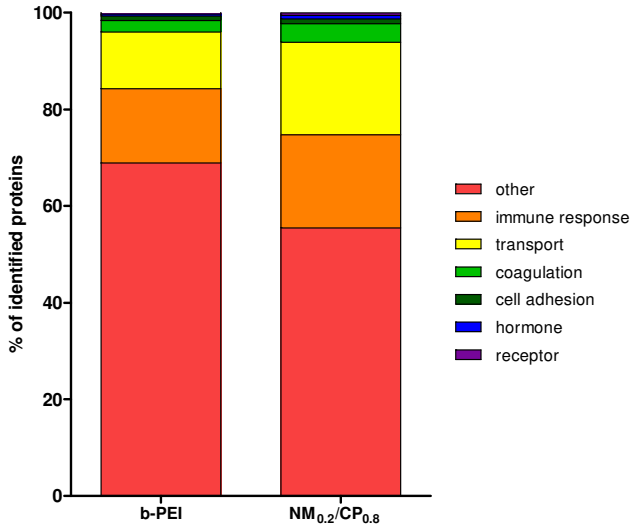

Figure 5. Functions of proteins quantified by LC-MS-MS in the hard PC of purified b-PEI and $NM_{0.2}/CP_{0.8}$ PXs after exposure to 10% FBS classified in 7 groups ("receptor", "hormone", "cell adhesion", "coagulation", "transport", "immune response" and "other").

The majority of proteins qunatified in the hard corona profiles of both formulations were immune response–related proteins and transport proteins. They were found with a percentage of 15.37 and 11.78 on b-PEI PXs and 19.26 and 19.10 on the surface of $NM_{0.2}/CP_{0.8}$ PXs, respectively. This is followed by coagulation and cell adhesion-related proteins detected with 2.36% and 0.93% on b-PEI PXs and 3.89% and 0.96% on $NM_{0.2}/CP_{0.8}$ PXs, respectively. The minority of detected proteins were hormones (0.37% found on b-PEI and 0.75% found on $NM_{0.2}/CP_{0.8}$ PXs) and receptors (0.3% detected for b-PEI and 0.53% detected for $NM_{0.2}/CP_{0.8}$ PXs). The remaining proteins determined in the hard corona protein profile of b-PEI (68.89%)

and $NM_{0.2}/CP_{0.8}$ PXs (55.51%) could be assigned to various other functions and were to this end grouped under the category "other". These data revealed, in line with previous observations, that the PC composition differs for both formulations possibly due to the hydrophobic content of $NM_{0.2}/CP_{0.8}$ PXs. Approximately 2-fold more transport proteins in the hard corona protein profile of $NM_{0.2}/CP_{0.8}$ PXs were detected than in the protein profile of b-PEI PXs, whereas the amounts of the other functional groups were virtually comparable. Transport proteins carry various substances through the body to their target sites. In many cases, they induce cellular uptake by interacting as ligands with specific receptors expressed by the cells of interest. This mechanism has been widely exploited in the field of selective drug targeting by modifying nanoparticulate systems with different proteins that act as ligands, thus achieving targeted cellular internalization of their payload into the site of action. Considerable success has already been achieved with a variety of nanoparticulate delivery systems modified with, for example, albumin [63], Transferrin [64], or Apolipoprotein E (ApoE) [65] through different strategies, from direct coating to the covalent binding. In a study conducted by Qi et al., dextran-chitosan NPs were modified via electrostatic attraction with BSA and loaded with the drug doxorubicin. The antitumor effects of doxorubicin-loaded NPs were investigated by the tumor inhibition and survivability of murine ascites hepatoma H22 tumor-bearing mice. The loaded NPs were found to largely decrease the toxicity of doxorubicin and significantly increase the survivability of the tumor-bearing mice [66]. The group of Xie et al. designed a novel pulmonary delivery system for siRNA by modifying PEI PXs with Transferrin. The formulation was able to significantly enhance cellular uptake and gene knockdown in Transferrin-receptor expressing human primary activated T cells and thus represents a promising siRNA delivery system for asthma [54].

ApoE also serves as a ligand for low-density lipoprotein (LDL) and the LDL receptor-related protein (LRP) receptors and can be used for selective drug targeting. Since LDL and LRP receptors are also expressed on the cells of the blood-brain barrier (BBB), it has been shown that modification of nanoparticles with ApoE can even lead to successful brain delivery. In the body, apolipoproteins form lipoproteins together with lipids, which are involved in plasma lipoprotein metabolism. ApoE is a component found in lipoprotein classes very low-density lipoproteins (VLDL) and chylomicrons. Therefore, the major function of ApoE is the transport of triglycerides and cholesterol from sites of synthesis or adsorption to sites of utilization (peripheral tissues) or excretion (liver) [67]. ApoE consists of two structural domains, the amino-terminal domain contains receptor-binding sites, while the carboxyl-terminal domain comprises the major lipid-binding sites, located in amphipathic alpha-helices [68]. It has been

shown that apolipoproteins, due to their lipid-binding domains, are increasingly adsorbed by nanoparticles containing hydrophobic components [39, 69]. The group of Blunk et al. utilized well-defined hydrophobic polystyrene beads using poloxamers and found over-proportional fractions of ApoE on particles with the highest hydrophobicity [56]. The group of Kreuter et al. used dalargin-loaded PBCA NPs modified with ApoE. The particles were precoated or not with polysorbate 80 (PS80) and demonstrated that PS80 precoated and ApoE-modified NPs achieved significantly higher analgesic effects in mice than other formulations. In addition, experiments with ApoE-deficient (ApoEtm1Unc) mice confirmed that ApoE plays a crucial role in mediating the delivery of the NPs across the BBB [70]. PS80 is theorized to act as a hydrophobic anchor for ApoE. Therefore, it has been used in several studies to investigate the delivery of different nanoparticle systems (e.g., poly(alyklcyanoacrylates) (PACA), poly(lactic-co-glycolic acid) (PLGA) and polycaprolactone (PCL) NPs) to the brain encapsulating small drug molecules, such as loperamide or doxorubicin, or proteins, like dalargine and others, as summarized in detail [65]. Further studies have revealed another interesting aspect of PS80-coated NPs. After intravenous administration of PS80–coated NPs, apolipoproteins present in the blood were adsorbed to the NPs and led to improved brain delivery [70, 71]. At this point, it was quite clear that a PC forms around the particles as soon as they are administered into a biological fluid. Moreover, this process can strongly influence the biodistribution of the particles.

There have been many studies in the past that have focused on the physicochemical properties and possible modifications of nanoparticulate systems and how to adapt them to achieve desired effects without considering the PC that forms after i.v. administration [16]. The group of Salvati et al. even demonstrated that the targeting ability of Transferrin conjugated silica nanoparticles disappeared when a biomolecule corona adsorbs on the surface, after placing them in a biological environment [24]. In comparison, some studies have addressed the question of whether adsorbed plasma proteins can induce specific targeting effects. Zhang et al. designed doxorubicin-loaded liposomes modified with a short nontoxic peptide that specifically interacts with the lipid-binding domain of exchangeable apolipoproteins. The absorption of plasma ApoE enabled a significant improvement in brain distribution and efficacy against brain tumors after i.v administration compared to doxorubicin-loaded plain liposomes. Furthermore, the corona-mediated targeting strategy also worked with modified PLGA NPs [72]. Apolipoproteins' role as specific targeting molecules was also investigated by Kim and collaborators. This study showed that poly(ethylene glycol) poly-hexadecylcyanoacrylate (PEG-PHDCA) NPs preferentially absorbed rat ApoE and ApoB-100 from the plasma on their

surface. They were effectively taken up by rat brain endothelial cells using the LDL receptor on the BBB [73].

In addition to the apolipoptroteins, it has been shown for many other molecules that they can lead to specific targeting via one component of the PC (e.g. vitronectin, albumin, Transferrin) [25]. Most of the studies mentioned above have been carried out with solid nanoparticles, which raises the question of whether this PC-based targeting strategy would also be applicable to dynamic systems such as PXs. Preliminary experiments were conducted to test whether the promising surfactant-based approach using PS80 and adsorbed ApoE from plasma to enable selective targeting into the brain could also be suitable for PXs. To determine the influence of PS precoating on the stability of the PXs, b-PEI PXs were incubated with PS concentrations from 0.01% to 0.5% and the sizes and PDIs were measured with DLS. As illustrated in Figure S1 (Supplementary Material), 0.1% was determined as the optimal PS 80 concentration that led to stable particles. A slight increase in size from 102.3 nm to 120 nm and a slight change in PDI value from 0.094 to 0.321 were observed. At higher concentrations, no particles could be measured by DLS, which may be explained by particle aggregation processes caused by the addition of surfactant.

In addition, an uptake experiment with b-PEI PXs with and without 0.1% PS80 precoating was performed in a human brain endothelial cell line (hCMEC) to determine the influence on the transfection efficiency. As shown in Figure S2 (Supplementary Material) uncoated b-PEI PXs displayed significantly higher cellular uptake compared to the pre-coated PEI PXs. Thus, it was hypothesized that pre-coating with a surfactant destabilizes the polymer-siRNA complexes once they are in the cell medium, leading to very low uptake by the cells. In summary, the preliminary experiments gave a first indication that the surfactant-based approach for PXs is only suitable to a limited extent. This is the main reason it was rejected for this study but would need to be further investigated in continuing experiments. As pointed out above, the presence of hydrophobic components plays a major role in the interaction with specific proteins. It led us to address the questions of i) how the profile of the absorbed proteins differs in detail between b-PEI PXs and the more hydrophobic $NM_{0.2}/CP_{0.8}$ PXs, and ii) whether hydrophobic subunits of $NM_{0.2}/CP_{0.8}$ PXs may lead to enhanced apolipoprotein adsorption.

For this purpose, the ratios of the mean values of abundances of the proteins identified on both PXs by LC-MS-MS were calculated ($NM_{0.2}/CP_{0.8}$ /b - PEI) (Table S1, Supplementary Material). As a threshold cutoff a 2-fold change in log2 values of ratios was used. P-values were additionally calculated and results are presented as a volcano plot comparison of protein levels

(y-axis: - log p-value, x-axis: log2 ratio) in Figure 5. As mentioned above, proteins that function as ligands for specific receptors potentially affecting the biodistribution and in particular the internalization of PXs into specific tissues are of special interest in this study. Therefore, only these proteins were considered in the following.

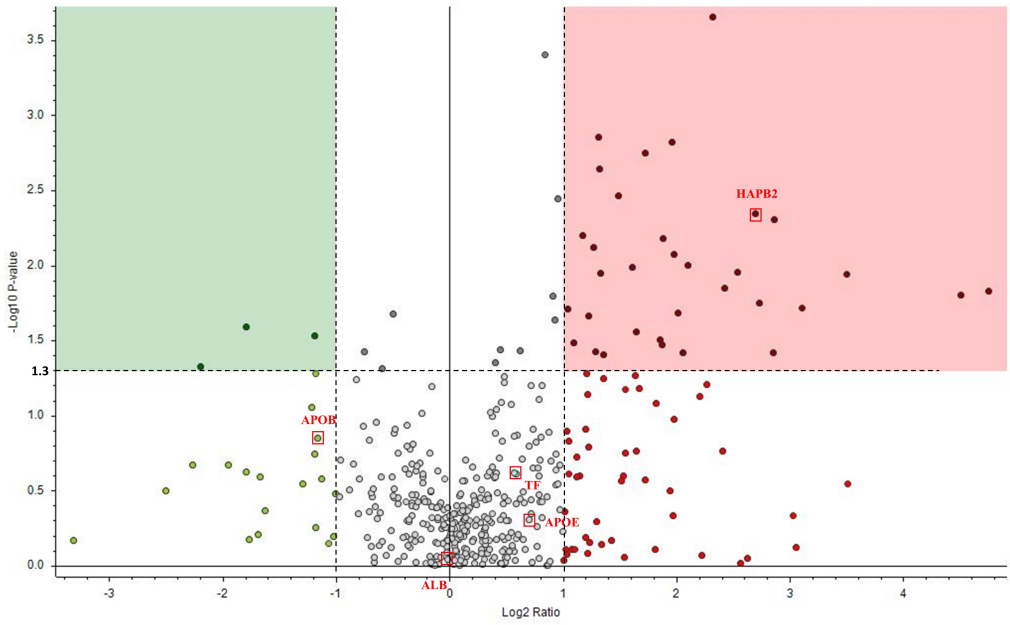

Figure 5. Volcano plot from the LC-MS-MS data demonstrates the differences of the protein levels bound on $NM_{0.2}/CP_{0.8}$ PXs compared to b-PEI PXs after exposure to 10% FBS. Log2 values of ratios of the normalized abundances from identified proteins present on PEI-PXs and $NM_{0.2}/CP_{0.8}$ PXs were calculated (x-axis) and a 2-fold change in ratio [log 2 (2) = 1 and log 2 [0.5] = - 1] was used as threshold cutoff (higher or lower abundance of proteins) indicated by vertical dashed lines. P-values were calculated with ANOVA and given as -log10 values (y-axis) to indicate the significance of differences in protein levels for each protein. As threshold cutoff a p-value of 0.05 [-log 10 (0.05) = 1.3] was used and indicated by the horizontal dash line. Therefore, the red box contains the most significant and most abundant proteins on $NM_{0.2}/CP_{0.8}$ PXs and the green box contains significantly lower bound proteins on $NM_{0.2}/CP_{0.8}$ PXs compared to PEI PXs.

Of all the proteins identified, 33 were found to be significantly more (red box) and three proteins were found to be significantly less abundant (green box) in the corona of $NM_{0.2}/CP_{0.8}$ PXs than in PEI-PXs. With regard to transport proteins, ApoB was found to a significantly lower extend in the protein corona of b-PEI PXs (log2 ratio = -1.17, -log p value: 0.85). Without significant differences in protein levels albumin (ALB) (log2 ratio = -0.02, -log p value: 0.09), Transferrin (Tf) (log2 ratio = 0.59, -log p value: 0.61) and ApoE (log2 ratio = 0.70, -log p value: 0.31) were found in both protein coronas. However, it was evidenced that one protein, namely the hyaluronan binding protein 2 (HABP2), was found to a significantly higher extent on $NM_{0.2}/CP_{0.8}$ PXs (log2 ratio = 2.69, -log p value: 2.3).

These observations point out that both, particle composition as well as surface chemistry influence the binding [74]. The hypothesis, that apolipoproteins can bind especially to $NM_{0.2}/CP_{0.8}$ PXs due to interactions between hydropbobic subunits of the PXs with the hydrophobic domains/lipid-binding sites present in the apolipoproteins [75] was refuted. However, the data also revealed that proteins with potential targeting effects accumulate on both PXs under physiological conditions. ApoB is an important protein in the lipoprotein metabolism as it is the major protein component of chylomicrons, LDL and very density lipoprotein (VDL) and functions as a recognition signal for the cellular binding and internalization of the lipoproteins by the LDL/LRP receptor. Due to its affinity to LDL/LRP receptors, ApoB has also been investigated as a component of selective drug delivery systems, especially for reaching the brain [70, 76]. Transferrin, as component of the PC of NPs, was able to selectively drive NPs to the cellular destination. The group of Santi et al., for example, utilized the spontaneous recruiting of Transferrin by gold NPs conjugated with a specifically designed peptide. The Tf-binding peptide efficiently interacted with plasma Transferrin, which led to enhanced internalization of peptide-functionalized NPs into Tf-receptor overexpressing cells [77]. HABP2, also called factor VII–activating protease (FASP) [78] or plasma hyaluronan binding protein (PHBP) [79], is an extracellular serine protease involved in the extrinsic pathway of blood coagulation (via activation of factor VII) and fibrinolysis (via activation of prourokinase type plasminogen activator) [78]. It is also involved in tissue remodeling processes, such as wound healing and tumor progression [80]. HABP2 is present in human plasma as a single polypeptide chain (70 kDa) as a proform [79]. It is auto-activated by its own serin protease activity through cleavage into the two-chain forms, including a heavy chain of 50 kDa and a light chain of 25 kDa linked by a disulfide bond [81]. Further cleavages of the chains, leading to the three- or four-chain structure, cause the inactivation of HAPB2 [79]. The structure of the protein shows three epidermal growth factor (EGF) domains, a kringle domain, and a serin protease domain, whereby the second and third epidermal growth factor-like domains form the polyanion-binding domain (PABD) [78]. The protease activity of HAPB2 is regulated by the binding of polyanionic structures such as hyaluronic acid, heparin, or heparan sulfate to the PABD. The reaction accelerates the autocleavage of the preform into the active two-chain form [81].

HAPB2 was originally discovered through its ability to bind to hyaluronic acid. Hyaluronan (HA) is a negatively charged glycosaminoglycan composed of repeating disaccharides of glucuronic acid and N-acetyl glucosamine [82] and can be found in biological fluids and tissues

in different content and size distributions. Moreover, transmembrane receptor-proteins exist that can interact with HA, mainly via hydrogen bonds or van der Waals forces. The most investigated ones are the cluster of differentiation 44 (CD44) receptor and the receptor of hyaluronan-mediated mobility (RHAMM), which is involved in altering migratory cell behavior [73]. CD44 receptor is a cell surface glycoprotein, which is involved in cell proliferation processes. Therefore, it is highly overexpressed in various tumors, including pancreatic, breast, ovary, brain and lung cancers what makes it a highly potent target for nanocarriers [83]. Numerous studies have focused on the development of various HA-modified nanocarriers that actively target the CD44 receptor to enable accumulation, uptake and release of therapeutic agents within the tumor cells or tissue. Initially, small molecules such as doxorubicin, docetaxel, and curcumin were used and afterward, nanocarrier systems that can deliver nucleic acids to the target site as effective drugs have also been successfully developed [73]. In the field of siRNA delivery, as shown, for example, by the group of Ganesh et al., HA-PEI-siRNA complexes were able to demonstrate selective uptake in CD44 overexpressing tumor cells as well as target specific gene knockdown in *in vivo* experiments. In line with many previous studies, it was concluded that HA-modified NPs exhibited enhanced therapeutic effects due to the selective binding of HA to the overexpressed CD44 receptor on the tumor cells [84].

Taken together, our results indicate that, in agreement with the literature, differences in the physicochemical properties of the PXs lead to distinct PC profiles. Due to the accumulation of selective targeted proteins such as albumin, Transferrin or various apolipoproteins in the hard PC of both $NM_{0.2}/CP_{0.8}$ and b-PEI PXs, their influence on the biodistribution of particles after intravenously injection need to be evaluated in future work. In summary, hydrophobic modification of the $NM_{0.2}/CP_{0.8}$ PXs did not, as might be expected from previous studies, result in an increased accumulation of apolipoproteins. Interestingly, we detected another protein, namely HAPB2, at a tremendously increased abundance in the PC of hydrophobically modified $NM_{0.2}/CP_{0.8}$ PXs. This evidence underpins that these proteins have a preferential affinity for this specifically modified PX. Adsorbed HAPB2 proteins and bound plasma HA may have the potential to selectively deliver the respective formulation via overexpressed CD44 receptors into various tumor cells. This hypothesis encouraged us to test the targeting potential of the PCPXs in correlation to present corona proteins using a CD44 receptor-expressing cell line.

3.5 Correlation of Protein Binding Profile with Cellular Uptake Ability in a Glioblastoma Cell Line

Once the previous LC-MS-MS results revealed different PC profiles for $NM_{0.2}/CP_{0.8}$ and b-PEI PXs, the next step was to investigate the effect of the adsorbed proteins on the cellular internalization ability of the PCPXs. The aim here was to investigate whether HAPB2 proteins, which are highly abundant in the corona of $NM_{0.2}/CP_{0.8}$ PXs, may induce selective targeting into a CD44 receptor positive cell line. In this regard, CD44 receptor overexpression of utilized U87 glioblastoma cells was confirmed by Western Blot analysis in comparison to the negative control cell line MCF7, as illustrated in Figure S3 (Supplementary Material). Figure 6 depicts the MFI of U87 cells transfected for 24 h with PXs formulated with b-PEI and $NM_{0.2}/CP_{0.8}$ PXs at preassigned N/P ratios. The samples were incubated either in FBS-free or in a 10% FBS culture medium and compared to untreated cells and free siRNA (as negative controls) and LF lipoplexes (as a positive control). Trypan quenching was additionally performed to exclude extracellular fluorescent signals from bound but not internalized nanoparticles.

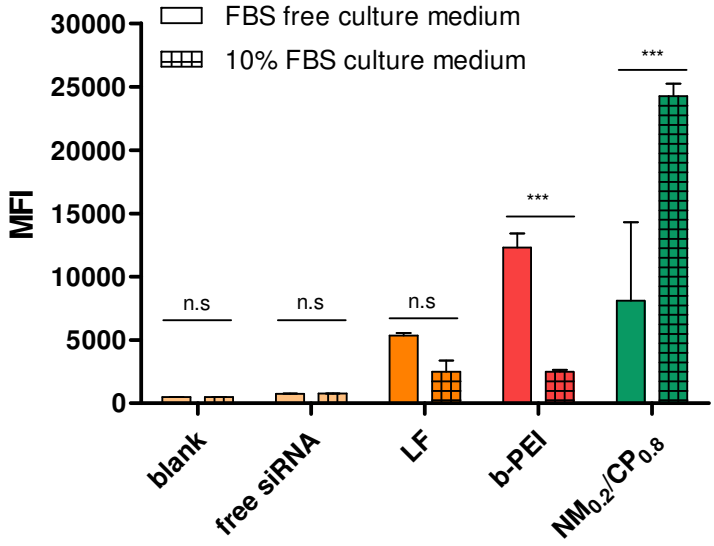

Figure 6. Cellular uptake of PXs (b-PEI PXs: N/P ratio = 7 and $NM_{0.2}/CP_{0.8}$ PXs: N/P ratio = 9) after 24 h incubation in either FBS-free or 10% FBS culture medium. Samples were trypan quenched, quantified by flow cytometry and presented as median fluorescence intensity (MFI). Negative control: untreated cells and free siRNA treated cells, positive control: with Lipofectamin (LF) lipoplexes transfected cells. (Results are shown as mean ± SD, n = 3, one-way ANOVA with Bonferroni post-hoc test, n.s (= not significant) $p > 0.05$, *** $p < 0.005$).

After incubation in 10% FBS containing medium, a PC adsorbed on the particles, which in the case of LF lipoplexes and b-PEI PXs led to reduced fluorescent signals within the measured cells dueto reduced particle internalization. The MFI of plain LF lipoplexes of 5358 decreased to 2495 for lipoplexes with proteins bound on their surface. B-PEI PXs displayed an MFI of

12283, which decreased significantly to 2488 for b-PEI PXs incubated in FBS. A remarkably opposite result was observed for the $NM_{0.2}/CP_{0.8}$ PXs, as the particles surrounded with proteins were internalized approximately 3 times more into the U87 cells than plain PXs. The observed MFI increased significantly from 8103 to 24250. The results for b-PEI PXs and lipoplexes are in agreement with previous literature that reported a remarkable decrease of transfection efficiency as soon as serum is present in the transfection medium [28, 30]. The group of Zhu et al. incubated b – PEI (25kDa) – DNA PXs with FBS at different concentrations and evaluated inter alia their transfection efficiencies in Hela cells using luciferase-encoding plasmid or enhanced green fluorescent protein (eGFP)-encoding plasmid as reporter genes. The data revealed that incubation in 10% FBS led to a serum-induced repression of transfection efficiency by 2-3 orders of magnitude. Hence, the authors suggested that adsorbed proteins may lead to PX dissociation or aggregation prior to the interaction of the PXs with cells inducing a considerably lowered cellular internalization capability [28]. The group of Maiolo et al. demonstrated similar results using 25 kDa b-PEI-DNA PXs that were incubated in a medium containing different concentrations of FBS (0 – 50%) prior to transfection. B-PEI PXs displayed a clear FBS-concentration dependency of transfection efficiency in HeLa cells with a sharp decrease at the highest FBS concentration of 50%. The authors hypothesized that the adsorption of proteins on the particles may influence either their physicochemical properties in an unfavorable way or hinders productive cell membrane–particle interactions [30]. In addition, previous studies reported a similar behavior for lipoplexes demonstrating that serum proteins also diminish lipoplex transfection abilities [85]. These results strongly support our finding that the adsorption of serum proteins to b-PEI PXs and LF lipoplexes remarkably reduce the cellular uptake into glioblastoma cells. Nevertheless, the exact mechanism remains unclear and gives rise to investigating this question in further studies.

In contrast, several studies revealed that binding of specific functional serum proteins, namely transport and binding proteins, to the nanoparticulate systems leads to active and highly selective targeting into cells that express the corresponding receptors. One of the first examples, as already mentioned, was the absorption of plasma ApoE on PS80-modified NPs that enabled the transport of surfactant-coated NPs across the BBB via LDL receptors [12, 86, 87].

Interestingly, in this study, we were able to identify a specific plasma component, the HAPB2 protein within the PC of $NM_{0.2}/CP_{0.8}$ PXs, that might be able to induce active targeting effects in CD44 receptor-bearing glioblastoma cells. This hypothesis was supported by the results of this experiment: $NM_{0.2}/CP_{0.8}$ PXs incubated in serum exhibited significantly increased

transfection efficiencies in glioblastoma cells in comparison to free-FBS medium. Several studies confirmed improved gene delivery activity by PXs containing hydrophobic segments, although, the explanations are still controversial and consider various aspects of the particles, e.g., physicochemical characteristics and stability of PXs including aggregation and sedimentation phenomena, particle-cell membrane interactions and the influence of the protein corona on PXs properties and protein-cell membrane interactions [88]. This underlines that the explanation of interaction of particles with cells is complicated because it can be influenced by many aspects of the particles, the environment, and the characteristics of selected cell lines and models. Taken together, we suggest, that PCPX – cell interactions may be involved in the enhanced uptake of $NM_{0.2}/CP_{0.8}$ PXs in glioblastoma cells. Whether absorbed HAPB2 proteins and expressed CD44 receptors of glioblastoma cells are involved in the cellular internalization of $NM_{0.2}/CP_{0.8}$ PXs needs to be further elucidated in future studies.

4. Conclusion

In recent decades, research in the field of nanomedicine has focused on the physicochemical characteristics and modification possibilities of NPs to achieve efficient targeting strategies. However, the interaction of NPs with the blood components after intravenous injection and the influence of the absorbed protein corona on the biodistribution of the particles has been an overlooked parameter. Hence, method development for PC investigations of various nanoparticulate systems caught the attention and introduced further knowledge of protein-NP and PCPX interactions. To date, most of the studies regarding protein adsorption have focused on hard materials and thus, the aim of this study was to develop appropriate methods for evaluating the PC formation on PXs. These formulations as well as siRNA-polymer complexes constitute dynamic systems. Herein, we successfully demonstrated that PCPXs can be isolated from loosely and not bound proteins after incubation in FBS via optimized centrifugation protocols (12.500g, 10 min, 3X), without destroying the PXs. Resuspending the pellets after the third centrifugation step led to the reassembly of PXs with acceptable sizes supplemented by narrow size distributions. Moreover, SYBR Gold assays confirmed that a very low amount of siRNA gets lost during the purification procedure. LDA experiments exhibited a reduction in zeta potential values for both formulations incubated in FBS in comparison to plain particles measured after the third centrifugation, indicating that adsorbed hard corona proteins are still present on the surface.

With the application of SDS-PAGE and LC-MS-MS methods, we were able to determine the composition of the PC with a special emphasis on functional proteins as a function of the NPs

material. Therefore, cationic b-PEI and hydrophobically modified $NM_{0.2}/CP_{0.8}$ polymers, both used as highly potent siRNA delivery agents, were used. It was shown that protein profiles differed mainly regarding the number of bound transport proteins, as approximately 2-fold more transport proteins in the hard corona protein profile of $NM_{0.2}/CP_{0.8}$ PXs were detected than in the protein profile of b-PEI PXs. Most proteins known to be able to induce targeting effects, such as albumin, Transferrin or apolipoproteins were found to a similar extent in the hard PC of both formulations. Interestingly, we detected one functional protein, namely the HABP2 protein, 6.5 times more frequently in the hard PC of $NM_{0.2}/CP_{0.8}$ PXs. In cellular uptake experiments, it was observed that PC formation in the case of b-PEI PXs induced attenuated cellular internalization capabilities of particles, indicating that no active protein-cell interactions occurred for this formulation. In the case of $NM_{0.2}/CP_{0.8}$ PXs, bound PC was correlated with tremendously increased cellular uptake ability, which was potentially induced by interactions between highly absorbed HABP2 proteins and CD44 receptors of glioblastoma cells.

In summary, we demonstrated that centrifugation is an appropriate purification method for PXs that could also be applied to other dynamic systems, laying the foundation for more in-depth studies in the future. Functional proteins with a high potential to influence the biodistribution of b-PEI and $NM_{0.2}/CP_{0.8}$ PXs *in vivo* have been identified. It highlights once again the importance of including PC investigations at an early stage of the development process to obtain the most efficient, safe, and precise drug carriers. However, continuing experiments are required to gain further knowledge about the correlation between PC composition and siRNA delivery efficacy. A wider understanding of the protein–PX and PCPXs-cell interactions could enable precise adjustment of NPs compositions to control the enrichment of desired proteins, thus, representing a novel strategy in the design of nanomedicines for targeted drug delivery.

References

[1] F. Pederzoli, G. Tosi, M.A. Vandelli, D. Belletti, F. Forni, B. Ruozi, Protein corona and nanoparticles: how can we investigate on?, WIREs Nanomedicine and Nanobiotechnology, 9 (2017) e1467.
[2] A.A. Halwani, Development of Pharmaceutical Nanomedicines: From the Bench to the Market, Pharmaceutics, 14 (2022) 106.
[3] S. Ren, M. Wang, C. Wang, Y. Wang, C. Sun, Z. Zeng, H. Cui, X. Zhao, Application of Non-Viral Vectors in Drug Delivery and Gene Therapy, Polymers, 13 (2021) 3307.
[4] M. Jinek, J.A. Doudna, A three-dimensional view of the molecular machinery of RNA interference, Nature, 457 (2009) 405-412.
[5] M.E. Davis, J.E. Zuckerman, C.H.J. Choi, D. Seligson, A. Tolcher, C.A. Alabi, Y. Yen, J.D. Heidel, A. Ribas, Evidence of RNAi in humans from systemically administered siRNA via targeted nanoparticles, Nature, 464 (2010) 1067-1070.
[6] T. Coelho, D. Adams, A. Silva, P. Lozeron, P.N. Hawkins, T. Mant, J. Perez, J. Chiesa, S. Warrington, E. Tranter, Safety and efficacy of RNAi therapy for transthyretin amyloidosis, New England Journal of Medicine, 369 (2013) 819-829.
[7] T. Zimmermann, V. Karsten, J. Harrop, A. Chan, J. Chiesa, G. Peters, R. Falzone, J. Cehelsky, S. Nochur, A. Vaishnaw, Phase I first-in-humans trial of ALN-TTRsc, a novel RNA interference therapeutic for the treatment of familial amyloidotic cardiomyopathy (FAC), Journal of Cardiac Failure, 19 (2013) S66.
[8] M.G. Kim, S.D. Jo, J.Y. Yhee, B.S. Lee, S.J. Lee, S.G. Park, S.-W. Kang, S.H. Kim, J.H. Jeong, Synergistic anti-tumor effects of bevacizumab and tumor targeted polymerized VEGF siRNA nanoparticles, Biochemical and biophysical research communications, 489 (2017) 35-41.
[9] G.R. Rettig, M.A. Behlke, Progress Toward In Vivo Use of siRNAs-II, Molecular Therapy, 20 (2012) 483-512.
[10] S. Patnaik, K.C. Gupta, Novel polyethylenimine-derived nanoparticles for in vivo gene delivery, Expert Opinion on Drug Delivery, 10 (2013) 215-228.
[11] B. Schwarz, O.M. Merkel, Functionalized PEI and its role in gene therapy, Mater Matters, 12 (2017) 2.
[12] P. Aggarwal, J.B. Hall, C.B. McLeland, M.A. Dobrovolskaia, S.E. McNeil, Nanoparticle interaction with plasma proteins as it relates to particle biodistribution, biocompatibility and therapeutic efficacy, Advanced drug delivery reviews, 61 (2009) 428-437.
[13] G. Caracciolo, Liposome–protein corona in a physiological environment: Challenges and opportunities for targeted delivery of nanomedicines, Nanomedicine: Nanotechnology, Biology and Medicine, 11 (2015) 543-557.
[14] S.-T. Yang, Y. Liu, Y.-W. Wang, A. Cao, Biosafety and Bioapplication of Nanomaterials by Designing Protein–Nanoparticle Interactions, Small, 9 (2013) 1635-1653.
[15] J. Wolfram, Y. Yang, J. Shen, A. Moten, C. Chen, H. Shen, M. Ferrari, Y. Zhao, The nano-plasma interface: Implications of the protein corona, Colloids and Surfaces B: Biointerfaces, 124 (2014) 17-24.
[16] D. Dutta, S.K. Sundaram, J.G. Teeguarden, B.J. Riley, L.S. Fifield, J.M. Jacobs, S.R. Addleman, G.A. Kaysen, B.M. Moudgil, T.J. Weber, Adsorbed Proteins Influence the Biological Activity and Molecular Targeting of Nanomaterials, Toxicological Sciences, 100 (2007) 303-315.
[17] A. Gessner, A. Lieske, B.R. Paulke, R.H. Müller, Influence of surface charge density on protein adsorption on polymeric nanoparticles: analysis by two-dimensional electrophoresis, European Journal of Pharmaceutics and Biopharmaceutics, 54 (2002) 165-170.
[18] T.M. Göppert, R.H. Müller, Adsorption kinetics of plasma proteins on solid lipid nanoparticles for drug targeting, International Journal of Pharmaceutics, 302 (2005) 172-186.

[19] M. Lück, B.-R. Paulke, W. Schröder, T. Blunk, R.H. Müller, Analysis of plasma protein adsorption on polymeric nanoparticles with different surface characteristics, Journal of Biomedical Materials Research, 39 (1998) 478-485.
[20] F.M. Musteata, J. Pawliszyn, M.G. Qian, J.-T. Wu, G.T. Miwa, Determination of drug plasma protein binding by solid phase microextraction, Journal of Pharmaceutical Sciences, 95 (2006) 1712-1722.
[21] M.J. Banker, T.H. Clark, J.A. Williams, Development and validation of a 96-well equilibrium dialysis apparatus for measuring plasma protein binding, Journal of Pharmaceutical Sciences, 92 (2003) 967-974.
[22] I. Kariv, H. Cao, K.R. Oldenburg, Development of a High Throughput Equilibrium Dialysis Method, Journal of Pharmaceutical Sciences, 90 (2001) 580-587.
[23] S. Sarre, K. Van Belle, I. Smolders, G. Krieken, Y. Michotte, The use of microdialysis for the determination of plasma protein binding of drugs, Journal of Pharmaceutical and Biomedical Analysis, 10 (1992) 735-739.
[24] A. Salvati, A.S. Pitek, M.P. Monopoli, K. Prapainop, F.B. Bombelli, D.R. Hristov, P.M. Kelly, C. Åberg, E. Mahon, K.A. Dawson, Transferrin-functionalized nanoparticles lose their targeting capabilities when a biomolecule corona adsorbs on the surface, Nature nanotechnology, 8 (2013) 137-143.
[25] R. Cagliani, F. Gatto, G. Bardi, Protein Adsorption: A Feasible Method for Nanoparticle Functionalization?, Materials (Basel), 12 (2019) 1991.
[26] D. Zhong, Y. Jiao, Y. Zhang, W. Zhang, N. Li, Q. Zuo, Q. Wang, W. Xue, Z. Liu, Effects of the gene carrier polyethyleneimines on structure and function of blood components, Biomaterials, 34 (2013) 294-305.
[27] D. Pezzoli, M. Zanda, R. Chiesa, G. Candiani, The yin of exofacial protein sulfhydryls and the yang of intracellular glutathione in in vitro transfection with SS14 bioreducible lipoplexes, Journal of Controlled Release, 165 (2013) 44-53.
[28] D. Zhu, H. Yan, Z. Zhou, J. Tang, X. Liu, R. Hartmann, W.J. Parak, N. Feliu, Y. Shen, Detailed investigation on how the protein corona modulates the physicochemical properties and gene delivery of polyethylenimine (PEI) polyplexes, Biomaterials Science, 6 (2018) 1800-1817.
[29] D. Zhu, H. Yan, Z. Zhou, J. Tang, X. Liu, R. Hartmann, W.J. Parak, Y. Shen, N. Feliu, Influence of the Modulation of the Protein Corona on Gene Expression Using Polyethylenimine (PEI) Polyplexes as Delivery Vehicle, Advanced Healthcare Materials, 10 (2021) 2100125.
[30] D. Maiolo, J. Colombo, J. Beretta, C. Malloggi, G. Candiani, F. Baldelli Bombelli, The polyplex, protein corona, cell interplay: Tips and drawbacks, Colloids and Surfaces B: Biointerfaces, 168 (2018) 60-67.
[31] R. Liu, K.S. Masters, S.H. Gellman, Polymer Chain Length Effects on Fibroblast Attachment on Nylon-3-Modified Surfaces, Biomacromolecules, 13 (2012) 1100-1105.
[32] N. Hartl, F. Adams, G. Costabile, L. Isert, M. Döblinger, X. Xiao, R. Liu, O.M. Merkel, The Impact of Nylon-3 Copolymer Composition on the Efficiency of siRNA Delivery to Glioblastoma Cells, Nanomaterials, 9 (2019) 986.
[33] R. Liu, X. Chen, Z. Hayouka, S. Chakraborty, S.P. Falk, B. Weisblum, K.S. Masters, S.H. Gellman, Nylon-3 Polymers with Selective Antifungal Activity, Journal of the American Chemical Society, 135 (2013) 5270-5273.
[34] B.P. Mowery, S.E. Lee, D.A. Kissounko, R.F. Epand, R.M. Epand, B. Weisblum, S.S. Stahl, S.H. Gellman, Mimicry of Antimicrobial Host-Defense Peptides by Random Copolymers, Journal of the American Chemical Society, 129 (2007) 15474-15476.
[35] R. Liu, X. Chen, S.P. Falk, B.P. Mowery, A.J. Karlsson, B. Weisblum, S.P. Palecek, K.S. Masters, S.H. Gellman, Structure–Activity Relationships among Antifungal Nylon-3 Polymers: Identification of Materials Active against Drug-Resistant Strains of Candida albicans, Journal of the American Chemical Society, 136 (2014) 4333-4342.

[36] J. Zhang, D.A. Kissounko, S.E. Lee, S.H. Gellman, S.S. Stahl, Access to Poly-β-Peptides with Functionalized Side Chains and End Groups via Controlled Ring-Opening Polymerization of β-Lactams, Journal of the American Chemical Society, 131 (2009) 1589-1597.
[37] T. Cedervall, I. Lynch, S. Lindman, T. Berggård, E. Thulin, H. Nilsson, K.A. Dawson, S. Linse, Understanding the nanoparticle–protein corona using methods to quantify exchange rates and affinities of proteins for nanoparticles, Proceedings of the National Academy of Sciences, 104 (2007) 2050.
[38] I. Lynch, T. Cedervall, M. Lundqvist, C. Cabaleiro-Lago, S. Linse, K.A. Dawson, The nanoparticle–protein complex as a biological entity; a complex fluids and surface science challenge for the 21st century, Advances in Colloid and Interface Science, 134-135 (2007) 167-174.
[39] T. Cedervall, I. Lynch, M. Foy, T. Berggård, S.C. Donnelly, G. Cagney, S. Linse, K.A. Dawson, Detailed Identification of Plasma Proteins Adsorbed on Copolymer Nanoparticles, Angewandte Chemie International Edition, 46 (2007) 5754-5756.
[40] E. Casals, T. Pfaller, A. Duschl, G.J. Oostingh, V. Puntes, Time Evolution of the Nanoparticle Protein Corona, ACS Nano, 4 (2010) 3623-3632.
[41] M. Lundqvist, J. Stigler, G. Elia, I. Lynch, T. Cedervall, K.A. Dawson, Nanoparticle size and surface properties determine the protein corona with possible implications for biological impacts, Proceedings of the National Academy of Sciences, 105 (2008) 14265.
[42] M.P. Monopoli, D. Walczyk, A. Campbell, G. Elia, I. Lynch, F. Baldelli Bombelli, K.A. Dawson, Physical–Chemical Aspects of Protein Corona: Relevance to in Vitro and in Vivo Biological Impacts of Nanoparticles, Journal of the American Chemical Society, 133 (2011) 2525-2534.
[43] D. Walczyk, F.B. Bombelli, M.P. Monopoli, I. Lynch, K.A. Dawson, What the Cell "Sees" in Bionanoscience, Journal of the American Chemical Society, 132 (2010) 5761-5768.
[44] M. Elsayed, V. Corrand, V. Kolhatkar, Y. Xie, N.H. Kim, R. Kolhatkar, O.M. Merkel, Influence of oligospermines architecture on their suitability for siRNA delivery, Biomacromolecules, 15 (2014) 1299-1310.
[45] P.K. Smith, R.I. Krohn, G.T. Hermanson, A.K. Mallia, F.H. Gartner, M.D. Provenzano, E.K. Fujimoto, N.M. Goeke, B.J. Olson, D.C. Klenk, Measurement of protein using bicinchoninic acid, Analytical Biochemistry, 150 (1985) 76-85.
[46] J.R. Wiśniewski, A. Zougman, N. Nagaraj, M. Mann, Universal sample preparation method for proteome analysis, Nature Methods, 6 (2009) 359-362.
[47] O.M. Merkel, D. Librizzi, A. Pfestroff, T. Schurrat, M. Béhé, T. Kissel, In Vivo SPECT and Real-Time Gamma Camera Imaging of Biodistribution and Pharmacokinetics of siRNA Delivery Using an Optimized Radiolabeling and Purification Procedure, Bioconjugate Chemistry, 20 (2009) 174-182.
[48] M. Kokkinopoulou, J. Simon, K. Landfester, V. Mailänder, I. Lieberwirth, Visualization of the protein corona: towards a biomolecular understanding of nanoparticle-cell-interactions, Nanoscale, 9 (2017) 8858-8870.
[49] A. Gessner, A. Lieske, B.-R. Paulke, R.H. Müller, Functional groups on polystyrene model nanoparticles: Influence on protein adsorption, Journal of Biomedical Materials Research Part A, 65A (2003) 319-326.
[50] H. de Martimprey, C. Vauthier, C. Malvy, P. Couvreur, Polymer nanocarriers for the delivery of small fragments of nucleic acids: Oligonucleotides and siRNA, European Journal of Pharmaceutics and Biopharmaceutics, 71 (2009) 490-504.
[51] V. Nadithe, R. Liu, B.A. Killinger, S. Movassaghian, N.H. Kim, A.B. Moszczynska, K.S. Masters, S.H. Gellman, O.M. Merkel, Screening Nylon-3 Polymers, a New Class of Cationic Amphiphiles, for siRNA Delivery, Molecular Pharmaceutics, 12 (2015) 362-374.
[52] C. Carrillo-Carrion, M. Carril, W.J. Parak, Techniques for the experimental investigation of the protein corona, Current Opinion in Biotechnology, 46 (2017) 106-113.

[53] E. Nicolì, M.I. Syga, M. Bosetti, V.P. Shastri, Enhanced gene silencing through human serum albumin-mediated delivery of polyethylenimine-siRNA polyplexes, PloS one, 10 (2015) e0122581-e0122581.
[54] Y. Xie, N.H. Kim, V. Nadithe, D. Schalk, A. Thakur, A. Kılıç, L.G. Lum, D.J.P. Bassett, O.M. Merkel, Targeted delivery of siRNA to activated T cells via transferrin-polyethylenimine (Tf-PEI) as a potential therapy of asthma, Journal of Controlled Release, 229 (2016) 120-129.
[55] V. Neuhoff, N. Arold, D. Taube, W. Ehrhardt, Improved staining of proteins in polyacrylamide gels including isoelectric focusing gels with clear background at nanogram sensitivity using Coomassie Brilliant Blue G 250 and r 250, ELECTROPHORESIS, 9 (1988).
[56] T. Blunk, D.F. Hochstrasser, J.-C. Sanchez, B.W. Müller, R.H. Müller, Colloidal carriers for intravenous drug targeting: Plasma protein adsorption patterns on surface-modified latex particles evaluated by two-dimensional polyacrylamide gel electrophoresis, Electrophoresis, 14 (1993) 1382-1387.
[57] X. Zheng, H. Baker, W.S. Hancock, F. Fawaz, M. McCaman, E. Pungor Jr, Proteomic Analysis for the Assessment of Different Lots of Fetal Bovine Serum as a Raw Material for Cell Culture. Part IV. Application of Proteomics to the Manufacture of Biological Drugs, Biotechnology Progress, 22 (2006) 1294-1300.
[58] M. Mahmoudi, I. Lynch, M.R. Ejtehadi, M.P. Monopoli, F.B. Bombelli, S. Laurent, Protein–Nanoparticle Interactions: Opportunities and Challenges, Chemical Reviews, 111 (2011) 5610-5637.
[59] D.E. Owens, N.A. Peppas, Opsonization, biodistribution, and pharmacokinetics of polymeric nanoparticles, International Journal of Pharmaceutics, 307 (2006) 93-102.
[60] M. Roser, D. Fischer, T. Kissel, Surface-modified biodegradable albumin nano- and microspheres. II: effect of surface charges on in vitro phagocytosis and biodistribution in rats, European Journal of Pharmaceutics and Biopharmaceutics, 46 (1998) 255-263.
[61] T.M. Göppert, R.H. Müller, Protein adsorption patterns on poloxamer- and poloxamine-stabilized solid lipid nanoparticles (SLN), European Journal of Pharmaceutics and Biopharmaceutics, 60 (2005) 361-372.
[62] J. Marrack, H. Hoch, Serum proteins: a review, Journal of Clinical Pathology, 2 (1949) 161.
[63] J. Mariam, S. Sivakami, P.M. Dongre, Albumin corona on nanoparticles – a strategic approach in drug delivery, Drug Delivery, 23 (2016) 2668-2676.
[64] C. Dufès, M. Al Robaian, S. Somani, Transferrin and the transferrin receptor for the targeted delivery of therapeutic agents to the brain and cancer cells, Therapeutic delivery, 4 (2013) 629-640.
[65] N. Hartl, F. Adams, O.M. Merkel, From Adsorption to Covalent Bonding: Apolipoprotein E Functionalization of Polymeric Nanoparticles for Drug Delivery Across the Blood–Brain Barrier, Advanced Therapeutics, 4 (2021) 2000092.
[66] J. Qi, P. Yao, F. He, C. Yu, C. Huang, Nanoparticles with dextran/chitosan shell and BSA/chitosan core—doxorubicin loading and delivery, International journal of pharmaceutics, 393 (2010) 177-185.
[67] R.W. Mahley, J. Stanley C. Rall, Apolipoprotein E: Far More Than a Lipid Transport Protein, Annual Review of Genomics and Human Genetics, 1 (2000) 507-537.
[68] J. Ribalta, J.-C. Vallvé, J. Girona, L. Masana, Apolipoprotein and apolipoprotein receptor genes, blood lipids and disease, Curr Opin Clin Nutr Metab Care, 6 (2003) 177-187.
[69] K. Partikel, R. Korte, D. Mulac, H.-U. Humpf, K. Langer, Serum type and concentration both affect the protein-corona composition of PLGA nanoparticles, Beilstein J Nanotechnol, 10 (2019) 1002-1015.
[70] J. Kreuter, D. Shamenkov, V. Petrov, P. Ramge, K. Cychutek, C. Koch-Brandt, R. Alyautdin, Apolipoprotein-mediated transport of nanoparticle-bound drugs across the blood-brain barrier, J Drug Target, 10 (2002) 317-325.

[71] D.A. Shamenkov, V.E. Petrov, R.N. Alyautdin, Effects of apolipoproteins on dalargin transport across the blood-brain barrier, Bulletin of Experimental Biology and Medicine, 142 (2006) 703-706.
[72] Z. Zhang, J. Guan, Z. Jiang, Y. Yang, J. Liu, W. Hua, Y. Mao, C. Li, W. Lu, J. Qian, C. Zhan, Brain-targeted drug delivery by manipulating protein corona functions, Nature Communications, 10 (2019).
[73] H.R. Kim, S. Gil, K. Andrieux, V. Nicolas, M. Appel, H. Chacun, D. Desmaële, F. Taran, D. Georgin, P. Couvreur, Low-density lipoprotein receptor-mediated endocytosis of PEGylated nanoparticles in rat brain endothelial cells, Cellular and Molecular Life Sciences, 64 (2007) 356-364.
[74] D. Chen, S. Ganesh, W. Wang, M. Amiji, The role of surface chemistry in serum protein corona-mediated cellular delivery and gene silencing with lipid nanoparticles, Nanoscale, 11 (2019) 8760-8775.
[75] S.G. Young, Recent progress in understanding apolipoprotein B, Circulation, 82 (1990) 1574-1594.
[76] J. Kreuter, T. Hekmatara, S. Dreis, T. Vogel, S. Gelperina, K. Langer, Covalent attachment of apolipoprotein A-I and apolipoprotein B-100 to albumin nanoparticles enables drug transport into the brain, Journal of Controlled Release, 118 (2007) 54-58.
[77] M. Santi, G. Maccari, P. Mereghetti, V. Voliani, S. Rocchiccioli, N. Ucciferri, S. Luin, G. Signore, Rational Design of a Transferrin-Binding Peptide Sequence Tailored to Targeted Nanoparticle Internalization, Bioconjugate Chemistry, 28 (2017) 471-480.
[78] N. Mambetsariev, T. Mirzapoiazova, B. Mambetsariev, S. Sammani, F.E. Lennon, J.G.N. Garcia, P.A. Singleton, Hyaluronic Acid Binding Protein 2 Is a Novel Regulator of Vascular Integrity, Arteriosclerosis, Thrombosis, and Vascular Biology, 30 (2010) 483-490.
[79] N.-H. Choi-Miura, K. Takahashi, M. Yoda, K. Saito, T. Mazda, M. Tomita, Proteolytic Activation and Inactivation of the Serine Protease Activity of Plasma Hyaluronan Binding Protein, Biological and Pharmaceutical Bulletin, 24 (2001) 448-452.
[80] M.K. Cowman, H.-G. Lee, K.L. Schwertfeger, J.B. McCarthy, E.A. Turley, The Content and Size of Hyaluronan in Biological Fluids and Tissues, Front Immunol, 6 (2015) 261-261.
[81] B. Altincicek, A. Shibamiya, H. Trusheim, E. Tzima, M. Niepmann, D. Linder, K.T. Preissner, S.M. Kanse, A positively charged cluster in the epidermal growth factor-like domain of Factor VII-activating protease (FSAP) is essential for polyanion binding, Biochem J, 394 (2006) 687-692.
[82] E.A. Turley, Hyaluronan-binding proteins and receptors, Advanced Drug Delivery Reviews, 7 (1991) 257-264.
[83] P. Kesharwani, R. Chadar, A. Sheikh, W.Y. Rizg, A.Y. Safhi, CD44-Targeted Nanocarrier for Cancer Therapy, Front Pharmacol, 2021, pp. 800481.
[84] S. Ganesh, A.K. Iyer, D.V. Morrissey, M.M. Amiji, Hyaluronic acid based self-assembling nanosystems for CD44 target mediated siRNA delivery to solid tumors, Biomaterials, 34 (2013) 3489-3502.
[85] J. Turek, C. Dubertret, G. Jaslin, K. Antonakis, D. Scherman, B. Pitard, Formulations which increase the size of lipoplexes prevent serum-associated inhibition of transfection, The Journal of Gene Medicine, 2 (2000) 32-40.
[86] R.N. Alyautdin, E.B. Tezikov, P. Ramge, D.A. Kharkevich, D.J. Begley, J. Kreuter, Significant entry of tubocurarine into the brain of rats by adsorption to polysorbate 80–coated polybutylcyanoacrylate nanoparticles: An in situ brain perfusion study, Journal of Microencapsulation, 15 (1998) 67-74.
[87] T.M. Göppert, R.H. Müller, Polysorbate-stabilized solid lipid nanoparticles as colloidal carriers for intravenous targeting of drugs to the brain: Comparison of plasma protein adsorption patterns, J Drug Target, 13 (2005) 179-187.

[88] Z. Liu, Z. Zhang, C. Zhou, Y. Jiao, Hydrophobic modifications of cationic polymers for gene delivery, Progress in Polymer Science, 35 (2010) 1144-1162.

Supplementary Material

1. Preliminary Experiments PS80 Precoating

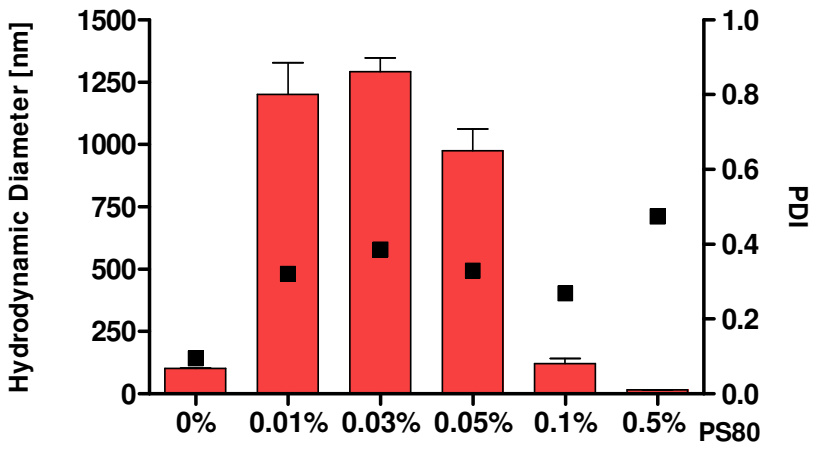

Figure S1. Hydrodynamic diameters (left y-axis) and polydispersity indices (PDI, right y-axis) of polysorbate 80 (0% - 0.5%) precaoted PXs formed with b-PEIat N/P ratio 8. (Data points indicate mean ± SD, n = 3).

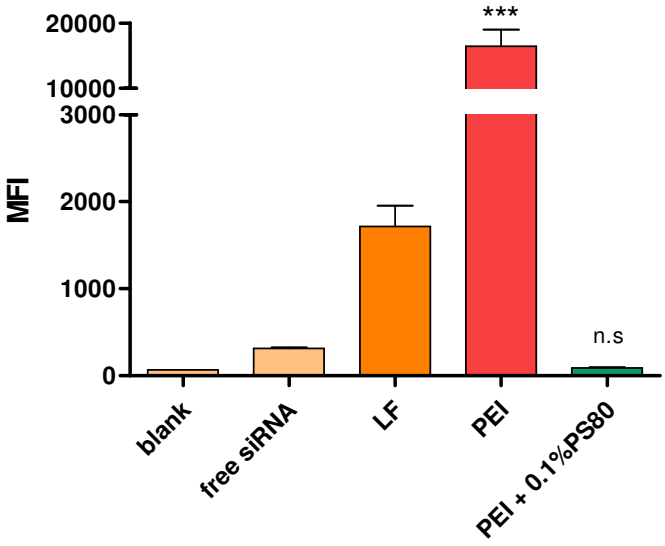

Figure S2. Cellular uptake of b-PEI PXs with and without PS80 (0.1%) precoating as quantified by flow cytometry and presented as median fluorescence intensitiy (MFI). Negative control: untreated cells and with free siRNA treated cells, positive control: with Lipofectamin (LF) lipoplexes transfected cells. (Results are shown as mean ± SD, n = 3, one-way ANOVA with Bonferroni post-hoc test, n.s (= not significant) $p > 0.05$, *** $p < 0.005$).

2. Comparison of Protein Corona Profiles

Table S1. List of calculated ratios ($NM_{0.2}/CP_{0.8}$ / b - PEI) from the mean values of abundances of proteins identified in the hard corona of purified b-PEI and $NM_{0.2}/CP_{0.8}$ PXs after exposure to 10 % FBS. The relative abundance of the proteins was analyzed by LC-MS-MS in three independent measurements.

Protein FDR Confidence: Combined	Accession	Description	Gene Symbol	# PSMs	# Unique Peptide	Abundance Ratio (log2): (Nylon) / (PEI)	Abundance Ratio: (Nylon) / (PEI)	Abundance Ratio P-Value: (Nylon) / (PEI)	Abundance Ratio Adj. P-Value: (Nylon) / (PEI)	Abundances (Normalized): F1: Sample, Nylon	Abundances (Normalized): F2: Sample, Nylon	Abundances (Normalized): F3: Sample, Nylon	Abundances (Normalized): F4: Sample, PEI	Abundances (Normalized): F5: Sample, PI	Abundances (Normalized): F6: Sample, PI	Abundance: F1: Sample, Nylon	Abundance: F2: Sample, Nylon	Abundance: F3: Sample, Nylon	Abundance: F4: Sample, PEI	Abundance: F5: Sample, PEI	Abundance: F6: Sample, PEI
High	ENSBTAP00(	SPP1 UniProtKB Gene Name|Bos taurus secreted ph	SPP1	7	2	4,75	26,89	0,0149	0,3438	472504	2026632	1868875	127663	69496	58411	177854	1369604	1064198			
High	ENSBTAP00(	POSTN UniProtKB Gene Name|Bos taurus periostin,	POSTN	328	4	4,51	22,79	0,0157	0,3438	3317524	13134635	11384822	625415	499667	373328	1477906	8855011	6444975	119684	257606	297025
High	ENSBTAP00(	TUBB3 UniProtKB Gene Name|Bos taurus tubulin, b	LOC11155	1	1	3,06	8,32	0,7579	0,9465	43024	833302	891049	1001151	100179	90008		563148	507392	203155		
High	ENSBTAP00(	SPARCL1 UniProtKB Gene Name|Bos taurus SPARC-l	SPARCL1	93	18	2,87	7,30	0,0049	0,2496	4342037	2577587	3004349	408868	439431	411764	1918579	1693406	1710773	67757	286651	340968
High	ENSBTAP00(	SPARC UniProtKB Gene Name|Bos taurus secreted p	SPARC	82	11	2,86	7,25	0,0382	0,4258	1132464	3382904	3149647	399471	526261	434270	463124	2286177	1793511	68482	324991	401609
High	ENSBTAP00(	OMD EntrezGene|Bos taurus osteomodulin (OMD),	OMD	27	5	2,74	6,66	0,0178	0,3650	1591296	1840688	1907441	276282	503272	207859	703393	1243942	1086158	40543	304011	137562
High	ENSBTAP00(	HABP2 UniProtKB Gene Name|Bos taurus hyalurona	HABP2	62	14	2,69	6,47	0,0045	0,2496	3232180	1405507	1289069	123492	235336	217404	1439886	897605	694223		88503	101166
High	ENSBTAP00(	Uncharacterized protein [Source:UniProtKB/TrEMBl		1290	11	2,62	6,16	0,8938	0,9874	273544	23147505	25380085	6279533	3755117	3452370	103414	15643153	14452238	1274253	2586969	3452370
High	ENSBTAP00(	Bos taurus complement component 4A (C4A), mRNA		2303	54	2,57	5,92	0,9731	0,9924	232665	76142316	76575164	13110071	12852212	10039097	63195	51457202	43604364	2660316	8854125	10039097
High	ENSBTAP00(	PSMA3 UniProtKB Gene Name|Bos taurus proteasor	PSMA3	11	4	2,54	5,82	0,0111	0,2922	368862	912352	842196	73593	144612	154404	122786	616570	479574			96527
High	ENSBTAP00(	SPP2 UniProtKB Gene Name|Bos taurus secreted ph	SPP2	34	7	2,43	5,38	0,0141	0,3426	1283930	2931886	2207819	461949	346798	410669	541214	1981377	1257203	79772	178757	379197
High	ENSBTAP00(	Bos taurus uncharacterized LOC790886 (LOC790886		11	2	2,41	5,31	0,1723	0,8722	133244	718580	734190	192489	89517	135453		485619	418071	29760		
High	ENSBTAP00(	VWF EntrezGene|Bos taurus von Willebrand factor (		118	25	2,32	4,98	0,0002	0,1105	1848797	2507722	2341742	380379	478103	470177	790464	1683452	1306288	68751	316956	403329
High	ENSBTAP00(	PSMB5 UniProtKB Gene Name|Bos taurus proteasor	PSMB5	4	2	2,27	4,83	0,0618	0,5495	197322	336671	379359	190431	66541	69711		227523	216019			
High	ENSBTAP00(	F2 UniProtKB Gene Name|Bos taurus coagulation fa	F2	554	32	2,22	4,67	0,8572	0,9874	129114	44030092	40968714	8394151	10325162	8773010		29755667	23328905	1703354	7113194	8773010
High	ENSBTAP00(	THBS4 UniProtKB Gene Name|Bos taurus thrombos	THBS4	135	19	2,2	4,60	0,0751	0,6065	4500153	1200331	1601063	756330	76466	347718	1988792	771264	868256	138890		210444
High	ENSBTAP00(	PSMA7 UniProtKB Gene Name|Bos taurus proteasor	PSMA7	7	6	2,1	4,28	0,0100	0,2922	414733	591484	565377	189441	91537	132053	129532	399727	321944	8664		29624
Medium	ENSBTAP00(	STAM UniProtKB Gene Name|Bos taurus signal tran:	STAM	7	1	2,06	4,17	0,0380	0,4258	2999998	3975270	1328669	485857	723520	719638	1336453	2686500	756587	98591	498446	719638
High	ENSBTAP00(	CFH EntrezGene|Bos taurus complement factor H ((		467	30	2,01	4,04	0,0207	0,3670	11131387	12903339	12991992	3196299	2297616	4820977	4934517	8720114	7398059	648598	1532772	4820977
Medium	ENSBTAP00(	MON2 HGNC Symbol|MON2 homolog (S. cerevisiae)		18	1	1,98	3,95	0,0085	0,2922	15032638	7895589	8193580	3305906	2074095	1482680	6696806	5335862	4665688	670840	1428882	1482680
High	ENSBTAP00(	PSMA5 UniProtKB Gene Name|Bos taurus proteasor	LOC10134	2	1	1,98	3,94	0,1068	0,7436	102195	293329	283875	136385	72000	40788		198232	161647			
High	ENSBTAP00(	Bos taurus BPI fold containing family A, member 2A	BPIFA2A;	5	3	1,97	3,92	0,4670	0,8813	86317	589452	552403	259521	139310	141060		398353	314556	31400		
High	ENSBTAP00(	PSMA6 UniProtKB Gene Name|Bos taurus proteasor		14	5	1,97	3,91	0,0015	0,1998	1064832	821784	788125	197434	297173	210408	442680	531753	426937	14763	160545	72619
High	ENSBTAP00(	LTBP4 HGNC Symbol|latent transforming growth fac		7	4	1,95	3,86	0,3176	0,8813	95527	654162	636225	115356	168831	165049		442084	362287			
High	ENSBTAP00(	LTBP1 EntrezGene|Bos taurus latent transforming g		18	8	1,88	3,69	0,0066	0,2618	602413	538699	529298	145876	197548	125509	249602	313164	288829			50110
Medium	ENSBTAP00(	PLEK HGNC Symbol|pleckstrin [Source:HGNC Symbo	PLEK	2	1	1,87	3,66	0,0339	0,4258	184987	446020	438964	128524	66287	119899		301421	249960			
High	ENSBTAP00(	PSMA1 UniProtKB Gene Name|Bos taurus proteasor	PSMA1	5	4	1,86	3,63	0,0313	0,4157	432200	245407	371088	184171	74768	102183	167927	123393	201014			
High	ENSBTAP00(	TAGLN2 UniProtKB Gene Name|Bos taurus transgeli	TAGLN2	7	2	1,82	3,54	0,0831	0,6318	431197	417426	383511	117834	198684	45629	192092	282098	218384			
High	ENSBTAP00(	CPN1 HGNC Symbol|carboxypeptidase N, polypeptic	CPN1	33	9	1,82	3,52	0,7849	0,9479	156180	4801807	4454657	661405	1265117	1373845		3193630	2536625	124761	853889	1373845
High	ENSBTAP00(	POSTN UniProtKB Gene Name|Bos taurus periostin,	POSTN	302	1	1,73	3,31	0,0018	0,1998	1473790	1126208	938622	340108	239720	351905	656550	761094	534481	69015	165147	351905
High	ENSBTAP00(	PROZ UniProtKB Gene Name|Vitamin K-dependent p		5	2	1,72	3,31	0,2684	0,8813	105381	566356	753556	94541	171333	174410		382745	429099		68645	
High	ENSBTAP00(	COMP EntrezGene|cartilage oligomeric matrix prote		117	19	1,67	3,18	0,0665	0,5579	3433426	4256735	4043567	2141675	696418	1270955	1497599	2876714	2302537	434592	479775	1212308
Medium	ENSBTAP00(	GPI UniProtKB Gene Name|Bos taurus glucose-6-ph	GPI	8	1	1,65	3,13	0,1723	0,8722	959700	615488	435226	196794	573713	89807	427531	415948	247832		395241	
High	ENSBTAP00(	PSAP UniProtKB Gene Name|Bos taurus prosaposin		9	4	1,65	3,13	0,0278	0,3989	489450	457700	452592	203776	100106	146346	209473	291328	243357			
High	ENSBTAP00(	PLVAP EntrezGene|Bos taurus plasmalemma vesicle	PLVAP	13	5	1,64	3,12	0,0542	0,5273	405847	1264180	957299	122457	310051	307061	150425	816480	522911		189029	244159
High	ENSBTAP00(	TNXB EntrezGene|tenascin-X precursor [Source:Ref		22	12	1,61	3,06	0,0103	0,2922	273887	441866	414191	107928	182723	135573	73977	298615	235854	5449		79000
High	ENSBTAP00(	NRP2 HGNC Symbol|neuropilin 2 [Source:HGNC Sym	NRP2	2	2	1,55	2,93	0,1775	0,8722	97548	286953	214641	73380	69135	153653		193924	122223			
High	ENSBTAP00(	PROC HGNC Symbol|protein C (inactivator of coagul	PROC	48	10	1,54	2,91	0,8784	0,9874	175060	2459413	2475817	1061414	748989	846262	48721	1662078	1409810	215384	495710	781109
High	ENSBTAP00(	NCAM1 HGNC Symbol|neural cell adhesion molecul		75	14	1,53	2,89	0,2513	0,8813	4029159	2581142	2569008	3680864	892596	625270	1770795	1732866	1440513	739003	532626	561486
High	ENSBTAP00(	GOLM1 HGNC Symbol|golgi membrane protein 1 [S(	GOLM1	30	7	1,52	2,87	0,2739	0,8813	426875	1291845	1098090	370262	813940	383065	159007	873033	625288	63028	560738	347286
High	ENSBTAP00(	CALM UniProtKB Gene Name|Bos taurus calmodulin	calm; CALI	11	2	1,49	2,82	0,0034	0,2235	612487	815633	896724	338424	230151	289736	259981	551207	510623	48964	134651	259192
High	ENSBTAP00(	PSMB1 EntrezGene|Bos taurus proteasome (prosom	PSMB1	5	3	1,36	2,56	0,0570	0,5349	752097	291969	308310	116961	120228	121265	307479	160819	122153			
High	ENSBTAP00(	AHCY UniProtKB Gene Name|Bos taurus adenosylho	AHCY	29	9	1,36	2,56	0,0394	0,4306	1735972	1032518	755726	315487	403393	608965	748895	697779	430335	50724	246398	608965
High	ENSBTAP00(	CLEC11A UniProtKB Gene Name|Bos taurus C-type l	CLEC11A	32	6	1,34	2,54	0,7223	0,9446	153881	1193676	1138990	348464	579351	448529		806690	648578	70711	399126	448529
High	ENSBTAP00(	CHST3 HGNC Symbol|carbohydrate (chondroitin 6)	CHST3	2	2	1,33	2,52	0,0114	0,2922	332423	281930	287223	106463	160734	113870	101332	190529	163554		44171	
High	ENSBTAP00(	CATB UniProtKB Gene Name|Bos taurus cathepsin B	CTSB	7	3	1,32	2,50	0,0023	0,2129	270199	349043	318913	158857	127831	116881	70237	235884	181599		50456	
High	ENSBTAP00(	COL12A1 HGNC Symbol|collagen, type XII, alpha 1 [S		9	4	1,31	2,49	0,0014	0,1998	438483	371637	331466	149500	146345	176583	195337	208974	159722	15850	86183	41740
High	ENSBTAP00(	TUBA1B EntrezGene|Bos taurus tubulin, alpha 1b (T	LOC10053	61	4	1,3	2,46	0,5097	0,8813	213653	1115357	1034277	522584	419829	305478		753762	588951	85126	277634	188226
High	ENSBTAP00(	ITIH1 HGNC Symbol|inter-alpha-trypsin inhibitor he		458	31	1,29	2,45	0,0376	0,4258	18578200	25513912	24406568	15763015	9964721	8754282	8258941	17242377	13897886	3198656	6852739	8709176
High	ENSBTAP00(	ACTN1 UniProtKB Gene Name|Bos taurus actinin, al	ACTN1	45	8	1,27	2,41	0,0076	0,2825	515548	487955	458912	149182	202536	209347	206683	282159	239222		74163	95980
Medium	ENSBTAP00(	NCKAP1 HGNC Symbol|NCK-associated protein 1 [Sc		13	1	1,24	2,36	0,6964	0,9251	142894	19803039	18779461	6098632	10015097	7966668		13382953	10693630	1237544	6899584	7966668
High	ENSBTAP00(	PSMA4 UniProtKB Gene Name|Bos taurus proteasor	CHRNA5;	14	4	1,23	2,34	0,1617	0,8660	585660	646691	586034	250044	578356	242985	251012	437036	333707	44977	345012	147313
High	ENSBTAP00(	C3 UniProtKB Gene Name|Bos taurus complement c		5689	137	1,22	2,34	0,0218	0,3685	117002094	68145215	61097108	29164700	13450486	29691286	52122612	46052738	34790660	5915648	9256302	29624163
High	ENSBTAP00(	TGFBI EntrezGene|Bos taurus transforming growth		71	13	1,22	2,32	0,8263	0,9792	89446	2099534	1846938	1265139	795051	750008		1418871	1051706	256724	523496	750008
High	ENSBTAP00(	COL5A1 HGNC Symbol|collagen, type V, alpha 1 [Sou		33	8	1,21	2,32	0,0724	0,5934	1007485	788229	904513	192186	389717	514835	441066	532688	515059	17972	235152	514835
High	ENSBTAP00(	ITIH3 UniProtKB Gene Name|Bos taurus inter-alpha	ITIH3	1163	36	1,21	2,32	0,0525	0,5221	60944675	29350256	25192861	12675415	13317490	10762891	27149904	19790820	14309190	2567368	9159951	10729255
High	ENSBTAP00(	DKK3 UniProtKB Gene Name|Bos taurus dickkopf hc	DKK3	7	4	1,2	2,30	0,1242	0,8045	210244	440445	790753	123944	191257	192541		249511	450280			
High	ENSBTAP00(	FBLN1 EntrezGene|Bos taurus fibulin 1 (FBLN1), mRI	FBLN1	482	26	1,2	2,30	0,6517	0,9208	172349	32012830	31117714	13557919	15548531	12590528	20654	21634365	17719428	2751194	10711668	12590528
High	ENSBTAP00(	P4HB UniProtKB Gene Name|Bos taurus prolyl 4-hyc	P4HB	14	6	1,18	2,26	0,0063	0,2618	367966	261049	292690	163208	108028	129435	136684	129281	135999			29698
High	ENSBTAP00(	C1QA UniProtKB Gene Name|Bos taurus compleme	C1QA	13	5	1,15	2,22	0,2525	0,8813	849091	221764	131262	213420	99763	81366	344563	74828	52981	23777		
Medium	ENSBTAP00(	GALM UniProtKB Gene Name|Bos taurus galactose r	GALM	1	1	1,12	2,18	0,1882	0,8813	278122	134087	72733	51658	61480	93302	123899					
High	ENSBTAP00(	CGREF1 UniProtKB Gene Name|Bos taurus cell grow	CGREF1	3	2	1,12	2,18	0,2583	0,8813	137734	349484	394198	118058	160633	210589		236183	224469			
High	ENSBTAP00(	PSMA2 UniProtKB Gene Name|Bos taurus proteasor	LOC10135	10	4	1,09	2,14	0,0326	0,4219	687235	368243	317019	172452	174658	123740	277145	207510	153112			37729
High	ENSBTAP00(	RCN3 UniProtKB Gene Name|Bos taurus reticulocalb	RCN3	8	2	1,08	2,11	0,7798	0,9479	74853	413486	450256	154809	260161	195789		279435	256390		113399	120690
Medium	ENSBTAP00(	PLXNB2 HGNC Symbol|plexin B2 [Source:HGNC Sym	PLXNB2	2	1	1,06	2,08	0,1490	0,8557	91569	208562	196555	53018	94531	113638		140947	111925			
High	ENSBTAP00(	PCOLCE UniProtKB Gene Name|Bos taurus procollag	PCOLCE	9	3	1,05	2,06	0,0197	0,3650	281709	457074	306490	146286	189543	148503	84677	279755	174525	11104	70731	127254
High	ENSBTAP00(	PCDH12 HGNC Symbol|protocadherin 12 [Source:H(	PCDH12	33	12	1,04	2,05	0,1280	0,8160	622688	1138344	1124849	669000	247146	547713	245166	769297	640525	135755	116591	547713
High	ENSBTAP00(	THBS1 EntrezGene|Bos taurus thrombospondin 1 (T	THBS1	194	35	1,03	2,05	0,8362	0,9842	135904	3450590	3437019	1214265	1692666	1678752		2331919	1957149	246401	1166109	1678752
High	ENSBTAP00(	TPM1 EntrezGene|Bos taurus tropomyosin 1 (alpha		22	1	1,02	2,03	0,4406	0,8813	79650	297392	365213	146595	193759	69063		200978	207964	29747		
High	ENSBTAP00(	Uncharacterized protein [Source:UniProtKB/TrEMBl		33	1	1,01	2,01	0,9164	0,9909	182366	2692736	1554350	1430951	772901	509398		1819759	885097	290371	532465	509398
High	ENSBTAP00(	COL5A2 HGNC Symbol|collagen, type V, alpha 2 [Sou		2	2	0,98	1,97	0,4271	0,8813	62578	221459	315403	76425	117357	112567		149663	179601	4923	21364	36677
Medium	ENSBTAP00(	PTPRZ1 HGNC Symbol|protein tyrosine phosphatase		1	1	0,97	1,96	0,2147	0,8813	426830	205719	92819	104989	134859	53051	190146	139025				
High	ENSBTAP00(	TPM4 HGNC Symbol|tropomyosin 4 [Source:HGNC S	LOC53527	49	3	0,96	1,94	0,2866	0,8813	513704	1329603	1462731	684286	709659	490144	182205	898550	832926	128972	488897	490144
High	ENSBTAP00(	FMOD UniProtKB Gene Name|Bos taurus fibromodu	FMOD	21	5	0,95	1,94	0,0036	0,2235	829786	710988	649498	342358	366975	442362	337076	442042	362121	61241	208287	398829
High	ENSBTAP00(	ST13 UniProtKB Gene Name|Bos taurus suppression	ST13	1	1	0,94	1,92	0,1797	0,8722	387281	186632	161123	210478	97322	62168	172528					
Medium	ENSBTAP00(	Uncharacterized protein [Source:UniProtKB/TrEMBl		1	1	0,94	1,92	0,2898	0,8813	65904	130334	218117	67990	99264	63181						63181
High	ENSBTAP00(	ACTN4 UniProtKB Gene Name|Bos taurus actinin, al	ACTN4	29	7	0,93	1,91	0,0231	0,3785	201893	279928	335203	150833	107172	146903	58597	189176	190875			79562
High	ENSBTAP00(	F10 UniProtKB Gene Name|Bos taurus coagulation f	F10	95	15	0,91	1,88	0,0160	0,3438	1642426	2204831	2162424	1193970	1045956	1152054	719657	1472359	1203590	238314	709502	1089832
High	ENSBTAP00(	HSPA1A UniProtKB Gene Name|Bos taurus heat sho	HSP70; HS	13	3	0,89	1,86	0,2017	0,8813	312521	225646	131859	121573	98159	182817	139223					134124
High	ENSBTAP00(	ACAN HGNC Symbol|aggrecan [Source:HGNC Symbc	ACAN	11	4	0,89	1,85	0,9318	0,9924	128131	706187	700079	1278514	163817	378791	22086	428575	380637	249892		344747
High	ENSBTAP00(	MYH9 EntrezGene|Bos taurus myosin, heavy chain !		36	17	0,87	1,83	0,1298	0,8160	802579	255288	203442	139290	173244	87938	325676	128261	80803			
High	ENSBTAP00(	CUTA UniProtKB Gene Name|Bos taurus cutA divale	CUTA	4	1	0,86	1,81	0,9996	0,9996	67028	423895	173047	95429	566351	91082		286470			390170	
Medium	ENSBTAP00(	CYP39A1 UniProtKB Gene Name|Bos taurus cytochr	CYP39A1;	26	1	0,86	1,81	0,3484	0,8813	2254979	1281900	2490783	2090107	167332	1244455	1004558	866312	1418332	424128		1244455
High	ENSBTAP00(	Uncharacterized protein [Source:UniProtKB/TrEMBl		3	1	0,81	1,76	0,4825	0,8813	39301	113604	2013280	154358	42084	64712			1146426			
High	ENSBTAP00(	YWHAQ UniProtKB Gene Name|Bos taurus tyrosine	LOC10075	13	2	0,81	1,76	0,0634	0,5495	170166	176317	172222	98055	81748	132383	58469		69806			69299
Medium	ENSBTAP00(	PSMB6 UniProtKB Gene Name|Bos taurus proteasor	PSMB6	3	1	0,8	1,75	0,1396	0,8344	180588	323437	378879	185231	200017	129275		218580	215746			
High	ENSBTAP00(	ACTA1 UniProtKB Gene Name|Bos taurus actin, alph	Acta1; ACT	187	1	0,8	1,74	0,3734	0,8813	3244614	2203483	2258079	204457	1298379	3531900	1445425	1489120	1285823		894477	3531900
High	ENSBTAP00(	RCN1 UniProtKB Gene Name|Bos taurus reticulocalb		6	3	0,8	1,74	0,1984	0,8813	328844	171256	306427	176571	198487	156466	133632	84799	154611		70007	81016
High	ENSBTAP00(	Histone H2A [Source:UniProtKB/TrEMBL;Acc:E1BIL5	H2AC8	4	1	0,79	1,73	0,8987	0,9874	370980	352346	307913	1536270	203264	89424	165266	238116	175335	311742	140032	89424
High	ENSBTAP00(	DAG1 HGNC Symbol|dystroglycan 1 (dystrophin-ass		2	1	0,79	1,73	0,3356	0,8813	92427	163330	169036	63562	94357	149846			96254		65004	149846
High	ENSBTAP00(	PSMB2 UniProtKB Gene Name|Bos taurus proteasor	PSMB2	6	3	0,79	1,73	0,0784	0,6237	206591	317460	244216	150749	141239	64164	73192	172787	123014			
High	ENSBTAP00(	NUCB1 UniProtKB Gene Name|Bos taurus nucleobin	NUCB1	10	6	0,79	1,73	0,2523	0,8813	470894	159379	285849	165746	163589	177714	179521	66324	138570			
Medium	ENSBTAP00(	B3GNT1 UniProtKB Gene Name|Bos taurus UDP-Glcl	B4GAT1	2	1	0,78	1,72	0,2238	0,8813	104713	168492	585283	109491	68885	97821			333279			
High	ENSBTAP00(	F13B UniProtKB Gene Name|Bos taurus coagulation	F13B	50	11	0,77	1,71	0,7441	0,9465	107152	889999	847034	385193	496889	953412		601464	482329	74555	310581	953412
Medium	ENSBTAP00(	TTC15 EntrezGene|Bos taurus tetratricopeptide rep	TRAPPC12	24	1	0,77	1,70	0,5492	0,9099	105115	177928138	174930292	48076413	134906175	102663958		120244362	99610941	9755741	92939336	102663958
High	ENSBTAP00(	C5 EntrezGene|complement C5a anaphylatoxin pre		528	69	0,76	1,70	0,1513	0,8598	9533540	6984166	6611763	7101948	4118988	3065309	4247044	4719920	3764951	1441138	2837647	3065309
High	ENSBTAP00(	ANGPTL3 UniProtKB Gene Name|Bos taurus angiop	ANGPTL3	11	6	0,74	1,67	0,1242	0,8045	781787	296113	300925	154960	247341	180514	348274	191811	164448	11259	82993	122489
High	ENSBTAP00(	TPM3 UniProtKB Gene Name|Bos taurus tropomyos	LOC10094	43	2	0,73	1,66	0,2253	0,8813	735487	806616	1049166	840247	485390	241740	315984	491258	597429	170504	261542	241740
High	ENSBTAP00(	MASP1 UniProtKB Gene Name|Bos taurus mannan-l	MASP1	26	8	0,73	1,65	0,9527	0,9924	72736	679624	562516	253227	340077	373206		459292	298121	32836	216306	373206
High	ENSBTAP00(	FLNA HGNC Symbol|filamin A, alpha [Source:HGNC S		42	15	0,72	1,65	0,0629	0,5495	467942	353873	280414	214324	270453	164216	193433	239148	119237	39172	186320	151036
High	ENSBTAP00(	THBS3 UniProtKB Gene Name|Bos taurus thrombos	THBS3	14	2	0,72	1,65	0,3633	0,8813	2350463	4998426	5189434	3575719	3036535	2192142	1047095	3323475	2912411	704629	2043850	2120353
High	ENSBTAP00(	TPI1 UniProtKB Gene Name|Bos taurus triosephosp	TPI1	11	4	0,72	1,64	0,4537	0,8813	138223	358543	352772	105981	268769	214691		242305	200880		144149	143233
High	ENSBTAP00(	APOE UniProtKB Gene Name|Bos taurus apolipopro	APOE	85	13	0,7	1,63	0,4949	0,8813	4084338	9117760	8662223	5318888	4785959	6564749	1782255	6161810	4932548	1079317	3297135	6564749
High	ENSBTAP00(	G3PDH UniProtKB Gene Name|Bos taurus glyceralde	GAPDH	12	5	0,7	1,63	0,1590	0,8660	634108	650898	658491	258613	574731	399617	265773	392683	332093	30532	377009	360993
High	ENSBTAP00(	Bos taurus amine oxidase, copper containing 3 (vasc		10	1	0,67	1,59	0,7795	0,9479	190334	839110	749392	471218	128708	991557		567073	426728	95620		991557
High	ENSBTAP00(	FGG UniProtKB Gene Name|Bos taurus fibrinogen g	FGG	112	17	0,66	1,58	0,3796	0,8813	1626425	3430454	2880184	1826345	2529645	1548696	686279	2318311	1640070	370605	1742719	1534009
High	ENSBTAP00(	VCAM1 UniProtKB Gene Name|Bos taurus vascular (	VCAM1	37	4	0,65	1,57	0,6736	0,9208	181223	110841	370172	115489	81616	361860	69324		163802			324584
High	ENSBTAP00(	COL1A1 UniProtKB Gene Name|Bos taurus collagen,	COL1A1	54	10	0,65	1,57	0,3222	0,8813	1743244	3597873	4298885	1279179	2712966	2298156	742471	2431453	2447924	259573	1869012	2298156
High	ENSBTAP00(	PRDX6 UniProtKB Gene Name|Bos taurus peroxired	Prdx6; PRI	3	2	0,64	1,56	0,1962	0,8813	895139	684887	541001	438506	474740	108123	398770	462848	308063	88982	327057	
High	ENSBTAP00(	F9 UniProtKB Gene Name|Bos taurus coagulation fa	F9	41	9	0,63	1,54	0,0369	0,4258	2166511	1593706	1502529	785165	1032410	1243351	951468	1038016	813705	150983	662894	1191101
High	ENSBTAP00(	F7 UniProtKB Gene Name|Bos taurus coagulation fa	F7	5	2	0,62	1,54	0,3614	0,8813	88915	168105	213989	94357	109192	123191		113606	121852	19147	75224	123191
High	ENSBTAP00(	Clusterin [Source:UniProtKB/TrEMBL;Acc:F1MWI1]|		32	2	0,6	1,52	0,6221	0,9208	217269	4711164	4527527	2978206	4138907	2219140		3183819	2578120	604342	2851369	2219140
High	ENSBTAP00(	APOD HGNC Symbol|apolipoprotein D [Source:HGN	APOD	85	4	0,59	1,51	0,1351	0,8267	6432342	5430345	4887046	3596288	5221342	3046848	2849977	3669843	2782841	729764	3597078	3046848
High	ENSBTAP00(	TF HGNC Symbol|transferrin [Source:HGNC Symbol;		5560	56	0,59	1,51	0,2463	0,8813	310187090	273935234	237695411	181928550	147879739	289440684	138183522	185126241	135351420	36917225	101877062	289440684
High	ENSBTAP00(	HIST3H2BB HGNC Symbol|histone cluster 3, H2bb [S		6	1	0,58	1,50	0,3859	0,8813	801103	639207	704551	889825	469791	333752	356879	431978	401194	180565	323647	333752
High	ENSBTAP00(	MT1E UniProtKB Gene Name|Bos taurus metallothic	LOC10500	5	1	0,58	1,50	0,9197	0,9909	272673	82822	136593	91182	498742	52854	121471		77780		343593	
High	ENSBTAP00(	SERPINB13 HGNC Symbol|serpin peptidase inhibitor		1	1	0,57	1,49	0,8031	0,9599	197445	210488	173787	132718	119379	761535						761535
High	ENSBTAP00(	PEBP1 UniProtKB Gene Name|Bos taurus phosphati	PEBP1	8	5	0,57	1,48	0,1370	0,8295	380327	403827	265307	135788	256264	264157	157452	272908	129277	22444	165878	223966
High	ENSBTAP00(	VCAM1 UniProtKB Gene Name|Bos taurus vascular (	VCAM1	34	3	0,57	1,48	0,2429	0,8813	250248	398691	395777	166597	266960	318690	91029	246036	186787	12091	149637	242657

Medium	ENSBTAP00(	MSN UniProtKB Gene Name|Bos taurus moesin (MS	MSN	1	1	0,55	1,46	0,7364	0,9465	212920	90877	226612	195552	105548	145491	94853					
High	ENSBTAP00(	TNC HGNC Symbol|tenascin C [Source:HGNC Symbo		3	2	0,55	1,46	0,5981	0,9208	269524	117871	188366	247538	101340	128902	81165	60407	57669	41700	48328	70166
High	ENSBTAP00(	F13A1 UniProtKB Gene Name|Bos taurus coagulatio	F13A1	49	10	0,54	1,46	0,0839	0,6318	1735994	1050145	1108751	530947	973804	761449	773358	709691	631359	78752	651321	761449
High	ENSBTAP00(	CALR UniProtKB Gene Name|Bos taurus calreticulin	CALR	2	1	0,53	1,44	0,7997	0,9599	224559	46497	193078	129017	133672	181582	100037					
High	ENSBTAP00(	CL43 EntrezGene|collectin-43 precursor [Source:Re		12	4	0,52	1,44	0,5048	0,8813	1419846	2382570	2203807	1317587	2244430	1535123	598940	1610148	1254918	267367	1546229	1535123
High	ENSBTAP00(	SERPIND1 UniProtKB Gene Name|Bos taurus serpin	SERPIND1	330	20	0,52	1,43	0,6524	0,9208	1378492	16844891	15972070	9465995	12900277	11161102	585166	11383827	9095011	1920854	8887237	11161102
High	ENSBTAP00(	KRT3 HGNC Symbol|keratin 3 [Source:HGNC Symbol	KRT3	156	1	0,51	1,42	0,8761	0,9874	83692	146093	760659	102887	58640	904864			433144			904864
High	ENSBTAP00(	PSMB7 EntrezGene|Bos taurus proteasome (proson	PSMB7	1	1	0,5	1,41	0,5004	0,8813	643733	90024	126995	86475	89879	202382	286773					
Medium	ENSBTAP00(	DSG1 EntrezGene|Bos taurus desmoglein 1 (DSG1),	DSG1; DSG	4	1	0,49	1,41	0,9565	0,9924	225322	103009	215356	152864	400587	89289					275972	
High	ENSBTAP00(	EFEMP1 UniProtKB Gene Name|Bos taurus EGF cont	EFEMP1	29	7	0,49	1,41	0,8803	0,9874	148950	524348	461107	222601	327562	629594		354356	262569	41790	148800	629594
High	ENSBTAP00(	PCDHGC3 UniProtKB Gene Name|Bos taurus protoc	PCDHGC3	7	4	0,49	1,40	0,0549	0,5273	169431	186488	231026	105244	156177	133148		126029	131554	12740	20000	
High	ENSBTAP00(	KRT12 HGNC Symbol|keratin 12 [Source:HGNC Symb		118	1	0,49	1,40	0,3461	0,8813	683939	207376	96964	68616	148084	161536	304684					
High	ENSBTAP00(	PGLYRP2 HGNC Symbol|peptidoglycan recognition p		29	5	0,48	1,40	0,7848	0,9479	150867	6746467	6034904	902337	5425034	4314423		4538898	3398349	177114	3737405	4314423
High	ENSBTAP00(	HSP90AA1 UniProtKB Gene Name|Bos taurus heat s	HSP90AA1	16	3	0,48	1,40	0,0603	0,5495	522120	331311	343278	245557	158035	270984	216852	137128	167003	34403	39535	167555
High	ENSBTAP00(	C1S EntrezGene|Bos taurus complement componen	C1S	17	5	0,48	1,40	0,6682	0,9208	136593	295855	299306	179541	214770	212027		199940	170434	20466	99580	151753
High	ENSBTAP00(	C6 HGNC Symbol|complement component 6 [Sourc	C6	3	1	0,48	1,39	0,9782	0,9924	57577	137562	119353	141698	85716	80089		92965	67963	28754	59051	80089
High	ENSBTAP00(	TLN1 HGNC Symbol|talin 1 [Source:HGNC Symbol;A		92	25	0,48	1,39	0,4650	0,8813	562121	548113	546392	200808	758865	393945	250416	370416	311133	23219	522796	393945
High	ENSBTAP00(	CNTN1 UniProtKB Gene Name|Bos taurus contactin	CNTN1	6	3	0,47	1,39	0,3878	0,8813	199236	180069	202026	67001	230881	143480		121691	115040		159058	143480
Medium	ENSBTAP00(	Uncharacterized protein [Source:UniProtKB/TrEMBl		7	1	0,47	1,38	0,1474	0,8554	1316735	696108	795930	278577	695147	575364	586585	470432	453228	56529	478900	575364
High	ENSBTAP00(	Uncharacterized protein [Source:UniProtKB/TrEMBl		8	1	0,46	1,38	0,6449	0,9208	124682	2109043	2148125	1530847	738031	2407893		1425298	1223212	310642	508443	2407893
Medium	ENSBTAP00(	GNB1 UniProtKB Gene Name|Bos taurus guanine nu	Gnb1; GNI	2	1	0,46	1,38	0,9664	0,9924	183910	41260	149174	96325	115928	108385			84945	19546	79865	108385
High	ENSBTAP00(	OGN UniProtKB Gene Name|Bos taurus osteoglycin		22	5	0,46	1,37	0,0820	0,6318	792695	560661	566908	542343	412634	373497	343570	378896	322815	110053	265401	341696
High	ENSBTAP00(	SFN UniProtKB Gene Name|Bos taurus stratifin (SFN	SFN	11	1	0,45	1,37	0,9678	0,9924	169597	214640	82198	52311	124256	506566						506566
High	ENSBTAP00(	SERPINA3-6 EntrezGene|Bos taurus endopin 1b (SE	SERPINA3-	1444	3	0,45	1,37	0,4963	0,8813	115636	5099243	5068174	6151008	2994168	3711934	8968	3446083	2844697	1234939	2022025	3711934
High	ENSBTAP00(	CDH6 UniProtKB Gene Name|Bos taurus cadherin 6,	CDH6	9	3	0,45	1,36	0,0367	0,4258	210296	214618	210199	142025	174999	154308	69649	109263	105803	10849	56319	140640
High	ENSBTAP00(	GSN HGNC Symbol|gelsolin [Source:HGNC Symbol;A	GSN	416	30	0,44	1,36	0,1917	0,8813	8353874	12800151	11448604	8694887	7993493	8449790	3713864	8650380	6519204	1764380	5506864	8449790
Medium	ENSBTAP00(	QSOX1 HGNC Symbol|quiescin Q6 sulfhydryl oxidas		6	1	0,42	1,34	0,3274	0,8813	193897	328777	289008	218981	211022	216049		222189	164571	44436		216049
High	ENSBTAP00(	KRT73 UniProtKB Gene Name|Bos taurus keratin 73	KRT73	44	1	0,42	1,34	0,6690	0,9208	209760	41881	1349953	74253	157149	220128			768707			
High	ENSBTAP00(	CHIA HGNC Symbol|chitinase, acidic [Source:HGNC		78	12	0,42	1,33	0,0913	0,6691	3471338	4831855	4283079	2913339	3444398	3209689	1536845	3265382	2438923	591179	2372909	3209689
High	ENSBTAP00(	Cationic trypsin Alpha-trypsin chain 1 Alpha-trypsin	LOC11389	7	2	0,41	1,33	0,2423	0,8813	1991930	3038096	4133153	2491832	1405502	2278632	848758	2053155	2353550	482143	935835	2278632
High	ENSBTAP00(	C1QB UniProtKB Gene Name|Bos taurus complemer	ADIA; C1Q	3	2	0,41	1,33	0,2570	0,8813	599743	205680	167619	236421	155050	56550	267176			47975		
High	ENSBTAP00(	CLU UniProtKB Gene Name|Bos taurus clusterin (CL	CLU; LOC1	252	11	0,41	1,33	0,0444	0,4753	8361712	9600166	9286519	7001300	7784580	6050446	3679183	6487821	5288043	1420715	5362940	6050446
High	ENSBTAP00(	YWHAE UniProtKB Gene Name|Bos taurus tyrosine	HEL2; LOC	25	4	0,4	1,32	0,1318	0,8160	695418	489776	485063	498310	370019	293010	309798	330992	276210	101118	254913	293010
High	ENSBTAP00(	TUBA4A UniProtKB Gene Name|Bos taurus tubulin,	LOC10133	70	4	0,39	1,31	0,8820	0,9874	387359	879944	781238	769388	594673	507103	129740	594669	444862	156125	409681	507103
High	ENSBTAP00(	C1R UniProtKB Gene Name|Bos taurus complement	C1R	1	1	0,38	1,30	0,2203	0,8813	318311	177229	227230	174924	53859	176601	141802					
High	ENSBTAP00(	LDHB UniProtKB Gene Name|Bos taurus lactate deh	LDHB	28	4	0,38	1,30	0,1020	0,7193	1075650	1201498	1093240	834299	1065286	841786	445763	811976	622526	169297	733895	841786
High	ENSBTAP00(	VTN UniProtKB Gene Name|Bos taurus vitronectin (	VTN	307	11	0,37	1,29	0,5160	0,8813	726754	34071905	29495812	30326857	22852580	20295898	299298	23025894	16795865	6153973	15743561	20295898
High	ENSBTAP00(	COL11A1 UniProtKB Gene Name|Bos taurus collager		7	1	0,35	1,28	0,7861	0,9479	96334	249175	301399	115286	195101	224371		168393	171626		134408	224371
High	ENSBTAP00(	COL6A1 EntrezGene|Bos taurus collagen, type VI, al	COL6A1	104	17	0,35	1,27	0,5022	0,8813	66349	2404480	2457495	2174415	1776952	1888473		1624955	1399377	433093	1224174	1888473
High	ENSBTAP00(	C1QTNF3 UniProtKB Gene Name|Bos taurus C1q an	C1QTNF3	17	4	0,35	1,27	0,2394	0,8813	1007244	688302	799824	809220	628425	594394	394070	465157	455445	160348	432933	520000
High	ENSBTAP00(	TTR UniProtKB Gene Name|Bos taurus transthyretin	TTR	79	7	0,35	1,27	0,3605	0,8813	14530276	4798941	5659935	4455331	3908910	6561989	6473012	3231923	3210402	901350	2674046	6508041
High	ENSBTAP00(	CA2 EntrezGene|Bos taurus carbonic anhydrase II (		6	3	0,34	1,26	0,8337	0,9839	374294	290227	219887	230013	549709	140278	137337	104929	101738	27505	353893	
High	ENSBTAP00(	ITIH2 EntrezGene|Bos taurus inter-alpha-trypsin inh	ITIH2	2778	45	0,33	1,26	0,2540	0,8813	82023404	115624870	110192269	87588722	92544085	77567889	36522883	78139629	62747026	17773640	63755316	77567889
High	ENSBTAP00(	Uncharacterized protein [Source:UniProtKB/TrEMBl		16	2	0,32	1,25	0,5603	0,9099	1883692	579349	1099530	529730	1163339	881676	839155	350850	626108	97505	801445	881676
High	ENSBTAP00(	VASN UniProtKB Gene Name|Bos taurus vasorin (VA		21	5	0,32	1,25	0,7224	0,9446	120275	604207	515226	293409	594650	413452		408325	293386	50952	409665	413452
High	ENSBTAP00(	CFP UniProtKB Gene Name|Bos taurus complement	CFP	57	8	0,32	1,25	0,6281	0,9208	137118	2077528	1926953	1033984	1546496	1579118		1403999	1097269	209818	1065410	1579118
High	ENSBTAP00(	CTSC EntrezGene|Bos taurus cathepsin C (CTSC), m	CTSC	7	2	0,32	1,25	0,3633	0,8813	246990	401864	357943	155130	333399	287524	96370	218689	164226		189905	266212
Medium	ENSBTAP00(	PPP3CC UniProtKB Gene Name|Bos taurus protein p	PPP3CC	3	1	0,31	1,24	0,5712	0,9116	186869	7073147	5184851	2658848	4175277	6555375		4780053	2952421	539538	2876425	6555375
High	ENSBTAP00(	Bos taurus hemoglobin, epsilon 1 (HBE1), mRNA. [S	HBE1; LOC	223	1	0,31	1,24	0,4685	0,8813	193933	1188461	319960	184254	258004	358531		803166	182196		177744	358531
High	ENSBTAP00(	SERPINA1 UniProtKB Gene Name|Bos taurus serpin	SERPINA1	7132	28	0,31	1,24	0,5928	0,9208	546010559	827133709	749884485	549900499	606593236	767828480	243239208	558979406	427008370	111586666	417893196	767828480
High	ENSBTAP00(	ANXA2 UniProtKB Gene Name|Bos taurus annexin A	ANXA2	7	6	0,3	1,23	0,7670	0,9479	135392	161698	115139	109897	89693	420745		19677	30586	11982	30433	420745
High	ENSBTAP00(	CSF1R UniProtKB Gene Name|Bos taurus colony stin	CSF1R	21	3	0,3	1,23	0,6231	0,9208	102643	731441	690565	404238	705536	561812		494310	393230	71913	486057	561812
High	ENSBTAP00(	AMBP EntrezGene|Bos taurus alpha-1-microglobulir		513	19	0,29	1,23	0,9866	0,9954	50356434	86146410	84103262	105332576	51183103	68676219	22433008	58217998	47891106	21374250	35260978	68676219
High	ENSBTAP00(	HBA UniProtKB Gene Name|Bos taurus hemoglobin,	GLNC1; HE	933	11	0,29	1,22	0,6539	0,9208	62793275	89478882	83769931	46917522	101078664	68660135	27973427	60470093	47701296	9520577	69634944	68660135
High	ENSBTAP00(	LGALS3BP UniProtKB Gene Name|Bos taurus lectin,	LGALS3BP	65	10	0,29	1,22	0,7820	0,9479	1452636	1653730	1755554	3798621	1356785	1165498	618661	1081066	973973	770822	923798	1099003
High	ENSBTAP00(	MASP2 HGNC Symbol|mannan-binding lectin serine		13	4	0,29	1,22	0,3146	0,8813	990741	642974	682572	559928	465899	805374	416449	382220	352262	87900	264221	778448
High	ENSBTAP00(	ADAMTS13 HGNC Symbol|ADAM metallopeptidase		23	9	0,28	1,22	0,8233	0,9778	152526	355794	340873	151275	335426	280491		240446	194104	7735	180308	242396
High	ENSBTAP00(	AGT UniProtKB Gene Name|Bos taurus angiotensin	AGT	333	15	0,28	1,21	0,6243	0,9208	17861194	20655427	20108291	24734598	16557876	13125180	7956884	13958999	11450308	5019183	11407025	13125180
High	ENSBTAP00(	Heat shock protein HSP 90-beta [Source:UniProtKB/		11	1	0,27	1,21	0,5203	0,8813	424558	81102	145365	71388	120410	176039	189134					
High	ENSBTAP00(	Uncharacterized protein [Source:UniProtKB/TrEMBl		1	1	0,27	1,21	0,3538	0,8813	195578	355933	285497	166208	252985	236446		240541	162571		174286	236446
High	ENSBTAP00(	YWHAB UniProtKB Gene Name|Bos taurus tyrosine	HEL-S-1; L	14	2	0,24	1,18	0,2613	0,8813	234399	226457	213605	123389	191918	216790	104421	95870				
High	ENSBTAP00(	CL46 EntrezGene|Bos taurus collectin -46 (CL46), m		5	2	0,24	1,18	0,3908	0,8813	837221	661304	525793	339547	714511	561312	340043	375996	286647	62717	425638	471959
High	ENSBTAP00(	APON UniProtKB Gene Name|ovarian and testicular	APON; LO	24	4	0,23	1,17	0,8712	0,9874	451380	1799905	1513023	815026	1290344	1504486	188852	1216381	861564	165386	888942	1504486
High	ENSBTAP00(	KRT4 UniProtKB Gene Name|Bos taurus keratin 4 (K	KRT4	81	2	0,23	1,17	0,5428	0,9052	118517	88033	1568516	53015	101160	348143			893164			313911
High	ENSBTAP00(	COTL1 UniProtKB Gene Name|Bos taurus coactosin-	COTL1	18	5	0,22	1,17	0,3895	0,8813	525664	507447	358083	213662	434914	451505	216487	342934	177762	29264	289610	451505
High	ENSBTAP00(	FGB UniProtKB Gene Name|Bos taurus fibrinogen b	FGB	109	15	0,22	1,17	0,3690	0,8813	4657180	3318176	2999280	2694869	3660996	2843835	2061479	2194842	1666029	537473	2488772	2768675
High	ENSBTAP00(	HSPG2 HGNC Symbol|heparan sulfate proteoglycan		31	11	0,22	1,17	0,9717	0,9924	104633	471368	424051	148137	414725	363877		277200	202870	25054	233194	320107
High	ENSBTAP00(	HIST1H4G HGNC Symbol|histone cluster 1, H4g [Sou		18	2	0,21	1,16	0,6709	0,9208	472899	720818	780836	668193	622359	498187	182635	487131	444633	116556	428754	498187
High	ENSBTAP00(	LUM UniProtKB Gene Name|Bos taurus lumican (LU	LUM	325	13	0,21	1,16	0,3438	0,8813	7998594	9940999	11092275	5652670	9685294	8590562	3550358	6718157	6316298	1147049	6672377	8590562
High	ENSBTAP00(	C8B EntrezGene|Bos taurus complement componer		33	9	0,21	1,15	0,6841	0,9208	81746	708052	762726	332207	620761	614259		478503	434321	55102	427653	614259
High	ENSBTAP00(	C4BPA UniProtKB Gene Name|Bos taurus compleme	C4BPA; LO	178	25	0,21	1,15	0,2214	0,8813	3328051	2466223	2477880	2148568	1078614	2407175	1482595	1666681	1410985	435991	699357	2407175
High	ENSBTAP00(	FABP1 UniProtKB Gene Name|Bos taurus fatty acid		10	2	0,2	1,15	0,8393	0,9842	582916	543352	217937	472092	556909	331746	259680	367199	124101	95798	383665	331746
High	ENSBTAP00(	MRC2 EntrezGene|Bos taurus mannose receptor, C		15	6	0,2	1,15	0,6879	0,9211	165440	279925	270745	289771	235669	235060	43153	142024	135772	35446	114256	164628
High	ENSBTAP00(	Uncharacterized protein [Source:UniProtKB/TrEMBl		21	1	0,17	1,13	0,4136	0,8813	1516336	1137601	1181639	776388	1428851	1046921	675504	768794	672863	157546	984362	1046921
High	ENSBTAP00(	PFN1 UniProtKB Gene Name|Bos taurus profilin 1 (P	PFN1	30	5	0,16	1,12	0,4286	0,8813	1274270	1212055	1036414	1240189	1083990	807438	544199	819110	590168	251661	746780	807438
High	ENSBTAP00(	IGFALS EntrezGene|Bos taurus insulin-like growth fa		50	11	0,16	1,11	0,5446	0,9055	167642	939067	829626	650547	903513	744838		634624	472416	129531	622446	744838
High	ENSBTAP00(	SERPINF1 UniProtKB Gene Name|Bos taurus serpin	SERPINF1	317	20	0,15	1,11	0,7842	0,9479	6745354	15565382	14812221	9937693	15384793	13331466	2984084	10519131	8434556	2016572	10598866	13331466
High	ENSBTAP00(	ACTB UniProtKB Gene Name|Bos taurus actin, beta		220	1	0,15	1,11	0,8710	0,9874	519461	173647	212558	154917	499916	191634	231412	117351	121037		344402	
High	ENSBTAP00(	Bos taurus amine oxidase, copper containing 3 (SAO		13	5	0,15	1,11	0,5965	0,9208	287230	260246	253107	234826	440563	61922	104636	149239	87182	29042	276988	
High	ENSBTAP00(	PLG UniProtKB Gene Name|Bos taurus plasminogen	PLG	740	53	0,15	1,11	0,1973	0,8813	26187972	15475341	14403036	7328363	14611509	13983134	11666334	10458281	8201552	1487083	10066137	13983134
High	ENSBTAP00(	CD109 HGNC Symbol|CD109 molecule [Source:HGN		27	9	0,14	1,11	0,8280	0,9792	476344	520851	471059	124178	4842841	431213	175495	315845	248624		3336322	395336
High	ENSBTAP00(	MST1 HGNC Symbol|macrophage stimulating 1 (hep	MST1	17	7	0,14	1,10	0,8463	0,9874	122353	435403	402052	212353	368494	364513		261881	196654	39695	253862	364513
High	ENSBTAP00(	SERPINA7 UniProtKB Gene Name|Bos taurus serpin	SERPINA7	325	14	0,14	1,10	0,4895	0,8813	3339776	7977660	7746532	7032301	9189619	6645188	1458307	5391326	4411125	1427005	6330897	6645188
High	ENSBTAP00(	VNN1 UniProtKB Gene Name|Bos taurus vanin 1 (VN	VNN1	128	14	0,14	1,10	0,4764	0,8813	174626	8482842	8144320	4668623	7400317	10136955		5732730	4637638	947364	5098214	10136955
High	ENSBTAP00(	ACTG1 UniProtKB Gene Name|Bos taurus actin, gam	ACTB; actg	291	3	0,13	1,10	0,5854	0,9208	1110576	1210803	1175664	825434	1072083	1353404	494744	801756	644838	152882	698156	1310868
High	ENSBTAP00(	SHBG UniProtKB Gene Name|Bos taurus sex hormo	SHBG	66	10	0,13	1,10	0,4930	0,8813	187843	2168294	1865510	2035072	1701053	1584969		1465339	1062281	412960	1171887	1584969
High	ENSBTAP00(	TG EntrezGene|Bos taurus thyroglobulin (TG), mRN		5	4	0,13	1,10	0,2718	0,8813	159795	240034	179937	145267	168686	164054		162216	60809	22882	58921	
High	ENSBTAP00(	Bos taurus hemoglobin, gamma 2 (LOC788610), mR	LOC10498	883	9	0,13	1,10	0,9467	0,9924	73893608	77504776	59620349	65985362	78407417	67393407	32918453	52377957	33949746	13389852	54016307	67393407
High	ENSBTAP00(	LCAT UniProtKB Gene Name|Bos taurus lecithin-cho	LCAT	17	3	0,13	1,10	0,7637	0,9479	492734	1048701	867011	400922	1000679	791312	160836	708715	493704	67116	689386	791312
High	ENSBTAP00(	APOC3 UniProtKB Gene Name|Bos taurus apolipopr	ApoC3; AF	4	1	0,13	1,09	0,5045	0,8813	219475	808404	725834	585265	927025	663775		546322	413313	118763	638645	663775
High	ENSBTAP00(	COL2A1 UniProtKB Gene Name|Bos taurus collagen,	COL2A1	17	3	0,13	1,09	0,6085	0,9208	114163	630247	525298	352767	602131	480928		425923	299122	71584	414819	480928
High	ENSBTAP00(	CRISP3 EntrezGene|Bos taurus cysteine-rich secreto		9	2	0,12	1,09	0,4974	0,8813	524190	233422	458225	420600	405180	638641	233518	114670	260928	75797	248184	638641
High	ENSBTAP00(	YWHAZ UniProtKB Gene Name|Bos taurus tyrosine	LOC10135	25	5	0,12	1,09	0,4373	0,8813	821157	479382	489177	602240	408325	449242	346087	277551	258019	110264	271008	392963
High	ENSBTAP00(	FN1 UniProtKB Gene Name|Bos taurus fibronectin 1		560	2	0,12	1,09	0,6371	0,9208	608014	1697525	1447566	1081494	1810354	1330780	270861	1147193	824291	219459	1247186	1330780
High	ENSBTAP00(	F5 HGNC Symbol|coagulation factor V (proaccelerin,		153	30	0,12	1,09	0,6156	0,9208	527641	1864305	1686121	1261133	1750132	1549533	201636	1259903	960132	243996	1205698	1549533
High	ENSBTAP00(	PKM2 UniProtKB Gene Name|Bos taurus pyruvate k	PKM	24	6	0,12	1,09	0,5578	0,9099	135667	635277	608464	560433	454543	597889		429322	346479	113724	281164	597889
High	ENSBTAP00(	HSPA8 UniProtKB Gene Name|Bos taurus heat shoc	HSPA8	26	7	0,12	1,09	0,4005	0,8813	312105	371016	334851	359042	197164	308389	80790	202774	154703	62392	80692	264234
High	ENSBTAP00(	CFB UniProtKB Gene Name|Bos taurus complement	CFB	612	40	0,12	1,09	0,2737	0,8813	18217496	13677694	11961124	8009915	13448309	12592164	8115611	9243426	6811049	1625384	9264786	12592164
High	ENSBTAP00(	MAP2K5 EntrezGene|Bos taurus mitogen-activated		22	1	0,11	1,08	0,4340	0,8813	12556213	12180130	9824339	11261900	6218242	11699328	5593597	8231368	5594295	2285282	4283861	11699328
High	ENSBTAP00(	CFD UniProtKB Gene Name|Bos taurus complement	CFD	14	4	0,11	1,08	0,6002	0,9208	152640	421253	422672	264065	521305	390468		284684	240683	41091	359137	390468
High	ENSBTAP00(	LRG1 UniProtKB Gene Name|Bos taurus leucine-rich	LRG1	150	13	0,11	1,08	0,5215	0,8813	1462639	4430596	3878732	3360590	4718039	3596903	596234	2994210	2208675	681936	3250344	3596903
High	ENSBTAP00(	BLVRB UniProtKB Gene Name|Bos taurus biliverdin	BLVRB	8	2	0,1	1,07	0,9248	0,9924	173013	403861	310121	231072	288945	298842		272931	160751	27134	185664	201972
High	ENSBTAP00(	ITIH4 HGNC Symbol|inter-alpha-trypsin inhibitor he		1443	38	0,1	1,07	0,4464	0,8813	130833	48207692	46978199	37229808	46414753	43819905		32578901	26750899	7554731	31975974	43819905
High	ENSBTAP00(	LDHA UniProtKB Gene Name|Bos taurus lactate deh	LDHA; LO(	29	5	0,1	1,07	0,3335	0,8813	426787	442521	401699	398355	335644	429598	161005	299057	228740	80835	178993	429598
High	ENSBTAP00(	Bos taurus endopin 2 (SERPINA3-7), mRNA. [Source:	SERPINA3-	597	6	0,1	1,07	0,6397	0,9208	3856072	19003475	17755872	9412475	20381383	16594853	1684910	12842605	10110765	1909994	14041108	16594853
High	ENSBTAP00(	Bos taurus enolase 1, (alpha) (ENO1), mRNA. [Sourc	ENO1	62	13	0,09	1,07	0,6226	0,9208	514234	1478841	1406867	915592	1320105	1668126	207383	999405	801116	179384	909445	1668126
High	ENSBTAP00(	C9 UniProtKB Gene Name|Bos taurus complement c	C9	139	20	0,09	1,06	0,9947	0,9983	2138842	3159455	2674697	3362565	2519389	2125582	909486	2135169	1523059	682337	1735653	2125582
High	ENSBTAP00(	Uncharacterized protein [Source:UniProtKB/TrEMBl		14	2	0,09	1,06	0,3428	0,8813	2952238	1365953	1147093	489474	1613292	1285728	1315176	856725	629543	86577	1070358	1260550
High	ENSBTAP00(	FETUB UniProtKB Gene Name|Bos taurus fetuin B (F	FETUB	1514	16	0,08	1,06	0,9701	0,9924	223734323	204754163	177110057	171418429	240662979	193842364	99670160	138373469	100852169	34784495	165797137	193842364
High	ENSBTAP00(	CD14 UniProtKB Gene Name|Bos taurus CD14 mole	CD14	21	5	0,07	1,05	0,8866	0,9874	407151	692722	579440	585855	550217	468130	127738	468143	329952	105519	379055	468130
High	ENSBTAP00(	APOH UniProtKB Gene Name|Bos taurus apolipopro	APOH	343	15	0,07	1,05	0,8780	0,9874	9199524	26464008	22588207	11671244	21453409	26921958	4050343	17884455	12862452	2368347	14779646	26921958
High	ENSBTAP00(	RGN UniProtKB Gene Name|Bos taurus regucalcin (s	RGN	24	4	0,07	1,05	0,3971	0,8813	885481	601962	627058	474913	721009	598789	394468	388787	357067	76121	496716	598789
High	ENSBTAP00(	Bos taurus SERPINA3-8 (SERPINA3-8), mRNA. [Sourc	LOC11387	330	4	0,06	1,05	0,6705	0,9208	521118	936141	842295	805416	755517	885347	218805	632647	479630	163436	520489	885347
High	ENSBTAP00(	SERPINA6 UniProtKB Gene Name|Corticosteroid-bin	SERPINA6	55	8	0,07	1,05	0,6077	0,9208	3536645	2838389	3172062	2299765	3570379	3031659	1575520	1918192	1806274	466672	2459700	3031659
High	ENSBTAP00(	APOA4 HGNC Symbol|apolipoprotein A-IV [Source:H	APOA4	68	14	0,06	1,04	0,8021	0,9599	434780	1078011	987653	578907	1121514	947230	150346	728523	562402	117473	772632	947230
High	ENSBTAP00(	PGK1 UniProtKB Gene Name|Bos taurus phosphogly	PGK1	7	1	0,06	1,04	0,9051	0,9904	684852	397677	465038	627416	417940	446623	305091	268752	264808	127316	287927	446623
High	ENSBTAP00(	CTSZ HGNC Symbol|cathepsin Z [Source:HGNC Symb		5	2	0,06	1,04	0,7978	0,9598	126675	225593	255148	166653	247506	217076		152456	145290		170512	217076
High	ENSBTAP00(	Uncharacterized protein [Source:UniProtKB/TrEMBl		69	6	0,05	1,03	0,9248	0,9924	1618602	4285654	3787074	1847116	3663454	4385457	679962	2896258	2156482	374820	2523820	4385457
High	ENSBTAP00(	Uncharacterized protein [Source:UniProtKB/TrEMBl		44	16	0,05	1,03	0,7026	0,9295	171960	492331	474321	269881	535302	459683	33270	332719	270093	50320	368780	389785
High	ENSBTAP00(	PPIA UniProtKB Gene Name|Bos taurus peptidylpro	LOC11290	13	2	0,04	1,03	0,7410	0,9465	738900	166199	139596	394276	161266	137940	317825	59006	43800	65714		76859
High	ENSBTAP00(	chymotrypsinogen B precursor [Source:RefSeq pep		11	4	0,04	1,03	0,5164	0,8813	167395	547424	681148	531348	633439	516727	27694	369951	387868	107822	436388	516727
High	ENSBTAP00(	KRT14 EntrezGene|Bos taurus keratin 14 (KRT14), m		273	8	0,04	1,03	0,9863	0,9954	6133331	712369	2485798	458619	2421259	10392112	2698978	425096	1400523	75955	1628257	10331631
High	ENSBTAP00(	CPB2 UniProtKB Gene Name|Bos taurus carboxypep	CPB2; LCP	24	7	0,04	1,03	0,5192	0,8813	532011	1433069	1236247	1031256	1593493	1203483	215747	968472	703959	209264	1097786	1203483
High	ENSBTAP00(	AFP UniProtKB Gene Name|Bos taurus alpha-fetopr	AFP	4597	43	0,04	1,03	0,4505	0,8813	3894684	114625813	104341931	89315839	101701425	114256742	1721314	77464463	59415655	18124109	70063976	114256742
High	ENSBTAP00(	21 ENSBTAG00000048094|ENSBTAT00000038516	LOC78493	663	9	0,03	1,02	0,5792	0,9208	11686944	15376855	14304393	10437836	13990799	13973020	5186730	10391724	8145382	2118062	9638518	13973020
High	ENSBTAP00(	ECM1 UniProtKB Gene Name|Bos taurus extracellul	ECM1	28	7	0,03	1,02	0,5237	0,8813	164527	639725	727903	375328	1087065	626002		410259	414492	52646	748899	626002
High	ENSBTAP00(	PYGL UniProtKB Gene Name|Bos taurus phosphoryl	PYGL	2	1	0,03	1,02	0,9145	0,9909	399322	56806	190819	187355	202748	140455	177892					
Medium	ENSBTAP00(	ROBO4 EntrezGene|Bos taurus roundabout homolo		1	1	0,02	1,02	0,8708	0,9874	135834	206450	181016	178226	210165	147352		139519	103076			
High	ENSBTAP00(	TUBB1 EntrezGene|Bos taurus tubulin, beta 1 class	TUBB1	8	3	0,02	1,02	0,6621	0,9208	134407	240756	364030	236874	371255	216608		132187	146134	48067	189446	164307
High	ENSBTAP00(	CSN2 UniProtKB Gene Name|Bos taurus casein beta	CSN2	4	1	0,02	1,01	0,5703	0,9116	159402	154910	340987	2980136	139110	157255			194169	604734	95836	
High	ENSBTAP00(	FERMT3 UniProtKB Gene Name|Bos taurus fermitin		4	1	0,01	1,01	0,6135	0,9208	148896	285511	243587	233410	260708	241547		192949	138706	47364	179607	241547
High	ENSBTAP00(	GPLD1 HGNC Symbol|glycosylphosphatidylinositol s		29	9	0,01	1,01	0,4872	0,8813	308720	656735	573799	569407	756241	502575	109875	443823	326740	115545	520988	468727
High	ENSBTAP00(	CD93 HGNC Symbol|CD93 molecule [Source:HGNC S		23	6	0,01	1,00	0,9501	0,9924	752657	726180	768834	936786	749955	580823	327913	490754	437799	190094	467370	580823
High	ENSBTAP00(	GNPTG UniProtKB Gene Name|Bos taurus N-acetylg	GNPTG	8	3	0,01	1,00	0,6449	0,9208	127556	321311	321554	191984	374226	319955		217143	183103	23649	257811	319955
High	ENSBTAP00(	MYRIP HGNC Symbol|myosin VIIA and Rab interacti		38	1	0	1,00	0,4677	0,8813	146065	22632798	19122726	11677704	23505500	19097817		15295312	10889096	2369658	16193370	19097817
High	ENSBTAP00(	ARF1 UniProtKB Gene Name|Bos taurus ADP-ribosyl	arf-1; arf1	6	1	-0,01	1,00	0,5577	0,9099	151431	263059	211634	345471	212705	184865		177776	120511	70103	146536	184865
High	ENSBTAP00(	CD59 UniProtKB Gene Name|Bos taurus CD59 mole	CD59	4	1	-0,01	0,99	0,9030	0,9901	196120	584480	502149	507089	195418	710217		394993	285940	102899		710217
High	ENSBTAP00(	C8A EntrezGene|Bos taurus complement componer	C8A	17	7	-0,02	0,99	0,4141	0,8813	79230	919486	916979	550952	926595	1673273		610687	494025	96088	610920	1673273
High	ENSBTAP00(	FGA UniProtKB Gene Name|Bos taurus fibrinogen al	FGA	108	18	-0,02	0,99	0,6844	0,9208	2147488	2200974	1811875	2176122	4500302	1413674	934349	1441792	988864	441582	3100341	1389898
High	ENSBTAP00(	ALB UniProtKB Gene Name|Bos taurus albumin (ALE	ALB	38975	78	-0,02	0,99	0,8175	0,9729	3278678930	2645204379	2142662739	2161900254	3711203406	2685319764	1460600446	1787636940	1220101152	438696169	2556716036	2685319764
High	ENSBTAP00(	CILP2 HGNC Symbol|cartilage intermediate layer pro	CILP2	7	4	-0,02	0,98	0,6791	0,9208	167443	352757	337126	80646	343760	342595		238394	191970		186025	342595
High	ENSBTAP00(	OSMR HGNC Symbol|oncostatin M receptor [Source		9	3	-0,03	0,98	0,7451	0,9465	479043	519472	261197	313495	570760	487874	166497	351061	109001	41710	382806	487874
High	ENSBTAP00(	C7 EntrezGene|Bos taurus complement component	C7	161	25	-0,04	0,98	0,5545	0,9099	1427789	3032746	2721534	2963371	2790132	2359272	572030	2049539	1549729	601332	1922173	2359272
High	ENSBTAP00(	RBP4 UniProtKB Gene Name|Bos taurus retinol bind	RBP4	100	9	-0,04	0,98	0,4821	0,8813	109164	6029615	4448991	2808857	4561318	6350314		4074832	2533399	569978	3099717	6350314
Medium	ENSBTAP00(	NFKB1 EntrezGene|Bos taurus nuclear factor of kap	NFKB1	5	1	-0,05	0,97	0,5512	0,9099	114075	1181848	856964	688268	887728	901927		798696	487983	139665	611572	901927
High	ENSBTAP00(	SERPINA10 UniProtKB Gene Name|Bos taurus serpin	SERPINA1(	69	9	-0,05	0,96	0,5296	0,8885	1836823	1993236	1930307	1785923	2418476	2002925	806343	1347035	1099179	348340	1666132	2002925
High	ENSBTAP00(	SERPINA5 UniProtKB Gene Name|Bos taurus serpin	SERPINA5	43	8	-0,06	0,96	0,7071	0,9333	3396292	4211066	4000779	1490114	5494384	4159556	1493467	2845851	2278173	302376	3785182	4159556
High	ENSBTAP00(	PLXDC2 UniProtKB Gene Name|Bos taurus plexin do	PLXDC2	1	1	-0,06	0,96	0,4913	0,8813	131792	334352	331009	346636	344993	266658		225956	188487	70340	237672	266658
High	ENSBTAP00(	IL1RAP UniProtKB Gene Name|Bos taurus interleuki		20	6	-0,07	0,96	0,5706	0,9116	430513	776758	658711	601233	767136	689125	181004	524935	375091	122003	528494	689125
High	ENSBTAP00(	CDH5 EntrezGene|Bos taurus cadherin 5, type 2 (va		52	9	-0,07	0,95	0,8856	0,9874	1100152	1625699	1478828	994524	1897552	1555921	460948	1098652	842092	201810	1307258	1555921

High	ENSBTAP00(	Uncharacterized protein [Source:UniProtKB/TrEMBl	LOC10084	106	5	-0,08	0,95	0,3829	0,8813	1105583	4679711	4006533	3953298	5690759	4230201	437878	3162562	2281449	802209	3920468	4230201
High	ENSBTAP00(	NID1 HGNC Symbol|nidogen 1 [Source:HGNC Symbo		5	3	-0,09	0,94	0,3946	0,8813	502750	112386	117740	171774	124897	54630	223967					
Medium	ENSBTAP00(	KIAA1033 HGNC Symbol|KIAA1033 [Source:HGNC Sy		73	1	-0,1	0,94	0,9749	0,9924	47679832	35826854	34712777	45074398	38290680	33909168	21240623	24211894	19766573	9146567	26379151	33909168
High	ENSBTAP00(	HGFAC EntrezGene|Bos taurus HGF activator (HGFA		23	7	-0,1	0,93	0,4027	0,8813	134539	1254289	1175359	1151834	1389861	1258034		847652	669288	226714	957501	1258034
High	ENSBTAP00(	MBL UniProtKB Gene Name|Bos taurus mannose-bi	MBL	7	2	-0,1	0,93	0,4919	0,8813	164986	702181	638059	431109	837803	683915	65306	474536	363331	78598	509376	683915
Medium	ENSBTAP00(	POF1B HGNC Symbol|premature ovarian failure, 1B		1	1	-0,1	0,93	0,2356	0,8813	225709	206109	140474	220980	212169	377585						377585
High	ENSBTAP00(	SPATA32 HGNC Symbol|spermatogenesis associated		5	1	-0,1	0,93	0,4774	0,8813	116903	171783	1141912	97944	198105	184469			650242			
High	ENSBTAP00(	TGFBR3 HGNC Symbol|transforming growth factor,		1	1	-0,11	0,93	0,4094	0,8813	144972	420577	374838	384742	405356	417994		284227	213445	78072	279257	417994
High	ENSBTAP00(	KLKB1 UniProtKB Gene Name|Bos taurus kallikrein E	KLKB1	86	12	-0,12	0,92	0,6976	0,9251	167618	3148517	1537128	576322	3069118	1666902		2127777	858748	95984	2114372	1604691
High	ENSBTAP00(	Uncharacterized protein [Source:UniProtKB/TrEMBl		67	7	-0,12	0,92	0,4099	0,8813	4880025	3026921	2962485	3603442	972818	3298155	2173975	2045602	1686934	731216	670192	3298155
High	ENSBTAP00(	Bos taurus keratin 6A (KRT6A), mRNA. [Source:RefSe	KRT6A	157	6	-0,13	0,91	0,9923	0,9977	2953952	597995	1405194	482196	1537919	3273088	1284621	404127	800163	91437	1059500	3273088
Medium	ENSBTAP00(	FAM83G HGNC Symbol|family with sequence simila	FAM83G	8	1	-0,15	0,90	0,9475	0,9924	8630322	6495411	5673814	7754450	7190461	5513942	3844674	4389618	3230852	1573545	4953641	5513942
High	ENSBTAP00(	KRT2 HGNC Symbol|keratin 2 [Source:HGNC Symbol		85	1	-0,15	0,90	0,8987	0,9874	12023530	1942952	6241600	2170963	13129369	6938033	5356296	1313053	3554168	440535	9045063	6938033
High	ENSBTAP00(	Uncharacterized protein [Source:UniProtKB/TrEMBl		13	2	-0,15	0,90	0,9782	0,9924	1333000	995269	874436	1107142	1159232	892148	593831	672606	497932	224663	798616	892148
High	ENSBTAP00(	Uncharacterized protein [Source:UniProtKB/TrEMBl		23	1	-0,16	0,90	0,9770	0,9924	607659	588592	274846	222477	701673	656743	270703	397772	156506		483396	656743
High	ENSBTAP00(	GC HGNC Symbol|group-specific component (vitami	GC	2168	33	-0,16	0,90	0,0641	0,5495	120347510	141345018	144783861	189683330	157321484	157681881	53584177	95521381	82444592	38490837	108381653	157681881
High	ENSBTAP00(	IGLL1 EntrezGene|Bos taurus immunoglobulin lamb		13	1	-0,16	0,90	0,4040	0,8813	198009	3308210	2958859	2181327	4935196	3304822		2235698	1684869	442638	3399947	3304822
High	ENSBTAP00(	Uncharacterized protein [Source:UniProtKB/TrEMBl		604	55	-0,16	0,90	0,3215	0,8813	2798645	5832904	5928248	5144467	7710063	6520434	1222334	3941894	3375735	1043923	5311603	6520434
High	ENSBTAP00(	SERPINA11 UniProtKB Gene Name|Bos taurus serpir	SERPINA1	6	2	-0,16	0,89	0,5685	0,9116	189034	222704	206419	408381	231093	160350	84212	150504	117542	82869	159204	160350
Medium	ENSBTAP00(	CUL4B HGNC Symbol|cullin 4B [Source:HGNC Symbo		1	1	-0,16	0,89	0,3157	0,8813	62357927	64365975	59331889	60648485	94387822	69832560	27779486	43498716	33785488	12306885	65025500	69832560
High	ENSBTAP00(	PPARD UniProtKB Gene Name|Bos taurus peroxison	PPARD	42	1	-0,16	0,89	0,9458	0,9924	34251463	46546297	37298301	31041985	44411411	41807294	15258494	31456125	21238854	6299088	30595835	41807294
Medium	ENSBTAP00(	RASGEF1A UniProtKB Gene Name|Bos taurus RasGE	RASGEF1A	50	1	-0,17	0,89	0,8745	0,9874	41309036	31798527	30559761	36285010	35834479	32542736	18402533	21489539	17401712	7363011	24687030	32542736
High	ENSBTAP00(	KRT1 HGNC Symbol|keratin 1 [Source:HGNC Symbol		282	4	-0,17	0,89	0,1785	0,8722	22732412	9478346	21182539	23871610	23872192	51806940	10126936	6376677	12062020	4844064	16423786	51806940
Medium	ENSBTAP00(	CRYZL1 UniProtKB Gene Name|Bos taurus crystallin,	CRYZL1	45	1	-0,19	0,88	0,3743	0,8813	150029352	106470178	118262819	123395747	177132009	134984543	66835742	71952861	67342657	25039657	122029487	134984543
High	ENSBTAP00(	A1BG UniProtKB Gene Name|Bos taurus alpha-1-B g	A1BG	701	18	-0,22	0,86	0,3774	0,8813	353976	51268713	48048569	53118313	76366772	55914468	146117	34647548	27360402	10778851	52610469	55914468
High	ENSBTAP00(	SERPINF2 UniProtKB Gene Name|Bos taurus serpin	SERPINF2	372	13	-0,23	0,86	0,3571	0,8813	25875262	35474522	33640339	28734063	48991012	39364285	11527027	23973787	19155892	5830761	33750806	39364285
High	ENSBTAP00(	KRT78 UniProtKB Gene Name|Bos taurus keratin 78	KRT78	28	2	-0,23	0,85	0,2451	0,8813	130130	78375	107876	126761	113003	166273		52966	61428		77850	166273
High	ENSBTAP00(	KRT18 UniProtKB Gene Name|Bos taurus keratin 18	KRT18	100	1	-0,23	0,85	0,2553	0,8813	28581710	8352561	31045420	28913209	33621968	56351992	12732707	5644686	17678262	5867114	23162790	56351992
High	ENSBTAP00(	IGLL1 EntrezGene|Bos taurus immunoglobulin lamb		105	7	-0,24	0,85	0,5217	0,8813	7640884	3234646	2845459	1738555	4363637	3809568	3403895	2133969	1589193	350088	2982431	3736607
Medium	ENSBTAP00(	PTAR1 HGNC Symbol|protein prenyltransferase alpl		19	1	-0,24	0,85	0,2816	0,8813	91629	5476710	5904476	31417624	6459010	5899462	40819	3701177	3362199	6375313	4449731	5899462
High	ENSBTAP00(	Uncharacterized protein [Source:UniProtKB/TrEMBl		63	9	-0,25	0,84	0,0967	0,6905	2045437	2186500	1713055	2650415	2185860	2425693	905221	1477643	975468	537826	1490797	2425693
High	ENSBTAP00(	COL9A1 HGNC Symbol|collagen, type IX, alpha 1 [So		2	2	-0,26	0,84	0,6678	0,9208	369750	87420	95750	114349	67157	185637	164718					
High	ENSBTAP00(	ICOSLG HGNC Symbol|inducible T-cell co-stimulator		8	2	-0,26	0,83	0,2064	0,8813	115342	297454	255929	273375	580568	307192		155818	130484	46654	399964	271519
Medium	ENSBTAP00(	RBM12B HGNC Symbol|RNA binding motif protein 1		19	1	-0,27	0,83	0,3754	0,8813	137874	7868487	7088581	6881800	11916689	8571123		5317547	4036466	1396466	8209626	8571123
High	ENSBTAP00(	SERPINC1 EntrezGene|Bos taurus serpin peptidase i	SERPINC1	895	28	-0,29	0,82	0,2166	0,8813	20907276	28447684	24366812	24904503	35345015	29810115	9281890	19225029	13875247	5053661	24349829	29810115
High	ENSBTAP00(	AFM EntrezGene|Bos taurus afamin (AFM), mRNA.	AFM	627	39	-0,3	0,82	0,4043	0,8813	4949005	11741280	10713938	8714842	13282984	13149829	2184499	7934792	6100862	1768429	9150891	13149829
High	ENSBTAP00(	HBB UniProtKB Gene Name|Bos taurus hemoglobin,	HBB; LOC1	319	7	-0,3	0,81	0,3372	0,8813	2662465	3993737	2922515	3172241	4847012	3589320	1152800	2698979	1664174	643716	3339196	3589320
High	ENSBTAP00(	PLTP UniProtKB Gene Name|Bos taurus phospholipi	PLTP	12	3	-0,3	0,81	0,2353	0,8813	198892	661719	602268	1065327	740047	679694		447192	342951	216178	509832	679694
High	ENSBTAP00(	APOA2 UniProtKB Gene Name|Bos taurus apolipopr	APOA2	84	7	-0,32	0,80	0,1540	0,8660	10202029	10682995	11845523	13352762	20166682	12579886	4544845	7219600	6745222	2709563	13893197	12579886
High	ENSBTAP00(	CREG1 HGNC Symbol|cellular repressor of E1A-stim	CREG1	4	2	-0,33	0,80	0,4630	0,8813	39199	336368	375420	195242	454828	421970		227319	213776	39619	313340	421970
High	ENSBTAP00(	HPX UniProtKB Gene Name|Bos taurus hemopexin (	HPX	1124	20	-0,33	0,80	0,3835	0,8813	204213	72781566	67477635	73214844	103922820	84700310	65179	49185997	38423938	14856870	71594335	84700310
High	ENSBTAP00(	IGF2R EntrezGene|cation-independent mannose-6-		155	34	-0,33	0,80	0,3364	0,8813	177500	13456950	12769405	27620759	15122076	16020444		9094246	7271310	5593715	10417875	16020444
High	ENSBTAP00(	RAP1B UniProtKB Gene Name|Bos taurus RAP1B, me	LOC10134	6	3	-0,33	0,79	0,3987	0,8813	213494	281626	403482	1000975	354603	259601		190324	229756	203119	244292	189910
High	ENSBTAP00(	COL3A1 EntrezGene|collagen alpha-1(III) chain prec		66	11	-0,33	0,79	0,2093	0,8813	711251	1770902	1597328	1789777	2611064	2013756	279750	1196781	909570	363184	1798810	2013756
Medium	ENSBTAP00(	CIT UniProtKB Gene Name|Uncharacterized protein		4	1	-0,35	0,79	0,1671	0,8722	95956	140349	165907	178328	224750	154458		94848	94473		154835	
High	ENSBTAP00(	KRT17 UniProtKB Gene Name|Bos taurus keratin 17	KRT17	136	1	-0,36	0,78	0,2448	0,8813	223895	172984	105189	187256	221839	292968			59898			292968
High	ENSBTAP00(	Bos taurus protein HP-25 homolog 1 (LOC511240), n		9	3	-0,36	0,78	0,5058	0,8813	17712111	476150	486875	308716	1122836	625242	7869914	252134	229626	49580	761919	591444
High	ENSBTAP00(	APOM UniProtKB Gene Name|Bos taurus apolipopr	APOM	76	8	-0,36	0,78	0,4912	0,8813	914493	4596061	2607013	2658749	4076668	3345480	396298	3106032	1474806	528674	2808491	3345480
High	ENSBTAP00(	CD9 UniProtKB Gene Name|Bos taurus CD9 molecul		8	2	-0,37	0,78	0,7301	0,9465	312043	279728	267334	546555	48708	360544	139010	189041	152228	110908		360544
High	ENSBTAP00(	CD44 UniProtKB Gene Name|Bos taurus CD44 mole		15	3	-0,37	0,77	0,1611	0,8660	351850	809224	780352	909338	1323469	1010732	123620	546876	444358	178355	911762	1010732
High	ENSBTAP00(	AHSG UniProtKB Gene Name|Bos taurus alpha-2-HS	AHSG	9250	27	-0,38	0,77	0,1166	0,7917	1038304086	1516120410	1662458880	1968283711	2298319658	1687665170	462532114	1024598656	946657613	399407198	1583354531	1687665170
High	ENSBTAP00(	CD5L HGNC Symbol|CD5 molecule-like [Source:HGN		56	10	-0,38	0,77	0,6434	0,9208	1559552	2016833	2611998	4103850	2622866	1332335	694756	1322867	1446674	823577	1796790	1308288
High	ENSBTAP00(	A2M UniProtKB Gene Name|Bos taurus alpha-2-ma	A2M	5897	93	-0,4	0,76	0,2284	0,8813	47155378	124108037	106341580	116606111	173791221	139936432	20975482	83872578	60554319	23661894	119727957	139936432
High	ENSBTAP00(	VIM UniProtKB Gene Name|Bos taurus vimentin (VI	VIM	21	5	-0,4	0,76	0,8641	0,9874	190797	132021	180775	238733	89184	263158	77492	15432	83565	36626		153875
High	ENSBTAP00(	F11 UniProtKB Gene Name|Bos taurus coagulation f	F11	30	5	-0,41	0,75	0,6538	0,9208	607791	570968	703220	144062	809548	839980	252906	385862	400436		523123	839980
High	ENSBTAP00(	EEF1A1 UniProtKB Gene Name|Elongation factor 1-a	EEF1A; EEI	8	2	-0,45	0,73	0,1783	0,8722	164194	339184	407141	464186	409336	612115		200972	231839	94193	281999	612115
High	ENSBTAP00(	COL6A3 HGNC Symbol|collagen, type VI, alpha 3 [So		112	34	-0,45	0,73	0,3554	0,8813	113842	1086144	958719	807697	1533761	1313462		734019	545925	156348	1056636	1313462
High	ENSBTAP00(	KRT19 UniProtKB Gene Name|Bos taurus keratin 19	KRT19	103	2	-0,46	0,73	0,9335	0,9924	103028	163177	278955	223842	91350	257477			128153			166369
High	ENSBTAP00(	B2M UniProtKB Gene Name|Beta-2-microglobulin [	B2M; LOC	6	2	-0,46	0,73	0,3895	0,8813	115206	169141	159445	117105	1607751	218617					1107609	137506
High	ENSBTAP00(	CAP1 UniProtKB Gene Name|Bos taurus CAP, adeny	CAP1	7	2	-0,48	0,72	0,1230	0,8045	88475	127342	105320	201111	146967	120501		86058	59973	32684	55808	120501
High	ENSBTAP00(	AMY2B EntrezGene|Bos taurus amylase, alpha 2B (p	AMY2B	61	10	-0,49	0,71	0,3083	0,8813	196748	1412231	1250148	1754173	2165843	1207238		941866	669917	344841	1492089	1207238
High	ENSBTAP00(	SERPINA3-1 UniProtKB Gene Name|Bos taurus serpi	SERPINA3-	1940	14	-0,49	0,71	0,3558	0,8813	155733	49517446	45523229	87831380	63966172	56801359	41706	33464036	25922393	17822881	44067468	56801359
High	MGC137211	EntrezGene|Bos taurus protein HP-25 homolog 2 (M	LOC11389	13	3	-0,49	0,71	0,1318	0,8160	280530	492955	408144	627559	499623	573708	100990	333140	232411	127345	310886	573708
High	ENSBTAP00(	Amine oxidase [Source:UniProtKB/TrEMBL;Acc:E1B.		24	4	-0,5	0,71	0,0211	0,3670	160750	218164	211277	297993	353359	284245		125086	103574	48578	243436	284245
High	ENSBTAP00(	Uncharacterized protein [Source:UniProtKB/TrEMBl		130	7	-0,5	0,71	0,3406	0,8813	216409	2477467	1864620	4822694	1435220	2638213		1674280	1061775	978629	988749	2638213
High	ENSBTAP00(	PROS1 UniProtKB Gene Name|Bos taurus protein S (	PROS1	107	14	-0,51	0,70	0,2572	0,8813	952907	2735671	2361145	2289712	3357976	3740693	395971	1848775	1344512	464632	2313371	3740693
High	ENSBTAP00(	PEPD UniProtKB Gene Name|Bos taurus peptidase D	PEPD	6	2	-0,51	0,70	0,7578	0,9465	128107	481154	261021	171321	371778	403665		325165	148634	21358	256125	403665
High	ENSBTAP00(	CFL1 UniProtKB Gene Name|Bos taurus cofilin 1 (no	Cfl1; CFL1;	14	3	-0,52	0,70	0,5857	0,9208	417629	303656	141716	434987	473637	188826	172076	185590	52030	60541	301864	81566
High	ENSBTAP00(	KRT77 HGNC Symbol|keratin 77 [Source:HGNC Symb		70	1	-0,56	0,68	0,8571	0,9874	155477	127213	353160	94169	229428	250649			201101		158057	250649
High	ENSBTAP00(	APOA1 UniProtKB Gene Name|Bos taurus apolipopr	APOA1	1638	22	-0,59	0,66	0,0486	0,5008	72553103	112675756	95572654	126290774	191516729	144252894	32321279	76146609	54422146	25627121	131939384	144252894
High	ENSBTAP00(	VCL UniProtKB Gene Name|Bos taurus vinculin (VCL	VCL	41	14	-0,6	0,66	0,6876	0,9211	8086255	5269153	5125630	7962198	8258939	4556419	3602301	3527925	2902716	1615702	5689735	4556419
High	ENSBTAP00(	CPN2 UniProtKB Gene Name|Bos taurus carboxypep	CPN2	47	9	-0,6	0,66	0,2568	0,8813	117610	1203701	1167199	1744275	2013687	1767641		801726	643424	353951	1387266	1767641
High	ENSBTAP00(	JUP UniProtKB Gene Name|Bos taurus junction plak	JUP	7	6	-0,61	0,66	0,4456	0,8813	159423	977554	1147404	390166	1493179	2662072		606462	616250	72022	976240	2662072
High	ENSBTAP00(	PTMA UniProtKB Gene Name|Prothymosin alpha [S	LOC11388	1	1	-0,62	0,65	0,7353	0,9465	113758	65252	575291	52976	174603	196560			327589			
High	ENSBTAP00(	C11H2orf81 EntrezGene|Bos taurus chromosome 1	C11H2orf8	31	1	-0,64	0,64	0,4890	0,8813	222446	92820	151239	235512	22108726	56600				47791	15231106	
High	ENSBTAP00(	Uncharacterized protein [Source:UniProtKB/TrEMBl		161	7	-0,64	0,64	0,1105	0,7601	2561024	2306531	2284330	5119958	3603509	2852033	1121875	1537601	1280719	1030049	2454262	2781732
High	ENSBTAP00(	CLEC3B UniProtKB Gene Name|Bos taurus C-type le	CLEC3B	33	7	-0,65	0,64	0,4037	0,8813	524166	526141	499765	396064	1099989	824798	200624	325652	243651	76258	757803	824798
Medium	ENSBTAP00(	INTB3 UniProtKB Gene Name|Bos taurus integrin, b	ITGB3	1	1	-0,67	0,63	0,9553	0,9924	87013	86784	115460	139664	48402	138065		58649	65747	28341		138065
High	MGC137014	EntrezGene|Bos taurus protein HP-20 homolog (MG	LOC10955	25	3	-0,67	0,63	0,3079	0,8813	129428	959169	615750	665258	1382919	977899		648209	338099	134995	952718	977899
High	ENSBTAP00(	CP HGNC Symbol|ceruloplasmin (ferroxidase) [Sour		90	20	-0,68	0,62	0,3503	0,8813	142945	938640	721418	586258	1227248	1159213		634335	410798	114573	845473	1159213
High	ENSBTAP00(	GGH UniProtKB Gene Name|Bos taurus gamma-glut	GGH	9	4	-0,69	0,62	0,7460	0,9465	581949	115520	175325	196256	372226	282801	259249		87341	21989	234258	175618
High	ENSBTAP00(	DSP HGNC Symbol|desmoplakin [Source:HGNC Sym		11	8	-0,69	0,62	0,3270	0,8813	154799	107997	81889	174657	101047	630187		15906	15795			630187
High	ENSBTAP00(	CSN1S1 UniProtKB Gene Name|Bos taurus casein al	CSN1S1	4	2	-0,71	0,61	0,4366	0,8813	173640	117606	250181	1362986	283920	111396		79479	142461	276579	195598	111396
High	ENSBTAP00(	AGP UniProtKB Gene Name|Bos taurus orosomucoi	agp; LOC1	1011	15	-0,71	0,61	0,1459	0,8552	26094975	57391675	61463380	57053549	113996749	93891572	11594553	38785463	34999228	11577395	78534450	93891572
High	ENSBTAP00(	CFI EntrezGene|Bos taurus complement factor I (CF	CFI	189	23	-0,73	0,61	0,6523	0,9208	1747291	2554133	1944608	1086183	5195936	3215907	745324	1690602	1096966	212980	3579576	3176035
High	ENSBTAP00(	ADIPOQ UniProtKB Gene Name|Adiponectin [Sourc	ADID; ADI	332	8	-0,75	0,59	0,0374	0,4258	13792147	21849798	18418538	30984046	33935454	26611014	6122681	14766158	10488109	6287331	23378756	26611014
High	ENSBTAP00(	DMBT1 HGNC Symbol|deleted in malignant brain tu		7	4	-0,76	0,59	0,1188	0,7971	140989	369244	382928	1272387	403976	624730		203968	157012	258195	219946	527779
High	ENSBTAP00(	COL1A2 UniProtKB Gene Name|Bos taurus collagen,	COL1A2	65	8	-0,8	0,58	0,2659	0,8813	77630	861401	1035611	1575075	1495261	1348221		572625	589711	319617	1030113	1348221
High	ENSBTAP00(	ALDOA UniProtKB Gene Name|Bos taurus aldolase A	ALDOA	19	4	-0,8	0,57	0,4508	0,8813	397583	325966	352687	257283	614503	690845	138597	193335	173291	37798	423343	690845
High	ENSBTAP00(	HRG EntrezGene|Bos taurus histidine-rich glycoprot		13	3	-0,82	0,57	0,0576	0,5349	210552	147353	136931	453964	259730	250713				92119	178933	250713
Medium	ENSBTAP00(	CDH11 UniProtKB Gene Name|Bos taurus cadherin	CDH11	3	1	-0,85	0,56	0,2096	0,8813	61284	317408	223343	226786	799122	402753		214505	127179		550530	402753
High	ENSBTAP00(	Bos taurus serotransferrin-like (LOC525947), mRNA.		296	20	-0,88	0,54	0,3131	0,8813	183767	15782615	13554290	18405216	29627591	24959288		10665938	7718249	3724949	20402290	24959288
High	ENSBTAP00(	KRT16 HGNC Symbol|keratin 16 [Source:HGNC Symb		38	1	-0,96	0,51	0,1980	0,8813	82515	124996	85974	167138	1053018	162354					725443	
High	ENSBTAP00(	KRT10 UniProtKB Gene Name|Bos taurus keratin 10	KRT10	326	8	-0,97	0,51	0,3473	0,8813	217168	14337880	22943907	13321302	28063500	42684780	50396	9689581	13064999	2703179	19333459	42684780
High	ENSBTAP00(	FABP5 HGNC Symbol|fatty acid binding protein 5 (ps		1	1	-1	0,50	0,3347	0,8813	162548	102875	76758	90036	206093	1010185						1010185
Medium	ENSBTAP00(	FLT4 HGNC Symbol|fms-related tyrosine kinase 4 [S		2	1	-1,02	0,49	0,6360	0,9208	36826	212931	81343	164761	247891	46696		143899		33434	170777	
High	ENSBTAP00(	KNG1 UniProtKB Gene Name|Bos taurus kininogen 1	KNG1	1002	24	-1,13	0,46	0,2632	0,8813	16476565	59324201	27697680	81358907	60477193	33503595	7324958	40091470	15771951	16509476	41663847	33473337
High	ENSBTAP00(	APOB HGNC Symbol|apolipoprotein B [Source:HGN		1554	185	-1,17	0,45	0,1408	0,8344	1271464	2850226	2483852	2359433	5570007	5591927	528053	1877266	1384151	474477	3837280	5591927
High	ENSBTAP00(	Uncharacterized protein [Source:UniProtKB/TrEMBl	LOC11387	1394	4	-1,18	0,44	0,5591	0,9099	1315243	658678	763665	489439	2128149	1727914	559182	394241	396337	86705	1466121	1727914
High	ENSBTAP00(	SERPING1 HGNC Symbol|serpin peptidase inhibitor,		433	16	-1,19	0,44	0,1801	0,8722	251888	8983759	7758773	58108310	17668201	16479517	64695	6071251	4418095	11791429	12171947	16479517
High	ENSBTAP00(	RPS27A UniProtKB Gene Name|Bos taurus ribosoma	HEL112; L(	8	3	-1,19	0,44	0,0294	0,3989	284013	263744	217600	601268	391181	684544	119894	158620	86073	107610	256539	684544
High	ENSBTAP00(	KRT24 EntrezGene|keratin, type I cytoskeletal 24 [S		101	2	-1,22	0,43	0,0883	0,6561	3325714	2074747	5518360	7724518	6993134	8886873	1435269	1402120	3142332	1567471	4817698	8886873
High	ENSBTAP00(	KRT75 UniProtKB Gene Name|Bos taurus keratin 75	KRT75	146	2	-1,29	0,41	0,2869	0,8813	129377	968768	2427712	1044263	2376051	5513200		654697	1382417	211903	1636905	5513200
High	ENSBTAP00(	PRDX2 UniProtKB Gene Name|Bos taurus peroxired	FARSA; PR	25	6	-1,62	0,33	0,4330	0,8813	194361	319328	5081369	11905282	869849	983056		165832	2885377	2415838	552073	937029
High	ENSBTAP00(	KRT79 UniProtKB Gene Name|Bos taurus keratin 79	KRT79	132	1	-1,67	0,32	0,2558	0,8813	1401390	2497177	7008801	2969364	14004334	7921663	624297	1687600	3991037	602548	9647842	7921663
High	ENSBTAP00(	PPIA HGNC Symbol|peptidylprolyl isomerase A (cycl	LOC61340	13	1	-1,69	0,31	0,6244	0,9208	87479	99968	260531	691234	322076	44344			148355	140266	221884	
High	ENSBTAP00(	Uncharacterized protein [Source:UniProtKB/TrEMBl		10	2	-1,76	0,29	0,6661	0,9208	134609	235596	140582	46864	726069	477513		159217			500203	477513
High	ENSBTAP00(	PTI EntrezGene|Bos taurus spleen trypsin inhibitor (		4	1	-1,79	0,29	0,2395	0,8813	124895	375169	215898	186124	930935	745776		253540	122939		641338	745776
High	ENSBTAP00(	GP1BA HGNC Symbol|glycoprotein Ib (platelet), alph		16	3	-1,79	0,29	0,0256	0,3989	414069	184863	239302	981822	827344	661649	176620	101505	102460	199233	569973	661649
High	ENSBTAP00(	KRT5 UniProtKB Gene Name|Bos taurus keratin 5 (K	KRT5	217	8	-1,95	0,26	0,2131	0,8813	270428	1838152	7801333	5438536	7077942	17373497	80627	1227052	4442330	1103596	4876124	17373497
Medium	ENSBTAP00(	E-CADHERIN UniProtKB Gene Name|Bos taurus cadh		2	1	-2,19	0,22	0,0475	0,4995	56426	41559	116425	120795	308039	257844			66296	24512	212214	257844
High	ENSBTAP00(	Uncharacterized protein [Source:UniProtKB/TrEMBl	LOC10499	6	1	-2,5	0,18	0,3166	0,8813	206564	580374	4559016	3283944	3698537	1648842		392218	2596051	666383	2547990	1648842
Medium	ENSBTAP00(	PEX19 UniProtKB Gene Name|Bos taurus peroxisom	PEX19	3	1	-3,31	0,10	0,6776	0,9208	112032	206912	4200583	135634	2503837	2052557			2391947		1724939	2052557

3. CD44 Receptor Expression of Glioblastoma Cells by Western Blot Analysis

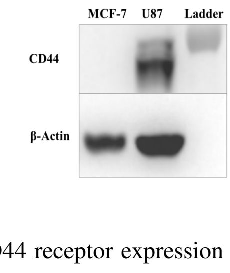

Figure S3. Western Blot confirming CD44 receptor expression of U87 glioblastoma cells. MCF-7 cell line was used as negative control and β-actin as loading control.

Chapter III

Proteins as Functional Components of Nanoparticles for Brain Targeting

III.3 ApoE - Functionalization of Nanoparticles for Targeted Brain Delivery - A Feasible Method for Polyplexes?

This chapter was submitted as research article in the Journal of Advanced Therapeutics (05/2023):

Natascha Hartl, Bettina Gabold, Philipp Uhl, Ximian Xiao, Walter Mier, Runhui Liu and Olivia M. Merkel

"ApoE – Functionalization of Nanoparticles for Targeted Brain Delivery – A Feasible Method for Polyplexes?"

Abstract

The blood- brain barrier (BBB) poses a major obstacle in the treatment of all types of central nervous system (CNS) diseases as it is a highly selective biological barrier that protects the brain from many substances. Small interfering RNA (siRNA) offers in principle a promising therapeutic approach, e.g., for brain tumors, by downregulating brain tumor-related genes and inhibiting tumor growth via RNA interference. However, the BBB is a formidable barrier for macromolecules such as nucleic acids. In an effort to develop a brain-targeted strategy for siRNA delivery systems formed by electrostatic interactions with cationic polymers (polyplexes, PXs), we investigated the suitability of the well-known surfactant-based approach for Apolipoprotein E (ApoE)-functionalization of nanoparticles (NPs). ApoE is a ligand for the low-density lipoprotein (LDL) receptor family, which is highly present at the BBB, and can mediate transport into the brain by receptor-mediated transcytosis (RMT). In the present work, we used cationic branched 25kDa poly(ethyleneimine) (b-PEI) and nylon-3 polymers to form PXs with siRNA and subsequently, we coated them with ApoE without or after precoating with polysorbate 80 (PS 80). We utilized highly hydrophobic $NM_{0.2}/CP_{0.8}$ nylon-3 polymers to evaluate the effects of hydrophobic cyclopentyl (CP) subunits on ApoE binding efficacy. The physicochemical characteristics of PS80+ApoE-PXs and ApoE-PXs, e.g., particle size and surface charge, were measured by dynamic light scattering and laser Doppler anemometry, whereas the binding of ApoE to the particle surfaces was confirmed by SDS-PAGE. Cellular internalization abilities of ApoE-PXs were investigated by flow cytometry and GAPDH knockdown abilities were evaluated by qPCR in an LDL and LDL receptor-related protein 1 (LRP1) receptor-positive model cell line. Furthermore, cellular tolerability was evaluated by CellTiter®-Blue assays and hemocompatibility of the polymers was confirmed by hemolysis and erythrocyte aggregation assays. Precoating of PXs with PS80 was not favorable for either formulation, whereas ApoE-$NM_{0.2}/CP_{0.8}$ PXs displayed significantly higher cellular internalization and successful GAPDH knockdown abilities *in vitro* compared with plain $NM_{0.2}/CP_{0.8}$ PXs and b-PEI formulations. Biodistribution studies of radiolabeled PXs in mice revealed that none of the formulations were able to reach the brain in appropriate concentrations. In conclusion, this study demonstrated that ApoE functionalization particularly of hydrophobically modified PXs is in principle possible and very promising for siRNA delivery based on *in vitro* results, but further optimization and more sophisticated *in vitro* models are required to achieve an appropriate *in vitro-in vivo* translation in future approaches.

1. Introduction

The ability of therapeutic agents to reach their target sites in the central nervous system (CNS) is very limited due to the strong protective function of the blood-brain barrier (BBB). However, according to the World Health Organization (WHO), approximately 20% of all humans suffer from CNS disorders such as depression, Parkinson's disease, Alzheimer's disease, dementia, epilepsy, stroke, cerebral cancer, or CNS-relevant metabolic diseases. According to recent estimates, the number of people suffering from CNS diseases worldwide will increase significantly in coming decades due to tremendous population growth, increasing life expectancy and in addition, due to risk factors such as obesity, smoking, high blood pressure or diabetes. Therefore, the development of highly efficient, safe and targeted pharmaceutical systems that are able to overcome the BBB is urgently needed in order to exert therapeutic effects in disease-specific regions of the brain. Macromolecular drugs, such as proteins, peptides or nucleic acids bear a very high potential to open up new perspectives for the treatment of CNS diseases. Less than 2% of small molecule drugs are able to cross the barrier to reach their target sides in the CNS [1]. When it comes to macromolecular drugs, the barrier is completely impermeable due to their high molecular weight [2]. A wide range of macromolecular drugs is embedded into nanocarriers to make them stable, safe and efficient drugs after administration into the human body. In an effort to design efficient nanocarriers that can enable controlled and targeted drug delivery into the brain, a promising option is to decorate the nanocarriers with ligands that can interact with specific binding sites of the BBB with subsequent internalization of the particles via receptor-mediated transcytosis (RMT) into the brain. Among the numerous potential targets at the BBB, the low-density lipoprotein (LDL) receptor family has been extensively investigated as highly efficient target for brain delivery in several studies using liposomes [3] or polymeric nanoparticles (NPs) [4] as drug carriers. In first attempts, it was found out that some drugs that are commonly unable to cross the BBB can be transported across this barrier and exhibit pharmacological effects after intravenous injection by encapsulating them into poly (butyl cyanoacrylate) (PBCA) NPs. By using PBCA NPs as drug carriers, substances such as the hexapeptide dalargin [5-11], the dipeptide kytorphin [9], loperamide [12], tubocurarine [13], the NMDA receptor antagonist MRZ 2/576 [14] and doxorubicin [15-17] have already been successfully transported into the brain. More continuing studies have confirmed that the brain targeting effect can be further enhanced by precoating the PBCA NPs with surfactants such as PS 20, 40, 60 and 80 [18]. Following the identification of Apolipoprotein E (ApoE) on the surface of PS precoated PBCA NPs after incubation in human

plasma [19], Kreuter et al. succeeded in confirming the involvement of plasma ApoE in the brain uptake mechanism of loperamide or dalargin-loaded PBCA NPs (both analgesics) after intravenous injection in mice by measuring the antinociceptive effects with the tail flick test [20]. Since then, numerous small molecule drugs, e.g., methotrexate [21] and cisplatin [22] for the treatment of cerebral cancer or tacrine [23, 24], rivastigmine [25] or rosmarinic acid [26] for treatment of Alzheimer's disease and peptide/protein drugs such as the nerve growth factor [27, 28] also for the treatment of Alzheimer's disease or arylsulfatase A [29] for metachromatic leukodystrophy have been successfully delivered into the brain using PS coated PBCA NPs. Subsequently, the ApoE targeting approach was successfully applied to several other matrix NPs, e.g., human and bovine serum albumin (HAS [30] and BSA [31]), poly(lactic acid) (PLA) [32, 33] and poly(lactic-co-glycolic acid) (PLGA) [34-37] NPs. Moreover, in addition to the surfactant-based approach, other types of ApoE-functionalization of NPs have been investigated such as direct coating of NPs with ApoE, adsorption of ApoE onto NPs by poly(ethylene glycol) (PEG) modification or covalent linkage of ApoE to NPs. In an effort to investigate whether the already established brain delivery strategy for solid NPs is also suitable for dynamic systems such as polymer-small interference RNA (siRNA) polyelectrolyte complexes (polyplexes) formed by electrostatic interactions, we evaluated the suitability of the surfactant-based approach with PS 80. The application of siRNA is a promising therapeutic approach in particular for brain tumors due to its ability to downregulate glioma-related genes and to induce tumor growth inhibition, as recently demonstrated *in vitro* as well as *in vivo* experiments [38-40]. Since PSs were shown to operate as hydrophobic anchors for binding ApoE, the question arose whether hydrophobic modification of polymers could lead to an enhancement of ApoE binding without surfactant precoating, what could be beneficial due to concerns and contradictions regarding surfactants' toxicity [41]. Therefore, besides branched poly(ethyleneimine) (b-PEI) polymers, this study utilized nylon-3 polymers synthesized by ring-opening polymerization (ROP) with an increased amount of hydrophobic subunits derived from β-lactam cyclopentyl (CP) and cationic subunits derived from β-lactam without ("no") methyl substitution (NM) with a subunit ratio of 1:4 (NM:CP), which have been previously investigated regarding efficacy of siRNA delivery into brain tumor cells [42]. Herein, we coated b-PEI and $NM_{0.2}/CP_{0.8}$ PXs with ApoE with and without PS 80 precoating and characterized the resulting PS80+ApoE-PXs and ApoE-PXs in terms of their physicochemical characteristics such as particle size, particle size distribution and surface charge. Sodium dodecylsulfate polyacrylamide gel electrophoresis (SDS-PAGE) was established as a suitable method to verify bound ApoE on b-PEI and $NM_{0.2}/CP_{0.8}$ PXs by visualizing them with Comassie Brilliant Blue

G staining. Furthermore, cell tolerability, cellular internalization ability and gene knockdown efficiency of modified and unmodified b-PEI and $NM_{0.2}/CP_{0.8}$ PXs were evaluated by CellTiter-Blue® assay, flow cytometry and real-time quantitative PCR (qPCR) using an LDL and LRP1 receptor expressing model cell line. Since we obtained very promising results in *in vitro* experiments particularly for ApoE-$NM_{0.2}/CP_{0.8}$ PXs, we first confirmed the hemocompatibility of polymers using a hemolysis assay and subsequently investigated their biodistribution in comparison to b-PEI and $NM_{0.2}/CP_{0.8}$ PXs by measuring the radioactive signals of encapsulated ^{177}Lu labeled DTPA-modified siRNA in the major organs and the brain after intravenous injection in SWISS mice.

2. Materials and Methods

2.1 Materials

Branched poly(ethylene imine) (b-PEI) 25 kDa, Apolipoprotein E (ApoE) from human plasma, HEPES (4-(2-hydroxyethyl)–1-piperazineethanesulfonic acid), Comassie Brilliant Blue G solution, sodium acetate, sodium chloride, sodium hydroxide, sodium hydrogen carbonate, Tween® 80, Dulbecco's Phosphate Buffered Saline (PBS), Triton-X, arsenazo(III), yttrium(III) chloride and for cell culture U87 cells (human glioblastoma astrocytoma), Eagle's Minimum Essential Medium (EMEM), Fetal Bovine Serum (FBS), Penicillin-Streptomycin solution, trypsin-EDTA solution 0.25% and dimethyl sulfoxide (DMSO) were purchased from Sigma-Aldrich (Taufkirchen, Germany). Novex™ 10% tris-glycine gel, PageRuler™ Plus Prestained Protein Ladder (10 to 250 kDA), Pierce™ Lane Marker Reducing Sample Buffer and absolute ethanol were purchased from Thermo Fisher Scientific (Waltham, MA, USA). Gibco® trypan blue solution 0.4% in phosphate buffered saline was obtained from FisherScientific (Hampton, New Hampshire, USA). Lipofectamin 2000 transfection reagent and AlexaFluor 488 (AF488) dye were purchased from Life Technologies (Carlsbad, California, USA). CellTiter-Blue® Cell Viability Assay was purchased from Promega (Madison, Wisconsin, USA). Rotiphorese®10x SDS-PAGE buffer was obtained from Carl Roth (Karlsruhe, Germany) and mouse ApoE was purchased from Abexxa (Cambridge, UK). 2-(4-Isothiocyanatobenzyl) diethylenetriaminepentaacetic acid (p-SCN-Bn-DTPA) was purchased from Macrocyclics (Dallas, TX, USA) and Hs_GAPDH_1_SG and Hs_ACTB_2_SG QuantiTect primer assays were obtained from Qiagen (Venlo, Netherlands). Fresh human blood was obtained from Blutspendedienst des Bayerischen Roten Kreuzes (Munich, Germany) and EndolucinBeta-Lu^{3+} in aqueous 0.04M HCl solution was purchased from ITG Isotope Technologies Garching

GmbH (Garching, Germany). The following antibodies were used: Anti-LRP antibody, Goat Anti-Mouse IgG H&L (Alexa Fluor® 488) antibody and Mouse IgG1 kappa monoclonal antibody – isotype control (Abcam, Cambridge, UK). Amine-modified eGFP siRNA (5′ - pACCCUGAAGUUCAUCUGCACCACcg, 3′- ACUGGGACUUCAAGUAGAC GGGUGGC), human glyceraldehyde 3–phosphate dehydrogenase (GAPDH) siRNA (5′- pGGUCGGAGUCAACGGAUUUGGUCgt, 3′- UUCCAGCCUCAGUUGCCUAAACCAGC A), and scrambled siRNA (5′-pCGUUAAUCGCGUAUAAUACGCGUat, 3′ - CAGCAAUUAGCGCAUAUUAUGCGCAUAp) were purchased from Integrated DNA Technologies (Leuven, Belgium). Indication of modified nucleotides: "p" denotes a phosphate residue, lower case letters are 2′-deoxyribonucleotides, capital letters are ribonucleotides, and underlined capital letters are 2′-O-methylribonucleotides.

2.2 Synthesis and characterization of Nylon-3 random copolymer

Nylon-3 copolymer $NM_{0.2}/CP_{0.8}$ was synthesized via anionic ring-opening polymerization (ROP) of racemic β-lactams as previously described by our group [42]. In brief, monomers β-NM (cationic monomer) and CP (hydrophobic monomer) were prepared according to literature procedures. Random copolymers from β-NM and CP were synthesized following previously reported procedures [43]. The polymerization was conducted in the presence of 4-tert-butyl-benzoyl chloride (II) as the co-initiator and lithium bis(trimethylsilylamide) as the base to afford the desired polymers with an N-terminal tert-butyl-benzoyl group [44]. Deprotection of Boc-protected polymers was performed in trifluoroacetic acid (TFA) to obtain the TFA-salts of the desired polymers [45]. ^{1}H - NMR spectra of $NM_{0.2}/CP_{0.8}$ polymer was measured on a Bruker AV500 in deuterium oxide with 128 scans and molar masses were directly calculated via ^{1}H-NMR in D_2O performed with unprotected TFA salts by comparing the signal between 4.0 and 4.5 ppm (one proton per repeating unit p (p = n + m)), and the tert-butyl group of the end-group (1.33 ppm) [42].

2.3 Preparation of polyplexes

To prepare polymer-siRNA complexes (PXs), aqueous b-PEI as well as $NM_{0.2}/CP_{0.8}$ polymer stock solutions were diluted with freshly filtered 10 mM HEPES buffer (pH = 7.2) to predetermined concentrations, added to a defined amount of siRNA in a microcentrifuge tube to obtain PXs at various N/P ratios and incubated for 30 min to allow for stable PX formation. The N/P ratio is defined as the molar ratio between the polymer amine groups (N) and the

siRNA phosphate groups (P). The amount of polymer needed to obtain different N/P ratios was calculated according to following equation:

m (polymer in pg) = n siRNA (pmol) x M protonable unit (g/mol) x N/P x number of nucleotides siRNA

The protonable unit of each polymer was calculated by dividing its molar mass by the number of protonable primary amines present in each polymer as illustrated in Scheme 1. The number of nucleotides of 25/27mer siRNA is set to 52.

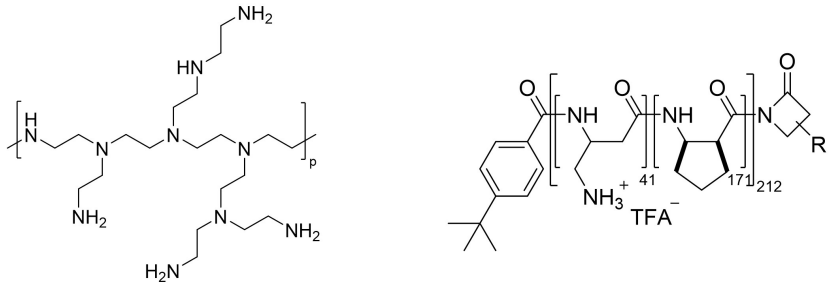

Branched PEI

M_n = 10 000 g/mol
$M_{n,\ protonable\ unit}$ = 43.07 g/mol

$NM_{0.2}/CP_{0.8}$

M_n = 28 000 g/mol
$M_{n,\ protonable\ unit}$ = 683 g/mol

Scheme 1. b-PEI and $NM_{0.2}/CP_{0.8}$ polymers used in this study.

2.4 Coating procedure

For coating of PXs, b-PEI and $NM_{0.2}/CP_{0.8}$ PXs were prepared as described above at preassigned N/P ratios. The PXs suspensions were divided into three microcentrifuge tubes; one tube was mixed with PS80 solution 1% to reach a final PS80 concentration of 0.1% (v/v) (PS80 precaoted samples) and the other samples were mixed with the same amount of 10 mM HEPES buffer (pH = 7.2) and stirred at 300rpm for 30 min. ApoE solution was mixed with the PS80 precoated PX solution (PS80 precaoted and ApoE overcoated samples: PS80+ApoE-PXs) and with one tube containing plain PXs to reach a final ApoE concentration of 12.5 µg/ml (ApoE coated samples: ApoE-PXs). The third tube was filled up to equal volumes with 10 mM HEPES buffer (pH = 7.2) (uncoated samples used as negative control: NC). Subsequently, all tubes were incubated for 1 h at room temperature (20 – 25°C) to allow protein adsorption in ApoE samples.

2.5 Size and Zeta Potential Analysis by Dynamic Light Scattering and Laser Doppler Anemometry

Particle size, polydispersity index (PDI) and zeta potential of PXs were measured using a Zetasizer Nano ZS (Malvern Instruments, Malvern, UK). PXs were formed at an N/P ratio of 8 and subsequently coated as described above. A total volume of 100 µl of each sample was added to a disposal cuvette (Malvern Instruments, Malvern; UK) and used for particle size and PDI measurements by dynamic light scattering (DLS) at 173° backscatter angle running 15 scans three times per sample. Zeta potentials were measured using a Zeta Cell (Zetasizer Nano series, Malvern, UK) containing a 7X dilution of another 100 µl sample aliquot by laser Doppler anemometry (LDA) with each run consisting of 30 scans. Results are expressed as mean ± standard deviation (n = 3).

2.6 Visualization of bound ApoE by sodium dodecylsulfate polyacrylamide gel electrophoresis (SDS-PAGE)

B-PEI and $NM_{0.2}/CP_{0.8}$ PXs were prepared at N/P 8 and coated as described above. PS80+ApoE-PXs and ApoE-PXs were purified from unbound ApoE analogous to centrifugation procedures optimized for a protein corona - PX approach as described in detail in *Subchapter III.2*. In brief, suspensions were centrifuged at 12.500g for 10 min, subsequently the supernatant was removed and the pellet was resuspended in 10 mM HEPES buffer (pH = 7.2) followed by an incubation period of 15 min to allow for equilibration. The centrifugation procedure was repeated to ensure removal of unbound ApoE. Samples (uncoated PXs, PS80+ApoE-PXs, ApoE-PXs) and ApoE reference solution (RS) were mixed with Pierce™ Lane Marker Reducing Sample Buffer and boiled at 95°C for 5 min to denaturate proteins in a Thermomixer (Eppendorf AG, Hamburg, Germany). A gel electrophoresis chamber Novex® Mini-Cell was prepared with a polyacrylamide-gel 10% placed in 10-fold diluted rotiphorese® 10x SDS PAGE buffer. The slots of the gel were loaded with 5 µl of PageRuler™ Plus Prestained protein ladder (10 to 250 kDA) as molecular marker, 25 µl ApoE RS as control and 25 µl of $NM_{0.2}/CP_{0.8}$ and b-PEI PX samples. The gel was run at 150 mV for 90 min, rinsed twice with deionized water , stained overnight in Comassie Brilliant Blue G solution to visualize the proteins and subsequently destained for 24 h in a mixture of 50% highly purificated water, 40% methanol and 10% acetic acid. The gel was scanned using a Biorad Chemidoc (Bio-Rad Laboratories, Hercules, CA, USA) and data were processed using Image Lab 6.0.1 software.

2.7 In vitro experiments

2.7.1 Cells and cell culture

U87 cells (human glioblastoma cell line) were cultured in EMEM media supplemented with heat inactivated FBS (10%) and Penicillin-Streptomycin (1%). All cells were subcultured, maintained and grown in an incubator in humidified air with 5% CO_2 at 37 °C.

2.7.2 Cytotoxicity measurements of PXs by CellTiter-Blue® Assay

Cytotoxicity of PXs was evaluated using a CellTiter-Blue® Cell Viability Assay Kit according to the manufacturer´s protocol based on the ability of living cells to convert a redox dye (resazurin) into a fluorescent end product (resorufin). Nonviable cells rapidly lose metabolic capacity and thus do not generate a fluorescent signal. In brief, 8.000 U87 cells per well were seeded in a transparent 96-well plate (FisherScientific, Hampton, NH, USA) and incubated for 24 h at 37 °C and 5% CO_2. B-PEI PXs were prepared at N/P ratios of 7 and 15 and $NM_{0.2}/CP_{0.8}$ PXs were prepared at N/P ratios of 5 and 15, respectively-and subsequently coated with ApoE as described above. After consumed medium was completely removed, 90 µL of fresh medium was added to each well and briefly mixed with 10 µL of uncoated PXs or ApoE $NM_{0.2}/CP_{0.8}$-PXs solutions. Pure 10 mM HEPES buffer was used as negative control and DMSO 25% in medium was utilized as a positive control. After a 24 h incubation period, 20 µL of CellTiter-Blue® substrate was added to each well followed by another incubation period of 4 h in the incubator. Subsequently, a volume of 100 µL of each sample was transferred to a white 96-well plate (FisherScientific, Hampton, NH, USA) and the fluorescence intensity was measured using a fluorescence plate reader (FLUOstar Omega, BMG Labtech, Ortenberg, Germany) at 560 nm and 590 nm excitation and emission wavelengths, respectively. The experiment was performed in triplicate, and the results are shown as mean ± standard deviation normalized to percentage of viable cells in comparison to untreated cells representing 100% viability.

2.7.3 Receptor expression of glioblastoma cells

The expression levels of LRP1 receptors on glioblastoma cells were evaluated by flow cytometry. Therefore, 100.000 U87 glioblastoma cells were transferred into an Eppendorf tube and spun down at 350g for 7 min and subsequently, the cell pellet was washed with PBS. The cell suspensions were mixed with Anti-LRP1 primary antibody and Mouse IgG1 monoclonal antibody as isotype control to reach a final concentration of 1 µg/ml, respectively. As negative control blank cells without antibody staining were used. All samples were vortexed and incubated for 30 min at 4° C, while protected from light. Subsequently, cells were spun down

at 300g for 5 min and washed with precooled PBS. After the third washing step, the supernatant was discarded and the cell pellet was resuspended in 100 µl of AF488-labeled secondary goat anti-mouse IgG H&L antibody solution, whereas cell pellets of control samples were resuspended in PBS buffer. After another incubation period of 30 min at 4° C, cells were washed three times via centrifugation at 400g for 5 mins, resuspended in 400 µL PBS with 2 mM EDTA and analyzed using an Attune R NxT flow cytometer (Thermo Fisher Scientific) by exciting the AF488-labeled secondary antibody at 488 nm and measuring the fluorescence signal with a 530/30 nm emission filter. The cells of all samples were gated according to morphology based on forward/sideward scattering. Samples were run in triplicates, each sample consisting of a minimum of 10.000 viable cells. Results are given as mean ± standard deviation (n = 3).

2.7.4 Quantification of cellular uptake into glioblastoma cells by Flow Cytometry

Flow cytometry was used to quantify the *in vitro* cellular uptake of b-PEI and $NM_{0.2}/CP_{0.8}$ PXs in glioblastoma cells as a function of PS80+ApoE or ApoE coating. Amine-modified siRNA was labeled with the fluorescent dye Alexa Fluor 488 (AF488) according to the manufacturer´s protocol and purified by ethanol precipitation and spin column binding as described previously [46]. U87 cells were seeded in 24 well plates, and for cell transfection, cell culture medium was replaced with FBS-free culture medium to prevent protein corona formation and thus potentially altered cellular internalization of PXs. B-PEI and $NM_{0.2}/CP_{0.8}$ PXs were prepared with 50 pmol siRNA-AF488 at previously optimized N/P ratios for cell transfection, specifically N/P 7 for b-PEI and N/P 5 for $NM_{0.2}/CP_{0.8}$ polyplexes and coated with PS80/ApoE as described above. Untreated cells and cells treated with free siRNA were used as negative controls. After a 24 h incubation period, incubation medium was removed, cells were washed with PBS and detached with 0.25% trypsin-EDTA. Samples were washed twice with PBS and resuspended in 500 µl PBS/2 mM EDTA. Additionally, trypan blue quenching was performed to exclude surface fluorescence signals of not completely internalized siRNA-complexes. Median fluorescence intensities (MFI) after quenching were analyzed using an Attune NxT Acoustic Focusing Cytometer (Thermo Fisher Scientific, Waltham, Massachusetts, USA) by exciting the siRNA-AF488 at 488 nm and measuring the fluorescence signal with a 530/30 nm emission filter. Samples were run in triplicates, each sample consisting of a minimum of 10000 viable cells. Results are given as mean ± standard deviation (n = 3).

2.7.5 GAPDH Knockdown measurements by real-time quantitative PCR (qPCR)

To investigate gene silencing of b-PEI and $NM_{0.2}/CP_{0.8}$ PXs with and without ApoE coating, 300.000 U87 glioblastoma cells per sample were seeded in a 6 well plate (Thermo Fisher Scientific) and grown for 24 h at 37 °C and 5% CO_2. After changing the medium with fresh FBS-free medium, cells were transfected with b-PEI PXs (N/P 7) and $NM_{0.2}/CP_{0.8}$ PXs (N/P 5), containing 100 pmol siRNA either directed against GAPDH (siGAPDH) or scrambled negative control siRNA (siNC), respectively. Samples were coated with ApoE as described above and uncoated samples were used as control. Additionally, Lipofectamine2000 lipoplexes were prepared according to manufacturer´s protocol with siGAPDH and siNC, respectively, and used as positive control. After 48 h incubation, cells were harvested, and total RNA was isolated with the PURELink RNA mini kit (Ambion, Kaufungen, Germany) according to the manufacturer´s protocol with additional DNase digestion. cDNA was synthesized from RNA and amplified with the high-capacity cDNA synthesis kit (Applied Biosystems, Waltham, MA, USA) and QuaniTect primer assays Hs_GAPDH_1_SG and Hs_ACTB_2_SG (Qiagen, Venlo, Netherlands) using a qTOWER real-time PCR thermal cycler (Analytik Jena, Jena, Germany). The RT-qPCR template consisted of an initial denaturation step of 10 min at 95° C and subsequent 40 cycles at 95° C for 15s for further denaturation followed by annealing and elongation step at 60° C for 1 min. Cycle threshold (Ct) values were obtained with the qPCRsoft software (Analytik Jena), and GAPDH gene expression was normalized by corresponding β-Actin expression for each sample. The relative quantity of transcripts was calculated according to the delta-delta Ct method. Results are given as mean ± standard deviation (n = 3).

2.7.6 Hemocompability of Polymers measured by Hemolysis and Erythrocyte Aggregation Assays

The hemocompatibility and endosomolytic activity of polymers was investigated by red blood cell (RBC) hemolysis and aggregation assays analogous to previous described protocols [47]. Briefly, human erythrocytes were isolated from fresh human blood by centrifugation at 900g for 10 min. RBCs were washed three times with 150 mM NaCl until the supernatant was clear and colourless. Erythrocytes were again centrifuged at 900g for 10 mins, and the supernatant was replaced with PBS buffer at defined pHs that mimic extracellular (pH 7.4) and late endosomal (pH 5.4) environments. A volume of 10 µl of 20X b-PEI and $NM_{0.2}/CP_{0.8}$ polymer solutions in different concentrations (1 mg/ml – 0.0078 mg/ml) was distributed in a 96-well plate. As controls, 20% Triton X-100 (100% lysis) and pure PBS (0% lysis) were used. A volume of 190 µl of the RBC suspension was added to each well, and the plate was incubated

for 30 min at 37 °C. RBCs were removed by centrifugation (500g, 5 min) and supernatant was investigated spectroscopically in a transparent FluoroNunc 96-well plate (FisherScientific, Hampton, NH, USA) by measuring the absorbance of released hemoglobin at 541 nm by using a multimode microplate reader (Tecan Spark, Tecan Group, Männedorf, Switzerland). Measurements were performed in triplicate, and the results are shown as mean values (n = 3). The degree of hemolysis induced by polymers (% hemolysis) was calculated according to the following equation:

$$\%\, Hemolysis = \frac{Hb - Hb0}{Hbtot}\, x\, 100$$

Hb is the amount of hemoglobin found in the sample, Hb0 is the amount of basal hemoglobin found in the negative control samples and Hbtot is the amount of hemoglobin after 100% hemolysis. In addition, to evaluate the aggregation of RBCs after treatment, images of them were taken after the centrifugation step using a Keyence BZ8100 Fluorescence microscope (Keyence, Osaka, Japan) equipped with a Nikon SPLan Fluor 10x/0.45 objective (Nikon, Japan) in the brightfield mode.

2.8 In vivo biodistribution experiments

2.8.1 Covalent modification of siRNA with pBn-SCN-Bn-DTPA

In an effort to examine the *in vivo* biodistribution of b-PEI and $NM_{0.2}/CP_{0.8}$ PXs in SWISS mice, siRNA was radioactively labeled with ^{177}Lutetium (^{177}Lu) following an adjusted protocol previously described by Jones et al. [48]. At first, amine-modified EGFP siRNA (siEGFP) was covalently coupled with the amine-reactive chelator p-Bn-SCN-Bn-DTPA according to a previously described method [49]. Briefly, 5.11 mg siEGFP was dissolved in a centrifuge tube in 2 ml RNase free water, 100 µl of 0.1 M $NaHCO_3$ solution were added and siEGFP solution was subsequently mixed with p-Bn-SCN-Bn-DTPA dissolved in DMSO. After thoroughly vortexing the tube and an incubation period of 6 h, siRNA-DTPA was precipitated by adding absolute ethanol. The siRNA-DTPA complex was isolated from free p-Bn-SCN-Bn-DTPA with the absolutely RNA miRNA Kit (Agilent, Santa Clara, CA, USA) according to manufacturer´s protocol. Concentration measurement of siRNA was performed by measuring the absorption at 280 nm with a spectrophotometer (Nanodrop One, Thermo Fisher Scientific, Waltham, MA, USA). The coupling degree after purification was determined by additional performed quantification of DTPA in a nonradioactive assay described by Pippin et al. [50]. Briefly, absorption of an yttrium(III)-arsenazo(III)-complex was measured at 652 nm with a UV/Vis

spectrophotometer (UV-1600PC, VWR, Ismaning, Germany), and sample DTPA content was calculated with the help of a calibration curve since the absorption of the complex decreases after addition of DTPA.

2.8.2 Labelling and purification

Radiolabelling of the p-SCN-Bn-DTPA-coupled siRNA with ^{177}Lutetium (^{177}Lu) was accomplished at room temperature in 0.4 M sodium acetate buffer (pH = 5) for 30 mins. The siRNA-Lutetium mixture was added to an equilibrated Illustra™ NAP™ 10 column Sephadex G-25 (GE Healthcare, Chicago, ILL, USA) for purification and elution. Fractions were collected and counts per minute were determined by a scintillation counter. The fraction with the highest radioactive signal was additionally investigated by HPLC analysis (Agilent 1100 Series, SEC column: TSK gel Super SW mAb HR) to ensure the presence of siRNA and the absence of free DTPA. The quantification of the siRNA in the final mixture was investigated spectrophotometrically with a UV visible sprectrophotometer (Cary 50 Conc, Varian) by measuring the absorbance at 260 nm.

2.8.3 In vivo biodistribution

All animal trials were approved by the Animal Care and Use committees at the University of Heidelberg, Heidelberg, Germany and the responsible government agency (Regierungspräsidium Karlsruhe, Germany, reference number 35-9185.81/G-111/16; approval date: 22 June 2016). For *in vivo* experiments, polyplexes with ^{177}Lu-labeled siRNA were prepared at N/P ratio of 7 with b-PEI polymer and at N/P ratio of 5 with $NM_{0.2}/CP_{0.8}$ polymers, respectively. One part of $NM_{0.2}/CP_{0.8}$ PX was additionally coated with mouse ApoE as described above. Free ^{177}Lu-labeled siRNA as control and PXs samples were injected intravenously to the tail vein of SWISS mice (2 nmol siRNA/animal), and biodistribution was investigated 1 h post injection. To this end, the animals were sacrificed, major organs were removed and weighed and the radioactivity of each sample was measured using a Cobra Auto γ-Counter (Packard BioScience Co., Meriden, CT, USA) in comparison with standards. The tissue-associated activity was related to the total injected dose (ID) and calculated as a percentage of the total injected dose per gram of the respective organ (ID%/g).

2.9 Statistics

Unless otherwise stated, results are given as mean value ± standard deviation. One-way ANOVA with Bonferroni multiple comparison test and two-way ANOVA were performed in

GraphPad Prism software (Graph Pad Software, La Jolla, CA) to calculate p-values at 95% confidence.

3. Results and Discussion

3.1 Synthesis and characterization of Nylon-3 random copolymer

$NM_{0.2}/CP_{0.8}$ polymer was prepared with hydrophobic and hydrophilic ß-lactams via anionic ring-opening polymerization (ROP) as described above. The synthesis led to a nylon-3 copolymer that contains randomly arranged hydrophobic and cationic subunits in a 1:4 ratio. The hydrophobic monomer was cyclopentadienyl ß-lactam (CP), the cationic monomer was a ß-lactam without a methyl group (NM). Molecular weight and subunit ratios were determined by ^{1}H-NMR spectroscopy as reported previously [42]. In this study, performed by our group, suitability for siRNA delivery into glioblastoma cells in comparison to various other nylon-3 polymers has been described and $NM_{0.2}/CP_{0.8}$ polymer was shown most promising regarding siRNA delivery into glioblastoma cells due to the high hydrophobic content [42]. Furthermore, since it was shown that hydrophobic moieties are able to induce adsorption of ApoE, the highly hydrophobic $NM_{0.2}/CP_{0.8}$ polymer was selected in this study to investigate the ApoE adsorption on $NM_{0.2}/CP_{0.8}$ PXs in comparison to cationic b-PEI PXs in an effort to examine the influence of ApoE adsorption on siRNA delivery efficiency of PXs across the BBB.

3.2 Size and Zeta Potential Analysis of PXs by Dynamic Light Scattering and Laser Doppler Anemometry

In order to investigate the hydrodynamic diameters, polydispersity indices and zeta potentials of uncoated particles in comparison to coated PXs, DLS and LDA measurements were performed. Particle size and charge are two major parameters of NPs that affect intracellular uptake and transfection ability. Therefore, the first step of our study was to investigate the influence of modifying the particles with ApoE or PS80+ApoE on the physicochemical characteristics of the PXs. For PS80 coating, we initially tested the optimal PS80 concentration by incubating the PXs with various PS80 concentrations ranging from 0.01% to 0.5% PS80 with subsequent measurement of sizes and PDIs of PS80-PXs by DLS. As illustrated in Figure S1 (Supplementary Material), $NM_{0.2}/CP_{0.8}$ PXs sizes were not affected at all by PS80 coating at the selected concentrations, whereas in the case of b-PEI PXs, only PS80 concentrations of 0.1% and higher led to appropriate particle sizes with low PDI values which were comparable to those of the reference particles. In the case of $NM_{0.2}/CP_{0.8}$ PXs, we suggest, that interactions

between hydrophobic CP parts of the polymer with oleic acid groups of PS80 molecules resulted in stable particles over a wide PS80 concentration rage. Furthermore, in the case of b-PEI, it is conceivable that low surfactant concentrations led to unstable aggregates due to interactions between cationic amino groups of the PEI molecule with carboxyl groups of the PS80 molecule before the optimal concentration for polyplex stabilization was reached. Moreover, excess surfactant at concentrations above the optimum contributed to self-assembly of the molecule chains in micelles, which increased the PDI values in the DLS measurement [51]. Therefore, a concentration of 0.1% PS80 was chosen for further experiments. For b-PEI PXs, as shown in Figure 1, coating with ApoE and PS80+ApoE resulted in a slight increase in particle size from 108.6 nm for the uncoated sample to 116.0 nm and 118.2 nm for the ApoE coated sample and the PS80+ApoE coated sample, respectively. The PDI values were in the same range for all b-PEI samples, in detail they amounted 0.095 for uncoated b-PEI PXs, 0.081 for ApoE b-PEI PXs and 0.120 for PS80+ApoE b-PEI PXs. The finding for the uncoated b-PEI PXs is in line with previously published results [52, 53]. The uncoated and ApoE coated $NM_{0.2}/CP_{0.8}$ PXs revealed similar sizes of 123.9 nm and 123.3 nm, respectively, whereas the size for PS80+ApoE coated PXs increased in comparison to other samples to 194.8 nm. The same trend was also observed for the PDI values of $NM_{0.2}/CP_{0.8}$ PXs as they increased from 0.260 (uncoated PXs) and 0.272 (ApoE coated PXs) to 0.401 for PS80+ApoE coated samples. The finding for uncoated $NM_{0.2}/CP_{0.8}$ PXs is in line with former studies [42]. The zeta potential of uncoated b-PEI PXs was +30.9 mV and decreased with ApoE coating to +28.23 mV and to +26.10 mV after PS80+ApoE coating. Uncoated $NM_{0.2}/CP_{0.8}$ PXs showed a zeta potential of +21.7 mV that also slightly decreased after ApoE and PS80+ApoE coating to +20.27 mV and +19.9 mV, respectively.

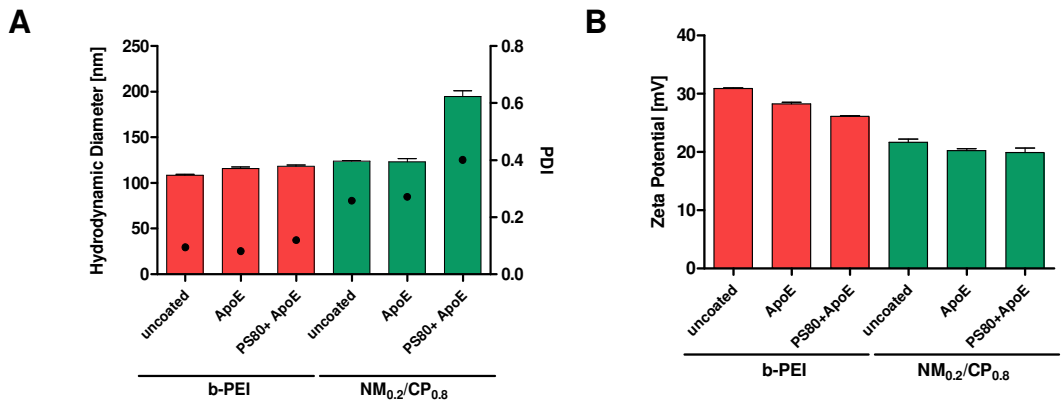

Figure 1. Hydrodynamic diameters (left y-axis) and polydispersity indices (PDI, right y-axis) (**A**) and Zeta potentials (**B**) of uncoated PXs, ApoE PXs and PS80+ApoE PXs formed with b-PEI and $NM_{0.2}/CP_{0.8}$ polymers at N/P ratio of 7 and 5, respectively. (Data points indicate mean ± SD, n = 3).

Since human ApoE has an isoelectric point of 5.55 [54] and is thus negatively charged at a pH of 7.2, it was concluded that ApoE molecules are adsorbed on the surface of positively charged PXs by electrostatic interactions and, in the case of $NM_{0.2}/CP_{0.8}$ PXs, additionally by hydrophobic interactions what might lead to the measurable size increase. ApoE is responsible for the redistribution of lipids among cells and tissues as parts of lipoproteins in the body and therefore bears a lipid binding region in the C-terminal domain [55]. For $NM_{0.2}/CP_{0.8}$ PXs, precoating with PS80 resulted in a higher size increase than for b-PEI PXs, which might occur due to more efficient interactions between PS80 and $NM_{0.2}/CP_{0.8}$ PXs. The zeta potential decrease after coating with ApoE and PS80+ApoE supports the assumption that negatively charged ApoE is adsorbed on the PXs' surface. In summary, coating of ApoE and PS80+ApoE showed little effect on the particle size, size distribution and zeta potentials of the PXs, resulting in particles with appropriate sizes and surface charges for further experiments.

3.3 Evaluation of bound ApoE by sodium dodecylsulfate polyacrylamide gel electrophoresis (SDS-PAGE)

SDS-PAGE is a commonly used electrophoretic technique for separation and analysis of proteins based on their molecular weight. Protein bands within the gel can be visualized by a colorimetric staining such as Comassie [56]. SDS-PAGE was hence performed to investigate whether and to which extent ApoE is indeed adsorbed on different formulations. Therefore b-PEI and $NM_{0.2}/CP_{0.8}$ PXs were coated with ApoE and PS80+ApoE, respectively as described above. Coated PXs were purified via centrifugation as described above to remove free and unbound ApoE. Purified PXs were resuspended after the last centrifugation step and 25 µl of each sample (uncoated, ApoE coated and PS80+ApoE coated b-PEI and $NM_{0.2}/CP_{0.8}$ PXs) and ApoE RS (34.2kDa) as reference, were loaded and run on a polyacrylamide gel for visualization of proteins by staining with Comassie Brilliant Blue G.

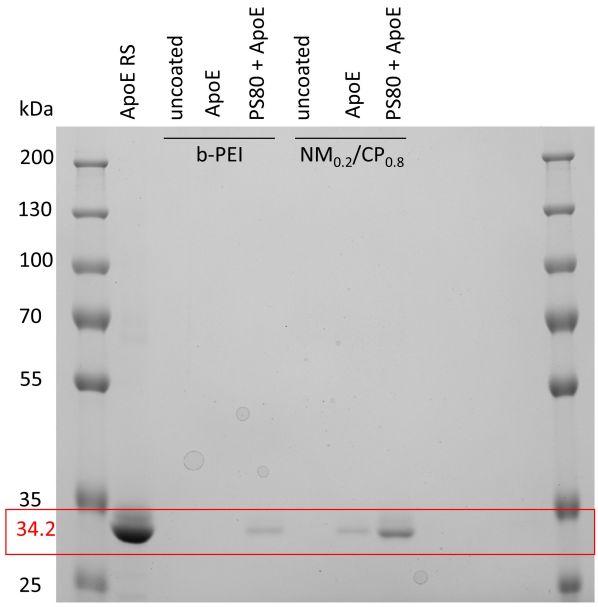

Figure 2. ApoE bound to $NM_{0.2}/CP_{0.8}$ and b-PEI polyplexes with and without PS80 precoating evaluated by SDS-PAGE performed with a polyacrylamide-gel 10%. The slots of the gel were loaded with a molecular marker (10 to 250 kDa), ApoE RS (34.2 kDa) as reference, uncoated PXs, ApoE-PXs and PS80+ApoE-PXs samples. Proteins were visualized by staining with Comassie Brilliant Blue G.

As displayed in Figure 2, no bound ApoE was detected by SDS-PAGE on ApoE coated b-PEI PXs, whereas a slight band of ApoE was visible for PS80 precoated b-PEI PXs. For $NM_{0.2}/CP_{0.8}$ PXs a slight band of ApoE appeared for ApoE coated NPs, while a more distinct ApoE band was observed for PS80 precoated samples, indicating that a larger amount of ApoE was attached to PS80+ApoE $NM_{0.2}/CP_{0.8}$ PX samples. These results are supported by the more visible size increase of PS80 precoated samples and led to the conclusions that the coating of PXs with ApoE was generally possible but the binding affinities of ApoE strongly depend on the underlying NP material and its modification, which is in line with previous reports. A former study of Blank assessed bound proteins on model polystyrene carriers as a function of their modification after incubation in plasma and described that on hydrophobically modified particles mainly apolipoproteins were found [57]. Subsequently, it was described for a wide variety of NPs that hydrophobicity facilitates the binding of specific proteins, such as ApoE [58]. Herein, we suggest that the C-terminal domain of the ApoE molecule that contains a lipid binding region [59] can directly interact with the hydrophobic CP subunits of the $NM_{0.2}/CP_{0.8}$ PX. Moreover, several other studies described that successful binding of ApoE was achieved by a surfactant-based approach in which poloxamers or PS were used as hydrophobic anchor [4]. Our results for PXs are in line with the literature, as adsorption of ApoE was not detected on cationic b-PEI PXs, while ApoE was found, albeit to a small extent, on more hydrophobic $NM_{0.2}/CP_{0.8}$ PXs. Moreover, PS80 precoating led for both, b-PEI and $NM_{0.2}/CP_{0.8}$ PXs to an

adsorption of ApoE. Herein, we hypothesize that the higher amount of ApoE on $NM_{0.2}/CP_{0.8}$ PXs can be explained by more efficient interactions with PS80. PS80 might adsorb with its hydrophobic part (oleic acid) to the CP subunits of the $NM_{0.2}/CP_{0.8}$ PXs, whereas the hydrophilic part ((poly(ethylene oxide) (PEO) sorbitan) protrudes into the dispersion medium (Figure 3) and facilitates the binding of ApoE, as similarly described for poloxamers by the group of Blunk et al. [57]. Taken together, SDS-PAGE results illustrated that functionalization of PXs with ApoE was successful by direct coating of $NM_{0.2}/CP_{0.8}$ PXs and by utilizing the surfactant-based approach with PS80 for both, b-PEI and $NM_{0.2}/CP_{0.8}$ PXs.

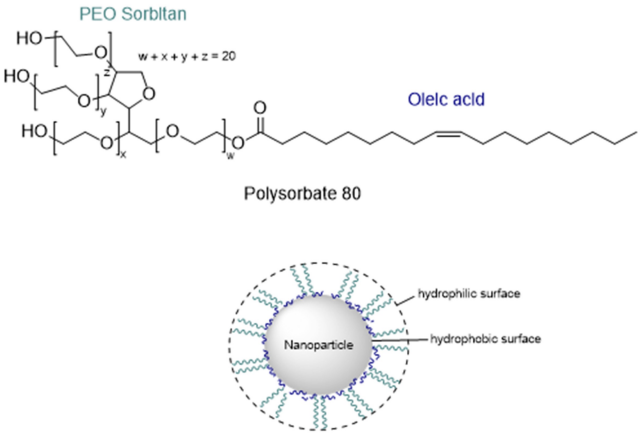

Figure 3. Polysorbate-coating of hydrophobic nanoparticles [adopted from [4]].

3.4 In vitro experiments

3.4.1 Quantification of cellular uptake into glioblastoma cells by flow cytometry

As successful coating of PXs with ApoE was confirmed, the next step was to investigate whether this may lead to selective uptake of NPs in an LDL and LRP1-receptor bearing human glioblastoma cell line. ApoE is a component in lipoprotein classes VLDL and chylomicrons and mediates lipid transport and delivery into cells mainly via LDL and LRP1 receptor-mediated pathways [60]. The N-terminal domain of the ApoE molecule contains a lysine- and arginine-rich receptor binding site, and interactions of this domain with the respective receptor initiate endocytotic uptake of the particles into cells [61]. LDL receptor expression of the U87 glioblastoma cell line used in this study was measured elsewhere [62] and expression of LRP1 receptors was confirmed by antibody staining and subsequent flow cytometry measurements as described above and shown in Figure S2 (Supplementary Material). Trypan blue quenching, which was additionally performed in order to exclude extracellular fluorescent signals caused by cell surface-bound siRNA, resulted in insignificantly lower MFI values for all tested b-PEI PXs, indicating that inconsiderable amounts of PXs were only bound to the outer cell

membranes, whereas significantly lower MFIs values were detected for all tested $NM_{0.2}/CP_{0.8}$ PXs, pointing out that $NM_{0.2}/CP_{0.8}$ PXs s adhered more strongly to the cells due to hydrophobic interactions (Figure S3, Supplementary Material). In order to exclude signals caused by surface-bound siRNA when quantifying cellular uptake of formulations, MFI values are presented after trypan quenching. As illustrated in Figure 4, PS80 coated particles showed, against our expectations, no differences in MFI values in comparison to negative control samples with free siRNA and therefore no measurable cellular internalization into glioblastoma cells. The MFI value for negative control was 646.5, for PS80+ApoE- b-PEI PXs 680.1 and for PS80+ApoE-$NM_{0.2}/CP_{0.8}$ PXs 651.8, respectively. Uncoated $NM_{0.2}/CP_{0.8}$ PXs (MFI =14852) revealed a slightly higher cell entry capability than b-PEI PXs (MFI = 8548), what goes in line with literature [63]. The most efficient siRNA delivery in glioblastoma cells was observed by the ApoE coated PXs, where significantly increased cellular uptake was detected in comparison to the uncoated particles. This effect, however, was even more pronounced for $NM_{0.2}/CP_{0.8}$ PXs than for b-PEI PXs. The MFI value for ApoE coated b-PEI PXs was 9957 (uncoated: 8548) and for ApoE coated $NM_{0.2}/CP_{0.8}$ PXs an average MFI value of 25216 (uncoated: 14852) was observed.

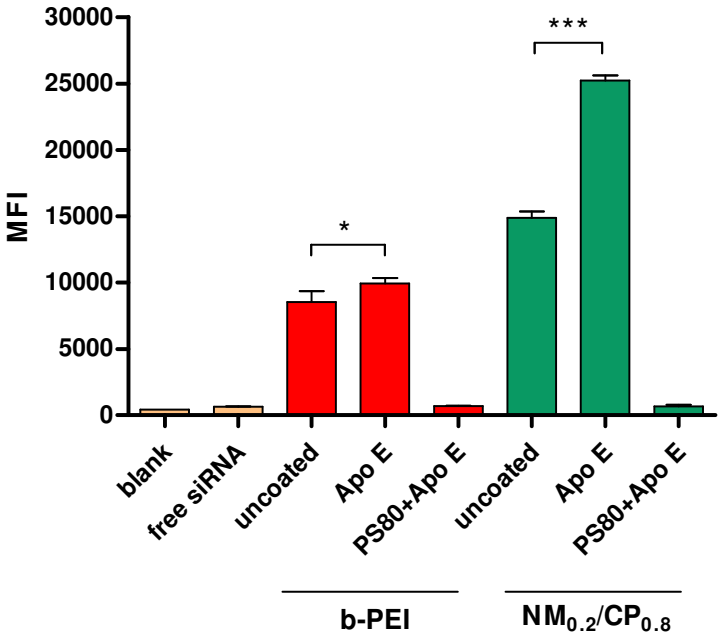

Figure 4. Cellular uptake of uncoated PXs, ApoE PXs and PS80+ApoE PXs (b-PEI PXs: N/P ratio = 7 and $NM_{0.2}/CP_{0.8}$ PXs: N/P ratio = 5) after 24 h incubation as quantified by flow cytometry performed with trypan quenching and presented as median fluorescence intensitiy (MFI). Negative control: untreated cells (blank) and with free siRNA treated cells. (Results are shown as mean ± SD, n = 3, one-way ANOVA with Bonferroni post-hoc test, * $p < 0.05$, *** $p < 0.005$).

The obtained results regarding the cellular uptake of PS80+ApoE PXs are not in line with our expectations that arose from the SDS-PAGE result, which indicated successful binding of ApoE on PXs especially on PS80 precoated particles as presented in 3.3. As no cellular uptake was detected for both, b-PEI and $NM_{0.2}/CP_{0.8}$ PS80 precoated samples, it may be speculated that PS80-ApoE modified PXs were destabilized in the complex environment of cell culture medium that was required for the uptake experiment, so that no functional particles were present to enter the cells. To exclude the possible influence of ApoE coating, we repeated the experiment exemplarily using PS80 precoated b-PEI PXs and uncoated b-PEI PXs. As displayed in Figure S4 (Supplementary Material), PS80 precoated b-PEI PXs were not able to enter glioblastoma cells in comparison to uncoated b-PEI PXs confirming that PS80 coating tremendously reduced the cellular uptake ability of PXs. Our hypothesis that in particular hydrophobic $NM_{0.2}/CP_{0.8}$ PXs constitute a promising system for the PS80-ApoE targeting approach, that were supported by promising SDS-PAGE and DLS results, was hereby disproved. Consequently, PS80 caoting does not seem to be a suitable approach for PXs in general, whereby the exact impact of PS80 caoting on PX destabilization remains unclear and gives rise to investigate this question in future studies. Consequently, PS80 precoated samples were not considered further in the following experiments. Notwithstanding, the uptake data revealed that modification of PXs with ApoE alone significantly enhanced the cellular internalization ability of both b-PEI and $NM_{0.2}/CP_{0.8}$ PXs, whereas this effect was more pronounced for $NM_{0.2}/CP_{0.8}$ PXs. Therefore, we suggest that adsorbed ApoE on the surface of the PXs interacted with LDL and LRP1-receptors and consequently induced selective receptor-mediated endocytosis of PXs into glioblastoma cells [64]. This goes in line with recently described data in the literature. Particularly the group of Kreuter et al. has described that coating of analgesic hexapeptide dalargin-loaded PBCA NPs with ApoE or ApoB alone mediated the delivery of the cargo across the BBB after intravenous injection. However, in their studies ApoE/B overcoating after PS80 precoating induced an even higher effect in the *in vivo* experiment [20]. Further, the group of Mulik et al. has shown that PBCA NPs loaded with the drug curcumin were more efficiently taken up by SH-SY5Y cells after caoting them with ApoE in comparison to plain PBCA NPs [65, 66]. These results underline our finding that ApoE coating of NPs alone could induce receptor-mediated endocytosis and that this approach can be translated from solid NPs to dynamic systems such as PXs at least in an *in vitro* setting. Interestingly, and in line with SDS-PAGE results, ApoE-$NM_{0.2}/CP_{0.8}$ PXs were more efficiently taken up in comparison to ApoE-treated b-PEI PXs what may be an indication that a higher amount of ApoE bound on $NM_{0.2}/CP_{0.8}$ PXs is able to induce more efficient receptor-mediated

cellular uptake. In conclusion, our results indicate that a surfactant-based targeting approach with PS80 precaoting for enhanced ApoE binding does not constitute an appropriate strategy for dynamic systems such as PXs due to suspected destabilization under *in vitro* conditions. However, direct caoting of PXs with ApoE resulted in remarkably increased receptor-mediated cell uptake, particulary for $NM_{0.2}/CP_{0.8}$ PXs, rendering them into highly promising candidates for ApoE-induced brain delivery.

3.4.2 GAPDH Knockdown measurements by PCR

Next, we investigated whether the significantly higher internalization of ApoE modified PXs correlated with the gene silencing of a targeted gene. Therefore, glioblastoma cells were transfected with ApoE-b-PEI PXs and ApoE-$NM_{0.2}/CP_{0.8}$ PXs prepared with siRNA against GAPDH (siGAPDH) or scrambled negative control siRNA (siNC), respectively. Uncoated samples were used as negative control and Lipofectamine 2000 lipoplexes were utilized as positive control samples. GAPDH gene expression was quantified by real time PCR (RT-qPCR) and normalized by β-actin gene expression and normalized to the values obtained after transfection with negative control siRNA for each sample. As displayed in Figure 5, significant downregulation of GAPDH expression was observed for uncoated $NM_{0.2}/CP_{0.8}$ PXs (knockdown of 34%) and more pronouncedly for ApoE-$NM_{0.2}/CP_{0.8}$ PXs (knockdown of 46%) compared with negative control samples. In contrast, there was no significant difference of GAPDH expression among b-PEI PX (uncoated and ApoE coated) treated cells and their respective negative controls. Positive control samples displayed a GAPDH gene silencing effect of 36% for Lipofectamine lipoplexes, reflecting the poor transfectability of U87 glioblastoma cells in general.

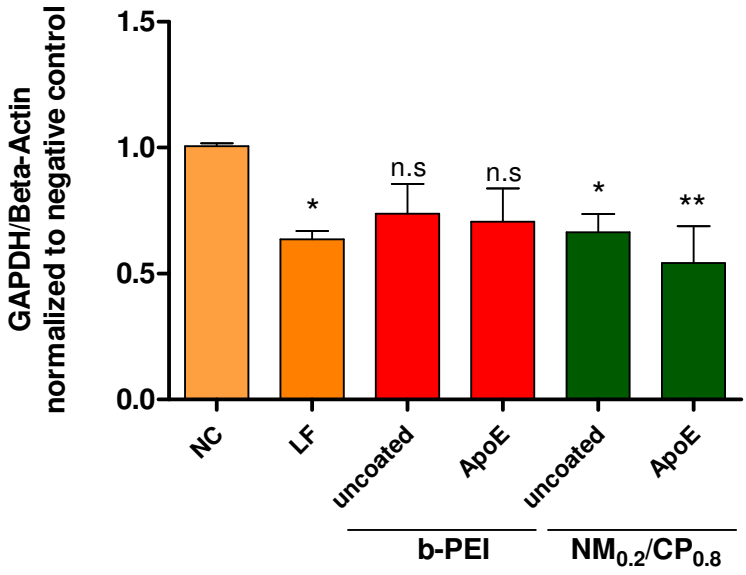

Figure 5. GAPDH knockdown in the human glioblastoma cell line U87 as quantified by RT-PCR 48 h after transfection with uncoated and ApoE coated b-PEI and $NM_{0.2}/CP_{0.8}$ PXs prepared with GAPDH siRNA or scrambled control siRNA as respective negative control (NC). The positive control consisted of Lipofectamine (LF) 2000 lipoplexes. The expression of GAPDH was normalized to the expression of β-actin and to cell samples transfected with the respective negative control PX. (Data points indicate mean ± SD, n = 3, one-way ANOVA with Bonferroni post-hoc test, n.s (= not significant) $p > 0.05$, *$p < 0.05$ **$p < 0.01$).

Unmodified b-PEI PXs can undergo endocytosis by electrostatic interactions between their positive surface charge and the negative charge of the cellular membrane, however, the internalization of b-PEI PXs was not sufficient to induce significant GAPDH gene silencing effects. A lack in GAPDH knockdown ability was also observed for ApoE modified b-PEI particles, implying that even receptor-mediated endocytosis of b-PEI particles did not lead to significant gene knockdown effects. This goes in line with literature, as high molecular weight b-PEI was shown to exhibit, besides low toxicity, poor transfection efficiencies [67]. In contrast, unmodified $NM_{0.2}/CP_{0.8}$ PXs demonstrated efficient gene knockdown, leading to the assumption that additional hydrophobic interactions with the outer cell membrane as well as with the endosomal membrane might have beneficial effects on the siRNA amount present in the cytoplasm, what is a prerequisite for successful gene silencing. As described in literature, endosome disruption can be caused by cationic as well as hydrophobic moieties of polymeric NPs, which are both present in $NM_{0.2}/CP_{0.8}$ polymers [68]. However, in accordance with cellular uptake results, ApoE modification of $NM_{0.2}/CP_{0.8}$ PXs mediated the most efficient gene knockdown effect, comparable to the commercially available transfection reagent Lipofectamine 2000, indicating that receptor-mediated endocytosis in combination with

favorable characteristics of the $NM_{0.2}/CP_{0.8}$ PXs provided most suitable conditions to induce sequence-specific gene silencing in a cell line, which is generally described to be hard to transfect [42]. Overall, the results presented here demonstrated efficient knockdown ability of ApoE-modified $NM_{0.2}/CP_{0.8}$ PXs, providing further evidence for the applicability of the targeted siRNA delivery system for potential treatment of brain diseases.

3.4.3 Cytotoxicity measurements

3.4.3.1 Cytotoxicity measurements of PXs by CTB Assay

In order to test the cytotoxicity of PXs, CTB assays were conducted with U87 cells that had been incubated for 24 h with uncoated b-PEI and $NM_{0.2}/CP_{0.8}$ PXs and ApoE $NM_{0.2}/CP_{0.8}$ PXs at two different N/P ratios. Thereby, lower N/P ratio of 5 (b-PEI) and 7 ($NM_{0.2}/CP_{0.8}$ PXs) represented treatment relevant conditions in *in vitro* experiments. The CTB assay is based on the ability of viable cells to reduce the nonfluorescent resazurin to fluorescent resorufin mainly by mitochondrial and cytosolic enzymes, while dead cells rapidly lose this capacity once their membrane integrity has been compromised [69]. All tested formulations resulted in favorable toxicity profiles, even at the higher N/P ratio of 15, as no considerable influence on cell viability was observed after PX treatment (Figure 6).

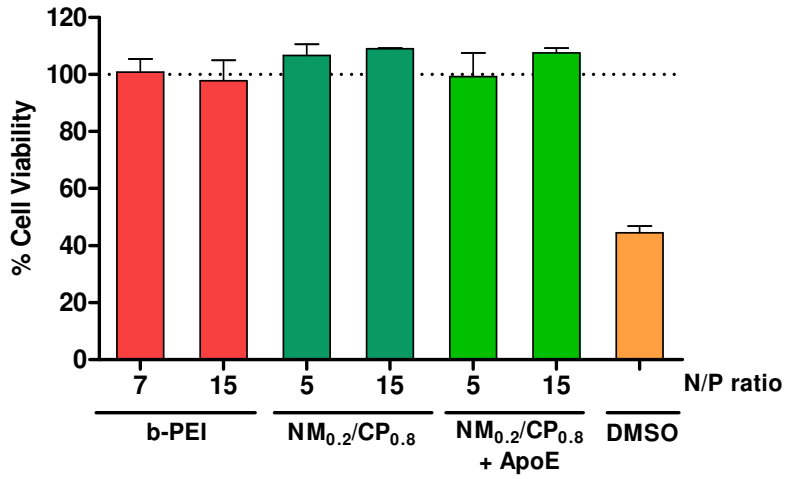

Figure 6. Cell viability as determined by CTB assay for formulated polyplexes at relevant N/P ratios after an incubation period of 24 h. DMSO 25% was used as positive control. (Results are shown as mean ± SD as percentage of viable cells in comparison to untreated cells representing 100% viability, n = 3).

A very low but still negligible effect on cell viability was demonstrated solely by b-PEI PXs at N/P 15 (97.82%) and ApoE $NM_{0.2}/CP_{0.8}$ PXs at N/P 5 (99.28%). The positive control of 25% DMSO resulted in a survival rate of 55.54%. Summing up, these data showed that neither b-PEI PXs nor $NM_{0.2}/CP_{0.8}$ PXs with or without ApoE coating are expected to have a noticeable

effect on U87 cell viability and therefore, are well tolerated in *in vitro* experiments. As nylon-3 polymers have been investigated in order to design an advanced delivery system with excellent compatibility, our results are in line with previous studies, that revealed high tolerability combined with efficient transfection efficacies especially for highly hydrophobic polymers [42, 63]. The functionalization of the $NM_{0.2}/CP_{0.8}$ PXs with ApoE was shown to not affect the cell tolerability in a significant manner. Although broadly used high molecular weight b-PEI is known for its high cellular toxicity due to its high cationic charge density [67], our findings demonstrated that b-PEI PXs do not exhibit significant cellular toxicity in our specific experimental setting. Altogether, these observations are especially important for future *in vivo* experiments as they demonstrate that our delivery systems are well tolerated after internalization into cells.

3.4.3.2 Hemocompability of polymers evaluated by Hemolytic and Erythrocyte Aggregation assay

The hemocompability of b-PEI and $NM_{0.2}/CP_{0.8}$ polymers was investigated by hemolysis and erythrocyte aggregation assays. These assays are an indispensable initial step in evaluating the blood compatibility of NPs in advance of administering the materials intravenously in animals or humans. Several studies have reported a good correlation between the results of *in vitro* hemolysis assays and *in vivo* toxicity studies identifying hemolysis as a toxic effect [70]. Hemolysis occurs due to disruption of erythrocytes leading to the release of intracellular components such as hemoglobin, which can be measured spectroscopically. We tested 1 mg/ml as the highest polymer concentration assuming that the test concentration *in vivo* will not exceed this concentration. For comparison, in *in vitro* studies polymer concentrations of 0.011 mg/ml of b-PEI polymer to obtain PXs with N/P 7 and 0.203 mg/ml of $NM_{0.2}/CP_{0.8}$ polymers to obtain PXs with N/P 5 were used. The results of the hemolysis assays are represented in Figure 7 and show that both formulations revealed no hemolysis at concentrations from 0.5 to 0.00781 mg/ml as the measured values were in the same range as the Hb0 value that represents the amount of basal hemoglobin found in the negative control sample. As shown in Figure 7A, b-PEI polymer displayed slight hemolytic activity at the highest concentration of 1 mg/ml, namely a final hemolysis of 0.58%. At the same polymer concentration, as shown in Figure 7B, $NM_{0.2}/CP_{0.8}$ polymers exhibited slightly higher hemolysis of 1.60%. Nevertheless, these values are still tolerable since substances are classified as non-hemolytic when hemolysis remains below 2% [71].

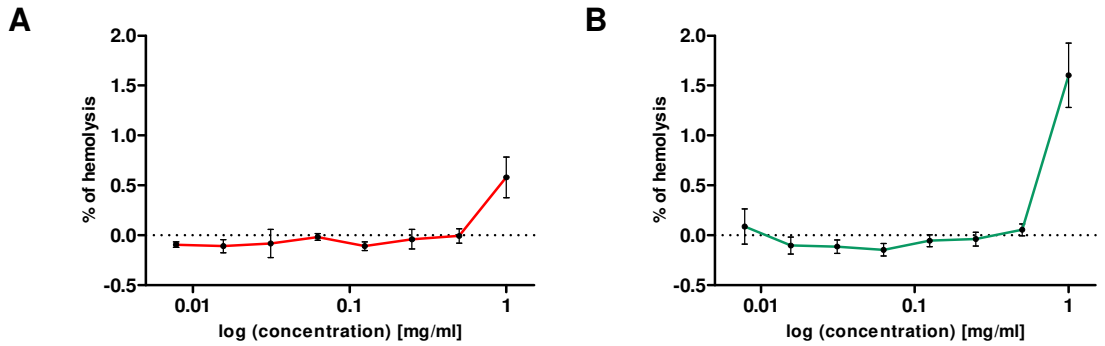

Figure 7. Hemolysis of human erythrocytes at pH 7.4 induced by b-PEI (**A**) and $NM_{0.2}/CP_{0.8}$ polymers (**B**) as a function of log concentration values. (Results are shown as mean ± SD as percentage of hemolysis in comparison to Triton-X treated cells representing 100% hemolysis, Hb0 represents the amount of basal hemoglobin found in the negative control samples, n = 3).

The erythrocyte aggregation assay allowed only semiquantitative estimations about the hemocompatibility of the polymers. Results in this study are displayed in Figure 8. Microscopic pictures of the erythrocytes are exemplarily shown for the concentrations of 1 mg/ml, 0.25 mg/ml and 0.01563 mg/ml for b-PEI and $NM_{0.2}/CP_{0.8}$ polymers, as well as for PBS as negative control. PBS control samples did not induce any aggregation of the erythrocytes, whereas polymer solutions, depending on the concentration, caused a slight (0.25 mg/ml and 0.01563 mg/ml) to strong (1 mg/ml) aggregation of the RBCs, respectively.

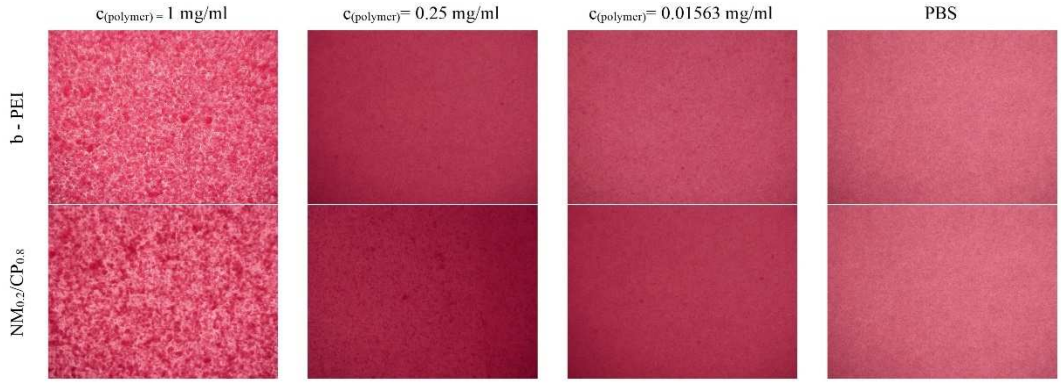

Figure 8. Erythrocyte aggregation profiles exemplarily shown for b-PEI and $NM_{0.2}/CP_{0.8}$ polymer concentrations of 1 mg/ml, 0.25 mg/ml and 0.01563 mg/ml in comparison to PBS used as negative control.

These results suggest that a higher amount polymer and thus positive charges induced stronger aggregation effects due to interactions with negatively charged components of the RBC membrane. Additional hydrophobic interactions with the CP subunits of the $NM_{0.2}/CP_{0.8}$ polymers might lead to slightly more aggregation effects as visible for $NM_{0.2}/CP_{0.8}$ polymer concentrations of 0.25 mg/ml and 1 mg/ml. Taken together, the favorable hemolytic profiles and the low tendency to induce erythrocyte aggregation indicated that both polymers are well

tolerated by RBCs, emphasizing the safe profile of these materials with regard to following *in vivo* experiments.

3.5 In vivo biodistribution experiments

After it was shown that ApoE-$NM_{0.2}/CP_{0.8}$ PXs in particular mediated targeted and efficient cellular uptake and *in vitro* knockdown in combination with favorable toxicity profiles, they were subsequently investigated *in vivo* in SWISS mice to evaluate their biodistribution behavior compared to non ApoE-coated $NM_{0.2}/CP_{0.8}$ PXs and in addition to b-PEI PXs. Therefore, siRNA was covalently coupled with DTPA to enable the labelling with ^{177}Lu as radioactive marker for biodistribution studies of formulations following an adjusted protocol previously described for ^{111}Indium-labeling of siRNA [48]. ApoE-$NM_{0.2}/CP_{0.8}$ PXs, $NM_{0.2}/CP_{0.8}$ PXs and b-PEI PXs were formed with ^{177}Lu-radiolabeled siRNA and intravenously administered through the tail vein, and biodistribution was investigated 1 h post injection in comparison to ^{177}Lu-labeled free siRNA as control. As measured by gamma scintillation counting of resected organs (Figure 9A), free siRNA exhibited a different biodistribution profile in comparison to PXs and accumulated preferentially in the kidney (50.65 %ID/g), as reported earlier [49]. Small amounts of siRNA were in addition found in the liver (7.44 %ID/g), as also described by the group of Braasch et al. [72], and in the spleen (5.48 %ID/g ratio). The results indicated that ^{177}Lu-labeled siRNA encapsulated with b-PEI accumulated mainly in the liver (106.41 %ID/g) and spleen (83.08 %ID/g), which is in good agreement with published data [73]. In contrast, with ^{177}Lu-labeled siRNA encapsulated with $NM_{0.2}/CP_{0.8}$ was preferentially detected in the lung, as 104.41 %ID/g and 138.87 %ID/g were found for $NM_{0.2}/CP_{0.8}$ and ApoE-$NM_{0.2}/CP_{0.8}$ PXs, respectively. In addition, $NM_{0.2}/CP_{0.8}$ and ApoE-$NM_{0.2}/CP_{0.8}$ complexed siRNA accumulated, although to a smaller extent, in the spleen ($NM_{0.2}/CP_{0.8}$ PXs: 75.74 %ID/g, ApoE-$NM_{0.2}/CP_{0.8}$ PXs: 72.98 %ID/g) and in the liver ($NM_{0.2}/CP_{0.8}$ PX: 75.92 %ID/g, ApoE-$NM_{0.2}/CP_{0.8}$ PXs: 66.54 % ID/g ratio). As illustrated in Figure 9B, only low concentrations of free ^{177}Lu-labeled siRNA and complexed with both, b-PEI and $NM_{0.2}/CP_{0.8}$ were detected in the brain. In fact, the lowest radioactive signal in the brain was observed in mice treated with ApoE-coated $NM_{0.2}/CP_{0.8}$ PXs 1 h post injection.

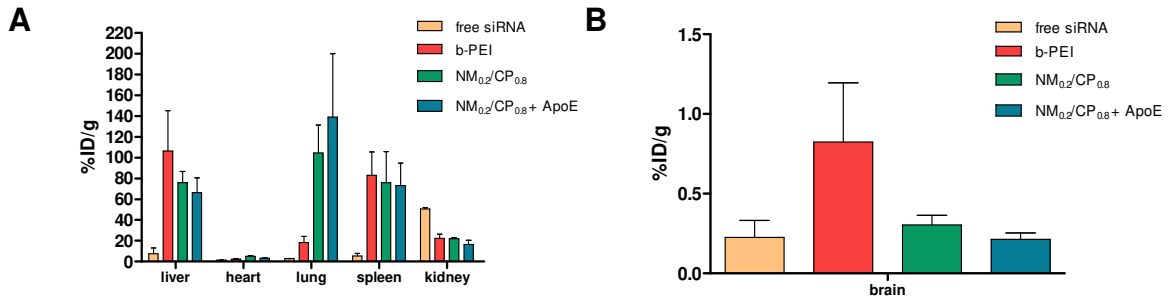

Figure 9. Biodistribution of ^{177}Lu-labeled siRNA, b-PEI PXs, $NM_{0.2}/CP_{0.8}$ PXs and ApoE-$NM_{0.2}/CP_{0.8}$ PXs in dissected organs (**A**) and the brain (**B**) of SWISS mice 1 h post injection. (Results are presented as %ID/g and shown as mean ± SD, n = 3, mice that urinated during the incubation period were excluded from the study to avoid falsification of the results due to undefined loss of radioactive material).

Several *in vivo* studies performed with polyplexes have shown that a variety of parameters influence the biodistribution of siRNA formulations. Physicochemical properties of the NPs such as particle size, surface charge and surface hydrophobicity further determine the stability of the polymer-siRNA complexes as well as interactions with proteins within the blood stream. Protein corona formation in turn can lead to recognition of the particles by the reticuloendothelial system (RES) determining the fate of the particles in the body after intravenous injection. Free labeled siRNA administered to mice was shown to be distributed to kidneys and the liver within minutes after injection, and a minor fraction of the siRNA was rapidly excreted via the urine so that levels of siRNA within the body decreased markedly after 24 h [72]. It is also known that siRNA is rapidly degraded by serum nucleases upon injection [74] implying that small fragments bearing the label might additionally circulate in the blood pool and show a different behavior than macromolecules, which needs to be considered as well when interpreting biodistribution data. Nevertheless, it was previously ascertained that renal clearance might occur more rapid than the degradation processes [75]. Moreover, free siRNA did not selectively accumulate in the other organs or in the brain, reflecting the poor ability of siRNA to penetrate the blood-brain barrier [49]. Taken together, our data for the biodistribution of ^{177}Lu-labeled free siRNA in mice were consistent with previous reports. Labeled siRNA complexed with PEI demonstrated accumulation in the liver and the spleen. This goes in line with earlier findings, which suggest that PEI-particles are cleared from the blood stream after opsonization very rapid by phagocytosing macrophages ending up in the organs of the RES, namely liver and spleen [76]. In a double labeling approach in which both, the siRNA and the polymer PEI were labeled with a radioactive marker via DTPA coupling to investigate the *in vivo* stability of the polyplexes, it was found that the polyplexes were taken up into the liver as a whole, but dissociation subsequently occurred during liver passage, resulting in the

accumulation of free siRNA in the interstitium while the polymer was taken up into hepatocytes [73, 77]. Our data underpins these assumptions, as b-PEI-encapsulated ^{177}Lu-labeled siRNA was detected mainly in the liver and the spleen. Small amounts of ^{177}Lu-labeled siRNA detected in the kidney after b-PEI PXs injection can possibly be explained by disintegration of the b-PEI-siRNA complex within the blood stream leading to free siRNA which consequently undergo renal clearance. A somewhat different picture emerged in the case of ^{177}Lu-labeled siRNA encapsulated with $NM_{0.2}/CP_{0.8}$ polymers, as it was detected in the liver and spleen to a smaller extent than b-PEI PXs siRNA, but to a higher extent in the lungs. Therefore, we suggest, that a lower proportion of the $NM_{0.2}/CP_{0.8}$ PXs was recognized after opsonization by RES cells leading to internalization in liver and spleen. A deposition in the lung was so far associated with the formation of aggregates due to interactions of polyplexes with blood components that subsequently get entrapped in the capillary bed of the lung [78]. In addition, it was shown that modification of particles with hydrophilic substances such es poly(ethylene glycol) (PEG) led to significantly decreased interactions with RBCs [73]. More hydrophobic NPs, as it is the case for $NM_{0.2}/CP_{0.8}$ PXs, seem to interact more easily with erythrocytes, what is also supported by the data of the erythrocyte aggregation assay described above, leading to accumulation of RBC-PX aggregates in the lung capillaries. Even though this effect was incisive, it did not lead to lethality of mice due to embolism incidents as described in previous investigations of biodistribution and kinetics of PXs [78, 79]. Against our expectations, no significant differences in biodistribution profiles, including no selective accumulation in the brain, were observed for $NM_{0.2}/CP_{0.8}$ PXs and ApoE-coated $NM_{0.2}/CP_{0.8}$ PXs. Subsequently, neither direct ApoE coating of $NM_{0.2}/CP_{0.8}$ PXs nor potential adsorption of ApoE from the blood to hydrophobic subunits of the $NM_{0.2}/CP_{0.8}$ PXs achieved selective or efficient siRNA delivery to the brain in this specific experimental setting at the time point investigated. One important aspect is related to potentially different pharmacokinetics of the various formulations injected. From our data, we conclude that while ApoE was shown to bind in particular to $NM_{0.2}/CP_{0.8}$ PXs, leading to successful internalization in LDL/LRP positive glioblastoma cells, used as model cell line *in vitro*, it did not lead to brain accumulation of the PXs *in vivo* within 1h. Therefore, we assumed that interactions between ApoE and PXs might not be stable enough in the biological environment of an *in vivo* setup and that the targeting ligand may be shed in the blood stream after injection before the system can reach the brain. To address this issue, we propose to develop a covalent coupling protocol of polymers with ApoE, as it was for example already described for HAS NPs in previous studies [41, 80]. It is likewise conceivable, that the ApoE concentration chosen for direct coating of PXs, following previous publications with solid NPs

[20], was too low to achieve efficient brain targeting effects *in vivo* with b-PEI and $NM_{0.2}/CP_{0.8}$ PXs and needs to be further optimized in future experiments. In case of our hypothesis that plasma ApoE might be part of the protein corona of $NM_{0.2}/CP_{0.8}$ PXs, that occurs on the surface of the PXs after intravenous injection due to hydrophobic interactions even without PS80 as hydrophobic anchor, additional experiments, for example mass spectrometry for the evaluation of the protein corona composition, are necessary to gain further insights into this topic. Taken together, the results pointed out that overcoming the blood-brain barrier *in vivo* remains a major bottleneck for siRNA delivery into the brain and that precisely designed delivery systems are needed for active targeting that fulfill the complex requirements present under physiological conditions. Specifically, in addition to appropriate properties of the delivery system, also sufficient residence in the circulation is required to allow interactions with respective receptors in target sites and thus uptake into targeted tissues.

4. Conclusion

RNAi is a promising technique for the treatment of several brain diseases such as brain tumors. In order to design safe and efficient polymeric siRNA delivery systems which overcome the BBB as major bottleneck of brain delivery, evaluation of a precise brain targeting strategy is needed to ensure that appropriate concentrations of siRNA are present at target sites within the brain. It has been shown that multiple cell surface receptors are overexpressed on brain endothelial cells which can be targeted by respective ligands to induce brain entry via RMT. Herein, we presented the first study investigating the feasibility of the PS80-ApoE brain targeting approach for PXs via LDL receptors, successfully applied for solid NPs. In addition to b-PEI polymers, $NM_{0.2}/CP_{0.8}$ polymers were selected for this study to evaluate the impact of hydrophobic subunits on the ApoE binding efficacy. Successful adsorption of ApoE on PS80 precaoted PXs and plain PXs was demonstrated by SDS-PAGE and it therefore appears that a higher hydrophobic content within the polymer has a beneficial effect on ApoE binding. DLS and LDA measurements revealed that modification with ApoE did not significantly influence particle sizes and surface charges in an unfavorable way. Negligible cytotoxic effects of all formulations were confirmed by CellTiter-Blue® assays. Cellular uptake experiments, which were conducted in an LDL- and LRP1-receptor overexpressing model cell line and measured by flow cytometry, exhibited a significantly increased internalization capacity of ApoE-PXs whereas this effect was more remarkable for $NM_{0.2}/CP_{0.8}$ PXs than for b-PEI PXs. In contrast, PS80 precoated formulations exhibited no cellular uptake at all, leading to the assumption that

PS80 coating of PXs induces a disintegration of the complex under *in vitro* conditions, indicating the ineptitude of the surfactant-based ApoE-functionalization approach for PXs. Knockdown experiments revealed that ApoE- $NM_{0.2}/CP_{0.8}$ PXs were able to reduce GAPDH gene expression to pproximately 50%, suggesting that ApoE modification leads not only to improved cellular internalization but also to an increased biological effect. Taken together, ApoE-$NM_{0.2}/CP_{0.8}$ PXs in particular yielded promising *in vitro* data regarding the capability of selective brain targeting. However, biodistribution studies performed with PXs containing ^{177}Lu-labeled DTPA-siRNA in mice were not consistent with *in vitro* results as virtually no radiolabeled siRNA was detected in the brain for any tested formulation. Overall, this study laid the foundation for investigations regarding selective siRNA delivery with PXs into the brain using the ApoE approach. PS80 precoating is not appropriate for ApoE adsorption on PXs, but this limitation can potentially be tackled by modifying polymers with hydrophobic modifications for enhanced ApoE binding. Nevertheless, since the *in vitro-in vivo* correlation was very poor, we suggest that, among other factors, the loose attachment of ApoE is not durable within complex biological environments and that more stable covalent linkage approaches for PXs should be addressed in future experiments. Furthermore, this study provides evidence for the need of appropriate *in vitro* models that better simulate physiological conditions and therefore provide more accurate estimates regarding the behavior of delivery systems *in vivo*. Ongoing work currently focuses on the establishment of a human BBB co-culture model mimicking the neurovascular unit using induced puri- and multipotent stem cells to provide a sophisticated tool for the development of effective drug delivery systems for CNS delivery in the future.

References

[1] W.M. Pardridge, Blood-brain barrier drug targeting: the future of brain drug development, Molecular interventions, 3 2 (2003) 90-105, 151.
[2] W.M. Pardridge, The blood-brain barrier: Bottleneck in brain drug development, NeuroRX, 2 (2005) 3-14.
[3] A. Cerletti, J. Drewe, G. Fricker, A. Eberle, J. Huwyler, Endocytosis and Transcytosis of an Immunoliposome-Based Brain Drug Delivery System, J Drug Target, 8 (2000) 435-446.
[4] N. Hartl, F. Adams, O.M. Merkel, From Adsorption to Covalent Bonding: Apolipoprotein E Functionalization of Polymeric Nanoparticles for Drug Delivery Across the Blood–Brain Barrier, Advanced Therapeutics, 4 (2021) 2000092.
[5] J. Kreuter, R.N. Alyautdin, D.A. Kharkevich, A.A. Ivanov, Passage of peptides through the blood-brain barrier with colloidal polymer particles (nanoparticles), Brain Research, 674 (1995) 171-174.
[6] R.N. Alyaudtin, A. Reichel, R. Löbenberg, P. Ramge, J. Kreuter, D.J. Begley, Interaction of Poly(butylcyanoacrylate) Nanoparticles with the Blood-Brain Barrier in vivo and in vitro, J Drug Target, 9 (2001) 209-221.
[7] U. Schröder, B.A. Sabel, Nanoparticles, a drug carrier system to pass the blood-brain barrier, permit central analgesic effects of i.v. dalargin injections, Brain Research, 710 (1996) 121-124.
[8] U. Schroeder, P. Sommerfeld, B.A. Sabel, Efficacy of Oral Dalargin-loaded Nanoparticle Delivery across the Blood–Brain Barrier, Peptides, 19 (1998) 777-780.
[9] U. Schroeder, P. Sommerfeld, S. Ulrich, B.A. Sabel, Nanoparticle technology for delivery of drugs across the blood–brain barrier, Journal of Pharmaceutical Sciences, 87 (1998) 1305-1307.
[10] P. Ramge, J. Kreuter, B. Lemmer, Circadian Phase-Dependent Antinociceptive Reaction in Mice Determined by the Hot-Plate test and the Tail-Flick Test After Intravenous Injection of Dalargin-Loaded Nanoparticles, Chronobiology International, 16 (1999) 767-777.
[11] J. Kreuter, Influence of the surface properties on nanoparticle-mediated transport of drugs to the brain, Journal of nanoscience and nanotechnology, 4 5 (2004) 484-488.
[12] R.N. Alyautdin, V.E. Petrov, K. Langer, A. Berthold, D.A. Kharkevich, J. Kreuter, Delivery of Loperamide Across the Blood-Brain Barrier with Polysorbate 80-Coated Polybutylcyanoacrylate Nanoparticles, Pharmaceutical Research, 14 (1997) 325-328.
[13] R.N. Alyautdin, E.B. Tezikov, P. Ramge, D.A. Kharkevich, D.J. Begley, J. Kreuter, Significant entry of tubocurarine into the brain of rats by adsorption to polysorbate 80–coated polybutylcyanoacrylate nanoparticles: An in situ brain perfusion study, Journal of Microencapsulation, 15 (1998) 67-74.
[14] A. Friese, E. Seiller, G. Quack, B. Lorenz, J. Kreuter, Increase of the duration of the anticonvulsive activity of a novel NMDA receptor antagonist using poly(butylcyanoacrylate) nanoparticles as a parenteral controlled release system, European Journal of Pharmaceutics and Biopharmaceutics, 49 (2000) 103-109.
[15] A.E. Gulyaev, S.E. Gelperina, I.N. Skidan, A.S. Antropov, G.Y. Kivman, J. Kreuter, Significant Transport of Doxorubicin into the Brain with Polysorbate 80-Coated Nanoparticles, Pharmaceutical Research, 16 (1999) 1564-1569.
[16] S.C.J. Steiniger, J. Kreuter, A.S. Khalansky, I.N. Skidan, A.I. Bobruskin, Z.S. Smirnova, S.E. Severin, R. Uhl, M. Kock, K.D. Geiger, S.E. Gelperina, Chemotherapy of glioblastoma in rats using doxorubicin-loaded nanoparticles, International Journal of Cancer, 109 (2004) 759-767.
[17] A. Ambruosi, S. Gelperina, A. Khalansky, S. Tanski, A. Theisen, J. Kreuter, Influence of surfactants, polymer and doxorubicin loading on the anti-tumour effect of poly(butyl cyanoacrylate) nanoparticles in a rat glioma model, Journal of Microencapsulation, 23 (2006) 582-592.

[18] J. Kreuter, V.E. Petrov, D.A. Kharkevich, R.N. Alyautdin, Influence of the type of surfactant on the analgesic effects induced by the peptide dalargin after its delivery across the blood–brain barrier using surfactant-coated nanoparticles, Journal of Controlled Release, 49 (1997) 81-87.
[19] M. Lück, B.-R. Paulke, W. Schröder, T. Blunk, R.H. Müller, Analysis of plasma protein adsorption on polymeric nanoparticles with different surface characteristics, Journal of Biomedical Materials Research, 39 (1998) 478-485.
[20] J. Kreuter, D. Shamenkov, V. Petrov, P. Ramge, K. Cychutek, C. Koch-Brandt, R. Alyautdin, Apolipoprotein-mediated transport of nanoparticle-bound drugs across the blood-brain barrier, J Drug Target, 10 (2002) 317-325.
[21] K. Gao, X. Jiang, Influence of particle size on transport of methotrexate across blood brain barrier by polysorbate 80-coated polybutylcyanoacrylate nanoparticles, International Journal of Pharmaceutics, 310 (2006) 213-219.
[22] H. Ebrahimi Shahmabadi, F. Movahedi, M. Koohi Moftakhari Esfahani, S.E. Alavi, A. Eslamifar, G. Mohammadi Anaraki, A. Akbarzadeh, Efficacy of Cisplatin-loaded polybutyl cyanoacrylate nanoparticles on the glioblastoma, Tumor Biology, 35 (2014) 4799-4806.
[23] B. Wilson, M.K. Samanta, K. Santhi, K.P.S. Kumar, N. Paramakrishnan, B. Suresh, Targeted delivery of tacrine into the brain with polysorbate 80-coated poly(n-butylcyanoacrylate) nanoparticles, European Journal of Pharmaceutics and Biopharmaceutics, 70 (2008) 75-84.
[24] B.A. Abdel-Wahab, M.M. Abdel-Latif, A.A. Abdel-Hafez, Comparative study for brain delivery of tacrine using polysorbate 80-coated poly(butylcyanoacrylate) and pegylated-poly(butylcyanoacrylate) nanoparticles, International Journal of Nano and Biomaterials, 2 (2009) 360-374.
[25] B. Wilson, M.K. Samanta, K. Santhi, K.P.S. Kumar, N. Paramakrishnan, B. Suresh, Poly(n-butylcyanoacrylate) nanoparticles coated with polysorbate 80 for the targeted delivery of rivastigmine into the brain to treat Alzheimer's disease, Brain Research, 1200 (2008) 159-168.
[26] Y.-C. Kuo, R. Rajesh, Targeted delivery of rosmarinic acid across the blood–brain barrier for neuronal rescue using polyacrylamide-chitosan-poly(lactide-co-glycolide) nanoparticles with surface cross-reacting material 197 and apolipoprotein E, International Journal of Pharmaceutics, 528 (2017) 228-241.
[27] K.B. Kurakhmaeva, I.A. Djindjikhashvili, V.E. Petrov, V.U. Balabanyan, T.A. Voronina, S.S. Trofimov, J. Kreuter, S. Gelperina, D. Begley, R.N. Alyautdin, Brain targeting of nerve growth factor using poly(butyl cyanoacrylate) nanoparticles, J Drug Target, 17 (2009) 564-574.
[28] K.B. Kurakhmaeva, T.A. Voronina, I.G. Kapica, J. Kreuter, L.N. Nerobkova, S.B. Seredenin, V.Y. Balabanian, R.N. Alyautdin, Antiparkinsonian effect of nerve growth factor adsorbed on polybutylcyanoacrylate nanoparticles coated with polysorbate-80, Bulletin of Experimental Biology and Medicine, 145 (2008) 259-262.
[29] T. Schuster, A. Mühlstein, C. Yaghootfam, O. Maksimenko, E. Shipulo, S. Gelperina, J. Kreuter, V. Gieselmann, U. Matzner, Potential of surfactant-coated nanoparticles to improve brain delivery of arylsulfatase A, Journal of Controlled Release, 253 (2017) 1-10.
[30] S. Wagner, J. Kufleitner, A. Zensi, M. Dadparvar, S. Wien, J. Bungert, T. Vogel, F. Worek, J. Kreuter, H.v. Briesen, Nanoparticulate transport of oximes over an in vitro blood-brain barrier model, PLoS One, 5 (2010).
[31] P. Girotra, S.K. Singh, A Comparative Study of Orally Delivered PBCA and ApoE Coupled BSA Nanoparticles for Brain Targeting of Sumatriptan Succinate in Therapeutic Management of Migraine, Pharmaceutical Research, 33 (2016) 1682-1695.
[32] M. Liu, H. Li, G. Luo, Q. Liu, Y. Wang, Pharmacokinetics and biodistribution of surface modification polymeric nanoparticles, Archives of Pharmacal Research, 31 (2008) 547-554.

[33] T. Ren, N. Xu, C. Cao, W. Yuan, X. Yu, J. Chen, J. Ren, Preparation and Therapeutic Efficacy of Polysorbate-80-Coated Amphotericin B/PLA-b-PEG Nanoparticles, Journal of Biomaterials Science, Polymer Edition, 20 (2009) 1369-1380.
[34] G. Mittal, H. Carswell, R. Brett, S. Currie, M.N.V.R. Kumar, Development and evaluation of polymer nanoparticles for oral delivery of estradiol to rat brain in a model of Alzheimer's pathology, Journal of Controlled Release, 150 (2011) 220-228.
[35] S. Gelperina, O. Maksimenko, A. Khalansky, L. Vanchugova, E. Shipulo, K. Abbasova, R. Berdiev, S. Wohlfart, N. Chepurnova, J. Kreuter, Drug delivery to the brain using surfactant-coated poly(lactide-co-glycolide) nanoparticles: Influence of the formulation parameters, European Journal of Pharmaceutics and Biopharmaceutics, 74 (2010) 157-163.
[36] S. Jose, B.C. Juna, T.A. Cinu, H. Jyoti, N.A. Aleykutty, Carboplatin loaded Surface modified PLGA nanoparticles: Optimization, characterization, and in vivo brain targeting studies, Colloids and Surfaces B: Biointerfaces, 142 (2016) 307-314.
[37] Y. Malinovskaya, P. Melnikov, V. Baklaushev, A. Gabashvili, N. Osipova, S. Mantrov, Y. Ermolenko, O. Maksimenko, M. Gorshkova, V. Balabanyan, J. Kreuter, S. Gelperina, Delivery of doxorubicin-loaded PLGA nanoparticles into U87 human glioblastoma cells, International Journal of Pharmaceutics, 524 (2017) 77-90.
[38] J. Bruun, T.B. Larsen, R.I. Jølck, R. Eliasen, R. Holm, T. Gjetting, T.L. Andresen, Investigation of enzyme-sensitive lipid nanoparticles for delivery of siRNA to blood–brain barrier and glioma cells, Int J Nanomedicine, 10 (2015) 5995.
[39] M. Grzelinski, B. Urban-Klein, T. Martens, K. Lamszus, U. Bakowsky, S. Höbel, F. Czubayko, A. Aigner, RNA Interference-Mediated Gene Silencing of Pleiotrophin Through Polyethylenimine-Complexed Small Interfering RNAs In Vivo Exerts Antitumoral Effects in Glioblastoma Xenografts, Human Gene Therapy, 17 (2006) 751-766.
[40] R. Zukiel, S. Nowak, E. Wyszko, K. Rolle, I. Gawronska, M.Z. Barciszewska, J. Barciszewski, Suppression of human brain tumor with interference RNA specific for tenascin-C, Cancer biology & therapy, 5 (2006) 1002-1007.
[41] K. Michaelis, M.M. Hoffmann, S. Dreis, E. Herbert, R.N. Alyautdin, M. Michaelis, J. Kreuter, K. Langer, Covalent Linkage of Apolipoprotein E to Albumin Nanoparticles Strongly Enhances Drug Transport into the Brain, Journal of Pharmacology and Experimental Therapeutics, 317 (2006) 1246.
[42] N. Hartl, F. Adams, G. Costabile, L. Isert, M. Döblinger, X. Xiao, R. Liu, O.M. Merkel, The Impact of Nylon-3 Copolymer Composition on the Efficiency of siRNA Delivery to Glioblastoma Cells, Nanomaterials, 9 (2019) 986.
[43] B.P. Mowery, S.E. Lee, D.A. Kissounko, R.F. Epand, R.M. Epand, B. Weisblum, S.S. Stahl, S.H. Gellman, Mimicry of Antimicrobial Host-Defense Peptides by Random Copolymers, Journal of the American Chemical Society, 129 (2007) 15474-15476.
[44] R. Liu, X. Chen, S.P. Falk, B.P. Mowery, A.J. Karlsson, B. Weisblum, S.P. Palecek, K.S. Masters, S.H. Gellman, Structure–Activity Relationships among Antifungal Nylon-3 Polymers: Identification of Materials Active against Drug-Resistant Strains of Candida albicans, Journal of the American Chemical Society, 136 (2014) 4333-4342.
[45] J. Zhang, D.A. Kissounko, S.E. Lee, S.H. Gellman, S.S. Stahl, Access to Poly-β-Peptides with Functionalized Side Chains and End Groups via Controlled Ring-Opening Polymerization of β-Lactams, Journal of the American Chemical Society, 131 (2009) 1589-1597.
[46] M.A. Behlke, Progress towards in vivo use of siRNAs, Molecular Therapy, 13 (2006) 644-670.
[47] H. Petersen, P.M. Fechner, A.L. Martin, K. Kunath, S. Stolnik, C.J. Roberts, D. Fischer, M.C. Davies, T. Kissel, Polyethylenimine-graft-Poly(ethylene glycol) Copolymers: Influence of Copolymer Block Structure on DNA Complexation and Biological Activities as Gene Delivery System, Bioconjugate Chemistry, 13 (2002) 845-854.

[48] S. Jones, O. Merkel, Indium-labeling of siRNA for small animal SPECT imaging, RNA Imaging, Springer2016, pp. 79-88.
[49] F.M. van de Water, O.C. Boerman, A.C. Wouterse, J.G.P. Peters, F.G.M. Russel, R. Masereeuw, Intravenously administered short interfering RNA accumulates in the kidney and selectively suppresses gene function in renal proximal tubules, Drug Metabolism and Disposition, 34 (2006) 1393.
[50] C.G. Pippin, T.A. Parker, T.J. McMurry, M.W. Brechbiel, Spectrophotometric method for the determination of a bifunctional DTPA ligand in DTPA-monoclonal antibody conjugates, Bioconjugate Chemistry, 3 (1992) 342-345.
[51] P.C. Mesquita, E. dos Santos-Silva, L. Streck, I.Z. Damasceno, A.M.S. Maia, M.F. Fernandes-Pedrosa, A.A. da Silva-Júnior, Cationic functionalized biocompatible polylactide nanoparticles for slow release of proteins, Colloids and Surfaces A: Physicochemical and Engineering Aspects, 513 (2017) 442-451.
[52] P.K.C. Chang, C.A. Prestidge, K.E. Bremmell, Interfacial analysis of siRNA complexes with poly-ethylenimine (PEI) or PAMAM dendrimers in gene delivery, Colloids and Surfaces B: Biointerfaces, 158 (2017) 370-378.
[53] L. Liu, M. Zheng, D. Librizzi, T. Renette, O.M. Merkel, T. Kissel, Efficient and Tumor Targeted siRNA Delivery by Polyethylenimine-graft-polycaprolactone-block-poly(ethylene glycol)-folate (PEI–PCL–PEG–Fol), Molecular Pharmaceutics, 13 (2016) 134-143.
[54] M. Eto, K. Watanabe, K. Ishii, A rapid flat gel isoelectric focusing method for the determination of apolipoprotein E phenotypes and its application, Clinica Chimica Acta, 149 (1985) 21-28.
[55] R.W. Mahley, T.L. Innerarity, S.C. Rall Jr, K.H. Weisgraber, Plasma lipoproteins: apolipoprotein structure and function, Journal of lipid research, 25 (1984) 1277-1294.
[56] V. Neuhoff, N. Arold, D. Taube, W. Ehrhardt, Improved staining of proteins in polyacrylamide gels including isoelectric focusing gels with clear background at nanogram sensitivity using Coomassie Brilliant Blue G 250 and r 250, ELECTROPHORESIS, 9 (1988).
[57] T. Blunk, D.F. Hochstrasser, J.-C. Sanchez, B.W. Müller, R.H. Müller, Colloidal carriers for intravenous drug targeting: Plasma protein adsorption patterns on surface-modified latex particles evaluated by two-dimensional polyacrylamide gel electrophoresis, ELECTROPHORESIS, 14 (1993) 1382-1387.
[58] M. Mahmoudi, I. Lynch, M.R. Ejtehadi, M.P. Monopoli, F.B. Bombelli, S. Laurent, Protein−Nanoparticle Interactions: Opportunities and Challenges, Chemical Reviews, 111 (2011) 5610-5637.
[59] J. Ribalta, J.-C. Vallvé, J. Girona, L. Masana, Apolipoprotein and apolipoprotein receptor genes, blood lipids and disease, Curr Opin Clin Nutr Metab Care, 6 (2003) 177-187.
[60] D. Kibuule, Advanced Pharmacology, (2012).
[61] Y.-H. Hsieh, C.-Y. Chou, Structural and functional characterization of human apolipoprotein E 72-166 peptides in both aqueous and lipid environments, Journal of biomedical science, 18 (2011) 1-9.
[62] L. Maletínská, E.A. Blakely, K.A. Bjornstad, D.F. Deen, L.J. Knoff, T.M. Forte, Human Glioblastoma Cell Lines: Levels of Low-Density Lipoprotein Receptor and Low-Density Lipoprotein Receptor-related Protein1, Cancer Research, 60 (2000) 2300-2303.
[63] V. Nadithe, R. Liu, B.A. Killinger, S. Movassaghian, N.H. Kim, A.B. Moszczynska, K.S. Masters, S.H. Gellman, O.M. Merkel, Screening Nylon-3 Polymers, a New Class of Cationic Amphiphiles, for siRNA Delivery, Molecular Pharmaceutics, 12 (2015) 362-374.
[64] B. Dehouck, M.-P. Dehouck, J.-C. Fruchart, R. Cecchelli, Upregulation of the low density lipoprotein receptor at the blood-brain barrier: intercommunications between brain capillary endothelial cells and astrocytes, Review & Expositor, 84 (1987) 465-473.

[65] R.S. Mulik, J. Mönkkönen, R.O. Juvonen, K.R. Mahadik, A.R. Paradkar, ApoE3 mediated polymeric nanoparticles containing curcumin: Apoptosis induced in vitro anticancer activity against neuroblastoma cells, International Journal of Pharmaceutics, 437 (2012) 29-41.
[66] R.S. Mulik, J. Mönkkönen, R.O. Juvonen, K.R. Mahadik, A.R. Paradkar, ApoE3 Mediated Poly(butyl) Cyanoacrylate Nanoparticles Containing Curcumin: Study of Enhanced Activity of Curcumin against Beta Amyloid Induced Cytotoxicity Using In Vitro Cell Culture Model, Molecular Pharmaceutics, 7 (2010) 815-825.
[67] S.M. Moghimi, P. Symonds, J.C. Murray, A.C. Hunter, G. Debska, A. Szewczyk, A two-stage poly(ethylenimine)-mediated cytotoxicity: implications for gene transfer/therapy, Molecular Therapy, 11 (2005) 990-995.
[68] Y. Xu, F.C. Szoka, Mechanism of DNA release from cationic liposome/DNA complexes used in cell transfection, Biochemistry, 35 (1996) 5616-5623.
[69] K. Bigl, A. Schmitt, I. Meiners, G. Münch, T. Arendt, Comparison of results of the CellTiter Blue, the tetrazolium (3-[4,5-dimethylthioazol-2-yl]-2,5-diphenyl tetrazolium bromide), and the lactate dehydrogenase assay applied in brain cells after exposure to advanced glycation endproducts, Toxicology in Vitro, 21 (2007) 962-971.
[70] M.A. Dobrovolskaia, S.E. McNeil, Understanding the correlation between in vitro and in vivo immunotoxicity tests for nanomedicines, Journal of Controlled Release, 172 (2013) 456-466.
[71] ASTM, Standard Test Method for Analysis of Hemolytic Properties of Nanoparticles, ASTM International West Conshohocken, PA, 2013.
[72] D.A. Braasch, Z. Paroo, A. Constantinescu, G. Ren, O.K. Öz, R.P. Mason, D.R. Corey, Biodistribution of phosphodiester and phosphorothioate siRNA, Bioorganic & Medicinal Chemistry Letters, 14 (2004) 1139-1143.
[73] O.M. Merkel, D. Librizzi, A. Pfestroff, T. Schurrat, K. Buyens, N.N. Sanders, S.C. De Smedt, M. Béhé, T. Kissel, Stability of siRNA polyplexes from poly(ethylenimine) and poly(ethylenimine)-g-poly(ethylene glycol) under in vivo conditions: Effects on pharmacokinetics and biodistribution measured by Fluorescence Fluctuation Spectroscopy and Single Photon Emission Computed Tomography (SPECT) imaging, Journal of Controlled Release, 138 (2009) 148-159.
[74] D. Bumcrot, M. Manoharan, V. Koteliansky, D.W.Y. Sah, RNAi therapeutics: a potential new class of pharmaceutical drugs, Nature Chemical Biology, 2 (2006) 711-719.
[75] O.M. Merkel, D. Librizzi, A. Pfestroff, T. Schurrat, M. Béhé, T. Kissel, In Vivo SPECT and Real-Time Gamma Camera Imaging of Biodistribution and Pharmacokinetics of siRNA Delivery Using an Optimized Radiolabeling and Purification Procedure, Bioconjugate Chemistry, 20 (2009) 174-182.
[76] D.E. Owens, N.A. Peppas, Opsonization, biodistribution, and pharmacokinetics of polymeric nanoparticles, International Journal of Pharmaceutics, 307 (2006) 93-102.
[77] R.S. Burke, S.H. Pun, Extracellular barriers to in vivo PEI and PEGylated PEI polyplex-mediated gene delivery to the liver, Bioconjugate chemistry, 19 (2008) 693-704.
[78] P. Chollet, M.C. Favrot, A. Hurbin, J.-L. Coll, Side-effects of a systemic injection of linear polyethylenimine–DNA complexes, The Journal of Gene Medicine, 4 (2002) 84-91.
[79] M. Ogris, S. Brunner, S. Schüller, R. Kircheis, E. Wagner, PEGylated DNA/transferrin–PEI complexes: reduced interaction with blood components, extended circulation in blood and potential for systemic gene delivery, Gene therapy, 6 (1999) 595-605.
[80] J. Kreuter, T. Hekmatara, S. Dreis, T. Vogel, S. Gelperina, K. Langer, Covalent attachment of apolipoprotein A-I and apolipoprotein B-100 to albumin nanoparticles enables drug transport into the brain, Journal of Controlled Release, 118 (2007) 54-58.

Supplementary Material

1. Size and Zeta Potential Analysis of PXs by Dynamic Light Scattering and Laser Doppler Anemometry

1.1 PS80-concentration optimization

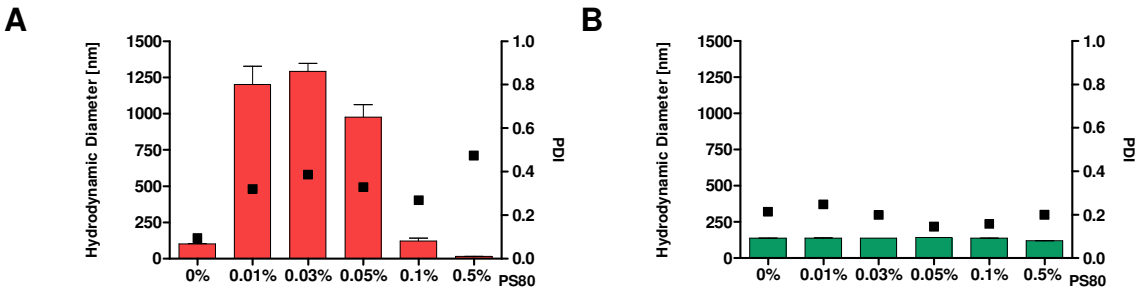

Figure S1. DLS measurements of PS80-b-PEI PXs (**A**) and PS80-$NM_{0.2}/CP_{0.8}$ PXs (**B**) coated with varying PS80 concentrations (0.01% - 0.5% PS80) in comparison to uncoated particles (0% PS80). (Data points indicate mean ± SD, n = 3).

2. Quantification of cellular uptake into glioblastoma cells by flow cytometry

2.1 LRP1-Receptor expression of glioblastoma cells

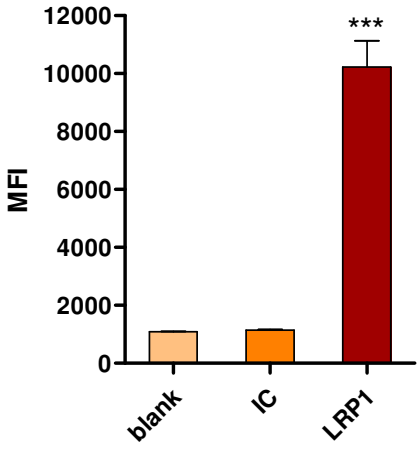

Figure S2. LRP1-receptor expression of U87 glioblastoma cells as determined by flow cytometry and presented as median fluorescence intensity (MFI): Cells were first stained with anti – LRP1 primary antibody or mouse IgG1 monoclonal antibody as isotype control (IC) to exclude unspecific binding and consequently reacted with AF488-labeled secondary goat anti-mouse IgG H&L antibody. Blank samples were left unstained. (Results are presented as median fluorescence intensity (MFI) and shown as mean ± SD, n = 3, one-way ANOVA with Bonferroni post-hoc test, *** $p < 0.005$).

2.2 Trypan quenching

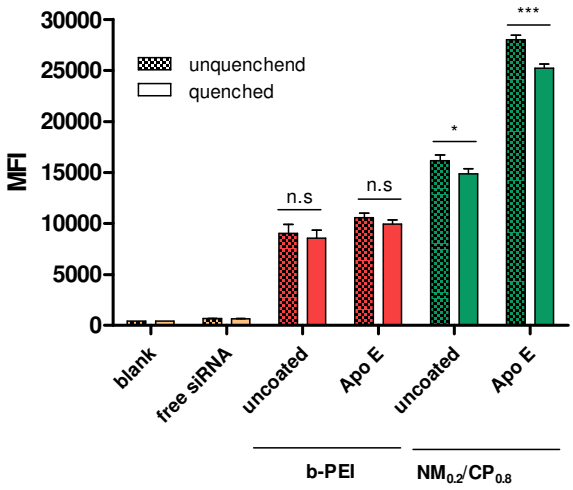

Figure S3. Cellular uptake of uncoated PXs and ApoE coated PXs after 24 h incubation as quantified by flow cytometry performed with and without trypan quenching and presented as median fluorescence intensitiy (MFI). Negative control: untreated cells (blank) and with free siRNA treated cells. (Results are shown as mean ± SD, n = 3, two-way ANOVA with Bonferroni post-hoc test, n.s (= not significant) $p > 0.05$, * $p < 0.05$, *** $p < 0.005$).

3. Influence of PS80 caoting on celllar uptake efficacy

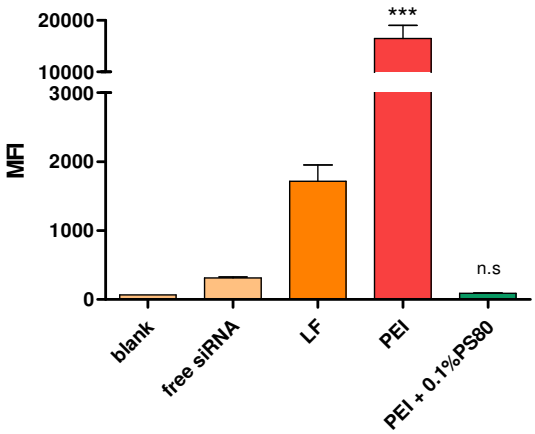

Figure S4. Cellular uptake of uncoated b-PEI and PS80-b-PEI PXs (b-PEI PXs: N/P ratio 7, final PS80 concentration = 0.1%) after 24 h incubation as quantified by flow cytometry and presented as median fluorescence intensitiy (MFI). Negative control: untreated cells (blank) and with free siRNA treated cells. Positive control: Lipofectamin 2000 lipoplexes (LF). (Results are shown as mean ± SD, n = 3, one-way ANOVA with Bonferroni post-hoc test, n.s (= not significant) $p > 0.05$, *** $p < 0.005$).

Chapter IV

Overcoming the Blood-Brain Barrier? - Evaluation of the Blood-Brain Permeability of Polyplexes

IV.1 Overcoming the BBB? - Prediction of Blood-Brain Permeability of Hydrophobically Modified Polyethylenimine Polyplexes for siRNA Delivery into the Brain with *in vitro* and *in vivo* Models

This chapter was submitted as research article in the Journal of Controlled Release (04/2023):

Natascha Hartl, Bettina Gabold, Friederike Adams, Philipp Uhl, Sabrina Oerter, Sabine Gätzner, Marco Metzger, Ann-Christine König, Stefanie M. Hauck, Antje Appelt-Menzel, Walter Mier, Gert Fricker and Olivia M. Merkel

"Overcoming the Blood-Brain Barrier? - Prediction of Blood-Brain Permeability of Hydrophobically Modified Polyethylenimine Polyplexes for siRNA Delivery into the Brain with *in vitro* and *in vivo* Models"

Abstract

The blood-brain barrier (BBB) is a highly selective biological barrier that represents a major bottleneck in the treatment of all types of central nervous system (CNS) disorders. Small interfering RNA (siRNA) offers in principle a promising therapeutic approach, e.g., for brain tumors, by downregulating brain tumor-related genes and inhibiting tumor growth via RNA interference. In an effort to develop efficient siRNA nanocarriers for crossing the BBB, we utilized polyethyleneimine (PEI) polymers hydrophobically modified with either stearic-acid (SA) or dodecylacrylamide (DAA) subunits and evaluated their suitability for delivering siRNA across the BBB in *in vitro* and *in vivo* BBB models depending on their structure. Physicochemical characteristics of siRNA-polymer complexes (polyplexes (PXs)), e.g., particle size and surface charge, were measured by dynamic light scattering and laser Doppler anemometry, whereas siRNA condensation ability of polymers and polyplex stability was evaluated by spectrophotometric methods. The composition of the biomolecule corona that absorbs on polyplexes upon encountering physiological fluids was investigated by sodium dodecyl sulfate polyacrylamide gel electrophoresis (SDS-PAGE) and by a liquid chromatography-tandem mass spectrometry (LC-MS-MS) method. Cellular internalization abilities of PXs into brain endothelial cells (hCMEC/D3) was confirmed, and a BBB permeation assay using a human induced pluripotent stem cell (hiPSC)–derived BBB model revealed similar abilities to cross the BBB for all formulations under physiological conditions. Biodistribution studies of radiolabeled PXs in mice were only partially consistent with *in vitro* results as the detected amount of radiolabeled siRNA in the brain delivered with PEI PXs was higher compared to PEI-SA PXs. Taken together, PEI PXs were shown to be a suitable nanocarrier to deliver small amounts of siRNA across the BBB into the brain but more sophisticated human BBB models that better represent physiological conditions are required to provide highly predictive *in vitro* data for human CNS drug development in the future.

1. Introduction

According to the World Health Organization (WHO), approximately 20% of all humans suffer from damages of the central nervous system (CNS) such as cerebral cancer, depression, Parkinson's disease, Alzheimer's disease, dementia, epilepsy, stroke, epilepsy or CNS-relevant metabolic diseases. With regard to the tremendous population growth and increased life expectations, the number of people suffering from CNS diseases will increase significantly in the next decades. To tackle this issue, there is an urgent need to develop highly efficient therapeutic systems for CNS diseases. A promising approach within the field of RNA therapeutics is the use of small interfering RNA (siRNA), which has shown therapeutic utility in the form of cellular nuclease-driven downregulation of mRNA levels of disease-related genes. Therapeutics based on siRNA have been already investigated for many genetically influenced CNS diseases such as Parkinson's disease, Alzheimer's disease, Huntington's disease, amyotrophic lateral sclerosis or brain tumors [1, 2]. Since siRNA is not suited for direct application into the body due to rapid degradation by nucleases, activation of immune response and low passive internalization into target cells, various nanocarriers have been investigated to provide protection for siRNA molecules. Encapsulation of siRNA by e.g., liposomes or cationic polymers resulted in longer retention time in the blood and improved cellular internalization in the target tissues. However, the administration of nanocarriers for the treatment of CNS disorders is known to be inherently limited, as the delivery of all substances to the brain is tightly regulated by the blood-brain barrier (BBB). The BBB is the major biological barrier between the bloodstream and the CNS and consists of specialized blood endothelial cells connected by very dense tight junctions, and surrounded by pericytes, astrocytes, neurons, and microglia [3]. To date, various nanoparticulate systems such as liposomes, polymeric nanoparticles (NPs) (e.g., poly(butyl cyanoacrylate) (PBCA), poly(lactic-co-glycolic acid) (PLGA), poly (lactic acid) (PLA), and carbon quantum dots (CD)) and inorganic systems (gold, zinc oxide and silver NPs) have been investigated for their potential to overcome the BBB in *in vitro* as well as *in vivo* models [4]. Initially primary porcine, bovine and rodent endothelial cells were utilized as cell-based *in vitro* models since they provide appropriate functionality and barrier integrity [5]. To overcome their limitations such as the time-consuming isolation processes and the high variability between cells of different isolations, immortalized endothelial cell lines from different species (mouse, rat, bovine, porcine, human) were established [6, 7] and integrated into more sophisticated models such as transwell- and dynamic-flow based models and microfluidic devices. To overcome their limitations in terms of low barrier tightness

with transendothelial resistance (TEER) values of 150-200 $\Omega \cdot cm^2$ and species differences in, e.g., BBB transporter expression and functionality, much emphasis has been placed on stem cells as alternative cell source. Since stem cells are self-renewable and able to differentiate into mature somatic cell types, they serve as virtually unlimited cell source with promising *in vivo*-like characteristics in BBB models, e.g., TEER values up to 5000 $\Omega \cdot cm^2$, that can be even further enhanced by co-culturing with other cell types such as pericytes, astrocytes and neural cells. *In vivo* methods to study the uptake of NPs into the brain include visualization methods such as fluorescence microscopy and imaging, behavioral tests and quantitative methods to determine pharmacokinetic parameters and biodistribution of formulations [8]. One of the most investigated polycations for the delivery of siRNA is polyethylenimine (PEI) [9], which is able to form a complex with nucleic acids through interactions between its positively charged amino groups and the negatively charged phosphate groups present in the backbone of the nucleic acid. Its success has been mainly attributed to its ability to escape the endosome by a process described as "proton-sponge" effect [10] leading to the release of the payload into the cytoplasm. However, PEI is disadvantaged by a sub-optimal balance between efficacy and toxicity. High molecular weight PEI (> 25 kDa) generates stable complexes with high transfection efficacies but high cytotoxicity, whereas low molecular weight PEI (2-10 kDa) possesses better toxicity profiles but is less efficient [11]. To address these drawbacks, various alterations of PEI have been explored, identifying hydrophobic modification as a suitable tool to improve gene delivery activity and cytocompatibility of polyplexes. Therefore, PEI was modified with acyl [12] or alkyl chains, from C4 up to larger "fatty" hydrocarbon chains and sterol compounds (cholesteryl-PEI) [13-15], forming micelle-like nanoparticles with nucleic acids that offer unique properties regarding self-assembly, condensation of nucleic acids, improved cell association and gene transfection accompanied by more appropriate toxicity profiles. In an effort to develop a suitable nanocarrier for siRNA delivery into the brain we examined the BBB permeation ability of highly promising PEI-siRNA complexes (polyplexes (PXs)) depending on their hydrophobic modifications derived from either stearic-acid (SA) or decylacrylamide (DAA) monomers. Modification of PEI with SA has previously been shown to be beneficial for siRNA delivery into B16 melanoma cells [16], while SA-modified chitosan particles even demonstrated improved brain targeting-ability evaluated in a rodent animal biodistribution experiment [17]. The hydrophobic monomer DAA has so far only been utilized in micellar approaches, in which an excellent balance between hydrophobicity and size was described, making it a promising modification for drug delivery approaches [18-20]. Consequently, for this study, we commercially obtained SA-functionalized PEI (PEI-SA),

while DAA-modified PEI (PEI-DAA) polymers were synthesized by our group. As a first step, PXs formed with siRNA were characterized in detail with respect to their physicochemical properties such as encapsulation ability, size, surface charge, and stability. Protein binding of PX is a previously often overlooked parameter in both cell-based experiments with serum-containing media and biodistribution of PXs in the body after intravenous injection into the blood, as it has an impact on particle toxicity, cell uptake, agglomeration [21] and the PXs' fate in the body. It has been shown that some proteins adsorbed from the blood on NPs surface, e.g., Apolipoprotein E (ApoE), can even facilitate the BBB penetration via interactions with receptors located in the BBB, inducing cellular internalization into brain endothelial cells by receptor-mediated endocytosis (RMT) [22]. In order to gain insight into the protein composition adsorbed on PXs, depending on their hydrophobic modification, we analyzed the adsorbed proteins after PXs' incubation in serum by sodium dodecyl sulfate polyacrylamide gel electrophoresis (SDS-PAGE) and liquid chromatography – mass spectrometry (LC-MS-MS) techniques. In addition, the ability of PXs to be internalized into brain endothelial cells in a serum-dependent manner was initially examined with the immortalized human brain endothelial capillary cell line hCMEC/D3. Moreover, we examined the BBB permeation ability of unmodified and modified PXs for the first time in a highly sophisticated human induced pluripotent stem cell (hiPSC)-derived BBB transwell-model. Since we obtained promising results in *in vitro* experiments, we finally investigated the biodistribution of PXs by measuring the radioactive signals of ^{177}Lutetium (^{177}Lu) labeled DTPA-modified siRNA in the major organs and the brain after intravenous injection of formulations in SWISS mice.

2. Materials and Methods

2.1 Materials

Branched poly(ethylene imine) (PEI, 10000 g/mol) and stearic acid-functionalized PEI (PEI-SA) were obtained from Sigma-Aldrich (Taufkirchen, Germany). For synthesis of decylacrylamide-modified PEI (PEI-DAA) all chemicals were purchased from Acros Organics, or TCl and used as received. Deuterated solvents were obtained from Sigma-Aldrich (Taufkirchen, Germany), Deutero (Kastellaun, Germany) or Eurisotop (Saarbrücken, Germany). Holo Transferrin, HEPES (4-(2-hydroxyethyl)–1-piperazineethanesulfonic acid), Comassie Brilliant Blue G solution, dithiothreitol, indole-3-acetic acid, sodium acetate, sodium chloride, sodium hydroxide, heparin sodium salt, hydrochloric acid, copper(II)-acetate, potassium acetate, Dulbecco's Phosphate Buffered Saline (PBS), Triton-X, arsenazo(III),

yttrium(III) chloride, Fetal Bovine Serum (FBS), trypsin-EDTA solution 0.25%, dimethyl sulfoxide (DMSO), rat tail collagen coating solution, collagen from human placenta and retinoic acid were purchased from Sigma-Aldrich (Taufkirchen, Germany). Immortalized human brain capillary endothelial cell line hCMEC/D3 was kindly provided by the Institute of Pharmacy and Molecular Biotechnology (IPMB) (Heidelberg, Germany). Human iPSC culture cell line IMR90-4 was obtained from WiCell (Madison, WI, USA). Endothelial cell growth medium 2 and endothelial cell growth medium MV2 were purchased from Promocell (Heidelberg, Germany). Human endothelial-serum free growth medium, B27™ serum free supplement (50X), human fibronectin protein, Novex™ 10% tris-glycine gel, PageRuler™ Plus Prestained Protein Ladder (10 to 250 kDA), Pierce™ Lane Marker Reducing Sample Buffer and absolute ethanol were purchased from Thermo Fisher Scientific (Waltham, MA, USA). Recombinant human fibroblast growth factor (basic) was purchased from PeproTech (Hamburg, Germany), and Gibco® trypan blue solution 0.4% in phosphate buffered saline was obtained from FisherScientific (Hampton, New Hampshire, USA). SYBR Gold Dye, Lipofectamine 2000 transfection reagent and AlexaFluor 488 (AF488) dye were purchased from Life Technologies (Carlsbad, California, USA). CellTiter-Blue® Cell Viability Assay, CellTiter-Glo® Cell Viability Assay and trypsin was purchased from Promega (Madison, Wisconsin, USA). Rotiphorese®10x SDS-PAGE buffer was obtained from Carl Roth (Karlsruhe, Germany) and Lys-C was obtained from Wako Chemicals (Neuss, Germany). 2-(4-Isothiocyanatobenzyl) diethylenetriaminepentaacetic acid (p-SCN-Bn-DTPA) was purchased from Macrocyclics (Dallas, TX, USA), and Hs_GAPDH_1_SG and Hs_ACTB_2_SG QuantiTect primer assays were obtained from Qiagen (Venlo, Netherlands). Fresh human blood was obtained from Blutspendedienst des Bayerischen Roten Kreuzes (Munich, Germany) and EndolucinBeta-Lu^{3+} in aqueous 0.04M HCl solution was purchased from ITG Isotope Technologies Garching GmbH (Garching, Germany). Amine-modified eGFP siRNA (5′ - pACCCUGAAGUUCAUCUGCACCACcg, 3′- ACUGGGACUUCAAGUAGAC GGGUGGC), human glyceraldehyde 3–phosphate dehydrogenase (GAPDH) siRNA (5′- pGGUCGGAGUCAACGGAUUUGGUCgt, 3′- UUCCAGCCUCAGUUGCCUAAACCAGC A), and scrambled siRNA (5′-pCGUUAAUCGCGUAUAAUACGCGUat, 3′ - CAGCAAUUAGCGCAUAUUAUGCGCAUAp) were purchased from Integrated DNA Technologies (Leuven, Belgium). Indication of modified nucleotides: “p” denotes a phosphate residue, lower case letters are 2′-deoxyribonucleotides, capital letters are ribonucleotides, and underlined capital letters are 2′-O-methylribonucleotides.

2.2 Synthesis and characterization of PEI-DAA polymer

The synthesis of PEI-DAA was performed as described in the Supporting Information (Scheme S1, Supplementary Material). Based on the ^{1}H-NMR spectrum (Figure S1, Supplementary Material) a content of 95 mol% and 79 wt.% of PEI was calculated.

2.3 Quantification of PEI amount by copper assay

For quantification of PEI content within the PEI-SA and PEI-DAA polymers, a copper assay as described previously was used [23]. In brief, a calibration curve of PEI in deionized water was created over the concentration range of 2.0 mg/mL to 0.0375 mg/mL. Aqueous PEI-SA and PEI-DAA polymer solutions (1 mg/mL) and PEI calibration curve samples were distributed into a transparent FluoroNunc 96-well plate (FisherScientific, Hampton, NH, USA) and equal volume of beforehand freshly prepared 0.02 M copper(II)-acetate solution (pH = 5.4) was added to each well. Upon addition of copper (II), primary amines of PEI formed a dark blue cuprammonium complex, which was detected spectrophotometrically by measuring the absorbance at 690 nm with a microplate reader ((FLUOstar Omega, BMG Labtech, Ortenberg, Germany). Based on the PEI standard curve, PEI content of PEI-SA and PEI-DAA polymers were calculated. Measurements were performed in triplicate (n = 3).

2.4 Buffer capacity of the modified polymers

To determine the buffer capacity of PEI-SA and PEI-DAA polymers in comparison to unmodified PEI, pH titration was performed as described previously [24]. A total of 5 mg of each polymer was dissolved in 5 mL highly purified water and adjusted to a pH of approximately 11.5 with 0.1 M NaOH. Aliquots (50 µL) of 0.1 M HCl were added, and the pH of the solution was measured with a pH meter (accumet® AB150, Fisher Scientific, Hampton, NH, USA) after each addition.

2.5 Preparation of polyplexes

To prepare polymer-siRNA complexes (polyplexes (PXs)), aqueous polymer stock solutions were diluted with freshly filtered 10 mM HEPES buffer (pH = 7.2) to predetermined concentrations, added to a defined amount of siRNA in a microcentrifuge tube to obtain PXs at various N/P ratios and incubated for 30 min to permit stable PX formation. The N/P ratio is defined as the molar ratio between the polymer amine groups (N) and the siRNA phosphate groups (P). The amount of polymer needed to obtain different N/P ratios was calculated according to following equation:

m (polymer in pg) = n siRNA (pmol) x M protonable unit (g/mol) x N/P x number of nucleotides siRNA

The protonable unit of each polymer was calculated by dividing its molar mass by number of protonable primary amines present in each polymer, as calculated from the results of the copper assay (Scheme 1). The number of nucleotides of 25/27mer siRNA is set to 52.

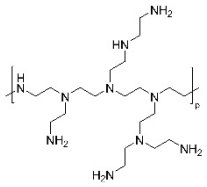

Branched PEI

Mn = 10000 g/mol

Mn, repeating unit = 43.07 g/mol

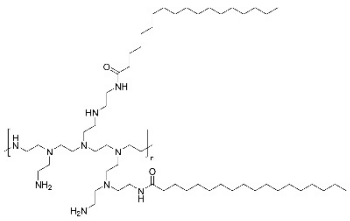

PEI-SA

Mn = 2132.67 g/mol

83 wt. % PEI

(calculated via copper assay)

Mn, protonable unit = 51.93 g/mol

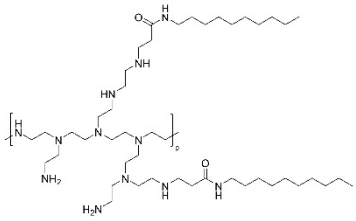

PEI-DAA

Mn = 12320 g/mol

86 wt. % PEI

(calculated via copper assay)

Mn, protonable unit = 50.12 g/mol

Scheme 1. Branched PEI, PEI-SA and PEI-DAA polymers used in this study. PEI content of modified polymers was calculated based on copper assay results, and molecular mass of one protonable unit (Mn, protonable unit) was calculated by dividing the molar mass (Mn) of the polymer by the number of protonable primary amines.

2.6 Physicochemical characterization of polyplexes

2.6.1 siRNA encapsulation ability by SYBR Gold Assay

SYBR Gold assay was used to evaluate the capacity of the polymers to encapsulate siRNA analogous to the procedures previously described [25]. PEI, PEI-SA and PEI-DAA PXs were prepared at various N/P ratios with scrambled siRNA in HEPES buffer, and 100 µL of each PX solution was distributed in a white FluoroNunc 96-well plate (FisherScientific, Hampton, NH, USA). A 4X SYBR Gold solution (30 µL) was added to each well, and the plate was incubated for 10 min in the dark. The fluorescence signal was determined by using a fluorescence plate reader (FLUOstar Omega, BMG Labtech, Ortenberg, Germany) at 492 and 555 nm excitation and emission wavelengths, respectively. An analogous procedure with free siRNA was used to obtain a 100% value. Measurements were performed in triplicate, and the results are shown as mean values (n = 3).

2.6.2 Size and Zeta Potential Analysis by Dynamic Light Scattering and Laser Doppler Anemometry

Particle size, polydispersity index (PDI) and zeta potential of PXs were measured using a Zetasizer Nano ZS (Malvern Instruments, Malvern, UK). PXs were formed at various N/P ratios, and a total volume of 100 µL of each sample was added to a disposal cuvette (Malvern Instruments, Malvern; UK) and used for particle size and PDI measurements by dynamic light scattering (DLS) at 173 ° backscatter angle running 15 scans three times per sample. Zeta potentials were measured using a Zeta Cell (Zetasizer Nano series, Malvern, UK) containing a 7X dilution of another 100 µL sample aliquot by laser Doppler anemometry (LDA) with each run consisting of 30 scans. Results are expressed as mean ± standard deviation (n = 3).

2.6.3 Polyplex stability measured by Heparin Competition Assay

To evaluate the PX stability in the presence of competing polyanions under neutral and acidic conditions, a heparin competition assay was performed as described previously [26]. In brief, PXs were prepared at N/P 7 in the presence of two different buffers: a 10 mM HEPES buffer (pH 7.4) and a 10 mM sodium acetate buffer (pH 4.5) to enable the comparison of PXs' stability at different pH values as well as at various ionic strengths. PXs sample aliquots of 60 µL were dispersed into a white FluoroNunc 96-well plate, and 10 µL of beforehand prepared heparin concentrations (0.12, 0.16, 0.21, 0.27, 0.35, 0.46, 0.59, 0.77, 1 USP units/well) were added to each well. After incubation for 30 min at room temperature, 30 µL of a 4X SYBR Gold solution was added to each well, and the plate was incubated for 10 min under light exclusion.

Fluorescence measurement and the calculation of a percentage of free siRNA were performed as described above. To obtain more precise results, each heparin concentration was added to the respective buffer and used as a blank for related samples. Measurements were performed in triplicate, and the results are shown as mean values (n = 3).

2.7 Protein corona investigations

2.7.1 Formation of the protein corona by FBS coating

PEI, PEI-SA and PEI-DAA PXs were incubated with FBS for protein coating at final concentrations of either 10% or 50% (v/v) FBS. Therefore, one part of the PX suspension was mixed with equal volumes of FBS to achieve a 50% FBS dilution and in addition one part of it was further diluted with 10 mM HEPES buffer (pH 7.2) to achieve a final concentration of 10% FBS, which corresponds to a particle-to-serum ratio used in the *in vitro* experiments performed in this study. PX – FBS mixtures were incubated at 37°C for 30 min in a Thermomixer (Eppendorf AG, Hamburg, Germany) and used for further experiments after cooling down to room temperature (20-25 °C).

2.7.2 Visualization of bound Proteins by sodium dodecyl sulfate polyacrylamide gel electrophoresis (SDS-PAGE)

PEI, PEI-SA and PEI-DAA PXs were prepared at N/P 7 and coated with FBS as described above. Subsequently, PXs were purified from unbound proteins analogous to centrifugation procedures optimized for a protein corona - PX approach as described in detail in *Subchapter III.2*. In brief, solutions were centrifuged at 12.500g for 10 min, subsequently the supernatant was removed, and the pellet was resuspended in 10 mM HEPES buffer (pH = 7.2) followed by an incubation period of 15 min to allow PX reformation. The centrifugation procedure was repeated to ensure removal of loosely attached proteins. Samples (FBS coated PXS and uncoated PXs as control), FBS and Transferrin reference solution (RS) were mixed with Pierce™ Lane Marker Reducing Sample Buffer and boiled at 95°C for 5 min to denature proteins in a Thermomixer (Eppendorf AG, Hamburg, Germany). Gel electrophoresis chamber Novex® Mini-Cell was prepared with a polyacrylamide-gel 10% placed in 10-fold diluted rotiphorese® 10x SDS PAGE buffer. The wells of the gel were loaded with 5 µL of PageRuler™ Plus Prestained protein ladder (10 to 250 kDA) as molecular marker, 25 µL FBS solution and 25 µL Transferrin RS as controls and 25 µL of PXs (uncoated, 10% FBS and 50% FBS) samples. The gel was run at 150 mV for 90 min, rinsed twice with deionized water , stained overnight in Comassie Brilliant Blue G solution to visualize the proteins and subsequently

destained for 24 h in a mixture of 50% highly purificated water, 40% methanol and 10% acetic acid. The gel was scanned using a Biorad Chemidoc (Bio-Rad Laboratories, Hercules, CA, USA) and data were processed using Image Lab 6.0.1 software.

2.7.3 Protein Identification by Mass Spectrometry (MS) measurements

2.7.3.1 Filter Aided Sample Preparation (FASP) Digest

PEI, PEI-SA and PEI- DAA PXs prepared with 100 pmol scrambled siRNA at N/P 7 were incubated in 10% FBS and purified by centrifugation as described above. The quantification of the total protein amount was investigated spectrophotometrically with a UV visible spectrophotometer (Nanodrop One, Thermo Fisher Scientific, Waltham, Massachusetts, USA) by measuring the absorbance at 280 nm, and aliquots containing 20 µg total protein were prepared for MS measurements. Therefore, protein corona – PX complexes (PCPXs) were reduced and alkylated using dithiothreitol (DTT) and indole-3-acetic acid (IAA) followed by using a modified FASP procedure [27]. The proteins were centrifuged on a 30 kDa cutoff filter device (Sartorius), washed thrice with UA buffer (8 M urea in 0.1 M Tris/HCl pH 8.5) and twice with 50 mM ammonium bicarbonate. The proteins were digested for 2 h at room temperature using 0.5 µg Lys-C and for 16 h at 37°C using 1 µg trypsin. After centrifugation (10 min, 14.000g), the eluted peptides were acidified with 0.5% trifluoroacetic acid solution and stored at -20 °C.

2.7.3.2 Mass Spectrometric (MS) Measurements

Liquid chromatography with tandem mass spectrometry (LC-MS-MS) analysis was performed in data-dependent acquisition (DDA) mode. MS data were acquired on a Q-Exactive HF-X mass spectrometer (Thermo Fisher Scientific, Waltham, Massachusetts, USA) each online coupled to a nano-RSLC (Ultimate 3000 RSLC; Dionex). Tryptic peptides were automatically loaded on a C18 trap column (300 µm inner diameter (ID) × 5 mm, Acclaim PepMap100 C18, 5 µm, 100 Å, LC Packings) at 30 µL/min flow rate. For chromatography, a C18 reversed phase analytical column (nanoEase MZ HSS T3 Column, 100Å, 1.8 µm, 75 µm x 250 mm, Waters) at 250 nL/min flow rate in a 95 min non-linear acetonitrile gradient from 3 to 40% in 0.1% formic acid was used. The high-resolution (60 000 full width at half-maximum) MS spectrum was acquired with a mass range from 300 to 1500 m/z with automatic gain control target set to 3 x 106 and a maximum of 30 ms injection time. From the MS prescan, the 15 most abundant peptide ions were selected for fragmentation (MS-MS) if at least doubly charged, with a dynamic exclusion of 30 seconds. MS-MS spectra were recorded at 15 000 resolutions with

automatic gain control target set to 5 x 102 and a maximum of 50 ms injection time. The normalized collision energy was 28, and the spectra were recorded in profile mode.

2.7.3.3 Data Processing - Protein Identification

Proteome Discoverer 2.5 software (Thermo Fisher Scientific; Waltham, Massachusetts, USA, version 2.5.0.400) was used for peptide and protein identification via a database search (Sequest HT search engine) against Ensemble Cow data base (Release 2014_75, 22118 sequences). Search settings were 10 ppm precursor tolerance, 0.02 Da fragment tolerance, one missed cleavage allowed. Carbamidomethylation of Cys was set as a static modification. Dynamic modifications included deamidation of Asn, Gln and Arg, oxidation of Pro and Met, and a combination of Met loss with acetylation on protein N-terminus. Percolator was used for validating peptide spectrum matches and peptides, accepting only the top-scoring hit for each spectrum, and satisfying the cutoff values for false discovery rate (FDR) < 1%, and posterior error probability < 0.01. The final list of proteins was complied with the strict parsimony principle.

2.7.3.4 Data Processing – Label-Free Quantification

The quantification of proteins was based on abundance values for unique peptides. Abundance values were normalized on the total peptide amount to account for sample loading errors. The protein abundances were calculated as the average of the three most abundant (Top 3N) distinct peptide groups. The final protein ratio was calculated from the grouped protein abundances, and an ANOVA was used for the determination of p-values (< 0.05). To overcome the problem of missing values, match between run (MBR) was used to transfer identified peptides in one run to another by inference based on 1ppm mass tolerance and 30sec retention time shift. Additionally missing values were replaced by low abundant imputation from the lower five percent of detected values.

2.8 In vitro monolayer experiments

2.8.1 Cells and Cell culture

The immortalized human brain capillary endothelial cell line ((hCMEC/D3) was cultured in ready-to-use endothelial cell growth medium supplemented with Penicillin-Streptomycin (1%). The cells were cultured, maintained and grown in an incubator in humidified air with 5% CO_2 at 37 °C. Culture flasks were coated with rat tail collagen coating solution for 2 h at 37 °C. Transfection experiments were performed using heparin-free endothelial cell growth medium

MV2. Human iPSC IMR90-4 cell culture line was differentiated into BBB hiPS-ECs and cultured as previously described elsewhere [28].

2.8.2 Cytotoxicity measurements of PXs by CellTiter-Blue® Assay

Cytotoxicity of PXs was evaluated using a CellTiter-Blue® Cell Viability Assay Kit according to the manufacturer's protocol based on the ability of living cells to convert a redox dye (resazurin) into a fluorescent end product (resorufin). Nonviable cells rapidly lose metabolic capacity and thus do not generate a fluorescent signal. In brief, 2.000 hCMEC/D3 cells per well were seeded in a transparent 96-well plate (FisherScientific, Hampton, NH, USA) and incubated for 24 h at 37 °C and 5% CO_2. PXs were prepared at N/P ratios of 7 and 15, and free polymer solutions containing respective polymer concentrations as used for PX preparation were additionally utilized. After consumed medium was completely removed, 90 µL of fresh medium was added to each well and briefly mixed with solutions containing PXs or free polymers. Pure 10 mM HEPES buffer was used as negative control, and DMSO 25% in medium was utilized as a positive control. After a 24 h incubation period, 20 µL of CellTiter-Blue® substrate was added to each well followed by another incubation period of 4 h in the incubator. Subsequently, a volume of 100 µL of each sample was transferred to a white 96-well plate (FisherScientific, Hampton, NH, USA), and the fluorescence intensity was measured using a fluorescence plate reader (FLUOstar Omega, BMG Labtech, Ortenberg, Germany) at 560 and 590 nm excitation and emission wavelengths, respectively. The experiment was performed in triplicate, and the results are shown as mean ± standard deviation normalized to percentage of viable cells in comparison to untreated cells representing 100% viability.

2.8.3 Quantification of cellular Internalization into hCMEC/D3 cells by Flow Cytometry

Flow cytometry was used to quantify the *in vitro* cellular uptake of PEI, PEI-SA and PEI-DAA PXs in the human brain capillary endothelial cell line (hCMEC/D3) with and without FCS present in the culture medium. Amine modified siRNA was labeled with the fluorescent dye Alexa Fluor 488 (AF488) according to the manufacturer's protocol and purified by ethanol precipitation and spin column binding as described previously [29]. The hCMEC/D3 cells were seeded in 24 well plates, cell culture medium was replaced with heparin-free cell culture medium with or without FCS to examine alteration in cellular internalization capability of PXs as a function of FCS presence. All PXs were prepared with 50 pmol siRNA-AF488 at N/P 7. Untreated cells and cells treated with free siRNA were used as negative controls. After a 24 h incubation period, incubation medium was removed, cells were washed with PBS and detached

with 0.25% trypsin-EDTA. Samples were washed twice with PBS and resuspended in 500 µL PBS/2 mM EDTA. Additionally, trypan blue quenching was performed to exclude surface fluorescent signals of not completely internalized siRNA-complexes. Median fluorescence intensities (MFI) after quenching were analyzed using an Attune NxT Acoustic Focusing Cytometer (Thermo Fisher Scientific, Waltham, Massachusetts, USA) by exciting the siRNA-AF488 at 488 nm and measuring the fluorescence signal with a 530/30 nm emission filter. Samples were run in triplicates, each sample consisting of a minimum of 10000 viable cells. Results are given as mean ± standard deviation (n = 3).

2.9 Blood-Brain permeability of PXs evaluated in hiPSC-derived BBB Model

2.9.1 Cytotoxicity measurements of PXs by CellTiter-Glo® Assay

Cell viability of the differentiated pluripotent stem cell line IMR90-4 after treatment with PEI, PEI-SA and PEI-DAA PXs at N/P 7 was evaluated using a CellTiter-Glo® Luminescent Cell Viability Assay Kit (Promega, Walldorf, Germany) based on quantification of ATP present, which reflects the presence of metabolically active cells. Therefore, the human induced pluripotent stem cell line IMR90-4 was differentiated into blood-brain barrier endothelial-like cells (EC) as previously described [28, 30]. Differentiated ECs were plated on a collagen IV/fibronectin coated 96-well black flat bottom plate (Greiner Bio-One, Kremsmünster, Austria) at a density of 10^6 cells/cm² in EC medium (human endothelial serum free medium supplemented with B27™) additionally containing human basic fibroblast growth factor (hbFGF) and retinoic acid. On the next day, medium was changed to EC medium without supplements. After 24 h, cells were treated with PEI, PEI-SA and PEI-DAA PXs at N/P 7 and incubated for further 24 h at 37 °C in a 5 % CO2 incubator at 37 °C. Cells treated with EC medium and 1 % sodium dodecyl sulfate (SDS) were used as negative and positive controls, respectively. Subsequently, wells were washed with PBS, and equal amounts of cell culture medium and CellTiter-Glo® reagent were added to the wells. The plate was transferred into a multimode plate reader (Infinite M200, Tecan, Männedorf, Switzerland) and mixed for 2 min to induce cell lysis and incubated for another 10 min at room temperature to stabilize the luminescent signal. The luminescence of each sample was measured (wavelength range 400 – 700 nm), and the cell viability was calculated using the negative control as a reference, representing 100% cell viability. Measurements were performed in duplicate and the results are shown as mean ± standard deviation (n = 2).

2.9.2 Evaluation of barrier integrity by TEER measurements

To investigate barrier integrity prior to transport studies, the transendothelial electrical resistance (TEER) was measured 48 h after seeding hiPSC-derived ECs on cell culture inserts. TEER values were determined 40 min after complete medium change with an Millicell ERS-2 (Merck Millipore, Burlington, MA, USA) electrical resistance system in combination with the electrode type STX3 (World Precision Instruments, Sarasota, FL, USA). To exclude additional barrier properties, empty inserts (blank sample) coated with collagen IV/fibronectin were measured. To receive the TEER values [$\Omega \cdot cm^2$] resulting from hiPSC-derived ECs, average TEER of the blank samples were subtracted, and values were multiplied by surface area of the inserts. Each insert was measured at three positions monitoring the entire surface area, duplicates were used for each model in three independent biological experiments.

2.9.3 Evaluation of PXs Blood-Brain Barrier Permeability

Transport assays were performed in a TTP 24-well cell culture plate (Faust Lab Science, Klettgau, Germany) with transwell inserts (ThinCert® cell culture inserts; Greiner Bio-One, Kremsmünster, Austria) on an orbital shaker (KM-2 Akku, Edmund Bühler, Bodelshausen, Germany) at 100 rpm, 37 °C, 95% humidity, and 5% CO2. PEI, PEI-SA and PEI-DAA PXs prepared at N/P 7 were diluted in EC medium with or without addition of serum and applied to the apical (top) side of the blood-brain barrier monoculture model with hiPSCs-derived endothelial-like cells. The basolateral (bottom) side was supplied with EC medium, and the permeation was evaluated after an incubation time of 24 h. Apical and basolateral media were analyzed by fluorescence measurements with an Infinite M200 fluorescence reader (Tecan, Männedorf, Switzerland) to quantify the transport of the PXs through the BBB model (λ_{em} = 524 nm, λ_{ex} = 490 nm). As a control, PXs were incubated on collagen IV-/fibronectin-coated inserts without cells to exclude adsorption effects on the membrane. The apparent permeability coefficient (Papp [cm/s]) was calculated from the observed transport rate of the PX over 24 h (dQ/dt [mg/min]) and normalized by the surface area of the cell culture insert membrane (A = 0.336 cm^2) and the initial concentration of the donor solution (D [mg/mL]) according to the following equation:

$$Papp\ \left[\frac{cm}{s}\right] = \frac{\Delta Q}{\Delta t}\ x\ \frac{1}{D\ x\ A}$$

All permeability studies were performed in duplicate and three independent biological replicates; results are presented as mean ± SD.

2.10 In vivo biodistribution experiments

2.10.1 Hemocompability of Polymers measured by Hemolysis and Erythrocyte Aggregation Assays

The hemocompatibility and endosomolytic activity of polymers was investigated by red blood cell (RBC) hemolysis and aggregation assays analogous to previous described protocols [31]. Briefly, human erythrocytes were isolated from fresh human blood by centrifugation at 900g for 10 min. RBCs were washed three times with 150mM NaCl until the supernatant was clear and colourless. Erythrocytes were again centrifuged at 900g for 10 mins and the supernatant was replaced with PBS buffer at defined pH values that mimic physiologically conditions in the blood (pH 7.4). A volume of 10 µL of 20X PEI, PEI-SA and PEI-DAA solutions in different concentrations (1 mg/mL – 0.0078 mg/mL) was distributed in a 96-well plate. 20% Triton X-100 (100% lysis) and pure PBS (0% lysis) were used as control. A volume of 190 µL of the RBC suspension was added to each well, and the plate was incubated for 30 min at 37 °C. RBCs were removed by centrifugation (500g, 5 min) and supernatant was investigated spectroscopically in a transparent FluoroNunc 96-well plate (FisherScientific, Hampton, NH, USA) by measuring the absorbance of released hemoglobin at 541 nm using a multimode microplate reader (Tecan Spark, Tecan Group, Männedorf, Switzerland). Measurements were performed in triplicate, and the results are shown as mean values (n = 3). The degree of hemolysis induced by polymers (% hemolysis) was calculated according to following equation:

$$\%\, Hemolysis = \frac{Hb - Hb0}{Hbtot}\, x\, 100$$

Hb is the amount of hemoglobin found in the sample, Hb0 is the amount of basal hemoglobin found in the negative control samples and Hbtot is the amount of hemoglobin after 100% hemolysis. In addition, to evaluate the aggregation of RBCs after treatment, images of the samples were taken after the centrifugation step using a Keyence BZ8100 Fluorescence microscope (Keyence, Osaka, Japan) equipped with a Nikon SPLan Fluor 10x/0.45 objective (Nikon, Minato, Japan) in the brightfield mode.

2.10.2 Covalent modification of siRNA with pBn-SCN-Bn-DTPA

In an effort to examine the *in vivo* biodistribution of unmodified and modified PEI PXs in SWISS mice, siRNA was radioactively labeled with ^{177}Lu following an adjusted protocol previously described by Jones et al. [32]. At first, amine-modified EGFP siRNA (siEGFP) was covalently coupled with the amine-reactive chelator p-Bn-SCN-Bn-DTPA according to a

previously described method [33]. Briefly, 5.11 mg siEGFP was dissolved in a centrifuge tube in 2 mL RNase free water, 100 µL of 0.1 M $NaHCO_3$ solution was added and siEGFP solution was subsequently mixed with p-Bn-SCN-Bn-DTPA dissolved in DMSO. After thoroughly vortexing the tube and an incubation period of 6 h, siRNA-DTPA was precipitated by adding absolute ethanol. The siRNA-DTPA complex was isolated from free p-Bn-SCN-Bn-DTPA with the absolutely RNA miRNA Kit (Agilent, Santa Clara, CA, USA) according to manufacturer´s protocol. Concentration measurement of siRNA was performed by measuring the absorption at 260 nm with a spectrophotometer (Nanodrop One, Thermo Fisher Scientific, Waltham, MA, USA). The coupling degree after purification was determined by additional quantification of DTPA in a nonradioactive assay described by Pippin et al. [34]. Briefly, absorption of an yttrium(III)-arsenazo(III)-complex was measured at 652 nm with a UV/Vis spectrophotometer (UV-1600PC, VWR, Ismaning, Germany) and sample DTPA content was calculated with the help of a calibration curve since the absorption of the complex decreases after addition of DTPA.

2.10.3 Labelling and purification

Radiolabelling of the p-SCN-Bn-DTPA-coupled siRNA with ^{177}Lu was accomplished at room temperature in 0.4 M sodium acetate buffer (pH = 5) for 30 mins. The siRNA-^{177}Lu mixture was added to an equilibrated Illustra™ NAP™ 10 column Sephadex G-25 (GE Healthcare, Chicago, ILL, USA) for purification and elution. Fractions were collected, and counts per minute were determined by a scintillation counter. The fraction with the highest radioactive signal was additionally investigated by HPLC analysis (Agilent 1100 Series, SEC column: TSK gel Super SW mAb HR) to ensure the presence of siRNA and the absence of free DTPA. The quantification of the siRNA in the final mixture was investigated spectrophotometrically with a UV visible spectrophotometer (Cary 50 Conc, Varian) by measuring the absorbance at 260 nm.

2.10.4 In vivo biodistribution

All animal experiments were approved by the Animal Care and Use committees at the University of Heidelberg, (Heidelberg, Germany) and the Regierungspräsidium Karlsruhe (Karlsruhe, Germany) (reference number 35-9185.81/G-111/16; date of approval: 22 June 2016). For *in vivo* experiments, polyplexes with ^{177}Lu-labeled siRNA were prepared at N/P ratio of 7 with PEI and PEI-SA polymers. Free ^{177}Lu-labeled siRNA as control and PXs samples were injected intravenously to the tail vein of SWISS mice (2 nmol siRNA/animal), and

biodistribution was investigated 1 h post injection. At this point, the animals were sacrificed, major organs were removed and weighed, and the radioactivity of each sample was measured using a Cobra Auto γ-Counter (Packard BioScience Co., Meriden, CT, USA) in comparison with standards. The tissue-associated activity was related to the total injected dose (ID) and calculated as a percentage of the total injected dose per gram of the respective organ (ID%/g). Measurements were performed in triplicate, and the results are shown as mean ± standard deviation (n = 3).

2.11 Statistics

Unless otherwise stated, results are given as mean value ± standard deviation. One-way ANOVA with Bonferroni multiple comparison test and two-way ANOVA were performed in GraphPad Prism software (Graph Pad Software, La Jolla, CA) to calculate p-values at 95% confidence.

3. Results and Discussion

3.1 Synthesis and characterization of polymers

The beneficial effects of hydrophobic modifications of cationic polymers on gene delivery efficiency, especially for fatty acids and linear alkyl chains have been previously reported in the literature [35]. Therefore, in this study, two different hydrophobically modified branched PEI polymers were selected to investigate their potential for siRNA delivery into the brain compared to cationic PEI PXs depending on the polymers' microstructure and the selected experimental setting. Stearic acid-modified branched PEI (PEI-SA) was purchased from Sigma-Aldrich and PEI-DAA was synthesized by our group by functionalization of branched PEI (M_n = 10kDa) with decylacrylamide (DAA) as described in Scheme S1 (Supplementary Material). Based on the ^{1}H-NMR spectrum (Figure S1, Supplementary Material), a content of 95 mol% and 79 wt.% of PEI was calculated. Quantification of PEI content in modified polymers was investigated using a copper assay and amounted to 83 wt% and 86 wt% for PEI-SA and PEI-DAA polymer, respectively. These data were further used to calculate the protonable unit of each modified polymer as described above ($M_{n(\text{protonable unit})}$ PEI-SA = 51.93 g/mol, $M_{n(\text{protonable unit})}$ PEI-DAA = 50.12 g/mol).

3.2 Buffer capacity

Buffer capacity constitutes an important property of polycations with respect to endosomal escape ability and cargo release into the cytoplasm. One of the postulated mechanisms for endosomal escape in the case of amine-containing polymers is the so-called "proton-sponge" effect [36, 37]. After internalization of the NPS into the cell via endocytosis, a low endosomal pH of approximately 4.5 leads to protonation of the residual non-protonated amino groups of the polymer, resulting in swelling of the particles, disruption of the endosomal membrane, and subsequent release of the cargo into the cytoplasm. The primary, secondary and tertiary amino groups present in the branched PEI molecule exhibit pKa values distributed over the entire physiological pH range, making PEI a molecule with large buffering capacity and endosomal escape ability. In an effort to examine the effect of functionalization of PEI with SA and DAA, acid/base titration with 0.1 M HCl was performed with PEI, PEI-SA and PEI-DAA polymers. As illustrated in Figure 1 only slight differences were detected in titration curves of the polymers.

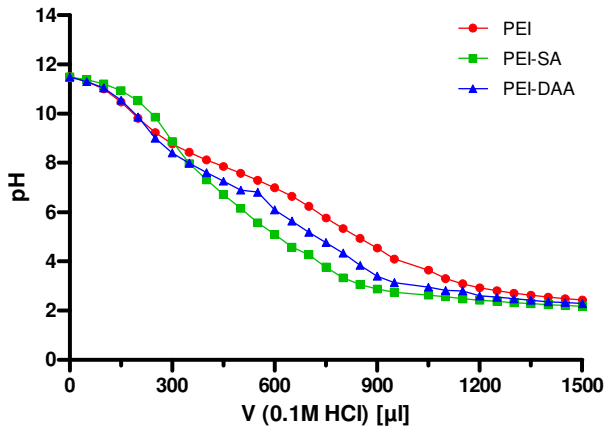

Figure 1. Titration curves of aqueous PEI, PEI-SA and PEI-DAA polymer solutions (1 mg/mL) titrated against 0.1 M HCl from pH 11.5 to 2. Solutions were adjusted to pH 11.5 with 0.1 M NaOH. (Data points indicate mean values).

The PEI polymer exhibited considerable buffering capacity over the entire pH range, while the PEI-SA and PEI-DAA polymers revealed a slightly lower buffer capacity, as they required lower amounts of HCl for the alteration of the pH value of the solution. This effect was even more pronounced for the PEI-SA polymer. These results are in line with our expectations since polymer functionalization converts a primary amine of the PEI into an amide with considerably higher pKa values, which is not protonated at endosomal pH. However, all polymers exhibited appropriate buffer capacities as only slight differences were observed between them. Therefore,

we suggest that modification of PEI polymers with SA as well as DAA subunits might not negatively affect the endosomal escape ability.

3.3 SYBR Gold Assay

SYBR Gold assays were performed at various N/P ratios to determine the optimal polymer amounts for complete siRNA condensation, and to evaluate the impact of hydrophobic modifications on encapsulation ability of polymers. Protection of siRNA molecules by charge complexation with cationic polymers is an effective method to circumvent the limitations in the application of naked siRNA caused by rapid degradation, immune response and low passive cell uptake [38]. Negatively charged phosphate groups present in siRNA molecules interact electrostatically with positive charges of protonated amine groups of the polymer [39] forming PXs. In the case of hydrophobic modified polymers, it is known that the polyplex formation process is synergistically driven by electrostatic as well as hydrophobic interactions, leading to thermodynamically highly stable micelle-like NPs [40]. The fluorescent dye SYBR Gold intercalates into free and unbound siRNA molecules causing a fluorescent signal that decreases as soon as the siRNA is condensed by the polymers. As shown in Figure 2, PEI exhibited lowest siRNA condensation ability from N/P 0.5 to 1.5 compared with modified polymers with 98%, 94% and 88% of free sRNA, respectively.

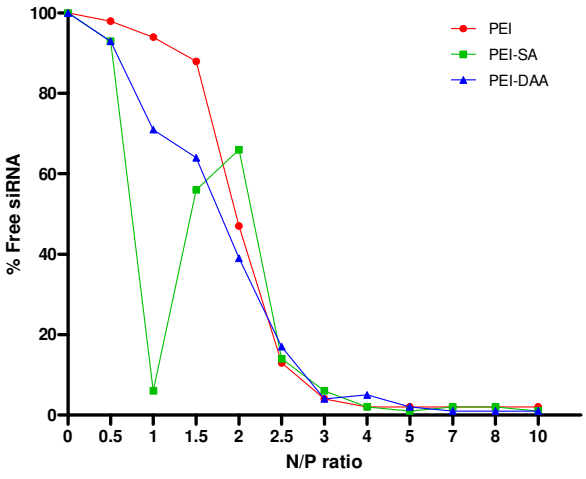

Figure 2. siRNA encapsulation profiles of polyplexes as measured by SYBR Gold assay at various N/P ratios. 100% values (N/P = 0) are represented by determined fluorescence of uncondensed siRNA. (Data points indicate mean, n = 3).

For PEI-DAA 93%, 71% and 64% non-encapsulated siRNA was detected at N/P ratios ranging from 0.5 to 1.5. Interestingly, only 6% of siRNA free remained uncomplexed from PEI-SA PXs at N/P 1, while higher N/P ratios were found to be less efficient in terms of encapsulation ability.

However, PEI, PEI-SA and PEI-DAA polymers showed comparable siRNA encapsulation profiles starting at a N/P ratio of 2.5. Maximum protection of the siRNA payload was reached at the same N/P ratio, namely N/P 5, with 2%, 1% and 2% free siRNA, respectively. These results indicate that the hydrophobic modifications of the PEI polymer did not significantly influence the amount of polymer required to achieve full siRNA condensation but, however, still might have an influence on the thermodynamical stability of the formed micelle-like PXs. In the literature, the influence of hydrophobic segments on particle formation has been investigated with variously modified polymers, for example, the group of Liu et al. reported that amphiphilic PEI-PCL-PEG polymers achieved full siRNA condensation at an N/P ratio of two and thus suggested that additional hydrophobic interactions increase nucleic-acid binding affinity [41]. Similar behavior was reported for amphiphilic nylon-3 polymers previously investigated by our group as siRNA delivery systems [26, 42]. In the case of hydrophobically modified PEI polymers, the group of Alshamsan et al. reported that stearic-acid functionalized PEI exhibited a left shift in binding vs. concentration curves in performed gel retardation assay and that less polymer was required than for unmodified PEI to achieve 50% binding of siRNA. Accordingly, the author suggested that modified PEI possess more efficient condensation ability compared to unmodified PEI. However, complete condensation of siRNA was only achieved with the same amount of both, PEI and stearic acid-modified PEI [16]. In regard of our results, especially for PEI-SA at N/P ratio of 1, we hypothesize that hydrophobically modified polymers initially form loose aggregates with transition to micelles upon exceeding the critical micelle concentration. The micelles might embed free siRNA molecules resulting in a decreased fluorescent signal. The same trend, albeit less pronounced, was found for PEI-DAA PXs at N/P ratios of 1 and 1.5. On the basis of this data, we hypothesize that conversion to stable polyplexes occurs only upon addition of higher amounts of polymer (as of N/P 5), which is a prerequisite for further experiments and successful siRNA delivery in general. Taken together, hydrophobic alkyl chains within the polymer were shown to not remarkably affect the electrostatic interactions between siRNA and amines. All polymers showed comparably efficient siRNA encapsulation abilities at rather low N/P ratios, which is beneficial in terms of PXs toxicity, unwanted side effects and economical aspects. PEI-SA and PEI-DAA polymers were demonstrated to possess amphiphilic properties, leading to micelle-like PXs, that might possess unique properties with beneficial effects for the siRNA delivery process.

3.4 Size and Zeta Potential Analysis of PXs by Dynamic Light Scattering and Laser Doppler Anemometry

As hydrodynamic diameters, size distributions and surface charges are major parameters that considerably contribute to the cell internalization ability and transfection efficacy of PXs, we evaluated them depending on the polymers' modifications in the next step of the study at N/P ratios from 0.5 to 10 with DLS and LDA techniques. In general, it is known that sizes smaller than 200 nm are suitable for *in vivo* and clinical applications and that a positive surface charge is a prerequisite for successful interaction with negatively charged cell membranes and subsequent internalization via endocytosis. Our data revealed, as illustrated in Figure 3, that sizes and PDI values and surface charges of the PXs formed with PEI, PEI-SA and PEI-DAA polymers changed in a similar manner as a function of the selected N/P ratio.

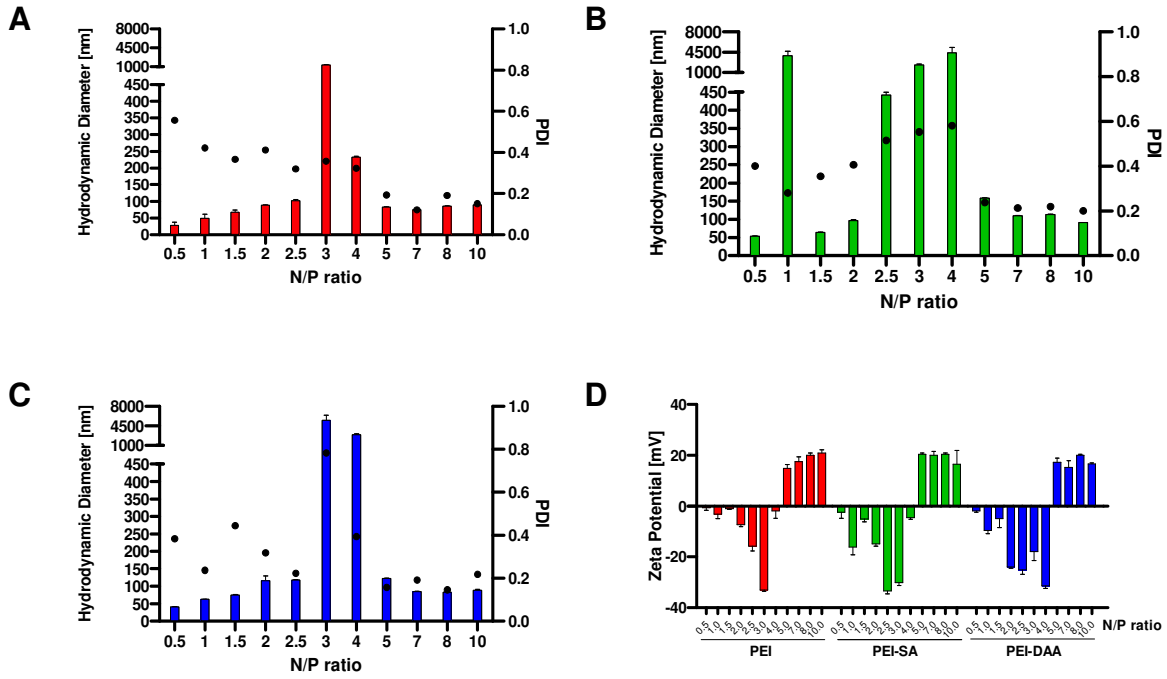

Figure 3. Hydrodynamic diameters (left y-axis) and polydispersity indices (PDI, right y-axis) of (**A**) PEI, (**B**) PEI-SA and (**C**) PEI-DAA PXs and (**D**) zeta potentials of all formulations formed at various N/P ratios (0.5 - 10). (Data points indicate mean ± SD, n = 3).

In detail, as shown in Figure 3A and 3C, sizes for PEI and PEI-DAA PXs at the smallest N/P ratios from 0.5 to 2.5 started at very low values (PEI: 27.35 nm, PEI-DAA: 40.65 nm at N/P 0.5) and increased with increasing polymer amounts ((PEI: 101.66 nm, PEI-DAA: 117.37 nm at N/P 2.5), whereas the respective PDI values were relatively high and inconsistent, indicating a non-stable system. In case of PEI-SA, as shown in Figure 3B, the values of hydrodynamic diameters revealed only slight increases from N/P 0.5 to N/P 2.0 (53.70 nm to 96.43 nm), except the value measured for N/P 1, that was tremendously higher (3858.67 nm, PDI: 0.28).

Sizes considerably enlarged with further increase of the N/P ratio and reached values of 1321.67 nm, 2295.67 and 5469.33 nm at N/P 3 and 232.67 nm, 4386.67 nm and 2925.33 nm at N/P 4 for PEI, PEI-SA and PEI-DAA, respectively. Sizes remarkably decreased for all PXs with further addition of polymer upon N/P ratio 5, exhibiting values of 82.47 nm, 158.00 nm and 122.07 nm for PEI, PEI-SA and PEI-DAA, respectively. A similar trend emerged regarding the PDI values which yielded in similar ranges from 0.12 to 0.22 for all PXs (N/P 5 to N/P 10). All polymers exhibited slightly decreased sizes and PDI values upon addition of more polymer, reaching an N/P value of 7 (PEI-PXs: 74.83 nm/0.12, PEI-SA PXs: 109.7 nm/0.21, PEI-DAA PXs: 84.6 nm/0.19) with no relevant changes by further increasing the N/P value to 8 and 10. The zeta potential at lower N/P ratios from 0.5 to 4 of PXs was negative for all formulations, while upon N/P ratio of 5, all the PXs revealed positive values ranging from 14.9 mV to 20.9 mV. Therefore, we conclude, in line with the results of the SYBR Gold assay, that the amount of polymer at low N/P ratios was not enough to efficiently embed the siRNA, whereas, by increasing the N/P ratio up to 5, a sufficient polymer excess was reached to form stable complexes with appropriate sizes, PDI values and positive surface charges. Effects of hydrophobic modification on size reduction due to additional hydrophobic interactions with siRNA, as described in the literature [43, 44], were not observed for PEI-SA and PEI-DAA PXs. We hypothesize that hydrophobic alkyl chains do not considerably affect the size of PXs possibly due to the free-rotation property of the saturated carbon atoms, leading to a high flexibility in condensation to siRNA-polymer complexes, what goes in line with a study described by Aliabadi et al. using a library of lipid-substituted PEI(2kDa)s [12]. However, since PEI-DAA PXS exhibited a slightly smaller size compared to PEI-SA PXs for the most efficient N/P ratio of 7, we hypothesize that the shorter hydrophobic alkyl chains in the PEI-DAA polymer enables a higher packing efficiency due to lower steric hinderance. In conclusion, N/P 7 was identified as the most appropriate N/P ratio and was subsequently used in all further experiments. Hydrophobic modification of PXs was not demonstrated to considerably affect siRNA packaging and the resulting sizes, PDI values and surface charges of PXs. All polymers formed PXs with suitable properties for further *in vitro* and in *vivo* testing upon reaching optimal polymer concentrations.

3.5 siRNA Release by Heparin Competition Assay

The stability of PXs is highly influenced by the presence of competing anions after addition to serum containing cell culture medium or administration *in vivo* and highly depends on the pH of the environment. Release assays were performed to investigate the protective capacity of

PEI, PEI-SA and PEI-DAA polymers at physiologically relevant conditions in blood (pH 7.4) and under acidic conditions (pH 4.5) that mimic the endosomal compartment in which siRNA must be released to successfully induce the RNAi machinery and leading to therapeutic effects. As shown in Figure 4A, siRNA displacement at pH 7.4 from PEI PXs was observed at low heparin concentrations and reached maximum release of approximately 25% at highest heparin concentration.

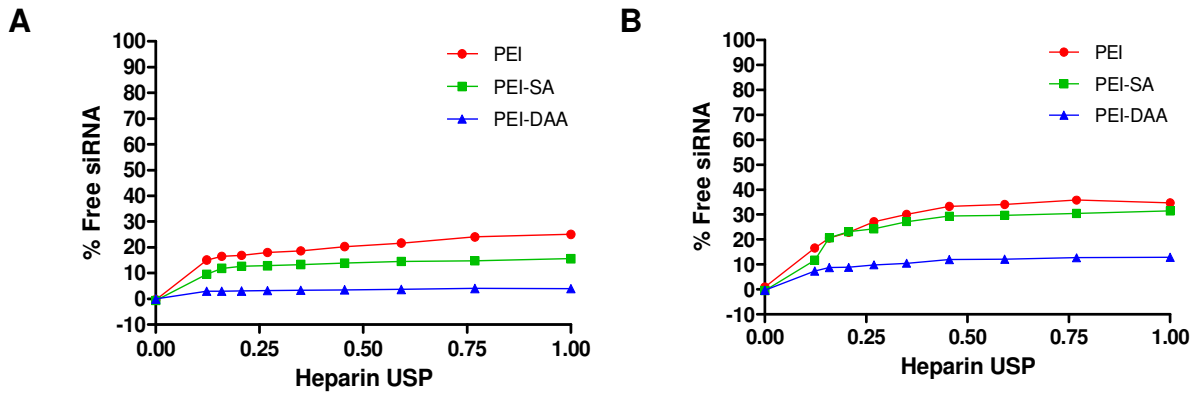

Figure 4. Release profiles of siRNA from PEI, PEI-SA and PEI-DAA PXs at N/P 7 as a function of heparin concentration (0.0 - 1.0 USP heparin per well) at pH (**A**) 7.4 and (**B**) 4.5. (Data points indicate mean normalized fluorescence, n = 3).

PEI-SA PXs displayed a comparable release profile albeit with generally lower siRNA displacement. Maximum release of approximately 16% was obtained upon addition of 1.00 USP units heparin per well. PEI-DAA PXs demonstrated to be the most stable complexes as only up to 4% siRNA was released when the maximum amount of heparin was added. This goes in line with our suggestion, that amphiphilic polymers interact with siRNA also based on hydrophobic interactions which are not affected by competing anions such as heparin. Great stability against competitive exchange reactions by polyanions was already described for triazine dendrimers modified with alkyl chains in comparison to PEI (25kDA) [45] as well as for spermine polymers modified with hydrophobic DAA subunits compared to unmodified spermine (see *Subchapter II.2*). As displayed in Figure 4B, siRNA was more easily released from all PXs under acidic conditions at a pH of 4.5. Interestingly, PEI-PXs and PEI-SA PXs showed very similar release profiles by reaching siRNA displacement of approximately 35% (PEI) and 31% (PEI-SA) at highest heparin concentration of 1.00 USP units per well. In contrast, PEI-DAA PXs exhibited a much lower siRNA release ability since maximum release of only 13% was measured at the highest heparin concentration. It is hypothesized that payload release from the complexes at lower pH values as present in the endosomes is caused by

protonation of amines what might lead to charge repulsion, complex destabilization and consequent endosomal escape of the siRNA, as already stated for PEI-PXs [46]. Our data is in agreement with this notion, as PEI polymers possess the highest number of primary amines, which can be easily protonated under acidic conditions. PEI-SA PXs demonstrated similar siRNA release ability despite the lower number of primary amines and additional hydrophobic interactions with siRNA. Therefore, it can be assumed that steric hindrance of long alkyl chains within the PEI-SA complex facilitates the complex destabilization by charge repulsion. Shorter alkyl chains present in the PEI-DAA polymer might enable more tightly ensembled complexes with siRNA even in the presence of a high charge density provided by protonated amines. These data indicate that especially PEI and PEI-SA PXs are able to efficiently release their payload in presence of competing anions at low pH upon being endocytosed. Taken together, especially PEI-SA PXs exhibited favorable properties both in terms of stability in the blood circulation and ability to escape from the endosome.

3.6 Protein corona investigations

3.6.1 Evaluation of hard corona proteins by sodium dodecyl sulfate polyacrylamide gel electrophoresis (SDS PAGE)

To gain insight into the profile of proteins bound on PEI, PEI-SA and PEI-DAA PXs after incubation in FBS an SDS-PAGE was performed. This is a common electrophoretic technique for separation and analysis of proteins based on their molecular weight and visualization by a colorimetric staining such as Comassie [47]. Therefore, all formulations were incubated either in 0% (as negative control (NC) samples), 10% or 50% FBS and subsequently purified by a centrifugation procedure optimized for PXs, as described in *Subchapter III.2* to remove unbound and loosely bound proteins. Purified PXs were resuspended after the final centrifugation step, and 25 µL of each sample and reference (pure FBS and Transferrin RS (80 kDa)) were loaded and separated on a polyacrylamide gel, and proteins were finally visualized by staining them with Comassie Brilliant Blue G. Transferrin RS was utilized based on preliminary experiments (*Subchapter III.2*) suggesting that Tf might be a component of the hard protein corona of PXs.

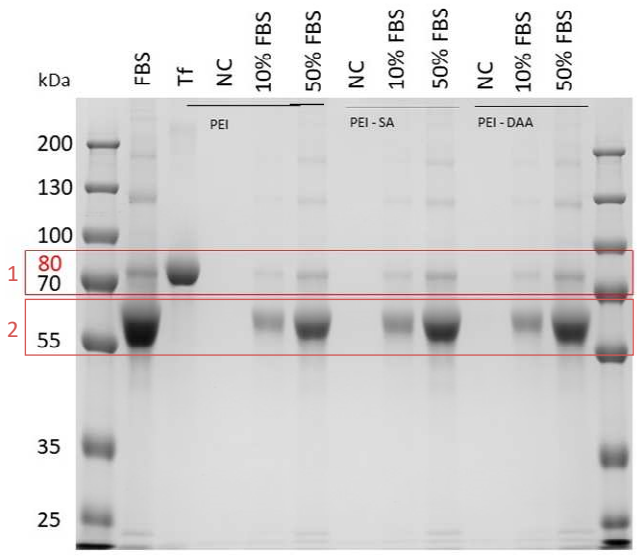

Figure 5. Proteins bound on PEI, PEI-SA and PEI-DAA PXs after incubation in 10% and 50% FBS as visualized by SDS-PAGE performed with a polyacrylamide-gel 10%. The wells of the gel were loaded with a molecular marker (10 to 250 kDa), pure FBS and Transferrin (80 kDa) as references, uncoated and FBS coated PEI, PEI-SA and PEI-DAA PXs. Proteins were visualized by a Comassie Brilliant Blue G staining.

As illustrated in Figure 5, SDS-PAGE revealed very similar protein bands for PEI, PEI-SA and PEI-DAA PXs. For all formulations slight bands appeared for 10% FBS, while more distinct bands were visible for 50% FBS samples. This led to the assumption that saturation of protein binding is probably to be reached at much higher FBS concentrations than 10% FBS. The molecular weights of the protein bands observed for PEI, PEI-SA and PEI-DAA PXs were approximately 80 kDa (lane 1) and 65 kDa (lane 2). Based on these results, the presence of Tf in the protein corona of all formulations was confirmed, since the molecular weight of the protein band of lane 1 corresponded to the molecular weight of the Tf RS (80 kDa). It is tempting to assume that lane 2 might depict albumin, a highly abundant protein in serum with a molecular weight of 66 kDa as interactions between albumin and PEI (25 kDa) have been already described in literature [48]. However, the SDS-PAGE performed can only provide a first insight into the protein corona profiles of PXs, since only highly abundant proteins can be visualized and were not truly identified. To this end, more specific investigations regarding the protein corona composition were conducted with mass spectrometry in the following.

3.6.2 Protein Identification by Mass Spectrometry (MS) measurements

An LC-MS-MS method was used in order to determine the composition of the protein corona for all formulations in more detail. PEI PXs, PEI-SA PXs and PEI-DAA PXs were incubated in 10% FBS, the PCPXs were isolated as described previously (*Subchapter III.2*), and the further purified proteins were subjected to trypsin digestion. Of special interest in this study are

proteins that function as ligands for specific receptors affecting the biodistribution and in particular the internalization of PXs into specific tissues. Several proteins were already identified, which can lead to specific targeting as a component of the protein corona [49]. In terms of BBB targeting, considerable success has already been achieved with, for example, Transferrin, ApoB and ApoE. The group of Santi et al., for example, utilized the spontaneous recruiting of Transferrin by gold NPs conjugated with a specifically designed peptide. The Tf-binding peptide efficiently interacted with plasma Transferrin, which led to enhanced internalization of peptide-functionalized NPs into Tf-receptor overexpressing cells [50]. Furthermore, the group of Zhang et al. designed doxorubicin-loaded liposomes modified with a short nontoxic peptide that specifically interacts with the lipid-binding domain of exchangeable apolipoproteins. The absorption of plasma ApoE enabled a significant improvement in brain distribution and efficacy against brain tumors after i.v administration compared to doxorubicin-loaded plain liposomes [51]. Apolipoproteins' role as specific targeting molecules was also investigated by Kim and collaborators. This study showed that poly(ethylene glycol) poly-hexadecylcyanoacrylate (PEG-PHDCA) NPs preferentially absorbed rat ApoE and ApoB-100 from the plasma on their surface. They were effectively taken up by rat brain endothelial cells via the Low-Density Lipoprotein (LDL) receptor on the BBB [52]. The group of Kreuter et al. used dalargin-loaded PBCA NPs modified with ApoE with and without polysorbate 80 (PS80) precoating and demonstrated that PS80 precoated and ApoE modified NPs achieved significantly higher analgetic effects in mice than the other formulations. In addition, experiments with ApoE-deficient (ApoEtm1Unc) mice confirmed that plasma ApoE has a crucial role in mediating the delivery of the NPs across the BBB [53]. These observations led us to address the questions of how the profile of the absorbed proteins differs in detail between PEI PXs and the more hydrophobic PEI-SA and PEI-DAA PXs with special emphasis to proteins that function as ligands. To gain insight into the differences of protein levels of the hard protein corona of PXs, we calculated the ratio of normalized abundances for all proteins that were identified for the respective pair of compared PXs (PEI-SA PXs vs PEI PXs, PEI-DAA PXs vs PEI PXs and PEI-DAA PXs vs PEI-SA PXs) and set a threshold cutoff of a 2-fold change in ratios. P-values were additionally calculated (Table S1, Supplementary Material) and results are presented as volcano plot comparison of protein levels (y-axis: - log p-value, x-axis: log2 ratio) in Figure 6.

A

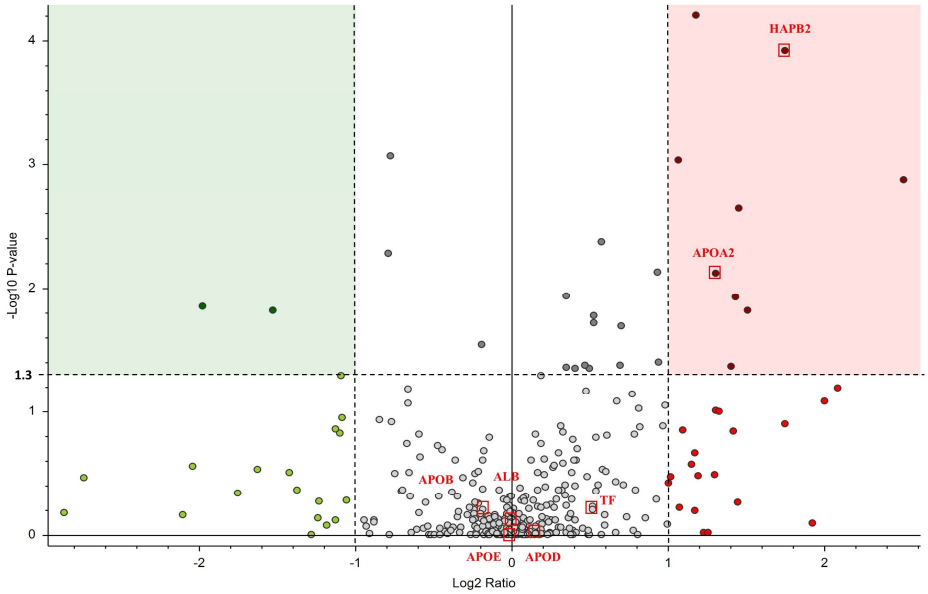
HAPB2
APOA2
APOB
ALB
TF
APOE
APOD
-Log10 P-value
Log2 Ratio
1.3

B

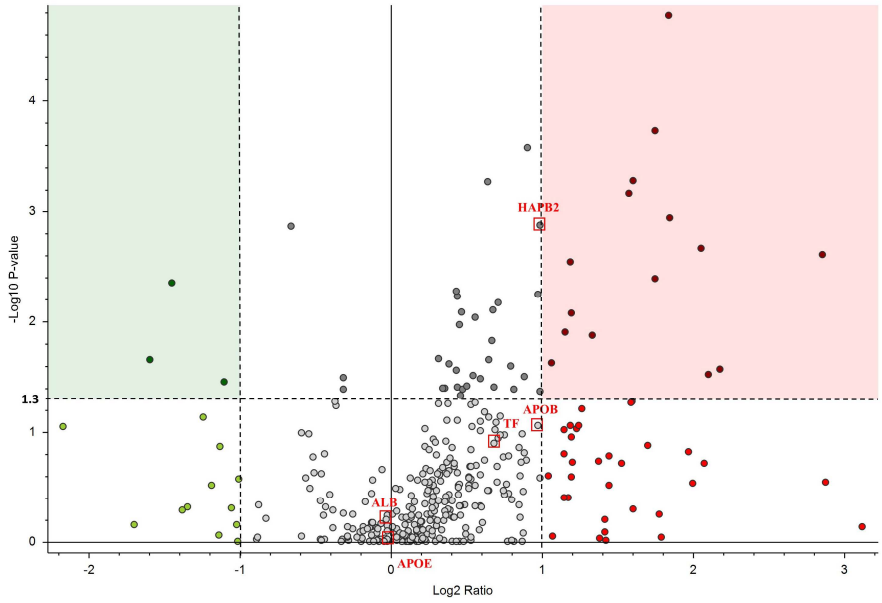
HAPB2
APOB
TF
ALB
APOE
-Log10 P-value
Log2 Ratio
1.3

C

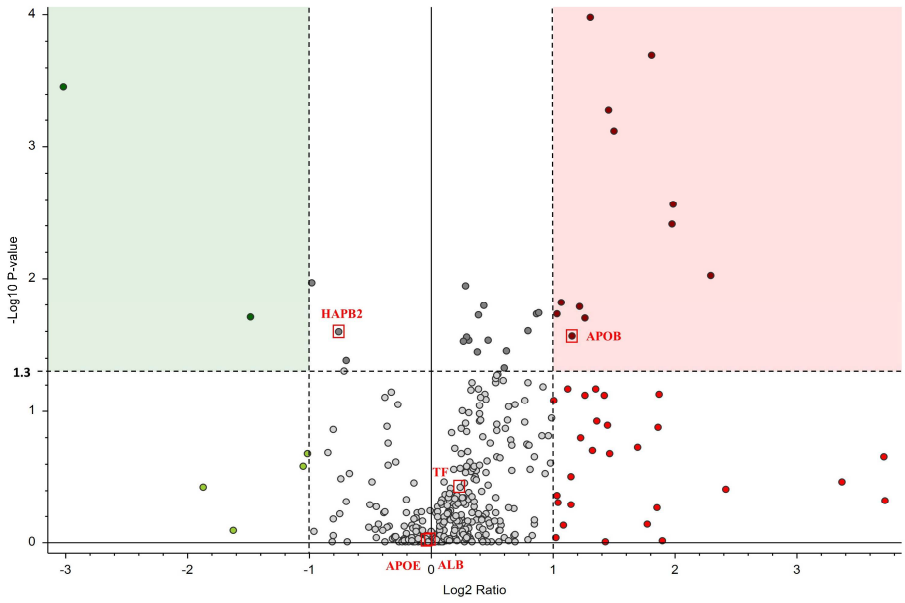
HAPB2
APOB
TF
APOE
ALB
-Log10 P-value
Log2 Ratio
1.3

Figure 6. Volcano plots from the LC-MSMS data demonstrate the differences of the protein levels for (**A**) PEI-SA vs PEI PXs (**B**) PEI-DAA vs PEI PXs and (**C**) PEI-DAA vs. PEI-SA PXs after exposure to 10% FBS. Log2 values of ratios of the normalized abundances from identified proteins present on respective pair of PXs were calculated (x-axis), and a 2-fold change in ratio [log 2 (2) = 1 and log 2 [0.5] = - 1] was used as threshold cutoff (higher or lower bound proteins) indicated by vertical dashed lines. P-values were calculated with ANOVA and given as -log10 values (y-axis) to indicate the significance of differences in protein levels on respective pair of PX for each protein. As threshold cutoff, a p-value of 0.05 [-log 10 (0.05) = 1.3] was used, indicated by the horizontal dash line. Therefore, the red boxes contain most significant and most abundant proteins on (**A**) PEI-SA PXs compared to PEI PXs (**B**) PEI-DAA PXs compared to PEI PXs and (**C**) PEI-DAA PXs compared to PEI-SA PXs and green boxes show significantly lower bound proteins on (**A**) PEI-SA PXs compared to PEI PXs (**B**) PEI-DAA PXs compared to PEI PXs, and (**C**) PEI-DAA PXs compared to PEI-SA PXs.

As illustrated in Figure 6A, of all the proteins identified, nine were found to be significantly higher abundant (red box), and two proteins were significantly lower (green box) present in the corona of PEI-SA PXs compared with PEI-PXs. The proteins with higher abundance included the hyaluronan binding protein (HAPB2) (log2 ratio: 1.75, -log10 p-value: 3.92) and Apolipoprotein AII (ApoA2) (log2 ratio: 1.3 , -log10 p-value: 2.12). In addition, albumin (ALB), Transferrin (Tf) and Apolipoproteins B (ApoB), and E (ApoE) were identified in the protein corona of both PXs with no significant differences in protein levels. Figure 6B exhibits the comparison of protein levels between PEI-DAA PXs and PEI-PXs and illustrates 15 proteins with significantly higher abundance and 3 proteins with significantly lower abundance in the protein corona of PEI-DAA PXs compared to PEI PXs. HAPB2 was found to a higher extent just below the threshold cutoff of 1 (log2 ratio: 0.99, -log10 p-value: 2.87) on PEI-DAA PXs. In line with the results for PEI-SA PXs vs. PEI-PXs, ALB, Tf, ApoB and ApoE were identified with similar abundances on both PXs. The volcano plot shown in Figure 6C demonstrates that 12 proteins were found on PEI-DAA PXs with a significantly higher and 2 proteins with a significantly lower abundance in the protein corona of PEI-DAA PXs compared to PEI-SA PXs, respectively. The proteins with higher abundance include ApoB (log 2 ratio: 1.16, -log10 p-value: 1.56), whereas albumin, Transferrin, HAPB2 and ApoE exhibited no significant differences in protein levels.

The data revealed that proteins with potential targeting effects accumulate to all PXs under physiological conditions. HABP2 was shown to exhibit great binding affinities to hydrophobically modified PEI-SA and PEI-DAA PXs. This protein was originally discovered through its ability to bind to hyaluronic acid (HA), that is present in human plasma [54]. Since HA also serves as ligand for CD44 receptors, which are highly overexpressed in various tumors [55], HA-modified nanocarriers were already used in the field of targeted drug delivery. In terms of siRNA delivery, as shown, for example, by the group of Ganesh et al., HA-PEI-siRNA

complexes were able to demonstrate selective uptake in CD44 overexpressing tumor cells resulting in target specific gene knockdown in *in vivo* experiments [56].

Taken together, our results indicate that, in agreement with the literature, differences in the physicochemical properties of the PXs lead to distinct protein corona profiles. In particular, hydrophobic modification of PXs resulted in binding of high amounts of HAPB2. The question of whether adsorbed HAPB2 proteins and bound plasma HA may have the potential to selectively deliver the respective PXs via overexpressed CD44 receptors into tumor cells needs to be further elucidated. Moreover, several other functional targeting proteins such as albumin, Transferrin or apolipoproteins were found in the protein corona of all PXs to similar extents. Their influence on protein – cell membrane interactions, biodistribution of PXs as well as their feasibility to induce active targeting effects after intravenously injection needs to be investigated in more detail in the future.

4. Quantification of cellular Uptake into hCMEC/D3 cells by flow cytometry

As previous experiments indicated that hydrophobically modified PEI-SA and PEI-DAA PXs have suitable properties in terms of siRNA condensation ability, physicochemical characteristics and stability, the next step of the study was to investigate their ability to internalize into immortalized hCMEC/D3 cells. This cell line was developed by immortalization of primary human brain capillary endothelial cells (BCEC) and was characterized in detail regarding the expression of endothelial markers, adhesion molecules and receptors, the formation of tight junction proteins and the capacity to exhaust drugs [6, 57-59]. Overall, hCMEC/D3 was described as the most promising immortalized human BBB cell line since it exhibits many of the characteristics that are essential for a predictive BBB *in vitro* model, and therefore it was selected in this study. Furthermore, as already mentioned, upon exposing PXs to biomolecules, a protein corona forms on the surface of the NPs, which depends on their physicochemical surface properties and affects their cellular internalization ability in *in vitro* experiments, but also the fate of the NPs *in vivo* after intravenous injection. In this regard, cellular internalization ability into hCMEC/D3 cells of PEI, PEI-SA and PEI-DAA PXs containing Alexa Fluor 488-labelled siRNA depending on serum present in the cell culture medium was quantified by flow cytometry. To ensure the compatibility of our formulations for hCMEC/D3 cells, Cell-Titer Blue® viability assays were performed in advance. This assay is based on the ability of viable cells to reduce the nonfluorescent resazurin to fluorescent resorufin mainly by mitochondrial and cytosolic enzymes, dead cells rapidly lose this capacity once their membrane has been compromised [60]. Thereby, N/P ratio of 7 represented

treatment-relevant conditions in *in vitro* experiments. Amounts of free polymer corresponded to the amounts required to form NPs with N/P 7 or 15, respectively. As illustrated in Figure S2, all free polymers tested, resulted in an acceptable toxicity profile, since no influence on cell viability was observed. Among the PXs at N/P ratio of 7, only PEI-DAA revealed a very low cytotoxic effect, as the survival rate was found to be 92.3 %, indicating that all PXs were well tolerated at conditions selected for the in vitro uptake experiments. However, PEI-DAA PXs did not show cytotoxicity at a higher N/P ratio of 15. In case of PEI and PEI-SA PXs, a higher N/P ratio of 15 resulted in survival rates of 93.9% and 85.2%, respectively, demonstrating a small and thus tolerable cytotoxic effect on hCMEC/D3 cells. Furthermore, trypan blue quenching was performed to exclude extracellular fluorescence signals caused by PXs adhering to the outer cell membranes. Figure S3 (Supplementary Material) shows trypan blue quenched MFI values of hCMEC/D3 cells transfected with PEI, PEI-SA and PEI-DAA PXs at N/P 7 in comparison to untreated cells and free siRNA treated cells as negative controls and Lipofectamine 2000 (LF) lipoplex-treated cells as positive control. The obtained results revealed that trypan blue quenched samples yielded insignificantly lower MFI values for all tested PEI-PXs with or without serum, suggesting that inconsiderable amounts of PXs adhered to the outer cell membranes.

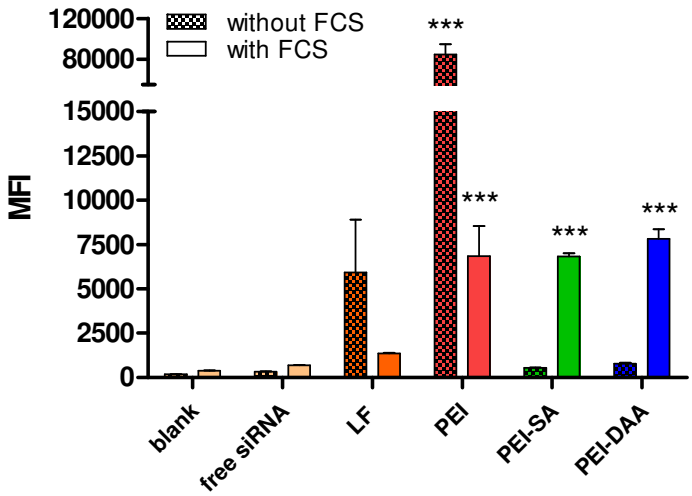

Figure 7. Cellular uptake of PEI, PEI-SA and PEI-DAA PXs into hCMEC/D3 cells at N/P 7 after 24 h in a serum-dependent manner as quantified by flow cytometry with trypan blue quenching and presented as median fluorescence intensity (MFI). Negative control: untreated cells (blank) and with free siRNA treated cells. Positive control: cells treated with lipoplexes (Lipofectamine 2000). (Results are shown as mean ± SD, n = 3, one-way ANOVA with Bonferroni post-hoc test related to free siRNA values, *** $p < 0.005$).

As shown in Figure 7, the addition of serum resulted in remarkable differences in the cellular internalization ability of respective PXs. In case of LF lipoplexes and PEI PXs it led to considerably reduced MFI values und thus to reduced NPs uptake. The MFI values for LF lipoplexes and PEI PXs decreased from 5912.3 to 1354.0 and from 84808.0 to 6856.7, respectively. Nevertheless, PEI PXs with and without serum revealed significantly increased uptake values in comparison to free siRNA negative control. But a somewhat different picture was seen in case of hydrophobically modified PEI-SA and PEI-DAA PXS, since the presence of serum within the cell culture medium yielded in highly increased uptake capabilities. Without serum, the cellular internalization ability of both formulations was rather low, namely 557.0 and 779.7 for PEI-SA and PEI-DAA PXs, respectively. With serum, both PXs achieved significantly increased MFI values in comparison to the free siRNA negative control and yielded in values of 6824.7 and 7830.7 for PEI-SA and PEI-DAA, respectively. The phenomenon of transfection efficacy reduction caused by serum for PEI PXs as well as for LF lipoplexes has already been described in the literature. Maiolo's group demonstrated an FBS-concentration dependency of transfection efficacy in Hela cells by using 25 kDa b - PEI – DNA PXs and also suggested that absorbed proteins may influence either their physicochemical characteristics or their interactions with cell membranes in an unfavorable way [61]. These results are also in line with observations of our group, as cellular internalization of PEI PXs and LF lipoplexes into glioblastoma cells was found to be significantly reduced as soon as a protein corona formed on the particles [*Subchapter III.2*]. A study by Zhu recently investigated the influence of the protein corona on the physicochemical properties and gene delivery of PEI-DNA PXs in detail. The authors hypothesized that reduced transfection efficacy of b – PEI (25kDa) – DNA PXs in Hela cells in presence of serum was caused by PX dissociation or aggregation induced by absorbed proteins. The authors found an 8-fold size increase of PEI PXs in a 150 mM NaCL solution, a 4-fold increase in FBS free medium, and a 2-fold increase of size in 10% FBS containing medium (in comparison to 10 mM HEPES solution). It was shown that no salt-induced dissociation, but salt-induced aggregation of particles occurred, and to this end, the author suggested that aggregation of particles led to sedimentation in the two-dimensional cell culture of Hela cells leading to enhanced cellular internalization capabilities. The study additionally revealed that a preformed protein corona was able to protect the PEI-DNA particles from salt-induced aggregation/sedimentation, leading to lower cellular uptake of particles [21]. Our findings for LF lipoplexes and PEI-siRNA PXs regarding the cellular uptake into hCMEC/D3 cells are in line with this argumentation. However, the completely opposite trend was observed for the modified PEI-SA and PEI-DAA PXs as significant uptake

into cells was only observed in the presence of serum. Several studies confirmed the improved gene delivery activity by PXs containing hydrophobic segments. However, the explanations are still diverse and consider just a few of the many important parameters, e.g., physicochemical characteristics and stability of PXs, particle-cell membrane interactions and the influence of the protein corona on PXs properties, stability as well as protein-cell membrane interactions [35]. For example, the group of Neamnark et al. reported a study investigating a fatty acid-substituted PEI (2 kDa) library for gene delivery. Improved cellular uptake of plasmids into 293T and bone marrow-derived stem/stromal cells (BMSC) cells was shown but not further explained [62]. A study using oleic and stearic acid-modified PEI derivatives (25 kDa) revealed that siRNA transport was increased several-fold in B16 melanoma cells compared with plain PEI [16]. Kim's group illustrated that a cholesteryl conjugated PEI (1800 kDa)/siRNA complex was able to silence vascular endothelial growth factor (VEGF) in a PC-3 cell line significantly, whereas unmodified PEI did not show any effect at all [63]. The authors suggested in both studies that this occurred probably due to altered particle – cell membrane interactions, however, they did not provide any details. The group of Furgeson et al. investigated the internalization of cholesteryl-l-PEI/DNA complexes into MCF-7 cells and included into the discussion of the results that the NPs might be able to interact with LDL receptors as saturation of this receptor inhibited the internalization efficacy [64]. Taken together the current state in literature underlines once more that the explanation of interaction of particles with cells is complicated because it can be influenced by many aspects of the particles, the environment, and the characteristics of selected cell lines. Previous experiments in this study revealed that hydrophobically modified PEI PXs behave similarly to PEI PXs in terms of encapsulation efficiency, size and surface charge as soon as N/P ratios are reached, that allow stable PX formations. To return to the topic of aggregation and sedimentation, it should be pointed out that this effect may explain the enhanced uptake as solely one factor among others. The hydrophobic moieties might confer the PXs with a protection against salt-induced aggregation in serum-free medium, hindering sedimentation, and thus successful particle internalization into cells, which in turn would mean that adsorbed proteins on modified PXs lead to particle aggregation instead of stabilization as argued for plain PEI PXs. In our opinion this explanation for enhanced uptake of hydrophobically modified PXs in presence of serum is highly questionable and should be addressed in future studies. MS measurements of the protein corona composition of the formulations used in this study confirmed that the protein identities differ depending on the PXs properties, what might have a significant impact on non-specific and specific protein – cell membrane interactions, thus affecting the cellular internalization abilities.

Therefore, to provide a detailed explanation of our results, it is of great need to investigate the effect of bound serum components on cellular internalization ability and the route of PXs uptake into hCMEC/D3 cells, which should be addressed in more detail. Altogether, the results of the uptake experiment indicate that the addition of serum to the experimental setting remarkably influences the internalization abilities of PXs. The uptake of unmodified PEI PXs was significantly inhibited by serum addition, whereas PEI-SA and PEI-DAA PXs reached significant internalization only in the presence of serum. Nevertheless, as the presence of serum constitutes the more physiological condition, all formulations demonstrated successful internalization into human brain endothelial cells, which is a highly promising result for further investigations regarding the BBB permeability of PXs in more sophisticated BBB models.

5. Blood- Brain Permeability of PXs through hiPSC-derived BBB model

As initial experiments indicated that PEI, PEI-SA and PEI-DAA PXs hold favorable characteristics regarding physicochemical properties and cellular internalization abilities into hCMEC/D3 cells, the next step of the study was to investigate their ability to permeate the BBB as this would be a prerequisite for successful siRNA delivery into the brain after e.g., intravenous injection. In an effort to develop highly predictive BBB models, intensive research on sophisticated models has been conducted in recent years. One promising approach is the use of human pluripotent stem cells, from which respective cell types for BBB modelling can be differentiated. By now, standardized protocols for the development of hiPSC-derived BBB models are available, and several studies have confirmed excellent *in vivo* like properties of the models, such as the upregulation of typical BBB genes, the formation of a physiological tight junction network and thus high TEER values up to 2500 $\Omega \cdot cm^2$ [28]. To investigate the applicability of a hiPSC-derived BBB model for evaluating the blood- brain permeability of PXs for the first time, we initially used the simplest setup with hiPSC-derived BBB endothelial-like cells as monoculture seeded on the top of a transwell insert. In order to measure the cytotoxicity of PEI, PEI-SA and PEI-DA PXs on highly sensitive ECs, we performed CellTiter-Glo® Assays in a serum-dependent manner in advance. This assay is used to determine the number of living cells by generating a luminescent signal proportional to the amount of ATP present in the cell. As illustrated in Figure S4 (Supplementary Material), neither PXs with nor PXs without serum exhibited any noticeable cytotoxic effect on ECs, ensuring that no unfavorable effects by toxicity on the barrier integrity occurred during the experiment. Subsequently, the hiPSC-derived BBB model was built according to recently published protocols [28], and barrier integrity was evaluated prior to permeability testing of PXs via

TEER measurements, as presented in Table S2 (Supplementary Material). TEER values ranging from 1795.93 – 3706.80 $\Omega \cdot cm^2$ confirmed appropriate barrier integrity values for each sample compartment and consequently, PEI, PEI-SA and PEI-DAA PXs containing Alexa Fluor 488-labeled siRNA diluted in EC medium with or without addition of serum were applied to the apical side of the respective sample compartment as illustrated in Scheme 2.

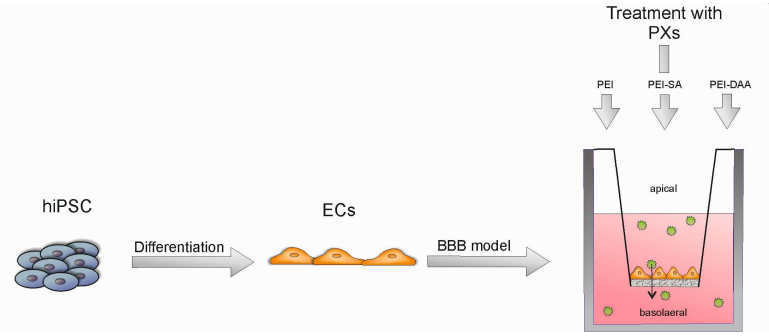

Scheme 2. Schematic representation of the hiPSC-derived *in vitro* BBB model used to investigate the BBB permeability of PEI, PEI-SA and PEI-DA PXs.

Additionally, PXs were administered in transwells without cells to correct permeation values for the barrier formed by the membrane support, resulting in values related only to the permeation through the BBB endothelial cell layer. After an incubation period of 24 h fluorescence signals in apical and basolateral media were evaluated, and Papp values for each formulation were calculated as illustrated in Figure 8.

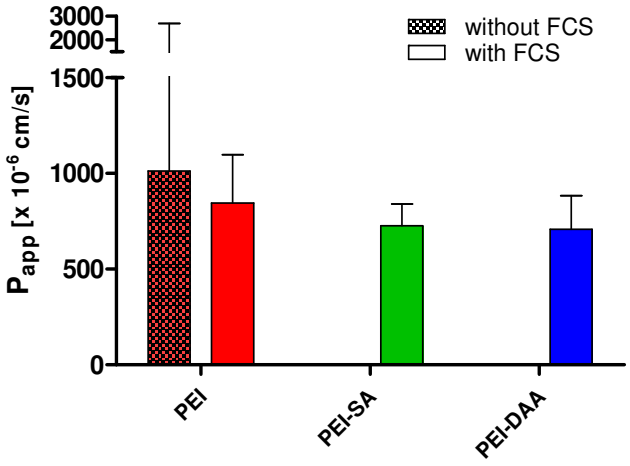

Figure 8. Permeation ability of PEI, PEI-SA and PEI-DAA PXs at N/P 7 after 24 h incubation with or without serum quantified in a blood-brain barrier model monoculture with hiPSCs-derived endothelial-like cells (ECs). Permeation ability of PXs through transwells without cells was measured as control. Permeation was determined in three individual transwell plates, each containing the respective samples in duplicates and calculated as apparent permeability coefficient (Papp [cm/s]). (Data are presented as mean ± SD, n = 3, statistical analysis was performed using two-way ANOVA with Bonferroni post-hoc test, no significant differences were observed between the samples with and without serum).

Calculated Papp values for PEI, PEI-SA and PEI-DAA PXs were slightly influenced by the presence of serum. For PEI PXs with and without serum and for PEI-SA and PEI-DAA PXs permeation through the BBB endothelial-like cells were observed only with addition of serum. Papp values for PEI PXs revealed to be 1010.8 and 844.4 ($x10^{-6}$ cm/s) without and with addition of serum, respectively. In the presence of serum, PEI-SA and PEI-DA PXs Papp values yielded 726.2 ($x10^{-6}$ cm/s) and 708.1 ($x10^{-6}$ cm/s), respectively. However, hydrophobically modified PXs were not able to cross the barrier without addition of serum. The trends observed for permeation abilities of PXs were in complete agreement with the cellular internalization abilities into hCMEC/D3 cells as described above. We therefore concluded that neither addition of formulations nor addition of serum adversely affected the barrier integrity. This implies that PEI-PXs with and without serum, as well as PEI-SA and PEI-DA PXs with serum successfully penetrated the endothelial cell layer by transcytosis with subsequent release at the abluminal cell surface into the basolateral compartment of the model. The data also revealed that the presence of serum has an inhibitory effect on the permeation ability of PEI-PXs. As the hiPSC-derived BBB model represents a static model as well, aggregation and sedimentation phenomena might play a non-negligible role in their cellular uptake ability. As mentioned above, the hydrophobic parts of the PXs are presumed to confer them greater salt compatibility, leading to highly stable particles [65, 66] that are suspended in the serum-free culture medium. These particles rarely sediment and consequently might get hardly internalized into cells. As soon as a protein corona adsorbed on the PXs surface, we speculate that effects of aggregation/sedimentation, as well as protein – cell membrane interactions, may have jointly evoked the highly increased transcytosis of PXs. As mentioned above under 3.6.2 , the protein corona profile of PEI, PEI-DA and PEI-SA PXs was affected by the PXs material and revealed compositional differences. It should be pointed out, that consideration of the surface modification of the PXs that would be present in physiological environments and its influence on the ability of the PX to cross the BBB is urgently needed to draw conclusions about its behavior *in vivo*. Bound proteins on PXs might be able to serve as ligands for receptors expressed on BBB endothelial cells via RMT processes. Potential RMT-mediating receptors expressed on hiPSC-derived EC are e.g., Transferrin receptor (TfR), Low-Density Lipoprotein Receptor (LDLR), Low-Density-Lipoprotein Receptor-related Protein 1 (LRP1), Insulin (INSR) and Insuline-like Growth Factor Receptors (IGFIR and IGFRIIR) [67]. As described above, several respective ligands for some of these receptors (Tf, Apo B and E) were detected in the protein corona of PXs. However, the influence of potential ligand - receptor interactions and permeation pathways of PEI, PEI-SA and PEI-DAA PXs through ECs needs to be further

elucidated. Nevertheless, the results implied that the hiPSC-derived BBB model described in this study is, in principle, a valuable tool for studying blood-brain permeability of PXs but needs further optimization in future approaches to enhance reproducibility of the data. So far, just a few other groups used comparable models to investigate the interactions of substances with the BBB. Recently, the group of Lübtow et al. successfully applied the hiPSC-derived BBB model as presented in this study to evaluate the BBB penetration ability of micelles loaded with atorvastatin [68]. The group of Ribecco-Lutkiewicz et al. developed a BBB model derived from human amniotic fluid-derived induced pluripotent stem cells and confirmed its applicability to study antibody triggered receptor-mediated transcytosis [67]. In addition, the group of Onyema et al. stated previously that the hiPSC-based BBB model bridges the gap between already existing immortalized cell culture models and animal experiments in studying the effects of PLGA and Poly-L-lactic acid (PLLA) NPs on the integrity of the BBB barrier as a function of size, material and protein corona [69]. Taken together, hiPSC-derived BBB models are a useful tool to mimic the human BBB physiology *in vitro* and can be used to examine the blood-brain permeability of PXs. By mimicking physiologically relevant conditions through the addition of serum, we demonstrated comparable barrier penetration abilities of PEI, PEI-SA and PEI-DA PXs, making them promising siRNA carriers for the treatment of CNS disorders.

6. In vivo biodistribution

Since successful cellular internalization into immortalized hCMEC/D3 cells and permeation capability through the BBB barrier were demonstrated in the hiPSCS-derived BBB model for PEI, PEI-SA and PEI-DAA PXs, the next step of the study was to investigate their *in vivo* biodistribution behavior in a mouse animal model to test the correlation of the cell-based *in vitro* model with *in vivo* settings. In advance of administering the materials intravenously into animals, the hemocompatibility of PEI, PEI-SA and PEI-DAA PXs must be guaranteed. Assays with RBCs as a model for mammalian cells have been widely investigated since they possess a very good *in vitro – in vivo* correlation [70] and therefore are highly predictive power regarding potential toxic effects of substances in animals. Especially amphiphilic compounds hold great potential to interact with biological and artificial membranes due to hydrophobic interactions and therefore, investigating their interactions with RBCs in hemolysis and erythrocyte aggregation assays is an important prerequisite to perform animal experiments. As illustrated in Figure S5 (Supplementary Material), all tested polymers exhibited different hemocompatibility profiles. The best tolerated polymer was unmodified PEI, as no hemolysis occurred at PEI concentrations ranging from 0.5 to 0.00781 mg/mL. A slight but neglectable

value of 0.6% hemolysis was obtained at the highest polymer concentration of 1 mg/mL. In general, a substance is defined as non-hemolytic as long as the hemolytic effect remains below 2% as defined elsewhere [71]. Free PEI-SA polymer induced slightly more hemolytic events than unmodified PEI, especially at higher polymer concentrations, namely 5.9%, 5.8% and 3.1% at concentrations of 1 mg/mL, 0.5 mg/mL and 0.25 mg/mL, respectively. The hemolytic effect of PEI-SA was less than 2% at all lower concentrations tested. The most unfavorable hemocompatibility profile was observed for PEI-DAA polymers. Relatively high values regarding the hemolytic effect were observed at the three highest concentrations, namely 24.8%, 16.1% and 12.8%. Values lower than 2% were obtained only from a concentration of 0.03125 mg/mL. Erythrocyte aggregation studies were in line with the trends found by the hemolytic assay, as shown in Figure S6. These results are consistent with our expectations, as hydrophobic moieties are inserted into polymers with the aim to enhance the interactions with cell membranes in order to improve delivery properties. Also in good agreement with our suggestion are some studies in literature that reported adverse effects of hydrophobic modifications in terms of cell toxicity [62, 72]. Herein, the effect was even more pronounced with DAA side chains than with SA side chains, what caused us to exclude PEI-DAA polymers from the animal study for safety reasons, even if the polymer concentrations of the dose administered into the mice would be much lower. For the animal biodistribution experiment, siRNA was covalently coupled with DTPA to enable the labelling with ^{177}Lu as radioactive marker following an adjusted protocol previously described for ^{111}Indium-labeling of siRNA [32]. PEI and PEI-SA PXs were formed with ^{177}Lu-radiolabeled siRNA and were intravenously administered through the tail vein in SWISS mice and subsequently, biodistribution was investigated 1 h post injection in comparison to ^{177}Lu-labeled free siRNA as control.

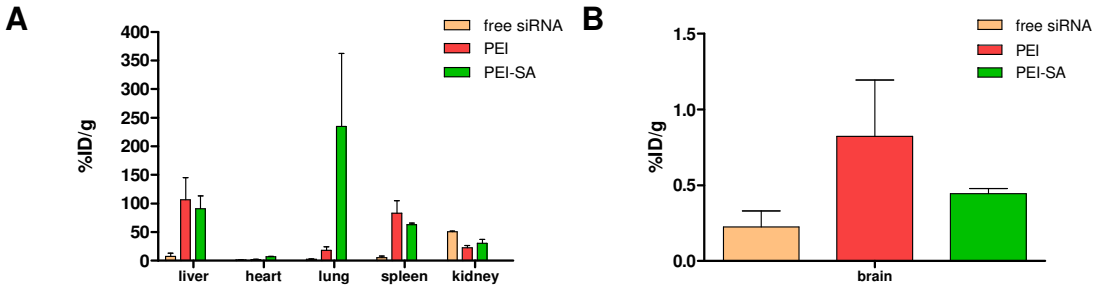

Figure 9. Biodistribution of ^{177}Lu-labeled siRNA, PEI, PEI-SA and PEI-DAA PXs in (**A**) dissected organs and (**B**) the brain of SWISS mice 1 h post injection. (Results are presented as %ID/g and shown as mean ± SD, n = 3, mice that urinated during the incubation period were excluded from the study to avoid falsification of the results due to undefined loss of radioactive material).

As measured by gamma scintillation counting of resected organs (Figure 9A), free siRNA exhibited a different biodistribution profile in comparison to PXs and accumulated preferentially in the kidney (50.65 %ID/g), as reported earlier [33], small amounts of siRNA were in addition found in the liver (7.44 %ID/g), as also described from van der Water's group [33] and in the spleen (5.48 %ID/g). The results indicated that PEI-encapsulated ^{177}Lu-labeled siRNA accumulated mainly in the liver (106.41 %ID/g) and spleen (83.08 %ID/g), which is in good agreement with published data [73]. In contrast, PEI-SA-encapsulated ^{177}Lu-labeled siRNA was preferentially detected in the lung (234.73 %ID/g), what goes in line with the study by Xie's group performed with stearic acid – grafted chitosan micelles [17]. In addition, PEI-SA-complexed siRNA accumulated, although to a smaller extent, in the spleen (63.14 %ID/g) and in the liver (90.84 %ID/g). As illustrated in Figure 9B, only low concentrations of free ^{177}Lu-labeled siRNA and PEI- and PEI-SA-complexed ^{177}Lu-labeled siRNA, were detected in the brain. In fact, the highest radioactive signal in the brain 1 h post injection was determined in mice treated with PEI-PXs (0.82 %ID/g) followed by PEI-SA PXs (0.44 %ID/g), and the lowest signal was obtained for free siRNA (0.23 %ID/g). The biodistribution of siRNA formulations is generally influenced by a variety of parameters, such as the physicochemical properties of the NPs, their interactions with proteins and their stability within the blood stream, as well as by the recognition of the particles by the reticuloendothelial system (RES). Our data for the biodistribution of ^{177}Lu-labeled free siRNA in mice were consistent with previous reports. It was already shown that free siRNA administered to mice is rapidly distributed to the kidneys and liver and that level of free siRNA within the body also decreases sharply within the first 24 h after injection due to the excretion via the urine [74]. Moreover, free siRNA did not selectively accumulate in the other organs or in the brain, reflecting the poor ability of siRNA to penetrate the blood-brain barrier [33]. Accumulation of PEI-PXs in the organs of the RES (liver and spleen) are in agreement with an earlier report, which suggests that PEI-particles are rapidly removed from the blood stream after opsonization by phagocytosing macrophages [75]. A somewhat different picture was seen for ^{177}Lu-labeled siRNA encapsulated with PEI-SA PXs, as it was detected to a remarkably higher extent in the lungs. A deposition in the lung was so far associated with the formation of aggregates due to interactions of PXs with blood components that subsequently entrap in the capillary bed of the lung [17, 76]. This is in line with the data of the erythrocyte aggregation assay, which showed that that more hydrophobic PXs seem to interact more easily with erythrocytes, potentially leading to accumulation of RBC-PX aggregates in the lung capillaries. When it comes to the delivery of nanoparticles into the brain, it was already shown in literature that the amounts found in the brain tissue are often

below 0.5% and can be even as low as 0.01% ID/g brain. For example, in a study by Schnyder et al, tissue biodistribution experiments with biotinylated immunoliposomes conjugated to the OX26 monoclonal antibody directed against the Transferrin receptor in rats revealed that the brain accumulation of OX26-immunoliposomes after intravascular content correction were two-fold higher (0.01 %ID/g) than compared to control liposomes (0.005 %ID/g) [77]. Another report by the group of We et al. investigated the biodistribution of poly(amidoamine) - poly(ethylene glycol) (PAMAM-PEG) NPs modified with an angiopep peptide directed against the LRP1- receptor and reported 8.42-fold higher brain accumulation values (0.25 %ID/g) of modified NPs in comparison to unmodified PAMAM dendrimers [78]. Herein, it was demonstrated that encapsulation of free siRNA with polymers induced an enhanced brain uptake that was 3.56 and 1.91-fold higher in case of PEI PXs and PEI-SA PXs, respectively. Lower values of PEI-SA PXs might be explained by the high accumulation in the lung that reduces the number of particles in the blood stream and thus available PXs for brain accumulation. Although the values of ^{177}Lu-labeled siRNA encapsulated with both polymers in the brain are rather low, it is not known whether this low amount of siRNA is yet sufficient to induce a therapeutic effect.

4. Conclusion

The delivery of drugs and in particular nucleic acids into the brain has been a challenging task since the brain is protected by the very selective BBB characterized by extremely tight junctions and expression of export proteins. Therefore, the aim of this study was to evaluate the BBB permeability of nanocarriers formed with hydrophobically modified PEI polymers (PEI-SA and PEI-DAA) as especially promising siRNA delivery agents in comparison to unmodified PEI. The assembly of PXs with an optimal amount of polymers led to particles with appropriate sizes and surface charges. With the application of SDS-PAGE and LC-MS-MS methods, we were able to determine the composition of the protein corona with a special emphasis on functional proteins depending on the NPs material. Most proteins known to be able to induce active targeting effects, such as albumin, Transferrin or apolipoproteins were found to a similar extent in the protein corona of all formulations. Moreover, one functional protein, namely the HABP2 protein, was found to exhibit increased binding affinity to the amphiphilic PXs. Cellular internalization experiments, which were conducted in a human brain endothelial cell line (hCMEC/D3) in a serum-dependent manner, exhibited remarkably different effects on cellular uptake ability of PXs. A significant serum-induced reduction of cellular internalization ability

was observed for PEI PXs, whereas amphiphilic PXs only achieved significant cellular uptake in the presence of serum. The role of adsorbed proteins regarding aggregation and sedimentation phenomena and cellular internalization processes in static *in vitro* settings needs to be elucidated in future experiments to find an explanation for enhanced cell uptake of hydrophobically modified PXs. Nevertheless, all formulations demonstrated auspicious cellular internalization into hCMEC/D3 cells under physiological conditions. Furthermore, a hiPSC-derived BBB *in vitro* model demonstrated that all tested PXs were in addition able to permeate a tight EC layer in the presence of serum to similar extents, predicting potential BBB permeability of all PXs *in vivo*. However, biodistribution studies performed with PXs containing ^{177}Lu-labeled DTPA-siRNA in mice were only partially consistent with *in vitro* results as the detected amount of radiolabeled siRNA in the brain delivered with PEI PXs was approximately 2-fold higher compared to PEI-SA PXs. Due to high accumulation in the lung, the hydrophobic modification of PEI was shown to be detrimental to successful siRNA delivery into the brain. Taken together, the results pointed out that successful delivery into the brain *in vivo* is not only limited by the BBB but also highly influenced by several additional parameters such as sufficient residence time of the formulation in the circulation to allow uptake into target sites. However, with keeping an eye on the big picture regarding CNS drug development for humans, clinical studies have pointed out a low translation between first-in-human studies and the approval of novel therapeutics, even though the clinical candidates have indicated high potential for passing the BBB in preliminary *in vitro* and *in vivo* investigations. The use of animal models has faced increasing criticism for both ethical and scientific reasons as not only do millions of animals suffer pain, distress and death but the efficacy of animal testing in predicting expected outcomes in humans is highly questionable due to significant differences among species. Consequently, this study pointed out the urgent need for the development of appropriate and standardized human BBB models that better represent physiological conditions, thus providing highly relevant data for human CNS drug development.

References

[1] P.S. Ramachandran, M.S. Keiser, B.L. Davidson, Recent Advances in RNA Interference Therapeutics for CNS Diseases, Neurotherapeutics, 10 (2013) 473-485.
[2] A. Dessy, J. Gorman, The Emerging Therapeutic Role of RNA Interference in Disorders of the Central Nervous System, Clinical Pharmacology & Therapeutics, 89 (2011) 450-454.
[3] B.T. Hawkins, T.P. Davis, The blood-brain barrier/neurovascular unit in health and disease, Pharmacological reviews, 57 (2005) 173-185.
[4] Y. Zhou, Z. Peng, E.S. Seven, R.M. Leblanc, Crossing the blood-brain barrier with nanoparticles, Journal of Controlled Release, 270 (2018) 290-303.
[5] M. Vastag, G.M. Keseru, Current in vitro and in silico models of blood-brain barrier penetration: a practical view, Current opinion in drug discovery & development, 12 (2009) 115-124.
[6] D.E. Eigenmann, G. Xue, K.S. Kim, A.V. Moses, M. Hamburger, M. Oufir, Comparative study of four immortalized human brain capillary endothelial cell lines, hCMEC/D3, hBMEC, TY10, and BB19, and optimization of culture conditions, for an in vitro blood–brain barrier model for drug permeability studies, Fluids and Barriers of the CNS, 10 (2013) 1-17.
[7] A. Avdeef, M.A. Deli, W. Neuhaus, In vitro assays for assessing BBB permeability: artificial membrane and cell culture models, Blood-Brain Barrier in Drug Discovery: Optimizing Brain Exposure of CNS Drugs and Minimizing Brain Side Effects for Peripheral Drugs, (2015) 188-237.
[8] I. van Rooy, S. Cakir-Tascioglu, W.E. Hennink, G. Storm, R.M. Schiffelers, E. Mastrobattista, In Vivo Methods to Study Uptake of Nanoparticles into the Brain, Pharmaceutical Research, 28 (2011) 456-471.
[9] F. Hao, Y. Li, J. Zhu, J. Sun, B. Marshall, J.R. Lee, L. Teng, Z. Yang, J. Xie, Polyethylenimine-based Formulations for Delivery of Oligonucleotides, Current Medicinal Chemistry, 26 (2019) 2264-2284.
[10] L. Wanling, K.W.L. Jenny, Endosomal Escape Pathways for Non-Viral Nucleic Acid Delivery Systems, in: C. Brian (Ed.) Molecular Regulation of Endocytosis, IntechOpen, Rijeka, 2012, pp. Ch. 17.
[11] C.L. Gebhart, A.V. Kabanov, Evaluation of polyplexes as gene transfer agents, Journal of Controlled Release, 73 (2001) 401-416.
[12] H.M. Aliabadi, B. Landry, R.K. Bahadur, A. Neamnark, O. Suwantong, H. Uludağ, Impact of Lipid Substitution on Assembly and Delivery of siRNA by Cationic Polymers, Macromolecular Bioscience, 11 (2011) 662-672.
[13] D.Y. Furgeson, R.N. Cohen, R.I. Mahato, S.W. Kim, Novel water insoluble lipoparticulates for gene delivery, Pharmaceutical research, 19 (2002) 382-390.
[14] R.N. Cohen, M.A. van der Aa, N. Macaraeg, A.P. Lee, F.C. Szoka Jr, Quantification of plasmid DNA copies in the nucleus after lipoplex and polyplex transfection, Journal of Controlled Release, 135 (2009) 166-174.
[15] M. Mahato, P. Kumar, A.K. Sharma, Amphiphilic polyethylenimine polymers mediate efficient delivery of DNA and siRNA in mammalian cells, Molecular BioSystems, 9 (2013) 780-791.
[16] A. Alshamsan, A. Haddadi, V. Incani, J. Samuel, A. Lavasanifar, H. Uludağ, Formulation and Delivery of siRNA by Oleic Acid and Stearic Acid Modified Polyethylenimine, Molecular Pharmaceutics, 6 (2009) 121-133.
[17] Y.-T. Xie, Y.-Z. Du, H. Yuan, F.-Q. Hu, Brain-targeting study of stearic acid–grafted chitosan micelle drug-delivery system, Int J Nanomedicine, 7 (2012) 3235.
[18] T.J. Prazeres, M. Beija, M.-T. Charreyre, J.P.S. Farinha, J.M. Martinho, RAFT polymerization and self-assembly of thermoresponsive poly (N-decylacrylamide-bN, N-diethylacrylamide) block copolymers bearing a phenanthrene fluorescent α-end group, Polymer, 51 (2010) 355-367.

[19] G. Marcelo, T. JV Prazeres, M.-T. Charreyre, J.M. Martinho, J.P.S. Farinha, Thermoresponsive Micelles of Phenanthrene-α-end-labeled Poly (N-decylacrylamide-b-N, N-diethylacrylamide) in Water, Macromolecules, 43 (2010) 501-510.
[20] T.J. Prazeres, M. Beija, F.V. Fernandes, P.G. Marcelino, J.P.S. Farinha, J. Martinho, Determination of the critical micelle concentration of surfactants and amphiphilic block copolymers using coumarin 153, Inorganica Chimica Acta, 381 (2012) 181-187.
[21] D. Zhu, H. Yan, Z. Zhou, J. Tang, X. Liu, R. Hartmann, W.J. Parak, N. Feliu, Y. Shen, Detailed investigation on how the protein corona modulates the physicochemical properties and gene delivery of polyethylenimine (PEI) polyplexes, Biomaterials Science, 6 (2018) 1800-1817.
[22] J. Kreuter, Mechanism of polymeric nanoparticle-based drug transport across the blood-brain barrier (BBB), Journal of microencapsulation, 30 (2013) 49-54.
[23] F. Ungaro, G. De Rosa, A. Miro, F. Quaglia, Spectrophotometric determination of polyethylenimine in the presence of an oligonucleotide for the characterization of controlled release formulations, Journal of pharmaceutical and biomedical analysis, 31 (2003) 143-149.
[24] N.P. Gabrielson, D.W. Pack, Acetylation of Polyethylenimine Enhances Gene Delivery via Weakened Polymer/DNA Interactions, Biomacromolecules, 7 (2006) 2427-2435.
[25] M. Elsayed, V. Corrand, V. Kolhatkar, Y. Xie, N.H. Kim, R. Kolhatkar, O.M. Merkel, Influence of oligospermines architecture on their suitability for siRNA delivery, Biomacromolecules, 15 (2014) 1299-1310.
[26] N. Hartl, F. Adams, G. Costabile, L. Isert, M. Döblinger, X. Xiao, R. Liu, O.M. Merkel, The Impact of Nylon-3 Copolymer Composition on the Efficiency of siRNA Delivery to Glioblastoma Cells, Nanomaterials, 9 (2019) 986.
[27] J.R. Wiśniewski, A. Zougman, N. Nagaraj, M. Mann, Universal sample preparation method for proteome analysis, Nature Methods, 6 (2009) 359-362.
[28] A. Appelt-Menzel, A. Cubukova, K. Günther, F. Edenhofer, J. Piontek, G. Krause, T. Stüber, H. Walles, W. Neuhaus, M. Metzger, Establishment of a Human Blood-Brain Barrier Co-culture Model Mimicking the Neurovascular Unit Using Induced Pluri- and Multipotent Stem Cells, Stem Cell Reports, 8 (2017) 894-906.
[29] O.M. Merkel, D. Librizzi, A. Pfestroff, T. Schurrat, M. Béhé, T. Kissel, In Vivo SPECT and Real-Time Gamma Camera Imaging of Biodistribution and Pharmacokinetics of siRNA Delivery Using an Optimized Radiolabeling and Purification Procedure, Bioconjugate Chemistry, 20 (2009) 174-182.
[30] A. Appelt-Menzel, A. Cubukova, M. Metzger, Establishment of a Human Blood-Brain Barrier Co-Culture Model Mimicking the Neurovascular Unit Using Induced Pluripotent Stem Cells, Current Protocols in Stem Cell Biology, 47 (2018) e62.
[31] H. Petersen, P.M. Fechner, A.L. Martin, K. Kunath, S. Stolnik, C.J. Roberts, D. Fischer, M.C. Davies, T. Kissel, Polyethylenimine-graft-Poly(ethylene glycol) Copolymers: Influence of Copolymer Block Structure on DNA Complexation and Biological Activities as Gene Delivery System, Bioconjugate Chemistry, 13 (2002) 845-854.
[32] S. Jones, O. Merkel, Indium-labeling of siRNA for small animal SPECT imaging, RNA Imaging, Springer2016, pp. 79-88.
[33] F.M. van de Water, O.C. Boerman, A.C. Wouterse, J.G.P. Peters, F.G.M. Russel, R. Masereeuw, Intravenously Administered Short Interfering Rna Accumulates In The Kidney And Selectively Suppresses Gene Function In Renal Proximal Tubules, Drug Metabolism and Disposition, 34 (2006) 1393.
[34] C.G. Pippin, T.A. Parker, T.J. McMurry, M.W. Brechbiel, Spectrophotometric method for the determination of a bifunctional DTPA ligand in DTPA-monoclonal antibody conjugates, Bioconjugate Chemistry, 3 (1992) 342-345.
[35] Z. Liu, Z. Zhang, C. Zhou, Y. Jiao, Hydrophobic modifications of cationic polymers for gene delivery, Progress in Polymer Science, 35 (2010) 1144-1162.

[36] B. Winkeljann, D.C. Keul, O.M. Merkel, Engineering poly- and micelleplexes for nucleic acid delivery - A reflection on their endosomal escape, J Control Release, 353 (2023) 518-534.
[37] B. Winkeljann, D.C. Keul, O.M. Merkel, Engineering poly- and micelleplexes for nucleic acid delivery – A reflection on their endosomal escape, Journal of Controlled Release, 353 (2023) 518-534.
[38] Y. Wan, P.M. Moyle, M.P. Christie, I. Toth, Nanosized, peptide-based multicomponent DNA delivery systems: optimization of endosome escape activity, Nanomedicine, 11 (2016) 907-919.
[39] H. de Martimprey, C. Vauthier, C. Malvy, P. Couvreur, Polymer nanocarriers for the delivery of small fragments of nucleic acids: Oligonucleotides and siRNA, European Journal of Pharmaceutics and Biopharmaceutics, 71 (2009) 490-504.
[40] T. Bronich, A.V. Kabanov, L.A. Marky, A thermodynamic characterization of the interaction of a cationic copolymer with DNA, The Journal of Physical Chemistry B, 105 (2001) 6042-6050.
[41] L. Liu, M. Zheng, D. Librizzi, T. Renette, O.M. Merkel, T. Kissel, Efficient and Tumor Targeted siRNA Delivery by Polyethylenimine-graft-polycaprolactone-block-poly(ethylene glycol)-folate (PEI–PCL–PEG–Fol), Molecular Pharmaceutics, 13 (2016) 134-143.
[42] V. Nadithe, R. Liu, B.A. Killinger, S. Movassaghian, N.H. Kim, A.B. Moszczynska, K.S. Masters, S.H. Gellman, O.M. Merkel, Screening Nylon-3 Polymers, a New Class of Cationic Amphiphiles, for siRNA Delivery, Molecular Pharmaceutics, 12 (2015) 362-374.
[43] M. Grzelczak, J. Vermant, E.M. Furst, L.M. Liz-Marzán, Directed self-assembly of nanoparticles, ACS nano, 4 (2010) 3591-3605.
[44] M. Zheng, D. Librizzi, A. Kılıç, Y. Liu, H. Renz, O.M. Merkel, T. Kissel, Enhancing in vivo circulation and siRNA delivery with biodegradable polyethylenimine-graft-polycaprolactone-block-poly(ethylene glycol) copolymers, Biomaterials, 33 (2012) 6551-6558.
[45] O.M. Merkel, M.A. Mintzer, D. Librizzi, O. Samsonova, T. Dicke, B. Sproat, H. Garn, P.J. Barth, E.E. Simanek, T. Kissel, Triazine Dendrimers as Nonviral Vectors for in Vitro and in Vivo RNAi: The Effects of Peripheral Groups and Core Structure on Biological Activity, Molecular Pharmaceutics, 7 (2010) 969-983.
[46] T.F. Martens, K. Remaut, J. Demeester, S.C. De Smedt, K. Braeckmans, Intracellular delivery of nanomaterials: how to catch endosomal escape in the act, Nano Today, 9 (2014) 344-364.
[47] V. Neuhoff, N. Arold, D. Taube, W. Ehrhardt, Improved staining of proteins in polyacrylamide gels including isoelectric focusing gels with clear background at nanogram sensitivity using Coomassie Brilliant Blue G 250 and r 250, ELECTROPHORESIS, 9 (1988).
[48] R. Cagliani, F. Gatto, G. Bardi, Protein Adsorption: A Feasible Method for Nanoparticle Functionalization?, Materials (Basel), 12 (2019) 1991.
[49] D. Zhong, Y. Jiao, Y. Zhang, W. Zhang, N. Li, Q. Zuo, Q. Wang, W. Xue, Z. Liu, Effects of the gene carrier polyethyleneimines on structure and function of blood components, Biomaterials, 34 (2013) 294-305.
[50] M. Santi, G. Maccari, P. Mereghetti, V. Voliani, S. Rocchiccioli, N. Ucciferri, S. Luin, G. Signore, Rational Design of a Transferrin-Binding Peptide Sequence Tailored to Targeted Nanoparticle Internalization, Bioconjugate Chemistry, 28 (2017) 471-480.
[51] Z.-A. Zhang, X. Xin, C. Liu, Y.-h. Liu, H.-X. Duan, L.-l. Qi, Y.-Y. Zhang, H.-m. Zhao, L.-Q. Chen, M.-J. Jin, Z.-G. Gao, W. Huang, Novel brain-targeted nanomicelles for anti-glioma therapy mediated by the ApoE-enriched protein corona in vivo, Journal of Nanobiotechnology, 19 (2021) 453.
[52] H.R. Kim, K. Andrieux, S. Gil, M. Taverna, H. Chacun, D. Desmaële, F. Taran, D. Georgin, P. Couvreur, Translocation of Poly(ethylene glycol-co-hexadecyl)cyanoacrylate Nanoparticles into Rat Brain Endothelial Cells: Role of Apolipoproteins in Receptor-Mediated Endocytosis, Biomacromolecules, 8 (2007) 793-799.

[53] J. Kreuter, D. Shamenkov, V. Petrov, P. Ramge, K. Cychutek, C. Koch-Brandt, R. Alyautdin, Apolipoprotein-mediated transport of nanoparticle-bound drugs across the blood-brain barrier, J Drug Target, 10 (2002) 317-325.
[54] N.-H. Choi-Miura, K. Takahashi, M. Yoda, K. Saito, T. Mazda, M. Tomita, Proteolytic Activation and Inactivation of the Serine Protease Activity of Plasma Hyaluronan Binding Protein, Biological and Pharmaceutical Bulletin, 24 (2001) 448-452.
[55] P. Kesharwani, R. Chadar, A. Sheikh, W.Y. Rizg, A.Y. Safhi, CD44-Targeted Nanocarrier for Cancer Therapy, Front Pharmacol, 2021, pp. 800481.
[56] S. Ganesh, A.K. Iyer, D.V. Morrissey, M.M. Amiji, Hyaluronic acid based self-assembling nanosystems for CD44 target mediated siRNA delivery to solid tumors, Biomaterials, 34 (2013) 3489-3502.
[57] B. Poller, H. Gutmann, S. Krähenbühl, B. Weksler, I. Romero, P.-O. Couraud, G. Tuffin, J. Drewe, J. Huwyler, The human brain endothelial cell line hCMEC/D3 as a human blood-brain barrier model for drug transport studies, Journal of Neurochemistry, 107 (2008) 1358-1368.
[58] S. Ohtsuki, C. Ikeda, Y. Uchida, Y. Sakamoto, F. Miller, F. Glacial, X. Decleves, J.-M. Scherrmann, P.-O. Couraud, Y. Kubo, Quantitative targeted absolute proteomic analysis of transporters, receptors and junction proteins for validation of human cerebral microvascular endothelial cell line hCMEC/D3 as a human blood–brain barrier model, Molecular pharmaceutics, 10 (2013) 289-296.
[59] K. Vu, B. Weksler, I. Romero, P.-O. Couraud, A. Gelli, Immortalized human brain endothelial cell line HCMEC/D3 as a model of the blood-brain barrier facilitates in vitro studies of central nervous system infection by Cryptococcus neoformans, Eukaryotic cell, 8 (2009) 1803-1807.
[60] K. Bigl, A. Schmitt, I. Meiners, G. Münch, T. Arendt, Comparison of results of the CellTiter Blue, the tetrazolium (3-[4,5-dimethylthioazol-2-yl]-2,5-diphenyl tetrazolium bromide), and the lactate dehydrogenase assay applied in brain cells after exposure to advanced glycation endproducts, Toxicology in Vitro, 21 (2007) 962-971.
[61] D. Maiolo, J. Colombo, J. Beretta, C. Malloggi, G. Candiani, F. Baldelli Bombelli, The polyplex, protein corona, cell interplay: Tips and drawbacks, Colloids and Surfaces B: Biointerfaces, 168 (2018) 60-67.
[62] A. Neamnark, O. Suwantong, R.B. K. C, C.Y.M. Hsu, P. Supaphol, H. Uludağ, Aliphatic Lipid Substitution on 2 kDa Polyethylenimine Improves Plasmid Delivery and Transgene Expression, Molecular Pharmaceutics, 6 (2009) 1798-1815.
[63] W.J. Kim, C.-W. Chang, M. Lee, S.W. Kim, Efficient siRNA delivery using water soluble lipopolymer for anti-angiogenic gene therapy, Journal of controlled release, 118 (2007) 357-363.
[64] D.Y. Furgeson, W.S. Chan, J.W. Yockman, S.W. Kim, Modified Linear Polyethylenimine−Cholesterol Conjugates for DNA Complexation, Bioconjugate Chemistry, 14 (2003) 840-847.
[65] H. Wei, L.R. Volpatti, D.L. Sellers, D.O. Maris, I.W. Andrews, A.S. Hemphill, L.W. Chan, D.S. Chu, P.J. Horner, S.H. Pun, Dual responsive, stabilized nanoparticles for efficient in vivo plasmid delivery, Angewandte Chemie (International ed. in English), 52 (2013) 5377.
[66] S.K. Filippov, Č. Koňák, P. Kopečková, L. Starovoytova, M. Špírková, P. Štěpánek, Effect of Hydrophobic Interactions on Properties and Stability of DNA−Polyelectrolyte Complexes, Langmuir, 26 (2010) 4999-5006.
[67] M. Ribecco-Lutkiewicz, C. Sodja, J. Haukenfrers, A.S. Haqqani, D. Ly, P. Zachar, E. Baumann, M. Ball, J. Huang, M. Rukhlova, M. Martina, Q. Liu, D. Stanimirovic, A. Jezierski, M. Bani-Yaghoub, A novel human induced pluripotent stem cell blood-brain barrier model: Applicability to study antibody-triggered receptor-mediated transcytosis, Scientific Reports, 8 (2018) 1873.

[68] M.M. Lübtow, S. Oerter, S. Quader, E. Jeanclos, A. Cubukova, M. Krafft, M.S. Haider, C. Schulte, L. Meier, M. Rist, O. Sampetrean, H. Kinoh, A. Gohla, K. Kataoka, A. Appelt-Menzel, R. Luxenhofer, In Vitro Blood–Brain Barrier Permeability and Cytotoxicity of an Atorvastatin-Loaded Nanoformulation Against Glioblastoma in 2D and 3D Models, Molecular Pharmaceutics, 17 (2020) 1835-1847.
[69] H.N. Onyema, M. Berger, A. Musyanovych, C. Bantz, M. Maskos, C. Freese, Uptake of polymeric nanoparticles in a human induced pluripotent stem cell-based blood–brain barrier model: Impact of size, material, and protein corona, Biointerphases, 16 (2021) 021004.
[70] M.A. Dobrovolskaia, S.E. McNeil, Understanding the correlation between in vitro and in vivo immunotoxicity tests for nanomedicines, Journal of Controlled Release, 172 (2013) 456-466.
[71] ASTM, Standard Test Method for Analysis of Hemolytic Properties of Nanoparticles, ASTM International West Conshohocken, PA, 2013.
[72] H. Eliyahu, A. Makovitzki, T. Azzam, A. Zlotkin, A. Joseph, D. Gazit, Y. Barenholz, A. Domb, Novel dextran–spermine conjugates as transfecting agents: comparing water-soluble and micellar polymers, Gene therapy, 12 (2005) 494-503.
[73] O.M. Merkel, D. Librizzi, A. Pfestroff, T. Schurrat, K. Buyens, N.N. Sanders, S.C. De Smedt, M. Béhé, T. Kissel, Stability of siRNA polyplexes from poly(ethylenimine) and poly(ethylenimine)-g-poly(ethylene glycol) under in vivo conditions: Effects on pharmacokinetics and biodistribution measured by Fluorescence Fluctuation Spectroscopy and Single Photon Emission Computed Tomography (SPECT) imaging, Journal of Controlled Release, 138 (2009) 148-159.
[74] D.A. Braasch, Z. Paroo, A. Constantinescu, G. Ren, O.K. Öz, R.P. Mason, D.R. Corey, Biodistribution of phosphodiester and phosphorothioate siRNA, Bioorganic & Medicinal Chemistry Letters, 14 (2004) 1139-1143.
[75] D.E. Owens, N.A. Peppas, Opsonization, biodistribution, and pharmacokinetics of polymeric nanoparticles, International Journal of Pharmaceutics, 307 (2006) 93-102.
[76] P. Chollet, M.C. Favrot, A. Hurbin, J.-L. Coll, Side-effects of a systemic injection of linear polyethylenimine–DNA complexes, The Journal of Gene Medicine, 4 (2002) 84-91.
[77] A. Schnyder, S. Krähenbühl, J. Drewe, J. Huwyler, Targeting of daunomycin using biotinylated immunoliposomes: Pharmacokinetics, tissue distribution and in vitro pharmacological effects, J Drug Target, 13 (2005) 325-335.
[78] W. Ke, K. Shao, R. Huang, L. Han, Y. Liu, J. Li, Y. Kuang, L. Ye, J. Lou, C. Jiang, Gene delivery targeted to the brain using an Angiopep-conjugated polyethyleneglycol-modified polyamidoamine dendrimer, Biomaterials, 30 (2009) 6976-6985.

Supplementary Material

1. Polymer synthesis and characterization

The synthesis of PEI-DAA was performed as illustrated in Scheme S1. The decylacrylamide monomer DAA was synthesized starting from acryloyl chloride, triethylamine and N-decylamine according to a modified procedure described in literature [1].

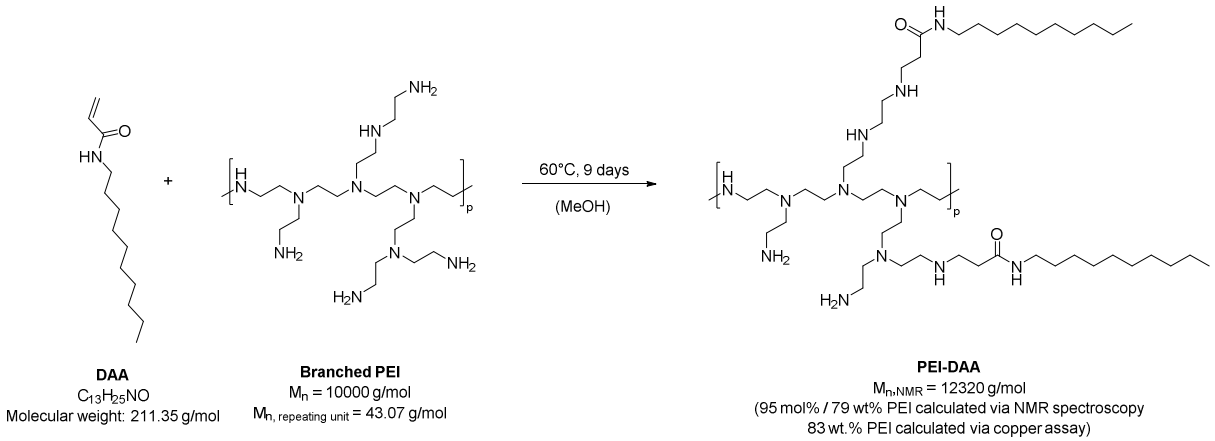

Scheme S1. Synthesis of decylacrylamide – modified poly (ethylene imine) (PEI-DAA) polymer.

Subsequently, 190 mg decylacrylamide (0.9 mmol, 30 eq.) were slowly added to a solution of 300 mg branched PEI (0.03 mmol, 1.0 eq.) in 60 mL methanol. The reaction mixture was stirred at 60°C for 9 days. Conversion of N-decylacrylamide was monitored via ^{1}H-NMR spectroscopy and reached a maximum conversion of 80%. The reaction mixture was precipitated from diethyl ether, centrifugated and the crude product was isolated as a colorless oil. After dissolving the substance in 10 mL high-purity water, filtration with a syringe filter (PES, 1 µm) and freeze-drying, the pure product was isolated as a viscous oil. NMR spectra were recorded on a Bruker 500 MHz spectrometer at Ludwig-Maximilians University at the Pharmacy NMR facility. ^{1}H-NMR spectroscopic chemical shifts δ are reported in ppm. δ (^{1}H) is calibrated to the residual proton signal. Successful linkage was proven by ^{1}H-NMR spectroscopy by the absence of vinylic protons. Based on the ^{1}H-NMR spectrum (Figure S1) a content of 95 mol% and 79 wt.% of PEI was calculated.

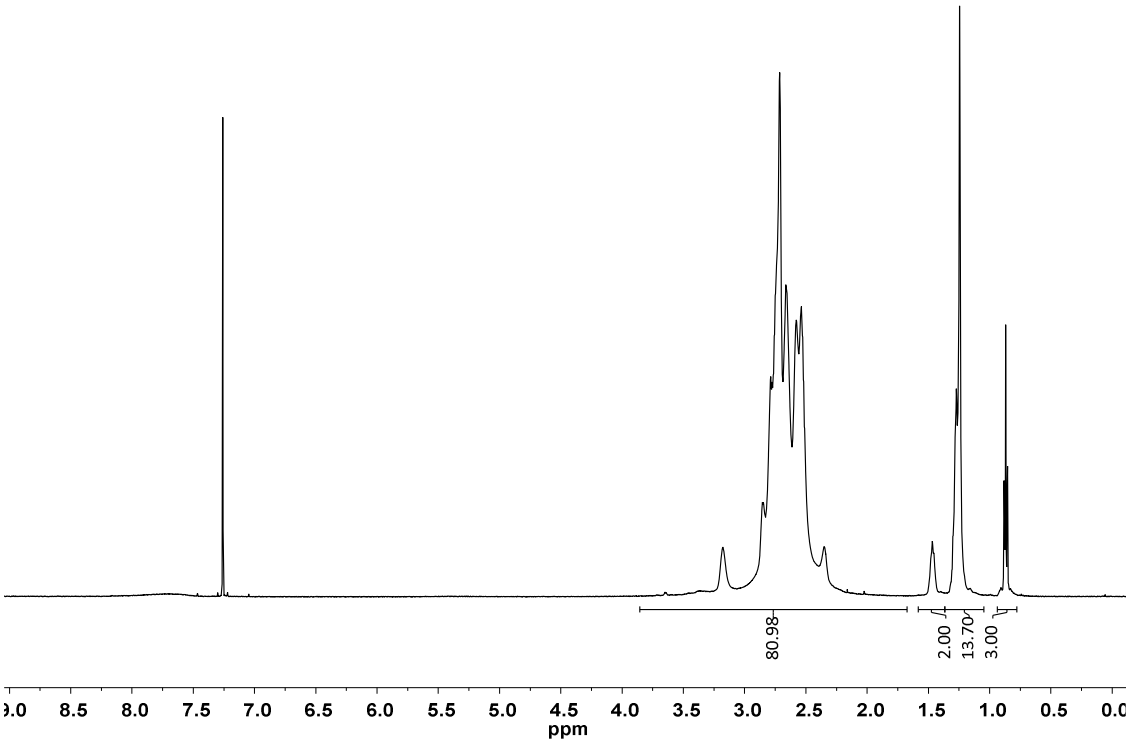

Figure S1. ^{1}H-NMR spectrum of PEI-DAA (500 MHz, CDCl3, 298 K): δ (ppm) = 3.84 – 1.88 (m, 81H, CH_2, $_{PEI}$ (4H per repeating unit), 3xCH_2, $_{DAA}$), 1.46 (m, 2H, CH_2, $_{DAA}$), 1.26 (m, 14H, 7xCH_2, $_{DAA}$), 0.87 (t, 3H, CH_3, $_{DAA}$).

2. Comparison of Protein Corona Profiles

Table S1. List of log2 values of calculated ratios (PEI-DAA vs. PEI PXs, PEI-SA vs. PEI PXs and PEI-DAA vs. PEI-SA PXs) from the mean values of abundances of proteins identified in the hard corona of purified PXs after exposure to 10 % FBS observed from three independent LC-MS-MS measurements.

Protein FDR Confidence: Combined	Accessi	Description	Gene symbol	# Unique Peptides	Abundance Ratio (log2): (PEI_DA) / (PEI)	Abundance Ratio (log2): (SA_Mod PEI) / (PEI)	Abundance Ratio (log2): (PEI_DA) / (SA_Mod PEI)	Abundance Ratio: (PEI_DA) / (PEI)	Abundance Ratio: (SA_Mod PEI) / (PEI)	Abundance Ratio: (PEI_DA) / (SA_Mod PEI)	Abundance Ratio P-Value: (PEI_DA) / (PEI)	Abundance Ratio P-Value: (SA_Mod PEI) / (PEI)	Abundance Ratio P-Value: (PEI_DA) / (SA_Mod PEI)	Abundance Ratio Adj. P-Value: (PEI_DA) / (PEI)	Abundance Ratio Adj. P-Value: (SA_Mod PEI) / (PEI)	Abundance Ratio Adj. P-Value: (PEI_DA) / (SA_Mod PEI)
High	ENSBTAP0	SPP1 UniProtKB Gene Name|Bos taurus secreted phosphoprotein 1 (SPP1), mRNA. [	SPP1	2	-0,51	2,51	-3,01	0,70	5,68	0,12	0,2315	0,0013	0,0003	0,7037	0,1300	0,0678
Medium	*ENSBTAP0*	*SOD1 UniProtKB Gene Name|Bos taurus superoxide dismutase 1, soluble (SOD1), mR*	*SOD1*	*1*	*1,97*	*2,09*	*-0,12*	*3,92*	*4,25*	*0,92*	*0,1519*	*0,0642*	*0,7838*	*0,7037*	*0,9626*	*1,0000*
Medium	*ENSBTAP0*	*PSMB6 UniProtKB Gene Name|Bos taurus proteasome (prosome, macropain) subunit,*	*PSMB6*	*1*	*1,20*	*2,00*	*-0,80*	*2,29*	*4,00*	*0,57*	*0,2545*	*0,0820*	*0,6633*	*0,7037*	*1,0000*	*1,0000*
High	ENSBTAP0	KRT16 HGNC Symbol|keratin 16 [Source:HGNC Symbol;Acc:6423]|19|ENSBTAG0000	KRT16	2	0,30	1,92	-1,62	1,23	3,79	0,32	0,9997	0,7957	0,8087	1,0000	1,0000	1,0000
Medium	*ENSBTAP0*	*EVPL EntrezGene|Bos taurus envoplakin (EVPL), mRNA. [Source:RefSeq mRNA;Acc:NM*	*EVPL*	*1*	*1,53*	*1,75*	*-0,22*	*2,89*	*3,36*	*0,86*	*0,1904*	*0,1253*	*0,9428*	*0,7037*	*1,0000*	*1,0000*
High	ENSBTAP0	HABP2 UniProtKB Gene Name|Bos taurus hyaluronan binding protein 2 (HABP2), m	HABP2	7	0,99	1,75	-0,76	1,98	3,36	0,59	0,0013	0,0001	0,0253	0,0574	0,0235	0,5105
High	ENSBTAP0	SPP2 UniProtKB Gene Name|Bos taurus secreted phosphoprotein 2, 24kDa (SPP2), m	SPP2	5	1,06	1,51	-0,45	2,09	2,85	0,73	0,0237	0,0150	0,9158	0,3293	0,4902	1,0000
High	ENSBTAP0	PROS1 UniProtKB Gene Name|Bos taurus protein S (alpha) (PROS1), mRNA. [Source:	PROS1	19	0,65	1,45	-0,80	1,57	2,73	0,57	0,0218	0,0023	0,1398	0,3121	0,1920	0,8275
High	ENSBTAP0	Bos taurus SERPINA3-8 (SERPINA3-8), mRNA. [Source:RefSeq mRNA;Acc:NM_001081	Bos	4	1,78	1,44	0,33	3,43	2,72	1,26	0,5555	0,5423	0,9997	0,9502	1,0000	1,0000
High	ENSBTAP0	GOLM1 HGNC Symbol|golgi membrane protein 1 [Source:HGNC Symbol;Acc:15451]|	GOLM1	7	0,99	1,44	-0,45	1,98	2,71	0,73	0,0428	0,0117	0,5302	0,4037	0,4558	1,0000
High	ENSBTAP0	PLEK HGNC Symbol|pleckstrin [Source:HGNC Symbol;Acc:9070]|11|ENSBTAG00000	PLEK	2	1,20	1,42	-0,23	2,29	2,68	0,86	0,1110	0,1452	0,9761	0,6496	1,0000	1,0000
High	ENSBTAP0	Uncharacterized protein [Source:UniProtKB/TrEMBL;Acc:F1MP09]|23|ENSBTAG000	Uncharacterized	10	0,74	1,41	-0,66	1,67	2,65	0,63	0,3362	0,0425	0,2962	0,7805	0,8999	1,0000
High	*ENSBTAP0*	*PTX3 EntrezGene|Bos taurus pentraxin 3, long (PTX3), mRNA. [Source:RefSeq mRNA;*	*PTX3*	*1*	*1,59*	*1,33*	*0,27*	*3,02*	*2,51*	*1,21*	*0,0531*	*0,0999*	*0,8730*	*0,4677*	*1,0000*	*1,0000*
High	*ENSBTAP0*	*TPM1 EntrezGene|Bos taurus tropomyosin 1 (alpha) (TPM1), mRNA. [Source:RefSeq r*	*TPM1*	*1*	*-0,17*	*1,31*	*-1,48*	*0,89*	*2,48*	*0,36*	*0,4323*	*0,0987*	*0,0197*	*0,8766*	*1,0000*	*0,4358*
High	ENSBTAP0	APOA2 UniProtKB Gene Name|Bos taurus apolipoprotein A-II (APOA2), mRNA. [Sou	APOA2	8	0,33	1,30	-0,98	1,25	2,47	0,51	0,9334	0,0075	0,0109	1,0000	0,3473	0,4358
High	ENSBTAP0	CDH13 EntrezGene|Bos taurus cadherin 13, H-cadherin (heart) (CDH13), mRNA. [So	CDH13	3	1,70	1,30	0,40	3,25	2,46	1,32	0,1325	0,3242	0,7629	0,6918	1,0000	1,0000
High	ENSBTAP0	TAGLN2 UniProtKB Gene Name|Bos taurus transgelin 2 (TAGLN2), mRNA. [Source:R	TAGLN2	3	2,07	1,26	0,81	4,21	2,39	1,76	0,1922	0,9528	0,2781	0,7037	1,0000	1,0000
High	*ENSBTAP0*	*MT1E UniProtKB Gene Name|Bos taurus metallothionein 1E (MT1E), mRNA. [Source:R*	*MT1E*	*1*	*1,61*	*1,23*	*0,37*	*3,05*	*2,35*	*1,30*	*0,5080*	*0,9524*	*0,6730*	*0,9031*	*1,0000*	*1,0000*
High	ENSBTAP0	PLVAP EntrezGene|Bos taurus plasmalemma vesicle associated protein (PLVAP), mR	PLVAP	4	1,23	1,19	0,04	2,34	2,28	1,03	0,0929	0,3311	0,5959	0,6038	1,0000	1,0000
High	ENSBTAP0	F2 UniProtKB Gene Name|Bos taurus coagulation factor II (thrombin) (F2), mRNA. [S	F2	28	0,91	1,18	-0,27	1,87	2,26	0,83	0,0003	0,0001	0,0887	0,0362	0,0182	0,7248
High	ENSBTAP0	RCN1 UniProtKB Gene Name|Bos taurus reticulocalbin 1, EF-hand calcium binding d	RCN1	4	2,18	1,17	1,01	4,53	2,25	2,01	0,0266	0,6376	0,0838	0,3454	1,0000	0,7006
High	ENSBTAP0	COL1A1 UniProtKB Gene Name|Bos taurus collagen, type I, alpha 1 (COL1A1), mRNA	COL1A1	12	0,87	1,17	-0,30	1,83	2,25	0,81	0,3434	0,2152	0,9230	0,7847	1,0000	1,0000
High	*ENSBTAP0*	*PSMA4 UniProtKB Gene Name|Bos taurus proteasome (prosome, macropain) subunit,*	*PSMA4*	*1*	*1,44*	*1,15*	*0,29*	*2,72*	*2,22*	*1,23*	*0,1635*	*0,2686*	*0,9182*	*0,7037*	*1,0000*	*1,0000*
High	ENSBTAP0	RCN3 UniProtKB Gene Name|Bos taurus reticulocalbin 3, EF-hand calcium binding d	RCN3	4	1,05	1,10	-0,05	2,06	2,14	0,97	0,2486	0,1407	0,8956	0,7037	1,0000	1,0000

High	ENSBTAP0	ACAN HGNC Symbol|aggrecan [Source:HGNC Symbol;Acc:319]|21|ENSBTAG00000	ACAN		5	1,07	1,07	0,00	2,10	2,10	1,00	0,8854	0,6053	0,8638	1,0000	1,0000	1,0000
High	ENSBTAP0	CALM UniProtKB Gene Name|Bos taurus calmodulin 1 (phosphorylase kinase, delta)	CALM		2	0,71	1,07	-0,36	1,64	2,10	0,78	0,0068	0,0009	0,1320	0,1657	0,1077	0,8275
High	ENSBTAP0	OMD EntrezGene|Bos taurus osteomodulin (OMD), mRNA. [Source:RefSeq mRNA;A	OMD		5	0,86	1,02	-0,16	1,81	2,02	0,90	0,2473	0,3371	0,9647	0,7037	1,0000	1,0000
High	ENSBTAP0	SPARCL1 UniProtKB Gene Name|Bos taurus SPARC-like 1 (hevin) (SPARCL1), mRNA. [	SPARCL1		13	0,50	1,00	-0,51	1,41	2,00	0,70	0,7521	0,3799	0,7692	1,0000	1,0000	1,0000
High	ENSBTAP0	Bos taurus amine oxidase, copper containing 3 (SAO), mRNA. [Source:RefSeq mRNA	Bos		4	1,45	0,99	0,45	2,73	1,99	1,37	0,3064	0,8108	0,6048	0,7418	1,0000	1,0000
High	ENSBTAP0	SPARC UniProtKB Gene Name|Bos taurus secreted protein, acidic, cysteine-rich (oste	SPARC		12	0,53	0,98	-0,45	1,44	1,97	0,73	0,2037	0,0900	0,8034	0,7037	1,0000	1,0000
High	ENSBTAP0	CA2 EntrezGene|Bos taurus carbonic anhydrase II (CA2), mRNA. [Source:RefSeq mR	CA2		2	0,99	0,97	0,02	1,98	1,96	1,01	0,2605	0,1304	0,8510	0,7037	1,0000	1,0000
High	ENSBTAP0	CLEC11A UniProtKB Gene Name|Bos taurus C-type lectin domain family 11, member	CLEC11A		5	0,60	0,94	-0,35	1,51	1,92	0,79	0,0983	0,0395	0,7552	0,6186	0,8999	1,0000
High	ENSBTAP0	Bos taurus complement component 4A (C4A), mRNA. [Source:RefSeq mRNA;Acc:NM	Bos		42	0,23	0,93	-0,71	1,17	1,91	0,61	0,2838	0,0075	0,0501	0,7197	0,3473	0,6976
Medium	*ENSBTAP0*	*PCDH18 HGNC Symbol|protocadherin 18 [Source:HGNC Symbol;Acc:14268]|17|ENSB*	*PCDH18*		*1*	*0,23*	*0,92*	*-0,69*	*1,18*	*1,90*	*0,62*	*0,9974*	*0,5186*	*0,4831*	*1,0000*	*1,0000*	*1,0000*
High	ENSBTAP0	ACTA1 UniProtKB Gene Name|Bos taurus actin, alpha 1, skeletal muscle (ACTA1), m	ACTA1		3	1,15	0,86	0,29	2,21	1,81	1,22	0,3927	0,7329	0,8035	0,8333	1,0000	1,0000
High	ENSBTAP0	DKK3 UniProtKB Gene Name|Bos taurus dickkopf homolog 3 (Xenopus laevis) (DKK3	DKK3		4	0,87	0,82	0,05	1,82	1,76	1,03	0,1873	0,1343	0,9633	0,7037	1,0000	1,0000
High	ENSBTAP0	F11 UniProtKB Gene Name|Bos taurus coagulation factor XI (F11), mRNA. [Source:R	F11		6	1,24	0,82	0,42	2,36	1,76	1,34	0,0876	0,0950	0,9978	0,5953	1,0000	1,0000
High	ENSBTAP0	HSPG2 HGNC Symbol|heparan sulfate proteoglycan 2 [Source:HGNC Symbol;Acc:52	HSPG2		9	1,15	0,79	0,36	2,22	1,73	1,28	0,0954	0,4290	0,4858	0,6124	1,0000	1,0000
High	ENSBTAP0	PSMA6 UniProtKB Gene Name|Bos taurus proteasome (prosome, macropain) subur	PSMA6		2	0,39	0,78	-0,39	1,31	1,72	0,76	0,5146	0,1540	0,5952	0,9031	1,0000	1,0000
Medium	*ENSBTAP0*	*Uncharacterized protein [Source:UniProtKB/TrEMBL;Acc:F1MV78]|9|ENSBTAG00000*	*Uncharacterized*		*1*	*1,42*	*0,78*	*0,64*	*2,68*	*1,72*	*1,56*	*0,8167*	*0,9254*	*0,9692*	*1,0000*	*1,0000*	*1,0000*
High	ENSBTAP0	COMP EntrezGene|cartilage oligomeric matrix protein precursor [Source:RefSeq pe	COMP		17	1,84	0,77	1,07	3,59	1,70	2,10	0,0012	0,0717	0,0154	0,0563	0,9985	0,4358
High	ENSBTAP0	TPM3 UniProtKB Gene Name|Bos taurus tropomyosin 3 (TPM3), mRNA. [Source:Ref	TPM3		4	-0,07	0,73	-0,80	0,96	1,66	0,57	0,9423	0,7202	0,8903	1,0000	1,0000	1,0000
High	ENSBTAP0	TPM4 HGNC Symbol|tropomyosin 4 [Source:HGNC Symbol;Acc:12013]|7|ENSBTAG0	TPM4		3	-0,13	0,71	-0,84	0,92	1,64	0,56	0,8615	0,3937	0,2087	1,0000	1,0000	0,9709
Medium	*ENSBTAP0*	*MFAP5 UniProtKB Gene Name|Bos taurus microfibrillar associated protein 5 (MFAP5)*	*MFAP5*		*1*	*1,19*	*0,70*	*0,49*	*2,29*	*1,63*	*1,40*	*0,0083*	*0,0203*	*0,7050*	*0,1743*	*0,5643*	*1,0000*
High	ENSBTAP0	AMBP EntrezGene|Bos taurus alpha-1-microglobulin/bikunin precursor (AMBP), mR	AMBP		15	0,68	0,70	-0,01	1,61	1,62	0,99	0,0388	0,0419	0,9979	0,3927	0,8999	1,0000
Medium	*ENSBTAP0*	*STAM UniProtKB Gene Name|Bos taurus signal transducing adaptor molecule (SH3 do*	*STAM*		*1*	*0,44*	*0,67*	*-0,23*	*1,36*	*1,60*	*0,85*	*0,0780*	*0,0823*	*0,9990*	*0,5768*	*1,0000*	*1,0000*
High	ENSBTAP0	VIM UniProtKB Gene Name|Bos taurus vimentin (VIM), mRNA. [Source:RefSeq mRN	VIM		7	2,00	0,67	1,33	4,00	1,59	2,51	0,2940	0,9490	0,2005	0,7367	1,0000	0,9695
High	*ENSBTAP0*	*Uncharacterized protein [Source:UniProtKB/TrEMBL;Acc:G3N3P6]|29|ENSBTAG0000*	*Uncharacterized*		*1*	*0,75*	*0,67*	*0,08*	*1,68*	*1,59*	*1,06*	*0,3675*	*0,3740*	*0,9999*	*0,8204*	*1,0000*	*1,0000*
High	ENSBTAP0	APON UniProtKB Gene Name|ovarian and testicular apolipoprotein N precursor [So	APON		4	0,88	0,61	0,27	1,84	1,53	1,21	0,0312	0,1548	0,4525	0,3630	1,0000	1,0000
High	ENSBTAP0	VWF EntrezGene|Bos taurus von Willebrand factor (VWF), mRNA. [Source:RefSeq m	VWF		18	0,80	0,60	0,20	1,74	1,52	1,15	0,0252	0,3040	0,1908	0,3347	1,0000	0,9302
High	ENSBTAP0	F13B UniProtKB Gene Name|Bos taurus coagulation factor XIII, B polypeptide (F13B)	F13B		14	1,59	0,60	0,99	3,01	1,51	1,99	0,0541	0,8314	0,1135	0,4677	1,0000	0,8275
High	ENSBTAP0	EFEMP1 UniProtKB Gene Name|Bos taurus EGF containing fibulin-like extracellular r	EFEMP1		9	1,26	0,59	0,67	2,40	1,51	1,59	0,0620	0,6889	0,1822	0,5040	1,0000	0,9034
High	ENSBTAP0	HBA UniProtKB Gene Name|Bos taurus hemoglobin, alpha 2 (HBA), mRNA. [Source:	HBA		10	0,38	0,58	-0,20	1,30	1,50	0,87	0,4167	0,2918	0,9502	0,8674	1,0000	1,0000
High	ENSBTAP0	PROC HGNC Symbol|protein C (inactivator of coagulation factors Va and VIIIa) [Sour	PROC		9	0,46	0,58	-0,12	1,37	1,49	0,92	0,0107	0,0043	0,6509	0,2011	0,3124	1,0000
Medium	*ENSBTAP0*	*POF1B HGNC Symbol|premature ovarian failure, 1B [Source:HGNC Symbol;Acc:13711*	*POF1B*		*1*	*1,42*	*0,57*	*0,85*	*2,68*	*1,49*	*1,80*	*0,6274*	*0,9966*	*0,6717*	*1,0000*	*1,0000*	*1,0000*
High	ENSBTAP0	GSTA1 UniProtKB Gene Name|Bos taurus glutathione S-transferase alpha 3 (GSTA3)	GSTA1		2	2,85	0,56	2,30	7,24	1,47	4,92	0,0025	0,3921	0,0096	0,0906	1,0000	0,4309
High	*ENSBTAP0*	*APOC3 UniProtKB Gene Name|Bos taurus apolipoprotein C-III (APOC3), mRNA. [Sourc*	*APOC3*		*1*	*0,19*	*0,54*	*-0,35*	*1,14*	*1,45*	*0,79*	*0,9287*	*0,1617*	*0,2569*	*1,0000*	*1,0000*	*1,0000*
High	ENSBTAP0	FMOD UniProtKB Gene Name|Bos taurus fibromodulin (FMOD), mRNA. [Source:Ref	FMOD		4	0,11	0,54	-0,43	1,08	1,45	0,74	0,8690	0,4442	0,7215	1,0000	1,0000	1,0000
High	ENSBTAP0	SERPIND1 UniProtKB Gene Name|Bos taurus serpin peptidase inhibitor, clade D (he	SERPIND1		19	0,46	0,53	-0,06	1,38	1,44	0,96	0,0459	0,0168	0,6847	0,4263	0,5186	1,0000
High	ENSBTAP0	PEPD UniProtKB Gene Name|Bos taurus peptidase D (PEPD), mRNA. [Source:RefSeq	PEPD		3	1,84	0,52	1,31	3,57	1,44	2,48	0,0000	0,0190	0,0001	0,0049	0,5557	0,0594
High	*ENSBTAP0*	*C1orf68 HGNC Symbol|chromosome 1 open reading frame 68 [Source:HGNC Symbol;*	*C1orf68*		*1*	*0,78*	*0,52*	*0,26*	*1,72*	*1,43*	*1,20*	*0,3597*	*0,6219*	*0,8634*	*0,8168*	*1,0000*	*1,0000*
High	ENSBTAP0	TF HGNC Symbol|transferrin [Source:HGNC Symbol;Acc:11740]|1|ENSBTAG000000	TF		41	0,76	0,52	0,24	1,69	1,43	1,18	0,1074	0,5947	0,3789	0,6345	1,0000	1,0000
High	ENSBTAP0	F10 UniProtKB Gene Name|Bos taurus coagulation factor X (F10), mRNA. [Source:Re	F10		11	0,31	0,50	-0,18	1,24	1,41	0,88	0,0552	0,0446	0,9837	0,4677	0,8999	1,0000
Medium	*ENSBTAP0*	*B3GNT1 UniProtKB Gene Name|Bos taurus UDP-GlcNAc:betaGal beta-1,3-N-acetylglu*	*B3GNT1*		*1*	*1,19*	*0,49*	*0,69*	*2,28*	*1,41*	*1,62*	*0,0871*	*0,9996*	*0,0901*	*0,5953*	*1,0000*	*0,7248*
High	ENSBTAP0	AHCY UniProtKB Gene Name|Bos taurus adenosylhomocysteinase (AHCY), mRNA. [S	AHCY		7	0,42	0,49	-0,07	1,34	1,40	0,95	0,5993	0,9246	0,8109	0,9812	1,0000	1,0000
High	ENSBTAP0	JUP UniProtKB Gene Name|Bos taurus junction plakoglobin (JUP), mRNA. [Source:Re	JUP		7	-0,56	0,49	-1,05	0,68	1,40	0,48	0,2625	1,0000	0,2643	0,7037	1,0000	1,0000
High	*ENSBTAP0*	*LTBP4 HGNC Symbol|latent transforming growth factor beta binding protein 4 [Source*	*LTBP4*		*1*	*1,75*	*0,48*	*1,27*	*3,37*	*1,40*	*2,41*	*0,0041*	*0,3382*	*0,0201*	*0,1258*	*1,0000*	*0,4358*
High	ENSBTAP0	F9 UniProtKB Gene Name|Bos taurus coagulation factor IX (F9), mRNA. [Source:RefS	F9		9	0,44	0,47	-0,03	1,36	1,39	0,98	0,0387	0,0678	0,8943	0,3927	0,9680	1,0000
High	ENSBTAP0	ITIH3 UniProtKB Gene Name|Bos taurus inter-alpha-trypsin inhibitor heavy chain 3 (	ITIH3		31	0,43	0,47	-0,04	1,35	1,39	0,97	0,0272	0,0418	0,9311	0,3454	0,8999	1,0000
High	ENSBTAP0	TNXB EntrezGene|tenascin-X precursor [Source:RefSeq peptide;Acc:NP_777128]|23	TNXB		3	0,61	0,45	0,15	1,53	1,37	1,11	0,6714	0,8910	0,4253	1,0000	1,0000	1,0000
High	ENSBTAP0	COL12A1 HGNC Symbol|collagen, type XII, alpha 1 [Source:HGNC Symbol;Acc:2188]|	COL12A1		5	0,56	0,42	0,14	1,48	1,34	1,11	0,0545	0,2015	0,5849	0,4677	1,0000	1,0000
High	ENSBTAP0	COL5A1 HGNC Symbol|collagen, type V, alpha 1 [Source:HGNC Symbol;Acc:2209]|11	COL5A1		6	0,74	0,41	0,33	1,67	1,33	1,26	0,1672	0,2472	0,9485	0,7037	1,0000	1,0000
High	ENSBTAP0	PLXNB2 HGNC Symbol|plexin B2 [Source:HGNC Symbol;Acc:9104]|5|ENSBTAG00000	PLXNB2		2	0,19	0,41	-0,22	1,14	1,33	0,86	0,8831	0,9626	0,7481	1,0000	1,0000	1,0000
High	ENSBTAP0	Bos taurus hemoglobin, gamma 2 (LOC788610), mRNA. [Source:RefSeq mRNA;Acc:N	Bos		9	0,53	0,41	0,12	1,45	1,33	1,09	0,0565	0,0446	0,9799	0,4723	0,8999	1,0000
High	ENSBTAP0	ITIH1 HGNC Symbol|inter-alpha-trypsin inhibitor heavy chain 1 [Source:HGNC Symb	ITIH1		29	-0,10	0,41	-0,50	0,94	1,33	0,71	0,9724	0,4014	0,5122	1,0000	1,0000	1,0000
High	ENSBTAP0	F7 UniProtKB Gene Name|Bos taurus coagulation factor VII (serum prothrombin cor	F7		2	0,28	0,41	-0,12	1,22	1,33	0,92	0,3867	0,7567	0,7732	0,8333	1,0000	1,0000
High	ENSBTAP0	FGB UniProtKB Gene Name|Bos taurus fibrinogen beta chain (FGB), mRNA. [Source:	FGB		16	0,26	0,40	-0,13	1,20	1,32	0,91	0,2257	0,2478	0,9969	0,7037	1,0000	1,0000
High	ENSBTAP0	FSTL1 UniProtKB Gene Name|Bos taurus follistatin-like 1 (FSTL1), mRNA. [Source:Re	FSTL1		3	1,19	0,39	0,80	2,28	1,31	1,74	0,0029	0,1695	0,0248	0,0997	1,0000	0,5105
High	*ENSBTAP0*	*KRT73 UniProtKB Gene Name|Bos taurus keratin 73 (KRT73), mRNA. [Source:RefSeq n*	*KRT73*		*1*	*0,46*	*0,39*	*0,06*	*1,37*	*1,31*	*1,05*	*0,9896*	*0,9205*	*0,8609*	*1,0000*	*1,0000*	*1,0000*
Medium	*ENSBTAP0*	*Uncharacterized protein [Source:UniProtKB/TrEMBL;Acc:G3X7H8]|23|ENSBTAG0000*	*Uncharacterized*		*1*	*1,42*	*0,39*	*1,03*	*2,68*	*1,31*	*2,04*	*0,9744*	*0,9823*	*0,9176*	*1,0000*	*1,0000*	*1,0000*
High	*ENSBTAP0*	*PTGR1 EntrezGene|Bos taurus prostaglandin reductase 1 (PTGR1), mRNA. [Source:Re*	*PTGR1*		*1*	*0,25*	*0,39*	*-0,14*	*1,19*	*1,31*	*0,91*	*0,7603*	*0,9849*	*0,6667*	*1,0000*	*1,0000*	*1,0000*
High	ENSBTAP0	TG EntrezGene|Bos taurus thyroglobulin (TG), mRNA. [Source:RefSeq mRNA;Acc:NM	TG		6	0,85	0,39	0,46	1,80	1,31	1,38	0,4626	0,5137	0,9945	0,9031	1,0000	1,0000
High	ENSBTAP0	ADAMTS13 HGNC Symbol|ADAM metallopeptidase with thrombospondin type 1 mo	ADAMTS13		9	1,15	0,38	0,77	2,23	1,30	1,71	0,0124	0,3104	0,0837	0,2274	1,0000	0,7006
High	*ENSBTAP0*	*CATHL1 UniProtKB Gene Name|Bos taurus cathelicidin 1 (CATHL1), mRNA. [Source:Re*	*CATHL1*		*1*	*0,53*	*0,38*	*0,15*	*1,45*	*1,30*	*1,11*	*0,9068*	*0,9952*	*0,9418*	*1,0000*	*1,0000*	*1,0000*
High	ENSBTAP0	VNN1 UniProtKB Gene Name|Bos taurus vanin 1 (VNN1), mRNA. [Source:RefSeq mR	VNN1		14	0,59	0,38	0,21	1,51	1,30	1,16	0,2447	0,6806	0,6337	0,7037	1,0000	1,0000
High	ENSBTAP0	Uncharacterized protein [Source:UniProtKB/TrEMBL;Acc:G3MXD9]|7|ENSBTAG000	Uncharacterized		2	0,85	0,37	0,47	1,80	1,30	1,39	0,1375	0,7204	0,3667	0,6918	1,0000	1,0000
High	ENSBTAP0	CFH EntrezGene|Bos taurus complement factor H (CFH), mRNA. [Source:RefSeq mR	CFH		31	0,81	0,37	0,45	1,76	1,29	1,36	0,0407	0,8761	0,0752	0,3927	1,0000	0,7006
High	ENSBTAP0	IGFBP3 UniProtKB Gene Name|Bos taurus insulin-like growth factor binding protein	IGFBP3		2	0,62	0,36	0,26	1,54	1,29	1,20	0,1788	0,7261	0,4567	0,7037	1,0000	1,0000
High	ENSBTAP0	Uncharacterized protein [Source:UniProtKB/TrEMBL;Acc:G3MZL1]|18|ENSBTAG000	Uncharacterized		3	0,23	0,35	-0,12	1,17	1,28	0,92	0,0925	0,0438	0,8261	0,6038	0,8999	1,0000
High	ENSBTAP0	ITIH2 EntrezGene|Bos taurus inter-alpha-trypsin inhibitor heavy chain 2 (ITIH2), mR	ITIH2		33	0,64	0,35	0,29	1,56	1,27	1,23	0,0005	0,0115	0,0281	0,0362	0,4558	0,5134
High	ENSBTAP0	BLVRB UniProtKB Gene Name|Bos taurus biliverdin reductase B (flavin reductase (N	BLVRB		2	0,53	0,35	0,18	1,45	1,27	1,14	0,2031	0,5726	0,6579	0,7037	1,0000	1,0000
Medium	*ENSBTAP0*	*NCKAP1 HGNC Symbol|NCK-associated protein 1 [Source:HGNC Symbol;Acc:7666]|2|*	*NCKAP1*		*1*	*0,33*	*0,35*	*-0,02*	*1,26*	*1,27*	*0,99*	*0,2775*	*0,4777*	*0,8862*	*0,7153*	*1,0000*	*1,0000*
High	ENSBTAP0	VASN UniProtKB Gene Name|Bos taurus vasorin (VASN), mRNA. [Source:RefSeq mR	VASN		6	-0,04	0,34	-0,38	0,98	1,27	0,77	0,9210	0,3898	0,5863	1,0000	1,0000	1,0000
High	ENSBTAP0	CDH6 UniProtKB Gene Name|Bos taurus cadherin 6, type 2, K-cadherin (fetal kidney	CDH6		3	0,54	0,33	0,21	1,45	1,26	1,16	0,0894	0,2638	0,6853	0,5953	1,0000	1,0000
High	*ENSBTAP0*	*YWHAQ UniProtKB Gene Name|Bos taurus tyrosine 3-monooxygenase/tryptophan 5-*	*YWHAQ*		*1*	*0,59*	*0,33*	*0,26*	*1,51*	*1,26*	*1,20*	*0,0328*	*0,1471*	*0,4938*	*0,3688*	*1,0000*	*1,0000*
High	ENSBTAP0	OGN UniProtKB Gene Name|Bos taurus osteoglycin (OGN), mRNA. [Source:RefSeq m	OGN		4	0,28	0,32	-0,04	1,22	1,25	0,97	0,4147	0,4312	0,9993	0,8665	1,0000	1,0000
High	*ENSBTAP0*	*CUTA UniProtKB Gene Name|Bos taurus cutA divalent cation tolerance homolog (E. c*	*CUTA*		*1*	*0,88*	*0,32*	*0,56*	*1,83*	*1,25*	*1,47*	*0,8392*	*0,8705*	*0,9977*	*1,0000*	*1,0000*	*1,0000*
High	ENSBTAP0	HSP90AA1 UniProtKB Gene Name|Bos taurus heat shock protein 90kDa alpha (cytos	HSP90AA1		4	0,29	0,32	-0,02	1,23	1,25	0,98	0,1240	0,1321	0,9987	0,6699	1,0000	1,0000
Medium	*ENSBTAP0*	*COL18A1 HGNC Symbol|collagen, type XVIII, alpha 1 [Source:HGNC Symbol;Acc:2195]*	*COL18A1*		*1*	*-0,04*	*0,30*	*-0,35*	*0,97*	*1,23*	*0,79*	*0,9845*	*0,2156*	*0,1743*	*1,0000*	*1,0000*	*0,8981*
High	ENSBTAP0	CADM1 UniProtKB Gene Name|Bos taurus cell adhesion molecule 1 (CADM1), mRN	CADM1		2	0,19	0,30	-0,11	1,14	1,23	0,93	0,8046	0,8630	0,9926	1,0000	1,0000	1,0000
High	*ENSBTAP0*	*CD59 UniProtKB Gene Name|Bos taurus CD59 molecule, complement regulatory prote*	*CD59*		*1*	*0,78*	*0,30*	*0,48*	*1,72*	*1,23*	*1,40*	*0,1640*	*0,4289*	*0,7200*	*0,7037*	*1,0000*	*1,0000*
High	ENSBTAP0	KRT17 UniProtKB Gene Name|Bos taurus keratin 17 (KRT17), mRNA. [Source:RefSeq	KRT17		3	-0,19	0,29	-0,48	0,88	1,22	0,72	0,9293	0,5126	0,3416	1,0000	1,0000	1,0000
High	ENSBTAP0	CD44 UniProtKB Gene Name|Bos taurus CD44 molecule (Indian blood group) (CD44	CD44		3	0,14	0,29	-0,14	1,10	1,22	0,91	0,9071	0,9484	0,9930	1,0000	1,0000	1,0000
High	ENSBTAP0	RBP4 UniProtKB Gene Name|Bos taurus retinol binding protein 4, plasma (RBP4), m	RBP4		9	0,51	0,28	0,24	1,43	1,21	1,18	0,3274	0,7600	0,6898	0,7679	1,0000	1,0000
High	ENSBTAP0	Uncharacterized protein [Source:UniProtKB/TrEMBL;Acc:G3MY71]|21|ENSBTAG000	Uncharacterized		2	0,56	0,27	0,29	1,47	1,21	1,22	0,3069	0,5985	0,8174	0,7418	1,0000	1,0000
High	ENSBTAP0	PCOLCE UniProtKB Gene Name|Bos taurus procollagen C-endopeptidase enhancer (	PCOLCE		4	0,69	0,27	0,42	1,62	1,21	1,34	0,0822	0,2713	0,6348	0,5865	1,0000	1,0000
High	ENSBTAP0	QSOX1 HGNC Symbol|quiescin Q6 sulfhydryl oxidase 1 [Source:HGNC Symbol;Acc:97	QSOX1		3	0,42	0,27	0,15	1,34	1,20	1,11	0,2044	0,2819	0,9637	0,7037	1,0000	1,0000
High	ENSBTAP0	Clusterin [Source:UniProtKB/TrEMBL;Acc:F1MWI1]|8|ENSBTAG00000015027|ENSBT	Clusterin		2	-0,44	0,25	-0,69	0,74	1,19	0,62	0,1590	0,5696	0,0419	0,7037	1,0000	0,6444
High	ENSBTAP0	HBB UniProtKB Gene Name|Bos taurus hemoglobin, beta (HBB), mRNA. [Source:Ref	HBB		5	0,10	0,25	-0,15	1,07	1,19	0,90	0,9995	0,7594	0,7432	1,0000	1,0000	1,0000
High	ENSBTAP0	DAG1 HGNC Symbol|dystroglycan 1 (dystrophin-associated glycoprotein 1) [Source:	DAG1		3	0,35	0,24	0,11	1,28	1,18	1,08	0,4306	0,9799	0,3459	0,8766	1,0000	1,0000
High	ENSBTAP0	MST1 HGNC Symbol|macrophage stimulating 1 (hepatocyte growth factor-like) [Sou	MST1		9	0,51	0,24	0,27	1,43	1,18	1,21	0,2527	0,9609	0,3496	0,7037	1,0000	1,0000
High	ENSBTAP0	CD109 HGNC Symbol|CD109 molecule [Source:HGNC Symbol;Acc:21685]|9|ENSBTA	CD109		9	0,43	0,24	0,20	1,35	1,18	1,15	0,9976	0,7824	0,8177	1,0000	1,0000	1,0000
High	ENSBTAP0	FGA UniProtKB Gene Name|Bos taurus fibrinogen alpha chain (FGA), mRNA. [Source	FGA		13	0,64	0,23	0,41	1,56	1,17	1,33	0,3388	0,9874	0,4035	0,7834	1,0000	1,0000
High	ENSBTAP0	PSAP UniProtKB Gene Name|Bos taurus prosaposin (PSAP), mRNA. [Source:RefSeq r	PSAP		4	2,10	0,23	1,88	4,30	1,17	3,67	0,0300	0,7480	0,0745	0,3630	1,0000	0,7006
High	ENSBTAP0	LDHB UniProtKB Gene Name|Bos taurus lactate dehydrogenase B (LDHB), mRNA. [S	LDHB		4	0,12	0,22	-0,11	1,09	1,17	0,93	0,9976	0,7394	0,7760	1,0000	1,0000	1,0000
High	*ENSBTAP0*	*FABP5 HGNC Symbol|fatty acid binding protein 5 (psoriasis-associated) [Source:HGNC*	*FABP5*		*1*	*0,01*	*0,22*	*-0,21*	*1,01*	*1,17*	*0,86*	*0,5627*	*0,5810*	*0,9994*	*0,9561*	*1,0000*	*1,0000*
High	ENSBTAP0	TUBB3 UniProtKB Gene Name|Bos taurus tubulin, beta 3 class III (TUBB3), mRNA. [S	TUBB3		2	0,53	0,22	0,31	1,45	1,16	1,24	0,2670	0,4053	0,9340	0,7037	1,0000	1,0000
High	ENSBTAP0	PGK1 UniProtKB Gene Name|Bos taurus phosphoglycerate kinase 1 (PGK1), mRNA. [	PGK1		3	0,27	0,21	0,06	1,21	1,16	1,05	0,4289	0,3230	0,9671	0,8766	1,0000	1,0000
High	*ENSBTAP0*	*ROBO4 EntrezGene|Bos taurus roundabout homolog 4, magic roundabout (Drosophila*	*ROBO4*		*1*	*0,69*	*0,21*	*0,48*	*1,61*	*1,15*	*1,40*	*0,0963*	*0,2417*	*0,7582*	*0,6124*	*1,0000*	*1,0000*
Medium	*ENSBTAP0*	*MON2 HGNC Symbol|MON2 homolog (S. cerevisiae) [Source:HGNC Symbol;Acc:2917*	*MON2*		*1*	*0,68*	*0,20*	*0,49*	*1,61*	*1,15*	*1,40*	*0,1258*	*0,9639*	*0,1750*	*0,6699*	*1,0000*	*0,8981*
Medium	*ENSBTAP0*	*GNB1 UniProtKB Gene Name|Bos taurus guanine nucleotide binding protein (G protei*	*GNB1*		*1*	*-0,08*	*0,20*	*-0,27*	*0,95*	*1,15*	*0,83*	*0,9468*	*0,8145*	*0,9506*	*1,0000*	*1,0000*	*1,0000*
High	ENSBTAP0	YWHAE UniProtKB Gene Name|Bos taurus tyrosine 3-monooxygenase/tryptophan 5	YWHAE		4	0,04	0,19	-0,15	1,03	1,14	0,90	0,9116	0,7106	0,9177	1,0000	1,0000	1,0000
High	ENSBTAP0	CD14 UniProtKB Gene Name|Bos taurus CD14 molecule (CD14), mRNA. [Source:RefS	CD14		5	0,44	0,19	0,25	1,36	1,14	1,19	0,0059	0,0506	0,2104	0,1510	0,9015	0,9709
High	ENSBTAP0	COL2A1 UniProtKB Gene Name|Bos taurus collagen, type II, alpha 1 (COL2A1), trans	COL2A1		3	0,59	0,19	0,40	1,51	1,14	1,32	0,0799	0,9725	0,1064	0,5768	1,0000	0,7978
High	ENSBTAP0	CILP2 HGNC Symbol|cartilage intermediate layer protein 2 [Source:HGNC Symbol;Ac	CILP2		5	0,73	0,19	0,54	1,65	1,14	1,45	0,0717	0,8984	0,1261	0,5590	1,0000	0,8275
High	ENSBTAP0	SERPINA7 UniProtKB Gene Name|Bos taurus serpin peptidase inhibitor, clade A (alp	SERPINA7		14	0,34	0,19	0,15	1,27	1,14	1,11	0,0396	0,1823	0,4879	0,3927	1,0000	1,0000
High	ENSBTAP0	TUBA1B EntrezGene|Bos taurus tubulin, alpha 1b (TUBA1B), mRNA. [Source:RefSeq	TUBA1B		3	0,27	0,19	0,09	1,21	1,14	1,06	0,8719	0,8994	0,9979	1,0000	1,0000	1,0000
High	ENSBTAP0	PKM2 UniProtKB Gene Name|Bos taurus pyruvate kinase, muscle (PKM), mRNA. [So	PKM2		6	0,48	0,19	0,29	1,39	1,14	1,22	0,0409	0,6062	0,1429	0,3927	1,0000	0,8275
High	ENSBTAP0	YWHAZ UniProtKB Gene Name|Bos taurus tyrosine 3-monooxygenase/tryptophan 5	YWHAZ		4	0,49	0,18	0,31	1,40	1,14	1,24	0,4596	0,9998	0,4694	0,9031	1,0000	1,0000
High	ENSBTAP0	Bos taurus protein HP-25 homolog 1 (LOC511240), mRNA. [Source:RefSeq mRNA;Ac	Bos		2	0,12	0,18	-0,06	1,08	1,13	0,96	0,9866	0,9774	0,9988	1,0000	1,0000	1,0000
Medium	*ENSBTAP0*	*DSG1 EntrezGene|Bos taurus desmoglein 1 (DSG1), mRNA. [Source:RefSeq mRNA;Acc*	*DSG1*		*1*	*-1,70*	*0,18*	*-1,87*	*0,31*	*1,13*	*0,27*	*0,6918*	*0,8244*	*0,3784*	*1,0000*	*1,0000*	*1,0000*
High	ENSBTAP0	LUM UniProtKB Gene Name|Bos taurus lumican (LUM), mRNA. [Source:RefSeq mRN	LUM		12	0,46	0,17	0,29	1,37	1,13	1,22	0,4715	0,9963	0,5136	0,9031	1,0000	1,0000
High	ENSBTAP0	TPI1 UniProtKB Gene Name|Bos taurus triosephosphate isomerase 1 (TPI1), mRNA.	TPI1		4	0,08	0,17	-0,09	1,06	1,13	0,94	0,9971	0,8634	0,8960	1,0000	1,0000	1,0000
High	ENSBTAP0	HSPA1A UniProtKB Gene Name|Bos taurus heat shock 70kDa protein 1A (HSPA1A), r	HSPA1A		2	0,45	0,17	0,28	1,36	1,12	1,21	0,3695	0,4362	0,9881	0,8204	1,0000	1,0000
High	MGC1372	EntrezGene|Bos taurus protein HP-25 homolog 2 (MGC137211), mRNA. [Source:Ref	EntrezGene|Bos		3	0,42	0,17	0,25	1,34	1,12	1,19	0,1928	0,5885	0,6181	0,7037	1,0000	1,0000
High	ENSBTAP0	APOD HGNC Symbol|apolipoprotein D [Source:HGNC Symbol;Acc:612]|1|ENSBTAG0	APOD		4	-0,03	0,17	-0,20	0,98	1,12	0,87	0,9673	0,9531	0,8538	1,0000	1,0000	1,0000
High	ENSBTAP0	CLU UniProtKB Gene Name|Bos taurus clusterin (CLU), mRNA. [Source:RefSeq mRNA	CLU		13	0,43	0,16	0,27	1,35	1,12	1,20	0,0053	0,3102	0,0298	0,1469	1,0000	0,5134
High	ENSBTAP0	GSN HGNC Symbol|gelsolin [Source:HGNC Symbol;Acc:4620]|8|ENSBTAG000000199	GSN		24	0,56	0,15	0,41	1,48	1,11	1,33	0,0091	0,1537	0,1178	0,1774	1,0000	0,8275
High	ENSBTAP0	CD5L HGNC Symbol|CD5 molecule-like [Source:HGNC Symbol;Acc:1690]|3|ENSBTAG	CD5L		8	-0,22	0,15	-0,38	0,86	1,11	0,77	0,9134	0,8572	0,9911	1,0000	1,0000	1,0000
High	ENSBTAP0	FBLN1 EntrezGene|Bos taurus fibulin 1 (FBLN1), mRNA. [Source:RefSeq mRNA;Acc:N	FBLN1		24	1,61	0,15	1,46	3,05	1,11	2,75	0,0005	0,9999	0,0005	0,0362	1,0000	0,0678
High	ENSBTAP0	C3 UniProtKB Gene Name|Bos taurus complement component 3 (C3), mRNA. [Sourc	C3		99	0,67	0,14	0,53	1,59	1,10	1,45	0,0150	0,5290	0,0570	0,2581	1,0000	0,7006
Medium	*ENSBTAP0*	*NDC80 HGNC Symbol|NDC80 kinetochore complex component [Source:HGNC Symbol;*	*NDC80*		*1*	*0,37*	*0,13*	*0,25*	*1,30*	*1,09*	*1,19*	*0,0778*	*0,2480*	*0,6518*	*0,5768*	*1,0000*	*1,0000*
High	ENSBTAP0	CPB2 UniProtKB Gene Name|Bos taurus carboxypeptidase B2 (plasma) (CPB2), mRN	CPB2		8	0,29	0,12	0,16	1,22	1,09	1,12	0,4697	0,9982	0,4419	0,9031	1,0000	1,0000
High	ENSBTAP0	FGG UniProtKB Gene Name|Bos taurus fibrinogen gamma chain (FGG), mRNA. [Sour	FGG		15	0,01	0,12	-0,10	1,01	1,09	0,93	0,7338	0,7642	0,9983	1,0000	1,0000	1,0000
Medium	*ENSBTAP0*	*PEX19 UniProtKB Gene Name|Bos taurus peroxisomal biogenesis factor 19 (PEX19), m*	*PEX19*		*1*	*0,26*	*0,12*	*0,15*	*1,20*	*1,08*	*1,11*	*0,6383*	*0,9390*	*0,4561*	*1,0000*	*1,0000*	*1,0000*
Medium	*ENSBTAP0*	*TTC15 EntrezGene|Bos taurus tetratricopeptide repeat domain 15 (TTC15), mRNA. [S*	*TTC15*		*1*	*0,29*	*0,11*	*0,18*	*1,22*	*1,08*	*1,13*	*0,6236*	*0,9314*	*0,4331*	*1,0000*	*1,0000*	*1,0000*
High	ENSBTAP0	21 ENSBTAG00000048094|ENSBTAT00000038516		21	7	0,36	0,11	0,25	1,28	1,08	1,19	0,0395	0,6074	0,1371	0,3927	1,0000	0,8275
High	ENSBTAP0	ANXA5 EntrezGene|Bos taurus annexin A5 (ANXA5), mRNA. [Source:RefSeq mRNA;A	ANXA5		3	0,37	0,11	0,26	1,29	1,08	1,20	0,3886	0,8147	0,7156	0,8333	1,0000	1,0000
High	ENSBTAP0	DSP HGNC Symbol|desmoplakin [Source:HGNC Symbol;Acc:3052]|23|ENSBTAG0000	DSP		10	-0,18	0,11	-0,29	0,88	1,08	0,82	0,7982	0,9696	0,9110	1,0000	1,0000	1,0000

High	ENSBTAP0	APOM UniProtKB Gene Name|Bos taurus apolipoprotein M (APOM), mRNA. [Source	APOM	6	0,50	0,10	0,40	1,42	1,07	1,32	0,0380	0,7731	0,0904	0,3927	1,0000	0,7248
High	ENSBTAP0	NEO1 HGNC Symbol|neogenin 1 [Source:HGNC Symbol;Acc:7754]|10|ENSBTAG0000	NEO1	5	0,20	0,10	0,10	1,15	1,07	1,07	0,8986	0,9991	0,8811	1,0000	1,0000	1,0000
High	*ENSBTAP0*	*TRAP1 UniProtKB Gene Name|Bos taurus TNF receptor-associated protein 1 (TRAP1),*	*TRAP1*	*1*	*0,25*	*0,10*	*0,15*	*1,19*	*1,07*	*1,11*	*0,2973*	*0,8251*	*0,5755*	*0,7401*	*1,0000*	*1,0000*
High	ENSBTAP0	TLN1 HGNC Symbol|talin 1 [Source:HGNC Symbol;Acc:11845]|8|ENSBTAG0000025	TLN1	26	0,17	0,09	0,07	1,12	1,07	1,05	0,9112	0,9085	0,6971	1,0000	1,0000	1,0000
High	ENSBTAP0	Bos taurus uncharacterized LOC790886 (LOC790886), mRNA. [Source:RefSeq mRNA;	Bos	3	0,73	0,09	0,63	1,65	1,07	1,55	0,1053	0,9950	0,0933	0,6285	1,0000	0,7375
High	ENSBTAP0	APOH UniProtKB Gene Name|Bos taurus apolipoprotein H (beta-2-glycoprotein I) (A	APOH	14	0,32	0,09	0,23	1,25	1,07	1,17	0,4250	0,9864	0,5033	0,8728	1,0000	1,0000
High	*ENSBTAP0*	*PRDX6 UniProtKB Gene Name|Bos taurus peroxiredoxin 6 (PRDX6), mRNA. [Source:Re*	*PRDX6*	*1*	*0,06*	*0,09*	*-0,03*	*1,04*	*1,07*	*0,98*	*0,3282*	*0,4832*	*0,9374*	*0,7679*	*1,0000*	*1,0000*
High	ENSBTAP0	MYH9 EntrezGene|Bos taurus myosin, heavy chain 9, non-muscle (MYH9), mRNA. [S	MYH9	15	0,25	0,09	0,16	1,19	1,06	1,12	0,2819	0,9630	0,3842	0,7197	1,0000	1,0000
High	ENSBTAP0	COL6A1 EntrezGene|Bos taurus collagen, type VI, alpha 1 (COL6A1), mRNA. [Source:	COL6A1	19	0,97	0,09	0,88	1,96	1,06	1,85	0,0056	0,5361	0,0183	0,1500	1,0000	0,4358
High	ENSBTAP0	THBS4 UniProtKB Gene Name|Bos taurus thrombospondin 4 (THBS4), mRNA. [Sourc	THBS4	18	0,87	0,08	0,79	1,83	1,06	1,73	0,1048	0,9085	0,1791	0,6285	1,0000	0,9034
High	ENSBTAP0	APOA4 HGNC Symbol|apolipoprotein A-IV [Source:HGNC Symbol;Acc:602]|15|ENSB	APOA4	15	0,37	0,08	0,29	1,29	1,06	1,22	0,1870	0,9593	0,2638	0,7037	1,0000	1,0000
High	ENSBTAP0	LTBP1 EntrezGene|Bos taurus latent transforming growth factor beta binding protei	LTBP1	7	1,57	0,08	1,50	2,98	1,05	2,83	0,0007	0,9859	0,0008	0,0362	1,0000	0,0678
High	ENSBTAP0	LRG1 UniProtKB Gene Name|Bos taurus leucine-rich alpha-2-glycoprotein 1 (LRG1),	LRG1	13	0,39	0,08	0,31	1,31	1,05	1,24	0,0242	0,5062	0,1026	0,3293	1,0000	0,7898
High	ENSBTAP0	VCAM1 UniProtKB Gene Name|Bos taurus vascular cell adhesion molecule 1 (VCAM	VCAM1	2	0,28	0,08	0,20	1,21	1,05	1,15	0,7892	0,8267	0,4620	1,0000	1,0000	1,0000
High	ENSBTAP0	AFP UniProtKB Gene Name|Bos taurus alpha-fetoprotein (AFP), mRNA. [Source:RefS	AFP	34	0,47	0,07	0,39	1,38	1,05	1,31	0,0083	0,7352	0,0189	0,1743	1,0000	0,4358
Medium	*ENSBTAP0*	*BCR HGNC Symbol|breakpoint cluster region [Source:HGNC Symbol;Acc:1014]|17|EN*	*BCR*	*1*	*0,46*	*0,07*	*0,39*	*1,38*	*1,05*	*1,31*	*0,5749*	*0,9980*	*0,6083*	*0,9582*	*1,0000*	*1,0000*
High	ENSBTAP0	C9 UniProtKB Gene Name|Bos taurus complement component 9 (C9), mRNA. [Sourc	C9	19	0,32	0,07	0,25	1,25	1,05	1,19	0,2288	0,7917	0,4954	0,7037	1,0000	1,0000
High	ENSBTAP0	CTSC EntrezGene|Bos taurus cathepsin C (CTSC), mRNA. [Source:RefSeq mRNA;Acc:	CTSC	3	0,70	0,07	0,63	1,63	1,05	1,55	0,2055	0,8998	0,1172	0,7037	1,0000	0,8275
High	ENSBTAP0	MRC2 EntrezGene|Bos taurus mannose receptor, C type 2 (MRC2), mRNA. [Source:F	MRC2	6	-0,14	0,07	-0,21	0,91	1,05	0,86	0,9918	0,9243	0,9642	1,0000	1,0000	1,0000
High	ENSBTAP0	POSTN UniProtKB Gene Name|Bos taurus periostin, osteoblast specific factor (POST	POSTN	4	2,05	0,07	1,98	4,15	1,05	3,96	0,0022	0,9602	0,0027	0,0841	1,0000	0,1454
High	ENSBTAP0	CL43 EntrezGene|collectin-43 precursor [Source:RefSeq peptide;Acc:NP_001002237	CL43	5	0,62	0,07	0,55	1,53	1,05	1,46	0,0652	0,9852	0,0532	0,5228	1,0000	0,7006
High	ENSBTAP0	IGF2R EntrezGene|cation-independent mannose-6-phosphate receptor precursor [	IGF2R	37	0,21	0,07	0,14	1,15	1,05	1,10	0,9587	0,8586	0,9650	1,0000	1,0000	1,0000
High	ENSBTAP0	GGH UniProtKB Gene Name|Bos taurus gamma-glutamyl hydrolase (conjugase, foly	GGH	4	0,17	0,07	0,11	1,13	1,05	1,08	0,7935	0,9594	0,6396	1,0000	1,0000	1,0000
High	ENSBTAP0	FETUB UniProtKB Gene Name|Bos taurus fetuin B (FETUB), mRNA. [Source:RefSeq m	FETUB	13	0,30	0,06	0,24	1,23	1,05	1,18	0,3426	0,9793	0,2712	0,7847	1,0000	1,0000
High	*ENSBTAP0*	*IGLL1 EntrezGene|Bos taurus immunoglobulin lambda-like polypeptide 1 (IGLL1), mRN*	*IGLL1*	*1*	*0,23*	*0,06*	*0,17*	*1,17*	*1,05*	*1,12*	*0,9448*	*0,8496*	*0,6748*	*1,0000*	*1,0000*	*1,0000*
High	ENSBTAP0	SERPINA1 UniProtKB Gene Name|Bos taurus serpin peptidase inhibitor, clade A (alp	SERPINA1	24	0,13	0,06	0,07	1,09	1,04	1,05	0,2619	0,5290	0,8155	0,7037	1,0000	1,0000
High	ENSBTAP0	CFP UniProtKB Gene Name|Bos taurus complement factor properdin (CFP), mRNA. [	CFP	8	-0,02	0,06	-0,08	0,99	1,04	0,95	0,9512	0,8986	0,9890	1,0000	1,0000	1,0000
High	ENSBTAP0	COL6A3 HGNC Symbol|collagen, type VI, alpha 3 [Source:HGNC Symbol;Acc:2213]|3	COL6A3	38	0,68	0,05	0,62	1,60	1,04	1,54	0,0078	0,4137	0,0355	0,1743	1,0000	0,5677
High	ENSBTAP0	SHBG UniProtKB Gene Name|Bos taurus sex hormone-binding globulin (SHBG), mRN	SHBG	9	0,38	0,05	0,33	1,31	1,04	1,26	0,2224	0,6729	0,5980	0,7037	1,0000	1,0000
High	*ENSBTAP0*	*COLEC11 UniProtKB Gene Name|Bos taurus collectin sub-family member 11 (COLEC11*	*COLEC11*	*1*	*0,36*	*0,05*	*0,31*	*1,28*	*1,03*	*1,24*	*0,5234*	*0,8940*	*0,7771*	*0,9113*	*1,0000*	*1,0000*
High	ENSBTAP0	CAP1 UniProtKB Gene Name|Bos taurus CAP, adenylate cyclase-associated protein 1	CAP1	3	0,02	0,04	-0,02	1,02	1,03	0,99	0,9142	0,9746	0,9803	1,0000	1,0000	1,0000
High	ENSBTAP0	C8B EntrezGene|Bos taurus complement component 8, beta polypeptide (C8B), mR	C8B	8	0,71	0,04	0,67	1,64	1,03	1,59	0,1130	0,7611	0,2801	0,6543	1,0000	1,0000
Medium	*ENSBTAP0*	*RBM12B HGNC Symbol|RNA binding motif protein 12B [Source:HGNC Symbol;Acc:323*	*RBM12B*	*1*	*0,18*	*0,04*	*0,14*	*1,13*	*1,03*	*1,10*	*0,7971*	*0,9346*	*0,6000*	*1,0000*	*1,0000*	*1,0000*
High	ENSBTAP0	B2M UniProtKB Gene Name|Beta-2-microglobulin [Source:UniProtKB/Swiss-Prot;Ac	B2M	2	0,87	0,04	0,83	1,83	1,03	1,78	0,9947	0,9321	0,8929	1,0000	1,0000	1,0000
High	ENSBTAP0	COTL1 UniProtKB Gene Name|Bos taurus coactosin-like 1 (Dictyostelium) (COTL1), m	COTL1	6	-0,32	0,04	-0,36	0,80	1,03	0,78	0,9434	0,9228	0,7662	1,0000	1,0000	1,0000
High	*ENSBTAP0*	*COL9A1 HGNC Symbol|collagen, type IX, alpha 1 [Source:HGNC Symbol;Acc:2217]|9|E*	*COL9A1*	*1*	*0,65*	*0,04*	*0,61*	*1,57*	*1,03*	*1,53*	*0,0739*	*0,8830*	*0,1360*	*0,5613*	*1,0000*	*0,8275*
High	ENSBTAP0	RAP1B UniProtKB Gene Name|Bos taurus RAP1B, member of RAS oncogene family (	RAP1B	4	0,11	0,04	0,07	1,08	1,03	1,05	0,9113	0,9998	0,9194	1,0000	1,0000	1,0000
High	ENSBTAP0	GC HGNC Symbol|group-specific component (vitamin D binding protein) [Source:HG	GC	29	0,19	0,03	0,16	1,14	1,02	1,12	0,7620	0,9427	0,5769	1,0000	1,0000	1,0000
High	ENSBTAP0	Uncharacterized protein [Source:UniProtKB/TrEMBL;Acc:F1MH40]|11|ENSBTAG000	Uncharacterized	8	0,24	0,03	0,21	1,18	1,02	1,16	0,8487	0,9631	0,7080	1,0000	1,0000	1,0000
High	ENSBTAP0	LRP1 HGNC Symbol|low density lipoprotein receptor-related protein 1 [Source:HGN	LRP1	7	0,23	0,03	0,20	1,17	1,02	1,15	0,4542	0,8251	0,7823	0,9031	1,0000	1,0000
High	*ENSBTAP0*	*MAP2K5 EntrezGene|Bos taurus mitogen-activated protein kinase kinase 5 (MAP2K5)*	*MAP2K5*	*1*	*0,04*	*0,03*	*0,01*	*1,03*	*1,02*	*1,01*	*0,5210*	*0,8416*	*0,8337*	*0,9098*	*1,0000*	*1,0000*
Medium	*ENSBTAP0*	*FAM83G HGNC Symbol|family with sequence similarity 83, member G [Source:HGNC*	*FAM83G*	*1*	*-0,29*	*0,03*	*-0,32*	*0,82*	*1,02*	*0,80*	*0,9050*	*0,9966*	*0,9353*	*1,0000*	*1,0000*	*1,0000*
High	ENSBTAP0	KNG1 UniProtKB Gene Name|Bos taurus kininogen 1 (KNG1), transcript variant I, mR	KNG1	23	0,10	0,03	0,07	1,07	1,02	1,05	0,8601	0,9802	0,7611	1,0000	1,0000	1,0000
High	ENSBTAP0	ECM1 UniProtKB Gene Name|Bos taurus extracellular matrix protein 1 (ECM1), mRN	ECM1	10	-0,19	0,03	-0,22	0,87	1,02	0,86	0,9976	0,9472	0,9664	1,0000	1,0000	1,0000
High	ENSBTAP0	ACTG1 UniProtKB Gene Name|Bos taurus actin, gamma 1 (ACTG1), mRNA. [Source:F	ACTG1	2	1,14	0,02	1,12	2,21	1,02	2,17	0,1566	0,7929	0,0675	0,7037	1,0000	0,7006
High	*ENSBTAP0*	*CD97 UniProtKB Gene Name|Bos taurus CD97 molecule (CD97), mRNA. [Source:RefSe*	*CD97*	*1*	*0,57*	*0,02*	*0,54*	*1,48*	*1,02*	*1,46*	*0,1993*	*0,9624*	*0,1424*	*0,7037*	*1,0000*	*0,8275*
High	ENSBTAP0	TUBB1 EntrezGene|Bos taurus tubulin, beta 1 class VI (TUBB1), mRNA. [Source:RefS	TUBB1	4	0,70	0,02	0,68	1,63	1,01	1,61	0,2840	0,8242	0,5557	0,7197	1,0000	1,0000
High	ENSBTAP0	VTN UniProtKB Gene Name|Bos taurus vitronectin (VTN), mRNA. [Source:RefSeq mR	VTN	11	0,41	0,02	0,39	1,33	1,01	1,31	0,1389	0,8440	0,0680	0,6918	1,0000	0,7006
High	ENSBTAP0	Uncharacterized protein [Source:UniProtKB/TrEMBL;Acc:F1MLW8]|17|ENSBTAG000	Uncharacterized	5	0,13	0,02	0,11	1,09	1,01	1,08	0,9775	0,8469	0,9343	1,0000	1,0000	1,0000
High	ENSBTAP0	FLNA HGNC Symbol|filamin A, alpha [Source:HGNC Symbol;Acc:3754]|X|ENSBTAG00	FLNA	17	1,17	0,02	1,15	2,25	1,01	2,22	0,3931	0,9810	0,3163	0,8333	1,0000	1,0000
High	ENSBTAP0	TUBA4A UniProtKB Gene Name|Bos taurus tubulin, alpha 4a (TUBA4A), mRNA. [Sou	TUBA4A	4	0,17	0,02	0,15	1,13	1,01	1,11	0,7792	0,8746	0,9807	1,0000	1,0000	1,0000
High	*ENSBTAP0*	*C6 HGNC Symbol|complement component 6 [Source:HGNC Symbol;Acc:1339]|20|ENS*	*C6*	*1*	*-0,13*	*0,01*	*-0,14*	*0,92*	*1,01*	*0,91*	*0,7243*	*0,6753*	*0,9959*	*1,0000*	*1,0000*	*1,0000*
High	ENSBTAP0	IL1RAP UniProtKB Gene Name|Bos taurus interleukin 1 receptor accessory protein (I	IL1RAP	6	0,18	0,01	0,17	1,13	1,01	1,12	0,2746	0,8765	0,1477	0,7109	1,0000	0,8307
High	ENSBTAP0	ICOSLG HGNC Symbol|inducible T-cell co-stimulator ligand [Source:HGNC Symbol;Ac	ICOSLG	2	0,14	0,01	0,13	1,10	1,01	1,09	0,9750	0,8612	0,9481	1,0000	1,0000	1,0000
High	ENSBTAP0	HRG EntrezGene|Bos taurus histidine-rich glycoprotein (HRG), mRNA. [Source:RefSe	HRG	5	0,34	0,01	0,33	1,26	1,01	1,25	0,7735	0,6178	0,2896	1,0000	1,0000	1,0000
High	ENSBTAP0	VCAM1 UniProtKB Gene Name|Bos taurus vascular cell adhesion molecule 1 (VCAM	VCAM1	2	1,79	0,01	1,78	3,45	1,01	3,43	0,9019	0,9387	0,7296	1,0000	1,0000	1,0000
High	ENSBTAP0	SERPINA11 UniProtKB Gene Name|Bos taurus serpin peptidase inhibitor, clade A (al	SERPINA11	4	-0,02	0,01	-0,03	0,99	1,01	0,98	0,7066	0,7498	0,9967	1,0000	1,0000	1,0000
High	ENSBTAP0	CFD UniProtKB Gene Name|Bos taurus complement factor D (adipsin) (CFD), mRNA.	CFD	5	0,29	0,01	0,29	1,22	1,01	1,22	0,4715	0,6583	0,9375	0,9031	1,0000	1,0000
High	ENSBTAP0	THBS1 EntrezGene|Bos taurus thrombospondin 1 (THBS1), mRNA. [Source:RefSeq n	THBS1	32	0,12	0,01	0,12	1,09	1,01	1,08	0,4852	0,9931	0,4300	0,9031	1,0000	1,0000
High	ENSBTAP0	CHIA HGNC Symbol|chitinase, acidic [Source:HGNC Symbol;Acc:17432]|3|ENSBTAG	CHIA	9	0,31	0,00	0,31	1,24	1,00	1,24	0,0215	0,9587	0,0297	0,3121	1,0000	0,5134
High	ENSBTAP0	Bos taurus endopin 2 (SERPINA3-7), mRNA. [Source:RefSeq mRNA;Acc:NM_0010122	Bos	6	0,31	0,00	0,31	1,24	1,00	1,24	0,2365	0,9917	0,2027	0,7037	1,0000	0,9709
High	ENSBTAP0	PTI EntrezGene|Bos taurus spleen trypsin inhibitor (LOC404103), mRNA. [Source:Re	PTI	2	0,31	0,00	0,30	1,24	1,00	1,24	0,6446	0,9958	0,6944	1,0000	1,0000	1,0000
High	ENSBTAP0	CLEC3B UniProtKB Gene Name|Bos taurus C-type lectin domain family 3, member B	CLEC3B	7	0,31	0,00	0,30	1,24	1,00	1,23	0,7057	0,9259	0,8991	1,0000	1,0000	1,0000
High	ENSBTAP0	SERPINF1 UniProtKB Gene Name|Bos taurus serpin peptidase inhibitor, clade F (alph	SERPINF1	17	0,13	0,00	0,13	1,10	1,00	1,10	0,3751	0,9511	0,5212	0,8248	1,0000	1,0000
Medium	*ENSBTAP0*	*NFKB1 EntrezGene|Bos taurus nuclear factor of kappa light polypeptide gene enhance*	*NFKB1*	*1*	*0,53*	*0,00*	*0,53*	*1,44*	*1,00*	*1,44*	*0,1439*	*0,7859*	*0,0611*	*0,6918*	*1,0000*	*0,7006*
High	ENSBTAP0	Uncharacterized protein [Source:UniProtKB/TrEMBL;Acc:G3N0V0]|20|ENSBTAG000	Uncharacterized	6	0,13	0,00	0,13	1,10	1,00	1,10	0,5695	0,9970	0,6108	0,9582	1,0000	1,0000
High	ENSBTAP0	CFB UniProtKB Gene Name|Bos taurus complement factor B (CFB), mRNA. [Source:F	CFB	30	0,54	0,00	0,54	1,46	1,00	1,46	0,0309	0,8934	0,0537	0,3630	1,0000	0,7006
High	ENSBTAP0	SERPINA10 UniProtKB Gene Name|Bos taurus serpin peptidase inhibitor, clade A (al	SERPINA10	11	0,37	0,00	0,38	1,30	1,00	1,30	0,2372	0,9574	0,3340	0,7037	1,0000	1,0000
High	ENSBTAP0	Uncharacterized protein [Source:UniProtKB/TrEMBL;Acc:E1B805]|7|ENSBTAG0000	Uncharacterized	20	0,19	0,00	0,19	1,14	1,00	1,14	0,5681	0,9918	0,5028	0,9582	1,0000	1,0000
High	*ENSBTAP0*	*FERMT3 UniProtKB Gene Name|Bos taurus fermitin family member 3 (FERMT3), mRN*	*FERMT3*	*1*	*0,38*	*0,00*	*0,38*	*1,30*	*1,00*	*1,30*	*0,0548*	*0,9366*	*0,0359*	*0,4677*	*1,0000*	*0,5677*
High	ENSBTAP0	F13A1 UniProtKB Gene Name|Bos taurus coagulation factor XIII, A1 polypeptide (F1	F13A1	12	0,17	0,00	0,17	1,12	1,00	1,13	0,9918	0,4829	0,4230	1,0000	1,0000	1,0000
High	ENSBTAP0	SERPINA5 UniProtKB Gene Name|Bos taurus serpin peptidase inhibitor, clade A (alp	SERPINA5	9	0,52	-0,01	0,52	1,43	1,00	1,44	0,2604	0,6491	0,6939	0,7037	1,0000	1,0000
High	ENSBTAP0	KLKB1 UniProtKB Gene Name|Bos taurus kallikrein B, plasma (Fletcher factor) 1 (KLK	KLKB1	14	0,56	-0,01	0,57	1,47	0,99	1,48	0,4755	0,8250	0,8054	0,9031	1,0000	1,0000
High	ENSBTAP0	PLXDC2 UniProtKB Gene Name|Bos taurus plexin domain containing 2 (PLXDC2), mR	PLXDC2	2	0,28	-0,01	0,29	1,21	0,99	1,22	0,5333	0,4856	0,1241	0,9230	1,0000	0,8275
High	ENSBTAP0	APOA1 UniProtKB Gene Name|Bos taurus apolipoprotein A-I (APOA1), mRNA. [Sour	APOA1	20	0,20	-0,01	0,21	1,15	0,99	1,16	0,8943	0,7420	0,4906	1,0000	1,0000	1,0000
High	ENSBTAP0	CSF1R UniProtKB Gene Name|Bos taurus colony stimulating factor 1 receptor (CSF1F	CSF1R	4	0,24	-0,01	0,26	1,18	0,99	1,19	0,3659	0,5810	0,1001	0,8202	1,0000	0,7808
Medium	*ENSBTAP0*	*AZGP1 UniProtKB Gene Name|Bos taurus alpha-2-glycoprotein 1, zinc-binding (AZGP1*	*AZGP1*	*1*	*0,02*	*-0,01*	*0,04*	*1,02*	*0,99*	*1,03*	*0,9404*	*0,7950*	*0,9449*	*1,0000*	*1,0000*	*1,0000*
High	ENSBTAP0	CRISP3 EntrezGene|Bos taurus cysteine-rich secretory protein 3 (CRISP3), mRNA. [Sc	CRISP3	2	0,19	-0,02	0,20	1,14	0,99	1,15	0,7701	0,8972	0,5205	1,0000	1,0000	1,0000
High	ENSBTAP0	PCDH12 HGNC Symbol|protocadherin 12 [Source:HGNC Symbol;Acc:8657]|7|ENSBT	PCDH12	7	0,07	-0,02	0,09	1,05	0,99	1,06	0,6021	0,9865	0,5164	0,9812	1,0000	1,0000
High	ENSBTAP0	HSPA8 UniProtKB Gene Name|Bos taurus heat shock 70kDa protein 8 (HSPA8), mRN	HSPA8	6	0,24	-0,02	0,26	1,18	0,99	1,20	0,5579	0,9611	0,7092	0,9515	1,0000	1,0000
High	ENSBTAP0	IGLL1 EntrezGene|Bos taurus immunoglobulin lambda-like polypeptide 1 (IGLL1), m	IGLL1	5	0,12	-0,03	0,15	1,09	0,98	1,11	0,6251	0,9998	0,6154	1,0000	1,0000	1,0000
High	ENSBTAP0	Cationic trypsin Alpha-trypsin chain 1 Alpha-trypsin chain 2 [Source:UniProtKB/Swis	Cationic	2	0,03	-0,03	0,06	1,02	0,98	1,04	0,3257	0,8545	0,5850	0,7679	1,0000	1,0000
Medium	*ENSBTAP0*	*Uncharacterized protein [Source:UniProtKB/TrEMBL;Acc:G5E5V1]|17|ENSBTAG0000*	*Uncharacterized*	*1*	*-0,13*	*-0,03*	*-0,10*	*0,91*	*0,98*	*0,93*	*0,3602*	*0,5286*	*0,9348*	*0,8168*	*1,0000*	*1,0000*
High	ENSBTAP0	ALB UniProtKB Gene Name|Bos taurus albumin (ALB), mRNA. [Source:RefSeq mRNA	ALB	79	-0,03	-0,03	0,00	0,98	0,98	1,00	0,6195	0,6720	0,9953	1,0000	1,0000	1,0000
High	ENSBTAP0	APOE UniProtKB Gene Name|Bos taurus apolipoprotein E (APOE), mRNA. [Source:R	APOE	13	-0,04	-0,03	-0,01	0,97	0,98	0,99	0,9318	0,9025	0,9969	1,0000	1,0000	1,0000
High	*ENSBTAP0*	*SERPINB13 HGNC Symbol|serpin peptidase inhibitor, clade B (ovalbumin), member 13*	*SERPINB13*	*1*	*0,81*	*-0,03*	*0,85*	*1,76*	*0,98*	*1,80*	*0,9983*	*0,6937*	*0,7249*	*1,0000*	*1,0000*	*1,0000*
High	ENSBTAP0	A1BG UniProtKB Gene Name|Bos taurus alpha-1-B glycoprotein (A1BG), mRNA. [Sou	A1BG	17	0,08	-0,03	0,11	1,06	0,98	1,08	0,8455	0,6014	0,8988	1,0000	1,0000	1,0000
High	*ENSBTAP0*	*Uncharacterized protein [Source:UniProtKB/TrEMBL;Acc:G3N1H5]|21|ENSBTAG0000*	*Uncharacterized*	*1*	*0,45*	*-0,03*	*0,48*	*1,36*	*0,98*	*1,39*	*0,3196*	*0,8848*	*0,5406*	*0,7630*	*1,0000*	*1,0000*
High	ENSBTAP0	MBL UniProtKB Gene Name|Bos taurus mannose-binding lectin (protein C) 2, solubl	MBL	2	0,32	-0,04	0,36	1,25	0,98	1,28	0,2444	0,9685	0,3277	0,7037	1,0000	1,0000
High	ENSBTAP0	CTSZ HGNC Symbol|cathepsin Z [Source:HGNC Symbol;Acc:2547]|13|ENSBTAG0000	CTSZ	2	0,38	-0,04	0,42	1,30	0,97	1,33	0,4999	0,9500	0,6686	0,9031	1,0000	1,0000
High	ENSBTAP0	ANGPTL3 UniProtKB Gene Name|Bos taurus angiopoietin-like 3 (ANGPTL3), mRNA. [	ANGPTL3	6	0,30	-0,04	0,34	1,23	0,97	1,27	0,1608	0,7360	0,0609	0,7037	1,0000	0,7006
High	*ENSBTAP0*	*CL46 EntrezGene|Bos taurus collectin -46 (CL46), mRNA. [Source:RefSeq mRNA;Acc:N*	*CL46*	*1*	*0,06*	*-0,04*	*0,10*	*1,04*	*0,97*	*1,08*	*0,8367*	*0,9660*	*0,7005*	*1,0000*	*1,0000*	*1,0000*
High	ENSBTAP0	CPN1 HGNC Symbol|carboxypeptidase N, polypeptide 1 [Source:HGNC Symbol;Acc:2	CPN1	7	0,90	-0,04	0,94	1,86	0,97	1,92	0,1815	0,9157	0,2991	0,7037	1,0000	1,0000
High	ENSBTAP0	F5 HGNC Symbol|coagulation factor V (proaccelerin, labile factor) [Source:HGNC Syr	F5	27	0,28	-0,04	0,32	1,21	0,97	1,25	0,1157	0,8344	0,2418	0,6636	1,0000	1,0000
High	ENSBTAP0	A2M UniProtKB Gene Name|Bos taurus alpha-2-macroglobulin (A2M), mRNA. [Sour	A2M	74	-0,37	-0,04	-0,32	0,78	0,97	0,80	0,0523	0,9658	0,0716	0,4677	1,0000	0,7006
High	ENSBTAP0	PCDHGC3 UniProtKB Gene Name|Bos taurus protocadherin gamma subfamily B, 4 (I	PCDHGC3	3	0,05	-0,05	0,10	1,04	0,97	1,07	0,9054	0,9352	0,7285	1,0000	1,0000	1,0000
High	ENSBTAP0	SERPINC1 EntrezGene|Bos taurus serpin peptidase inhibitor, clade C (antithrombin)	SERPINC1	22	0,20	-0,05	0,25	1,15	0,97	1,19	0,6485	0,9476	0,4781	1,0000	1,0000	1,0000
High	ENSBTAP0	GPLD1 HGNC Symbol|glycosylphosphatidylinositol specific phospholipase D1 [Sourc	GPLD1	9	0,28	-0,05	0,33	1,21	0,96	1,26	0,3013	0,5149	0,0696	0,7418	1,0000	0,7006
High	ENSBTAP0	chymotrypsinogen B precursor [Source:RefSeq peptide;Acc:NP_001098924]|18|ENS	chymotrypsinogen	3	0,04	-0,06	0,09	1,03	0,96	1,07	0,7635	0,8555	0,4672	1,0000	1,0000	1,0000
High	ENSBTAP0	PLTP UniProtKB Gene Name|Bos taurus phospholipid transfer protein (PLTP), mRNA	PLTP	3	0,02	-0,06	0,07	1,01	0,96	1,05	0,8504	0,9899	0,7802	1,0000	1,0000	1,0000
High	ENSBTAP0	IGFALS EntrezGene|Bos taurus insulin-like growth factor binding protein, acid labile	IGFALS	10	0,15	-0,06	0,22	1,11	0,96	1,16	0,7047	0,8750	0,4361	1,0000	1,0000	1,0000
High	*ENSBTAP0*	*POSTN UniProtKB Gene Name|Bos taurus periostin, osteoblast specific factor (POSTN)*	*POSTN*	*1*	*1,75*	*-0,06*	*1,81*	*3,36*	*0,96*	*3,51*	*0,0002*	*0,9910*	*0,0002*	*0,0362*	*1,0000*	*0,0594*
Medium	*ENSBTAP0*	*SH3BGRL3 UniProtKB Gene Name|Bos taurus SH3 domain binding glutamic acid-rich p*	*SH3BGRL3*	*1*	*-0,28*	*-0,07*	*-0,21*	*0,82*	*0,95*	*0,86*	*0,9646*	*0,9973*	*0,9812*	*1,0000*	*1,0000*	*1,0000*
High	ENSBTAP0	SERPINA3-6 EntrezGene|Bos taurus endopin 1b (SERPINA3-3), mRNA. [Source:RefSe	SERPINA3-6	3	0,35	-0,07	0,42	1,27	0,95	1,34	0,9652	0,9988	0,9518	1,0000	1,0000	1,0000
High	ENSBTAP0	INTB3 UniProtKB Gene Name|Bos taurus integrin, beta 3 (platelet glycoprotein IIIa, a	INTB3	2	0,52	-0,08	0,60	1,43	0,95	1,51	0,3065	0,4366	0,0583	0,7418	1,0000	0,7006
Medium	*ENSBTAP0*	*AP3B1 UniProtKB Gene Name|Bos taurus adaptor-related protein complex 3, beta 1 su*	*AP3B1*	*1*	*0,11*	*-0,08*	*0,19*	*1,08*	*0,95*	*1,14*	*0,7929*	*0,9894*	*0,8635*	*1,0000*	*1,0000*	*1,0000*
High	ENSBTAP0	LCP1 HGNC Symbol|lymphocyte cytosolic protein 1 (L-plastin) [Source:HGNC Symbol	LCP1	3	-0,02	-0,08	0,06	0,99	0,95	1,04	0,5792	0,9966	0,5366	0,9625	1,0000	1,0000
High	ENSBTAP0	C5 EntrezGene|complement C5a anaphylatoxin precursor [Source:RefSeq peptide;/	C5	54	-0,09	-0,08	-0,01	0,94	0,95	0,99	0,7573	0,7968	0,9971	1,0000	1,0000	1,0000
High	ENSBTAP0	AGP UniProtKB Gene Name|Bos taurus orosomucoid 1 (ORM1), mRNA. [Source:RefS	AGP	11	0,12	-0,08	0,20	1,09	0,95	1,15	0,9929	0,9708	0,9368	1,0000	1,0000	1,0000
High	ENSBTAP0	HPX UniProtKB Gene Name|Bos taurus hemopexin (HPX), mRNA. [Source:RefSeq mF	HPX	18	0,20	-0,08	0,29	1,15	0,94	1,22	0,6514	0,7426	0,2908	1,0000	1,0000	1,0000
High	ENSBTAP0	CFI EntrezGene|Bos taurus complement factor I (CFI), mRNA. [Source:RefSeq mRNA	CFI	23	-0,06	-0,08	0,02	0,96	0,94	1,02	0,6792	0,8460	0,9497	1,0000	1,0000	1,0000
High	ENSBTAP0	OSMR HGNC Symbol|oncostatin M receptor [Source:HGNC Symbol;Acc:8507]|20|EN	OSMR	2	0,14	-0,09	0,23	1,10	0,94	1,17	0,5037	0,9038	0,7436	0,9031	1,0000	1,0000
High	ENSBTAP0	G3PDH UniProtKB Gene Name|Bos taurus glyceraldehyde-3-phosphate dehydrogen	G3PDH	4	-0,29	-0,09	-0,20	0,82	0,94	0,87	0,7333	0,9680	0,5955	1,0000	1,0000	1,0000
High	MGC1370	EntrezGene|Bos taurus protein HP-20 homolog (MGC137014), mRNA. [Source:RefSe	EntrezGene|Bos	3	0,27	-0,09	0,36	1,20	0,94	1,28	0,5498	0,7935	0,2609	0,9433	1,0000	1,0000
High	*ENSBTAP0*	*PPIA UniProtKB Gene Name|Bos taurus peptidylprolyl isomerase A (cyclophilin A) (PPI*	*PPIA*	*1*	*0,19*	*-0,09*	*0,28*	*1,14*	*0,94*	*1,21*	*0,9903*	*0,9993*	*0,9843*	*1,0000*	*1,0000*	*1,0000*
High	*ENSBTAP0*	*PPIA HGNC Symbol|peptidylprolyl isomerase A (cyclophilin A) [Source:HGNC Symbol;A*	*PPIA*	*1*	*0,19*	*-0,09*	*0,28*	*1,14*	*0,94*	*1,21*	*0,9903*	*0,9993*	*0,9843*	*1,0000*	*1,0000*	*1,0000*
High	ENSBTAP0	SERPINA6 UniProtKB Gene Name|Corticosteroid-binding globulin [Source:UniProtKE	SERPINA6	7	0,16	-0,09	0,25	1,11	0,94	1,19	0,4331	0,9960	0,4747	0,8766	1,0000	1,0000
High	ENSBTAP0	PLG UniProtKB Gene Name|Bos taurus plasminogen (PLG), mRNA. [Source:RefSeq m	PLG	40	-0,20	-0,10	-0,11	0,87	0,94	0,93	0,8165	0,9018	0,9823	1,0000	1,0000	1,0000
High	ENSBTAP0	LCAT UniProtKB Gene Name|Bos taurus lecithin-cholesterol acyltransferase (LCAT),	LCAT	3	-0,02	-0,10	0,08	0,98	0,93	1,05	0,9960	0,8512	0,8906	1,0000	1,0000	1,0000
High	ENSBTAP0	SERPINF2 UniProtKB Gene Name|Bos taurus serpin peptidase inhibitor, clade F (alpl	SERPINF2	13	0,05	-0,11	0,15	1,03	0,93	1,11	0,8788	0,6850	0,4237	1,0000	1,0000	1,0000
High	*ENSBTAP0*	*PPARD UniProtKB Gene Name|Bos taurus peroxisome proliferator-activated receptor*	*PPARD*	*1*	*-0,25*	*-0,11*	*-0,15*	*0,84*	*0,93*	*0,90*	*0,5638*	*0,9181*	*0,7859*	*0,9561*	*1,0000*	*1,0000*
High	ENSBTAP0	C7 EntrezGene|Bos taurus complement component 7 (C7), mRNA. [Source:RefSeq n	C7	25	0,80	-0,11	0,91	1,74	0,93	1,88	0,4087	0,7175	0,1543	0,8601	1,0000	0,8569
High	ENSBTAP0	CDH5 EntrezGene|Bos taurus cadherin 5, type 2 (vascular endothelium) (CDH5), mR	CDH5	9	0,29	-0,11	0,40	1,22	0,93	1,32	0,5254	0,8139	0,2587	0,9120	1,0000	1,0000
High	ENSBTAP0	ANXA2 UniProtKB Gene Name|Bos taurus annexin A2 (ANXA2), mRNA. [Source:RefS	ANXA2	7	0,48	-0,12	0,60	1,39	0,92	1,52	0,9829	0,8509	0,9277	1,0000	1,0000	1,0000
Medium	*ENSBTAP0*	*H3F3A UniProtKB Gene Name|Bos taurus H3 histone, family 3B (H3F3B), mRNA. [Sour*	*H3F3A*	*1*	*-0,38*	*-0,12*	*-0,26*	*0,77*	*0,92*	*0,84*	*0,7444*	*0,7865*	*0,9968*	*1,0000*	*1,0000*	*1,0000*

High	ENSBTAP0	LDHA UniProtKB Gene Name|Bos taurus lactate dehydrogenase A (LDHA), mRNA. [S	LDHA	4	-0,08	-0,14	0,06	0,95	0,91	1,04	0,9983	0,9995	0,9959	1,0000	1,0000	1,0000
High	ENSBTAP0	Bos taurus serotransferrin-like (LOC525947), mRNA. [Source:RefSeq mRNA;Acc:NM_	Bos	19	0,20	-0,14	0,34	1,15	0,91	1,27	0,8308	0,7616	0,4412	1,0000	1,0000	1,0000
High	ENSBTAP0	C8A EntrezGene|Bos taurus complement component 8, alpha polypeptide (C8A), m	C8A	6	0,07	-0,14	0,21	1,05	0,91	1,16	0,8507	0,7414	0,9768	1,0000	1,0000	1,0000
High	ENSBTAP0	Amine oxidase [Source:UniProtKB/TrEMBL;Acc:E1BJN3]|19|ENSBTAG00000039321|	Amine	4	-0,06	-0,14	0,08	0,96	0,91	1,06	0,2186	0,1621	0,9697	0,7037	1,0000	1,0000
High	ENSBTAP0	AFM EntrezGene|Bos taurus afamin (AFM), mRNA. [Source:RefSeq mRNA;Acc:NM_	AFM	29	0,23	-0,15	0,37	1,17	0,90	1,30	0,1363	0,8375	0,2809	0,6918	1,0000	1,0000
High	*ENSBTAP0*	*Bos taurus amine oxidase, copper containing 3 (vascular adhesion protein 1) (AOC3), r*	*Bos*	*1*	*-0,20*	*-0,15*	*-0,05*	*0,87*	*0,90*	*0,97*	*0,9841*	*0,9990*	*0,9753*	*1,0000*	*1,0000*	*1,0000*
High	ENSBTAP0	PEBP1 UniProtKB Gene Name|Bos taurus phosphatidylethanolamine binding protei	PEBP1	3	0,39	-0,15	0,54	1,31	0,90	1,46	0,1719	0,9758	0,2243	0,7037	1,0000	0,9901
High	ENSBTAP0	C1QTNF3 UniProtKB Gene Name|Bos taurus C1q and tumor necrosis factor related	C1QTNF3	4	0,25	-0,15	0,40	1,19	0,90	1,32	0,3361	0,7043	0,1205	0,7805	1,0000	0,8275
High	ENSBTAP0	Uncharacterized protein [Source:UniProtKB/TrEMBL;Acc:G3N0S9]|16|ENSBTAG000	Uncharacterized	8	0,10	-0,16	0,25	1,07	0,90	1,19	0,8581	0,9388	0,6746	1,0000	1,0000	1,0000
High	*ENSBTAP0*	*Histone H2A [Source:UniProtKB/TrEMBL;Acc:E1BIL5]|23|ENSBTAG00000031768|EN*	*Histone*	*1*	*0,53*	*-0,16*	*0,69*	*1,44*	*0,89*	*1,62*	*0,9609*	*0,9689*	*0,9995*	*1,0000*	*1,0000*	*1,0000*
High	ENSBTAP0	C1QA UniProtKB Gene Name|Bos taurus complement component 1, q subcompone	C1QA	2	0,41	-0,16	0,57	1,33	0,89	1,49	0,6009	0,9697	0,7349	0,9812	1,0000	1,0000
High	ENSBTAP0	COL3A1 EntrezGene|collagen alpha-1(III) chain precursor [Source:RefSeq peptide;A	COL3A1	10	1,20	-0,16	1,37	2,30	0,89	2,58	0,1886	0,9319	0,1193	0,7037	1,0000	0,8275
High	ENSBTAP0	C8G UniProtKB Gene Name|Bos taurus complement component 8, gamma polypept	C8G	2	0,19	-0,17	0,36	1,14	0,89	1,29	0,7145	0,7176	0,3151	1,0000	1,0000	1,0000
High	ENSBTAP0	AHSG UniProtKB Gene Name|Bos taurus alpha-2-HS-glycoprotein (AHSG), mRNA. [S	AHSG	22	-0,31	-0,17	-0,14	0,80	0,89	0,91	0,0316	0,2074	0,3539	0,3630	1,0000	1,0000
High	ENSBTAP0	CD9 UniProtKB Gene Name|Bos taurus CD9 molecule (CD9), mRNA. [Source:RefSeq	CD9	2	0,27	-0,18	0,45	1,21	0,89	1,37	0,4969	0,7697	0,8776	0,9031	1,0000	1,0000
High	ENSBTAP0	VCL UniProtKB Gene Name|Bos taurus vinculin (VCL), mRNA. [Source:RefSeq mRNA;	VCL	15	-1,14	-0,18	-0,96	0,46	0,89	0,51	0,8691	0,9948	0,8214	1,0000	1,0000	1,0000
High	*ENSBTAP0*	*COL5A2 HGNC Symbol|collagen, type V, alpha 2 [Source:HGNC Symbol;Acc:2210]|2|E*	*COL5A2*	*1*	*0,13*	*-0,18*	*0,30*	*1,09*	*0,88*	*1,23*	*0,8974*	*0,9945*	*0,8514*	*1,0000*	*1,0000*	*1,0000*
High	ENSBTAP0	APOB HGNC Symbol|apolipoprotein B [Source:HGNC Symbol;Acc:603]|11|ENSBTAG	APOB	177	0,97	-0,18	1,16	1,96	0,88	2,23	0,0877	0,6293	0,0272	0,5953	1,0000	0,5134
High	ENSBTAP0	CD55 UniProtKB Gene Name|Bos taurus CD55 molecule, decay accelerating factor fc	CD55	2	0,26	-0,18	0,44	1,20	0,88	1,36	0,1443	0,2457	0,0161	0,6918	1,0000	0,4358
High	*ENSBTAP0*	*ARF1 UniProtKB Gene Name|Bos taurus ADP-ribosylation factor 1 (ARF1), mRNA. [Sou*	*ARF1*	*1*	*0,13*	*-0,18*	*0,32*	*1,10*	*0,88*	*1,24*	*0,9997*	*0,4257*	*0,4150*	*1,0000*	*1,0000*	*1,0000*
High	ENSBTAP0	AGT UniProtKB Gene Name|Bos taurus angiotensinogen (serpin peptidase inhibitor,	AGT	15	-0,09	-0,19	0,10	0,94	0,88	1,07	0,8222	0,8549	0,9976	1,0000	1,0000	1,0000
Medium	*ENSBTAP0*	*MYH14 HGNC Symbol|myosin, heavy chain 14, non-muscle [Source:HGNC Symbol;Acc*	*MYH14*	*1*	*0,09*	*-0,19*	*0,29*	*1,07*	*0,88*	*1,22*	*0,7012*	*0,0288*	*0,0114*	*1,0000*	*0,7648*	*0,4358*
High	ENSBTAP0	Bos taurus enolase 1, (alpha) (ENO1), mRNA. [Source:RefSeq mRNA;Acc:NM_17404	Bos	10	-0,15	-0,19	0,04	0,90	0,88	1,03	0,7569	0,7365	0,9993	1,0000	1,0000	1,0000
High	ENSBTAP0	HGFAC EntrezGene|Bos taurus HGF activator (HGFAC), mRNA. [Source:RefSeq mRN	HGFAC	7	0,21	-0,20	0,41	1,16	0,87	1,33	0,2413	0,6682	0,0785	0,7037	1,0000	0,7006
High	ENSBTAP0	ITIH4 HGNC Symbol|inter-alpha-trypsin inhibitor heavy chain family, member 4 [Sou	ITIH4	32	-0,02	-0,21	0,19	0,98	0,87	1,14	0,9967	0,3048	0,2775	1,0000	1,0000	1,0000
High	*ENSBTAP0*	*YWHAB UniProtKB Gene Name|Bos taurus tyrosine 3-monooxygenase/tryptophan 5-r*	*YWHAB*	*1*	*-0,25*	*-0,21*	*-0,04*	*0,84*	*0,87*	*0,97*	*0,7695*	*0,5561*	*0,9242*	*1,0000*	*1,0000*	*1,0000*
High	ENSBTAP0	PFN1 UniProtKB Gene Name|Bos taurus profilin 1 (PFN1), mRNA. [Source:RefSeq mF	PFN1	4	-0,13	-0,22	0,09	0,91	0,86	1,06	0,6653	0,8872	0,9089	1,0000	1,0000	1,0000
High	*ENSBTAP0*	*Uncharacterized protein [Source:UniProtKB/TrEMBL;Acc:G3MXG6]|21|ENSBTAG000*	*Uncharacterized*	*1*	*0,13*	*-0,23*	*0,36*	*1,10*	*0,86*	*1,28*	*0,5990*	*0,9918*	*0,5322*	*0,9812*	*1,0000*	*1,0000*
High	ENSBTAP0	C1S EntrezGene|Bos taurus complement component 1, s subcomponent (C1S), mRN	C1S	6	-0,52	-0,23	-0,29	0,70	0,86	0,82	0,1699	0,9553	0,2443	0,7037	1,0000	1,0000
High	ENSBTAP0	SERPING1 HGNC Symbol|serpin peptidase inhibitor, clade G (C1 inhibitor), member	SERPING1	15	0,41	-0,23	0,64	1,33	0,85	1,56	1,0000	0,5456	0,5477	1,0000	1,0000	1,0000
Medium	*ENSBTAP0*	*CIT UniProtKB Gene Name|Uncharacterized protein [Source:UniProtKB/TrEMBL;Acc:F*	*CIT*	*1*	*0,23*	*-0,23*	*0,47*	*1,18*	*0,85*	*1,38*	*0,2121*	*0,3197*	*0,0292*	*0,7037*	*1,0000*	*0,5134*
High	ENSBTAP0	Uncharacterized protein [Source:UniProtKB/TrEMBL;Acc:F1MI18]|5|ENSBTAG0000	Uncharacterized	54	0,12	-0,23	0,35	1,09	0,85	1,28	0,8734	0,8545	0,5798	1,0000	1,0000	1,0000
High	ENSBTAP0	RGN UniProtKB Gene Name|Bos taurus regucalcin (senescence marker protein-30) (	RGN	5	0,37	-0,23	0,60	1,29	0,85	1,52	0,1201	0,7459	0,0469	0,6699	1,0000	0,6976
High	ENSBTAP0	GP1BA HGNC Symbol|glycoprotein Ib (platelet), alpha polypeptide [Source:HGNC Sy	GP1BA	6	-0,38	-0,24	-0,14	0,77	0,85	0,91	0,5083	0,6296	0,9734	0,9031	1,0000	1,0000
High	ENSBTAP0	HIST1H4G HGNC Symbol|histone cluster 1, H4g [Source:HGNC Symbol;Acc:4792]|6|	HIST1H4G	2	-0,43	-0,24	-0,19	0,74	0,85	0,88	0,4771	0,6731	0,9322	0,9031	1,0000	1,0000
High	*ENSBTAP0*	*TGFBR3 HGNC Symbol|transforming growth factor, beta receptor III [Source:HGNC Sy*	*TGFBR3*	*1*	*0,21*	*-0,25*	*0,46*	*1,16*	*0,84*	*1,37*	*0,9231*	*0,3810*	*0,2407*	*1,0000*	*1,0000*	*1,0000*
Medium	*ENSBTAP0*	*E-CADHERIN UniProtKB Gene Name|Bos taurus cadherin 1, type 1, E-cadherin (epithe*	*E-CADHERIN*	*1*	*0,10*	*-0,25*	*0,35*	*1,07*	*0,84*	*1,27*	*0,6047*	*0,7577*	*0,2719*	*0,9827*	*1,0000*	*1,0000*
High	ENSBTAP0	PROZ UniProtKB Gene Name|Vitamin K-dependent protein Z [Source:UniProtKB/Sw	PROZ	2	-0,32	-0,26	-0,07	0,80	0,84	0,96	0,9865	0,9931	0,9610	1,0000	1,0000	1,0000
High	ENSBTAP0	NID1 HGNC Symbol|nidogen 1 [Source:HGNC Symbol;Acc:7821]|28|ENSBTAG00000	NID1	3	0,77	-0,27	1,04	1,71	0,83	2,06	0,9808	0,5981	0,4967	1,0000	1,0000	1,0000
High	ENSBTAP0	SERPINA3-1 UniProtKB Gene Name|Bos taurus serpin peptidase inhibitor, clade A (a	SERPINA3-1	9	0,04	-0,28	0,32	1,03	0,82	1,25	0,8787	0,6817	0,9274	1,0000	1,0000	1,0000
High	ENSBTAP0	NCAM1 HGNC Symbol|neural cell adhesion molecule 1 [Source:HGNC Symbol;Acc:7	NCAM1	13	-0,47	-0,31	-0,16	0,72	0,81	0,90	0,4252	0,3420	0,9802	0,8728	1,0000	1,0000
High	ENSBTAP0	CP HGNC Symbol|ceruloplasmin (ferroxidase) [Source:HGNC Symbol;Acc:2295]|1|E	CP	21	0,44	-0,33	0,77	1,36	0,80	1,70	0,2333	0,8691	0,1222	0,7037	1,0000	0,8275
High	ENSBTAP0	PGLYRP2 HGNC Symbol|peptidoglycan recognition protein 2 [Source:HGNC Symbol;	PGLYRP2	7	0,65	-0,33	0,98	1,57	0,80	1,97	0,3427	0,9618	0,2484	0,7847	1,0000	1,0000
High	ENSBTAP0	Uncharacterized protein [Source:UniProtKB/TrEMBL;Acc:G3N3V1]|2|ENSBTAG0000	Uncharacterized	2	-1,02	-0,34	-0,69	0,49	0,79	0,62	0,7005	0,6477	0,9953	1,0000	1,0000	1,0000
High	ENSBTAP0	FABP1 UniProtKB Gene Name|Bos taurus fatty acid binding protein 1, liver (FABP1),	FABP1	3	-0,54	-0,34	-0,20	0,69	0,79	0,87	0,1050	0,4835	0,4676	0,6285	1,0000	1,0000
High	ENSBTAP0	HIST3H2BB HGNC Symbol|histone cluster 3, H2bb [Source:HGNC Symbol;Acc:20514]	HIST3H2BB	2	-0,46	-0,35	-0,11	0,73	0,79	0,93	0,2390	0,7124	0,5914	0,7037	1,0000	1,0000
High	ENSBTAP0	KRT1 HGNC Symbol|keratin 1 [Source:HGNC Symbol;Acc:6412]|5|ENSBTAG0000004	KRT1	4	-1,10	-0,36	-0,74	0,47	0,78	0,60	0,0345	0,2465	0,3275	0,3808	1,0000	1,0000
High	ENSBTAP0	C4BPA UniProtKB Gene Name|Bos taurus complement component 4 binding protein	C4BPA	24	0,28	-0,37	0,65	1,21	0,77	1,57	0,3081	0,8745	0,1658	0,7418	1,0000	0,8815
High	ENSBTAP0	TTR UniProtKB Gene Name|Bos taurus transthyretin (TTR), mRNA. [Source:RefSeq m	TTR	6	-0,45	-0,38	-0,07	0,73	0,77	0,95	0,5705	0,4512	0,9717	0,9582	1,0000	1,0000
Medium	*ENSBTAP0*	*UBAC2 UniProtKB Gene Name|Bos taurus UBA domain containing 2 (UBAC2), mRNA.*	*UBAC2*	*1*	*0,04*	*-0,39*	*0,42*	*1,03*	*0,77*	*1,34*	*0,9648*	*0,9217*	*0,8028*	*1,0000*	*1,0000*	*1,0000*
High	ENSBTAP0	GNPTG UniProtKB Gene Name|Bos taurus N-acetylglucosamine-1-phosphate transfe	GNPTG	4	0,39	-0,41	0,80	1,31	0,75	1,74	0,3713	0,8326	0,1816	0,8204	1,0000	0,9034
High	ENSBTAP0	MASP2 HGNC Symbol|mannan-binding lectin serine peptidase 2 [Source:HGNC Sym	MASP2	5	-0,59	-0,41	-0,18	0,66	0,75	0,88	0,8847	0,9761	0,9619	1,0000	1,0000	1,0000
High	ENSBTAP0	ALDOA UniProtKB Gene Name|Bos taurus aldolase A, fructose-bisphosphate (ALDO.	ALDOA	5	-0,83	-0,43	-0,40	0,56	0,74	0,76	0,6186	0,9394	0,8075	1,0000	1,0000	1,0000
High	ENSBTAP0	COL1A2 UniProtKB Gene Name|Bos taurus collagen, type I, alpha 2 (COL1A2), mRNA	COL1A2	9	0,35	-0,45	0,80	1,27	0,73	1,74	0,6343	0,2032	0,0613	1,0000	1,0000	0,7006
High	ENSBTAP0	COL11A1 UniProtKB Gene Name|Bos taurus collagen, type XI, alpha 1 (COL11A1), m	COL11A1	3	0,77	-0,46	1,23	1,70	0,73	2,34	0,2942	0,8830	0,1617	0,7367	1,0000	0,8728
High	ENSBTAP0	MASP1 UniProtKB Gene Name|Bos taurus mannan-binding lectin serine peptidase 1	MASP1	6	0,34	-0,46	0,80	1,27	0,73	1,75	0,2106	0,9920	0,1808	0,7037	1,0000	0,9034
High	ENSBTAP0	CNTN1 UniProtKB Gene Name|Bos taurus contactin 1 (CNTN1), mRNA. [Source:RefS	CNTN1	5	0,45	-0,47	0,92	1,37	0,72	1,89	0,3057	0,4825	0,0654	0,7418	1,0000	0,7006
High	ENSBTAP0	ADIPOQ UniProtKB Gene Name|Adiponectin [Source:UniProtKB/Swiss-Prot;Acc:Q3Y	ADIPOQ	7	-0,02	-0,47	0,45	0,99	0,72	1,37	0,7942	0,1905	0,0823	1,0000	1,0000	0,7006
High	*ENSBTAP0*	*KRT3 HGNC Symbol|keratin 3 [Source:HGNC Symbol;Acc:6440]|5|ENSBTAG00000045*	*KRT3*	*1*	*2,88*	*-0,49*	*3,37*	*7,36*	*0,71*	*10,37*	*0,2842*	*0,9864*	*0,3432*	*0,7197*	*1,0000*	*1,0000*
High	*ENSBTAP0*	*ACTB UniProtKB Gene Name|Bos taurus actin, beta (ACTB), mRNA. [Source:RefSeq m*	*ACTB*	*1*	*1,38*	*-0,51*	*1,90*	*2,61*	*0,70*	*3,73*	*0,9325*	*0,9855*	*0,9793*	*1,0000*	*1,0000*	*1,0000*
Medium	*ENSBTAP0*	*Uncharacterized protein [Source:UniProtKB/TrEMBL;Acc:F1MQM5]|18|ENSBTAG000*	*Uncharacterized*	*1*	*-0,19*	*-0,53*	*0,34*	*0,88*	*0,70*	*1,27*	*0,7267*	*0,9990*	*0,7031*	*1,0000*	*1,0000*	*1,0000*
High	ENSBTAP0	CFL1 UniProtKB Gene Name|Bos taurus cofilin 1 (non-muscle) (CFL1), mRNA. [Sourc	CFL1	4	0,89	-0,54	1,43	1,85	0,69	2,69	0,1555	0,8447	0,0761	0,7037	1,0000	0,7006
High	*ENSBTAP0*	*KRT19 UniProtKB Gene Name|Bos taurus keratin 19 (KRT19), mRNA. [Source:RefSeq r*	*KRT19*	*1*	*-0,08*	*-0,55*	*0,47*	*0,95*	*0,68*	*1,39*	*0,9720*	*0,5455*	*0,6726*	*1,0000*	*1,0000*	*1,0000*
Medium	*ENSBTAP0*	*PPP3CC UniProtKB Gene Name|Bos taurus protein phosphatase 3, catalytic subunit, g*	*PPP3CC*	*1*	*0,58*	*-0,57*	*1,15*	*1,50*	*0,68*	*2,22*	*0,7853*	*0,8774*	*0,5118*	*1,0000*	*1,0000*	*1,0000*
High	*ENSBTAP0*	*KRT18 UniProtKB Gene Name|Bos taurus keratin 18 (KRT18), mRNA. [Source:RefSeq r*	*KRT18*	*1*	*-1,59*	*-0,58*	*-1,01*	*0,33*	*0,67*	*0,50*	*0,0219*	*0,2359*	*0,2124*	*0,3121*	*1,0000*	*0,9709*
High	ENSBTAP0	ACTN1 UniProtKB Gene Name|Bos taurus actinin, alpha 1 (ACTN1), mRNA. [Source:F	ACTN1	4	-0,14	-0,59	0,45	0,91	0,66	1,37	0,7406	0,6599	0,2949	1,0000	1,0000	1,0000
High	ENSBTAP0	TGFBI EntrezGene|Bos taurus transforming growth factor, beta-induced, 68kDa (TG	TGFBI	13	0,27	-0,59	0,87	1,21	0,66	1,82	0,2727	0,1542	0,0187	0,7109	1,0000	0,4358
High	*ENSBTAP0*	*KRT77 HGNC Symbol|keratin 77 [Source:HGNC Symbol;Acc:20411]|5|ENSBTAG00000*	*KRT77*	*1*	*0,39*	*-0,64*	*1,03*	*1,31*	*0,64*	*2,05*	*0,5748*	*0,9614*	*0,4360*	*0,9582*	*1,0000*	*1,0000*
High	ENSBTAP0	NUCB1 UniProtKB Gene Name|Bos taurus nucleobindin 1 (NUCB1), mRNA. [Source:F	NUCB1	9	1,33	-0,65	1,98	2,52	0,64	3,95	0,0133	0,4868	0,0039	0,2364	1,0000	0,1911
High	ENSBTAP0	P4HB UniProtKB Gene Name|Bos taurus prolyl 4-hydroxylase, beta polypeptide (P4H	P4HB	2	-0,09	-0,66	0,57	0,94	0,63	1,48	0,7371	0,3092	0,6860	1,0000	1,0000	1,0000
High	ENSBTAP0	LGALS3BP UniProtKB Gene Name|Bos taurus lectin, galactoside-binding, soluble, 3 b	LGALS3BP	9	-0,59	-0,66	0,07	0,66	0,63	1,05	0,1026	0,0850	0,9881	0,6285	1,0000	1,0000
High	ENSBTAP0	FN1 UniProtKB Gene Name|Bos taurus fibronectin 1 (FN1), mRNA. [Source:RefSeq m	FN1	3	0,37	-0,67	1,03	1,29	0,63	2,05	0,5718	0,0660	0,0187	0,9582	0,9659	0,4358
High	ENSBTAP0	AMY2B EntrezGene|Bos taurus amylase, alpha 2B (pancreatic) (AMY2B), mRNA. [So	AMY2B	10	-0,40	-0,67	0,26	0,76	0,63	1,20	0,3717	0,1817	0,8323	0,8204	1,0000	1,0000
High	ENSBTAP0	Uncharacterized protein [Source:UniProtKB/TrEMBL;Acc:G5E5T5]|21|ENSBTAG000	Uncharacterized	6	-0,29	-0,70	0,41	0,82	0,62	1,33	0,8960	0,4324	0,6734	1,0000	1,0000	1,0000
High	ENSBTAP0	RPS27A UniProtKB Gene Name|Bos taurus ribosomal protein S27a (RPS27A), mRNA.	RPS27A	3	-1,00	-0,71	-0,30	0,50	0,61	0,81	0,2657	0,4375	0,9059	0,7037	1,0000	1,0000
High	ENSBTAP0	ITGA2B UniProtKB Gene Name|Bos taurus integrin, alpha 2b (platelet glycoprotein II	ITGA2B	4	0,60	-0,75	1,35	1,52	0,60	2,55	0,4831	0,3185	0,0683	0,9031	1,0000	0,7006
High	ENSBTAP0	Uncharacterized protein [Source:UniProtKB/TrEMBL;Acc:G3N3Q3]|21|ENSBTAG000	Uncharacterized	2	0,45	-0,77	1,22	1,37	0,59	2,33	0,2947	0,1217	0,0164	0,7367	1,0000	0,4358
High	ENSBTAP0	CPN2 UniProtKB Gene Name|Bos taurus carboxypeptidase N, polypeptide 2 (CPN2),	CPN2	9	-0,66	-0,77	0,11	0,63	0,59	1,08	0,0014	0,0009	0,8185	0,0574	0,1077	1,0000
High	ENSBTAP0	KRT14 EntrezGene|Bos taurus keratin 14 (KRT14), mRNA. [Source:RefSeq mRNA;Acc	KRT14	9	-0,59	-0,78	0,19	0,67	0,58	1,14	0,8961	0,9998	0,8884	1,0000	1,0000	1,0000
High	ENSBTAP0	Uncharacterized protein [Source:UniProtKB/TrEMBL;Acc:G5E513]|8|ENSBTAG0000	Uncharacterized	6	-0,36	-0,79	0,42	0,78	0,58	1,34	0,0578	0,0053	0,1580	0,4765	0,3438	0,8640
High	ENSBTAP0	CD93 HGNC Symbol|CD93 molecule [Source:HGNC Symbol;Acc:15855]|13|ENSBTAG	CD93	6	-0,31	-0,84	0,53	0,81	0,56	1,44	0,5450	0,1165	0,4502	0,9377	1,0000	1,0000
High	ENSBTAP0	Uncharacterized protein [Source:UniProtKB/TrEMBL;Acc:G8JKW7]|21|ENSBTAG000	Uncharacterized	4	0,59	-0,88	1,47	1,51	0,54	2,77	0,4658	0,7903	0,2120	0,9031	1,0000	0,9709
High	ENSBTAP0	Uncharacterized protein [Source:UniProtKB/TrEMBL;Acc:G5E604]|17|ENSBTAG000	Uncharacterized	2	-0,47	-0,88	0,42	0,72	0,54	1,33	0,9435	0,7537	0,9139	1,0000	1,0000	1,0000
High	*ENSBTAP0*	*MVP EntrezGene|Bos taurus major vault protein (MVP), mRNA. [Source:RefSeq mRNA*	*MVP*	*1*	*-0,11*	*-0,91*	*0,79*	*0,92*	*0,53*	*1,73*	*0,9985*	*0,9658*	*0,9505*	*1,0000*	*1,0000*	*1,0000*
High	*ENSBTAP0*	*CSN2 UniProtKB Gene Name|Bos taurus casein beta (CSN2), mRNA. [Source:RefSeq m*	*CSN2*	*1*	*0,50*	*-0,93*	*1,43*	*1,41*	*0,53*	*2,69*	*0,8419*	*0,8418*	*1,0000*	*1,0000*	*1,0000*	*1,0000*
High	*ENSBTAP0*	*KRT75 UniProtKB Gene Name|Bos taurus keratin 75 (KRT75), mRNA. [Source:RefSeq r*	*KRT75*	*1*	*-1,05*	*-0,94*	*-0,11*	*0,48*	*0,52*	*0,93*	*0,4947*	*0,7604*	*0,8833*	*0,9031*	*1,0000*	*1,0000*
High	*ENSBTAP0*	*KRT78 UniProtKB Gene Name|Bos taurus keratin 78 (KRT78), mRNA. [Source:RefSeq r*	*KRT78*	*1*	*0,39*	*-1,06*	*1,45*	*1,31*	*0,48*	*2,72*	*0,5097*	*0,5232*	*0,1285*	*0,9031*	*1,0000*	*0,8275*
High	ENSBTAP0	EEF1A1 UniProtKB Gene Name|Elongation factor 1-alpha 1 [Source:UniProtKB/Swis	EEF1A1	3	0,18	-1,09	1,27	1,13	0,47	2,41	0,9484	0,1124	0,0757	1,0000	1,0000	0,7006
High	*ENSBTAP0*	*FAP UniProtKB Gene Name|Bos taurus fibroblast activation protein, alpha (FAP), mRN.*	*FAP*	*1*	*-0,12*	*-1,09*	*0,97*	*0,92*	*0,47*	*1,95*	*0,6739*	*0,0513*	*0,1553*	*1,0000*	*0,9015*	*0,8569*
High	ENSBTAP0	PRDX2 UniProtKB Gene Name|Bos taurus peroxiredoxin 2 (PRDX2), mRNA. [Source:F	PRDX2	6	-0,54	-1,10	0,56	0,69	0,47	1,48	0,3280	0,1486	0,8061	0,7679	1,0000	1,0000
High	ENSBTAP0	KRT10 UniProtKB Gene Name|Bos taurus keratin 10 (KRT10), mRNA. [Source:RefSeq	KRT10	8	-1,24	-1,12	-0,12	0,42	0,46	0,92	0,0733	0,1397	0,8708	0,5613	1,0000	1,0000
Medium	*ENSBTAP0*	*S100A1 UniProtKB Gene Name|Bos taurus S100 calcium binding protein A1 (S100A1),*	*S100A1*	*1*	*-0,44*	*-1,13*	*0,69*	*0,74*	*0,46*	*1,61*	*0,9567*	*0,7536*	*0,8964*	*1,0000*	*1,0000*	*1,0000*
High	*ENSBTAP0*	*KRT79 UniProtKB Gene Name|Bos taurus keratin 79 (KRT79), mRNA. [Source:RefSeq r*	*KRT79*	*1*	*-1,19*	*-1,18*	*0,00*	*0,44*	*0,44*	*1,00*	*0,3031*	*0,8299*	*0,5791*	*0,7418*	*1,0000*	*1,0000*
Medium	*ENSBTAP0*	*CDH11 UniProtKB Gene Name|Bos taurus cadherin 11, type 2, OB-cadherin (osteoblas*	*CDH11*	*1*	*-1,38*	*-1,23*	*-0,15*	*0,39*	*0,43*	*0,90*	*0,5156*	*0,5378*	*0,9990*	*0,9031*	*1,0000*	*1,0000*
High	ENSBTAP0	GPR116 HGNC Symbol|G protein-coupled receptor 116 [Source:HGNC Symbol;Acc:1	GPR116	2	0,46	-1,24	1,70	1,37	0,42	3,24	0,4740	0,7277	0,1875	0,9031	1,0000	0,9219
High	ENSBTAP0	Bos taurus keratin 6A (KRT6A), mRNA. [Source:RefSeq mRNA;Acc:NM_001083510]|5	Bos	9	-0,89	-1,28	0,39	0,54	0,41	1,31	0,9572	0,9828	0,8916	1,0000	1,0000	1,0000
High	ENSBTAP0	KRT5 UniProtKB Gene Name|Bos taurus keratin 5 (KRT5), mRNA. [Source:RefSeq mR	KRT5	7	-0,87	-1,37	0,50	0,55	0,39	1,41	0,4628	0,4356	0,9983	0,9031	1,0000	1,0000
High	*ENSBTAP0*	*KRT2 HGNC Symbol|keratin 2 [Source:HGNC Symbol;Acc:6439]|5|ENSBTAG00000039*	*KRT2*	*1*	*-2,17*	*-1,42*	*-0,75*	*0,22*	*0,37*	*0,60*	*0,0895*	*0,3127*	*0,6067*	*0,5953*	*1,0000*	*1,0000*
High	ENSBTAP0	KRT24 EntrezGene|keratin, type I cytoskeletal 24 [Source:RefSeq peptide;Acc:NP_0	KRT24	2	-1,45	-1,53	0,08	0,37	0,35	1,06	0,0044	0,0151	0,4939	0,1291	0,4902	1,0000
Medium	*ENSBTAP0*	*C11H2orf81 EntrezGene|Bos taurus chromosome 11 open reading frame, human C2o*	*C11H2orf81*	*1*	*0,80*	*-1,63*	*2,42*	*1,74*	*0,32*	*5,37*	*0,9706*	*0,2957*	*0,3889*	*1,0000*	*1,0000*	*1,0000*
High	*ENSBTAP0*	*Uncharacterized protein [Source:UniProtKB/TrEMBL;Acc:G3MWT1]|7|ENSBTAG0000*	*Uncharacterized*	*1*	*0,11*	*-1,75*	*1,86*	*1,08*	*0,30*	*3,64*	*0,5989*	*0,4567*	*0,1343*	*0,9812*	*1,0000*	*0,8275*
High	ENSBTAP0	DMBT1 HGNC Symbol|deleted in malignant brain tumors 1 [Source:HGNC Symbol;A	DMBT1	4	-1,13	-1,98	0,85	0,46	0,25	1,80	0,1366	0,0140	0,2213	0,6918	0,4902	0,9882
Medium	*ENSBTAP0*	*CYP2W1 HGNC Symbol|cytochrome P450, family 2, subfamily W, polypeptide 1 [Sourc*	*CYP2W1*	*1*	*-1,35*	*-2,04*	*0,69*	*0,39*	*0,24*	*1,62*	*0,4851*	*0,2757*	*0,8773*	*0,9031*	*1,0000*	*1,0000*
High	*ENSBTAP0*	*SFN UniProtKB Gene Name|Bos taurus stratifin (SFN), mRNA. [Source:RefSeq mRNA;A*	*SFN*	*1*	*-1,02*	*-2,10*	*1,09*	*0,49*	*0,23*	*2,13*	*0,9942*	*0,6889*	*0,7467*	*1,0000*	*1,0000*	*1,0000*
Medium	*ENSBTAP0*	*Uncharacterized protein [Source:UniProtKB/TrEMBL;Acc:G3N1R8]|29|ENSBTAG0000*	*Uncharacterized*	*1*	*-0,88*	*-2,73*	*1,85*	*0,54*	*0,15*	*3,61*	*0,9060*	*0,3409*	*0,5435*	*1,0000*	*1,0000*	*1,0000*
High	*ENSBTAP0*	*PGLYRP1 UniProtKB Gene Name|Bos taurus peptidoglycan recognition protein 1 (PGLY*	*PGLYRP1*	*1*	*0,86*	*-2,86*	*3,72*	*1,81*	*0,14*	*13,14*	*0,6000*	*0,6676*	*0,2208*	*0,9812*	*1,0000*	*0,9882*

3. Trypan quenching

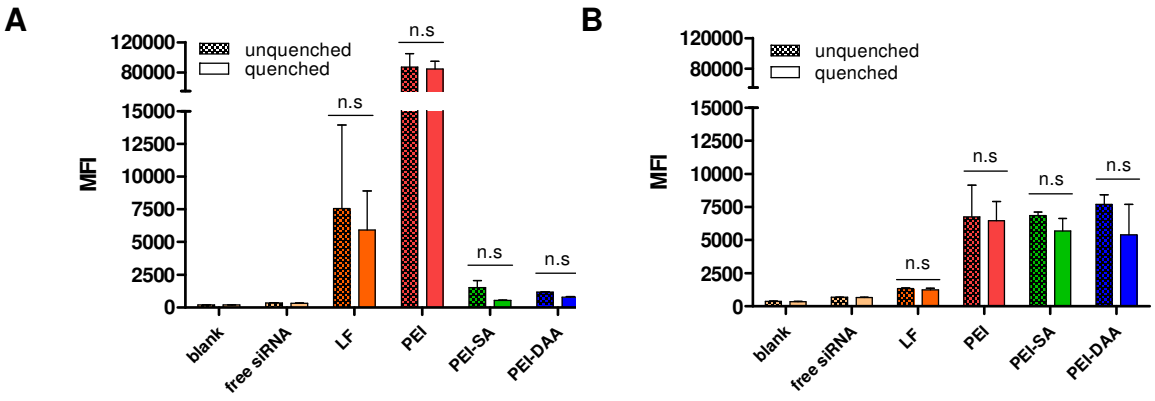

Figure S3. Cellular uptake of PEI, PEI-SA and PEI-DAA PXs into hCMEC/D3 cells after 24 h incubation in medium without (A) and with (B) serum as quantified by flow cytometry performed with and without trypan quenching and presented as median fluorescence intensitiy (MFI). Negative control: untreated cells (blank) and with free siRNA treated cells. (Results are shown as mean ± SD, n = 3, two-way ANOVA with Bonferroni post-hoc test, n.s = not significant).

4. Transport Assay

4.1 Cytotoxicity measurements of PXs by CellTiter-Glo® Assay

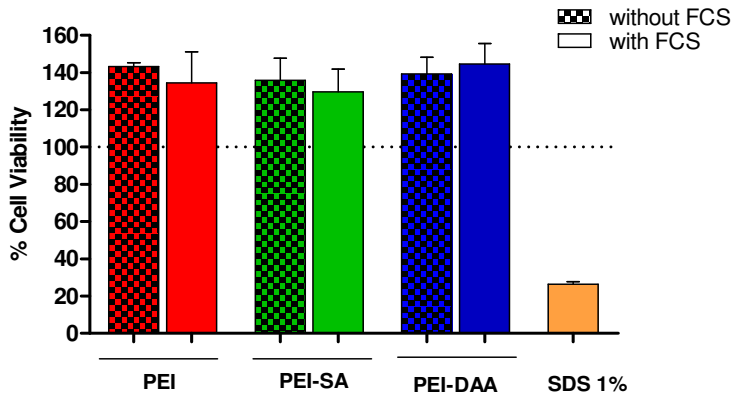

Figure S4. Cell viability of hiPSC-derived endothelial cells as determined by CellTiter-Glo® Assay after treatment with PEI, PEI-SA and PEI-DAA PXs with or without addition of serum after an incubation period of 24 h. Cells treated with medium were used as negative control and cells treated with 1% SDS were used as positive control. (Results are presented as mean ± SD as percentage of viable cells in comparison to negative control cells representing 100% viability, n = 3).

4.2 TEER measurements

Table S2. Barrier integrity of hiPSC-derived ECS evaluated by TEER measurements with a Millicell ERS-2 electrical resistance system and a STX3 electrode before addition of respective formulations. Each insert was measured at three positions monitoring the entire surface area of the insert. Duplicates were used for each model in three independent biologicals experiments (n = 1-3) and results are shown as mean ± SD.

Polyplex	TEER values [Ω·cm²]		
	n=1	n=2	n=3
Without Serum			
PEI	2073.79 ± 153.23	3013.25 ± 316.81	2969.52 ± 93.18
PEI-SA	2247.21 ± 537.39	3519.03 ± 262.82	2955.77 ± 57.56
PEI-DAA	2143.37 ± 355.38	3075.67 ± 661.92	2962.54 ± 30.57
With Serum			
PEI	1795.93 ± 1085.83	3134.41 ± 569.52	2949.78 ± 22.32
PEI-SA	1808.97 ± 164.20	2967.05 ± 562.91	2970.73 ± 6.22
PEI-DAA	1957.30 ± 787.62	3706.80 ± 203.09	2982.50 ± 230.23

5. Animal testing

5.1 Hemocompatibility measurements

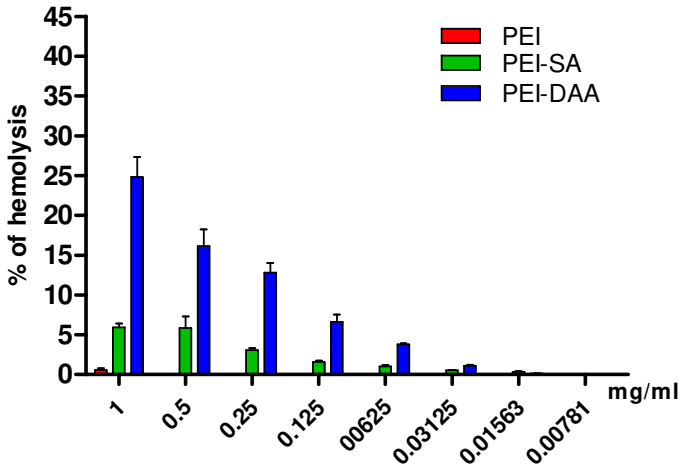

Figure S5. Hemolysis of human erythrocytes at pH 7.4 induced by PEI, PEI-SA and PEI-DAA polymers at various concentrations (1 – 0.00781 mg/mL). (Results are shown as mean ± SD as percentage of hemolysis in comparison to Triton-X treated cells representing 100% hemolysis, n = 3).

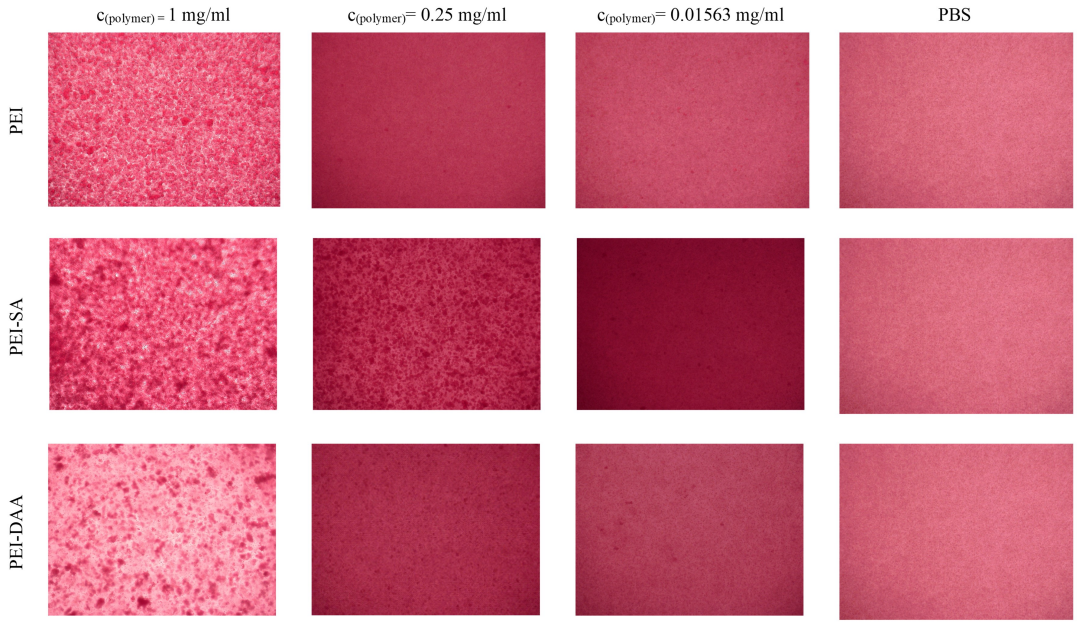

Figure S6. Erythrocyte aggregation profiles of PEI, PEI-SA and PEI-DAA polymers at pH 7.4 shown for concentrations of 1 mg/mL, 0.25 mg/mL and 0.01563 mg/mL in comparison to PBS used as negative control.

References

[1] F. Adams, C.M. Zimmermann, D. Baldassi, Amphiphilic poly(spermine acrylamides): A new class of sophisticated non-viral vectors for pulmonary siRNA delivery, Advanced Healthcare Materials, (to be submitted for publication).

Chapter V

Summary and Perspectives

Within this thesis, various aspects of polymer-based siRNA transport into the brain were investigated to expand the general understanding of important parameters of delivery of macromolecules across the blood-brain barrier (BBB), thus enabling the development of effective RNAi-based CNS drugs in the future.

Although RNAi offers an auspicious novel treatment option for several CNS diseases by silencing disease-related genes, it is also accompanied with major hurdles. The unfavorable physico-chemical characteristics of siRNA such as the negative charges of the phosphate backbone and instability toward serum nucleases constitutes the need for an appropriate siRNA delivery system capable of protecting siRNA from degradation in the bloodstream and initiating particle-cell membrane interaction for successful internalization into target cells. Moreover, the transport of high-molecular-weight compounds to the brain is considerably restricted by the protective function of the BBB, making it a particularly difficult target site to reach within the body.

Cationic polymers have been successfully utilized as siRNA carriers since the high positive charge densities confer efficient cellular entry and endosomal escape abilities to the formed polymer-siRNA complexes, resulting in acceptable transfection efficiency. However, cationic polymers have also been demonstrated to possess remarkable cytotoxic effects and poor biocompatibility profiles, which considerably limits their clinical translation. In an effort to develop advantageous siRNA delivery systems, that can be also administered repeatedly, special emphasis is laid on reducing cytotoxic effects, e.g., through insertion of hydrophobic modifications to cationic polymers as well as on evaluating novel and in particular biodegradable types of polymers.

Within **Chapter II** of the thesis, two polymer types, namely nylon-3 polymers (*Subchapter II.1*) and spermine-based poly(acrylamides) (*Subchapter II.2*) were tested regarding their suitability for siRNA delivery into glioblastoma cells as a function of their content of hydrophobic subunits. All polyplexes exhibited very favorable characteristics such as efficient siRNA encapsulation, particle sizes below 250 nm, slightly positive zeta potentials and appropriate toxicity profiles. Most amphiphilic polyplexes were confirmed to possess optimal cellular internalization abilities resulting in successful gene silencing effects.

Since the development of active targeting strategies for polyplexes would be of great benefit for siRNA delivery into the brain, in the further course, the role of proteins as potential targeting ligands for the BBB was evaluated in **Chapter III**.

It has been previously shown that specific plasma proteins adsorbed on particles upon encountering physiological environments are capable to initiate uptake of particles into the brain through the receptor-mediated endocytosis pathway. Moreover, the formed protein corona considerably dictates the fate of the particle in the body, thus representing a highly important parameter that needs to be considered for the development of precise siRNA delivery systems.

So far, relatively little is known about the composition of the protein corona of polyplexes caused inter alia by a lack of methodology. Therefore, a strategy to analyze the protein corona formed on polyplexes after incubation in plasma has been developed within the scope of this thesis (*Subchapter III.2*). Isolation of protein – polyplex complexes from loosely bound proteins was successfully achieved by an optimized centrifugation protocol ensuring stability of complexes with appropriate sizes and low losses of siRNA payload after purification steps. With the application of SDS-PAGE and LC-MS-MS methods, the protein corona composition was determined with a particular emphasis on functional proteins as a function of the polyplex material (cationic PEI polyplexes vs amphiphilic nylon-3 polyplexes). Various proteins known to induce active targeting effects, such as albumin, Transferrin or ApoE were identified to similar extents in both protein corona profiles. Moreover, hyaluronan binding protein 2 (HAPB2) was found to be significantly higher abundant in the protein corona formed around amphiphilic polyplexes. The successfully developed methods for studying the protein corona not only provided interesting insights into the protein corona composition of polyplexes but could also be applied to other dynamic systems in the future.

In *Subchapter III.3*, the feasibility of the PS80-ApoE brain targeting approach via LDL receptors, which has been successfully applied to solid nanoparticles (as reviewed in *Subchapter III.1*), was evaluated for polyplexes for the first time. In line with our expectations, precoating with surfactants as anchors for ApoE is not applicable for polyplexes due to potential disintegration of the complexes under *in vitro* conditions. Coating of amphiphilic polyplexes with ApoE revealed very promising *in vitro* results regarding cellular internalization and gene knockdown abilities in an LDL overexpressing cell line, however, *in vitro-in vivo* correlations remained rather poor.

Chapter IV aimed to evaluate the blood-brain barrier permeability of unmodified and hydrophobically modified PEI polyplexes in a serum dependent manner with BBB models *in vitro* and *in vivo*. The assembly of polyplexes led to particles with favorable sizes and surface charges. Protein corona composition of polyplexes was determined by applying the methods developed in *Subchapter III.2,* and results confirmed that the protein profile is predominantly determined by the material of the utilized polymers. In line with results of *Subchapter III.2* various functional proteins were detected in the protein corona of all formulations, whereas HABP2 was detected significantly more frequently in the protein corona of amphiphilic PEI polyplexes, indicating that high binding affinities to amphiphilic compounds are caused by their hydrophobic properties. Serum-induced reduction of cellular internalization abilities into a human brain endothelial cell line (hCMEC/D3) was observed for unmodified PEI polyplexes, whereas amphiphilic PEI polyplexes only reached significant cell uptake under physiological conditions. Since the results of *Subchapter III.3* provide evidence for the need of more appropriate *in vitro* models to better predict the outcome in *in vivo* settings, a BBB model derived from human induced pluripotent stem cells (hiPSC) was utilized for the first time within the framework of this thesis to evaluate the BBB permeation ability of polyplexes. All formulations demonstrated auspicious BBB permeation abilities under physiological conditions, which, however, was only partially confirmed *in vivo* since high accumulation of amphiphilic polyplexes in the lung possibly hampered their delivery into the brain.

In continuation of the topics described, several further investigations and developments need to be addressed in the future.

Since the relatively novel siRNA carrier systems introduced in **Chapter II** were well suited for delivery into glioblastoma cells, their use for other potential targets is conceivable. Based on the data presented in this work, optimized amphiphilic poly(spermine acrylamides) have recently been successfully applied for pulmonary siRNA delivery. In future investigations, the question of the underlying mechanism for enhanced uptake capabilities of amphiphilic polyplexes as well as biocompatibility of novel polymeric materials needs to be further elucidated. We suggest evaluating *in vitro* biodegradability of designed polymeric materials for instance *via* gel permeation chromatography after incubation in degrading conditions for various time points. *In vivo* pharmacokinetic studies can be realized by pursuing the distribution of radiolabeled polymeric materials, most elegantly with non-invasive nuclear imaging

approaches such as single photon emission computed tomography (SPECT) and positron emission tomography (PET).

The methods optimized in *Subchapter III.2* for investigating the protein corona can also be applied to other dynamic systems, since this important aspect needs to be considered when designing precise and effective carrier systems. At this point, it should be briefly noted that the use of differential centrifugal sedimentation (DCS) in future studies would allow the characterization of protein-polyplex complexes, leading to a deeper understanding of, for example, aggregation issues and thus the behavior of the systems under physiological conditions *in vitro* and *in vivo*. Dynamic light scattering (DLS), one of the standard particle characterization methods, is of limited use for this purpose. Moreover, correlations between polymer properties and binding affinities to specific proteins as well as the effects of bound proteins on biodistribution and targeting effects require further research efforts.

Regarding active targeting approaches for brain delivery, the results of *Subchapter III.3* revealed that loose attachment of ApoE by simply coating of polyplexes is not durable within complex biological environments. Therefore, we suggest that more stable covalent linkage approaches should be investigated, for example, with the use of a sulfhydryl-modified PEG cross-linker, which could be coupled to primary amines present in both, polymers and ApoE. Another approach, already established but not described in this work in order not to go beyond the scope, is the coupling of nylon-3 polymers to Transferrin via a heterobifunctional succinimidyl 3-(2-pyridyldithio) propionate (SPDP) linker. Resulting conjugates of advanced polymers and Transferrin, as another potent targeting ligand for the BBB, are certainly worth to be tested as siRNA nanocarrier for brain delivery in future experiments.

Although the hiPSC-derived BBB model offers great in-human like properties in terms of BBB tightness, the results described in **Chapter IV** pointed out that several additional parameters, such as the residence time in the circulation, needs to be considered to accurately assess the permeation of the formulations into the brain. Therefore, also with regard to disadvantages of animal models, it would be of great benefit to invest more research efforts into systems that combine various relevant parameters, e.g., microfluidic brain-on-a-chip models. Nevertheless, although the formulations described here delivered just small amounts of siRNA into the brain, it is not yet known if this would be enough to achieve therapeutic effects. The use of siRNA

sequences against disease-related genes in *in vitro* gene silencing experiments or in *in vivo* pharmacological disease models could clarify this issue in the future.

Taken together, within this work, efforts were made to broaden the understanding of several relevant issues related to the development of a suitable approach for targeted siRNA delivery to the brain. Evaluation of advanced polymeric materials, the influence of hydrophobic modifications and the composition of the protein corona profile may allow precise adjustment of polymer composition in future approaches. The application of a hiPSC-derived BBB model to evaluate the BBB permeation ability of polyplexes provides a valuable tool for further development of siRNA-based CNS drugs. Although the strategies for targeted delivery of siRNA to the brain investigated in this work were not as successful as hypothesized, the gathered findings are expected to lay the foundation for achieving this ambitious goal in the near future.

Chapter VI

Appendix

VI.1 List of publications

1. Articles

Natascha Hartl, Friederike Adams, Gabriella Costabile, Lorenz Isert, Markus Döblinger, Ximian Xiao, Runhui Liu and Olivia M. Merkel

"The Impact of Nylon-3 Copolymer Composition on the Efficiency of siRNA Delivery to Glioblastoma Cells"

Nanomaterials 2019, 9(7), 986; https://doi.org/10.3390/nano9070986

Natascha Hartl, Friederike Adams and Olivia M. Merkel

"From Adsorption to Covalent Bonding: Apolipoprotein E Functionalization of polymeric Nanoparticles for Drug Delivery across the Blood-Brain Barrier"

Advanced Therapeutics 2021,4: 2000092, https://doi.org/10.1002/adtp.202000092

Top Cited Article 2021/2022

Natascha Hartl, David C. Jürgens, Simone Carneiro, Ann-Chrisitne König, Stefanie M. Hauck, Philipp Uhl, Ximian Xiao, Runhui Liu and Olivia M. Merkel

"Protein Corona Investigations of Polyplexes with Varying Hydrophobicity – from Method Development to *in vitro* Studies"

International Journal of Pharmaceutics 2023, submitted 04/2023

Natascha Hartl, Bettina Gabold, Philipp Uhl, Ximian Xiao, Walter Mier, Runhui Liu and Olivia M. Merkel

"ApoE - Functionalization of Nanoparticles for Targeted Brain Delivery - A Feasible Method for Polyplexes?"

Advanced Therapeutics 2023, submitted 05/2023

Natascha Hartl, Bettina Gabold, Friederike Adams, Philipp Uhl, Sabrina Oerter, Sabine Gätzner, Marco Metzger, Ann-Christine König, Stefanie M. Hauck, Antje Appelt-Menzel, Walter Mier, Gert Fricker and Olivia M. Merkel

"Overcoming the Blood-Brain Barrier? - Prediction of Blood-Brain Permeability of Hydrophobically Modified Polyethylenimine Polyplexes for siRNA Delivery into the Brain with *in vitro* and *in vivo* Models"

Journal of Controlled Release 2023, submitted 04/2023

2. Abstracts or/and Poster Presentations

Natascha Hartl, Friederike Adams, Runhui Liu, Olivia M. Merkel

"Performance of Differently Composed Nylon-3 Copolymers in Targeted siRNA Delivery"

16th European Symposium on Controlled Drug Delivery, Egmond aan Zee, Netherlands April 8 - 10, 2020

Natascha Hartl, Friederike Adams, Olivia M. Merkel

"Amphiphilic Nylon-3 Polymers for Enhanced siRNA Delivery into Glioblastoma Cells"

12th World Meeting on Pharmaceutics, Biopharmaceutics and Pharmaceutical Technology, Vienna, Austria, March 23 - 26, 2020

Natascha Hartl, Friederike Adams, Olivia M. Merkel

"Amphiphilic Nylon-3 Polymers for Enhanced siRNA Delivery into Glioblastoma Cells"

CRS German Chapter Annual Meeting 2020, Munich, Germany, February 20 - 21, 2020

Friederike Adams, Natascha Hartl, Runhui Liu, Olivia M. Merkel

"The Impact of Nylon-3 Copolymer Composition on the Efficiency in siRNA Delivery"

International Conference on Nanomedicine and Nanobiotechnology (ICONAN) Munich, Germany. October 16 - 18, 2019

Natascha Hartl, Friederike Adams, Gabriella Costabile, Olivia M. Merkel

"Amphiphilic Nylon-3 Polymers for Enhanced siRNA Delivery into Glioblastoma Cells"

Symposium on Innovative Polymers for the Nanomedicine of the 21st Century, Jena, Germany, July 15 - 17, 2019

Natascha Hartl, Friederike Adams, Gabriella Costabile, Olivia M. Merkel

"Amphiphilic Nylon-3 Polymers for Enhanced siRNA Delivery into Glioblastoma Cells"

Bad Herrenalber Transporter und Barrieretage, Bad Herrenalb (Germany), May 27 – 29, 2019

Natascha Hartl, Gabriella Costabile, Olivia M. Merkel

"Transferrin Conjugated Nylon-3 Polymers for Delivering siRNA Across the BBB in the Treatment of Glioblastoma"

NIM Conference "The future of nanoscience" Tutzing (Germany), September 4 – 6, 2018

Natascha Hartl, Gabriella Costabile, Olivia M. Merkel

"Transferrin Conjugated Nylon-3 Polymers for Delivering siRNA Across the BBB in the Treatment of Glioblastoma"

ESCDD, Egmond aan Zee/Netherlands, April 11 – 13, 2018